Toward an innovative treatment of Alzheimer's disease : Design of novel multi-target directed ligands

Mégane Pons

Normandie Université

THÈSE

Pour obtenir le diplôme de doctorat

Spécialité Chimie

Préparée au sein de l'Université de Rouen Normandie

Toward an innovative treatment of Alzheimer's disease: Design of novel multi-target directed ligands

Présentée et soutenue par
Mégane PONS

Thèse soutenue publiquement le 06 Décembre 2019 devant le jury composé de		
Pr. Diego MUÑOZ-TORRERO	Professeur, Université de Barcelone	Rapporteur
Dr. Catherine GUILLOU	Directrice de recherche, Université de Paris-Saclay	Rapporteur
Pr. Sylvain ROUTIER	Professeur, Université d'Orléans	Examinateur
Pr. Maria Laura BOLOGNESI	Professeur, Université de Bologne	Examinateur
Dr. Rómulo ARAOZ	Chargé de recherche, Institut de Neurosciences Paris-Saclay	Membre invité
Pr. Pierre-Yves RENARD	Professeur, Université de Rouen	Examinateur (Directeur de thèse)
Dr. Ludovic JEAN	Maitre de conférences, Université de Rouen	Examinateur (Co-directeur de thèse)

Thèse dirigée par Pierre-Yves RENARD et Ludovic JEAN, laboratoire COBRA, UMR 6014

UNIVERSITÉ DE ROUEN NORMANDIE

ED 508 NC Normande de Chimie

Laboratoire Cobra

Normandie Université

THÈSE

Pour obtenir le diplôme de doctorat

Spécialité Chimie

Préparée au sein de l'Université de Rouen Normandie

Toward an innovative treatment of Alzheimer's disease: Design of novel multi-target directed ligands

Présentée et soutenue par
Mégane PONS

Thèse soutenue publiquement le 06 Décembre 2019 devant le jury composé de		
Pr. Diego MUÑOZ-TORRERO	Professeur, Université de Barcelone	Rapporteur
Dr. Catherine GUILLOU	Directrice de recherche, Université de Paris-Saclay	Rapporteur
Pr. Sylvain ROUTIER	Professeur, Université d'Orléans	Examinateur
Pr. Maria Laura BOLOGNESI	Professeur, Université de Bologne	Examinateur
Dr. Rómulo ARAOZ	Chargé de recherche, Institut de Neurosciences Paris-Saclay	Membre invité
Pr. Pierre-Yves RENARD	Professeur, Université de Rouen	Examinateur (Directeur de thèse)
Dr. Ludovic JEAN	Maitre de conférences, Université de Rouen	Examinateur (Co-directeur de thèse)

Thèse dirigée par Pierre-Yves RENARD et Ludovic JEAN, laboratoire COBRA, UMR 6014

UNIVERSITÉ DE ROUEN NORMANDIE

ED 508 NC Normande de Chimie

Laboratoire Cobra

Remerciements

To begin with, I would like to thank all the member of the jury who kindly accepted to judge and evaluated the work I have done in the past wonderful three years. You are all inspirational experts to look up to and I feel lucky to have crossed your paths during my PhD adventure.

Je voudrais chaleureusement remercier mes deux directeurs de thèse, le professeur Pierre-Yves Renard et le docteur Ludovic Jean qui m'ont fait confiance et donné ma chance pour porter ce nouveau projet. Merci à vous deux pour l'autonomie que vous m'avez accordée, je me souviens d'une phrase très importante prononcée par vous Pierre-Yves pendant mon entretien : «Le but ici est de former des chercheurs », alors un immense merci pour cette formation durant laquelle j'ai beaucoup appris.
Ludo, merci d'avoir toujours été présent malgré ton emploi du temps chargé (et tous tes soucis de voiture :-)), tu es un encadrant rêvé qui a toujours de bons conseils et tu es toujours ouvert à la discussion pour la chimie mais aussi pour pleins d'autres sujets.

Je voudrais aussi adresser mes remerciements à tous nos collaborateurs sans qui ce projet n'aurait pas pu se faire, merci au Pr. Sylvain Routier, au Pr. Sylvie Chalon, au Pr. Manuela Bartolini et au Pr. Diego Muñoz-Torrero et à leurs équipes pour leur grande expertises (en chimie ou biologie) et leur disponibilité.

Mes remerciements vont aussi à tous les permanents du 2ème étage mais aussi à Tia[2] et Emilie, les reines de la purification qui se souviendront longtemps des galères que j'ai pu leur faire endurer avec mes huprines.

Evidemment, je voudrais aussi remercier du fond du cœur tous les doctorants, post-doctorants (anciens et nouveaux) et stagiaires que j'ai eu la chance de côtoyer et sans qui ces 3 années n'auraient pas eu la même saveur. Pour les anciens, merci à Pierrick qui va pouvoir arrêter de m'appeler la bleue, à Arnaud qui n'arrêtera certainement pas de m'appeler paupiette, à Pepito le roi pour m'embêter en salle de pause, à Pauline pour les pauses clopes à râler principalement mais aussi à rire, à Wiwi dit la panthère pour ses blagues douteuses et sa tête toute rouge qui suivait, à Kevin Bescherelle pour ses jeux de mots pourris qui me faisaient bien rire même si je levais les yeux au ciel et à Morgane pour nos discussions (souvent devant la semi-prep) qui me faisaient toujours beaucoup de bien. Je souhaite aussi remercier Justine, ma super stagiaire, avec qui j'ai beaucoup rigolé (malgré toi souvent), je ne pouvais pas rêver mieux pour mon premier job d'encadrante.

Au tour des nouveaux, ceux que j'ai croisé le long de mon parcours, je voudrais commencer par remercier grandement Julien qui a su me soutenir et beaucoup m'aider pendant ma rédaction, merci aussi au trio de copains d'apéro et de randos (plus souvent d'apéro quand même ^^) : Steven (monsieur je -pinaille), Maxime le roukmoute roi de l'organisation de voyage et Madelein à qui je dois certainement mes plus gros fous rires à l'IRCOF. Olé !!! Merci aussi à Pierre, Margot et Alexis. Bon courage pour la suite, tenez bon !
A ceux de ma promo, Speedy pour tes conseils (pas si) avisés de rédaction, Mahmoud, Batoul, Dorra et Matthieu dit Kim Jung Hun ou le champion du monde de tetris (TUT !).

Mes remerciements vont aussi tout particulièrement à deux anciennes de l'IRCOF, des collègues devenues amies, Flo et Elo. Merci pour vos conseils, votre soutien et merci d'avoir su me redonner confiance dans les moments difficiles ou je ne croyais plus en moi et surtout merci pour les soirées à pleurer de rire. Vous êtes les meilleures !

Et parce que ma vie ne se trouve pas qu'à l'IRCOF, je voudrais aussi remercier mes deux amies Caro (ma tâche de vin préférée) et Laeti qui m'ont laissée les saouler avec mes histoires du monde un peu fou de la chimie.

Merci aussi évidemment à mes amis de toujours, ceux avec qui j'ai commencé cette grande aventure de la chimie et qui m'ont fait connaître la vie étudiante (un peu dans l'excès parfois) et qui m'ont initiée à la contrée, vous êtes mon capot cœur, cette thèse est aussi pour vous, Thibault, Maxence, Quentin, Emilie, Orion et Valou, ne changez jamais les copaings! BAGDOU 4EVER !

Mes pensées vont aussi à mes parents sans qui tout cela ne serait jamais arrivé. Merci à vous d'avoir cru en moi, de m'avoir toujours soutenue, aidée et poussée à toujours aller plus loin depuis le jeune âge ou je vous ai fièrement dit que je voulais être chercheuse. Vous êtes le pilier de ma réussite, je vous dois tellement, MERCI !

Enfin, le reste de mes remerciements et de mon cœur vont à mon amour, mon meilleur ami (oui je sais, c'est cliché et alors ? :-)), à toi Kevin. Tu as su me faire rire quand je voulais pleurer et tu m'as convaincue que je pouvais déplacer des montagnes. Merci d'avoir supporté mon caractère de cochon et rendu la fin de cette aventure plus douce et merci d'avoir partagé mes peines autant que mes réussites. Si dans tes yeux, je lis de la fierté, sache que dans les miens, tu peux lire une immense gratitude et un amour sans faille.

“Ever tried.

Ever failed.

No matter.

Try again.

Fail again.

FAIL BETTER”

Samuel Becket

« Dans la vie, rien n’est à craindre tout est à comprendre. »

Marie Curie

Abbreviations

5HT	5-hydroxytryptamine receptors
µg	microgram
µM	micromolar
Å	Angstrom
ACh	Acetylcholine
AChBP	Acetylcholine binding protein
AChE	Acetylcholinesterase
AChEI	Acetylcholinesterase inhibitor
Ac_2O	Acetic anhydride
AcOH	Acetic acid
AD	Alzheimer's disease
Ala	Alanine
AMBER	Assisted model building with energy refinement
AMPA	α-amino-3-hydroxy-5-methyl-4-isoxazoleprpionic acid
AMPK	5' adenosine monophosphate-activated protein kinase
Arg	Arginine
ATCh	acetylthiocholine iodide
Asn	Asparagine
Asp	Aspartic acid
APP	Amyloid Precursor Protein
Aβ	beta amyloid
BACE-1	Beta-site APP Cleaving Enzyme 1 or β-secretase
BBB	Blood brain barrier
9-BBN	9-Borabicyclo[3.3.1]nonane
BCh	Butyrylcholine
BChE	Butyrylcholinesterase
Boc_2O	tert-Butoxycarbonyle
BTCh	butyrylthiocholine iodide
CADD	Computer aided drug design
CAM	Cerium ammonium molybdate
CDK-5	Cyclin-dependent kinase 5
ChE	Cholinesterase

CK1	Casein kinase 1
CNS	Central nervous system
CNS MPO	Central nervous system multiparameter optimisation
CO	Carbon monoxide
CSA	Camphorsulfonic acid
CuAAC	Copper-catalysed alkyne-azide cycloaddition
CuI	Copper iodide
Cys	Cysteine
*d*AChE	*drosophila* acetylcholinesterase
DavePhos	2-Dicyclohexylphosphino-2'-biphenyl
DCM	Dichloromethane
DNA	Deoxyribonucleic acid
DMSO	Dimethylsulfoxyde
DMF	Dimethylformamide
1,2-DCE	1,2-dichloroethane
DPPH	2,2-diphenyl-1-picrylhydrazyl
E_{bind}	Binding energy
EC	Extracellular
EC_{50}	Half maximal effective concentration
EDC.HCl	1-Ethyl-3-(3-diméthylaminopropyl)carbodiimide chlorhydrate
*ee*AChE	*Electrophorus Electricus* acetylcholinesterase
EEDQ	N-Ethoxycarbonyl-2-ethoxy-1,2-dihydroquinoline
Equiv	Equivalent
Et_3N	Triethylamine
EtOAc	Ethyl acetate
EtOH	Ethanol
Et_2O	Diethyl ether
FDA	Food and Drugs Administration
FDG	Fluorodeoxyglucose
Fu	Fraction unbound in brain tissue
GDP	Gross domestic product
Gln	Glutamine
Glu	Glutamate
GSK3	Glycogen synthase kinase 3

Gly	Glycine
GRK-5	G protein-coupled receptor kinase 5
GTO	Granular tau oligomer
*h*AChE	*human* acetylcholinesterase
*h*BACE-1	Human β-secretase
HBD	Hydrogen bond donor
His	Histidine
HMG-coA	3-hydroxy-3-methyl-glutaryl coenzyme A
HNO_3	Nitric acid
HPLC	High performance liquid chromatography
H_3R	Type 3 histamine receptor
H_2SO_4	Sulfonic acid
IBX	2-Iodoxybenzoic acid
IC_{50}	Half maximal inhibitory concentration
Ile	Isoleucine
Kcal	kilocalorie
KDa	Kilo Dalton
Leu	Leucine
LiHMDS	Lithium Bis(trimethylsilyl)amide
LiTMP	Lithium tetramethlpiperidide
LOF	Large open-field
LogPS	Permeability surface
LTP	Long-term potentiation
Lys	Lysine
*m*AChE	*Mouse* acetylcholinesterase
mAChR	Acetylcholine muscarinic receptors
MAO	Monoamine oxidases
MARK	Microtubule affinity-regulating kinase
MAP	Microtubule associated protein
Me	Methyl
MeOH	Methanol
MeCN	Acetonitrile
Met	Methionine
Me_3SiI	Trimethylsilyl chloride
mg	milligram

mM	millimolar
MMFF	Merck Molecular Force Field
mmol	millimole
MRI	Magnetic resonance imaging
MsCl	Methanesulfonyl chloride
MTDL	Multi-Target Directed Ligand
mw	microwave
MW	Molecular weight
nAChR	Acetylcholine nicotinic receptors
NaHMDS	Sodium bis(trimethylsilyl)amide
NaOMe	Sodium methanolate
n-BuLi	N-butyllithium
NFT	Neurofibrillary tangle
NH_2OH	Hydroxylamine
NMJ	Neuromuscular junction
nM	nanomolar
NMDA	N-methyl-D-aspartate
NMDAR	N-methyl-D-aspartate receptor
NOL	Novel object localization
NOR	Novel object recognition
ORAC	Oxygen radical absorbance capacity
PAM	Positive allosteric modulator
PAS	Peripheral Anionic Site
PBS	Phosphate-buffered saline
PDB	Protein data bank
Pd/C	Palladium on carbon
$PdCl_2(dppf)$	[1 ,1'-Bis(diphenylphosphino)ferrocene]dichloropalladium(II)
$Pd_2(dba)_3$	Tris(dibenzylideneacetone)dipalladium(0)
$Pd(PPh_3)_2Cl_2$	Bis(triphenylphosphine)palladium(II) dichloride
$Pd(OAc)_2$	Palladium(II) acetate
$Pd(PPh_3)_4$	Palladium(0) triphenylphosphine tetrakis
PE	Petroleum ether
P_e	*In vitro* permeability
PET	Positron emission tomography
PKA	Cyclic AMP-dependent protein kinase A

Phe	Phenylalanine
PHF	Paired helical filament
PhMe	Toluene
PIB	Pittsburgh compound
PK	Pharmacokinetic
PMA	Phosphomolybdic acid
PMP	1-[^{11}C]MEthylpiperidin-4-yl propionate
PPh_3	Triphenylphosphine
PTSA	paratoluenesulfonic acid
QSAR	Quantitative structure activity relationship
*rh*AChE	Recombinant human acetylcholinesterase
RNA	Ribonucleic acid
RNS	Reactive nitrogen species
ROS	Reactive oxygen species
rt	Room temperature
SAR	Structure activity relationship
Ser	Serine
TBAB	Tetra-n-butylammonium bromide
TBAF	Tetrabutylammonium fluoride
TBDMSCl (or TBSCl)	tert-Butyldimethylsilyl chloride
t-BuOH	tert-butanol
TBTA	Tris((1-benzyl-4-triazolyl)methyl)amine
*Tc*AChE	*Torpedo californica* acetylcholinesterase
THF	Tetrahydrofuran
Tf	Triflate
TFA	Trifluoroacetic acid
TfN_3	Trifluoromethanesulfonyl azide
Tf_2O	Triflic anhydride
$TiOEt_4$	Titanium (IV) ethoxyde
TLC	Thin-layer chromatography
TM	Transmembrane
TMS	Tetramethylsilane
TPSA	Topological polar surface area
Trp	Tryptophan

Tyr	Tyrosine
THF	Tetrahydrofuran
Val	Valine
XPhos Pd G3	(2-Dicyclohexylphosphino-2′,4′,6′-triisopropyl-1,1′-biphenyl)[2-(2′-amino-1,1′-biphenyl)]palladium(II) methanesulfonate

Summary

General introduction

Chapter I: Huprine-Capsaicin hybrid design and biological evaluations

Chapter II: Development of combined MTDLs based on the Rivastigmine scaffold

General conclusion

Experimental part

Preamble

Alzheimer's disease is complex neurodegenerative disease characterised by a progressive loss of memory and cognition. AD is the first cause of dementia of people over 75 years old and affects around 20% of people of more than 75 years old. With more than 4.6 million new cases of dementia per year in the world, finding a treatment against AD is real public health issue. We estimate that 46.8 million people were affected with dementia in 2015 and this number will grow to reach 135.5 million in 2050. AD is a multifactorial disease with diverse metabolic consequences such as the apparition of "senile plaques" formed by the *β*-amyloid peptide (Amyloid cascade hypothesis), the neuroinflammation, the oxidative stress, the hyperphosphorylation of the Tau protein leading to neurofibrillary tangles, and finally a diminution of the levels of Acetylcholine (Cholinergic hypothesis).

Despite the apparition of biomarkers allowing an early diagnosis, there is no existing curative treatment of the disease to date. Indeed, actual treatments only have a palliative action, their goal is to improve the patient's life and to slow down the progression of AD.

In view of the complexity of AD, the therapeutic paradigm "one compound-one-target" has shown its limits in the treatment of AD. Thus, new strategies are emerging to overcome the lack of efficiency of the current pharmacotherapy in the last past decade.

My PhD subject consisted in designing and developing series of original multi-target directed ligands (MTDL). Indeed, this therapeutic strategy appears to be the most promising and efficient approach to obtain innovative drugs against CNS-related pathologies. Over the past few years, numerous MTDLs targeting AChE and another therapeutic target of AD such as kinases, MAO-A and B, oxidative stress and α7 nicotinic receptors were designed and synthetized by Professor Renard's team. In collaboration with the Professor Routier (ICOA, Orléans), we developed new combined MTDLs able to act simultaneously on two targets involved in AD: acetylcholinesterase and α7 nicotinic receptors. The *in vitro* affinities of the compounds toward α7 nicotinic receptors were assayed by Professor Chalon's team (CHU of Tours) who has a great expertise in the domain of nicotinic receptors, and the cholinesterases inhibition assays were performed by Professor Bartolini's team (University of Bologna).

Another part of my PhD consisted in preparing a heterodimer Huprine-Capsaicin targeting acetylcholinesterase and oxidative stress induced by AD, based on the previous work of Dr. Sovy Chao, Dr. Killian Oukoloff and Dr. Monika Bouet, former researchers and in collaboration with the Professor Diego Muñoz-Torrero, pioneer in the development of huprine compounds as anti-AD drugs.

This manuscript is made up of a general introduction, three chapters, a conclusion and an experimental part. The introduction will be dedicated to general information concerning AD, its histopathology, the

known therapeutic targets, the several approved or awaiting approval drugs, the multi-target directed ligand concept and a non-exhaustive bibliographic study of the various MTDLs designed in the past years. The first chapter will concern the design, synthesis and biological *in vitro* evaluation of a heterodimer linking a huprine fragment able to inhibit AChE and a capsaicin fragment with antioxidant properties whose *in vivo* elevations are ongoing in the laboratory of Pr. Inestrosa in Chile. Then, the chapter II will be dedicated to the *in silico* assays, design, synthesis and *in vitro* evaluation of a new family of combined MTDLs based on the Rivastigmine scaffold, an AChE inhibitor, combined to a quinuclidine fragment, an α7 nicotinic receptors agonist designed by our collaborators, the Professor Routier's team. Finally, the chapter III will expose our synthetic efforts in order to develop another new family of combined MTDLs targeting AChE and α7 nicotinic receptor by combining Donepezil's structure and the quinuclidine scaffold from the α7 nAChR ligands developed by our partner in Orleans. Finally, in the conclusion, we will summarize the main results (syntheses and biological evaluations) and the perspectives of this project.

General introduction

1. History of Alzheimer's disease[1]

In 1901, the German psychiatrist and neuropathologist Aloïs Alzheimer studied the case of a 51 years old woman. Auguste Deter was admitted in the Frankfort hospital for dementia. Her symptoms were various, she was suffering from memory troubles, mutism, disorientation and hallucinations. These symptoms were already well known in cases of dementia, but it was the first time they were observed in such a young patient.

Picture 1: Picture of Alois Alzheimer

After her death, in 1906, Aloïs Alzheimer performed an autopsy of her brain and discovered two major neuropathologic lesions: senile plaques and neurofibrillary deterioration.

He observed a cortex's atrophy and the loss of grey matter layers. This peripherical part of the brain is involved in memory, reflexion and language associated mechanisms. Moreover, he discovered, using a brain's slice coloured with silver salt observed with a microscope, the presence of two abnormal residues, one intracellular and another extracellular. Once again, these residues had already been noticed inside the brains of older patients[2].

In 1910, the name "Alzheimer's disease" was given to the pathology by Emil Kraeplin, a professor in psychiatry and director of the Ludwig-Maximilians-Universität München psychiatry laboratory. Other scientists are not to be neglected in the discovery:

- Oskar Fischer, a Czech psychiatrist and neuropathologist, described the existence of senile plaques in the brains of 12 patients diagnosed with dementia[3],

[1] Historique de la maladie d'Alzheimer : découverte, identification ... *Fondation Vaincre Alzheimer*.

[2] Alzheimer, A. über eigenartige Krankheitsfälle des späteren Alters. *Z. Für Gesamte Neurol. Psychiatr.* **1911**, *4* (1), 356.

[3] Fischer, O. Miliare Nekrosen mit drusigen Wucherungen der Neurofibril-len, eine regelma¨ssige Vera¨nderung der Hirnrinde bei seniler. *R DemenzMonatsschr Psychiat Neurol* **1907**, *22*, 361–372.

- Gaetano Perusini, collaborator of Aloïs Alzheimer, also helped a lot to the discovery of AD[4].

In the 80's, thanks to the progress in medicine and particularly in the development of new analytical tools, the biological constituents of the AD's lesions were characterised:

- the beta-amyloid protein was described as the major constituent of the senile plaques in 1984 by George Glenner, an American pathologist[5],
- in 1985, the Belgian Jean-Pierre Brion brought to light the implication of Tau protein hyperphosphorylation in the neurofibrillary deterioration[6].

2. Worldwide impact and epidemiology

AD is the first cause of dementia in the elderly patients and affects at least 20% of the elders over 75 years of age. With more than 4.6 million of new cases of dementia each year worldwide, finding a treatment for AD is a global public health challenge. An estimate of 46.8 million people was diagnosed with dementia in 2015. Moreover, with an aging population, this number could raise to 135.5 million in 2050[7]. Dementia is a general term which includes AD but also vascular dementia, fronto-temporal dementia and Lewi's body dementia. The prevalence of the various pathologies is substantially different, indeed, AD is diagnosed in 50% to 75% of cases whereas vascular dementia is diagnosed in 20% to 30% of cases, the average is 5% to 10% for the fronto-temporal dementia and less than 5% for the Lewi's body dementia.
Moreover, even if AD is a worldwide public health issue (Figure 1), it seems that people over 60 years of age in developing countries are less impacted by these disorders.

[4] Perusini, G. U˙ber klinisch und histologisch eigenartige psychischeErkrankungen des spa¨teren Lebensalters. *Nissl-Alzheimers HistolHistopathol Arb Hirnr* **1909**, *3*, 297–351.
[5] Glenner, G. G.; Wong, C. W. Alzheimer's Disease: Initial Report of the Purification and Characterization of a Novel Cerebrovascular Amyloid Protein. *Biochem. Biophys. Res. Commun.* **1984**, *120* (3), 885–890.
[6] Brion, J. P.; Passareiro, H.; Nunez, J.; Flament Durand, J. Mise en évidence immunologique de la protéine tau au niveau des lésions de dégénérescence neurofibrillaire de la maladie d'Alzheimer. *Arch. Biol. (Liege)* **1985**, *95*, 229–235.
[7] World Alzheimer Report 2015: The Global Impact of Dementia | Alzheimer's Disease International https://www.alz.co.uk/research/world-report-2015.

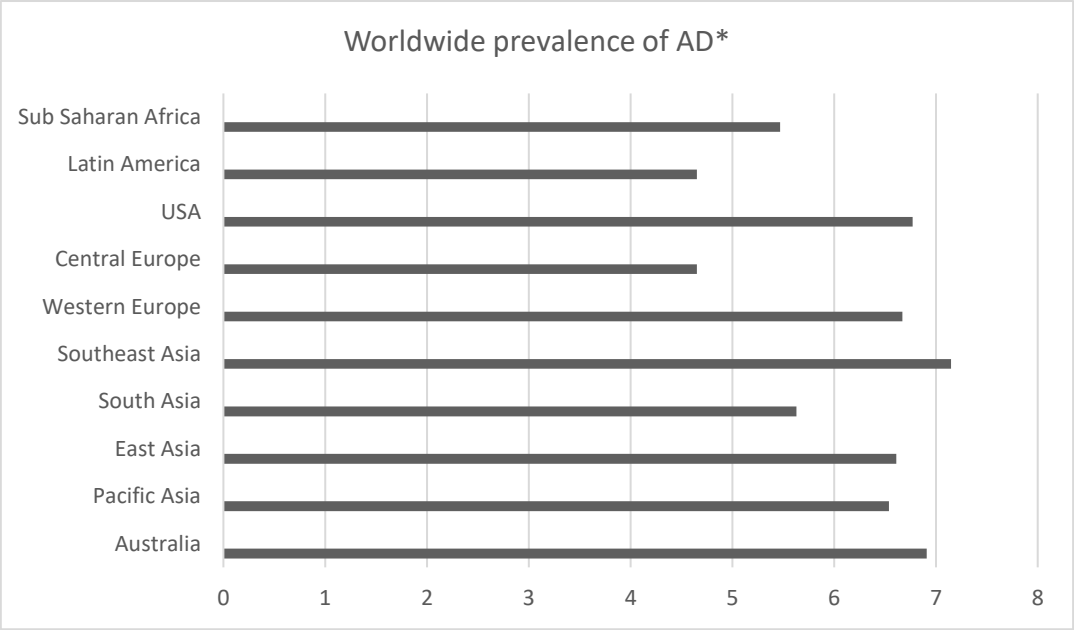

*Values were standardized to the values of Western Europe

Figure 1: Worldwide prevalence of AD

Another issue needing to be raised is the economic impact associated with these pathologies. Indeed, in 2010, the cost of the patients' care was evaluated at 604 billion US dollars, which is comparable to 1% of the global GDP. As an example, 70% of global costs are represented by western Europe and USA. These figures emphasize the fact that the patients' care is not the same internationally.

3. Disease symptoms[8]

Concerning AD 's symptoms, they can be divided in two types:

- the cognitive symptoms,
- the behavioural and psychological symptoms.

Being aware of these disruptions is a way to detect the pathology and diagnose its progress, but also to adapt the patient's care.

[8] Les symptômes de la maladie d'Alzheimer https://www.francealzheimer.org/maladie-dalzheimer-vos-questions-nos-reponses/symptomes-de-maladie-dalzheimer/.

3.1. Cognitive symptoms

The memory loss is usually the first visible cognitive AD's symptom. At first, the episodic memory of the patient is lost, the person forgets recent events but not older memories. Because AD is a neurodegenerative disease, the symptoms are evolutionary, and at some point, the other types of memories are affected (work memory, loss of words, etc). Thus, it starts to be complex to remember immediate information, to learn new skills and to orient oneself in space.

After the memory symptoms, the other important troubles are related to the language and are called aphasia. The patient progressively loses the communicating, understanding and finally talking abilities. First, the vocabulary is reduced, then, the person speaks with less and less words until he reaches a total muteness. Then, usual moves begin to be challenging to perform. It usually begins with complex actions like writing but ends with easy tasks like masticating or swallowing. Moreover, people with AD tend to forget faces they knew, it is called agnosia. After this, the executive functions' dysfunction will occur, and it is more and more complicated for the patient to plan, think and focus. The patient slowly abandons these kinds of tasks and relies on other people for each one of every day's life actions.

3.2. Behavioural and psychological symptoms of dementia

Behavioural symptoms can also occur in patients with AD, like rapid and violent mood change, anxiety, irrational fear, apathy or depression and negative thought. Therefore, patients need to be taken care of at almost every moment and are not independent anymore, which contributes to the high social costs for AD.

4. Diagnosis of AD[9]

Establishing a diagnosis during the pathology's early stages is a significant challenge. Indeed, an early detection of the pathology allows a good patient's care, but differentiating AD's symptoms from normal ageing, especially during preclinical phase (Figure 2) is a major challenge.

The first warning usually comes from the patient himself or his family, they will describe a memory loss that will lead to a neuropsychological overview. The doctor will perform a series of tests to evaluate memory, but also, orientation in space and time, language, comprehension and attention.

The second way to perform AD diagnosis is the use of biochemical and imaging tools able to evaluate the different pathology biomarkers:

[9] Diagnostic de la maladie d'Alzheimer. *Fondation pour la Recherche sur Alzheimer*.

- MRI imaging,
- PET scan,
- lumbar puncture.

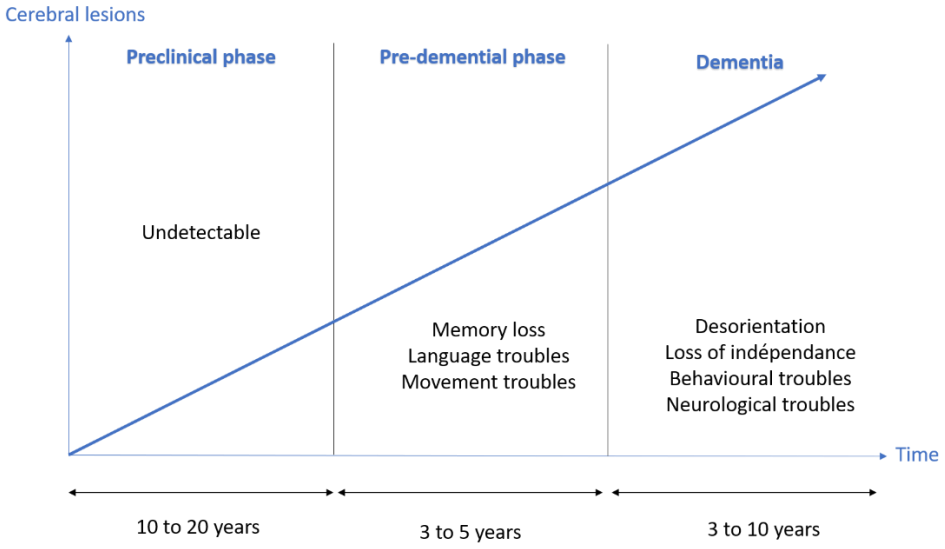

Figure 2: Evolution of AD (adapted from Dr. Alain Buisson's presentation – University of Grenoble Alpes)

4.1. MRI imaging

MRI study is a non-invasive and affordable technique allowing the doctors to visualize atrophies of certain parts of the brain like a cortical atrophy or a hippocampus atrophy. It is also used to discriminate AD from other pathologies, by visualizing a cerebral tumour for example[10]. For a few years, it has been employed to detect neuronal degeneration of AD patients and to follow the evolution of the disease in clinical trials[11].

[10] Salvatore, C.; Cerasa, A.; Castiglioni, I. MRI Characterizes the Progressive Course of AD and Predicts Conversion to Alzheimer's Dementia 24 Months Before Probable Diagnosis. *Front. Aging Neurosci.* **2018**, *10*.
[11] Sperling, R. A.; Jack, C. R.; Black, S. E.; Frosch, M. P.; Greenberg, S. M.; Hyman, B. T.; Scheltens, P.; Carrillo, M. C.; Thies, W.; Bednar, M. M.; Black, R. S.; Brashear, H. R.; Grundman, M.; Siemers, E. R.; Feldman, H. H.; Schindler, R. J. Amyloid-Related Imaging Abnormalities in Amyloid-Modifying Therapeutic Trials: Recommendations from the Alzheimer's Association Research Roundtable Workgroup. *Alzheimers Dement.* **2011**, *7* (4), 367–385.

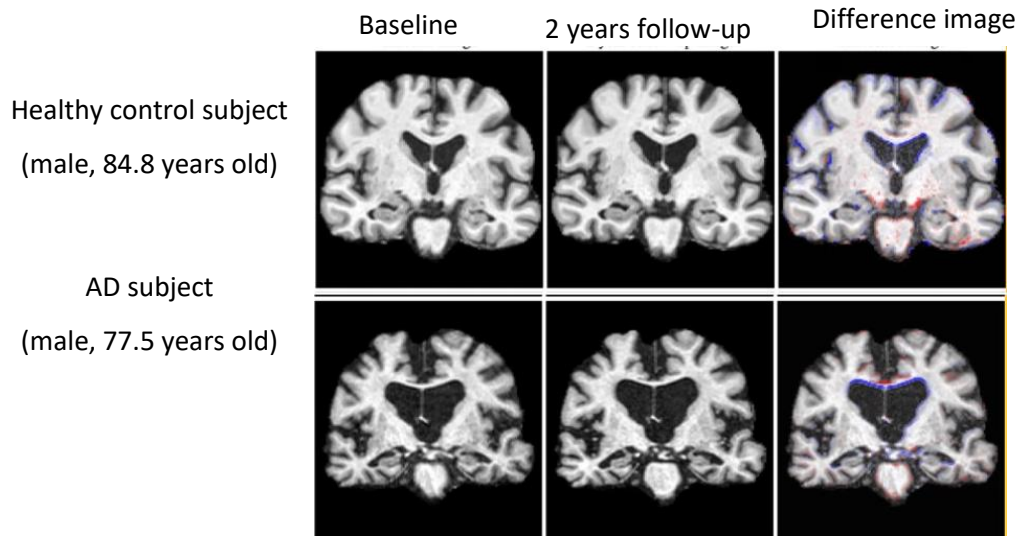

Figure 3: MR images (brain-extracted)[12]

As shown on Figure 3 [12], we can see the use of MRI to detect AD. As a matter of fact, there is a blatant difference between the healthy control brain and the AD subject's brain. MRI imaging also provides crucial information concerning the neuronal degeneration's evolution by monitoring the patient's brain.

4.2. PET scan

PET scan is a functional imaging process and is used to highlight an abnormally low effective functioning brain and to visualize neuronal lesions. Indeed, PET scan can be used to find early AD diagnosis markers[13]. Numerous brain systems can be monitored, like cerebral glucose metabolism, neurotransmitters systems, neuroinflammation and protein aggregates (beta amyloid deposits).

[12] Ledig, C.; Schuh, A.; Guerrero, R.; Heckemann, R. A.; Rueckert, D. Structural Brain Imaging in Alzheimer's Disease and Mild Cognitive Impairment: Biomarker Analysis and Shared Morphometry Database. *Sci. Rep.* **2018**, *8* (1), 11258.

[13] Oukoloff, K.; Cieslikiewicz-Bouet, M.; Chao, S.; Da Costa Branquinho, E.; Bouteiller, C.; Jean, L.; Renard, P.-Y. PET and SPECT Radiotracers for Alzheimer's Disease. *Curr. Med. Chem.* **2015**, *22* (28), 3278–3304.

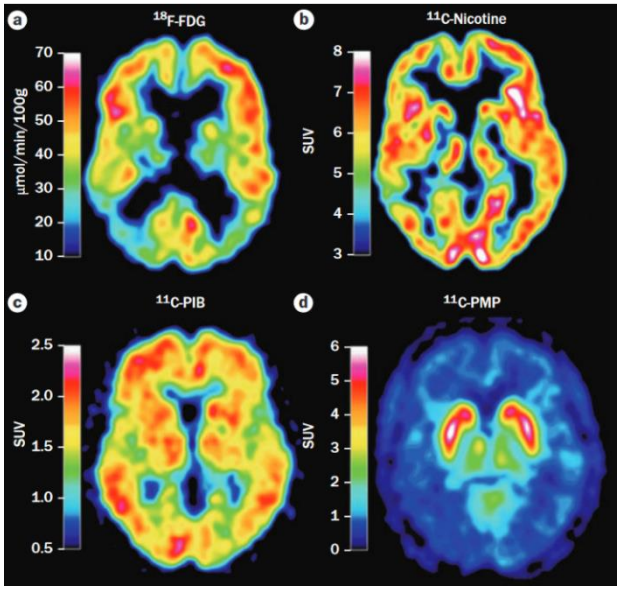

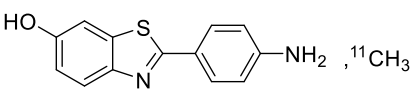

PIB: Pittsburgh compound B

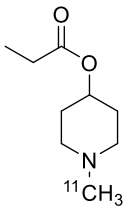

PMP: 1-[11C]Methylpiperidin-4-yl propionate

Figure 4: PET scan of an AD patient's brain[14] (discussed below) and structures of ^{11}C-PIB and ^{11}C-PMP

Low ^{18}F-FDG uptake (Figure 4 - a) is the sign of a deficit in glucose metabolism, particularly in the right hemisphere. Low ^{11}C-nicotinic binding (Figure 4 - b), reflects a deficit of cholinergic activity, a major marker of AD. High ^{11}C-PIB retention ((Figure 4 - c) is connected to the measure of fibrillar amyloid load. And finally, a high ^{11}C-PMP binding ((Figure 4 - d) leads to the conclusion that AChE activity is oddly high[14]. The monitoring of all these markers allows the doctors to diagnose patients with AD and researchers to better understand the disease thanks to a "coloured map of the brain activity".

More recently, other radiotracers[15] such as Amivid[16], Neuraceq[17] or Vizamyl[18] have been developed and FDA-approved to quantify Aβ plaques in brains of patients with AD with more accuracy (Figure 5).

[14] Nordberg, A.; Rinne, J. O.; Kadir, A.; Långström, B. The Use of PET in Alzheimer Disease. *Nat. Rev. Neurol.* **2010**, *6* (2), 78–87.

[15] Schilling, L. P.; Zimmer, E. R.; Shin, M.; Leuzy, A.; Pascoal, T. A.; Benedet, A. L.; Borelli, W. V.; Palmini, A.; Gauthier, S.; Rosa-Neto, P. Imaging Alzheimer's Disease Pathophysiology with PET. *Dement. Neuropsychol.* **2016**, *10* (2), 79–90.

[16] Fischer, F. U.; Wolf, D.; Scheurich, A.; Fellgiebel, A.; Alzheimer's Disease Neuroimaging Initiative. Altered Whole-Brain White Matter Networks in Preclinical Alzheimer's Disease. *NeuroImage Clin.* **2015**, *8*, 660–666.

[17] Syed, Y. Y.; Deeks, E. [(18)F]Florbetaben: A Review in β-Amyloid PET Imaging in Cognitive Impairment. *CNS Drugs* **2015**, *29* (7), 605–613.

[18] Thal, D. R.; Beach, T. G.; Zanette, M.; Heurling, K.; Chakrabarty, A.; Ismail, A.; Smith, A. P. L.; Buckley, C. [(18)F]Flutemetamol Amyloid Positron Emission Tomography in Preclinical and Symptomatic Alzheimer's Disease: Specific Detection of Advanced Phases of Amyloid-β Pathology. *Alzheimers Dement. J. Alzheimers Assoc.* **2015**, *11* (8), 975–985.

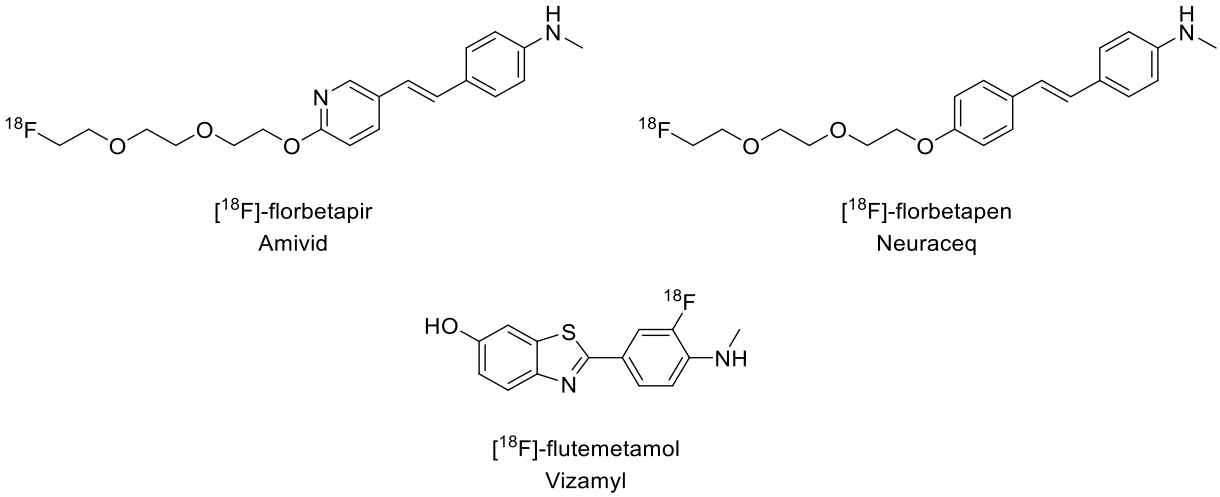

Figure 5: Structures of Aβ plaques biomarkers

In addition, Tau-specific PET tracers are currently in early stages of clinical trials, Flortaucipir[19] and THK5317[20] have displayed promising *in vivo* results as biomarkers for Tau pathology (Figure 6).

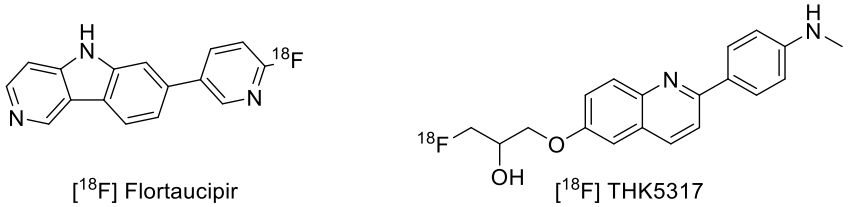

Figure 6: Structures of Tau pathology biomarkers

4.3. Lumbar puncture

The lumbar puncture is used with increasing frequency since it gives major information for the diagnosis of AD. This procedure begins with a sample collection of the cerebrospinal fluid, followed by a fluid's dosage to detect specific AD biomarkers levels such as hyperphosphorylated and normal Tau protein and beta-amyloid peptide. It helps the early stage diagnosis of the pathology, indeed, it has been observed that, rapidly, the Tau protein concentration raises to 2 or 3 times compared to a normal concentration and the hyperphosphorylated Tau protein is a major biomarker of the disease[21].

---

[19] Schonhaut, D. R.; McMillan, C. T.; Spina, S.; Dickerson, B. C.; Siderowf, A.; Devous, M. D.; Tsai, R.; Winer, J.; Russell, D. S.; Litvan, I.; Roberson, E. D.; Seeley, W. W.; Grinberg, L. T.; Kramer, J. H.; Miller, B. L.; Pressman, P.; Nasrallah, I.; Baker, S. L.; Gomperts, S. N.; Johnson, K. A.; Grossman, M.; Jagust, W. J.; Boxer, A. L.; Rabinovici, G. D. 18F-Flortaucipir Tau PET Distinguishes Established Progressive Supranuclear Palsy from Controls and Parkinson's Disease: A Multicenter Study. *Ann. Neurol.* **2017**, *82* (4), 622–634.

[20] Chiotis, K.; Saint-Aubert, L.; Savitcheva, I.; Jelic, V.; Andersen, P.; Jonasson, M.; Eriksson, J.; Lubberink, M.; Almkvist, O.; Wall, A.; Antoni, G.; Nordberg, A. Imaging In-Vivo Tau Pathology in Alzheimer's Disease with THK5317 PET in a Multimodal Paradigm. *Eur. J. Nucl. Med. Mol. Imaging* **2016**, *43*, 1686–1699.

[21] Having a lumbar puncture https://www.alzheimers.org.uk/research/take-part-research/lumbar-puncture.

5. Histopathology of AD

AD histopathology is not fully known, nevertheless, we can observe 3 aspects of the neuropathology:

- the cholinergic system,
- the amyloid cascade,
- the neurofibrillary degeneration.

5.1 The neurotransmission

5.1.1. Mechanism of the neurotransmission

The neurotransmission's mechanism is a vital process for the CNS accurate functioning (Figure 7). ACh, is the most ubiquitous neurotransmitter of the human body and is synthesized by a single step reaction from choline and acetyl coenzyme A through choline acetyltransferase catalysis (Scheme 1)[22].
ACh is formed inside the neurones, then stocked within synaptic vesicles. Its transfer to the synaptic cleft is done by an energy-dependent pump acidifying the vesicle. The neurotransmitter's purpose is to activate the synapses through binding to nicotinic and muscarinic receptors on the post-synaptic cell[22] once released into the synaptic cleft.

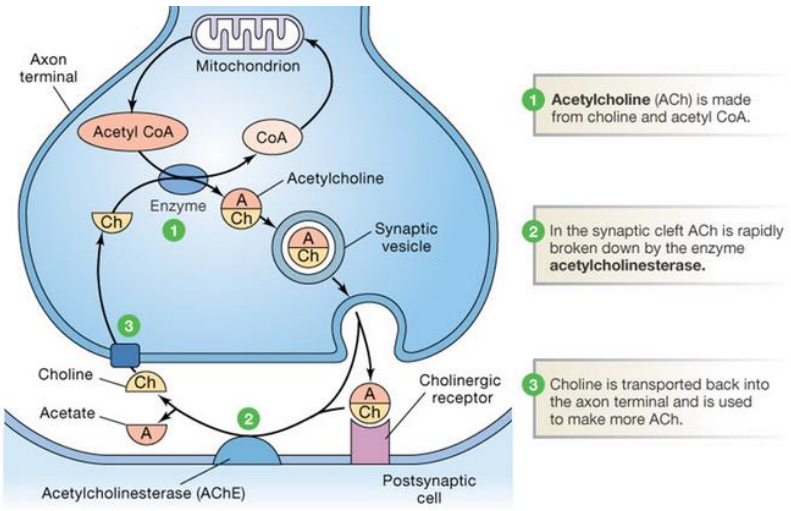

Figure 7: Mechanism of the neurotransmission[23]

Aiming at restoring the resting levels of neurotransmitter in the synaptic cleft, ACh must be hydrolysed by following a mechanism catalysed by a specific enzyme, named AChE (Scheme 1).

[22] Colovic, M. B.; Krstic, D. Z.; Lazarevic-Pasti, T. D.; Bondzic, A. M.; Vasic, V. M. Acetylcholinesterase Inhibitors: Pharmacology and Toxicology. *Curr. Neuropharmacol.* **2013**, *11* (3), 315–335.
[23] Acetylcholine Transmitter | Physiology Plus http://physiologyplus.com/acetylcholine-transmitter/.

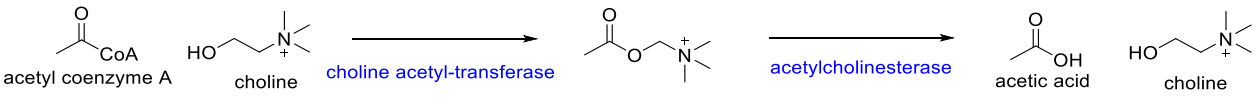

Scheme 1: Mechanism of ACh formation and hydrolysis

5.1.2. Cholinergic hypothesis

The cholinergic hypothesis was the first stated hypothesis to explain the mechanism of AD. Since 1976, numerous studies showed a misfunctioning of cholinergic system of patients with AD[24]. It has been shown that in patients with AD, ACh levels decrease in the CNS leading to a decrease of neuronal activity[25].

In 1983, Sims *et al*.[26] brought to light that ACh synthesis was significantly reduced in brain samples of patients with dementia and especially with AD (Figure 8-A). It has also been shown that choline acetyltransferase activity's decrease was linked to an increase of all kinds of dementia[27]. Indeed, Sims et *al*. showed that choline acetyltransferase activity tends to decrease in patients with AD (Figure 8-B).

[24] Bowen, D. M.; Smith, C. B.; White, P.; Davison, A. N. NEUROTRANSMITTER-RELATED ENZYMES AND INDICES OF HYPOXIA IN SENILE DEMENTIA AND OTHER ABIOTROPHIES. *Brain* **1976**, *99* (3), 459–496.

[25] Sugimoto, H.; Yamanishi, Y.; Iimura, Y.; Kawakami, Y. Donepezil Hydrochloride (E2020) and Other Acetylcholinesterase Inhibitors. *Curr. Med. Chem.* **2000**, *7* (3), 303–339.

[26] Sims, N. R.; Bowen, D. M.; Allen, S. J.; Smith, C. C. T.; Neary, D.; Thomas, D. J.; Davison, A. N. Presynaptic Cholinergic Dysfunction in Patients with Dementia. *J. Neurochem.* **1983**, *40* (2), 503–509.

[27] Ladner, C. J.; Lee, J. M. Pharmacological Drug Treatment of Alzheimer Disease: The Cholinergic Hypothesis Revisited. *J. Neuropathol. Exp. Neurol.* **1998**, *57* (8), 719–731.

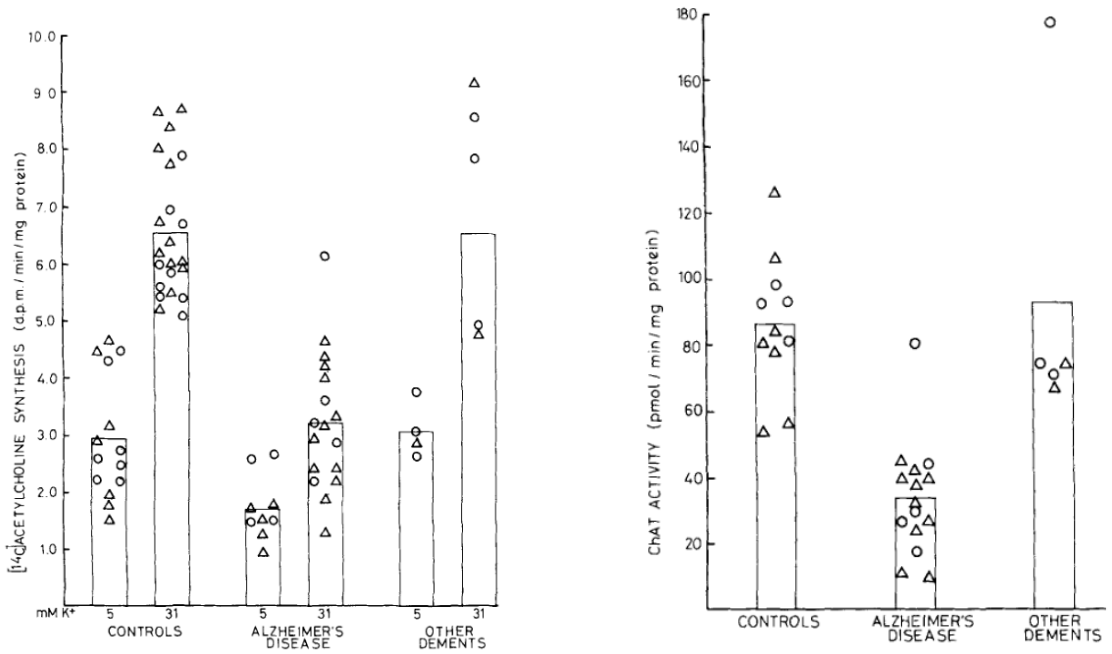

A) [^{14}C] ACh synthesis measured in the presence of either 5 mM K^+ or 31 mM K^+ in samples of temporal neocortex (Δ) and frontal neocortex (O) from neurosurgical controls, patients with AD and another dementia

B) Choline acetyltransferase activity in samples of temporal neocortex (Δ) and frontal neocortex (O) from neurosurgical controls, patients with AD and another dementia

Figure 8: Results of Sims et al. on cholinergic dysfunction in patients with dementia[26]

5.2. Amyloid cascade

Since Dr. Alzheimer's first studies in 1906, it has been shown that senile plaques and neurofibrillary deterioration are involved in AD. In the past years, different groups have investigated the role of the Aβ extracellular peptides in AD pathogenesis[28]. The APP (Amyloid Precursor Protein) is a transmembrane glycoprotein which seems to play different roles[29]:

- surface receptor,
- interactions between the cells,
- useful in the cytoskeleton formation,

[28] Hardy, J. The Amyloid Hypothesis for Alzheimer's Disease: A Critical Reappraisal. *J. Neurochem.* **2009**, *110* (4), 1129–1134.

[29] Les plaques amyloïdes — Site des ressources d'ACCES pour enseigner la Science de la Vie et de la Terre http://acces.ens-lyon.fr/acces/thematiques/neurosciences/actualisation-des-connaissances/maladies-et-traitements/alzheimer/la-maladie-dalzheimer-a-lechelle-cellulaire-et-moleculaire/les-palques.

- useful in the intracellular Ca^{2+} levels regulation,
- synapses formation,
- neurones protection against oxidative stress and interaction with the Tau protein,
- neuronal plasticity and neurotransmission in the cholinergic system.

The APP is made of up of 770 amino acids coded by only one gene found in the chromosome 21 and is found in three major forms according to the number of amino acids constituting the protein:

- APP 695 which the most common form of the young and non-pathologic brain,
- APP 751,
- APP 770 which is found in brains of premature child and in genetic forms of AD.

It has been found in 1999 that the protein is cleaved by three secretases (α, β and γ) to give amyloid peptides. The cleavage can follow two pathways: the non-amyloidogenic pathway and the amyloidogenic pathway[30].

5.2.1. The non-amyloidogenic pathway

The cleavage is initiated by an α-secretase in the cytosolic domain at the 687th amino acid of the chain to give a N-terminal peptide (APP α) and a C-terminal fragment (C83). In a second time, the γ-secretase cleaves the resulting C-terminal fragment (C83) producing a small and soluble peptide (p3) (Figure 9).

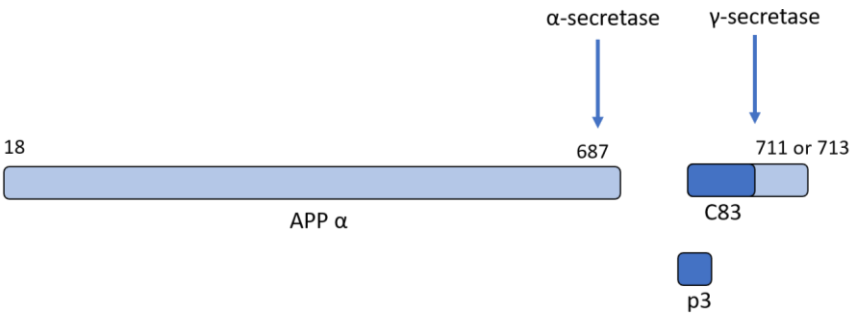

Figure 9: Non-amyloidogenic pathway of the APP cleavage

5.2.2. The amyloidogenic pathway

The amyloidogenic pathway's first step is the APP cleavage by the β-secretase at the 671th amino acid to give a N-terminal peptide (APP β) and another C-terminal fragment (C99). Then, the residual

[30] De Strooper, B. Proteases and Proteolysis in Alzheimer Disease: A Multifactorial View on the Disease Process. *Physiol. Rev.* **2010**, *90* (2), 465–494.

fragment C99 is cleaved by the γ-secretase to give two types of Aβ peptides (Figure 10). The first one is the $A\beta_{40}$ (40 amino acids) which represents normally 80-90% of the Aβ peptides in the brain and $A\beta_{42}$ (42 amino acids), produced normally in small amounts. Unfortunately, this second peptide is insoluble and cytotoxic and tends to aggregate spontaneously in oligomers leading to fibrils and senile plaques (Figure 11)[31].

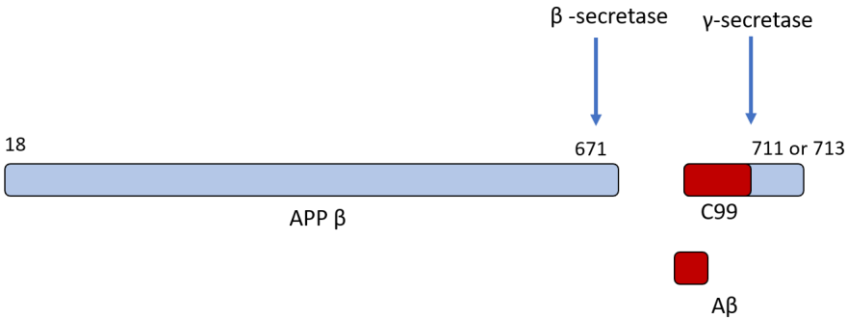

Figure 10: Amyloidogenic pathway of the APP cleavage

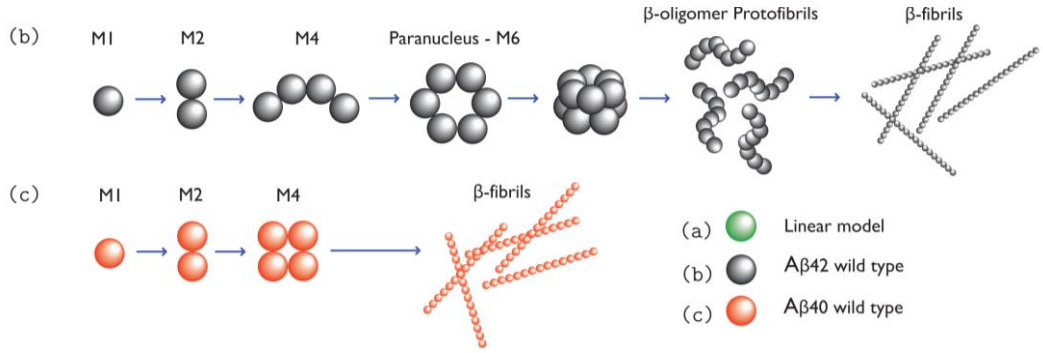

Figure 11: Formation of the senile plaques from Aβ[32]

It is well known that, in young brains, Aβ concentrations are maintained in steady-state levels because an equilibrium between its production and its elimination has been observed, this equilibrium is regulated *via* a cascade of degradative enzymes. Nevertheless, in aging brains, Aβ formation and elimination are impaired, which leads to an accumulation of the peptide and senile plaques formation causing a neuronal activity alteration induced by the neuronal cell death[33]. Moreover, studies have shown that there is a strong affinity between the Aβ peptide and the homomeric α7 nAChR facilitating

[31] Ubhi, K.; Masliah, E. Alzheimer's Disease: Recent Advances and Future Perspectives. *J. Alzheimers Dis. JAD* **2013**, *33 Suppl 1*, S185-194.
[32] Schreck, J. S.; Yuan, J.-M. Statistical Mechanical Treatments of Protein Amyloid Formation. *Int. J. Mol. Sci.* **2013**, *14* (9), 17420–17452.
[33] Shankar, G. M.; Walsh, D. M. Alzheimer's Disease: Synaptic Dysfunction and Aβ. *Mol. Neurodegener.* **2009**, *4* (1), 48.

the peptide's aggregation and an inhibition of the neuroprotection signals[34]. As shown on Figure 12, a normal low concentration of Aβ (picomolar range) does not affect the α7 nAChR activity. At higher concentration of Aβ (nanomolar range), the oligomerisation and aggregation of Aβ leads to the antagonization of nicotinic receptors.

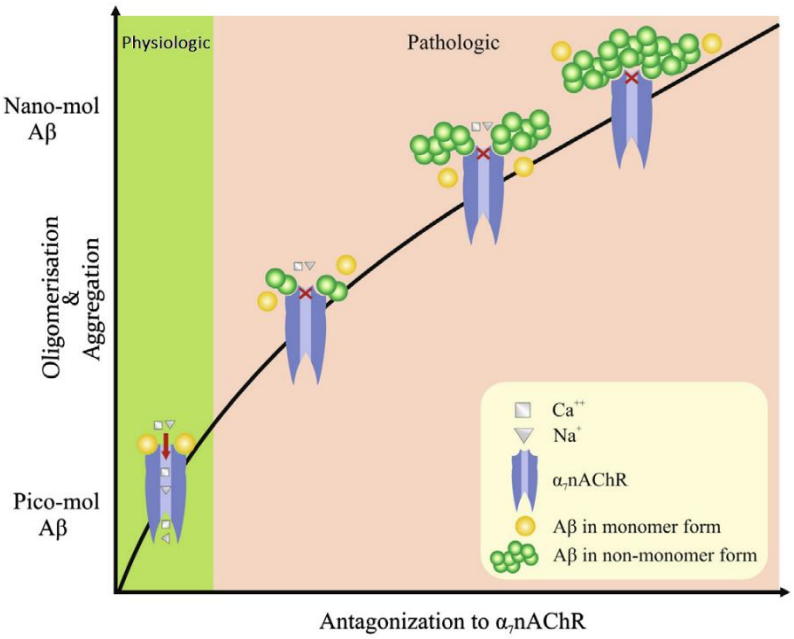

Figure 12: Interactions between the Aβ and α7 nAChR according to the concentration of Aβ[35]

5.3. Neurofibrillary degeneration

Tau proteins belong to the family of microtubule associated proteins (MAPs) and are found in many animal species. In the human case, they are mainly found in neurones where they play a major role in the formation of microtubules from tubular monomers. They also help the regulation of microtubules stability and connexion between the tubules and other elements of the cytoskeleton. They are part of a family of 6 isoforms going from 352 to 441 amino acids, these variants of the protein differ from each other by the presence of "repeat-regions" (3 or 4, R1-R4 Figure 13) in the C-terminal part of the protein. Another variation is the presence or not of one or two inserts (29 or 58 amino acids, E2 or E2/E3 Figure

[34] Yu, W.; Mechawar, N.; Krantic, S.; Chabot, J.-G.; Quirion, R. Upregulation of Astrocytic A7 Nicotinic Receptors in Alzheimer's Disease Brain- Possible Relevant to Amyloid Pathology. *Mol. Neurodegener.* **2012**, *7* (1), O7.
[35] Sadigh-Eteghad, S.; Talebi, M.; Farhoudi, M.; Golzari, S. E. J.; Sabermarouf, B.; Mahmoudi, J. Beta-Amyloid Exhibits Antagonistic Effects on Alpha 7 Nicotinic Acetylcholine Receptors in Orchestrated Manner. *J. Med. Hypotheses Ideas* **2014**, *8* (2), 49–52.

13) in the N-terminal part[36]. Because of all these differences, it might be rational to hypothesize that each isoform of the Tau protein has a different role and repartition in the body.

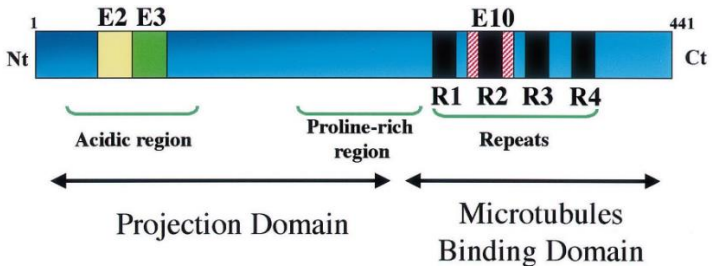

Figure 13: Schematic representation of a tau isoform[36]

The tau protein (Figure 13) is composed of two main parts:

- a projection domain with an acidic region and a Proline-rich region. This part of the protein is useful to interact with cytoskeleton elements in order to determine spacing between microtubules in axons. Thanks to a phosphorylation of serine and threonine, it allows a regulation of the interaction between the microtubules,
- a microtubule binding domain with a C-terminal part which regulates the rate of microtubules polymerisation and is also involved in the binding with proteins like protein phosphatase 2A or presenilin 1.

Tau proteins are highly hydrophilic and so, highly soluble and heat stable. In patients with AD, it has been observed that the protein is abnormally hyperphosphorylated. Indeed, Tau protein has approximately 79 sites of possible phosphorylation[37]. Concerning patients with AD, it has been observed the presence of 3 isoforms of hyperphosphorylated Tau protein: Tau_{55}, Tau_{64} and Tau_{69}. The major consequence of these insoluble and pathological isoforms formation is the loss of affinity with the microtubules, weakening the cytoskeleton and leading to neuronal death[38].
Moreover, the tau protein aggregates and polymerize to give paired helical filaments (PHF) and then neurofibrillary tangles (NFTs) (Figure 14).

[36] Buée, L.; Bussière, T.; Buée-Scherrer, V.; Delacourte, A.; Hof, P. R. Tau Protein Isoforms, Phosphorylation and Role in Neurodegenerative Disorders11These Authors Contributed Equally to This Work. *Brain Res. Rev.* **2000**, *33* (1), 95–130.
[37] Morishima-Kawashima, M.; Hasegawa, M.; Takio, K.; Suzuki, M.; Yoshida, H.; Titani, K.; Ihara, Y. Proline-Directed and Non-Proline-Directed Phosphorylation of PHF-Tau. *J. Biol. Chem.* **1995**, *270* (2), 823–829.
[38] Drechsel, D. N.; Hyman, A. A.; Cobb, M. H.; Kirschner, M. W. Modulation of the Dynamic Instability of Tubulin Assembly by the Microtubule-Associated Protein Tau. *Mol. Biol. Cell* **1992**, *3* (10), 1141–1154.

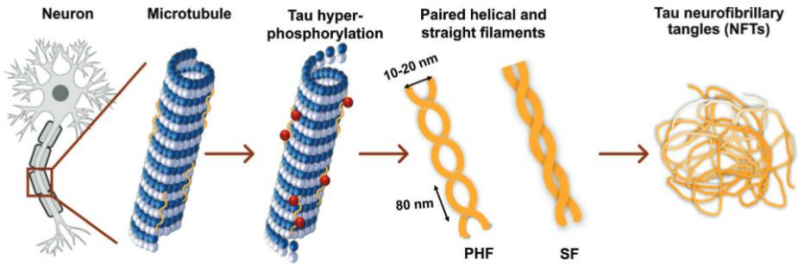

Figure 14: Illustration of the Tau protein polymerization[39]

Beginning by the monomer form of the protein, it will assemble to give a dimer with a PHF core, then a soluble oligomer and then an insoluble granular tau oligomer (GTO) which is the direct precursor of PHFs and thus of NFTs[40].

6. Therapeutic targets

Given the multifactorial nature of the pathology, a very large number of targets are studied to cure AD. Unfortunately, it would be too tedious to develop all the therapeutic targets. Hence, a choice to present the more advanced projects concerning the most widespread targets in the pharmaceuticals industries has been made. The choice was made according to the data given in Alzforum.org.

From this point of view, we observed that the main targets are:

- AChE inhibition,
- cholinergic receptors activation,
- amyloid-related strategy,
- neurofibrillary degeneration strategy,
- oxidative stress decrease.

Along with the development of new molecules related with these targets, another approach should not be disregarded, the repositioning of molecules already used in other pathologies. This approach allows the industries to gain time and money because the compounds already passed the early stages of clinical trials.

[39] Verwilst, P.; Kim, H. S.; Kim, S.; Kang, C.; Kim, J. S. Shedding Light on Tau Protein Aggregation: The Progress in Developing Highly Selective Fluorophores. *Chem. Soc. Rev.* **2018**, *47* (7), 2249–2265.

[40] Luna-Muñoz, J.; R, C.; M, C.; Flores-Rodriguez, P.; Avila, J.; R, S.; De la Cruz, F.; Mena, R.; A, M.; Floran, B. Phosphorylation of Tau Protein Associated as a Protective Mechanism in the Presence of Toxic, C-Terminally Truncated Tau in Alzheimer's Disease; **2013**.

6.1. AChE inhibition

Historically, the first studied target was AChE. Indeed, as it was explained in the beginning of this chapter, the first histopathological hypothesis was the cholinergic one. Since AChE hydrolyses ACh, the rational approach is to inhibit this enzyme to restore ACh levels in the CNS. Hence, in the 90's, the first AChE inhibitors (AChEI) were developed (

Figure 15). Today, 3 of them are still in the market (Tacrine was withdrawn because of its hepatotoxicity).

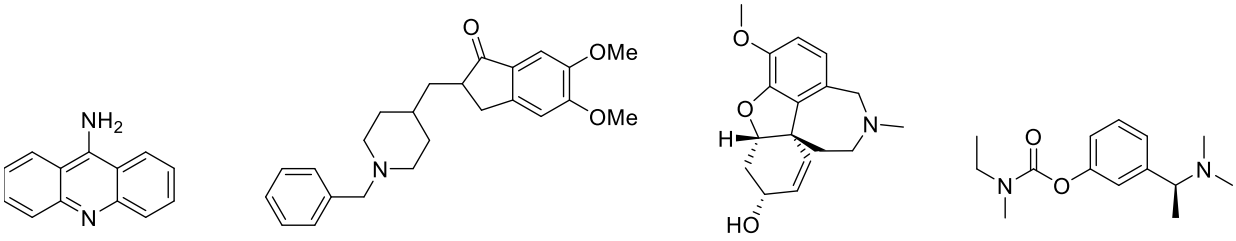

Tacrine
Pfizer
1993

Donepezil
Pfizer
1996

Galantamine
Janssen
2000

Rivastigmine
Novartis
1997

Figure 15: Commercially available AChE inhibitors

The first AChEI is Tacrine[41] described as a reversible AChEI in 1953 by Shaw and Bentley and developed by Pfizer in 1993 (and withdrawn in 2004). Tacrine causes allosteric reversible inhibition of the enzyme through its binding to a hydrophobic region near the anionic site on the enzyme's surface. Pharmacokinetic studies showed the ability of the molecule to easily cross the BBB and to inhibit the cholinesterases in the CNS. Indeed, Tacrine is not selective for AChE as compared to BChE, on the contrary the *K*i obtained for *h*AChE inhibition are of 424 nM whereas the results for *h*BChE are of 45.8 nM[42]. Even though clinical trials[43,44] have shown that doses of 120 and 160 mg/day had beneficial effects on patients, they were only palliative and failed to induce any decline of the pathology. Moreover, it has been proven that a treatment with Tacrine causes adverse effects and hepatotoxicity

[41] Tumiatti, V.; Minarini, A.; Bolognesi, M. L.; Milelli, A.; Rosini, M.; Melchiorre, C. Tacrine Derivatives and Alzheimers Disease. *Curr. Med. Chem.* **2010**, *17* (17), 1825–1838.
[42] Bolognesi, M. L.; Cavalli, A.; Valgimigli, L.; Bartolini, M.; Rosini, M.; Andrisano, V.; Recanatini, M.; Melchiorre, C. Multi-Target-Directed Drug Design Strategy: From a Dual Binding Site Acetylcholinesterase Inhibitor to a Trifunctional Compound against Alzheimer's Disease. *J. Med. Chem.* **2007**, *50* (26), 6446–6449.
[43] Arrieta, J. L.; Artalejo, F. R. Methodology, Results and Quality of Clinical Trials of Tacrine in the Treatment of Alzheimer's Disease: A Systematic Review of the Literature. *Age Ageing* **1998**, *27* (2), 161–179.
[44] Summers, W. K.; Majovski, L. V.; Marsh, G. M.; Tachiki, K.; Kling, A. Oral Tetrahydroaminoacridine in Long-Term Treatment of Senile Dementia, Alzheimer Type. *N. Engl. J. Med.* **1986**, *315* (20), 1241–1245.

due to the formation of several hydroxyderivatives during the liver metabolization by microsomal cytochrome P450 enzymes family[45].

The second well known commercially available reversible AChEI is Donepezil also developed by Pfizer, in 1996. It was a new class of AChEIs bearing an indanone moiety showing a longer and more selective activity toward AChE than Tacrine. Indeed, an IC_{50} for *h*AChE of 5.7 nM was found compared to an IC_{50} *h*BChE of 4100 nM[25]. Moreover, early clinical trials in 1996 have demonstrated that Donepezil at a dosage of 5 mg/day for 12 weeks improves cognitive functions in patients with AD. These studies have also shown that administration is not compromised by adverse events or hepatotoxicity, unlike Tacrine[46].

The third molecule is Galantamine commercialized in 2000 by Janssen. It is known to be a centrally acting, selective, reversible and competitive AChEI[47]. *In vitro* studies have brought to light that Galantamine has an IC_{50} of 0.8 µM toward *h*AChE which is ten times more effective than toward *h*BChE (IC_{50} = 7.3 µM). Moreover, it has shown an activity as an allosteric modulator of the neuronal nicotinic receptors nAChR or ACh[48], allowing a better sensitivity for the ionic canal opening during the ACh fixation and also a slower receptors desensitization[49].

The last commercially available AChEI is Rivastigmine commercialised in 1997 by the pharmaceutical company Novartis and as a patch since 2007. Because it generates significantly few gastrointestinal side effects[50], it enables patients to receive high therapeutic doses. It is currently the most used drug against dementia in a galenic form. Rivastigmine has an indirect parasympathomimetic way of action, it increases the ACh levels inside the synaptic cleft, causes the same effects toward nicotinic and muscarinic receptors of the CNS than ACh and is a pseudo-irreversible cholinesterases inhibitor[51]. Indeed, its mechanism of action is based on the presence of a carbamate in the structure, the

[45] Patocka, J.; Jun, D.; Kuca, K. Possible Role of Hydroxylated Metabolites of Tacrine in Drug Toxicity and Therapy of Alzheimer's Disease. *Curr. Drug Metab.* **2008**, *9* (4), 332–335.

[46] Rogers, S. L.; Friedhoff, L. T. The Efficacy and Safety of Donepezil in Patients with Alzheimer's Disease: Results of a US Multicentre, Randomized, Double-Blind, Placebo-Controlled Trial. *Dement. Geriatr. Cogn. Disord.* **1996**, *7* (6), 293–303.

[47] Marco-Contelles, J.; do Carmo Carreiras, M.; Rodríguez, C.; Villarroya, M.; García, A. G. Synthesis and Pharmacology of Galantamine. *Chem. Rev.* **2006**, *106* (1), 116–133.

[48] Lilienfeld, S. Galantamine--a Novel Cholinergic Drug with a Unique Dual Mode of Action for the Treatment of Patients with Alzheimer's Disease. *CNS Drug Rev.* **2002**, *8* (2), 159–176.

[49] Maelicke, A.; Samochocki, M.; Jostock, R.; Fehrenbacher, A.; Ludwig, J.; Albuquerque, E. X.; Zerlin, M. Allosteric Sensitization of Nicotinic Receptors by Galantamine, a New Treatment Strategy for Alzheimer's Disease. *Biol. Psychiatry* **2001**, *49* (3), 279–288.

[50] Cummings, J.; Lefèvre, G.; Small, G.; Appel-Dingemanse, S. Pharmacokinetic Rationale for the Rivastigmine Patch. *Neurology* **2007**, *69* (4 Suppl 1), S10-13.

[51] Jann, M. W. Rivastigmine, a New-Generation Cholinesterase Inhibitor for the Treatment of Alzheimer's Disease. *Pharmacotherapy* **2000**, *20* (1), 1–12.

carbamate function will lead to AChE inhibition by a slowly reversible carbamoylation of the enzyme's catalytic serine (Ser203).

The mechanism is the same for ACh and Rivastigmine, the first step is a deacylation (ACh) or decarbamoylation (Rivastigmine) by cholinesterase active serine residue, and a cleavage of the ligand. In the Rivastigmine case, the carbamate transfer from the stigmine to the residual serine of AChE is a slow process, thus, the IC_{50} values of this inhibitor are low (*h*AChE IC_{50} = 48 µM and IC_{50} *h*BChE = 54 µM). However, where the deacylation step is fast in the case of ACh, for the stigmine, the dissociation of the AChE's carbamoyl group is a slow process, which leaves AChE inactive for a long time[51,52] (Figure 16). Indeed, studies on the human cerebrospinal fluid have shown that a dose of 3 mg of Rivastigmine leads to an effective AChE inhibition for 10 h[53]. This long enzyme inactivation by Rivastigmine compensates for the low IC_{50} values toward the two cholinesterases.

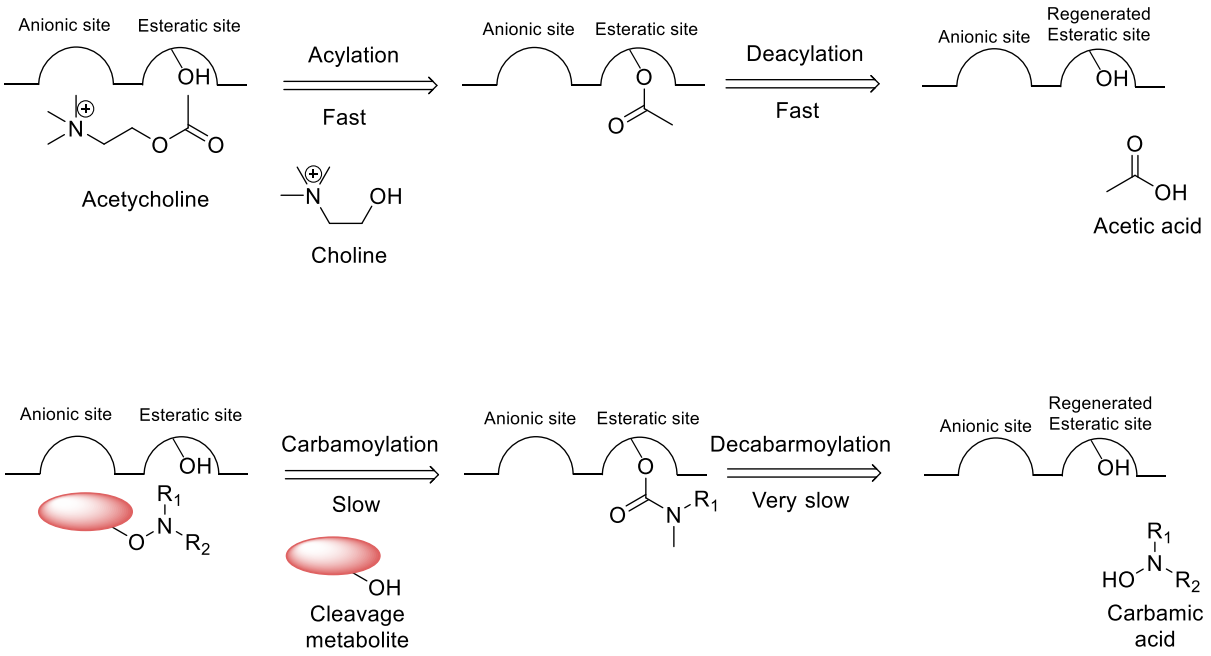

Figure 16: Mechanism of ACh and Rivastigmine decarbamoylation[53]

Besides these four molecules, other structures have been investigated to develop cholines inhibitors, especially AChE (Figure 17). Even if we can observe various structures, most of them failed during the clinical trials due to a lack of activity, efficiency or a high toxicity. For example, the Metrifonate

[52] Bar-On, P.; Millard, C. B.; Harel, M.; Dvir, H.; Enz, A.; Sussman, J. L.; Silman, I. Kinetic and Structural Studies on the Interaction of Cholinesterases with the Anti-Alzheimer Drug Rivastigmine. *Biochemistry* **2002**, *41* (11), 3555–3564.

[53] Polinsky, R. J. Clinical Pharmacology of Rivastigmine: A New-Generation Acetylcholinesterase Inhibitor for the Treatment of Alzheimer's Disease. *Clin. Ther.* **1998**, *20* (4), 634–647.

developed by Bayer in 2006, was discontinued because of its side effects on neuromuscular transmission and respiratory paralysis.

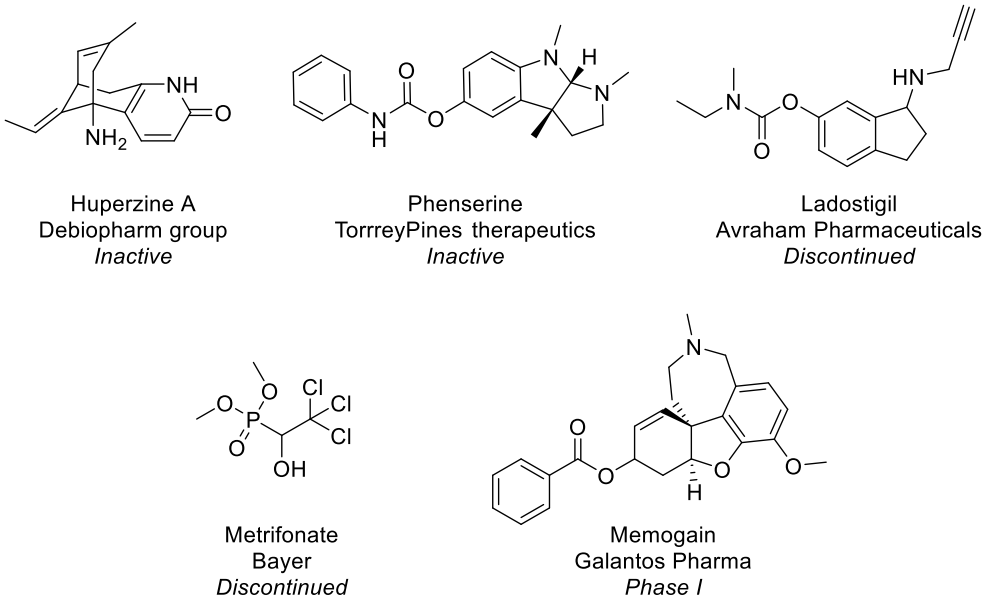

Figure 17: Examples of other AChE inhibitors investigated

Yet, Memogain developed by Galantos Pharma, is still in phase I. Memogain (or GLN-1062) is an inactive prodrug of Galantamine. Developing a Galantamine prodrug enabled to increase the compound's lipophilicity as compared to the first-generation drug in order to facilitate its BBB crossing ability, and its capacity to be enzymatically cleaved in the brain and release the active drug. The development of a prodrug also helped reducing adverse effects[54]. Indeed, studies on ferrets have proven that the prodrug's adverse effects are lower than the one induced by Galantamine (Figure 18 – A). This decrease allows to administrate higher drugs doses to patients of AD, the dose could be increased from 16-24 mg/day (for Galantamine) to 226 mg/day (for Memogain)[55], the performance recovery also seems to be improved with Memogain (Figure 18 – B).

[54] Maelicke, A. Memogain, a Pleasant, Highly Potent and Neuroprotective Novel Drug Treatment in Alzheimer's Disease. *Alzheimers Dement.* **2011**, *7* (4), S799.

[55] Maelicke, A.; Hoeffle-Maas, A.; Ludwig, J.; Maus, A.; Samochocki, M.; Jordis, U.; Koepke, A. K. E. Memogain Is a Galantamine Pro-Drug Having Dramatically Reduced Adverse Effects and Enhanced Efficacy. *J. Mol. Neurosci.* **2010**, *40* (1–2), 135–137.

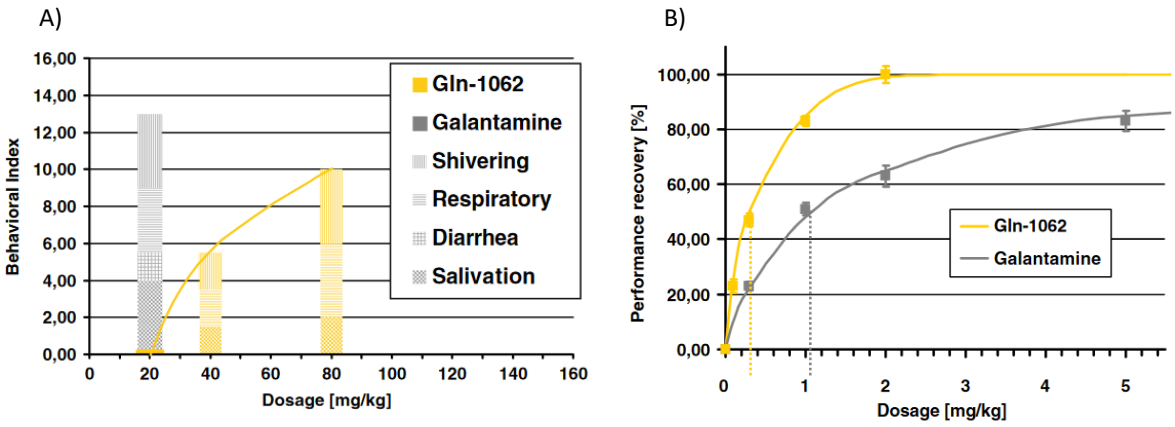

Figure 18: Studies of adverse effects of Memogain (A) and performance recovery (B)[55]

6.2. Activation of the cholinergic receptors

Another approach to develop treatments against AD is to explore the synthesis of molecules able to activate acetylcholine receptors. They are ligand-activated neurotransmitter receptors composed of two major types:

- the metabotropic muscarinic receptors,
- the ionotropic nicotinic receptors.

6.2.1. Nicotinic receptors activation

Nicotinic receptors are ionotropic receptors directly linked to ion channels. They are composed of five subunits symmetrically arranged around a central pore. Where muscle-type receptors are made up of α, β, γ, δ and ε subunits, neuronal-types are composed of only α and β subunits. Neuronal receptors are either homomeric (only α or only β) or heteromeric (different subunits with at least one α and one β)[56] (Figure 19).

[56] Zouridakis, M.; Zisimopoulou, P.; Poulas, K.; Tzartos, S. J. Recent Advances in Understanding the Structure of Nicotinic Acetylcholine Receptors. *IUBMB Life* **2009**, *61* (4), 407–423.

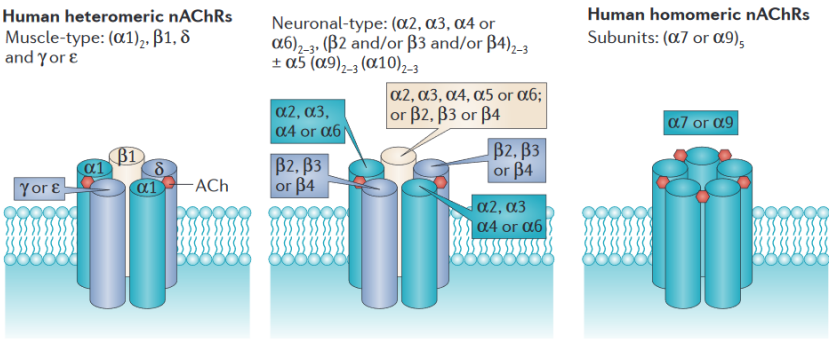

Figure 19: Schematic view of homomeric and heteromeric nAChR[57]

When ACh binds to the nAChR, it leads to a conformation change of the structure which opens the ion channel leading to the cations crossing (K^+, Ca^{2+} and Na^+). The flux of entering Na^+ and exiting K^+ leads to a brief membrane depolarization and thus a nervous transmission or muscular contraction. The next step is the desensitization followed by a return of the receptor in a state of rest[58] (Figure 20).

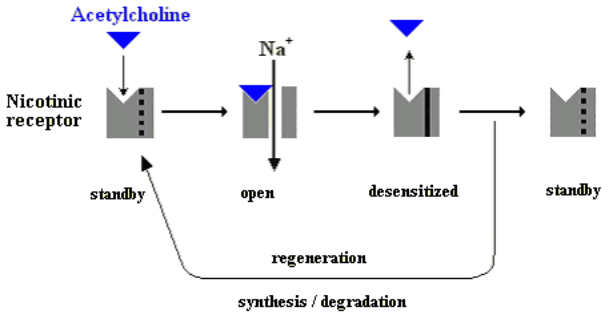

Figure 20: Mechanism of action of a nAChR with ACh[59]

Because of the high number of different nAChRs (combinations of up to 12 different subunits), the nAChRs are not very well known. However, 17 vertebrate nAChRs have been discovered (12 neuronal-type and 5 muscle-type). Among these identified receptors, three are widely expressed in the CNS and are involved in the post and presynaptic excitation: α4β2, α3β4, α7 [60].

In addition to having a strong affinity toward Aβ peptide leading to an acceleration of the senile plaques' formation, studies have shown that the number of α7 (and α4β2) receptors are reduced at

[57] Grando, S. A. Connections of Nicotine to Cancer. *Nat. Rev. Cancer* **2014**, *14* (6), 419–429.
[58] Karlin, A. Emerging Structure of the Nicotinic Acetylcholine Receptors. *Nat. Rev. Neurosci.* **2002**, *3* (2), 102–114.
[59] Metabolism http://www.chm.bris.ac.uk/motm/nicotine/E-metabolisme.html.
[60] Graham, A.; Court, J. A.; Martin-Ruiz, C. M.; Jaros, E.; Perry, R.; Volsen, S. G.; Bose, S.; Evans, N.; Ince, P.; Kuryatov, A.; Lindstrom, J.; Gotti, C.; Perry, E. K. Immunohistochemical Localisation of Nicotinic Acetylcholine Receptor Subunits in Human Cerebellum. *Neuroscience* **2002**, *113* (3), 493–507.

the frontal cortex and hippocampus levels in brains of patients with AD[61]. For these two main reasons, it was rational to investigate new molecules with an agonist activity toward nAChRs (Figure 21).

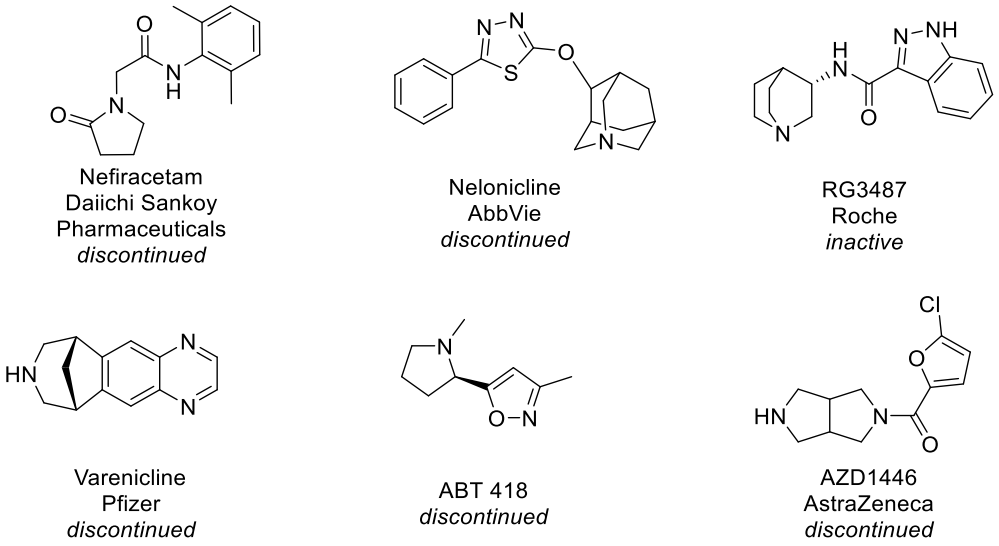

Figure 21: Example of nAChRs agonists

Unfortunately, either α4β2 (Nefiracetam, ABT418, AZD1446) or α7 agonists (Nelonicline, RG3487) failed in advanced phases of clinical trials. The major issue in the nAChRs agonists development is the rapid desensitization of the receptors when these agonists are dispensed.

6.2.2. Promising nAChR agonists – The quinuclidine scaffold

In 2017, Yang et *al*.[62] wrote a well-documented review about agonists and positive allosteric modulators of α7 nAChRs modulators in clinical trials for CNS related diseases. Among the different modulators like PAMs (Positive Allosteric Modulators) and ago-PAMs (Ago- Positive Allosteric Modulators, which are both orthosteric agonists and allosteric modulators), they developed the state of the art in the progress in the development of agonists of these receptors.

As shown on Figure 22, quinuclidine derivatives like spirooxazolidinones and quinuclidine ethers, amides and carbamates have been widely used in the research of full or partial α7 nAChR agonists. Currently, most of the existing compounds are partial agonists; Unlike full agonists, they can only produce a small maximum current even if all the receptors are occupied. Indeed, since 1957, it has

[61] Paterson, D.; Nordberg, A. Neuronal Nicotinic Receptors in the Human Brain. *Prog. Neurobiol.* **2000**, *61* (1), 75–111.

[62] Yang, T.; Xiao, T.; Sun, Q.; Wang, K. The Current Agonists and Positive Allosteric Modulators of α 7 NAChR for CNS Indications in Clinical Trials. *Acta Pharm. Sin. B* **2017**, *7* (6), 611–622.

been supposed that this small response is explained by their inefficiency at eliciting the conformational change between shut and open states of the ion channel in the case of a ligand-activated ion channel[63].

One of the first developed α7 nAChR partial agonist bearing a quinuclidine was AZD0328 by AstraZeneca which is a derivative of an existing spirooxazolidinone series. It exhibits an EC_{50} of 338 nM and an efficacy of 65% on *Xenopus* oocytes expressing human α7 nAChR. In contrast, its maximal activities are only of 12% on *h*$5HT_{3A}$, 4% on $\alpha_4\beta_2$ nAChR and no activity on $\alpha_3\beta_4$ nAChR[64]. Studies have also shown that the compound is stable and has good pharmacokinetic properties which suggests it could be a good compound for clinical trial[65]. As a matter of fact, a phase I clinical trial for AD was completed in 2008 and AZD0328 was repositioned as a drug for schizophrenia and went to phase II clinical trial. However, the company stopped the trials because the drug was "unlikely to meet the current target product profile"[66].

Reported in 2016, another pirooxazolidinone derivative was developed, BMS-933043, by Bristol-Myers Squibb as a selective α7 nAChR partial agonist. Preclinical studies showed a cognition enhancement[67] and a phase I clinical trial was started for schizophrenia.

The most famous example of α7 nAChR agonist is Encenicline developed by FORUM Pharmaceuticals Inc., and reached the phase III clinical trial for the treatment of AD. It is a partial selective agonist and as shown on Figure 22, Encenicline bears a quinuclidine fragment and has an amide bond. It has been developed for the treatment of cognitive deficits in AD but also in Schizophrenia. Rationally, selective α7 nAChR agonists like Encenicline enhance cognition without any side effects associated with an over-activation of other receptors like $\alpha_4\beta_2$ nAChR or muscarinic AChRs[68]. It has been proven that

[63] Lape, R.; Colquhoun, D.; Sivilotti, L. G. On the Nature of Partial Agonism in the Nicotinic Receptor Superfamily. *Nature* **2008**, *454* (7205), 722–727.
[64] Sydserff, S.; Sutton, E. J.; Song, D.; Quirk, M. C.; Maciag, C.; Li, C.; Jonak, G.; Gurley, D.; Gordon, J. C.; Christian, E. P.; Doherty, J. J.; Hudzik, T.; Johnson, E.; Mrzljak, L.; Piser, T.; Smagin, G. N.; Wang, Y.; Widzowski, D.; Smith, J. S. Selective A7 Nicotinic Receptor Activation by AZD0328 Enhances Cortical Dopamine Release and Improves Learning and Attentional Processes. *Biochem. Pharmacol.* **2009**, *78* (7), 880–888.
[65] Zhou, D.; Zhang, M.; Ye, X.; Gu, C.; Piser, T. M.; Lanoue, B. A.; Schock, S. A.; Cheng, Y.-F.; Grimm, S. W. In Vitro Metabolism of A7 Neuronal Nicotinic Receptor Agonist AZD0328 and Enzyme Identification for Its N-Oxide Metabolite. *Xenobiotica* **2011**, *41* (3), 232–242.
[66] Study to Asses Pharmacodynamics, Pharmacokinetics, Safety and Tolerability of AZD0328 in Patients With Schizophrenia - Full Text View - ClinicalTrials.gov https://clinicaltrials.gov/ct2/show/NCT00669903.
[67] Bristow, L. J.; Easton, A. E.; Li, Y.-W.; Sivarao, D. V.; Lidge, R.; Jones, K. M.; Post-Munson, D.; Daly, C.; Lodge, N. J.; Gallagher, L.; Molski, T.; Pieschl, R.; Chen, P.; Hendricson, A.; Westphal, R.; Cook, J.; Iwuagwu, C.; Morgan, D.; Benitex, Y.; King, D.; Macor, J. E.; Zaczek, R.; Olson, R. The Novel, Nicotinic Alpha7 Receptor Partial Agonist, BMS-933043, Improves Cognition and Sensory Processing in Preclinical Models of Schizophrenia. *PLOS ONE* **2016**, *11* (7), e0159996.
[68] Therapeutics | ALZFORUM https://www.alzforum.org/therapeutics.

Encenicline penetrates the BBB and it has shown improvement in the memory performances in rats, by potentiating the ACh response. Indeed, it enhances dopamine, glutamate and ACh efflux in the rat cortex[69,70] because it is also an antagonist at 5-HT_3 receptors (IC_{50} < 10 nM)[71]. It has been reported that this compound acts like a co-agonist with ACh and sensitizes the α7 nAChR receptor to its natural ligand. That is why lower doses of AChEIs, when administrated with Encenicline, are effective enough to restore the memory function in an object recognition task[71]. However, the phase III clinical trials conducted from 2012 to 2016 for schizophrenia were not conclusive and the phase III clinical trial for AD was suspended in 2017.

[69] Huang, M.; Felix, A. R.; Flood, D. G.; Bhuvaneswaran, C.; Hilt, D.; Koenig, G.; Meltzer, H. Y. The Novel A7 Nicotinic Acetylcholine Receptor Agonist EVP-6124 Enhances Dopamine, Acetylcholine, and Glutamate Efflux in Rat Cortex and Nucleus Accumbens. *Psychopharmacology (Berl.)* **2014**, *231* (23), 4541–4551.

[70] Huang, M.; Felix, A. R.; Bhuvaneswaran, C.; Hilt, D.; König, G.; Meltzer, H. Y. The Alpha-7 Receptor Agonist EVP-6124 Increases Dopamine and Glutamate Efflux in Rat Medial Prefrontal Cortex and Nucleus Accumbens. *Biochem. Pharmacol.* **2011**, *82* (8), 1040.

[71] Prickaerts, J.; van Goethem, N. P.; Chesworth, R.; Shapiro, G.; Boess, F. G.; Methfessel, C.; Reneerkens, O. A. H.; Flood, D. G.; Hilt, D.; Gawryl, M.; Bertrand, S.; Bertrand, D.; König, G. EVP-6124, a Novel and Selective A7 Nicotinic Acetylcholine Receptor Partial Agonist, Improves Memory Performance by Potentiating the Acetylcholine Response of A7 Nicotinic Acetylcholine Receptors. *Neuropharmacology* **2012**, *62* (2), 1099–1110.

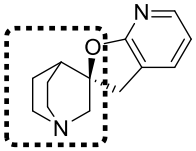

AZ0328

Partial agonist

K_i : 3.0 and 4.7 nmol/L (in *h*α-7 nAChR and *r*α-7 nAChR)
EC_{50} = 338 nmol/L ; $Ema_{x\,=}$ 64.7% (*h*α-7 nAChR in oocytes)
EC_{50} = 150 nmol/L ; $Ema_{x\,=}$ 61.0% (*r*α-7 nAChR in in oocytes)

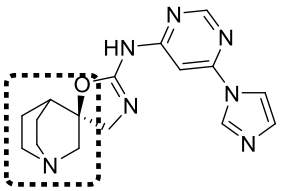

BMS-933043

Partial agonist

K_i : 8.1 and 3.3 nmol/L (*h*α-7 nAChR and *r*α-7 nAChR)
EC_{50} = 0.29 µmol/L ; E_{max} = 24% (*h*α-7 nAChR in oocytes)
EC_{50} = 0.14 µmol/L ; E_{max} = 27% (*r*α-7 nAChR in oocytes)

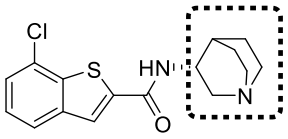

EVP-6124 (Encenicline)

Partial agonist

K_i : 9.98 nmol/L (*r*α-7 nAChR)
EC_{50} = 0.39 µmol/L ; E_{max} = 42% (*h*α-7 nAChR in oocytes)

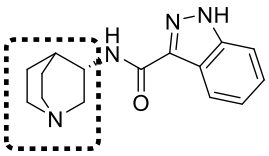

MEM3454/RG3487

Partial agonist
K_i : 6 nmol/L (in ra7)
EC_{50} = 0.8 µmol/L ; E_{max} = 63% (*h*α-7 nAChR in oocytes)
EC_{50} = 7.7 µmol/L ; E_{max} = 69% (*h*α-7 nAChR in QM cells)

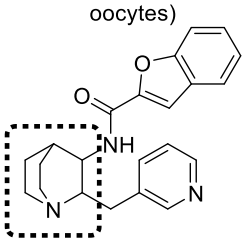

TC-5619

Full agonist

K_i : 1 and 1.4 nmol/L (in *h*a-7 nAChR and *ra*-7 nAChR)
EC_{50} = 33 nmol/L ; E_{max} = 100% (*h*α-7 nAChR in oocytes)
EC_{50} = 17 nmol/L ; E_{max} = 76% (*r*α-7 nAChR in GH4Cl cell line)

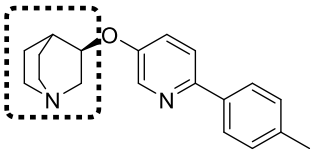

AQW051

Partial agonist

K_i : 27 nmol/L (*r*a-7 nAChR)
EC_{50} = 7.5 µmol/L ; E_{max} = 75% (*h*α-7 nAChR in oocytes)

Figure 22: examples of α7 nAChR agonists with a quinuclidine[62]

MEM3454 developed by Memory Pharmaceutical, like Encenicline, also shows an antagonist activity toward 5-HT_3 receptors and enhances dopamine efflux *via* a stimulation of nAChR and ACh efflux[72].

[72] Huang, M.; Felix, A. R.; Kwon, S.; Lowe, D.; Wallace, T.; Santarelli, L.; Meltzer, H. Y. The Alpha-7 Nicotinic Receptor Partial Agonist/5-HT3 Antagonist RG3487 Enhances Cortical and Hippocampal Dopamine and Acetylcholine Release. *Psychopharmacology (Berl.)* **2014**, *231* (10), 2199–2210.

However, MEM3454 did not improve cognitive deficits in patients with schizophrenia but mild negative symptoms were improved[73].

Then, TC-5619 (Bradanicline), an α7 nAChR full agonist, was developed in 2013 by Targacept. As shown on Figure 22**,** it has an excellent affinity and activity on α7 nAChRs[74]. On top of its good values of EC_{50}, TC-5619 has shown promising properties during *in vivo* studies, like good pharmacokinetic profile and rapid BBB permeability. Nevertheless, during phase II clinical trial, TC-5619 failed to improve cognitive deficits and negative symptoms in schizophrenia[75,76]. However, the good safety profile of TC-5619 in the clinical trials for schizophrenia and hyperactivity disorder could justify its use for further clinical trials for other diseases like AD[77].

Finally, a quinuclidine ether partial agonist of α7 nAChR has been recently developed by Novartis. AQW051 has shown promising results[78], a good pharmacokinetic profile and could also be useful in Parkinson's disease. AQW051 has been in phase II clinical trial for schizophrenia, AD and Parkinson's disease but failed to reduce dyskinesia or parkinsonian severity[79].

[73] Umbricht, D.; Keefe, R. S.; Murray, S.; Lowe, D. A.; Porter, R.; Garibaldi, G.; Santarelli, L. A Randomized, Placebo-Controlled Study Investigating the Nicotinic *α*7 Agonist, RG3487, for Cognitive Deficits in Schizophrenia. *Neuropsychopharmacology* **2014**, *39* (7), 1568–1577.

[74] Hauser, T. A.; Kucinski, A.; Jordan, K. G.; Gatto, G. J.; Wersinger, S. R.; Hesse, R. A.; Stachowiak, E. K.; Stachowiak, M. K.; Papke, R. L.; Lippiello, P. M.; Bencherif, M. TC-5619: An Alpha7 Neuronal Nicotinic Receptor-Selective Agonist That Demonstrates Efficacy in Animal Models of the Positive and Negative Symptoms and Cognitive Dysfunction of Schizophrenia. *Biochem. Pharmacol.* **2009**, *78* (7), 803–812.

[75] Lieberman, J. A.; Dunbar, G.; Segreti, A. C.; Girgis, R. R.; Seoane, F.; Beaver, J. S.; Duan, N.; Hosford, D. A. A Randomized Exploratory Trial of an Alpha-7 Nicotinic Receptor Agonist (TC-5619) for Cognitive Enhancement in Schizophrenia. *Neuropsychopharmacology* **2013**, *38* (6), 968–975.

[76] Hosford, D.; Dvergsten, C.; Beaver, J.; Segreti, A. C.; Toler, S.; Farr, M. G.; Joseph, M.; Jett, J.; Lippiello, P.; Bencherif, M. P.3.d.018 Phase 2 Clinical Trial of TC-5619, an Alpha 7 Nicotinic Receptor Agonist in the Treatment of Negative and Cognitive Symptoms in Schizophrenia. *Eur. Neuropsychopharmacol.* **2014**, *24*, S531–S532.

[77] Walling, D.; Marder, S. R.; Kane, J.; Fleischhacker, W. W.; Keefe, R. S. E.; Hosford, D. A.; Dvergsten, C.; Segreti, A. C.; Beaver, J. S.; Toler, S. M.; Jett, J. E.; Dunbar, G. C. Phase 2 Trial of an Alpha-7 Nicotinic Receptor Agonist (TC-5619) in Negative and Cognitive Symptoms of Schizophrenia. *Schizophr. Bull.* **2016**, *42* (2), 335–343.

[78] Di Paolo, T.; Grégoire, L.; Feuerbach, D.; Elbast, W.; Weiss, M.; Gomez-Mancilla, B. AQW051, a Novel and Selective Nicotinic Acetylcholine Receptor A7 Partial Agonist, Reduces l-Dopa-Induced Dyskinesias and Extends the Duration of l-Dopa Effects in Parkinsonian Monkeys. *Parkinsonism Relat. Disord.* **2014**, *20* (11), 1119–1123.

[79] Trenkwalder, C.; Berg, D.; Rascol, O.; Eggert, K.; Ceballos-Baumann, A.; Corvol, J.-C.; Storch, A.; Zhang, L.; Azulay, J.-P.; Broussolle, E.; Defebvre, L.; Geny, C.; Gostkowski, M.; Stocchi, F.; Tranchant, C.; Derkinderen, P.; Durif, F.; Espay, A. J.; Feigin, A.; Houeto, J.-L.; Schwarz, J.; Paolo, T. D.; Feuerbach, D.; Hockey, H.-U.; Jaeger, J.; Jakab, A.; Johns, D.; Linazasoro, G.; Maruff, P.; Rozenberg, I.; Sovago, J.; Weiss, M.; Gomez-Mancilla, B. A Placebo-Controlled Trial of AQW051 in Patients With Moderate to Severe Levodopa-Induced Dyskinesia. *Mov. Disord.* **2016**, *31* (7), 1049–1054.

Even though the majority of developed α7 nAChR agonists failed to pass the high phases of clinical trials, we can notice that all of them seems to have good results toward the receptors (good K_i, good EC_{50}, promising PK profiles, rapid CNS penetration) and they all have a common quinuclidine fragment.

6.2.3. Muscarinic receptors activation[80]

mAChRs forms G protein-coupled receptor complexes in the membrane of neurons, G-proteins are used in their signalling mechanism. They are made up of seven transmembrane regions and 5 of these receptors have been identified: M_1, M_2, M_3, M_4 and M_5. When M_1, M_3 and M_5 couple preferentially to G-proteins G_q/G_{11} and activate phospholipases, M_2 and M_4 couple to G_i/G_0 G-proteins and inhibit the adenylcyclase activity and modulate the ionic channels conductance[81,82]. Apart from M_5, all the receptors are abundant in the brain, and therefore, important in CNS function like memory and learning activities. In the pathology of AD, mAChRs could be divided in two groups based on their effects:

- the "M_2/M_4" group,
- the "M_1/M_3" group.

Studies have shown a M_2 mAChR decrease in patients with AD and it has been suggested that a M_2 receptor stimulation decreases β-secretase expression[83]. Therefore, a logical extrapolation could be that an impoverishment of the receptor could lead to an Aβ peptide increase. Besides, G protein-coupled receptor kinase 5 (GRK-5) deficiency impairs the "M_2/M_4" group and leads to a cholinergic hypofunction[84].

Moreover, the "M_1/M_3" group has been involved in ACh-mediated cognition. Studies have suggested that stimulation of the two receptors promotes the APP cleavage by the non-amyloidogenic pathway

[80] Avila, J. Muscarinic Receptors and Alzheimer's Disease. *Neurodegener. Dis. Manag.* **2011**, *1* (4), 267–269.
[81] Wess, J.; Eglen, R. M.; Gautam, D. Muscarinic Acetylcholine Receptors: Mutant Mice Provide New Insights for Drug Development. *Nat. Rev. Drug Discov.* **2007**, *6* (9), 721–733.
[82] Conn, P. J.; Jones, C. K.; Lindsley, C. W. Subtype-Selective Allosteric Modulators of Muscarinic Receptors for the Treatment of CNS Disorders. *Trends Pharmacol. Sci.* **2009**, *30* (3), 148–155.
[83] Züchner, T.; Perez-Polo, J. R.; Schliebs, R. Beta-Secretase BACE1 Is Differentially Controlled through Muscarinic Acetylcholine Receptor Signaling. *J. Neurosci. Res.* **2004**, *77* (2), 250–257.
[84] Liu, J.; Rasul, I.; Sun, Y.; Wu, G.; Li, L.; Premont, R. T.; Suo, W. Z. GRK5 Deficiency Leads to Reduced Hippocampal Acetylcholine Level via Impaired Presynaptic M2/M4 Autoreceptor Desensitization. *J. Biol. Chem.* **2009**, *284* (29), 19564–19571.

which decreases Aβ peptide levels. Another aspect is the neurons protection from Aβ peptide toxicity through a pathway involving GSK3 kinases regulation[85].

Thus, there is a strong hypothesis that the Aβ peptide, Tau protein and mAChRs are linked in the pathology of AD (Figure 23).

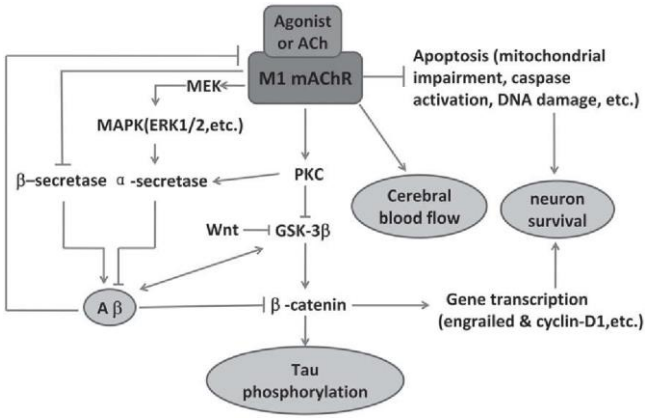

Figure 23: Putative role of M1 mAChR in AD[86]

For all these reasons, mAChRs modulators have been investigated in the treatment of AD (Figure 24). The major targeted receptor is the M_1 mAChR and among the recent developed compounds, only one seems to be promising (HTL0018318).

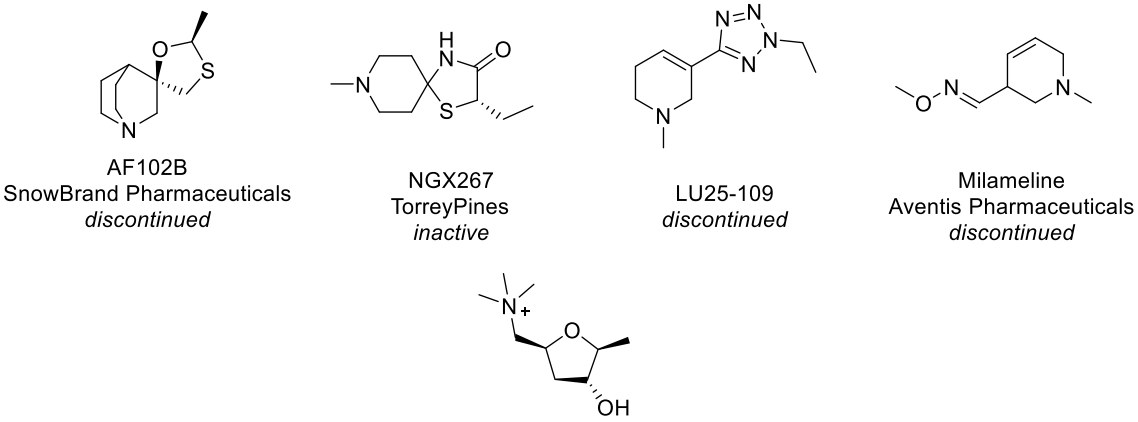

Figure 24: Example of M1 mAChR agonists

[85] Farías, G. G.; Godoy, J. A.; Hernández, F.; Avila, J.; Fisher, A.; Inestrosa, N. C. M1 Muscarinic Receptor Activation Protects Neurons from Beta-Amyloid Toxicity. A Role for Wnt Signaling Pathway. *Neurobiol. Dis.* **2004**, *17* (2), 337–348.

[86] Jiang, S.; Li, Y. L.; Zhang, C.; Zhao, Y.; Bu, G. D.; Xu, H.; Zhang, Y.-W. M1 Muscarinic Acetylcholine Receptor in Alzheimer's Disease. *Neurosci. Bull.* **2013**, *30*, 295–307.

Indeed, HTL0018318, a M_1 mAChRs selective agonist, was developed in 2016 by Allergan plc. A phase I clinical trial was ran in 2016, but unfortunately in 2018, the phase II trial was temporary put on hold by the company because of toxicology results from an animal study in non-human primates[87].

6.3. NMDA receptors antagonists

N-methyl-D-aspartate receptor (NMDA), found in nerve cells, is known to be an ion channel protein and part of the ionotropic glutamate receptor family with the AMPA and kainate receptors. NMDA is a heterodimeric complex made up of three different subunits (at least two GluN1 and GluN2 or GluN3 subunits). Moreover, GluN2 has four isoforms (GluN2A-D) and GluN3 has two (GluN3A and GluN3B). This variety of isoforms and possible assembling leads to a various number of combinations for the receptor (Figure 25).

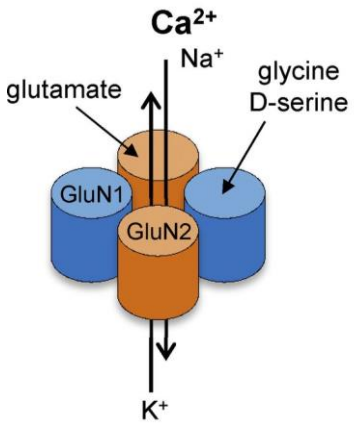

Figure 25: Structure and mechanism of a GluN1/GluN2 NMDA receptor[88]

NMDA receptors are expressed in the CNS and play an important role in synaptic functions like learning and memory activity or synaptic plasticity. Indeed, they allow the crossing of cations as Ca^{2+} responsible for a fast synaptic transmission[89]. For the channel to open and let the Ca^{2+} cross, the NMDA receptor needs to be activated by L-glutamate (binding with a GluN2 subunit), bound to a co-agonist like glycine

[87] Alzheimer Europe - News - Science watch - Tuesday 18 September 2018 - Sosei and Allergan suspend clinical activities of HTL0018318 in AD https://www.alzheimer-europe.org/News/Science-watch/Tuesday-18-September-2018-Sosei-and-Allergan-suspend-clinical-activities-of-HTL0018318-in-AD.

[88] Hansen, K. B.; Yi, F.; Perszyk, R. E.; Furukawa, H.; Wollmuth, L. P.; Gibb, A. J.; Traynelis, S. F. Structure, Function, and Allosteric Modulation of NMDA Receptors. *J. Gen. Physiol.* **2018**, *150* (8), 1081–1105.

[89] Gielen, M. Fonctionnement des récepteurs-canaux du glutamate - Des proteines responsables de la transmission synaptique excitatrice. *médecine/sciences* **2010**, *26* (1), 65–72.

or D-serine (at the GluN1 subunit level)[90,91] but it also undergoes a depolarization of the dendrite (Figure 25).

Moreover, studies have brought to light that Aβ peptide's oligomers interact with the receptor by inhibiting the long-term potentiation[92], which is a crucial function for the synaptic efficiency, leading to a loss of synapses and therefore a cognition deficit.

Neramexane
Forest laboratory
discontinued

Memantine
Forest Laboratories
approved

Figure 26: Examples of NMDA receptors antagonists

Forest laboratories developed two NMDA receptors channel blockers: Neramexane and Memantine (Figure 26). Even though Neramexane has been shown to block ACh-evoked responses by antagonizing α9 and α10 nAChRs[93] besides its moderate effect as a cation channel blocker, it failed to pass the clinical trials and was discontinued. However, Memantine, another channel blocker of NMDA receptors successfully passed through all phases clinical trials and has been approved for the treatment of AD. It has been shown that Memantine helps treating and preventing behavioural symptoms like hallucinations, agitation, aggression and irritability.

6.4. Inhibition of the formation of senile plaques

Another approach against AD is to directly fight the senile plaques formation by either developing anti-aggregates or modulating the different secretases (α, β and γ).

[90] Panatier, A.; Theodosis, D. T.; Mothet, J.-P.; Touquet, B.; Pollegioni, L.; Poulain, D. A.; Oliet, S. H. R. Glia-Derived D-Serine Controls NMDA Receptor Activity and Synaptic Memory. *Cell* **2006**, *125* (4), 775–784.

[91] Kleckner, N. W.; Dingledine, R. Requirement for Glycine in Activation of NMDA-Receptors Expressed in Xenopus Oocytes. *Science* **1988**, *241* (4867), 835–837.

[92] Snyder, E. M.; Nong, Y.; Almeida, C. G.; Paul, S.; Moran, T.; Choi, E. Y.; Nairn, A. C.; Salter, M. W.; Lombroso, P. J.; Gouras, G. K.; Greengard, P. Regulation of NMDA Receptor Trafficking by Amyloid-Beta. *Nat. Neurosci.* **2005**, *8* (8), 1051–1058.

[93] Plazas, P. V.; Savino, J.; Kracun, S.; Gomez-Casati, M. E.; Katz, E.; Parsons, C. G.; Millar, N. S.; Elgoyhen, A. B. Inhibition of the Alpha9alpha10 Nicotinic Cholinergic Receptor by Neramexane, an Open Channel Blocker of N-Methyl-D-Aspartate Receptors. *Eur. J. Pharmacol.* **2007**, *566* (1–3), 11–19.

6.4.1. Anti-aggregates of Aβ

As it was explained before, the Aβ peptide spreading and aggregation is a key trigger of AD, therefore, finding a way to avoid the peptide assembly or induce its clearance in the organism could be a viable strategy. With this approach, small molecules have been developed in the past years, a combination of two already approved drugs, Cromolyn (ALZT-OP1a) and Ibuprofen (ALZT-OP1b) is currently in phase III (Figure 27). Recently, Ibuprofen was shown to help lowering the Aβ peptides effects in cell-based and animal models of AD[94,95]. Moreover, cromolyn, a mast cell stabilizer usually used to treat asthma, acts as an anti-inflammatory compound. In 2015, a study showed that Cromolyn inhibits Aβ aggregation *in vitro* and decreases soluble Aβ levels in the brain *in vivo*[96].

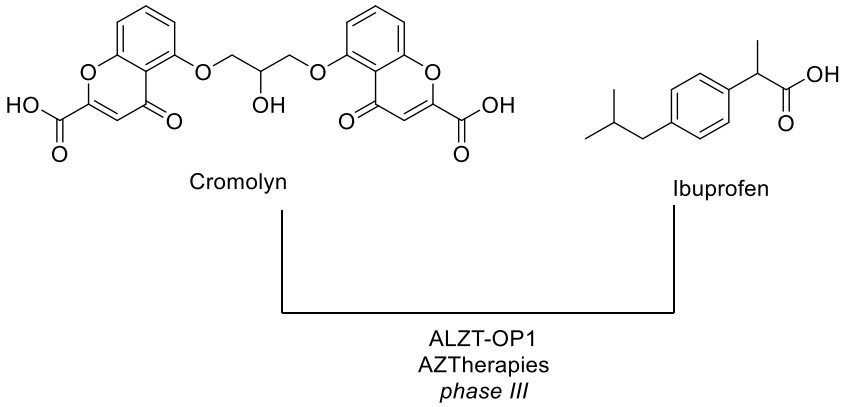

Figure 27: Anti-aggregate "drug cocktail"

6.4.2. α-secretase activation

As it was explained before, α-secretase is involved in the APP cleavage in a non-amyloidogenic pathway giving small soluble and non-cytotoxic peptides. Thus, activating this secretase seems rational to

[94] Lleó, A.; Berezovska, O.; Herl, L.; Raju, S.; Deng, A.; Bacskai, B. J.; Frosch, M. P.; Irizarry, M.; Hyman, B. T. Nonsteroidal Anti-Inflammatory Drugs Lower Abeta42 and Change Presenilin 1 Conformation. *Nat. Med.* **2004**, *10* (10), 1065–1066.

[95] Lim, G. P.; Yang, F.; Chu, T.; Chen, P.; Beech, W.; Teter, B.; Tran, T.; Ubeda, O.; Ashe, K. H.; Frautschy, S. A.; Cole, G. M. Ibuprofen Suppresses Plaque Pathology and Inflammation in a Mouse Model for Alzheimer's Disease. *J. Neurosci. Off. J. Soc. Neurosci.* **2000**, *20* (15), 5709–5714.

[96] Hori, Y.; Takeda, S.; Cho, H.; Wegmann, S.; Shoup, T. M.; Takahashi, K.; Irimia, D.; Elmaleh, D. R.; Hyman, B. T.; Hudry, E. A Food and Drug Administration-Approved Asthma Therapeutic Agent Impacts Amyloid β in the Brain in a Transgenic Model of Alzheimer Disease. *J. Biol. Chem.* **2015**, *290* (4), 1966–1978.

promote the APPα formation and block the Aβ peptides development. Moreover, APPα has another role which is to increase the mechanisms of neuroprotection to reduce the Aβ peptide action[97]. Different promising molecules have been developed for this purpose (Figure 28) and are currently in phase II or III clinical trials. For instance, Acitretin was reported to reduce Aβ peptide levels and promote the non-amyloidogenic pathway of the APP cleavage in mice[98] and increase α-secretases activity in humans[99].

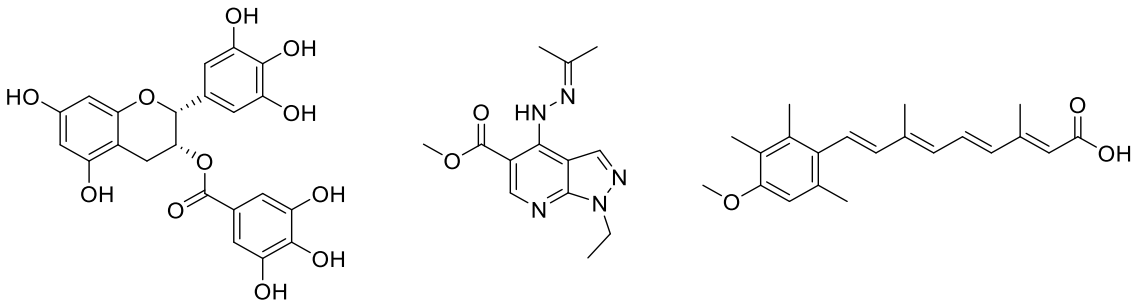

Figure 28: Examples of α-secretase activators

6.4.3. β-secretase inhibitors

The β-secretase (or BACE-1 for « Beta-site APP Cleaving Enzyme 1 ») plays a major role in Aβ peptides formation during the APP cleavage through the amyloidogenic pathway. Inhibiting this enzyme would be a way to avoid the amyloidogenic APP cleavage and reduce the Aβ peptides levels in the brain of patients with AD. Various small molecules failed to pass the clinical trials and were discontinued or found inactive[100], nevertheless, three are still in study and advanced phases of clinical trials (Figure 29).

[97] Stein, T. D.; Anders, N. J.; DeCarli, C.; Chan, S. L.; Mattson, M. P.; Johnson, J. A. Neutralization of Transthyretin Reverses the Neuroprotective Effects of Secreted Amyloid Precursor Protein (APP) in APPSw Mice Resulting in Tau Phosphorylation and Loss of Hippocampal Neurons: Support for the Amyloid Hypothesis. *J. Neurosci.* **2004**, *24* (35), 7707–7717.
[98] Tippmann, F.; Hundt, J.; Schneider, A.; Endres, K.; Fahrenholz, F. Up-Regulation of the Alpha-Secretase ADAM10 by Retinoic Acid Receptors and Acitretin. *FASEB J. Off. Publ. Fed. Am. Soc. Exp. Biol.* **2009**, *23* (6), 1643–1654.
[99] Endres, K.; Fahrenholz, F.; Lotz, J.; Hiemke, C.; Teipel, S.; Lieb, K.; Tüscher, O.; Fellgiebel, A. Increased CSF APPs-α Levels in Patients with Alzheimer Disease Treated with Acitretin. *Neurology* **2014**, *83* (21), 1930–1935.
[100]https://www.alzforum.org/therapeutics/.

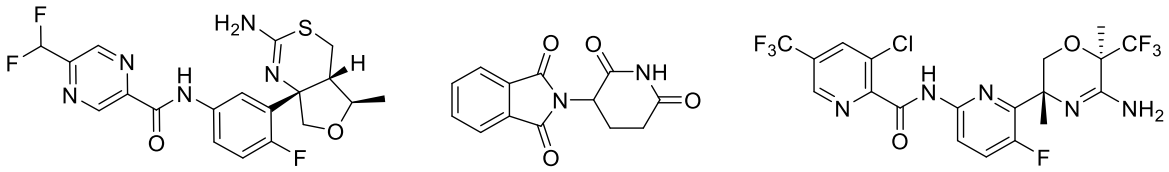

Elenbecestat
Biogen
phase III

Thalidomide
Celgene Corporation
phase II/III

Umibecestat
Novartis
phase II/III

Figure 29: Examples of BACE-1 inhibitors

For example, Thalidomide and Umibecestat have shown promising results concerning the BACE-1 inhibition and therefore the diminution of cytotoxic Aβ deposits. Indeed, despite its known teratogenic activity[101], Thalidomide reduces Aβ levels (Figure 30), lowers BACE-1 activity and reduces β-site cleavage of APP[102].

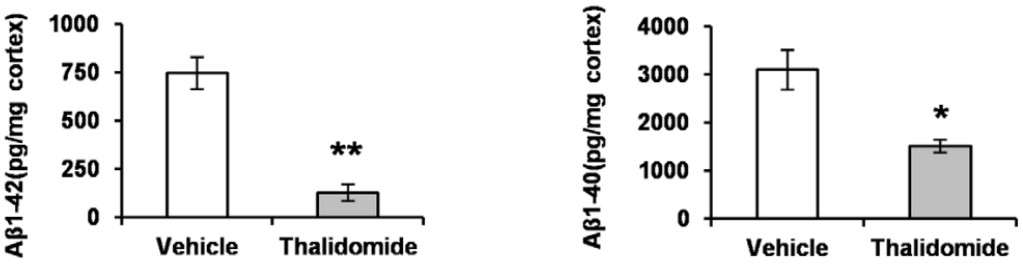

Figure 30: levels of Aβ in mice's neocortex exposed 100mg/kg of thalidomide for 3 months[102]

Regarding Umibecestat, studies have shown a good IC_{50} toward *h*BACE-1 (11 +/- 0.4 nM) with no relevant adverse side effects and induces a long-lasting Aβ level reduction in animals (Figure 31)[103].

[101] Maier, W. A. Thalidomide Embryopathy and Limb Defects. *Arch. Dis. Child.* **1965**, *40* (210), 154–157.

[102] He, P.; Cheng, X.; Staufenbiel, M.; Li, R.; Shen, Y. Long-Term Treatment of Thalidomide Ameliorates Amyloid-like Pathology through Inhibition of β-Secretase in a Mouse Model of Alzheimer's Disease. *PloS One* **2013**, *8* (2), e55091.

[103] Neumann, U.; Ufer, M.; Jacobson, L. H.; Rouzade-Dominguez, M.-L.; Huledal, G.; Kolly, C.; Lüönd, R. M.; Machauer, R.; Veenstra, S. J.; Hurth, K.; Rueeger, H.; Tintelnot-Blomley, M.; Staufenbiel, M.; Shimshek, D. R.; Perrot, L.; Frieauff, W.; Dubost, V.; Schiller, H.; Vogg, B.; Beltz, K.; Avrameas, A.; Kretz, S.; Pezous, N.; Rondeau, J.-M.; Beckmann, N.; Hartmann, A.; Vormfelde, S.; David, O. J.; Galli, B.; Ramos, R.; Graf, A.; Lopez Lopez, C. The BACE-1 Inhibitor CNP520 for Prevention Trials in Alzheimer's Disease. *EMBO Mol. Med.* **2018**, *10* (11).

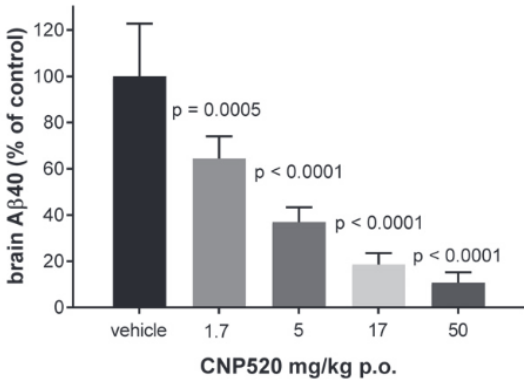

Figure 31: levels of Aβ 4h after Umibecestat administration[103]

6.4.4. γ-secretase modulation

Like the α and β secretases, the γ-secretase plays a key role in the APP cleavage and is involved in the two different cleavage process. The first objective was to develop γ-secretase inhibitors, but the adverse effects were important. Indeed, the inhibitors were efficient toward the γ-secretase but also toward the Notch protein, which was leading to a strong toxicity and an increase of infections[104]. That is why the second approach was to develop γ-secretase modulators and one is currently in clinical trial (Figure 32).

[104] Wong, G. T.; Manfra, D.; Poulet, F. M.; Zhang, Q.; Josien, H.; Bara, T.; Engstrom, L.; Pinzon-Ortiz, M.; Fine, J. S.; Lee, H.-J. J.; Zhang, L.; Higgins, G. A.; Parker, E. M. Chronic Treatment with the γ-Secretase Inhibitor LY-411,575 Inhibits β-Amyloid Peptide Production and Alters Lymphopoiesis and Intestinal Cell Differentiation. *J. Biol. Chem.* **2004**, *279* (13), 12876–12882.

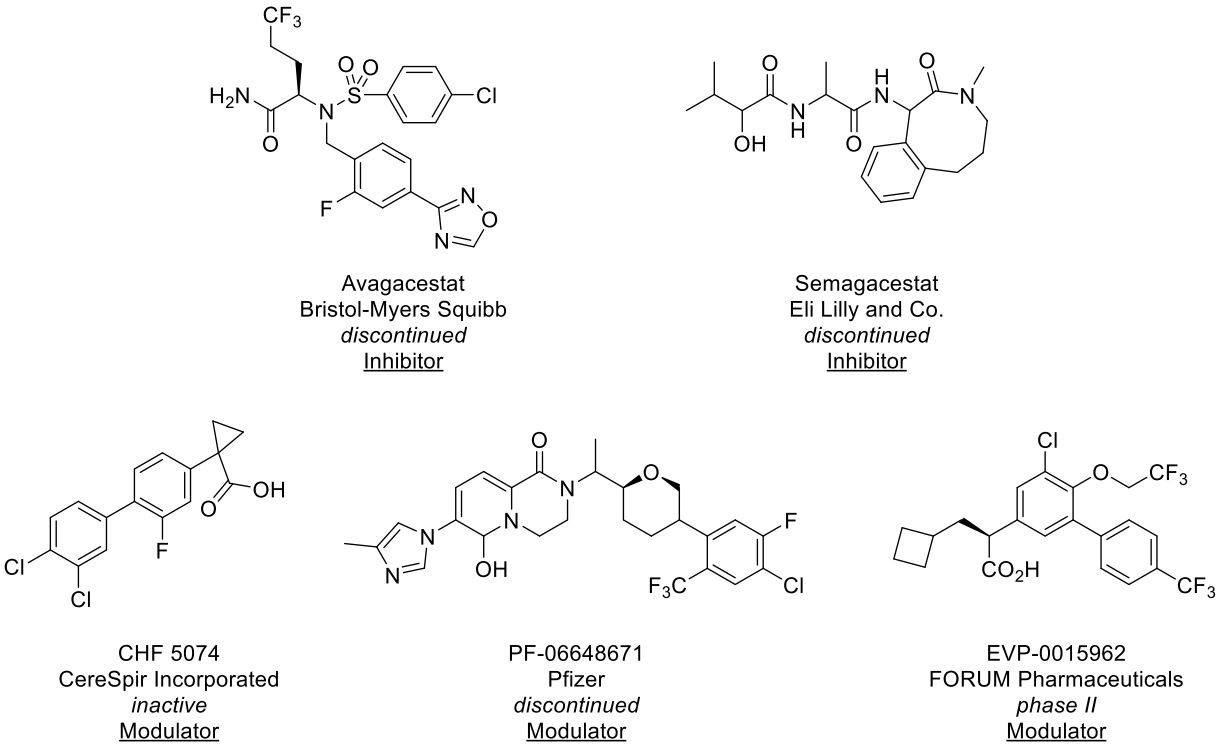

Figure 32: Examples of γ-secretase inhibitors and modulators

Indeed, EVP-0015962 was shown to be an orally bioavailable drug, detected in the brain and well tolerated after chronic treatment. Moreover, it has shown to decrease specifically $A\beta_{42}$ levels (Figure 33-A) during *in vitro* studies (IC_{50} = 67 +/- 5 nM) and there were no observed effects on $A\beta_{total}$ (Figure 33-B) until the EVP-0015962 concentration reaches levels at which cytotoxicity was detected. Other studies have shown that chronic treatment with EVP-0015962 also helps preventing plaque formation and inflammation in transgenic mice models expressing high levels of APP and Aβ[105].

[105] Rogers, K.; Felsenstein, K. M.; Hrdlicka, L.; Tu, Z.; Albayya, F.; Lee, W.; Hopp, S.; Miller, M.-J.; Spaulding, D.; Yang, Z.; Hodgdon, H.; Nolan, S.; Wen, M.; Costa, D.; Blain, J.-F.; Freeman, E.; De Strooper, B.; Vulsteke, V.; Scrocchi, L.; Zetterberg, H.; Portelius, E.; Hutter-Paier, B.; Havas, D.; Ahlijanian, M.; Flood, D.; Leventhal, L.; Shapiro, G.; Patzke, H.; Chesworth, R.; Koenig, G. Modulation of γ-Secretase by EVP-0015962 Reduces Amyloid Deposition and Behavioral Deficits in Tg2576 Mice. *Mol. Neurodegener.* **2012**, *7*, 61.

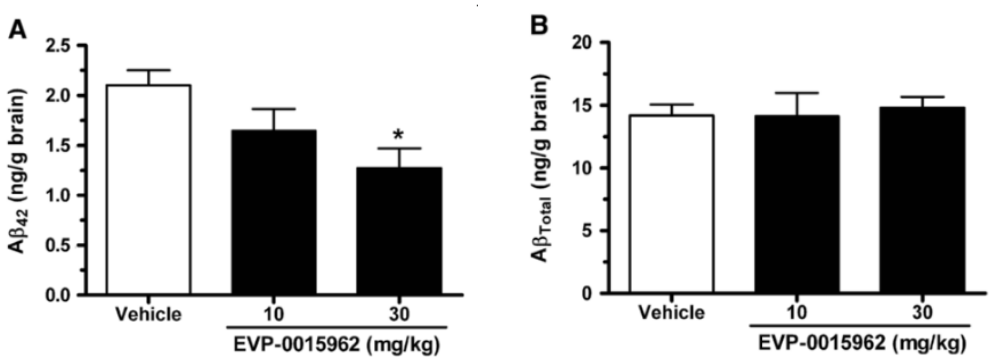

Figure 33: Brain concentrations of $A\beta_{42}$ (A) and $A\beta_{total}$ (B) measured 4h after administration of a 10 or 30 mg/kg dose of EVP-0015962[105]

6.5. Neurofibrillary degeneration strategy

6.5.1. Reduction of the hyperphosphorylation of the Tau protein

As it was outlined in the beginning of this chapter, the Tau protein is modified in brains of patients with AD and this alteration is leading to the NFTs formation. Numerous kinases and phosphatases have been identified to regulate the protein phosphorylation. The kinases can be divided in three groups:

- the proline-directed kinases made up of glycogen synthase kinase-3 (GSK-3), 5' adenosine monophosphate-activated protein kinase (AMPK) and the cyclin-dependent kinase 5 (CDK5),
- the non-proline-directed kinases like microtubule affinity-regulating kinases (MARKs), cyclic AMP-dependent protein kinase A (PKA) or casein kinase 1 (CK1),
- tyrosine kinases composed of Fyn, Abl and Syk.

Even if many of these enzymes play an important role in the Tau protein phosphorylation, the most important kinases in the hyperphosphorylation process are CDK5 and GSK3β, responsible of the phosphorylation of numerous tau protein's residues and promoting the insoluble oligomers formation[106]. Moreover, GSK-3 inhibition has been shown to lower deficits in long term potentiation[107]. This is probably why most of the drug developments in tau hyperphosphorylation focus on GSK-3[108].

[106] Nübling, G.; Bader, B.; Levin, J.; Hildebrandt, J.; Kretzschmar, H.; Giese, A. Synergistic Influence of Phosphorylation and Metal Ions on Tau Oligomer Formation and Coaggregation with α-Synuclein at the Single Molecule Level. *Mol. Neurodegener.* **2012**, *7* (1), 35.

[107] Hooper, C.; Markevich, V.; Plattner, F.; Killick, R.; Schofield, E.; Engel, T.; Hernandez, F.; Anderton, B.; Rosenblum, K.; Bliss, T.; Cooke, S. F.; Avila, J.; Lucas, J. J.; Giese, K. P.; Stephenson, J.; Lovestone, S. Glycogen Synthase Kinase-3 Inhibition Is Integral to Long-Term Potentiation. *Eur. J. Neurosci.* **2007**, *25* (1), 81–86.

[108] Gong, C.-X.; Iqbal, K. Hyperphosphorylation of Microtubule-Associated Protein Tau: A Promising Therapeutic Target for Alzheimer Disease. *Curr. Med. Chem.* **2008**, *15* (23), 2321–2328.

But all the developed small molecules inhibiting GSK-3 have been discontinued, the latest molecule being Tideglusib (Figure 34).Indeed, studies on DN-GSK-3β have shown that an extensive GSK-3 inhibition was correlated to neuronal apoptosis and impaired motor coordination[109].

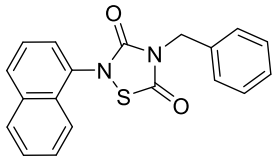

Figure 34: Structure of Tideglusib, a GSK3 inhibitor

6.5.2. Anti-aggregate of the Tau protein

Another approach is to inhibit the Tau protein oligomerisation by developing small molecules able to interact with the Tau protein core. Indeed, *in cellulo* and *in vitro* studies have shown that it is possible to inhibit the oligomers formation by interacting with the main protein residues (Tyr197, Tyr310, Phe346, Phe378 and Tyr394)[110]. For that purpose, two compounds have been developed (Figure 35).

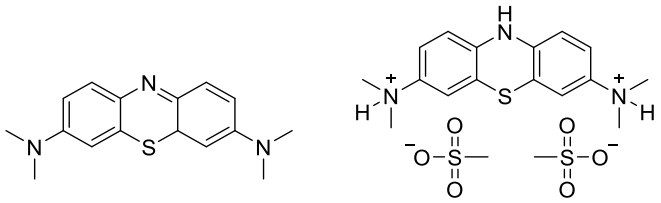

Figure 35: Anti-aggregate inhibitors

Firstly, Rember TM was tested in humans and showed good results concerning the cognition level improvements during a phase II clinical trial. Unfortunately, the main issue with this compound was the weak bioavailability. Rember TM was discontinued and the firm developed another molecule, LMTM, based on the same scaffold, able to act as a bioavailable prodrug of Rember TM. The compound is currently in phase III clinical trial.

[109] Avila, J.; Hernández, F. GSK-3 Inhibitors for Alzheimer's Disease. *Expert Rev. Neurother.* **2007**, *7* (11), 1527–1533.

[110] Akoury, E.; Gajda, M.; Pickhardt, M.; Biernat, J.; Soraya, P.; Griesinger, C.; Mandelkow, E.; Zweckstetter, M. Inhibition of Tau Filament Formation by Conformational Modulation. *J. Am. Chem. Soc.* **2013**, *135* (7), 2853–2862.

6.5.3. Microtubules stabilisation

Another consequence of the Tau hyperphosphorylation is a destabilisation of the microtubules leading to neuronal death (Figure 36). Microtubules are formed *via* a heterodimeric polymerization of two globular protein, alpha and beta tubulin, into protofilaments (usually 13 protofilaments) creating a hollow pipe of approximatively 24 nm. In neurons, they are essential for structure maintenance, axonal transport and synaptic plasticity[111].

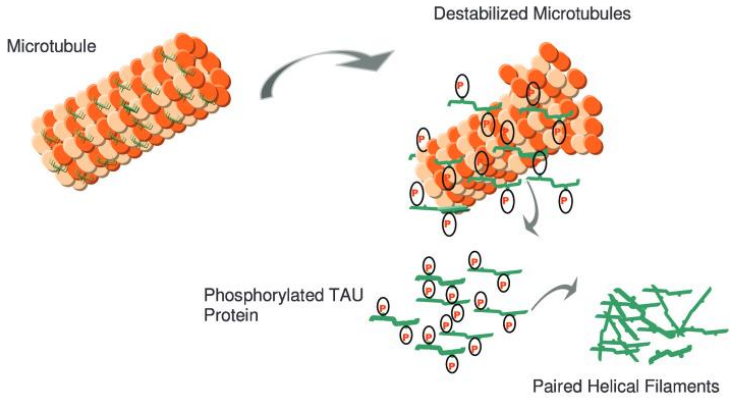

Figure 36: Microtubule destabilisation[111]

In CNS-related disorders, especially in AD, microtubule loss from axons and dendrites is a major contributor to neurodegeneration. One hypothesis is that abnormally phosphorylated Tau detaches from the microtubules and leads to a tubule's density decrease. Therefore, this loss of mass directly impacts the neuron capacity to maintain synaptic connections and axonal transport. However, there is very little information proving that the tubules simply disassembly by normal dynamic properties. Another hypothesis includes a microtubule protecting effect of the Tau protein against various proteins able to disassembly the microtubules[112]. Developing molecules stabilising the microtubules could counteract the abnormal detachment of the Tau protein and help maintaining microtubules' organisation and dynamic. Numerous drugs like taxanes used in oncology could be able to stabilise the microtubules by binding to the β-tubulin[113]. Hence, anti-cancer analogues have been developed to this end (Figure 37).

---

[111] de Paula, V. de J. R.; Guimarães, F. M.; Diniz, B. S.; Forlenza, O. V. Neurobiological Pathways to Alzheimer's Disease: Amyloid-Beta, TAU Protein or Both? *Dement. Neuropsychol.* **2009**, *3* (3), 188–194.
[112] Jean, D. C.; Baas, P. W. It Cuts Two Ways: Microtubule Loss during Alzheimer Disease: Microtubule Loss during Alzheimer Disease. *EMBO J.* **2013**, *32* (22), 2900–2902.
[113] Nogales, E.; Wolf, S. G.; Khan, I. A.; Ludueña, R. F.; Downing, K. H. Structure of Tubulin at 6.5 Å and Location of the Taxol-Binding Site. *Nature* **1995**, *375* (6530), 424.

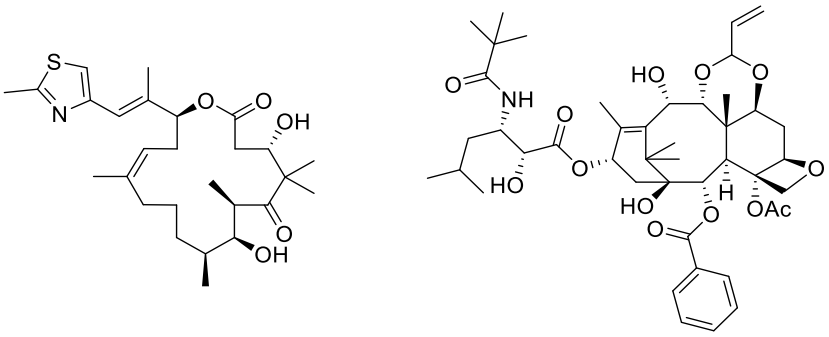

Epothilone D
Bristol-Myers Squibb
discontinued

TPI-287
Cortice Biosciences
phase I

Figure 37: Microtubules stabilizers

Only one stabilizer is still in clinical trial, TPI-287. It is a synthetic taxane diterpenoid drugs derivative, unlike most of the taxanes, TPI-287 crosses the BBB. Currently, the phase I clinical trial has the purpose of evaluating tolerance and pharmacokinetics of the drug. Consequently, further information concerning its activity are not available yet.

6.6. Oxidative stress reduction

Oxidative stress is a key factor of AD. Reactive oxygen species (ROS) and reactive nitrogen species (RNS) production appear to abnormally increase in patients with AD. Indeed, a mitochondria's malfunction leading to a significant production of superoxide ions could explain this behaviour[114]. The direct consequence is a hydrogen peroxide increase in the cytoplasm causing free radicals' formation *via* a Fenton reaction (Scheme 2)[115]. Studies have brought to light that because of a ferritin diminution in patients with AD, free iron ions are more present, therefore, free radicals' formation is promoted[116].

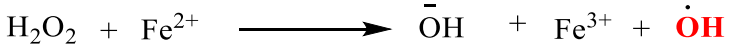

Scheme 2: Fenton reaction

ROS can oxidize lipids, proteins, DNA and RNA in vulnerable cells which leads to cellular death. Moreover, it has been suggested that oxidative stress could promote the Tau protein phosphorylation

[114] Petersen, R. B.; Nunomura, A.; Lee, H.; Casadesus, G.; Perry, G.; Smith, M. A.; Zhu, X. Signal Transduction Cascades Associated with Oxidative Stress in Alzheimer's Disease. *J. Alzheimers Dis. JAD* **2007**, *11* (2), 143–152.
[115] Sutton, H. C.; Winterbourn, C. C. On the Participation of Higher Oxidation States of Iron and Copper in Fenton Reactions. *Free Radic. Biol. Med.* **1989**, *6* (1), 53–60.
[116] Connor, J. R.; Snyder, B. S.; Arosio, P.; Loeffler, D. A.; LeWitt, P. A Quantitative Analysis of Isoferritins in Select Regions of Aged, Parkinsonian, and Alzheimer's Diseased Brains. *J. Neurochem.* **1995**, *65* (2), 717–724.

and its polymerization[117] and upregulate the production of both secretases (β-secretase and γ-secretase) involved in the amyloidogenic pathway leading to an increased production of Aβ[118]. Hence, it would seem wise to take an interest in the development of antioxidant to counteract this aspect of the pathology by trapping the free radicals. Well known antioxidants have been studied and seem promising (Figure 38). Indeed, Resveratrol[119,120], a polyphenol, can improve the patients' cognitive functions for mild to moderate stages of AD with a dose of 200 mg/day[121]. Regarding Melatonin, which is a sleeping hormone, it is currently in phase II and appears to help protecting the cells from oxidative stress by tackling free radicals.

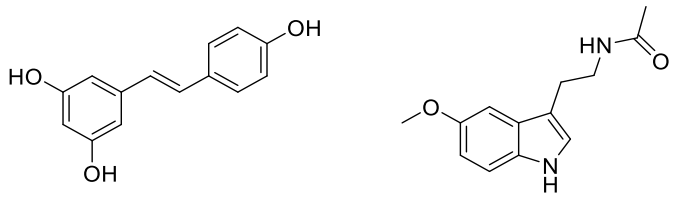

Resveratrol
phase III

Melatonin
phase II

Figure 38: Antioxidants in clinical trials

6.7. Other strategies

We have presented various therapeutic targets and the development of numerous small molecules intended to overcome the main abnormal behaviour of CNS-related pathologies. Nevertheless, even though, some molecules seem promising, the majority fails to pass the late stage of clinical development because of their inactivity or adverse effects. In the past years, other strategies have been investigated, like immunotherapy (vaccines) or drug repositioning.

---

[117] Dias-Santagata, D.; Fulga, T. A.; Duttaroy, A.; Feany, M. B. Oxidative Stress Mediates Tau-Induced Neurodegeneration in *Drosophila*. *J. Clin. Invest.* **2007**, *117* (1), 236–245.

[118] Paola, D.; Domenicotti, C.; Nitti, M.; Vitali, A.; Borghi, R.; Cottalasso, D.; Zaccheo, D.; Odetti, P.; Strocchi, P.; Marinari, U. M.; Tabaton, M.; Pronzato, M. A. Oxidative Stress Induces Increase in Intracellular Amyloid β-Protein Production and Selective Activation of BI and BII PKCs in NT2 Cells. *Biochem. Biophys. Res. Commun.* **2000**, *268* (2), 642–646.

[119] Wang, H.; Jiang, T.; Li, W.; Gao, N.; Zhang, T. Resveratrol Attenuates Oxidative Damage through Activating Mitophagy in an in Vitro Model of Alzheimer's Disease. *Toxicol. Lett.* **2018**, *282*, 100–108.

[120] Sawda, C.; Moussa, C.; Turner, R. S. Resveratrol for Alzheimer's Disease. *Ann. N. Y. Acad. Sci.* **2017**, *1403* (1), 142–149.

[121] Resveratrol Improves Memory in Overweight Adults | ALZFORUM https://www.alzforum.org/news/research-news/resveratrol-improves-memory-overweight-adults.

6.7.1. Immunotherapy

So far, three therapies targeting the Aβ peptide are in phase III clinical trials. First, BAN2401 which is a monoclonal antibody that binds selectively to Aβ protofibrils. The first clinical study proved that BAN2401 was well tolerated and safe in mild to moderate AD[122]. More recent studies have shown that BAN2401 reduces Aβ protofibrils concentrations in brain and reduces their toxicity by tackling abnormal accumulation of the protofibrils in astrocytes[123]. Secondly, Gantenerumab has shown promising results by preferentially interacting with brain Aβ but also by neutralizing oligomeric Aβ-mediated effects on LTP in rat brains. Finally, Solanezumab is a monoclonal antibody against the Aβ peptide's mid-domain and showed encouraging results by reversing memory deficits in APP-transgenic mouse models[124].

6.7.2. Repositioning[125]

Drug discovery is a laborious, costly, time-consuming and high-risk field of research. According to a report of the Eastern Research group, it takes usually 10-15 years to develop a new compound and only 2.01%[126] of the developed molecules will encounter success. Therefore, drug repositioning is a strategy appreciated by the pharmaceutical companies. By using the "old drug for new uses" approach, companies can save time and money because there are less steps to fulfil than in traditional drug development. Moreover, drug repositioning is not only timesaving but also a low risk and cheaper approach (Figure 39).

[122] Logovinsky, V.; Satlin, A.; Lai, R.; Swanson, C.; Kaplow, J.; Osswald, G.; Basun, H.; Lannfelt, L. Safety and Tolerability of BAN2401 - a Clinical Study in Alzheimer's Disease with a Protofibril Selective Aβ Antibody. *Alzheimers Res. Ther.* **2016**, *8* (1), 14.

[123] Söllvander, S.; Nikitidou, E.; Gallasch, L.; Zyśk, M.; Söderberg, L.; Sehlin, D.; Lannfelt, L.; Erlandsson, A. The Aβ Protofibril Selective Antibody MAb158 Prevents Accumulation of Aβ in Astrocytes and Rescues Neurons from Aβ-Induced Cell Death. *J. Neuroinflammation* **2018**, *15* (1), 98.

[124] Dodart, J.-C.; Bales, K. R.; Gannon, K. S.; Greene, S. J.; DeMattos, R. B.; Mathis, C.; DeLong, C. A.; Wu, S.; Wu, X.; Holtzman, D. M.; Paul, S. M. Immunization Reverses Memory Deficits without Reducing Brain Abeta Burden in Alzheimer's Disease Model. *Nat. Neurosci.* **2002**, *5* (5), 452–457.

[125] Xue, H.; Li, J.; Xie, H.; Wang, Y. Review of Drug Repositioning Approaches and Resources. *Int. J. Biol. Sci.* **2018**, *14* (10), 1232–1244.

[126] Pammolli, F.; Magazzini, L.; Riccaboni, M. The Productivity Crisis in Pharmaceutical R&D. *Nat. Rev. Drug Discov.* **2011**, *10* (6), 428–438.

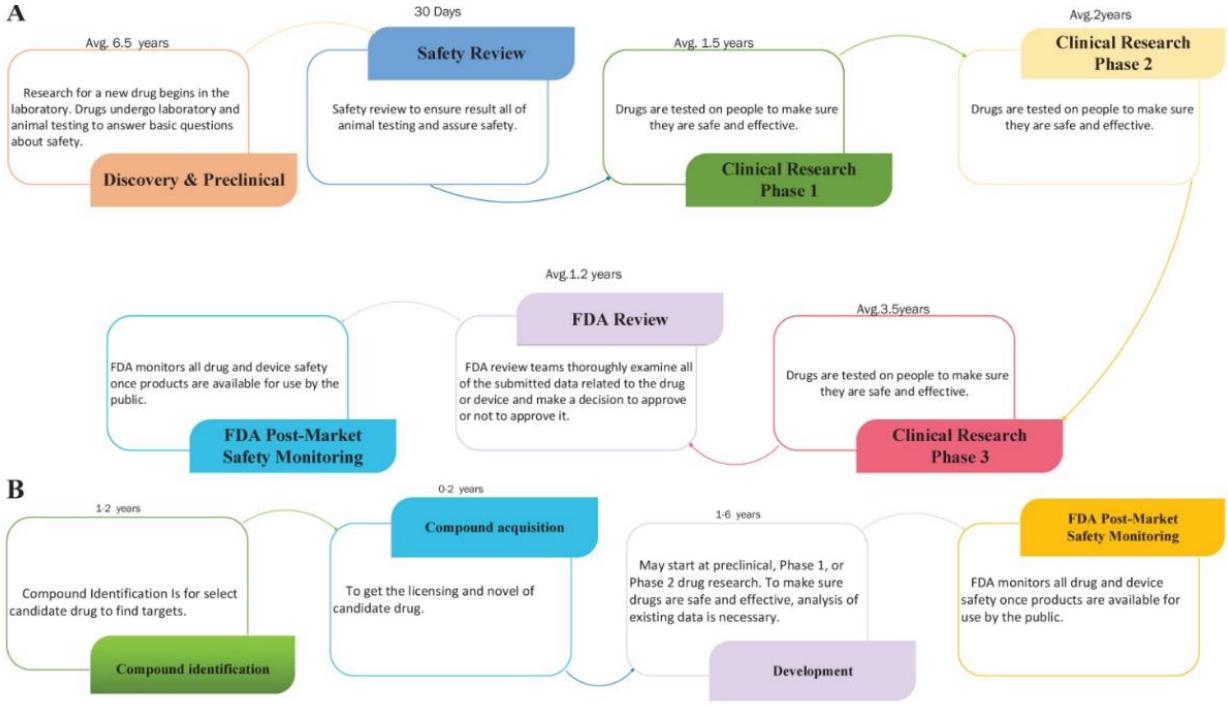

Figure 39: The contrast of traditional drug development (A) and drug repositioning (B)[125]

Currently, numerous drugs have been repositioned for AD treatment (approximatively 40 are listed on Alzforum.org), and three of them are in phase IV clinical trial (Figure 40). Carvedilol, a non-selective α/β-adrenergic receptor antagonist and vasodilator has been proven to significantly attenuate Aβ peptide fibrillation and oligomerization by interfering with early stage Aβ dimer, trimer and tetramer or pentamer and hexamer formation[127]. Simvastatin is an HMG-coA reductase inhibitor widely prescribed for hypercholesterolemia treatment. A large body of studies have shown that long-term statin treatments affect APP processing, might have neuroprotective effects and lower Aβ peptide levels. Simvastatin has demonstrated modest but still significant effects on brain cholesterol metabolism in a small number of AD patients when a high dose is administered[128]. Finally, Prazosin which is an α-blocker has been studied to counter aggressive agitation in the moderate stages of CNS-related pathologies. It has also been reported to reduce Aβ generation and counteract Aβ-induced vasoconstriction mediated via α-1 adrenergic receptor signalling[129].

[127] Wang, J.; Ono, K.; Dickstein, D. L.; Arrieta-Cruz, I.; Zhao, W.; Qian, X.; Lamparello, A.; Subnani, R.; Ferruzzi, M.; Pavlides, C.; Ho, L.; Hof, P. R.; Teplow, D. B.; Pasinetti, G. M. Carvedilol as a Potential Novel Agent for the Treatment of Alzheimer's Disease. *Neurobiol. Aging* **2011**, *32* (12), 2321.e1-2321.e12.

[128] Serrano-Pozo, A.; Vega, G. L.; Lütjohann, D.; Locascio, J. J.; Tennis, M. K.; Deng, A.; Atri, A.; Hyman, B. T.; Irizarry, M. C.; Growdon, J. H. Effects of Simvastatin on Cholesterol Metabolism and Alzheimer Disease Biomarkers: *Alzheimer Dis. Assoc. Disord.* **2010**, 1.

[129] Haase, N.; Herse, F.; Spallek, B.; Haase, H.; Morano, I.; Qadri, F.; Szijártó, I. A.; Rohm, I.; Yilmaz, A.; Warrington, J. P.; Ryan, M. J.; Gollasch, M.; Müller, D. N.; Dechend, R.; Wallukat, G. Amyloid-β Peptides Activate A1-Adrenergic Cardiovascular Receptors. *Hypertens. Dallas Tex 1979* **2013**, *62* (5), 966–972.

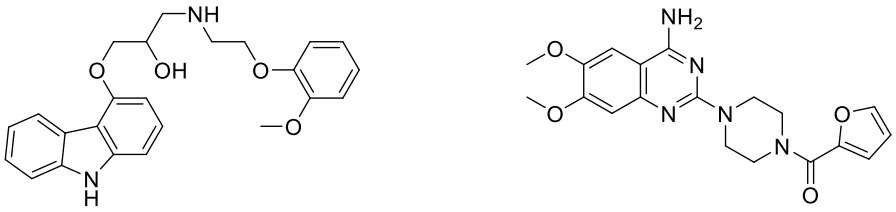

Carvedilol
Procter and Gamble
approved for hypertension, heart failure, angina pectoris
phase IV (AD)

Prazosin
approved for hypertension
phase IV (AD)

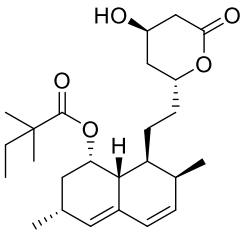

Simvastatin
Merck
approved for hypercholesterolemia and diabetic cardiomyopathy
phase IV (mild cognitive impairment)

Figure 40: Example of drugs repositioned for AD

As a conclusion, the multifactorial character of the pathology involving a large number of enzymes and receptors, could explain the high number of drugs that failed to pass all the clinical trials. The "one molecule for one target" does not seem to be a suitable solution for this kind of disorder. Therefore, in the past decade, besides the drug cocktail acting on different therapeutic targets, a new approach has emerged, the "multi-target directed ligand (MTDLs)" approach[130].

7. The "multi-target directed ligand" approach

7.1. Different therapeutic "multi-target" approaches

In view of the complexity of AD, the "one molecule for one target" concept, implying the use of a drug bearing only one pharmacophore acting selectively on a sole target, seems to have reached its limits. Thus, for the past decade, other approaches are emerging and are both in the private and academic laboratories (Figure 41):

- the « Drug cocktail » approach consists in the prescription of different drugs (usually 2 or 3) to the patient. This approach has proved successful for the treatment of AIDS for instance. This kind of therapy has two major issues, principally problems of therapeutic

[130] Design of Hybrid Molecules for Drug Development - 1st Edition https://www.elsevier.com/books/design-of-hybrid-molecules-for-drug-development/decker/978-0-08-101011-2.

observance and the fact that it is a heavy treatment, especially for people with cognitive disorders, requiring to take each drug at a definite time depending on its pharmacokinetics and pharmacodynamics parameters.

- the "single-pill drug combination" which only one medicine composed of different active substances in order to avoid the problems of therapeutic observance. However, this approach is very complicated because it is mandatory to know very well the reactivity of each compound to avoid or predict the secondary effects. Moreover, the active substances must have close pharmaceutical and pharmacodynamics profiles,

- the "Multitarget directed ligands (MTDLs)". Here, the aim is to pair several pharmacophores acting on different enzymes or receptors involved in the disease. One of the advantages of the treatment "one molecule, several targets" is to reduce the secondary effects induced by the interactions between different active substances. Moreover, it gives a less heavy treatment to the patients of AD.

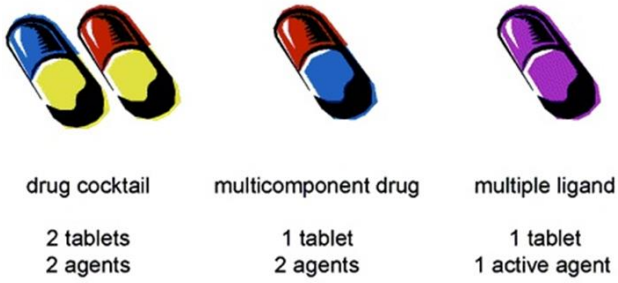

Figure 41: Three main clinical scenarios for multitarget therapy[131]

7.2. MTDLs conception

There are five types of pharmacophores' combinations to obtain different MTDLs with a variable synthetic complexity (Figure 42). They can be divided in two groups: MTDLs with a distinct linker and MTDLs without a linker.

[131] Morphy, R.; Rankovic, Z. Designed Multiple Ligands. An Emerging Drug Discovery Paradigm. *J. Med. Chem.* **2005**, *48* (21), 6523–6543.

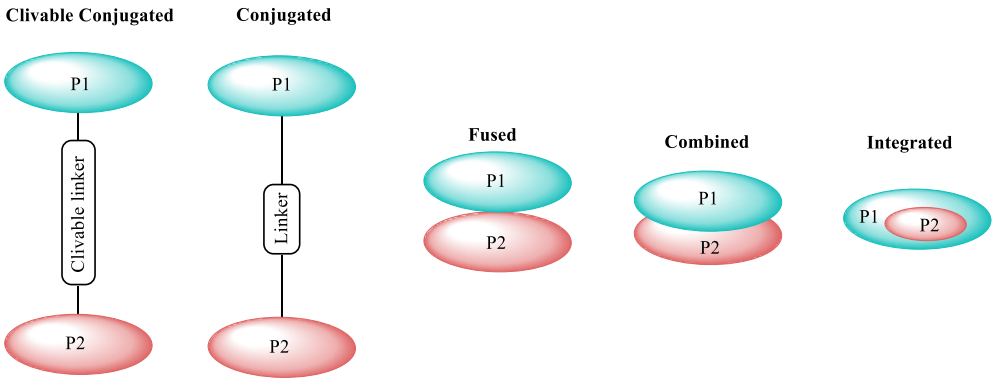

Figure 42: Different types of MTDLs

For the first group, there is major difference between the two types of MTDLs. Cleavable conjugates use a linker designed to be cleaved in the organism to release two independent ligands. Concerning the second group no linker is used to bind the two pharmacophores, the molecules are merged to some degree thanks to a common moiety. The blend's degree between the two pharmacophores will determine if the MTDLs is fused, combined or even integrated[131] to give MTDLs with lower molecular weights.

When developing MTDLs, specifications must be respected:

- the pharmacophores' choice must lead to a ligand with optimal pharmacokinetic and physicochemical properties,
- affinities and/or efficacies toward the two targets must be similar. Indeed, unlike a "drug cocktail", a 1/1 stoichiometry of a MTDL does not allow a therapeutic doses adjustment,
- Affinities of the MTDL toward each target must be in the same range of the observed affinities of each pharmacophore.

This kind of molecules in the treatment of multifactorial CNS-related pathologies like AD has numerous benefits:

- a better long-term efficacy of the treatment by limiting issues associated with low therapeutic observance,
- a limitation of adverse effects,
- simplified pharmacokinetic studies,
- simplified clinical trials,
- simplified drug formulation and production.

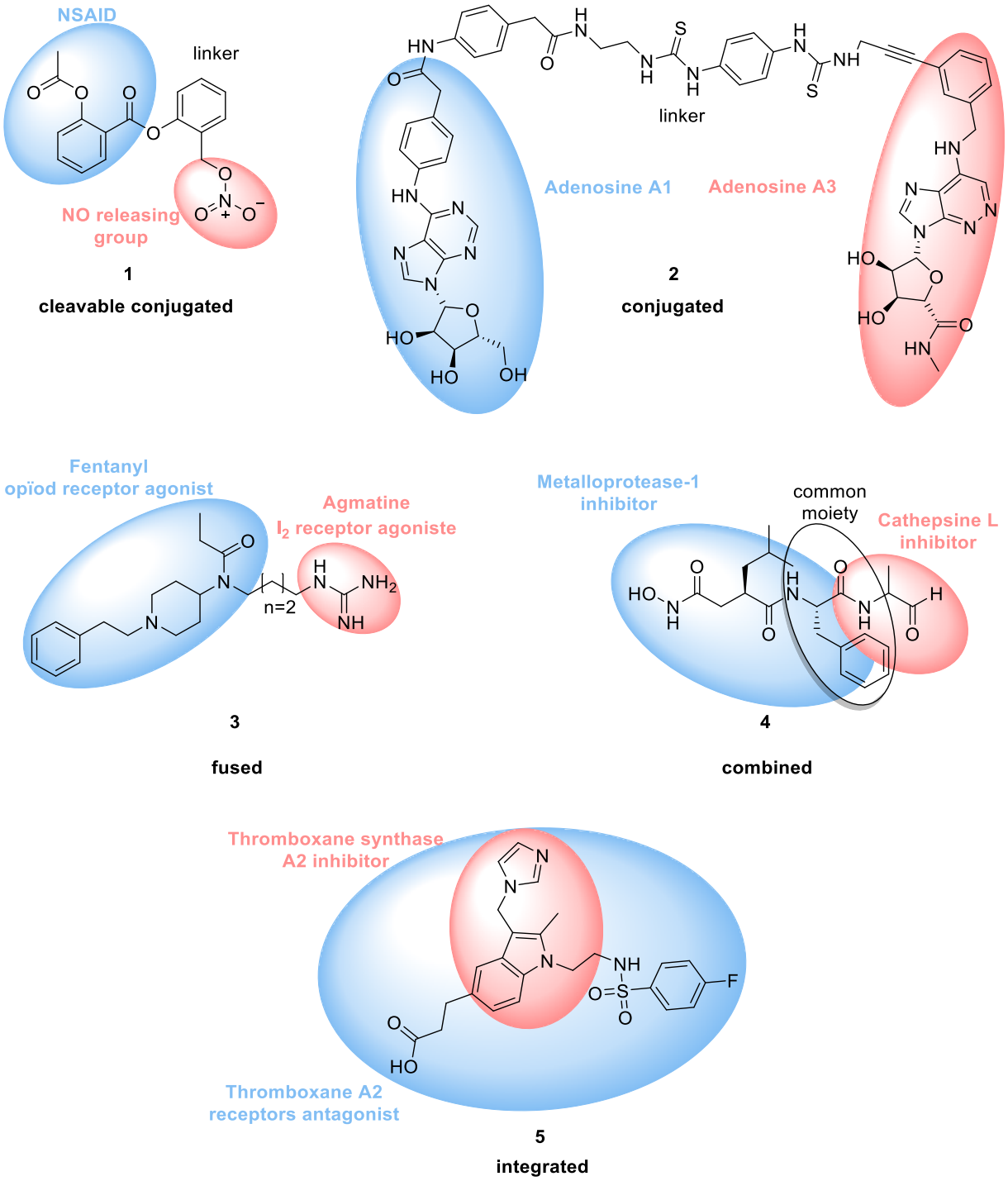

Figure 43: Example of various MTDLs' types[131] (NSAID: nonsteroidal anti-inflammatory drug)

A large variety of MTDLs have been described in the literature and used in various pathologies. Jacobson et *al*. described in 2000 the synthesis of a conjugated MTDLs (Figure 43 - **2**) using a rigid ethynyl-based spacer to link adenosine A1 and A3[132] to create a dual ligand with cardioprotective

[132] Jacobson, K. A.; Xie, R.; Young, L.; Chang, L.; Liang, B. T. A Novel Pharmacological Approach to Treating Cardiac Ischemia. Binary Conjugates of A1 and A3 Adenosine Receptor Agonists. *J. Biol. Chem.* **2000**, *275* (39), 30272–30279.

activity. Most of the cleavable conjugated MTDLs reported bear an ester-based linker cleavable by plasma esterase to release two independent drugs like NO-aspirin (Figure 43 – **1**). Moreover, in order to obtain an opioid analgesic with few adverse effects, Montero et *al*., worked on the association of a guanidium group from the I_2 ligand and the fentanyl, an opioid[133] (Figure 43 – **3**). MTDLs have also been investigated to develop combined drug able to bind and inhibit two proteases, in this example, a metalloprotease inhibitor and a cathepsin inhibitor (Figure 43 – **4**). Finally, the most complex and less developed MTDLs are the integrated ones. One example of this kind of ligands is a combination of a thromboxane synthase inhibitor pharmacophore and a thromboxane receptor antagonist (Figure 43 – **5**).

7.3. MTDLs designed for AD's treatment

Due to the rapid development of MTDLs synthesis in the past years and to the high number of publications on this topic, we made the choice to only take an interest on MTDLs designed against AD carrying an AChEI. More comprehensive reviews on MTDLs used for AD, have been published recently[134,135,136,137].

7.3.1. MTDLs targeting AChE and amyloid-related targets

7.3.1.1. Aβ aggregation inhibition

Different studies have identified a link between AChE and Aβ aggregation. Indeed, it has been brought to light that AChE peripheral site might contribute to amyloid deposits development by enhancing the

[133] Montero, A.; Goya, P.; Jagerovic, N.; Callado, L. F.; Callado, L. F.; Meana, J. J.; Girón, R.; Goicoechea, C.; Martín, M. I. Guanidinium and Aminoimidazolinium Derivatives of N-(4-Piperidyl)Propanamides as Potential Ligands for Mu Opioid and I2-Imidazoline Receptors: Synthesis and Pharmacological Screening. *Bioorg. Med. Chem.* **2002**, *10* (4), 1009–1018.

[134] Ortiz, C. J. C.; de Freitas Silva, M.; Gontijo, V. S.; Viegas, F. P. D.; Dias, K. S. T.; Viegas, C. Design of Multi-Target Directed Ligands as a Modern Approach for the Development of Innovative Drug Candidates for Alzheimer's Disease. In *Multi-Target Drug Design Using Chem-Bioinformatic Approaches*; Roy, K., Ed.; Methods in Pharmacology and Toxicology; Springer New York: New York, NY, 2019; pp 255–351.

[135] Rosini, M.; Simoni, E.; Bartolini, M.; Cavalli, A.; Ceccarini, L.; Pascu, N.; McClymont, D. W.; Tarozzi, A.; Bolognesi, M. L.; Minarini, A.; Tumiatti, V.; Andrisano, V.; Mellor, I. R.; Melchiorre, C. Inhibition of Acetylcholinesterase, β-Amyloid Aggregation, and NMDA Receptors in Alzheimer's Disease: A Promising Direction for the Multi-Target-Directed Ligands Gold Rush. *J. Med. Chem.* **2008**, *51* (15), 4381–4384.

[136] León, R.; Garcia, A. G.; Marco-Contelles, J. Recent Advances in the Multitarget-Directed Ligands Approach for the Treatment of Alzheimer's Disease. *Med. Res. Rev.* **2013**, *33* (1), 139–189.

[137] de Freitas Silva, M.; Dias, K. S. T.; Gontijo, V. S.; Ortiz, C. J. C.; Viegas, C. Multi-Target Directed Drugs as a Modern Approach for Drug Design Towards Alzheimer's Disease: An Update. *Curr. Med. Chem.* **2018**, *25* (29), 3491–3525.

Aβ peptide fragments aggregation[138] and accelerating the peptide assembly into fibrils conducting to the senile plaques' formation. Moreover, it appears that the $A\beta_{1-42}$ aggregates neurotoxicity depends on the amount of AChE linked to the complexes[139,140]. Building compounds with a dual activity toward AChE and Aβ aggregation could be an attractive therapeutic strategy against AD (Figure 44). The first example of MTDLs targeting AChE were Tacrine homodimer designed by Rodriguez-Franco et *al*.[141] such as compound **6** capable of interacting with the AChE catalytic site and the PAS simultaneously. This characteristic gave compound **6** various neuroprotective activities like a high and selective AChE inhibition compared to Tacrine and BACE-1 inhibition properties associated with AChE-induced Aβ aggregation[142]. In 2008, Kwon et *al*.[143] designed piperidine derivatives based on the Donepezil scaffold binding to the AChE catalytic site but also to the peripherical site. Compound **7** and **8** were the more promising MTDLs, indeed, they showed good inhibitory activity toward AChE and a promising percentage of aggregation inhibition. Moreover, **7** displayed a high inhibitory activity toward AChE and a good selectivity of AChE relative to BChE (120 times more selective). Compound **9** was developed by Camps et *al*. in 2008 by assembling two known AChEIs: Tacrine and Donepezil. It is a sub nanomolar AChEI and a potent BChE inhibitor. Like Donepezil, **9** can interact with the enzyme peripherical site to inhibit the peptide aggregation[144]. More recently, compound **10**, a curcumin like compound with a cyclohexanone moiety, was studied and showed a strong inhibitory activity and selectivity toward

[138] Alvarez, A.; Opazo, C.; Alarcón, R.; Garrido, J.; Inestrosa, N. C. Acetylcholinesterase Promotes the Aggregation of Amyloid-Beta-Peptide Fragments by Forming a Complex with the Growing Fibrils. *J. Mol. Biol.* **1997**, *272* (3), 348–361.

[139] De Ferrari, G. V.; Canales, M. A.; Shin, I.; Weiner, L. M.; Silman, I.; Inestrosa, N. C. A Structural Motif of Acetylcholinesterase That Promotes Amyloid Beta-Peptide Fibril Formation. *Biochemistry* **2001**, *40* (35), 10447–10457.

[140] Muñoz, F. J.; Inestrosa, N. C. Neurotoxicity of Acetylcholinesterase Amyloid Beta-Peptide Aggregates Is Dependent on the Type of Abeta Peptide and the AChE Concentration Present in the Complexes. *FEBS Lett.* **1999**, *450* (3), 205–209.

[141] Rodríguez-Franco, M. I.; Fernández-Bachiller, M. I.; Pérez, C.; Hernández-Ledesma, B.; Bartolomé, B. Novel Tacrine-Melatonin Hybrids as Dual-Acting Drugs for Alzheimer Disease, with Improved Acetylcholinesterase Inhibitory and Antioxidant Properties. *J. Med. Chem.* **2006**, *49* (2), 459–462.

[142] Fu, H.; Li, W.; Luo, J.; Lee, N. T. K.; Li, M.; Tsim, K. W. K.; Pang, Y.; Youdim, M. B. H.; Han, Y. Promising Anti-Alzheimer's Dimer Bis(7)-Tacrine Reduces β-Amyloid Generation by Directly Inhibiting BACE-1 Activity. *Biochem. Biophys. Res. Commun.* **2008**, *366* (3), 631–636.

[143] Kwon, Y. E.; Park, J. Y.; No, K. T.; Shin, J. H.; Lee, S. K.; Eun, J. S.; Yang, J. H.; Shin, T. Y.; Kim, D. K.; Chae, B. S.; Leem, J.-Y.; Kim, K. H. Synthesis, in Vitro Assay, and Molecular Modeling of New Piperidine Derivatives Having Dual Inhibitory Potency against Acetylcholinesterase and Aβ1–42 Aggregation for Alzheimer's Disease Therapeutics. *Bioorg. Med. Chem.* **2007**, *15* (20), 6596–6607.

[144] Camps, P.; Formosa, X.; Galdeano, C.; Gómez, T.; Muñoz-Torrero, D.; Scarpellini, M.; Viayna, E.; Badia, A.; Clos, M. V.; Camins, A.; Pallàs, M.; Bartolini, M.; Mancini, F.; Andrisano, V.; Estelrich, J.; Lizondo, M.; Bidon-Chanal, A.; Luque, F. J. Novel Donepezil-Based Inhibitors of Acetyl- and Butyrylcholinesterase and Acetylcholinesterase-Induced β-Amyloid Aggregation. *J. Med. Chem.* **2008**, *51* (12), 3588–3598.

AChE. Concerning the Aβ aggregates, **10** displayed promising inhibitory results and a 92% protection of PC12 cells against Aβ-induced apoptosis [145].

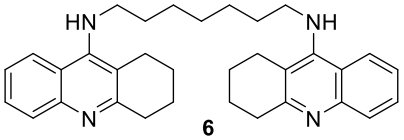

6

IC_{50} (AChE) = 0.40 nM
IC_{50} (BChE) = 390 nM
IC_{50} (AChE-induced Aβ aggregation) = 390 nM
IC_{50} (NMDAR) = 0.76 μM

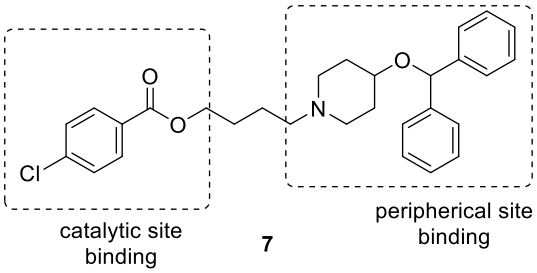

7

IC_{50} (AChE) = 0.32 ± 0.12 μM
IC_{50} (BChE) = 38.4 ± 3.72 μM
Aggregation inhibition = 55.5% at 100 μM

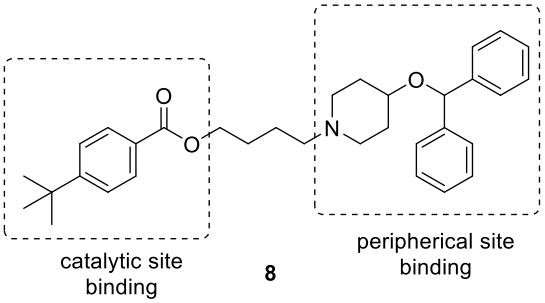

8

IC_{50} (AChE) = 2.41 ± 0.2 μM
IC_{50} (BChE) = 78.9 ± 5.44 μM
Aggregation inhibition = 72.4% 100 μM

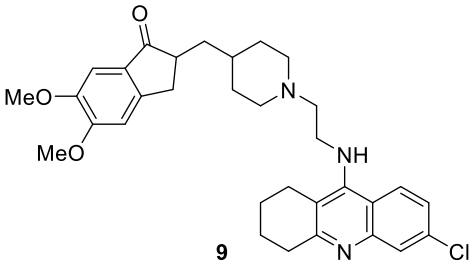

9

IC_{50} (*h*AChE) = 0.67 ± 0.06 nM
IC_{50} (*h*BChE) = 136 ± 9 nM
Aggregation inhibition = 37.6 ± 8.8% at 100 μM

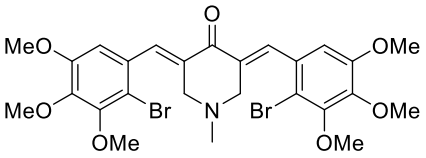

10

IC_{50} (AChE) = 0.037 ± 0.02 μM
IC_{50} (BChE) = 10.5 ± 2.2 μM
Aggregation inhibition = 76.6% at 10 μM

Figure 44: Example of MTDLs inhibiting AChE and Aβ aggregation

[145] Zha, G.-F.; Zhang, C.-P.; Qin, H.-L.; Jantan, I.; Sher, M.; Amjad, M. W.; Hussain, M. A.; Hussain, Z.; Bukhari, S. N. A. Biological Evaluation of Synthetic α,β-Unsaturated Carbonyl Based Cyclohexanone Derivatives as Neuroprotective Novel Inhibitors of Acetylcholinesterase, Butyrylcholinesterase and Amyloid-β Aggregation. *Bioorg. Med. Chem.* **2016**, *24* (10), 2352–2359.

7.3.1.2. BACE-1 inhibition[146]

Piazzi et *al*. designed in 2008 a series of coumarin derivatives[147] able to inhibit both AChE and BACE-1. Compound **11** was one of their best candidates with a balanced biological profile against the two targets. Six years later, the same group launched a screening of benzophenone derivatives to identify novel hybrids inhibiting AChE and BACE-1 but most of the compounds were proven to be inactive. Zha et *al*. synthesized and biologically evaluated a novel series of 26 Tacrine-benzofuran hybrids, amongst which compound **12** showed sub nanomolar inhibitory activity toward AChE and micromolar potency against BACE-1[148]. At the same time, Constanzo et *al*. designed a Donepezil-based series of derivatives and evaluated their selectivity toward AChE compared to BChE. Among all the derivatives, **13** had a promising inhibiting activity toward BACE-1 despite a less potent AChE inhibition potency as compared to the parent compound[149].

Another class of MTDLs inhibiting AChE and BACE-1 was investigated by different groups, the lead compounds not only modulated the two desired targets catalytic activity, but also acted on other targets of CNS-dependant pathologies. Firstly, Camps et *al*.[150] discovered a series of quinoline-chlorotacrine, the lead compound **14** proved to bind to both AChE catalytic and peripherical sites endowing the molecule with Aβ aggregation inhibition properties. **14** also displayed anti BACE-1 properties (80% of BACE-1 activity blocked with a 2.5 µM concentration).

---

[146] Prati, F.; Bottegoni, G.; Bolognesi, M. L.; Cavalli, A. BACE-1 Inhibitors: From Recent Single-Target Molecules to Multitarget Compounds for Alzheimer's Disease. *J. Med. Chem.* **2018**, *61* (3), 619–637.

[147] Piazzi, L.; Cavalli, A.; Colizzi, F.; Belluti, F.; Bartolini, M.; Mancini, F.; Recanatini, M.; Andrisano, V.; Rampa, A. Multi-Target-Directed Coumarin Derivatives: HAChE and BACE1 Inhibitors as Potential Anti-Alzheimer Compounds. *Bioorg. Med. Chem. Lett.* **2008**, *18* (1), 423–426.

[148] Zha, X.; Lamba, D.; Zhang, L.; Lou, Y.; Xu, C.; Kang, D.; Chen, L.; Xu, Y.; Zhang, L.; De Simone, A.; Samez, S.; Pesaresi, A.; Stojan, J.; Lopez, M. G.; Egea, J.; Andrisano, V.; Bartolini, M. Novel Tacrine–Benzofuran Hybrids as Potent Multitarget-Directed Ligands for the Treatment of Alzheimer's Disease: Design, Synthesis, Biological Evaluation, and X-Ray Crystallography. *J. Med. Chem.* **2016**, *59* (1), 114–131.

[149] Costanzo, P.; Cariati, L.; Desiderio, D.; Sgammato, R.; Lamberti, A.; Arcone, R.; Salerno, R.; Nardi, M.; Masullo, M.; Oliverio, M. Design, Synthesis, and Evaluation of Donepezil-Like Compounds as AChE and BACE-1 Inhibitors. *ACS Med. Chem. Lett.* **2016**, *7* (5), 470–475.

[150] Camps, P.; Formosa, X.; Galdeano, C.; Muñoz-Torrero, D.; Ramírez, L.; Gómez, E.; Isambert, N.; Lavilla, R.; Badia, A.; Clos, M. V.; Bartolini, M.; Mancini, F.; Andrisano, V.; Arce, M. P.; Rodríguez-Franco, M. I.; Huertas, Ó.; Dafni, T.; Luque, F. J. Pyrano[3,2-c]Quinoline−6-Chlorotacrine Hybrids as a Novel Family of Acetylcholinesterase- and β-Amyloid-Directed Anti-Alzheimer Compounds. *J. Med. Chem.* **2009**, *52* (17), 5365–5379.

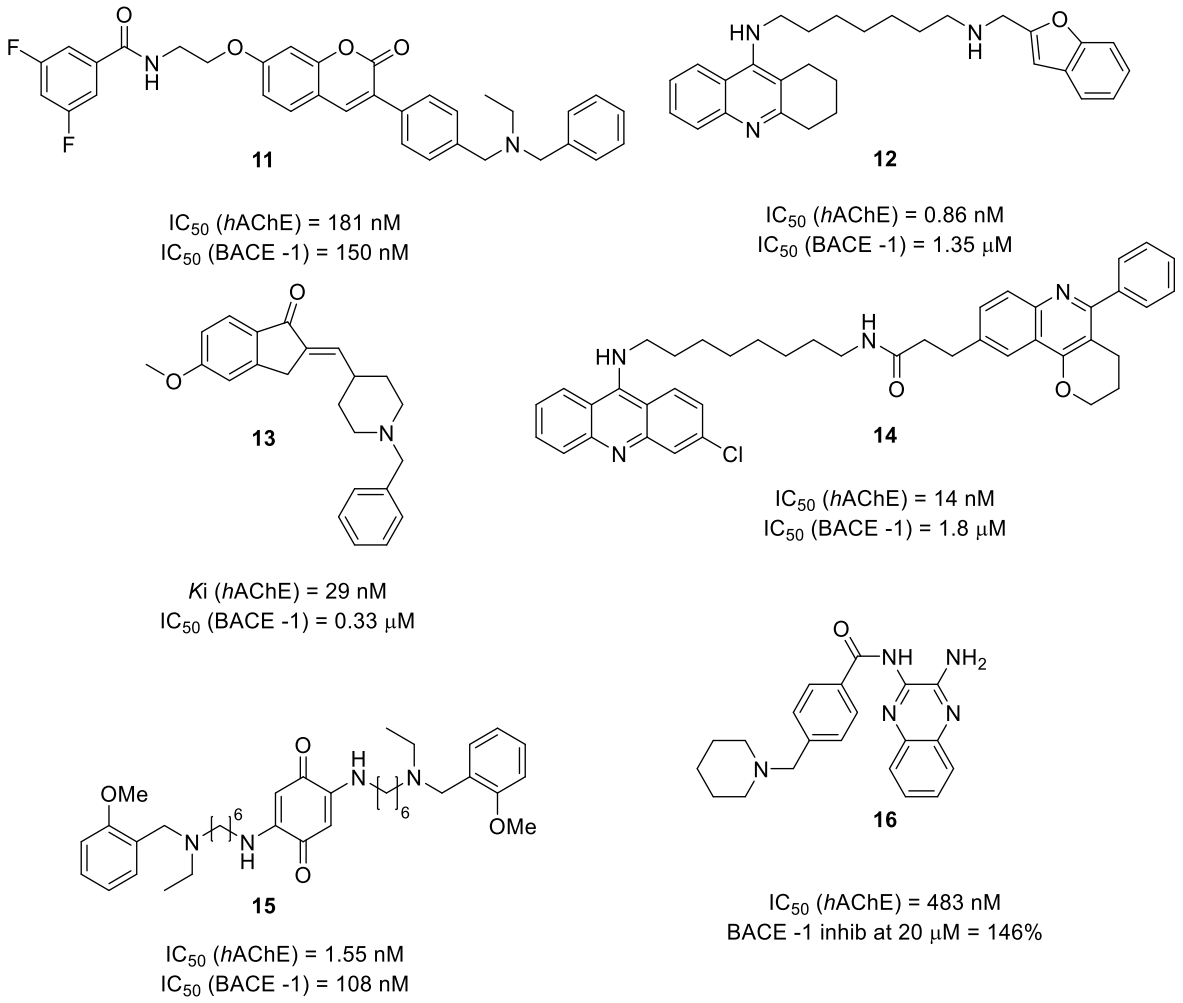

Figure 45: Example of MTDLs inhibiting AChE and BACE-1

Then, Cavalli et *al*. designed compound **15** called Memoquin acting on numerous targets involved in AD. Indeed, besides its inhibiting activity on AChE and BACE-1, Memoquin also turned out to prevent the Aβ aggregates to assembly automatically (IC_{50} = 5.93 μM) or by AChE induction (IC_{50} = 28.3 μM). Moreover, Memoquin proved to possess antioxidant properties, lowering the free radicals' formation by 44% and helps reducing Tau hyperphosphorylation[151]. *In vivo* studies have shown that Memoquin was able to restore cholinergic deficit and invert neuronal apoptosis in mice[152]. Finally, Huang et *al*. designed a quinoxaline derivatives series of 17 compounds expressing BACE-1 and AChE inhibition and some of them displayed H_3 receptor antagonist activity. Among the 17 molecules, only one, compound

[151] Cavalli, A.; Bolognesi, M. L.; Capsoni, S.; Andrisano, V.; Bartolini, M.; Margotti, E.; Cattaneo, A.; Recanatini, M.; Melchiorre, C. A Small Molecule Targeting the Multifactorial Nature of Alzheimer's Disease. *Angew. Chem. Int. Ed Engl.* **2007**, *46* (20), 3689–3692.

[152] Bolognesi, M. L.; Cavalli, A.; Melchiorre, C. Memoquin: A Multi-Target-Directed Ligand as an Innovative Therapeutic Opportunity for Alzheimer's Disease. *Neurotherapeutics* **2009**, *6* (1), 152–162.

16, proved to be a modulator of the three targets with promising results (IC_{50}(H_3R antagonism) = 280 nM and IC_{50}(H_3R inverse agonism) = 189 nM) [153].

7.3.2. MTDLs targeting NMDA receptors[154]

In 2012, a series of Galantamine and memantine hybrids was designed and investigated by Melchiorre et *al*. in order to obtain MTDLs able to inhibit AChE and to block NMDA receptors. Compound **17** called memagal showed a good affinity towards AChE and turned out to be a NMDA-mediated neurotoxicity inhibitor at the sub nanomolar range[154]. Rook et *al*. developed a novel series of bivalent β-carbolines (pyrido[3,4b]indoles) based on the structure of potent AChEIs, monovalent β-carbolines. Among all the derivatives, compound **18** turned out to be the most potent AChEI and a potent inhibitor of the Ca^{2+} glutamate-induced current with an IC_{50} 4 times stronger than memantine[155].

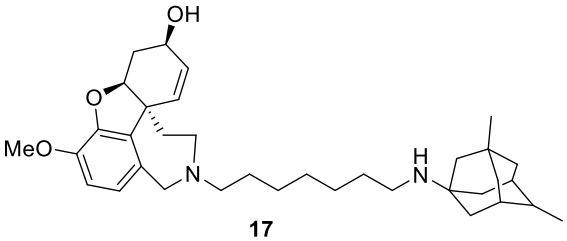

17

IC_{50} (AChE) = 1.16 nM
Ki NMDA NR_{1-a}/N_{2b} = 4.6 mM

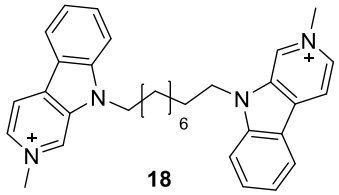

18

IC_{50} (AChE) = 0.50 nM
IC_{50} (BChE) = 5.7 nM
IC_{50} (NMDAR block NR_{1-a}/N_{2a}) = 1.4 mM
IC_{50} (NMDAR block NR_{1-a}/N_{2b}) = 2.9 mM

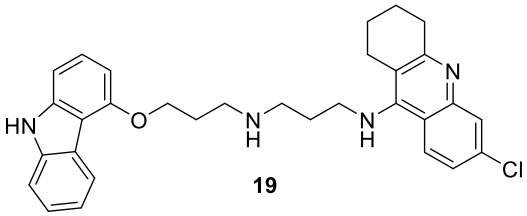

19

IC_{50} (AChE) = 2.15 nM
IC_{50} (BChE) = 296 nM
%AB $_{AChE\ agg.}$ = 57.7% at 100 mM
%AB $_{self\ agg.}$ = 36.0% at 50 mM
IC_{50} (NMDAR block) = 0.74 mM
IC_{50} (% protection ROS) = 23 mM

Figure 46: Examples of MTDLs inhibiting AChE and antagonizing NMDAR

---

[153] Huang, W.; Tang, L.; Shi, Y.; Huang, S.; Xu, L.; Sheng, R.; Wu, P.; Li, J.; Zhou, N.; Hu, Y. Searching for the Multi-Target-Directed Ligands against Alzheimer's Disease: Discovery of Quinoxaline-Based Hybrid Compounds with AChE, H3R and BACE 1 Inhibitory Activities. *Bioorg. Med. Chem.* **2011**, *19* (23), 7158–7167.

[154] Simoni, E.; Daniele, S.; Bottegoni, G.; Pizzirani, D.; Trincavelli, M. L.; Goldoni, L.; Tarozzo, G.; Reggiani, A.; Martini, C.; Piomelli, D.; Melchiorre, C.; Rosini, M.; Cavalli, A. Combining Galantamine and Memantine in Multitargeted, New Chemical Entities Potentially Useful in Alzheimer's Disease. *J. Med. Chem.* **2012**, *55* (22), 9708–9721.

[155] Rook, Y.; Schmidtke, K.-U.; Gaube, F.; Schepmann, D.; Wünsch, B.; Heilmann, J.; Lehmann, J.; Winckler, T. Bivalent β-Carbolines as Potential Multitarget Anti-Alzheimer Agents. *J. Med. Chem.* **2010**, *53* (9), 3611–3617.

Finally, Melchiorre et *al*. developed another promising MTDL, based on the structure of Carvedilol, an FDA-approved vasodilating β-blocker and antioxidant, and a carbazole known to inhibit Aβ fibril formation. Compound **19** showed an encouraging MTDL's profile because of its ability to act on various therapeutic targets of AD. Indeed, **19** turned out to be an effective AChEI with a nanomolar range activity with a good selectivity against AChE, an Aβ aggregation inhibitor, a NMDA receptors antagonist and **19** proved to have a neuroprotective activity by counteracting ROS formation in a significant manner[156].

7.3.3. MTDLs with antioxidant properties

7.3.3.1. ROS production inhibition

Compound **20** was designed by combining Tacrine, a well-known AChEI and lipoic acid, a potent antioxidant with neuroprotective effects. **20** proved to be a potent AChEI and decreased the production of ROS by 51%. Moreover, it has been shown that **20** was able to interact with the catalytic site but also with the peripheral site of the enzyme endowing the compound with an ability to decrease AChE-induced Aβ aggregation[157].

[156] Rosini, M.; Simoni, E.; Bartolini, M.; Cavalli, A.; Ceccarini, L.; Pascu, N.; McClymont, D. W.; Tarozzi, A.; Bolognesi, M. L.; Minarini, A.; Tumiatti, V.; Andrisano, V.; Mellor, I. R.; Melchiorre, C. Inhibition of Acetylcholinesterase, β-Amyloid Aggregation, and NMDA Receptors in Alzheimer's Disease: A Promising Direction for the Multi-Target-Directed Ligands Gold Rush. *J. Med. Chem.* **2008**, *51* (15), 4381–4384.

[157] Rosini, M.; Andrisano, V.; Bartolini, M.; Bolognesi, M. L.; Hrelia, P.; Minarini, A.; Tarozzi, A.; Melchiorre, C. Rational Approach to Discover Multipotent Anti-Alzheimer Drugs. *J. Med. Chem.* **2005**, *48* (2), 360–363.

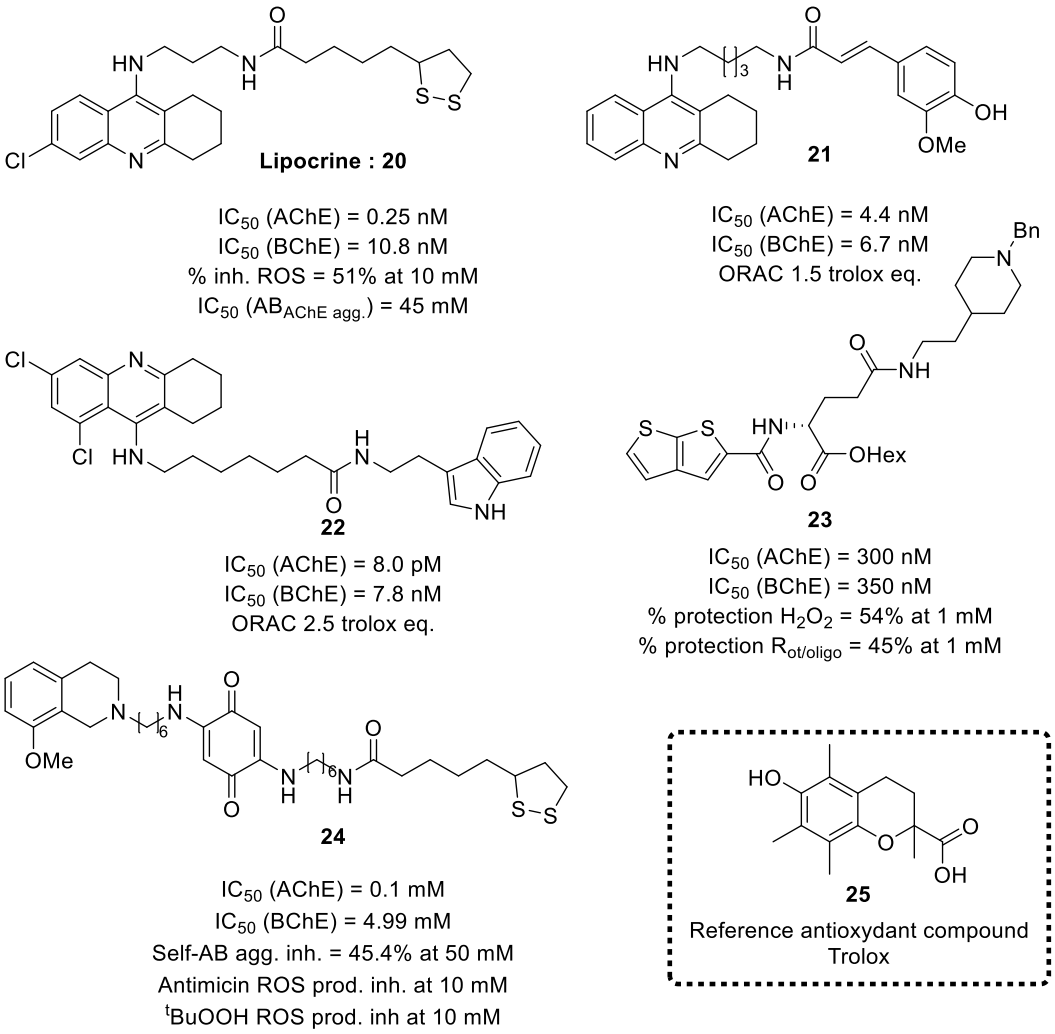

Figure 47: Examples of MTDLs inhibiting AChE with antioxidant properties

In addition, Tacrine was also used with feluric acid to develop compound **21** which turned out to reduce the toxicity in brains of rats exposed to $A\beta_{1-42}$ and to be a highly potent AChEI. Based on the oxygen radical absorbance capacity (ORAC) method, **21** showed a value of 1.5 trolox equivalent in its ability to decrease ROS species[158]. In 2006, Tacrine was also combined with melatonin to give compound **22**, a potent and selective AChEI[141]. It also turned out to have promising antioxidant properties and to cross the BBB with a permeability of 7.610^{-6} cm.s^{-1} [159]. Based on the Donepezil structure and a N-protecting group able to interact with the AChE PAS in order to protect neurons against oxidative stress, compound **23** was designed to inhibit AChE and to have a potent ability to decrease ROS species in

[158] Fang, L.; Kraus, B.; Lehmann, J.; Heilmann, J.; Zhang, Y.; Decker, M. Design and Synthesis of Tacrine-Ferulic Acid Hybrids as Multi-Potent Anti-Alzheimer Drug Candidates. *Bioorg. Med. Chem. Lett.* **2008**, *18* (9), 2905–2909.
[159] Fernández-Bachiller, M. I.; Pérez, C.; Campillo, N. E.; Páez, J. A.; González-Muñoz, G. C.; Usán, P.; García-Palomero, E.; López, M. G.; Villarroya, M.; García, A. G.; Martínez, A.; Rodríguez-Franco, M. I. Tacrine-Melatonin Hybrids as Multifunctional Agents for Alzheimer's Disease, with Cholinergic, Antioxidant, and Neuroprotective Properties. *ChemMedChem* **2009**, *4* (5), 828–841.

CNS-related disorders[160]. *In vitro* permeability experiments also demonstrated its potential to cross the BBB. Finally, based on the structure of Memoquin and Lipocrine, **24** was designed. **24** was shown to have good AChEI activity and selectivity[161]. Besides its ability to reduce ROS production, it also showed an ability to inhibit Aβ self-aggregation by 45%.

7.3.3.2. MAO inhibition

Monoamine oxidases are a group of oxidoreductases involved in the monoamines' catabolism. The two isoforms of the enzyme (MAO-A and MAO-B) are found in the CNS and involved in CNS-related functions. MAO-A is particularly important to protect the peripheral nervous system and the CNS of the ingested amines. MAO-B actives several neurotransmitters such as noradrenaline, serotonin or dopamine. Moreover, during the neurotransmitter catalytic deamination, MAOs tend to release ROS, therefore, MAOs inhibition could reduce ROS production, decreasing oxidative stress in AD patients. Based on this observation, a Rivastigmine/Rasagiline hybrid was developed by Avraham Pharmaceuticals, Ladostigil. It has been reported to be an AChE and BChE inhibitor and a MAO-A/B inhibitor, and to have neuroprotective and antidepressant effects.

[160] Arce, M. P.; Rodríguez-Franco, M. I.; González-Muñoz, G. C.; Pérez, C.; López, B.; Villarroya, M.; López, M. G.; García, A. G.; Conde, S. Neuroprotective and Cholinergic Properties of Multifunctional Glutamic Acid Derivatives for the Treatment of Alzheimer's Disease. *J. Med. Chem.* **2009**, *52* (22), 7249–7257.

[161] Bolognesi, M. L.; Cavalli, A.; Bergamini, C.; Fato, R.; Lenaz, G.; Rosini, M.; Bartolini, M.; Andrisano, V.; Melchiorre, C. Toward a Rational Design of Multitarget-Directed Antioxidants: Merging Memoquin and Lipoic Acid Molecular Frameworks. *J. Med. Chem.* **2009**, *52* (23), 7883–7886.

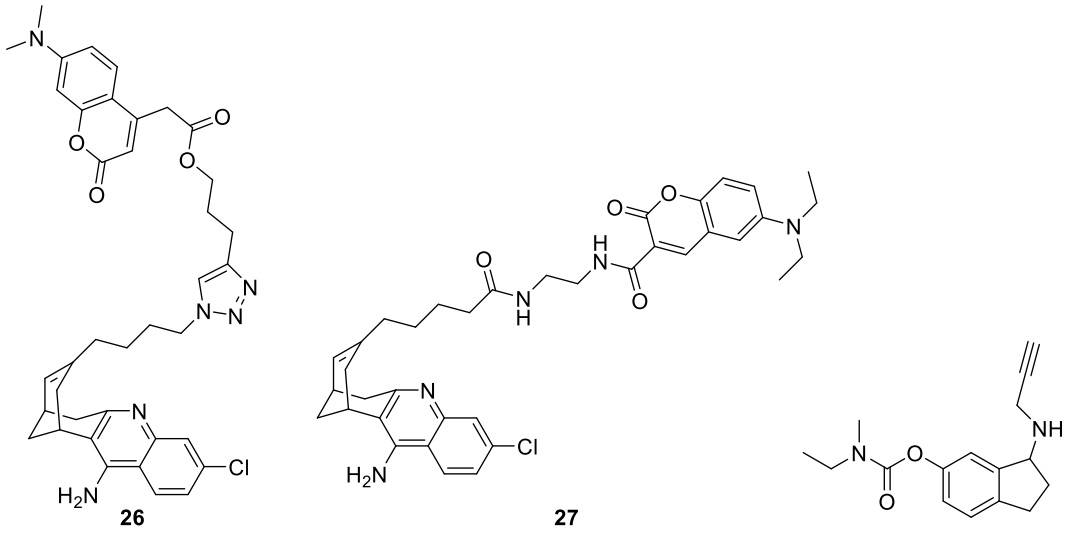

Figure 48: Example of MTDLs inhibiting AChE and MAOs

Within the professor Renard's team, Dr. Sovy Chao designed conjugated MTDLs aiming at inhibiting both AChE and MAOs during her PhD work (Figure 48). The two best candidates she obtained, **26** and **27**, were composed of a Huprine scaffold (potent AChEI) and 7-aminocoumarin derivatives (MAOs inhibitor and Aβ aggregation inhibitor). Promising activities against all the targets were obtained but optimisation investigations might be necessary to increase these results.

7.3.4. MTDLs targeting kinases

Another field of research in the professor Renard's team has been the development of conjugated MTDLs inhibiting AChE and kinases. Dr. Killian Oukoloff designed a series of Tacrine – Valmerin (GSK-3 inhibitor) derivatives as part of his PhD work (Figure 49). Among all the compound he synthesized, **28** and **29** were the most promising ligands. Especially **28** gave promising results against AChE with a good selectivity compared to BChE. It also turned out to be selective of GSK-3α/β compared to CDK5/p25[162].

[162] Oukoloff, K.; Coquelle, N.; Bartolini, M.; Naldi, M.; Le Guevel, R.; Bach, S.; Josselin, B.; Ruchaud, S.; Catto, M.; Pisani, L.; Denora, N.; Iacobazzi, R. M.; Silman, I.; Sussman, J. L.; Buron, F.; Colletier, J.-P.; Jean, L.; Routier, S.; Renard, P.-Y. Design, Biological Evaluation and X-Ray Crystallography of Nanomolar Multifunctional Ligands Targeting Simultaneously Acetylcholinesterase and Glycogen Synthase Kinase-3. *Eur. J. Med. Chem.* **2019**, *168*, 58–77.

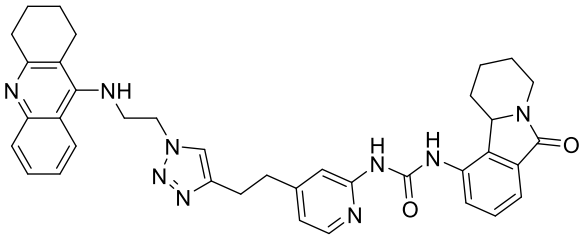

28

IC_{50} (hAChE) = 23.6 nM
IC_{50} (hBChE) = 65.7 nM
IC_{50} (Ssc_GSK-3) = 21 nM
IC_{50} (Hs_CDK5/p25) = 800 nM

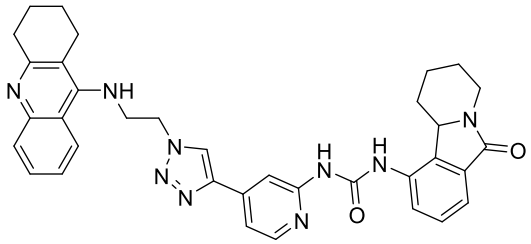

29

IC_{50} (hAChE) = 19.2 nM
IC_{50} (hBChE) = 301 nM
IC_{50} (Ssc_GSK-3) = 16 nM
IC_{50} (Hs_CDK5/p25) = 800 nM

Figure 49: Examples of MTDLs inhibiting AChE and kinases

Concerning all the previously described MTDLs, regardless of the therapeutic target, it could be noted that they were all designed with a linker, the direct consequence of it being that the molecular weight of this type of MTDLs is usually extremely high. When developing drugs against CNS-related pathologies, a high molecular weight could problematic because of issues to cross the BBB.

7.3.5. Other types of MTDLs – Combined molecules

5-hydroxytryptamine receptors ($5HT_4R$) is part of a family of serotonin receptors. It is a glycosylated transmembrane protein active in the CNS to modulate the release of neurotransmitters such as ACh. In patients with AD, *in vitro* studies using radiolabelled ligands on brain slices have shown an important decrease of $5HT_4R$ in the hippocampus and frontal cortex[163] suggesting that $5HT_4R$ were involved in cognitive learning and memory processes. Hence, targeting $5HT_4R$ in the development of anti-AD drugs appeared to be a promising approach. Indeed, $5HT_4R$ combined with AChEIs have been proven to be capable of repairing cholinergic damages through a promotion of ACh release in the prefrontal cortex and hippocampus. Moreover, activating $5HT_4R$ could promote the non-amyloidogenic pathway of the APP cleavage[164], lowering the levels of Aβ in brains of AD patients.

In that context, combined MTDLs targeting simultaneously AChE and $5HT_4R$ have been developed (Figure 50). In 2014, Donecopride **31**, a hybrid of Donepezil and RS67333 **30** which is a partial $5HT_4R$ agonist, was designed by Lecoutey et *al*.[165] and evaluated. Donecopride **31** appeared to be a viable

[163] Reynolds, G. P.; Mason, S. L.; Meldrum, A.; De Keczer, S.; Parnes, H.; Eglen, R. M.; Wong, E. H. 5-Hydroxytryptamine (5-HT)4 Receptors in Post Mortem Human Brain Tissue: Distribution, Pharmacology and Effects of Neurodegenerative Diseases. *Br. J. Pharmacol.* **1995**, *114* (5), 993–998.

[164] Robert, S. J.; Zugaza, J. L.; Fischmeister, R.; Gardier, A. M.; Lezoualc'h, F. The Human Serotonin 5-HT4 Receptor Regulates Secretion of Non-Amyloidogenic Precursor Protein. *J. Biol. Chem.* **2001**, *276* (48), 44881–44888.

[165] Lecoutey, C.; Hedou, D.; Freret, T.; Giannoni, P.; Gaven, F.; Since, M.; Bouet, V.; Ballandonne, C.; Corvaisier, S.; Fréon, A. M.; Mignani, S.; Cresteil, T.; Boulouard, M.; Claeysen, S.; Rochais, C.; Dallemagne, P. Design of

dual $5HT_4R$ agonist (K_i = 8.5 nM) and AChEI (IC_{50} = 16 nM) also promoting the non-amyloidogenic pathway of the APP cleavage.

Moreover, the same group designed compound **32** in 2018[166] by structurally modifying the already existing Donecopride **31** which demonstrated good AChE inhibition (IC_{50} = 28.8 nM) and promising affinities toward $5HT_4R$ (K_i = 37.5 nM) and σ_1 receptor (K_i = 5.1 nM) which is a transmembrane protein also involved in CNS-related pathologies. Several compounds acting on σ_1 receptor[167,168] have been designed and disclosed effective neuroprotection in transgenic mouse models of AD, probably because of the wide range of modulatory role of the receptor on neurotransmitter responses, ACh and glutamate systems and Ca^{2+} mobilisation[169].

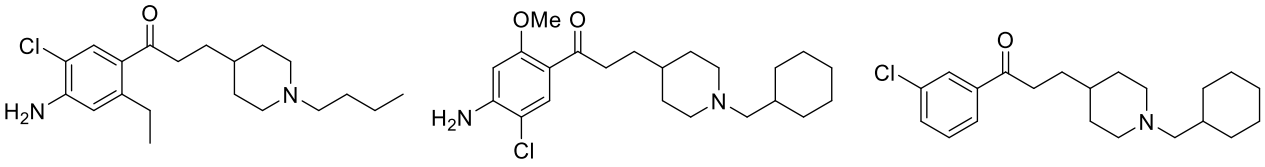

RS67333
30

IC_{50} (*h*AChE) = 403nM
K_i (*h*$5HT_4R$) = 13 nM
K_i (σ_2R) = 1.26 nM

Donecopride
31

IC_{50} (*h*AChE) = 16 nM
IC_{50} (*eq*BChE) = 3.53 nM
K_i (*h*$5HT_4R$) = 8.5 nM
K_i (σ_2R) = 1.6 nM

32

IC_{50} (*h*AChE) = 28.8 nM
K_i (*gp*$5HT_4R$) = 37.5 nM
K_i (σ_1R) = 5.1 nM

Figure 50: Examples of combined MTDLs against AD therapeutic targets

8. Conclusion

It has been brought to light in this introduction that AD is highly complex CNS-related pathology with several biological mechanisms involved. Despite numerous attempts of the pharmaceutical companies to design new drugs, only four palliative drugs managed to pass all the clinical trials to be FDA-approved (Figure 51). During the last decades, it has been assumed that the "one compound for one

Donecopride, a Dual Serotonin Subtype 4 Receptor Agonist/Acetylcholinesterase Inhibitor with Potential Interest for Alzheimer's Disease Treatment. *Proc. Natl. Acad. Sci.* **2014**, 201410315.

[166] Lalut, J.; Santoni, G.; Karila, D.; Lecoutey, C.; Davis, A.; Nachon, F.; Silman, I.; Sussman, J.; Weik, M.; Maurice, T.; Dallemagne, P.; Rochais, C. Novel Multitarget-Directed Ligands Targeting Acetylcholinesterase and Σ1 Receptors as Lead Compounds for Treatment of Alzheimer's Disease: Synthesis, Evaluation, and Structural Characterization of Their Complexes with Acetylcholinesterase. *Eur. J. Med. Chem.* **2019**, *162*, 234–248.

[167] Villard, V.; Espallergues, J.; Keller, E.; Vamvakides, A.; Maurice, T. Anti-Amnesic and Neuroprotective Potentials of the Mixed Muscarinic Receptor/Sigma 1 (Σ1) Ligand ANAVEX2-73, a Novel Aminotetrahydrofuran Derivative. *J. Psychopharmacol. Oxf. Engl.* **2011**, *25* (8), 1101–1117.

[168] Maurice, T. Protection by Sigma-1 Receptor Agonists Is Synergic with Donepezil, but Not with Memantine, in a Mouse Model of Amyloid-Induced Memory Impairments. *Behav. Brain Res.* **2016**, *296*, 270–278.

[169] Maurice, T.; Goguadze, N. Role of Σ1 Receptors in Learning and Memory and Alzheimer's Disease-Type Dementia. *Adv. Exp. Med. Biol.* **2017**, *964*, 213–233.

target" was not the optimal solution against a multifactorial pathology like AD, and research groups decided to design MTDLs tackling two or more therapeutic targets of AD.

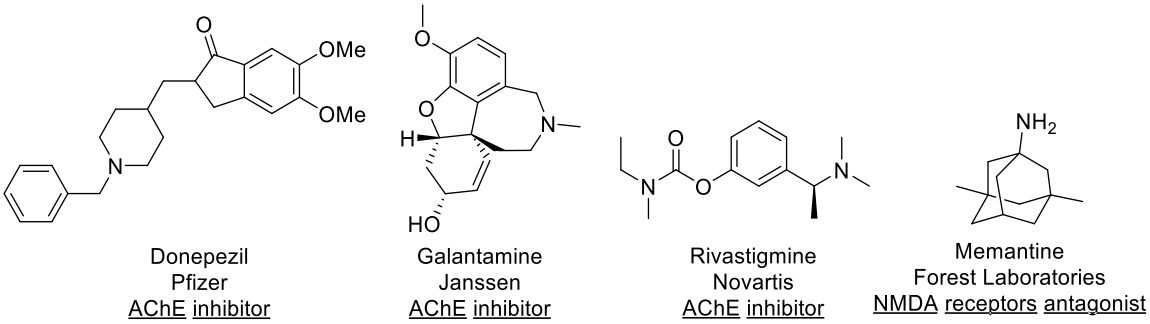

Figure 51: Approved AD drugs

For more than a decade, the professor Renard's team has been developing medicinal chemistry projects targeting AChE inhibition[170,171,172,173] and developing MTDLs in the treatment of AD. The therapeutic targets tackled by the group researchers were diverse as shown on Figure 52. Indeed, over the past few years, 41 MTDLs targeting AChE and another therapeutic target of AD were designed[174]. Moreover, the research group gained a strong expertise in the use of a key reaction in medicinal chemistry, such as the use of the Huisgen cycloaddition "click reaction" either in a classical pathway[170,172] or *in situ*[175].

[170] Ronco, C.; Foucault, R.; Gillon, E.; Bohn, P.; Nachon, F.; Jean, L.; Renard, P.-Y. New Huprine Derivatives Functionalized at Position 9 as Highly Potent Acetylcholinesterase Inhibitors. *ChemMedChem* **2011**, *6* (5), 876–888.

[171] Ronco, C.; Carletti, E.; Colletier, J.-P.; Weik, M.; Nachon, F.; Jean, L.; Renard, P.-Y. Huprine Derivatives as Sub-Nanomolar Human Acetylcholinesterase Inhibitors: From Rational Design to Validation by X-Ray Crystallography. *ChemMedChem* **2012**, *7* (3), 400–405.

[172] Ronco, C.; Sorin, G.; Nachon, F.; Foucault, R.; Jean, L.; Romieu, A.; Renard, P. Y. Synthesis and Structure-Activity Relationship of Huprine Derivatives as Human Acetylcholinesterase Inhibitors. *Bioorg. Med. Chem.* **2009**, *17* (13), 4523–4536.

[173] Galdeano, C.; Coquelle, N.; Cieslikiewicz-Bouet, M.; Bartolini, M.; Pérez, B.; Clos, M. V.; Silman, I.; Jean, L.; Colletier, J.-P.; Renard, P.-Y.; Muñoz-Torrero, D. Increasing Polarity in Tacrine and Huprine Derivatives: Potent Anticholinesterase Agents for the Treatment of Myasthenia Gravis. *Molecules* **2018**, *23* (3), 634.

[174] Aráoz, R.; Bouet, M.; Bartolini, M.; Coquelle, N.; Colletier, J.-P.; Servent, D.; Molgo, J.; Jean, L.; Renard, P.-Y. Multi-Target Directed Ligands: Electrophysiological Characterization of an Anticholinesterase Inhibitor Coupled to an Agonist of A7 Nicotinic Acetylcholine Receptor. *Biochem. Pharmacol.* **2015**, *97* (4), 621.

[175] Oueis, E.; Nachon, F.; Sabot, C.; Renard, P.-Y. First Enzymatic Hydrolysis/Thio-Michael Addition Cascade Route to Synthesis of AChE Inhibitors. *Chem. Commun.* **2014**, *50* (16), 2043–2045.

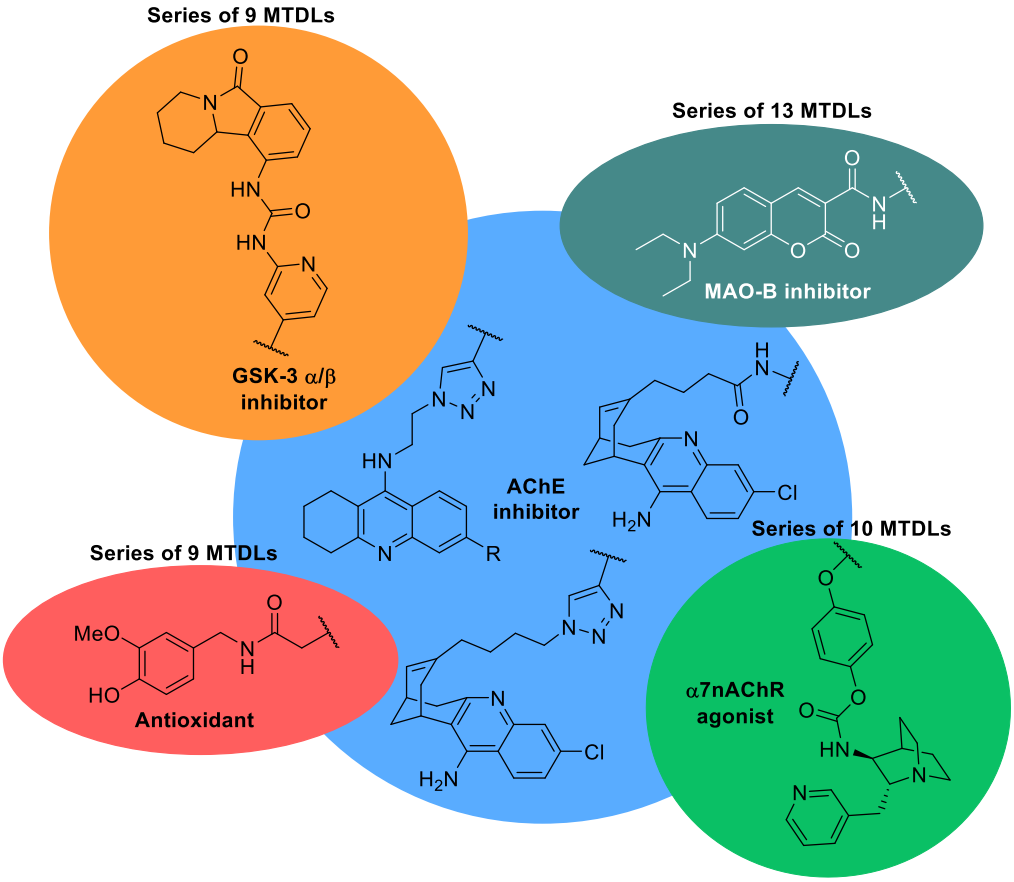

Figure 52: Team expertise in the design of MTDLs

In this context of developing innovative treatment of AD by designing MTDLs, we were interested in the synthesis of two types of ligands. First, in order to complete the series of AChEI and antioxidant MTDLs, we decided to work on conjugated MTDLs based on Huprine and Capsaicin to obtain a molecule with inhibiting activity against AChE coupled with antioxidant properties. This work will be presented in chapter I. Then, the focus of our work was to design smaller MTDLs by investigating the synthesis of combined MTDLs inhibiting AChE and activating α7 nAChR. Chapter II will be dedicated to the *in silico* assays, design, synthesis and *in vitro* evaluation of a new family of combined MTDLs based on a Rivastigmine scaffold, an AChEI, combined to a quinuclidine fragment, an α7 nicotinic receptors agonist designed by our collaborators, the Professor Routier's team. Finally, in chapter III will be about another new family of combined MTDLs targeting AChE and α7 nicotinic receptor, the variation will concern the choice of the pharmacophore inhibiting AChE. Indeed, in the last chapter, the two combined fragments will be a quinuclidine, for the α7 nicotinic receptors part, and a Donepezil fragment, for the AChE inhibition part.

The main challenge of the two last projects was the design and synthesis of combined MTDLs with a common moiety in order to obtain innovative MTDLs with a small molecular weight. Moreover, it has

been shown in this general introduction that the therapeutic targets of AD are numerous, however, working on MTDLs with α7 nAChR agonist properties is simultaneously a key challenge and an innovative way to design AD treatments. Indeed, the number of MTDLs combining an AChEI and an α7 nAChR agonist is small, nevertheless, as an example, Dr Monika Bouet designed a quinuclidine-Tacrine hybrid **33** (Figure 53) as part of her post-doctoral work. Conjugated MTDL **33** displayed a good inhibitory activity against AChE combined with a α7 nAChR partial agonist properties.

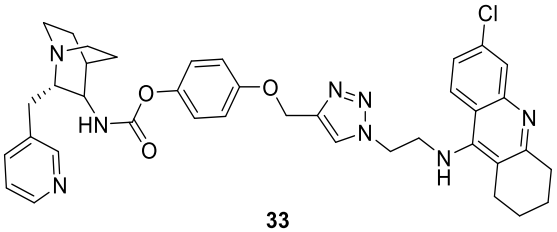

33

IC_{50} (*h*AChE) = 15 nM
Partial agonist of α7 nAChR (EC_{50} = 3 µM)
PAMPA-BBB : CNS+

Figure 53: Structure of a conjugated MTDL targeting AChE and α7 nAChR

Chapter I: Huprine-Capsaicin hybrid design and biological evaluations

1. Aim of the project

As explained in the general introduction of this thesis, since AD is a complex multifactorial disease, the best approach to find innovative and efficient treatment against this pathology seems to be the development of MTDLs targeting at least two therapeutic targets. One of the objectives of the ANR project "Multiclick" 2012-2017 involving our team, and the ones of Dr. Jacques-Philippe Colletier (IBS, Grenoble), Pr. Diego Muñoz-Torrero (University of Barcelona) and Pr. Jacques Rouen (University of Caen Normandy), consisted in synthesizing new MTDLs targeting the inhibition of AChE and targeting other landmarks of AD such as accumulation of reactive oxygen species, thus for instance bearing antioxidant properties (Figure 54). Thus, based on the expertise of Pr. Muñoz-Torrero's team[176,177] and ours in the synthesis of huprine derivatives, we planned to develop huprine-based MTDL with anti-AChE activity and antioxidant properties. This project was initiated by Dr. Monika Bouet, postdoctoral fellow in our group, who managed to design a new series of conjugated huprine-capsaicin MTDLs showing highly promising *in vitro* results[178] to be beneficial in the treatment of AD (see below).

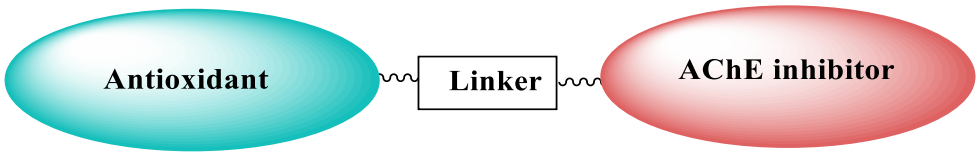

Figure 54: Conjugated MTDLs structure

The first part of my PhD consisted in synthesizing a new batch of MTDL **34**, the most promising analogue of this series (Figure 55) in order to extend the studies to *in vivo* investigations realized by Pr. Nibaldo Inestrosa's team in Chile (University Pontificia de Chile, Santiago de Chile).

[176] Viayna, E.; Sola, I.; Bartolini, M.; De Simone, A.; Tapia-Rojas, C.; Serrano, F. G.; Sabaté, R.; Juárez-Jiménez, J.; Pérez, B.; Luque, F. J.; Andrisano, V.; Clos, M. V.; Inestrosa, N. C.; Muñoz-Torrero, D. Synthesis and Multitarget Biological Profiling of a Novel Family of Rhein Derivatives as Disease-Modifying Anti-Alzheimer Agents. *J. Med. Chem.* **2014**, *57* (6), 2549–2567.

[177] Galdeano, C.; Viayna, E.; Sola, I.; Formosa, X.; Camps, P.; Badia, A.; Clos, M. V.; Relat, J.; Ratia, M.; Bartolini, M.; Mancini, F.; Andrisano, V.; Salmona, M.; Minguillón, C.; González-Muñoz, G. C.; Rodríguez-Franco, M. I.; Bidon-Chanal, A.; Luque, F. J.; Muñoz-Torrero, D. Huprine–Tacrine Heterodimers as Anti-Amyloidogenic Compounds of Potential Interest against Alzheimer's and Prion Diseases. *J. Med. Chem.* **2012**, *55* (2), 661–669.

[178] Badia, A.; Baños, J. E.; Camps, P.; Contreras, J.; Görbig, D. M.; Muñoz-Torrero, D.; Simón, M.; Vivas, N. M. Synthesis and Evaluation of Tacrine–Huperzine a Hybrids as Acetylcholinesterase Inhibitors of Potential Interest for the Treatment of Alzheimer's Disease. *Bioorg. Med. Chem.* **1998**, *6* (4), 427–440.

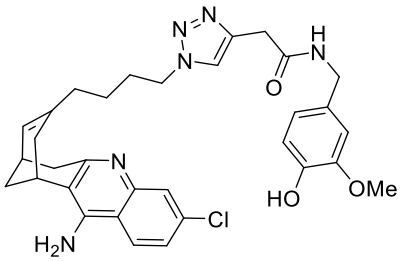

34

*Figure 55: Structure of **34***

Before presenting the synthesis of this MTDL and the *in vitro* results, the biological targets, namely AChE and BChE, their physiological roles and 3D structures will be exposed. Then, we'll present the structure of the huprine, its synthesis and the derivatives prepared by our group (e.g., selective AChE inhibitors, MTDLs, fluorescent probes, affinity chromatography for BChE purification). At the end, the interest of the use of antioxidant compounds in the treatment of AD and especially capsaicin will be discussed. Eventually, the optimized synthesis of **34** will be presented.

2. Biological targets

2.1. Acetylcholinesterase

2.1.1. Role of AChE

AChE (EC 3.1.1.7) is a serine esterase, highly selective for neurotransmitter Acetylcholine (ACh), and the key cholinesterase in the human body. Indeed, the enzyme can be found in erythrocytes, the spleen, the lungs or even muscular tissues, but AChE is more abundant in the cholinergic synapses and at neuromuscular junctions (NMJs). The primary role of AChE is to terminate the nerve impulse transmission in the cholinergic synapses in the CNS or at NMJs by hydrolysing ACh into choline and acetic acid (Scheme 3)[179].

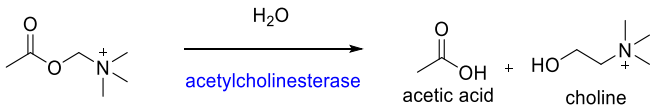

Scheme 3: AChE catalysed ACh hydrolysis

[179] Silman, I.; Sussman, J. L. Acetylcholinesterase: "classical" and "Non-Classical" Functions and Pharmacology. *Curr. Opin. Pharmacol.* **2005**, *5* (3), 293–302.

Indeed, during the nerve impulse, ACh is released from the neuronal cholinergic synapses and diffused in the synaptic cleft, thus neurotransmitters' concentration in this area becomes particularly high (around 500 mM)[180] and ACh binds to mAChRs and nAChRs receptors known to be involved in the nerve impulse. In the synaptic cleft, ACh hydrolysis into acetic acid and choline is then rapidly achieved by AChE with a particularly high turnover number of approximatively 25 000 molecules of neurotransmitter every second,[181] in order to end nerve impulse propagation AChE can thus be considered as the second fastest known enzyme, second to Carbonic Anhydrase[182].

2.1.2. Structural characteristic of AChE

Sussman et al. were the first to elucidate AChE structure from *Torpedo Californica* (*Tc*AChE) through AChE crystals X-ray diffraction images analysis in 1991 with a 2.8 Å resolution[183]. Later, AChE structures from other species were resolved, like the mouse AChE (*m*AChE)[184], *drosophila d*AChE[185] or *Electrophorus Electricus* AChE (*ee*AChE)[186]. In 2000, human AChE *(h*AChE) structure was obtained thanks to co-crystallisation of AChE with fasciculine-2 , a toxin acting as an inhibitor through interaction with the peripheral site, limiting the high flexibility of this part of the enzyme which prevented crystals formation[187]. Moreover, AChE peripheral site role in Aβ fibrils formation has been shed light[188], understanding this role was limited by the presence of this PAS binding toxin in the crystal structures. More recently, crystals structures of the enzyme without the PAS binding toxin were obtained by

[180] Van der Kloot, W.; Molgó, J.; Cameron, R.; Colasante, C. Vesicle Size and Transmitter Release at the Frog Neuromuscular Junction When Quantal Acetylcholine Content Is Increased or Decreased. *J. Physiol.* **2002**, *541* (Pt 2), 385–393.

[181] Colović, M. B.; Krstić, D. Z.; Lazarević-Pašti, T. D.; Bondžić, A. M.; Vasić, V. M. Acetylcholinesterase Inhibitors: Pharmacology and Toxicology. *Curr. Neuropharmacol.* **2013**, *11* (3), 315–335.

[182] Berg, J. M.; Tymoczko, J. L.; Stryer, L. Enzymes Are Powerful and Highly Specific Catalysts. *Biochem. 5th Ed.* **2002**.

[183] Sussman, J. L.; Harel, M.; Frolow, F.; Oefner, C.; Goldman, A.; Toker, L.; Silman, I. Atomic Structure of Acetylcholinesterase from Torpedo Californica: A Prototypic Acetylcholine-Binding Protein. *Science* **1991**, *253* (5022), 872–879.

[184] Marchot, P.; Ravelli, R. B.; Raves, M. L.; Bourne, Y.; Vellom, D. C.; Kanter, J.; Camp, S.; Sussman, J. L.; Taylor, P. Soluble Monomeric Acetylcholinesterase from Mouse: Expression, Purification, and Crystallization in Complex with Fasciculin. *Protein Sci. Publ. Protein Soc.* **1996**, *5* (4), 672–679.

[185] Harel, M.; Kryger, G.; Rosenberry, T. L.; Mallender, W. D.; Lewis, T.; Fletcher, R. J.; Guss, J. M.; Silman, I.; Sussman, J. L. Three-Dimensional Structures of Drosophila Melanogaster Acetylcholinesterase and of Its Complexes with Two Potent Inhibitors. *Protein Sci. Publ. Protein Soc.* **2000**, *9* (6), 1063–1072.

[186] Bourne, Y.; Grassi, J.; Bougis, P. E.; Marchot, P. Conformational Flexibility of the Acetylcholinesterase Tetramer Suggested by X-Ray Crystallography. *J. Biol. Chem.* **1999**, *274* (43), 30370–30376.

[187] Kryger, G.; Harel, M.; Giles, K.; Toker, L.; Velan, B.; Lazar, A.; Kronman, C.; Barak, D.; Ariel, N.; Shafferman, A.; Silman, I.; Sussman, J. L. Structures of Recombinant Native and E202Q Mutant Human Acetylcholinesterase Complexed with the Snake-Venom Toxin Fasciculin-II. *Acta Crystallogr. D Biol. Crystallogr.* **2000**, *56* (Pt 11), 1385–1394.

[188] Inestrosa, N. C.; Dinamarca, M. C.; Alvarez, A. Amyloid-Cholinesterase Interactions: Implications for Alzheimer's Disease. *FEBS J.* **2008**, *275* (4), 625–632.

Dr.M.C. Franklin[189] and Dr. Florian Nachon's (in collaboration with Pr. Renard) teams[190], thus allowing a more accurate determination of the structure and flexibility of this peripheral site. These various studies led to a precise visualisation of the enzyme conformation and mode of action (Figure 56).

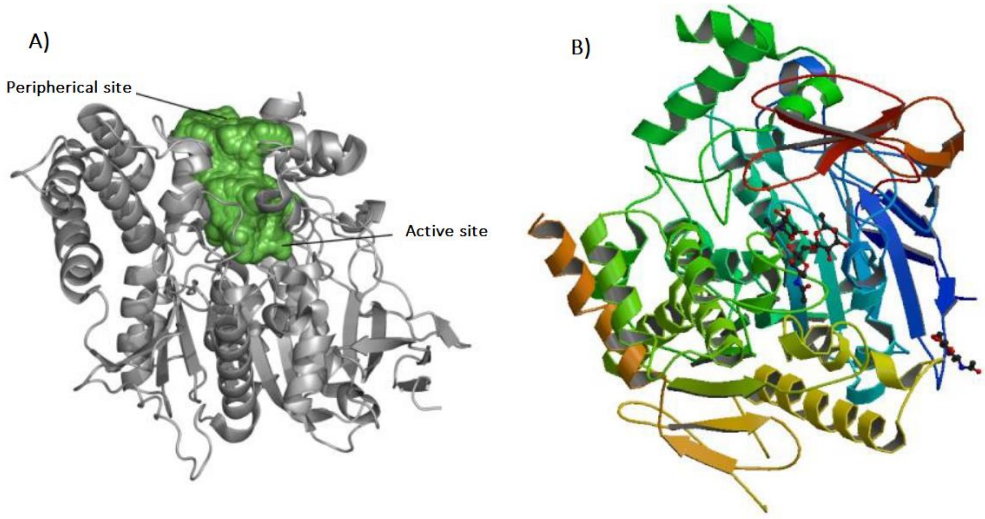

Figure 56: TcAChE (A) and hAChE (B) structures[187]

It is known now that *h*AChE is an ellipsoidal macromolecule of 45 x 60 x 65 Å. The enzyme monomer is an α/β protein containing 537 amino acids and made of 12-stranded mixed β sheets surrounded by 14 α helices[191]. AChE is a serine hydrolase part of the type B carboxylesterase family, even though AChE structure is strikingly resembling to several hydrolases, Sussman et al. discovered that, surprisingly, contrary to other serine hydrolases, the active site contains a glutamate residue and not an aspartate residue involved in the catalytic triade[183].

In 1993, Taylor et al. performed AChE structural atomic studies and brought to light that its structure presents two distinct regions directly involved in the enzymatic activity, linked by a hydrophobic gorge : an active site where the reaction takes place, deeply buried within the enzyme, and linked to the outer space by a peripheral site[192] (Figure 57).

---

[189] Cheung, J.; Rudolph, M. J.; Burshteyn, F.; Cassidy, M. S.; Gary, E. N.; Love, J.; Franklin, M. C.; Height, J. J. Structures of Human Acetylcholinesterase in Complex with Pharmacologically Important Ligands. *J. Med. Chem.* **2012**, *55* (22), 10282–10286.

[190] Ronco, C.; Carletti, E.; Colletier, J.-P.; Weik, M.; Nachon, F.; Jean, L.; Renard, P.-Y. Huprine Derivatives as Sub-Nanomolar Human Acetylcholinesterase Inhibitors: From Rational Design to Validation by X-Ray Crystallography. *ChemMedChem* **2012**, *7* (3), 400–405.

[191] Ollis, D. L.; Cheah, E.; Cygler, M.; Dijkstra, B.; Frolow, F.; Franken, S. M.; Harel, M.; Remington, S. J.; Silman, I.; Schrag, J. The Alpha/Beta Hydrolase Fold. *Protein Eng.* **1992**, *5* (3), 197–211.

[192] Radic, Z.; Pickering, N. A.; Vellom, D. C.; Camp, S.; Taylor, P. Three Distinct Domains in the Cholinesterase Molecule Confer Selectivity for Acetyl- and Butyrylcholinesterase Inhibitors. *Biochemistry* **1993**, *32* (45), 12074–12084.

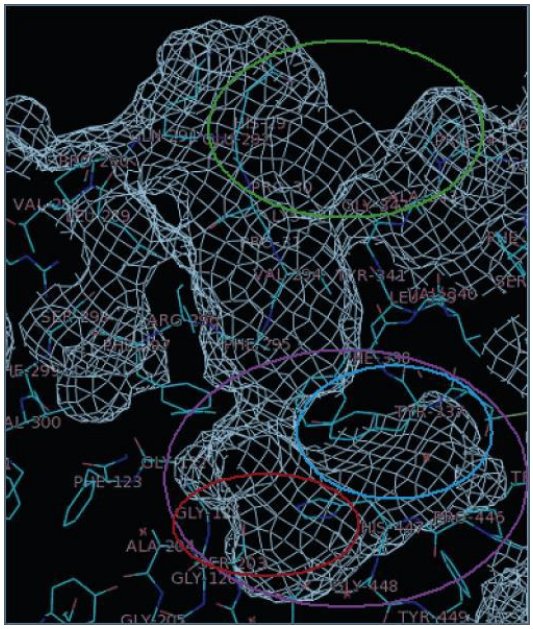

Figure 57: hAChE three-dimensional representation: in green, the peripherical site; in purple the active site; in red, the acylation site, in blue the π-cation site (figure extracted from Dr. Killian Oukoloff's PhD thesis)

2.1.2.1. Active site

The active site is made up of an acylation site where ACh is hydrolysed and a cation-π site in which the ACh quaternary ammonium is bound.

The acylation site can be divided in three sub-groups:

- a catalytic triad,
- an oxyanion hole,
- an acyl pocket.

Catalytic triad (Figure 58)

The triad plays a key role in the ACh hydrolysis and is formed by three residues: Glu334, Ser203 and His447. Ser203 and His447 are directly involved in the hydrolysis and used respectively as nucleophilic attacking group and general acid-base catalytic elements[193]. Indeed, Ser203's nucleophilic character is increased thanks to His447 and Glu334 assistance. After the acyl transfer from ACh to Ser203, stabilisation of the transition state is induced by Glu334 *via* electrostatic interactions[193] and *via* N-H amide residues contained in the oxyanion hole. Then, an acyl-enzyme intermediate is formed to

[193] Zhang, Y.; Kua, J.; McCammon, J. A. Role of the Catalytic Triad and Oxyanion Hole in Acetylcholinesterase Catalysis: An Ab Initio QM/MM Study. *J. Am. Chem. Soc.* **2002**, *124* (35), 10572–10577.

release choline and the enzyme is regenerated through a reaction between the intermediate and a molecule of water (which nucleophilic character is once again activated by His447 and Glu334)[194].

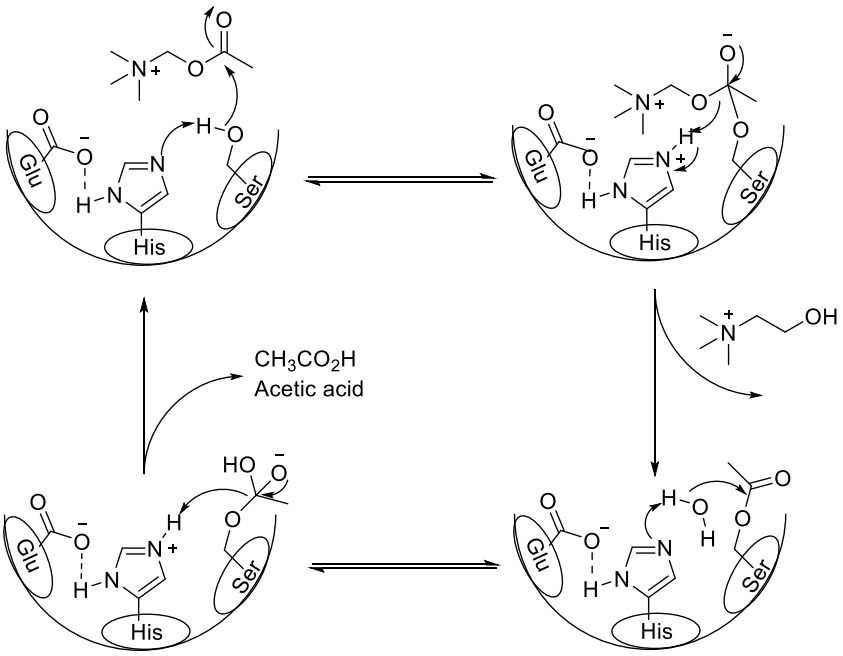

Figure 58: Catalytic cycle of ACh hydrolysis (extracted from Dr. Julien Renou's thesis)

Oxyanion hole

This part of the active site is made up of residues Gly121, Gly122 and Ala204 which allows the ACh's ester activation through H-bond formation between the N-H of their amide and the oxyanion. These residues are also used to stabilise the reaction intermediate[195].

Acyl pocket

The acyl pocket made up of Trp236, Phe295 and Phe297 interacts with the ester part of ACh and stabilise it *via* Van der Waals interactions with the methyl's acyl group [196].

[194] Froede, H. C.; Wilson, I. B. Direct Determination of Acetyl-Enzyme Intermediate in the Acetylcholinesterase-Catalyzed Hydrolysis of Acetylcholine and Acetylthiocholine. *J. Biol. Chem.* **1984**, *259* (17), 11010–11013.

[195] Bourne, Y.; Radić, Z.; Sulzenbacher, G.; Kim, E.; Taylor, P.; Marchot, P. Substrate and Product Trafficking through the Active Center Gorge of Acetylcholinesterase Analyzed by Crystallography and Equilibrium Binding. *J. Biol. Chem.* **2006**, *281* (39), 29256–29267.

[196] Saxena, A.; Raveh, L.; Ashani, Y.; Doctor, B. P. Structure of Glycan Moieties Responsible for the Extended Circulatory Life Time of Fetal Bovine Serum Acetylcholinesterase and Equine Serum Butyrylcholinesterase. *Biochemistry* **1997**, *36* (24), 7481–7489.

The cation-π site, made up of three aromatic residues (Trp86, Tyr337 and Phe338) which interact with the ACh ammonium group through cation-π bounds. The role of these interactions is to direct the ACh's acyl part to the catalytic triad and stabilize the substrate[197].

2.1.2.2. Hydrophobic gorge

The hydrophobic gorge has a depth of 20 Å and a width of 5 Å and is comprised of 14 aromatic residues. It links the acylation site and the peripheral site and helps guiding and orientating the enzyme's substrates. Moreover, the aromatic residues are able to bind to ACh quaternary ammonium through cation-π interactions [198].

2.1.2.3. Peripheral "anionic" site (PAS)

The peripheral anionic site is found in the hydrophobic moiety's entry of AChE gorge, and, despite its name, is made up of uncharged residues, a majority of aromatic residues (for example: Trp286, Tyr72, Tyr124, Tyr341) but also of non-aromatic residues like Asp74. The role of this PAS as ACh binding unit before it enters the gorge, through affinity with the ammonium has been identified long time ago, leading to a false interpretation that this positive charge binding moiety should be constituted of anionic residues giving the "anionic" part of the name, before resolutions of crystal structures proved that this affinity was due to cation –π interactions[199]. Studies have brought to light the importance of the PAS aromatic residues which are able to perform a first recognition of the ligands approaching the enzyme by interacting with them in π -π stacking or cation-π types interactions[200]. The PAS has also a major role in ACh hydrolysis, indeed, when ACh is close to the enzyme, its trimethylammonium group binds to the peripheral Trp286 which leads to a position and conformational change of the Trp86 in the active site. Thereafter, if the ligand is found in low concentrations, the hydrolysis is fast whereas a high ACh concentration a substrate inhibition of the enzyme occurs slowing down the hydrolysis process[201].

---

[197] Ma, J. C.; Dougherty, D. A. The Cation−π Interaction. *Chem. Rev.* **1997**, *97* (5), 1303–1324.

[198] Axelsen, P. H.; Harel, M.; Silman, I.; Sussman, J. L. Structure and Dynamics of the Active Site Gorge of Acetylcholinesterase: Synergistic Use of Molecular Dynamics Simulation and X-Ray Crystallography. *Protein Sci. Publ. Protein Soc.* **1994**, *3* (2), 188–197.

[199] Harel, M.; Schalk, I.; Ehret-Sabatier, L.; Bouet, F.; Goeldner, M.; Hirth, C.; Axelsen, P. H.; Silman, I.; Sussman, J. L. Quaternary Ligand Binding to Aromatic Residues in the Active-Site Gorge of Acetylcholinesterase. *Proc. Natl. Acad. Sci.* **1993**, *90* (19), 9031–9035.

[200] Barak, D.; Kronman, C.; Ordentlich, A.; Ariel, N.; Bromberg, A.; Marcus, D.; Lazar, A.; Velan, B.; Shafferman, A. Acetylcholinesterase Peripheral Anionic Site Degeneracy Conferred by Amino Acid Arrays Sharing a Common Core. *J. Biol. Chem.* **1994**, *269* (9), 6296–6305.

[201] Van Belle, D.; De Maria, L.; Iurcu, G.; Wodak, S. J. Pathways of Ligand Clearance in Acetylcholinesterase by Multiple Copy Sampling11Edited by I. B. Honig. *J. Mol. Biol.* **2000**, *298* (4), 705–726.

2.2. Butyrylcholinesterase

2.2.1. Role of the BChE

BChE (EC 3.1.1.8)) is a non-specific cholinesterase enzyme, part of the serine hydrolase family, and able to hydrolyse various choline-based esters. It is synthesised in several part of the human body (liver, plasma, pancreas) but its physiologic role remains unclear[202]. Nevertheless, due to its poor selectivity, BChE is capable to take over the role of AChE to hydrolyse ACh. Indeed, transgenic mice, knocked-out for the AChE coding gene can survive without AChE, meaning that BChE is able to replace AChE and protect the mice of an ACh excess[203]. In the case of CNS-related pathologies such as AD, while the AChE levels are increasing, the BChE levels remain unchanged and in advanced stages of the disease, BChE can substitute AChE[204]. Increased BChE levels in blood serum has thus been identified as a significant biomarker of AD development but is also involved in some cases of diabetes[205,206]. Very recently, some selective BChE inhibitors have shown promising results in AD treatment[207,208].

2.2.2. Structural characteristics

BChE structure (Figure 59) is close to AChE structure with 65% of sequence homology and the same disulphide bridges[209]. It has been observed that BChE active site is also made up of an acylation site and a cation -π site, however, its acylation site is larger (500 Å for BChE against 300 Å for AChE)[210].

---

[202] Chatonnet, A.; Lockridge, O. Comparison of Butyrylcholinesterase and Acetylcholinesterase. *Biochem. J.* **1989**, *260* (3), 625–634.

[203] Li, B.; Stribley, J. A.; Ticu, A.; Xie, W.; Schopfer, L. M.; Hammond, P.; Brimijoin, S.; Hinrichs, S. H.; Lockridge, O. Abundant Tissue Butyrylcholinesterase and Its Possible Function in the Acetylcholinesterase Knockout Mouse. *J. Neurochem.* **2000**, *75* (3), 1320–1331.

[204] Manoharan, I.; Boopathy, R.; Darvesh, S.; Lockridge, O. A Medical Health Report on Individuals with Silent Butyrylcholinesterase in the Vysya Community of India. *Clin. Chim. Acta Int. J. Clin. Chem.* **2007**, *378* (1–2), 128–135.

[205] Greig, N. H.; Lahiri, D. K.; Sambamurti, K. Butyrylcholinesterase: An Important New Target in Alzheimer's Disease Therapy. *Int. Psychogeriatr.* **2002**, *14 Suppl 1*, 77–91.

[206] Rao, A. A.; Sridhar, G. R.; Das, U. N. Elevated Butyrylcholinesterase and Acetylcholinesterase May Predict the Development of Type 2 Diabetes Mellitus and Alzheimer's Disease. *Med. Hypotheses* **2007**, *69* (6), 1272–1276.

[207] Meden, A.; Knez, D.; Jukič, M.; Brazzolotto, X.; Gršič, M.; Pišlar, A.; Zahirović, A.; Kos, J.; Nachon, F.; Svete, J.; Gobec, S.; Grošelj, U. Tryptophan-Derived Butyrylcholinesterase Inhibitors as Promising Leads against Alzheimer's Disease. *Chem. Commun.* **2019**, *55* (26), 3765–3768.

[208] Wajid, S.; Khatoon, A.; Khan, M. A.; Zafar, H.; Kanwal, S.; Atta-ur-Rahman; Choudhary, M. I.; Basha, F. Z. Microwave-Assisted Organic Synthesis, Structure–Activity Relationship, Kinetics and Molecular Docking Studies of Non-Cytotoxic Benzamide Derivatives as Selective Butyrylcholinesterase Inhibitors. *Bioorg. Med. Chem.* **2019**, *27* (18), 4030–4040.

[209] Allderdice, P. W.; Gardner, H. A.; Galutira, D.; Lockridge, O.; LaDu, B. N.; McAlpine, P. J. The Cloned Butyrylcholinesterase (BCHE) Gene Maps to a Single Chromosome Site, 3q26. *Genomics* **1991**, *11* (2), 452–454.

[210] Masson, P.; Lockridge, O. Butyrylcholinesterase for Protection from Organophosphorus Poisons: Catalytic Complexities and Hysteretic Behavior. *Arch. Biochem. Biophys.* **2010**, *494* (2), 107–120.

Moreover, BChE owns a catalytic triad with the same residues than the AChE triad, a serine (Ser198), a histidine (His438) and a glutamate (Glu325). The main difference between the two cholinesterases is found in the acyl pocket, indeed, where AChE owns two aromatic residues leading to the enzyme's specificity towards acetates BChE owns a leucine (Leu286) and a valine (Val288), two aliphatic residues giving BChE the opportunity to catalyse the hydrolysis of several choline-based esters[211]. Moreover, the BChE acyl pocket is larger than the AChE acyl pocket, due to the replacement of 6 aromatic residues (in the case of AChE) by aliphatic residues (in the case of BChE). This difference is known to be responsible of the poor selectivity of the enzyme as far as the acyl part is concerned, since it confers to larger molecules the possibility to enter and interact with the BChE active site[212].

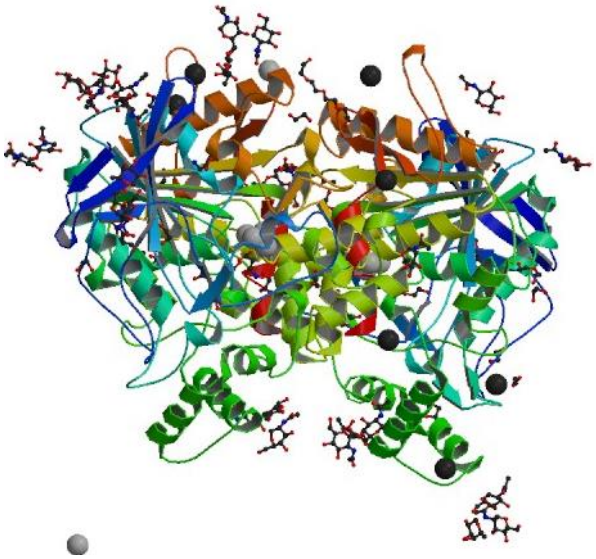

Figure 59: Structure of hBChE[213]

[211] Radic, Z.; Pickering, N. A.; Vellom, D. C.; Camp, S.; Taylor, P. Three Distinct Domains in the Cholinesterase Molecule Confer Selectivity for Acetyl- and Butyrylcholinesterase Inhibitors. *Biochemistry* **1993**, *32* (45), 12074–12084.

[212] Saxena, A.; Redman, A. M.; Jiang, X.; Lockridge, O.; Doctor, B. P. Differences in Active Site Gorge Dimensions of Cholinesterases Revealed by Binding of Inhibitors to Human Butyrylcholinesterase. *Biochemistry* **1997**, *36* (48), 14642–14651.

[213] Brazzolotto, X.; Wandhammer, M.; Ronco, C.; Trovaslet, M.; Jean, L.; Lockridge, O.; Renard, P. Y.; Nachon, F. Human Butyrylcholinesterase Produced in Insect Cells: Huprine-Based Affinity Purification and Crystal Structure. *FEBS J* **2012**, *279*, 2905–2916.

Concerning the peripheral site, which is larger than the AChE peripheral site, only two residues (Asp70 and Tyr332) interact with the quaternary ammonium of choline-based esters. A H-bond between these two amino acids is also capable to control the functional architecture of BChE[214,215].

3. Chosen structures

3.1. Huprine – a potent AChE inhibitor

3.1.1. Design of huprine scaffold

Pr. Camps and Pr. Muñoz-Torrero's team developed in 2000 an innovative and promising scaffold in order to obtain a more potent AChEI than those already existing[178]. Huprine was born from the fusion of the scaffolds of two well-known AChEIs, namely tacrine and (-)-huperzine A (Figure 60). The huprine structure combines the carbobicyclic moiety from the (-)-huperzine A and the 4-aminoquinoline moiety of tacrine.

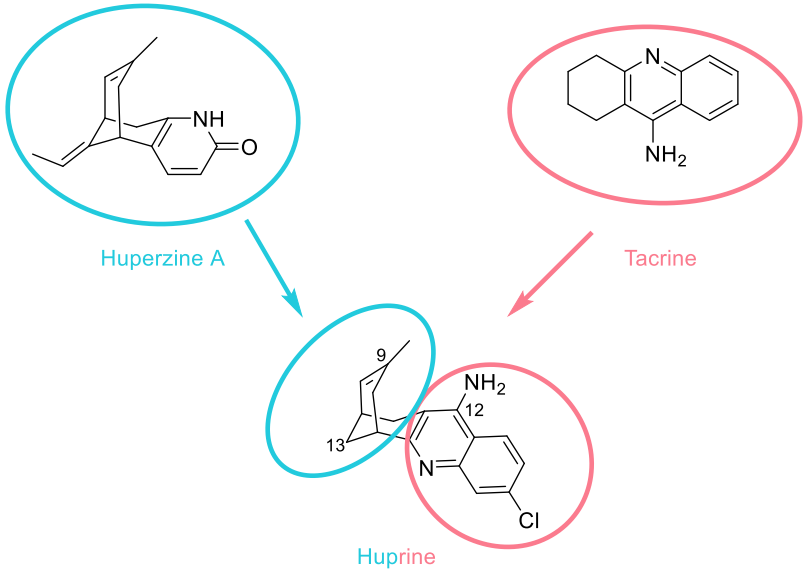

Figure 60: Design of huprine scaffold

The inhibitory potency (in the nanomolar range) of huprine toward AChE could be explained through several strong interactions within the active site of the human enzyme. As showed in the X-ray crystal

[214] Masson, P.; Xie, W.; Froment, M. T.; Levitsky, V.; Fortier, P. L.; Albaret, C.; Lockridge, O. Interaction between the Peripheral Site Residues of Human Butyrylcholinesterase, D70 and Y332, in Binding and Hydrolysis of Substrates. *Biochim. Biophys. Acta* **1999**, *1433* (1–2), 281–293.
[215] Masson, P.; Xie, W.; Froment, M. T.; Lockridge, O. Effects of Mutations of Active Site Residues and Amino Acids Interacting with the Omega Loop on Substrate Activation of Butyrylcholinesterase. *Biochim. Biophys. Acta* **2001**, *1544* (1–2), 166–176.

structure of *h*AChE in a complex with huprine W[216], the central aromatic ring of the quinolinium is facing Trp286 while the lateral aromatic ring is facing Tyr337. Moreover, chlorine atom interacts strongly with Trp439 and an additional stabilization of the quinolinium structure is provided by a hydrogen bond between the aromatic nitrogen and the main chain carbonyl of His447 (Figure 61).

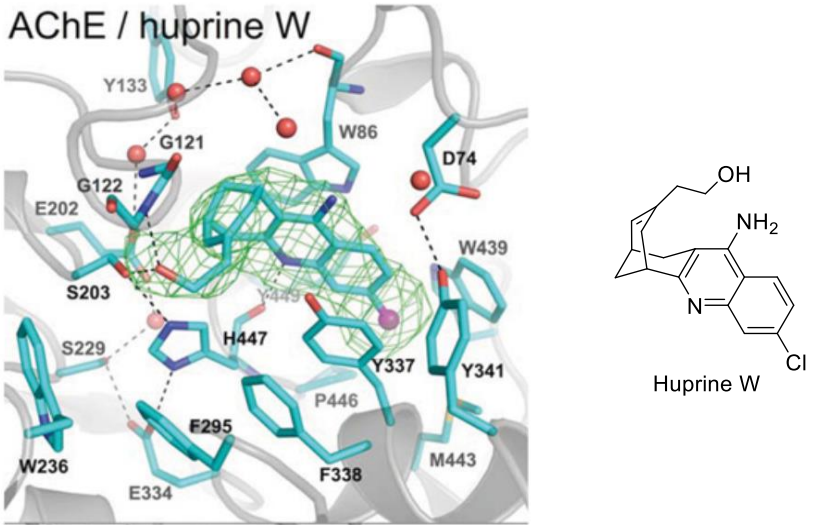

Figure 61: 3D structure of huprine W with hAChE[216]

Several *structure–activity relationship* (SAR) studies have been realized by Pr. Muñoz-Torrero's team and ours in order to optimize the structure of huprine's scaffold[217,218,219,220]. Structural modification studies have been performed in position 9, 12 and 13 and in the aromatic moiety of this structure.

The first structural modifications were performed on position 13 by adding alkoxy groups, alkyl groups, a ketone or even by changing the (E) isomer of the ethylene group by the (Z) isomer. Nevertheless, as

[216] Nachon, F.; Carletti, E.; Ronco, C.; Trovaslet, M.; Nicolet, Y.; Jean, L.; Renard, P.-Y. Crystal Structures of Human Cholinesterases in Complex with Huprine W and Tacrine: Elements of Specificity for Anti-Alzheimer's Drugs Targeting Acetyl- and Butyryl-Cholinesterase. *Biochem. J.* **2013**, *453* (3), 393–399.
[217] Ronco, C.; Foucault, R.; Gillon, E.; Bohn, P.; Nachon, F.; Jean, L.; Renard, P.-Y. New Huprine Derivatives Functionalized at Position 9 as Highly Potent Acetylcholinesterase Inhibitors. *ChemMedChem* **2011**, *6* (5), 876–888.
[218] Ronco, C.; Carletti, E.; Colletier, J. P.; Weik, M.; Nachon, F.; Jean, L.; Renard, P. Y. Huprine Derivatives as Sub-Nanomolar Human Acetylcholinesterase Inhibitors: From Rational Design to Validation by X-Ray Crystallography. *ChemMedChem* **2012**, *7* (3), 400–405.
[219] Camps, P.; El Achab, R.; Görbig, D. M.; Morral, J.; Muñoz-Torrero, D.; Badia, A.; Baños, J. E.; Vivas, N. M.; Barril, X.; Orozco, M.; Luque, F. J. Synthesis, in Vitro Pharmacology, and Molecular Modeling of Very Potent Tacrine−Huperzine A Hybrids as Acetylcholinesterase Inhibitors of Potential Interest for the Treatment of Alzheimer's Disease. *J. Med. Chem.* **1999**, *42* (17), 3227–3242.
[220] Camps, P.; El Achab, R.; Morral, J.; Muñoz-Torrero, D.; Badia, A.; Baños, J. E.; Vivas, N. M.; Barril, X.; Orozco, M.; Luque, F. J. New Tacrine−Huperzine A Hybrids (Huprines): Highly Potent Tight-Binding Acetylcholinesterase Inhibitors of Interest for the Treatment of Alzheimer's Disease. *J. Med. Chem.* **2000**, *43* (24), 4657–4666.

opposed to the huperzine A, the presence of a substituent in the position 13 decreased dramatically the inhibition potency of huprine analogues[178].

The second SAR study consisted in modifying the substituent in the position 9, Camps et *al*. replaced the methyl group of the huperzine A by different substituents such as alkyls groups, allyl, phenyl or a hydrogen atom. The various structural modifications brought to light that only the presence of a methyl or ethyl group was accepted in order to maintain good inhibitory activities against AChE[218,221].

Finally, an addition of a methyl group or a chlorine atom[219] on the benzene ring moiety displayed promising results. Through the various structural studies, it was possible to better understand the role of each hybrid's constituents and design the first two most potent monomeric AChE inhibitors, huprine X bearing an ethyl group in position 9, and huprine Y bearing a methyl group in the same position (Figure 62)[222,223].

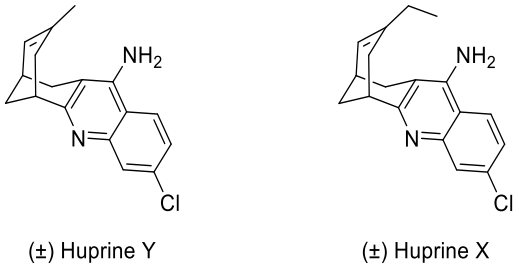

(±) Huprine Y (±) Huprine X

Figure 62: Huprine X and huprine Y structure

3.1.2. Biological properties

The biological properties of huprine X and Y have been evaluated and are reported in Figure 63. It was shown that huprine X and Y display a potent anti-AChE activity in the a subnanomolar scale (IC_{50} (*h*AChE) = 0.75 nM and 0.78 nM respectively). (-)-huperzine A is known to be more potent against AChE while tacrine is more effective against BChE. Concerning huprine Y and X, they display a high inhibitory activity and selectivity toward AChE and the levogyre enantiomer is always the most potent by a factor

[221] Ronco, C.; Sorin, G.; Nachon, F.; Foucault, R.; Jean, L.; Romieu, A.; Renard, P. Y. Synthesis and Structure-Activity Relationship of Huprine Derivatives as Human Acetylcholinesterase Inhibitors. *Bioorg. Med. Chem.* **2009**, *17* (13), 4523–4536.

[222] Ros, E.; Aleu, J.; Gómez de Aranda, I.; Muñoz-Torrero, D.; Camps, P.; Badia, A.; Marsal, J.; Solsona, C. The Pharmacology of Novel Acetylcholinesterase Inhibitors, (+/-)-Huprines Y and X, on the Torpedo Electric Organ. *Eur. J. Pharmacol.* **2001**, *421* (2), 77–84.

[223] Camps, P.; Cusack, B.; Mallender, W. D.; Achab, R. E.; Morral, J.; Muñoz-Torrero, D.; Rosenberry, T. L. Huprine X Is a Novel High-Affinity Inhibitor of Acetylcholinesterase That Is of Interest for Treatment of Alzheimer's Disease. *Mol. Pharmacol.* **2000**, *57* (2), 409–417.

2. Moreover, other investigations have proven that huprines have a slow on-rate constant (k_{on}), indeed, an incubation of 30 min between the enzyme and the inhibitor is mandatory during the inhibition assays[223]. Moreover, *ex vivo* studies on mice's brains have reported the huprine compounds have shown promising pharmacological profiles and a CNS activity[217].

Interestingly, this combination of two AChEIs has also displayed agonist activities toward mAChRs and nAChRs[224,225], antagonist activities toward NMDA receptors, giving a neuroprotective character[226] to these molecules. They have also proven their capacity to activate protein kinase C and mitogen activated protein kinase, proteins involved in the promotion of the non-amyloidogenic pathway for the APP cleavage[227].

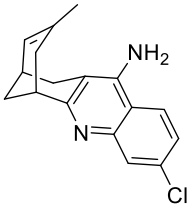

Huprine Y

(±) IC_{50} (*rh*AChE) = 0.78 +/- 0.02 nM
(±) IC_{50} (*rh*BChE) = 236 +/- 44 nM

(-) IC_{50} (*rh*AChE) = 0.32 +/- 0.10 nM
(-) IC_{50} (*rh*BChE) = 153 +/- 31 nM

(+) IC_{50} (*rh*AChE) = 123 +/- 18 nM
(+) IC_{50} (*rh*BChE) = 153 +/- 31 nM

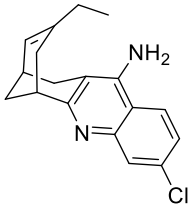

Huprine X

(±) IC_{50} (*rh*AChE) = 0.75 +/- 0.06 nM
(±) IC_{50} (*rh*BChE) = 15.8 +/- 2.4 nM

(-) IC_{50} (*rh*AChE) = 0.32 +/- 0.09 nM
(-) IC_{50} (*rh*BChE) = 159 +/- 10 nM

(+) IC_{50} (*rh*AChE) = 23.1 +/- 2.3 nM
(+) IC_{50} (*rh*BChE) = 58.3 +/- 5.9 nM

Figure 63: Inhibitory activities of huprine X and huprine Y toward cholinesterases

[224] Muñoz-Torrero, D.; Pera, M.; Relat, J.; Ratia, M.; Galdeano, C.; Viayna, E.; Sola, I.; Formosa, X.; Camps, P.; Badia, A.; Clos, M. V. Expanding the Multipotent Profile of Huprine-Tacrine Heterodimers as Disease-Modifying Anti-Alzheimer Agents. *Neurodegener. Dis.* **2012**, *10* (1–4), 96–99.

[225] Roman, S.; Badia, A.; Camps, P.; Clos, M. V. Potentiation Effects of (+/-)Huprine X, a New Acetylcholinesterase Inhibitor, on Nicotinic Receptors in Rat Cortical Synaptosomes. *Neuropharmacology* **2004**, *46* (1), 95–102.

[226] Canudas, A. M.; Pubill, D.; Sureda, F. X.; Verdaguer, E.; Camps, P.; Muñoz-Torrero, D.; Jiménez, A.; Camins, A.; Pallàs, M. Neuroprotective Effects of (±)-Huprine Y on in Vitro and in Vivo Models of Excitoxicity Damage. *Exp. Neurol.* **2003**, *180* (2), 123–130.

[227] Ratia, M.; Giménez-Llort, L.; Camps, P.; Muñoz-Torrero, D.; Clos, M.; Badia, A. Behavioural Effects and Regulation of PKCα and MAPK by Huprine X in Middle Aged Mice. *Pharmacol. Biochem. Behav.* **2010**, *95* (4), 485–493.

3.1.3. State of the art

3.1.3.1. Huprine functionalized in position 12

Due to their high potency against AChE, huprine scaffold has been used in the past years in the development of MTDLs against AD. For example, Pr. Muñoz-Torrero's team designed new hybrids by functionalising the position 12[176,177,228] (Figure 64). In 2010, they have designed a family of dual binding site AChEIs by conjugating a huprine scaffold and a donepezil moiety, compound **35**, the lead molecule of the series, proved to be a potent AChE inhibitor and turned out to moderately act on AChE-induced and self-induced Aβ aggregation and BACE-1[228]. Five years later, this lead MTDL was evaluated *in vivo* and showed that compound **35** had pro-cognitive effects on mice improving both short and long-term memory. Moreover, compound **35** exhibited anxiolytic-like actions and did not exerted significant adverse effects[229]. The same group also worked on the design of another AChE dual inhibitor, a huprine-tacrine heterodimer linked in position 12 of the huprine moiety, compound **36** exerted promising *in vitro* results by acting on several targets of CNS-related pathologies. Indeed, compound **36**, besides its potent inhibitory activity against AChE, also proved to be a good BACE-1 inhibitor and to reduce AChE-induced and self-induced Aβ aggregation[177]. Finally, compound **37** was designed by adding a Tau aggregation inhibiting moiety to the huprine moiety, the new hybrid gave promising *in vitro* results against AChE, BChE and BACE-1. Moreover, *ex vivo* studies in brain slices of mice revealed that compound **37** was efficient to protect against the Aβ self-aggregation and Tau protein aggregation, *in vivo* evaluations also showed an increase in the levels of mature APP and a central Aβ lowering effect[230].

---

[228] Viayna, E.; Gómez, T.; Galdeano, C.; Ramírez, L.; Ratia, M.; Badia, A.; Clos, M. V.; Verdaguer, E.; Junyent, F.; Camins, A.; Pallàs, M.; Bartolini, M.; Mancini, F.; Andrisano, V.; Arce, M. P.; Rodríguez-Franco, M. I.; Bidon-Chanal, A.; Luque, F. J.; Camps, P.; Muñoz-Torrero, D. Novel Huprine Derivatives with Inhibitory Activity toward β-Amyloid Aggregation and Formation as Disease-Modifying Anti-Alzheimer Drug Candidates. *ChemMedChem* **2010**, *5* (11), 1855–1870.

[229] Giménez-Llort, L.; Ratia, M.; Pérez, B.; Camps, P.; Muñoz-Torrero, D.; Badia, A.; Clos, M. V. AVCRI104P3, a Novel Multitarget Compound with Cognition-Enhancing and Anxiolytic Activities: Studies in Cognitively Poor Middle-Aged Mice. *Behav. Brain Res.* **2015**, *286*, 97–103.

[230] Viayna, E.; Sola, I.; Bartolini, M.; De Simone, A.; Tapia-Rojas, C.; Serrano, F. G.; Sabaté, R.; Juárez-Jiménez, J.; Pérez, B.; Luque, F. J.; Andrisano, V.; Clos, M. V.; Inestrosa, N. C.; Muñoz-Torrero, D. Synthesis and Multitarget Biological Profiling of a Novel Family of Rhein Derivatives as Disease-Modifying Anti-Alzheimer Agents. *J. Med. Chem.* **2014**, *57* (6), 2549–2567.

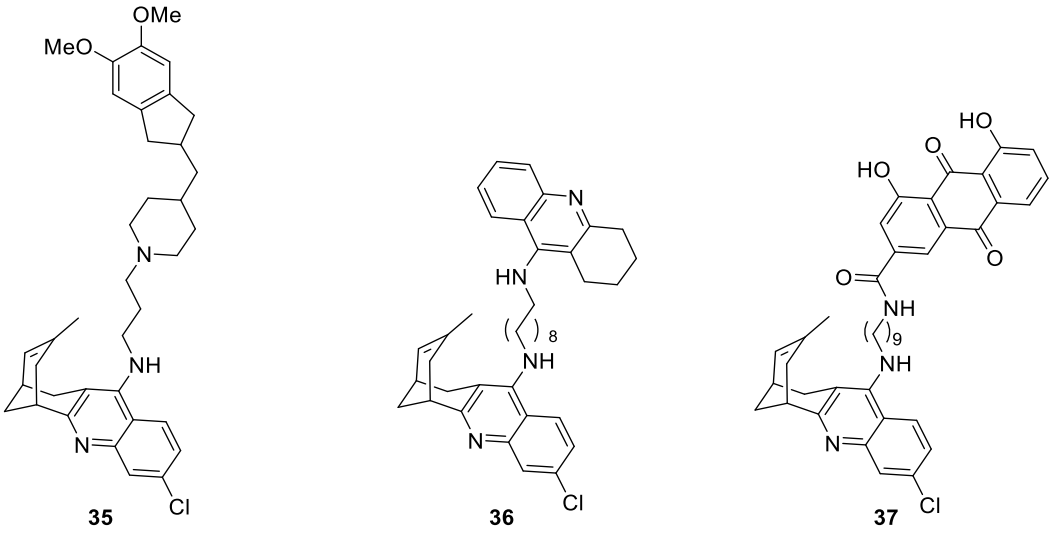

Figure 64: Examples of huprines functionalised in position 12

3.1.3.2. Huprine functionalized in position 9

Other functionalisation studies of huprine scaffold have been performed by Pr. Renard's team to develop a series of original potent dimeric AChEIs by functionalising the position 9 of the huprine scaffold[231]. After developing an efficient synthesis route to the huprine analogues functionalised in position 9[217,232,233], Ronco et *al.*[190] have synthesised many huprine analogues and some of which are bearing a substituent containing a 1,2,3- triazole moiety (Figure 10). The incorporation of this triazole moiety allowed us to develop efficient and convergent synthetises of heterodimeric AChEIs by using the copper-catalysed alkyne-azide cycloaddition (CuAAC). Moreover, as observed in the crystal structure of *m*AChE in complex with tacrine based MTDL anti-TZ2-PA6 (PDB 1Q84)[234] reported by Marchot and Bourne, the introduction of the triazole ring branched to the aniline moiety of tacrine (position 12 in huprine) would allow formation of favourable hydrogen bond interactions with well-identified residues (Tyr337, Tyr124, Tyr341) at the bottom of the gorge and within the active-site gorge

[231] Oukoloff, K.; Chao, S.; Cieslikiewicz-Bouet, M.; Mougeot, R.; Jean, L.; Renard, P.-Y. Improved Access to Huprine Derivatives Functionalized at Position 9. *Eur. J. Org. Chem.* **2016**, *2016* (7), 1337–1343.
[232] Ronco, C.; Jean, L.; Renard, P.-Y. Improved Synthetic Pathway for the Derivatization of Huprine Scaffold. *Tetrahedron* **2010**, *66* (37), 7399–7404.
[233] Patent WO2011124712A1
[234] Bourne, Y.; Kolb, H. C.; Radic, Z.; Sharpless, K. B.; Taylor, P.; Marchot, P. Freeze-Frame Inhibitor Captures Acetylcholinesterase in a Unique Conformation. *Proc.Natl.Acad.Sci.Usa* **2004**, *101*, 1449–1454.

of AChE. *In vitro* evaluations of their inhibitory activities against *h*AChE and the resolution of X-ray crystal structure of *m*AChE in complex with **43** (PDB 4A16) allowed us to rationally design potent AChE inhibitors at subnanomolar levels. Indeed, it was demonstrated that a linker possessing 4 carbon atoms (**41**, **42** and **43**) was favourable for a good placement of the triazole ring inside the enzyme leading to derivatives almost 500 times more potent than functionalised huprines bearing a 2 carbon atoms linker (**38**, **39** and **40**), and that the interaction occurred at another binding site situated at an upper place of the gorge closer to the PAS.

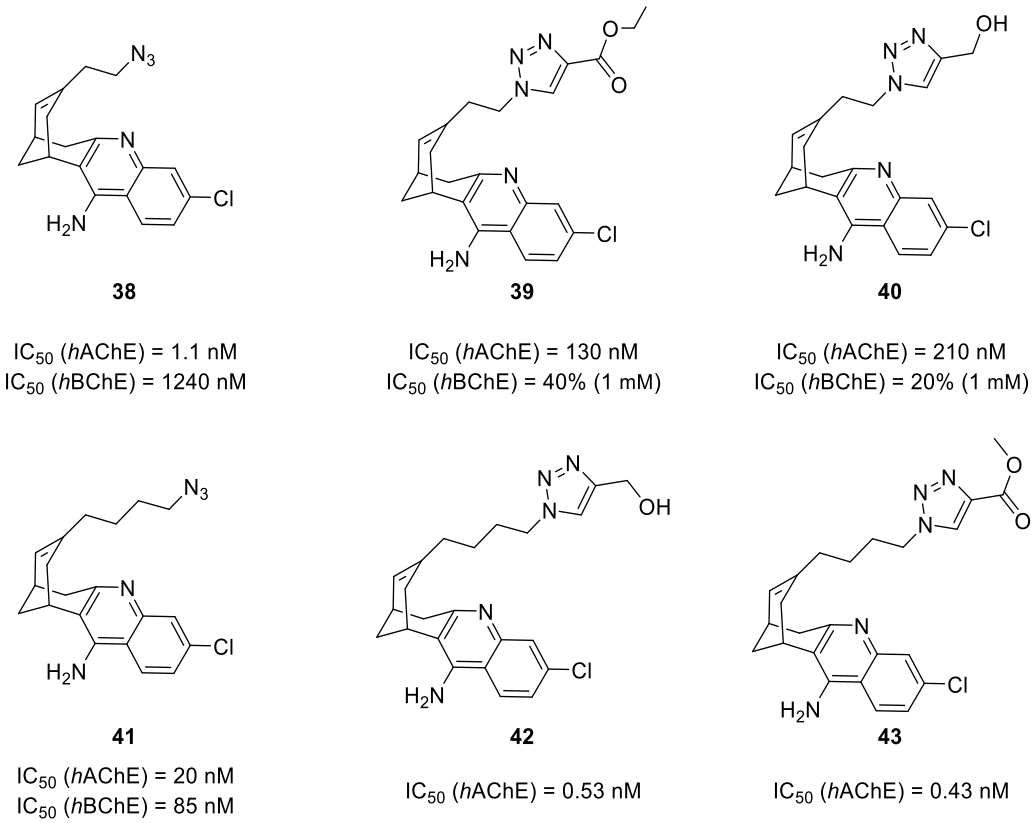

Figure 65: Examples of huprines functionalized in position 9

3.1.3.3. Others valorisation of huprine compounds

Based on these results, the bioorganic team has decided to develop several applications using huprine compound such as the preparation of an efficient resin (Hupresin® sold by a lab spin-off company ChemForase) for the purification of BChE and the preparation of a selective and sensitive near-infrared fluorescent probe for imaging AChE in the neuromuscular junction (NMJ) in muscles and in the brain.

3.1.3.3.1. Resin for the purification of BChE[235]

By grafting a huprine compound functionalised in position 9 on a solid support named Sepharose (Scheme 4), the team of Pr. Renard has developed an efficient resin to purify BChE from human plasma or transgenic plants[233,236,,237,238,239] by affinity chromatography. BChE is currently the most advanced bioscavenger as antidote against the intoxications with organophosphorus nerve agents and the use of this resin during the purification steps of the enzyme allowed decreasing the cost for the development of this bioscavenger in a large scale[240]. This innovative technology (Hupresin®) has been transferred to the start-up Chemforase[235] created in 2016 by Dr. Emilie David.

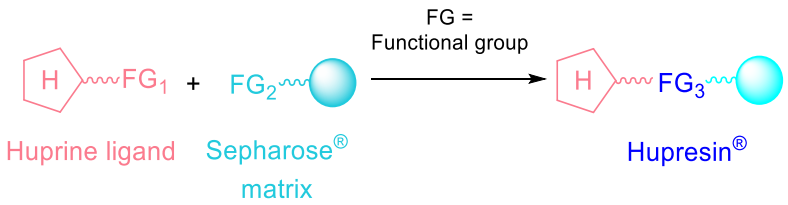

Scheme 4: Hupresin® formation

3.1.3.3.2. Synthesis of fluorescent probes for imaging AChE[241]

The second application using huprine compound is the development of a selective and sensitive fluorescent probe for imaging AChE. Based on the high selectivity of huprine for AChE versus BChE, Dr. Sovy Chao, during her PhD in Pr. Renard's bioorganic chemistry team, has synthesised two near-infrared fluorescent probes by coupling a huprine scaffold with the cyanine 5.0 leading to **HupNIR1** and **HupNIR2** (Figure 66). These two probes exhibited a high affinity toward AChE versus BChE (Table 1) (IC_{50} is 400-fold higher for AChE than BChE). The confocal fluorescence imaging showed a specific

[235] ChemForAse. Home http://www.chemforase.com/products/hupresin.
[236] Brazzolotto, X.; Wandhammer, M.; Ronco, C.; Trovaslet, M.; Jean, L.; Lockridge, O.; Renard, P.-Y.; Nachon, F. Human Butyrylcholinesterase Produced in Insect Cells: Huprine-Based Affinity Purification and Crystal Structure. *FEBS J.* **2012**, *279* (16), 2905–2916.
[237] Alkanaimsh, S.; Corbin, J. M.; Kailemia, M. J.; Karuppanan, K.; Rodriguez, R. L.; Lebrilla, C. B.; McDonald, K. A.; Nandi, S. Purification and Site-Specific N-Glycosylation Analysis of Human Recombinant Butyrylcholinesterase from Nicotiana Benthamiana. *Biochem. Eng. J.* **2019**, *142*, 58–67.
[238] Schopfer, L. M.; Lockridge, O.; David, E.; Hinrichs, S. H. Purification of Human Butyrylcholinesterase from Frozen Cohn Fraction IV-4 by Ion Exchange and Hupresin Affinity Chromatography. *PLOS ONE* **2019**, *14* (1), e0209795.
[239] Onder, S.; David, E.; Tacal, O.; Schopfer, L. M.; Lockridge, O. Hupresin Retains Binding Capacity for Butyrylcholinesterase and Acetylcholinesterase after Sanitation with Sodium Hydroxide. *Front. Pharmacol.* **2017**, *8*.
[240] Nachon, F.; Brazzolotto, X.; Trovaslet, M.; Masson, P. Progress in the Development of Enzyme-Based Nerve Agent Bioscavengers. *Chem. Biol. Interact.* **2013**, *206* (3), 536–544.
[241] Chao, S.; Krejci, E.; Bernard, V.; Leroy, J.; Jean, L.; Renard, P.-Y. A Selective and Sensitive Near-Infrared Fluorescent Probe for Acetylcholinesterase Imaging. *Chem. Commun.* **2016**, *52* (77), 11599–11602.

labelling of AChE in the NMJ in the muscles (mice) and even in the brain region displaying a low AChE concentration as striatum.

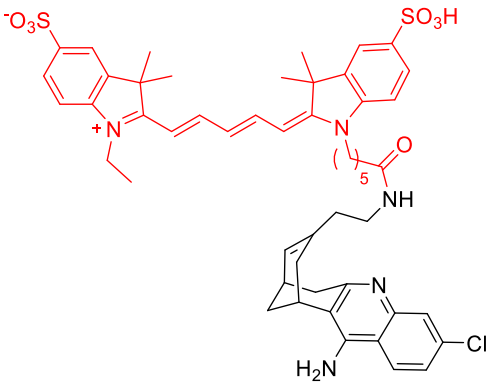

HupNIR1

IC_{50} (*h*AChE) = 80 nM
IC_{50} (*h*BChE) > 10^5 nM
Selectivity (*h*BChE/*h*AChE) > 1250

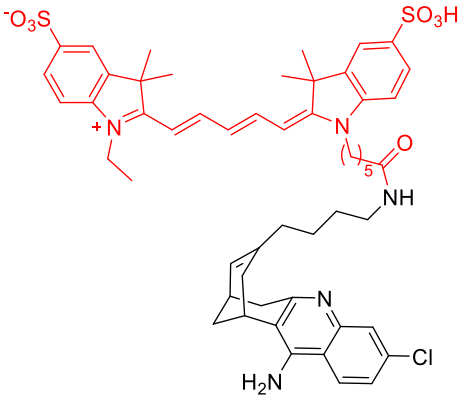

HupNIR2

IC_{50} (*h*AChE) = 31 nM
IC_{50} (*h*BChE) = > 12 500 nM
Selectivity (*h*BChE/*h*AChE) > 403

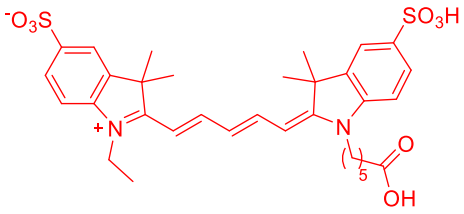

Cyanine 5.0

*Figure 66: Structure of **HupNR1**, **HupNR2** and cyanine 5.0*

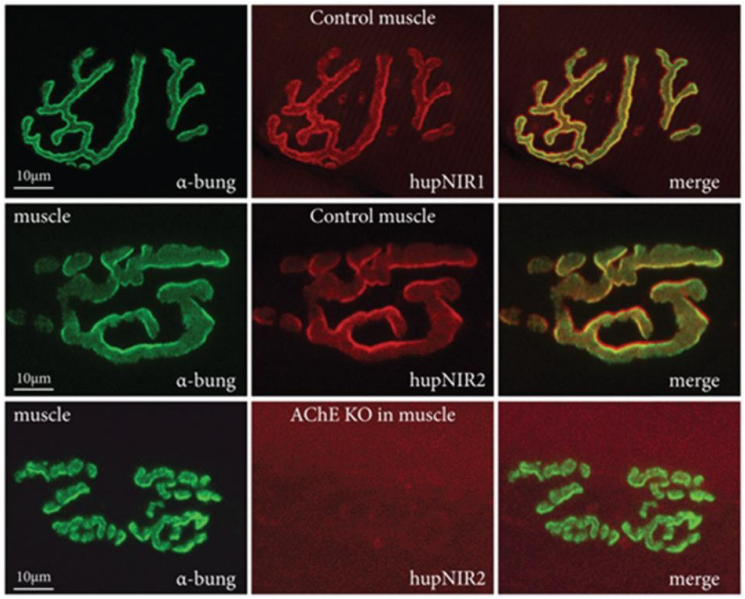

*Figure 67: **HupNIR1** and **HupNIR2** label specifically AChE at neuromuscular junctions. Confocal fluorescence imaging of NMJ in the muscle. NMJ were identified by Alexa488 α-BTX (green, left panel) and **HupNIR1** or **HupNIR2** as noted (middle panel). **HupNIR1** or **HupNIR2** are co-localised with Alexa488 α-BTX (producing a yellow image in the merged view on the right panel). When AChE is dramatically reduced in KO mice, the red signal is absent.*[241]

Entry	Compound	λmax_{Ab} (nm)	λmax_{Em} (nm)	ε ($L.mol^{-1}.cm^{-1}$)	ϕ_f	Brightness ($L.mol^{-1}.cm^{-1}$)
1	**HupNIR1**	649	668	299 794	0.41	122 915
2	**HupNIR2**	650	665	312 049	0.43	134 181

*Table 1: Fluorescence characterization of **HupNR1** and **HupNR2***

3.2. Antioxidants against AD – Use of natural compounds

Even though the use of antioxidants in the treatment of AD in clinical patients remains controversial[242,243], natural compounds and hybrids based on these molecules have been developed in the past years and have displayed interesting properties in the treatment of neurodegenerative diseases.

[242] Feng, Y.; Wang, X. Antioxidant Therapies for Alzheimer's Disease. *Oxid. Med. Cell. Longev.* **2012**, *2012*.
[243] Colizzi, C. The Protective Effects of Polyphenols on Alzheimer's Disease: A Systematic Review. *Alzheimers Dement. Transl. Res. Clin. Interv.* **2019**, *5*, 184–196.

3.2.1. Capsaicin – a well-known antioxidant

Capsaicin is the active substance of chili peppers obtained from the plants of genus *Capsicum* and is part of a chemical group called capsaicinoids. *Capsicum*'s effects on human body have been studied for more than a century, for example, Hogyes observed the burning sensation produced by an extract of *capsicum* when applied on human skin[244]. Indeed, over the years, Capsaicin and its analogues have been studied in the treatment of diverse pathologies including CNS-related diseases for its potent antioxidant properties[245] (Figure 68).

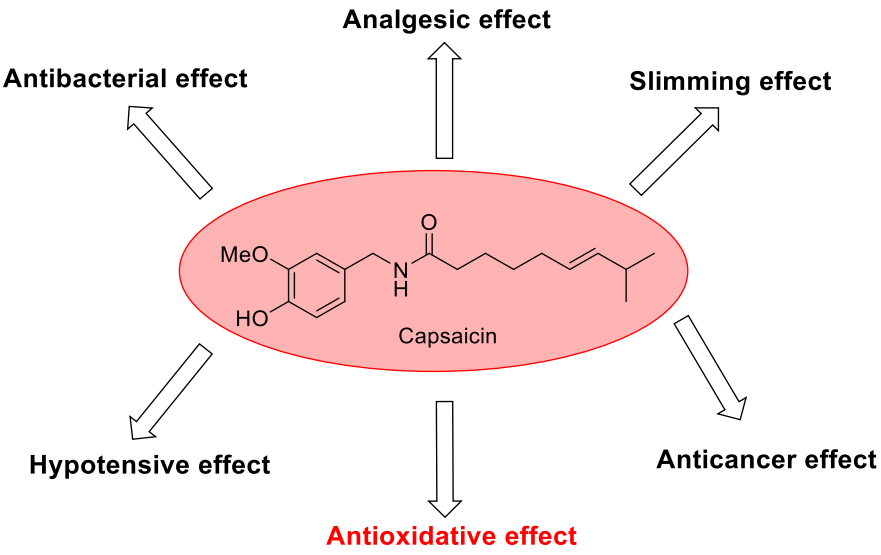

Figure 68: Structure and pharmacological properties of Capsaicin[245]

Due to its well-known antioxidative properties, capsaicin has been evaluated for its biological properties against CNS-related pathologies and it has been shown that using capsaicin moiety could have important implications in the prevention or treatment of neurodegenerative diseases such as AD[246]. As an illustration of its antioxidant property, it has been proven that, at 60 µg/mL, Capsaicin is able to scavenge 91.9% of the DPPH free radicals[247], it has been suggested that the C7-benzyl carbon was the important functional group responsible for the potent observed antioxidant properties.

[244] Sharma, S. K.; Vij, A. S.; Sharma, M. Mechanisms and Clinical Uses of Capsaicin. *Eur. J. Pharmacol.* **2013**, *720* (1), 55–62.
[245] Adaszek, Ł.; Gadomska, D.; Mazurek, Ł.; Łyp, P.; Madany, J.; Winiarczyk, S. Properties of Capsaicin and Its Utility in Veterinary and Human Medicine. *Res. Vet. Sci.* **2019**, *123*, 14–19.
[246] Delanty, N.; Dichter, M. A. Antioxidant Therapy in Neurologic Disease. *Arch. Neurol.* **2000**, *57* (9), 1265–1270.
[247] Dairam, A.; Fogel, R.; Daya, S.; Limson, J. L. Antioxidant and Iron-Binding Properties of Curcumin, Capsaicin, and S-Allylcysteine Reduce Oxidative Stress in Rat Brain Homogenate. *J. Agric. Food Chem.* **2008**, *56* (9), 3350–3356.

Besides Capsaicin's antioxidant properties, it has also been proven by Jiang et *al*. that this alkaloid was able to promote neuroprotection in rats[248].

3.2.2. Other antioxidants

3.2.2.1. Flavonoids

Flavonoids are part of the natural polyphenols family and have been widely investigated in the field of medicinal chemistry thanks to their proven health beneficial properties. Their antioxidant capacity has been used in the development of drugs against cancer[249], inflammatory pathologies[250] or neurodegenerative diseases[251]. The antioxidant activity of flavonoids is due to their chemical structure and particularly to the hydroxyl groups present in the molecules[252] and the high antioxidant potency of flavonoids is explained by the mechanisms in which they are involved. Indeed, they are able to scavenge free radicals (Scheme 5) through formation of less reactive phenol based radical, or even quinones, and inhibit enzymes known to be involved in ROS generation such as microsomal monooxygenase, glutathione-S transferase or NADH oxidase by chelating the metal ions.

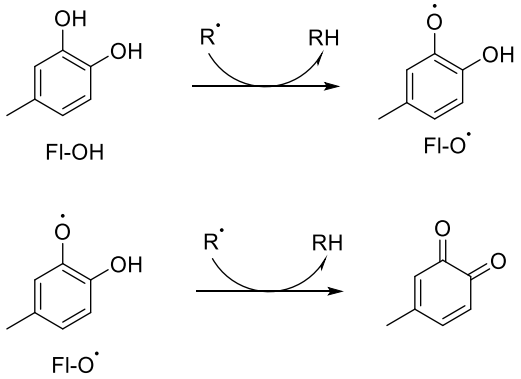

Scheme 5: ROS scavenging by flavonoids[251]

[248] Jiang, X.; Jia, L.-W.; Li, X.-H.; Cheng, X.-S.; Xie, J.-Z.; Ma, Z.-W.; Xu, W.-J.; Liu, Y.; Yao, Y.; Du, L.-L.; Zhou, X.-W. Capsaicin Ameliorates Stress-Induced Alzheimer's Disease-Like Pathological and Cognitive Impairments in Rats. *J. Alzheimers Dis.* **2013**, *35* (1), 91–105.

[249] Chen, D.; Daniel, K. G.; Kuhn, D. J.; Kazi, A.; Bhuiyan, M.; Li, L.; Wang, Z.; Wan, S. B.; Lam, W. H.; Chan, T. H.; Dou, Q. P. Green Tea and Tea Polyphenols in Cancer Prevention. *Front. Biosci. J. Virtual Libr.* **2004**, *9*, 2618–2631.

[250] Laughton, M. J.; Evans, P. J.; Moroney, M. A.; Hoult, J. R. S.; Halliwell, B. Inhibition of Mammalian 5-Lipoxygenase and Cyclo-Oxygenase by Flavonoids and Phenolic Dietary Additives. *Biochem. Pharmacol.* **1991**, *42* (9), 1673–1681.

[251] Kumar, S.; Pandey, A. K. Chemistry and Biological Activities of Flavonoids: An Overview. *Sci. World J.* **2013**, *2013*, 1–16.

[252] Bors, W.; Heller, W.; Michel, C.; Saran, M. [36] Flavonoids as Antioxidants: Determination of Radical-Scavenging Efficiencies. In *Methods in Enzymology*; Elsevier, 1990; Vol. 186, pp 343–355.

Thanks to their neuroprotective effects, flavonoids have been investigated as anti-AD drugs, the two main examples are represented in Figure 69. In 2008, Shimmyo et *al.* reported that myricetine, a flavonol, displayed inhibiting activity against BACE-1 inducing a decrease in the production of Aβ[253]. It must be added that myricetine also showed promising neuroprotective effects because of its ability to modulate NMDA receptors, and thus, to reduce Ca^{2+} influx and inhibit the ROS production induced by the glutamate[254]. Another promising therapeutic agent against AD is (-)-epigallocatechin (EGCG), a flavonol found in green tea, indeed, *in vitro* studies have shown that the molecule had a protective activity against Aβ-induced cytotoxicity by acting as an AChE inhibitor[255]. Moreover, EGCG displayed interesting ROS scavenging properties inducing neuroprotective effects against Aβ-induced neuronal apoptosis[256]. Finally, further studies have shown that ECGC was involved in the inhibition of aggregates induced by the hyperphosphorylated Tau protein[257].

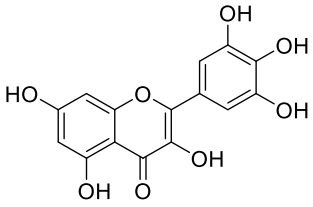

Myricetine

IC_{50} (BACE-1) = 2.8 μM
Inhibition of cell death = 30.81% at 1 μM
Inhibition of ROS generation = 77.07% at 1 μM
Scavenging of DPPH radical = 46.09% at 1 μM

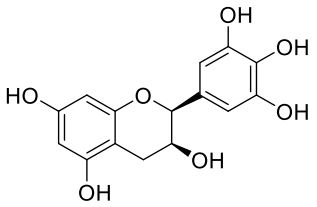

EGCG

IC_{50} (AChE) = 9.6 nM
Aβ inhibitior
Tau protein inhibitor
ROS scavenger

Figure 69: Structures of flavonoids as anti-AD agents

[253] Shimmyo, Y.; Kihara, T.; Akaike, A.; Niidome, T.; Sugimoto, H. Flavonols and Flavones as BACE-1 Inhibitors: Structure–Activity Relationship in Cell-Free, Cell-Based and in Silico Studies Reveal Novel Pharmacophore Features. *Biochim. Biophys. Acta BBA - Gen. Subj.* **2008**, *1780* (5), 819–825.

[254] Wang, J.; Yu, Z.; Yu, Q.; Kong, Q.; Zhang, N.; He, L.; Yi, Y. Study on Neuroprotective Capacity of Key Flavonoids of *Ampelopsis Grossedentata*. *J. Food Nutr. Res.* **2014**, *2* (12), 880–889.

[255] Okello, E. J.; Leylabi, R.; McDougall, G. J. Inhibition of Acetylcholinesterase by Green and White Tea and Their Simulated Intestinal Metabolites. *Food Funct.* **2012**, *3* (6), 651.

[256] Choi, Y.-T.; Jung, C.-H.; Lee, S.-R.; Bae, J.-H.; Baek, W.-K.; Suh, M.-H.; Park, J.; Park, C.-W.; Suh, S.-I. The Green Tea Polyphenol (−)-Epigallocatechin Gallate Attenuates β-Amyloid-Induced Neurotoxicity in Cultured Hippocampal Neurons. *Life Sci.* **2001**, *70* (5), 603–614.

[257] Wobst, H. J.; Sharma, A.; Diamond, M. I.; Wanker, E. E.; Bieschke, J. The Green Tea Polyphenol (−)-Epigallocatechin Gallate Prevents the Aggregation of Tau Protein into Toxic Oligomers at Substoichiometric Ratios. *FEBS Lett.* **2015**, *589* (1), 77–83.

3.2.2.2. Vitamin E

α-tocopherol (Figure 70) is the most studied and the most biologically active form of vitamin E, which includes different fat-soluble compounds, because it is the main form found in tissues and is an essential micronutrient for humans.

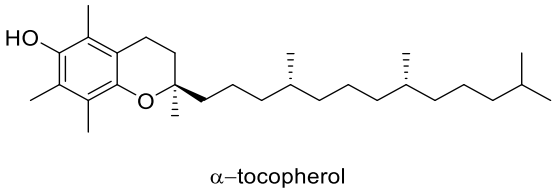

Figure 70: Structure of α-tocopherol

It has been shown that vitamin E has a pivotal role in the CNS because of its antioxidant properties, indeed, it is able to scavenge free radicals *via* a hydrogen atom transfer between the molecule and the free radicals resulting to a non-radical product and a less reactive vitamin E radical able to interact with a reducing agent such as vitamin C or ubiquinol to restore vitamin E (Scheme 6)[258]. Moreover, a low concentration of vitamin E in the CNS has been proven to cause cellular atrophy and cognitive deficit induced by a decrease of dendritic branching of Purkinje neurons[259].

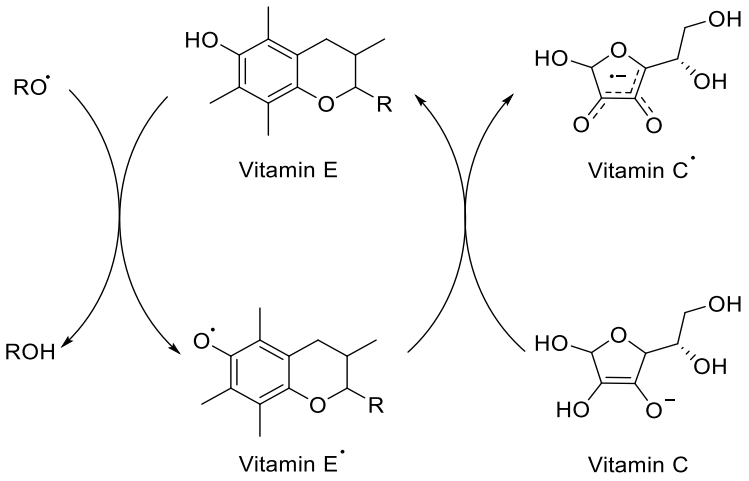

Scheme 6: Vitamin E radical oxygen species scavenging mechanism[260]

[258] Niki, E. Role of Vitamin E as a Lipid-Soluble Peroxyl Radical Scavenger: In Vitro and in Vivo Evidence. *Free Radic. Biol. Med.* **2014**, *66*, 3–12.
[259] Ulatowski, L.; Parker, R.; Warrier, G.; Sultana, R.; Butterfield, D. A.; Manor, D. Vitamin E Is Essential for Purkinje Neuron Integrity. *Neuroscience* **2014**, *260*, 120–129.
[260] Valko, M.; Izakovic, M.; Mazur, M.; Rhodes, C. J.; Telser, J. Role of Oxygen Radicals in DNA Damage and Cancer Incidence. *Mol. Cell. Biochem.* **2004**, *266* (1/2), 37–56.

Hence, vitamin E has been studied in the design of treatments against AD, it has been demonstrated that the molecule was capable to counteract Aβ-induced protein oxidation, ROS production and neurotoxicity[261] which might lead to an improvement of cognitive and memory deficit.
Moreover, "drug cocktail" approaches have been investigating to increase the activity of vitamin E by potentially having a synergic action with the additional compound. A combination of vitamin E and memantine[262] and a combination of vitamin E and selenium[263] have been put through phase III clinical trial in 2014 and 2017. Selenium was chosen due to studies correlating its decrease in elderly population's plasma and cognitive decline[264,265]. Concerning the first trial, no information following the trial has been displayed, and unfortunately, the vitamin E-Selenium cocktail was discontinued due to its inactivity to prevent dementia.

Moreover, because it has been shown that oxidative stress was linked to the rise of hyperphosphorylated Tau protein levels and Aβ aggregates levels[266], combining an anti-AChE activity with antioxidant properties could lead to the synthesis of heterodimers able to act on several therapeutic targets involved in AD. During her PhD in our team, Dr. Sovy Chao designed such conjugated heterodimers by combining a huprine fragment to an antioxidant moiety using the CuAAC. The lead compound of the series was **HUP-RES** (Figure 71), a hybrid conjugating huprine and a resveratrol moiety, indeed, it displayed promising inhibition properties against *h*AChE and *h*BChE combined to a good activity and selectivity against MAO-A compared to MAO-B. Studies of its inhibitory activity against Aβ auto-induced aggregation and ORAC determination are still ongoing.

---

[261] Yatin, S. M.; Varadarajan, S.; Butterfield, D. A. Vitamin E Prevents Alzheimer's Amyloid Beta-Peptide (1-42)-Induced Neuronal Protein Oxidation and Reactive Oxygen Species Production. *J. Alzheimers Dis. JAD* **2000**, *2* (2), 123–131.
[262] Dysken, M. W.; Guarino, P. D.; Vertrees, J. E.; Asthana, S.; Sano, M.; Llorente, M.; Pallaki, M.; Love, S.; Schellenberg, G. D.; McCarten, J. R.; Malphurs, J.; Prieto, S.; Chen, P.; Loreck, D. J.; Carney, S.; Trapp, G.; Bakshi, R. S.; Mintzer, J. E.; Heidebrink, J. L.; Vidal-Cardona, A.; Arroyo, L. M.; Cruz, A. R.; Kowall, N. W.; Chopra, M. P.; Craft, S.; Thielke, S.; Turvey, C. L.; Woodman, C.; Monnell, K. A.; Gordon, K.; Tomaska, J.; Vatassery, G. Vitamin E and Memantine in Alzheimer's Disease: Clinical Trial Methods and Baseline Data. *Alzheimers Dement. J. Alzheimers Assoc.* **2014**, *10* (1), 36–44.
[263] Kryscio, R. J.; Abner, E. L.; Caban-Holt, A.; Lovell, M.; Goodman, P.; Darke, A. K.; Yee, M.; Crowley, J.; Schmitt, F. A. Association of Antioxidant Supplement Use and Dementia in the Prevention of Alzheimer's Disease by Vitamin E and Selenium Trial (PREADViSE). *JAMA Neurol.* **2017**, *74* (5), 567–573.
[264] Gao, S.; Jin, Y.; Hall, K. S.; Liang, C.; Unverzagt, F. W.; Ji, R.; Murrell, J. R.; Cao, J.; Shen, J.; Ma, F.; Matesan, J.; Ying, B.; Cheng, Y.; Bian, J.; Li, P.; Hendrie, H. C. Selenium Level and Cognitive Function in Rural Elderly Chinese. *Am. J. Epidemiol.* **2007**, *165* (8), 955–965.
[265] Arnaud, J.; Akbaraly, N. T.; Hininger, I.; Roussel, A.-M.; Berr, C. Factors Associated with Longitudinal Plasma Selenium Decline in the Elderly: The EVA Study. *J. Nutr. Biochem.* **2007**, *18* (7), 482–487.
[266] Rodrigues, R.; Petersen, R. B.; Perry, G. Parallels between Major Depressive Disorder and Alzheimer's Disease: Role of Oxidative Stress and Genetic Vulnerability. *Cell. Mol. Neurobiol.* **2014**, *34* (7), 925–949.

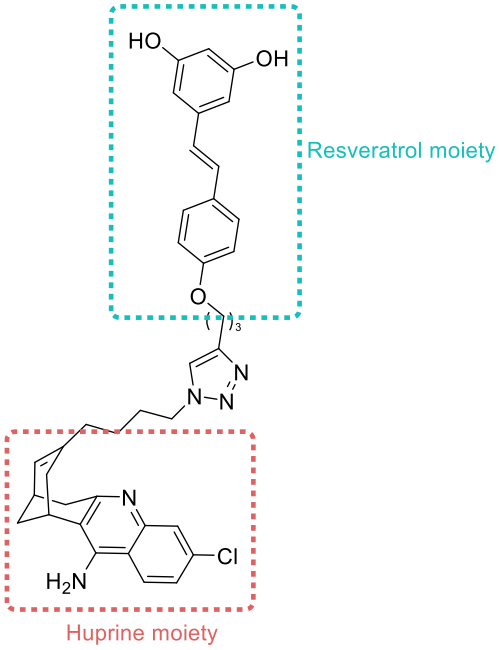

HUP-RES

IC_{50} (*h*AChE) = 94 nM
IC_{50} (*h*BChE) = 56 nM
IC_{50} (*h*MAO-A) = 140 nM
IC_{50} (*h*MAO-B) = 48% at 10 μM

*Figure 71: Structure of **HUP-RES***

As a conclusion, this overview of the chosen targets and pharmacophores has brought to light that designing MTDLs targeting simultaneously AChE and oxidative stress could lead to potent MTDLs against AD. Indeed, despite the fact that antioxidants used alone did not display high potency against neurodegenerative pathologies, conjugating an antioxidant pharmacophore to an AChEI could have a synergic effect increasing the properties of the chosen structures. Capsaicin was chosen as the antioxidant fragment because of its simple structure and its ability to scavenge DPPH free radicals, while huprine was chosen because of its high potency against AChE and BChE combined to the great expertise concerning huprine synthesis in the Professor Renard's team.

4. Hybrid's synthesis

In this context, in collaboration with the Professor Muñoz-Torrero's team, 9 new MTDLs combining an AChEI and an antioxidant have been developed and biological evaluated *in vitro* (Figure 72). Two compounds **44c** and **34** showed promising results and **34** was selected to be part of *in vivo* studies (currently ongoing in Pr. Inestrosa's team).

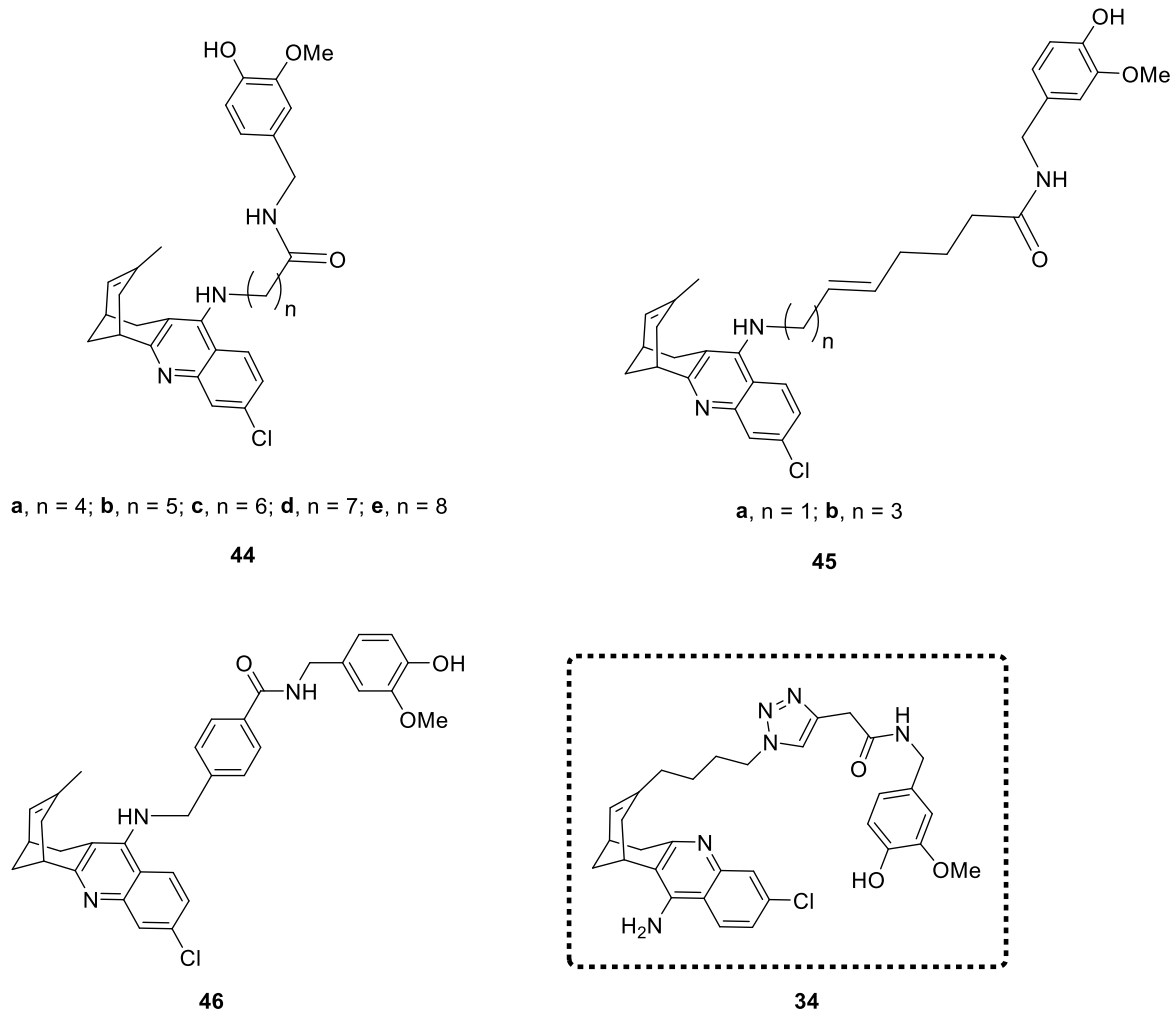

Figure 72: Huprine-Capsaicin hybrid conjugated MTDLs series

4.1. Retrosynthetic route to obtain the MTDL

In order to obtain MTDL 34 precursor, compound **47**, we worked on a convergent synthetic pathway where the key step is the 1,2,3-triazole ring formation by a copper catalysed Huisgen cycloaddition between azide **48** and alkyne **49** (Scheme 7). The synthetic pathway was firstly developed by the Doctor Monika Bouet (2013-2014) but, as part of the *in vivo* studies required for a publication, the compound had to be synthesized on a larger scale (approximatively 150 mg).

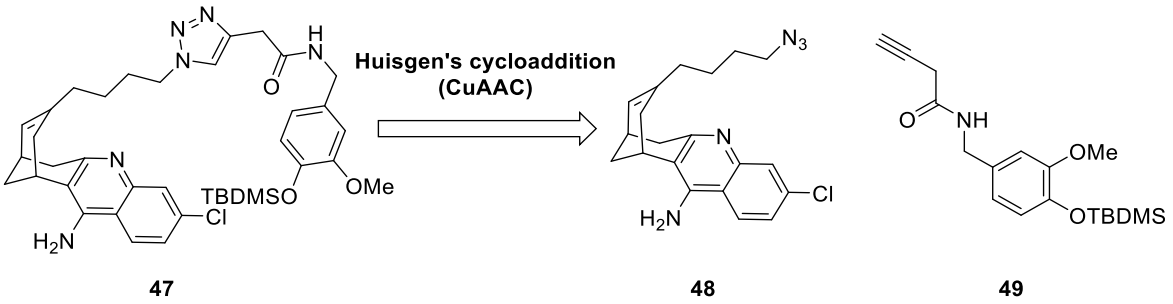

*Scheme 7: Retrosynthetic pathway to **47***

4.2. Alkyne's synthesis

The first step of the synthesis was to obtain alkyne **49** based on the capsaicin structure. The conversion of the aldehyde function of commercially available 4-hydroxy-3-methoxybenzaldehyde **50** into the corresponding nitrile **51** was obtained in an excellent yield by reaction of hydroxylamine in refluxed acetic acid. The phenol function of **51** was then protected as a *tert*-butyldimethylsilyl ether **52** in a quantitative yield after a reaction with *tert*-butyldimethylsilyl chloride and a catalytic amount of 4-dimethylaminopyridine and imidazole used as base in dichloromethane. Finally, after a reduction of the nitrile function of compound **52** using $LiAlH_4$ in THF, compound **53** carrying an amine was obtained with an excellent yield of 90% (Scheme 8).

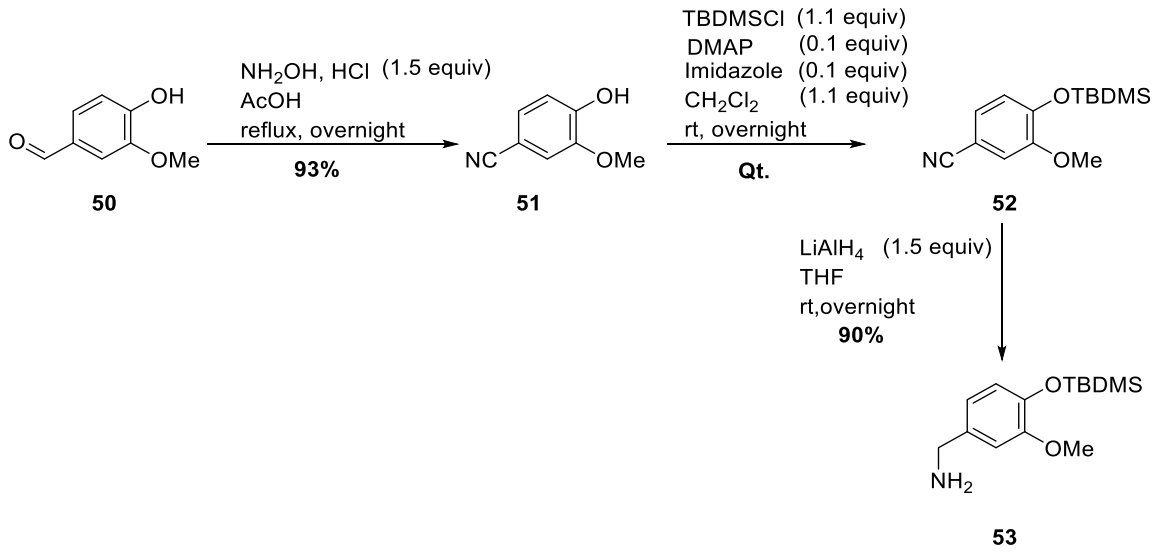

*Scheme 8: Synthesis of compound **53***

The next step consisted in synthesising 3-butynoic acid **55** from commercially available 3-butynol **54** in only one step with an excellent yield of 83% (Scheme 9). With compound **55** in hands, we tried to perform a coupling between carboxylic acid **55** and amine **53** with EEDQ (Scheme 10), unfortunately, the coupling failed to give compound **49** and only the starting materials were recovered. EEDQ was

used in order to limit the formation of the allenic form mainly observed when other usual peptide coupling reagents or conditions were used.

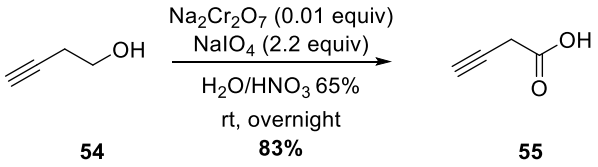

*Scheme 9: Synthesis of compound **55***

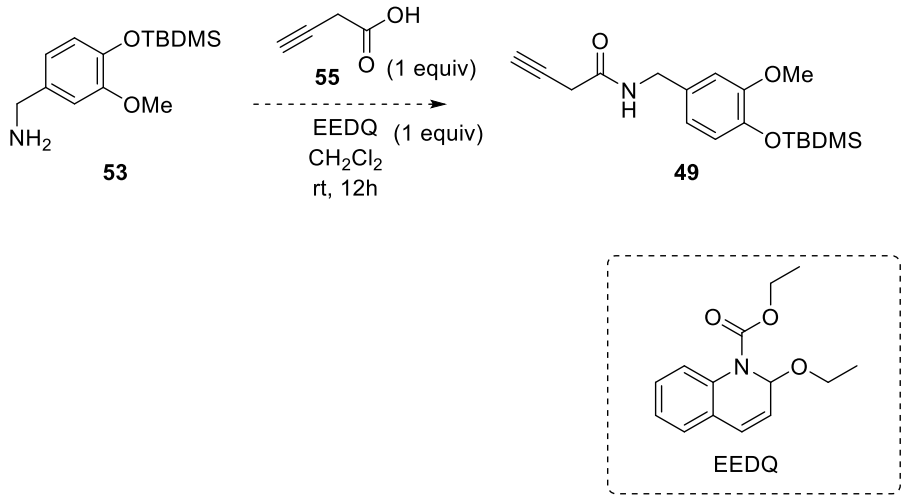

*Scheme 10: Attempted synthesis of **49** with EEDQ*

Our second attempt to couple compounds **53** and **55** was performed with EDC.HCl as an activation agent of the carboxylic acid (Scheme 11). We managed to obtain compound **49** with a low 20% yield. This low yield could be explained by the formation of the corresponding ketene as a side product of the reaction. Nevertheless, alkyne **49** was obtained in 4 steps with an overall yield of 18% on a 400 mg scale, our attempts to obtain higher amidation reaction yields failed.

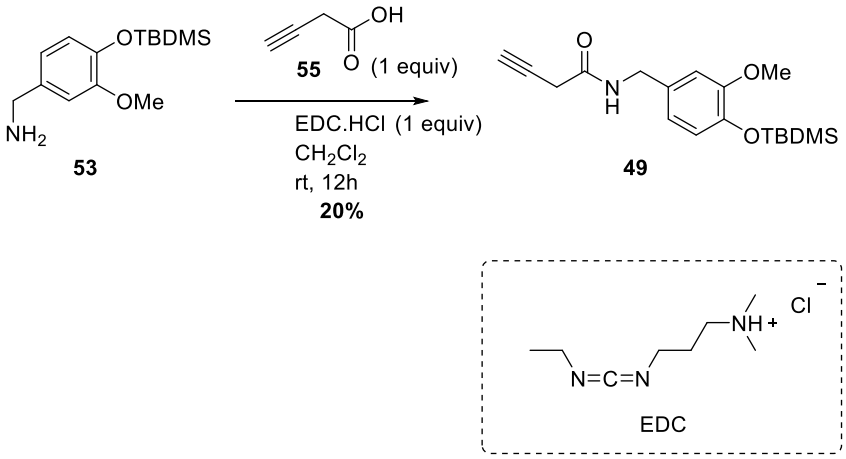

*Scheme 11: Synthesis of compound **49***

4.3. Azide synthesis

For the following of the synthesis, azide **48** was obtained in 10 steps according to a synthesis developed in the laboratory by Doctor Killian Oukoloff[231]. In the interest of clarity, the synthesis will be divided and discussed in four main steps.

4.3.1. Synthesis of intermediate 60

Diketone **60** was obtained in only 3 steps from commercially available 1,1,3,3-tetramethoxypropane and dimethyl-1,3-acetonedicarboxylate in a reaction of aldolization, crotonisation and intermolecular Michael addition (Scheme 12). The pH adjustment was primordial in the first step, because an acidic reaction mixture (pH = 5) could enable the 2,6-bis(methoxycarbonyl)phenol **58** to be formed while a neutral reaction mixture (7.45 < pH < 7.5) promoted the formation of **59.** Once the Michael addition was completed, pH was adjusted to 2.5 to precipitate compound **59** in a good yield of 58%. Then, compound **59** was put with hydrochloric acid and refluxed to obtain the first key intermediate **60** with an overall yield of 26% on a 10-gram scale.

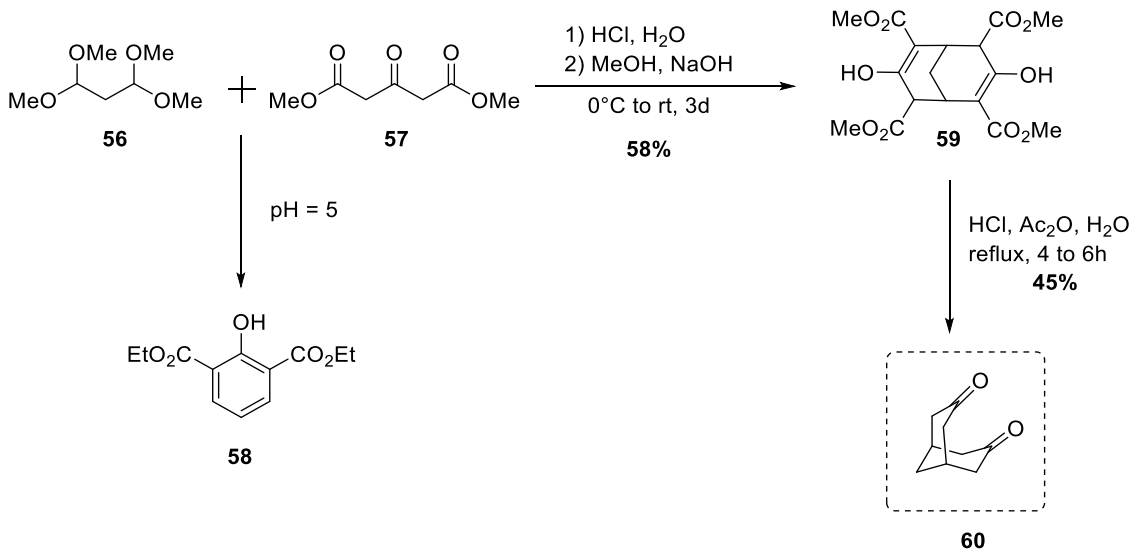

*Scheme 12: Synthesis of **60***

4.3.2. Synthesis of intermediate 65

The newly obtained diketone **60** was then, monoprotected as an acetal **61** in presence of boron trifluoride etherate and a large excess of ethylene glycol, the remaining ketone group was transformed into the corresponding vinyl triflate to obtain **62** in good yield (57% in two steps). To synthesise compound **61**, we performed a Suzuki-Miyaura coupling reaction between **62** and the 9-BBN borate prepared *in situ* through an addition of 9-BBN on tert-butyl 3-butenoate, the coupling reaction was catalysed with a catalytic amount of $Pd(dppf)Cl_2$ and performed in a mixture of THF and H_2O. A reduction of the synthesized ester **63** with $LiAlH_4$ in diethyl ether allowed us to obtain the corresponding alcohol **64**, then, the cyclic acetal was deprotected with PTSA in acetone to give compound **65** in 5 steps with an overall yield of 33% (Scheme 13).

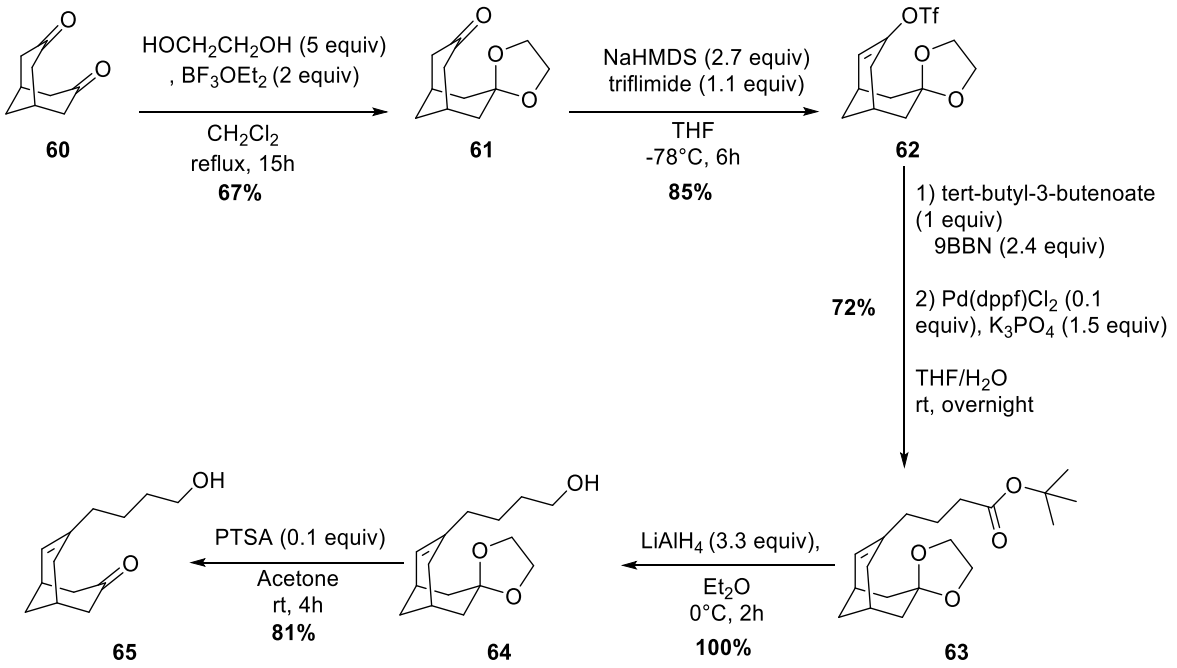

*Scheme 13: Synthesis of **65***

4.3.3. Synthesis of the huprine scaffold 67

Once we had compound **65** in hands, we were able to perform a Friedlander condensation with the 2-amino-4-chlorobenzonitrile **66** in presence of $AlCl_3$ in 1,2-dichloroethane to obtain the characteristic huprine scaffold **67** with a 40% yield.

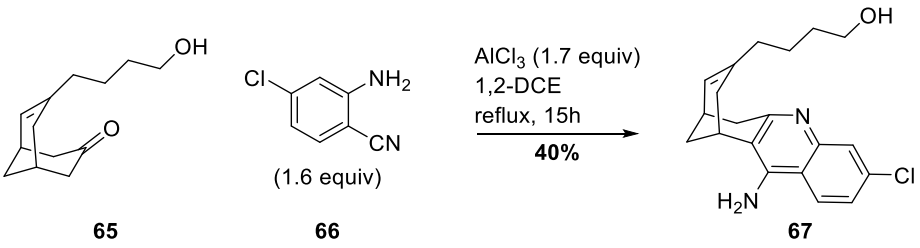

*Scheme 14: Synthesis of the huprine scaffold **67***

4.3.4. Final steps to obtain the azide 48

Once the newly obtained huprine scaffold's hydroxyl function was activated as a mesylate **68** with methanesulfonyl chloride and triethylamine in THF, we could perform a nucleophile substitution with sodium azide in DMF leading to the final azide **48** (Scheme 15). The huprine azide was obtained in 10 steps with an overall yield of 2% in a 600 mg scale.

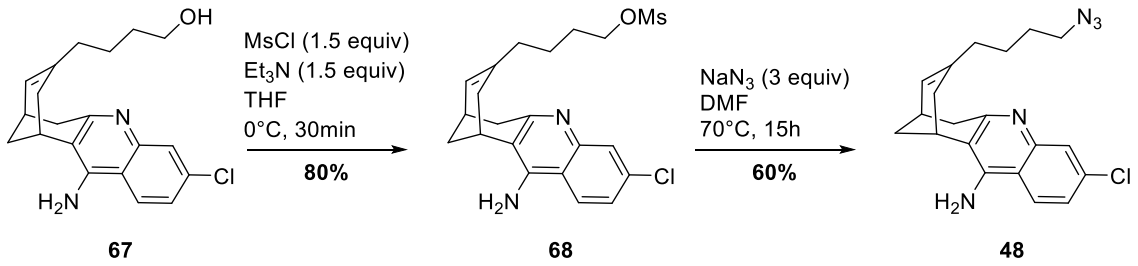

*Scheme 15: Synthesis of azide **48***

4.4. Coupling of the partners by CuAAC

The main step of this synthetic pathway consisted in associating the two partners, azide **48** and alkyne **49**, using a Copper(I) catalysed Huisgen cycloaddition to form a 1,2,3-triazole core (Scheme 16). We managed to obtain the protected compound **47** by performing the reaction with copper iodide in acetonitrile with an excellent yield of 71%.

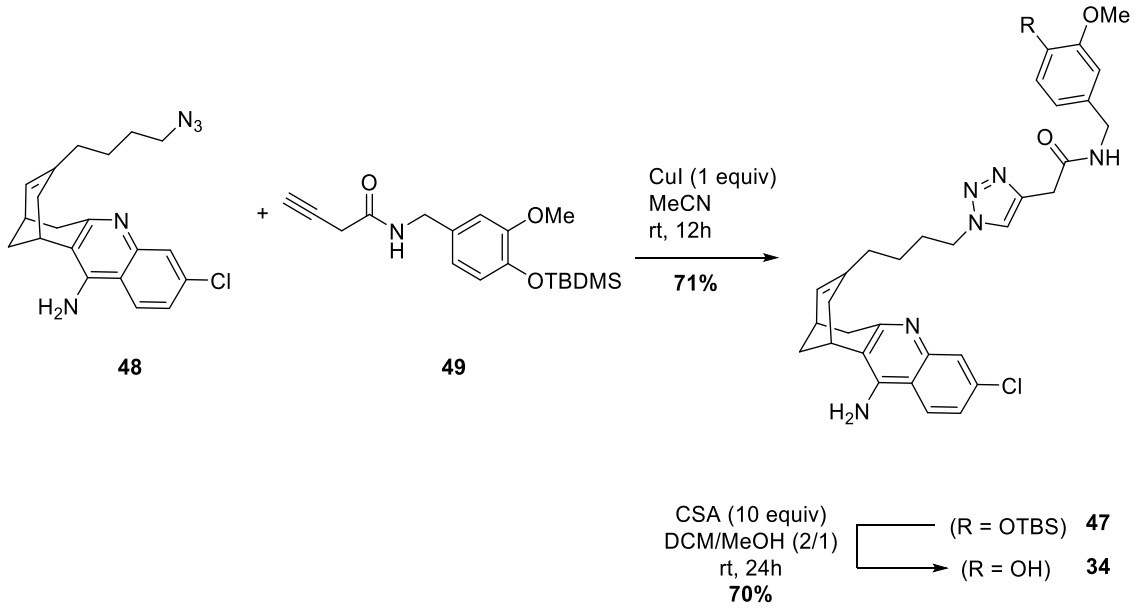

*Scheme 16: Synthesis of the MTDL **34***

The deprotection step had to be optimized compared to what had been done previously by Dr. Monika Bouet. Indeed, using a catalytic amount of CSA, as it was previously reported, was not effective enough to deprotect the hydroxyl group of **47** even after an extended time of reaction (more than 5 days). After several tests, we managed to deprotect **47** to obtain the final MTDL **34** with a good yield of 70% by using 10 equivalents of dried CSA.

Moreover, a final purification step by semi preparative RP-HPLC was required to obtain the pure MTDL (e.g. purity > 95%). The major issue was to understand the HPLC signals (Figure 73), we found out that signal (A) and (B) were given by the same compound **34** that seemed to take a protonated form in the TFA buffer we used for analytical HPLC.

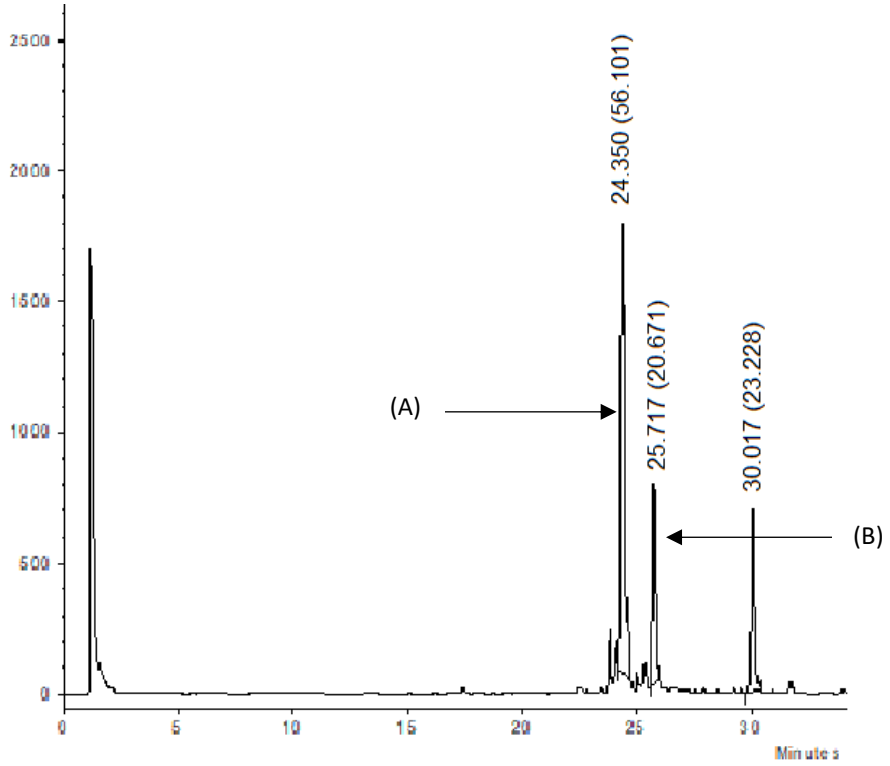

*Figure 73: **34** chromatogram with TFA buffer (analytic HPLC (Thermo Hypersil GOLD C_{18} column, 5 µm, 2.1 × 100 mm) with MeCN and TFA (aq. 0.1%; pH 2.0) as eluents [100% aq. TFA (5 min), then linear gradient from 0% to 100% (45 min) MeCN] at a flow rate of 0.25 mL.min^{-1}*

We thus managed to synthesize approximatively 150 mg of pure compound **34**, a new conjugated MTDL with a huprine pharmacophore and a capsaicin fragment, in 16 steps using a convergent pathway.

5. Biological evaluation

All 9 conjugated MTDLS (Figure 74) were tested for different biological activities:

- cholinesterases inhibition,
- BACE-1 inhibition,
- antioxidant properties,
- BBB permeability.

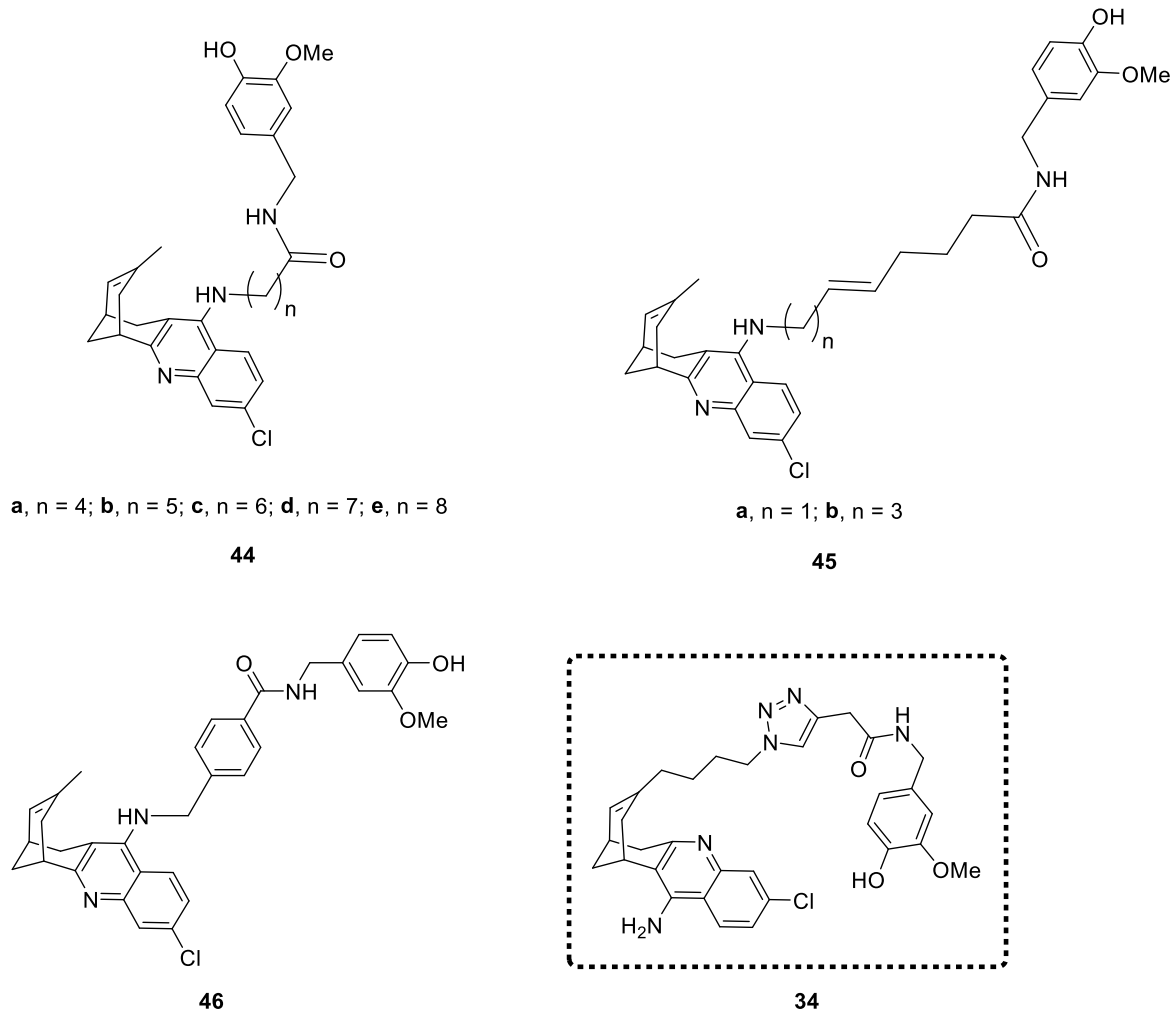

*Figure 74: Structures of the MTDLs **34**, **44a-e**, **45a-b** and **46** evaluated in vitro*

5.1. Cholinesterases inhibition

The inhibitory activities of the 9 conjugated MTDLs were evaluated on human AChE and BChE purified from human serum. Huprine Y results were extracted from the literature[230] (Table 2). IC_{50} on human cholinesterases was evaluated using the method of Ellman et *al*.[267].

As previously reported[268], capsaicin didn't show any inhibitory activity against AChE or BChE while huprine Y was a potent inhibitor of both cholinesterases with a high selectivity ratio of 169.2 in favour of AChE. The entire series displayed good inhibitory activities, especially compound **34** (entry 3), the only huprine-based hybrid functionalized in position 9 of the series, and **44c** (entry 6) functionalized in position 12. Moreover, compound **34** (entry 3) showed an interesting result, indeed this compound is

[267] Ellman, G. L.; Courtney, K. D.; Andres, V.; Featherstone, R. M. A New and Rapid Colorimetric Determination of Acetylcholinesterase Activity. *Biochem. Pharmacol.* **1961**, *7* (2), 88–95.

[268] Khorana, N.; Markmee, S.; Ingkaninan, K.; Ruchirawat, S.; Kitbunnadaj, R.; Pullagurla, M. R. Evaluation of a New Lead for Acetylcholinesterase Inhibition. *Med. Chem. Res.* **2008**, *18* (3), 231.

the only one of this series to present a similar inhibitory activity for both cholinesterases in the nanomolar range.

Entry	Compound	IC_{50} (nM) (*h*AChE)	IC_{50} (nM) (*h*BChE)	Selectivity ratio[b]
1	**Capsaicin**	>200 000	na[a]	/
2	**Huprine Y**	1.07 +/- 0.05	181 +/- 15	169.2
3	**34**	**1.06 +/- 0.26**	**7.3 +/- 0.6**	**6.9**
4	**44a**	5.48 +/- 0.28	52.2 +/- 1.3	9.5
5	**44b**	4.35 +/- 0.18	70.0 +/- 4.9	16.1
6	**44c**	**0.77 +- 0.06**	**30.6 +/-1.7**	**39.7**
7	**44d**	1.94 +/- 0.15	51.8 +/- 3.0	26.7
8	**44e**	2.94 +/- 0.16	36.1 +/- 2.2	12.3
9	**46**	24.9 +/- 1.9	290.+/- 19	11.6
10	**45a**	4.41 +/- 0.17	78.1 +/- 2.9	17.7
11	**45b**	5.64 +/- 0.30	53.1 +/- 2.4	9.4

[a] *not active*

[b] selectivity ration = IC_{50} hBChE/ IC_{50} hAChE

*Table 2: In vitro evaluation of **34**, **44a-e**, **45a-b** and **46** cholinesterases inhibition*

5.2. Other biological properties

Other properties of the conjugated MTDLs, capsaicin and huprine Y were assessed and reported in Table 3.

Entry	Compound	% inhibition (*h*BACE-1)	IC_{50} (μM) (DPPH)	P_e (10^{-6} cm s^{-1})
1	**Capsaicin**	na[a]	50.3 +/- 8.3	10.3 +/- 1.2 (CNS+)
2	**Huprine Y**	na[a]	nd[b]	23.8 +/- 2.7 (CNS+)
3	**34**	**na[a]**	**92.0 +/- 12.4**	**8.8 +/- 1.3 (CNS+)**
4	**44a**	55.6	68.5 +/- 8.2	11.5 +/- 1.1 (CNS+)
5	**44b**	34.3	62.6 +/- 11.6	14.9 +/- 1.2 (CNS+)
6	**44c**	**10.6**	**55.4 +/- 2.3**	**17.2 +/- 1.0 (CNS+)**
7	**44d**	3.6	70.8 +/- 20.8	20.1 +/- 1.1 (CNS+)
8	**44e**	23.7	64.6 +/- 8.6	21.8 +/- 1.3 (CNS+)
9	**46**	na	71.4 +/- 15.5	14.3 +/- 0.3 (CNS+)
10	**45a**	na	31.7 +/- 8.7	16.8 +/- 0.1 (CNS+)
11	**45b**	21.6	54.6 +/- 12.5	22.3 +/- 1.1 (CNS+)

[a] *not active*
[b] not determined

*Table 3: Other biological properties of **34**, **44a-e**, **45a-b** and **46***

5.2.1. BACE-1 inhibition

The percentage of BACE-1 inhibition was evaluated using a peptide mimicking APP sequence as substrate and fluorescence intensities with and without the inhibitor were compared to calculate the percentage of inhibition. Only 6 compounds showed inhibiting properties against BACE-1 with values from 3.6 for **44d** (entry 7) for the least potent to 55.6 for **44a** (entry 4) for the more active. Unfortunately, the main compounds of interest **34** didn't express an inhibitor character against BACE-1 (entry 3).

5.2.2. DPPH inhibition

Radical scavenging activities of the huprine-capsaicin hybrids were determined by DPPH assay[269], an assay based on electron-transfer. Indeed, if free radicals are scavenged by the tested compounds, the stable free radical DPPH will turn from purple to yellow (Scheme 17).

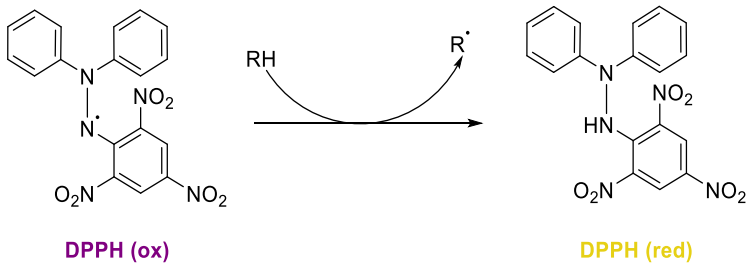

Scheme 17: Principle of DPPH scavenging capacity assay[270]

All compounds retained antioxidant properties from the parent compound capsaicin, nevertheless compound **34** proved slightly less active, (higher IC_{50} against DPPH) bringing to light that adding a triazole ring was disadvantageous for the antioxidant properties of the hybrid (entry 3).

5.2.3. BBB penetration

Finally, to determine the hybrids brain penetration, the parallel artificial membrane permeation for BBB developed by Di et *al.*[271] was used and lipid extract of porcine brain membrane was employed to

[269] Brand-Williams, W.; Cuvelier, M. E.; Berset, C. Use of a Free Radical Method to Evaluate Antioxidant Activity. *LWT - Food Sci. Technol.* **1995**, *28* (1), 25–30.
[270] Teixeira, J.; Gaspar, A.; Garrido, E. M.; Garrido, J.; Borges, F. Hydroxycinnamic Acid Antioxidants: An Electrochemical Overview. *BioMed Res. Int.* **2013**, *2013*, 1–11.
[271] Di, L.; Kerns, E. H.; Fan, K.; McConnell, O. J.; Carter, G. T. High Throughput Artificial Membrane Permeability Assay for Blood-Brain Barrier. *Eur. J. Med. Chem.* **2003**, *38* (3), 223–232.

perform *in vitro* permeability assays. All compounds were found CNS+ which suggests that they would be able to cross the BBB and reach the chosen therapeutic targets. It was also observed that increasing the linker's length enhanced the values, suggesting that increasing lipophilicity improved BBB crossing. This hypothesis was supported by the results obtained for compound **34** (entry 3), indeed, **34** was designed with a triazole core increasing the compound's hydrophilicity and seemed to be the least suited to cross the BBB.

6. Crystal structure with cholinesterases

34 crystallographic structures with *Tc*AChE and *h*BChE were solved, data were collected from crystal soaked for 12h in mother liquor solution with a 10 mM solution of **34.** Main interactions with the compound and cholinesterases are reported in Table 4.

Entry	**Type of interaction**	**Huprine Y moiety**		**Compound 34**	
		***Tc*AChE**	***h*BChE**	***Tc*AChE**	***h*BChE**
1	Hydrophobic interactions	Trp84 Phe330 Trp432 Ile439 Tyr442	Trp82 Phe329 Trp231 Ala328 Phe398	Phe330 Tyr334 Trp432 Met437	Tyr334
2	Parallel π-stacking	Trp84 Phe330		Trp84	
3	Perpendicular π-stacking		Trp82 Phe290	Phe290	Phe329 Trp231
4	H-Bond	His440	His440 Ser198	Phe288 Ser286 Tyr121 Tyr70	Asp70 Asn68

*Table 4: Interactions of Huprine and **34** with the cholinesterases main residues*

6.1. Crystal structure with *Tc*AChE

Crystal structure of *Tc*AChE in complex with **34** with (Figure 75) revealed that the MTDL's huprine moiety binds at the bottom of the enzyme, in the active site in a similar manner as the parent compound Huprine Y. π-stacking was observed between the aromatic system and Trp84, while the chlorine atom showed its importance by fitting in a hydrophobic cavity brought by Phe330, Tyr334, Trp432, Met437, and Ile439. Moreover, the triazole nitrogen was involved in a perpendicular π-stacking with Phe290 and a H-bond interaction with Phe288. Another H-bond interaction was displayed between the amide nitrogen atom of **34** and Ser286. Finally, the capsaicin moiety also interacted with the enzyme through the formation of a water bridge between its ether oxygen and Tyr121.

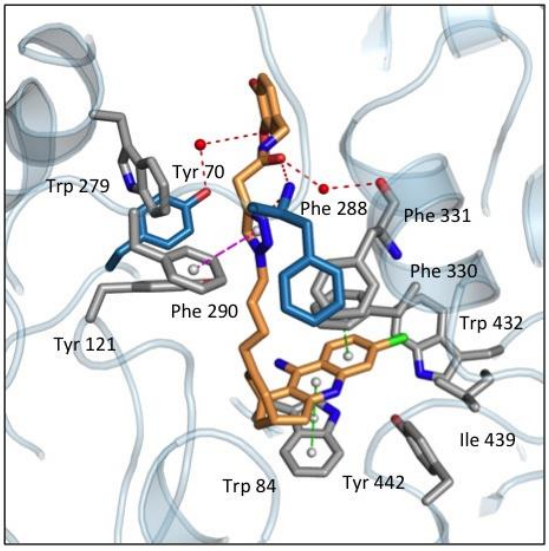

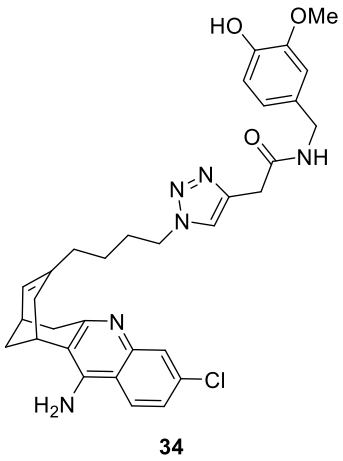

34

*Figure 75: Crystal structure of **34**-TcAChE*

6.2. Crystal structure with *h*BChE

A crystal structure of **34** with *h*BChE was also determined (Figure 76) and the chlorine of **34** was found in the active pocket of BChE at 4 Å from Leu286 and 4.1 Å from Trp231, this position lead to a π-stacking with Phe329. Moreover, the free aniline moiety of **34** in position 12 was positioned between Ser198 and His448 which effectively disrupted the catalytic triad. While the cyclohexene of **34** π-stacked with Trp84, the triazole ring interacted in the same way with Tyr334 but also did H-bonds with Asp70. Finally, the capsaicin moiety interacted through the formation of an H-bond with Asn68.

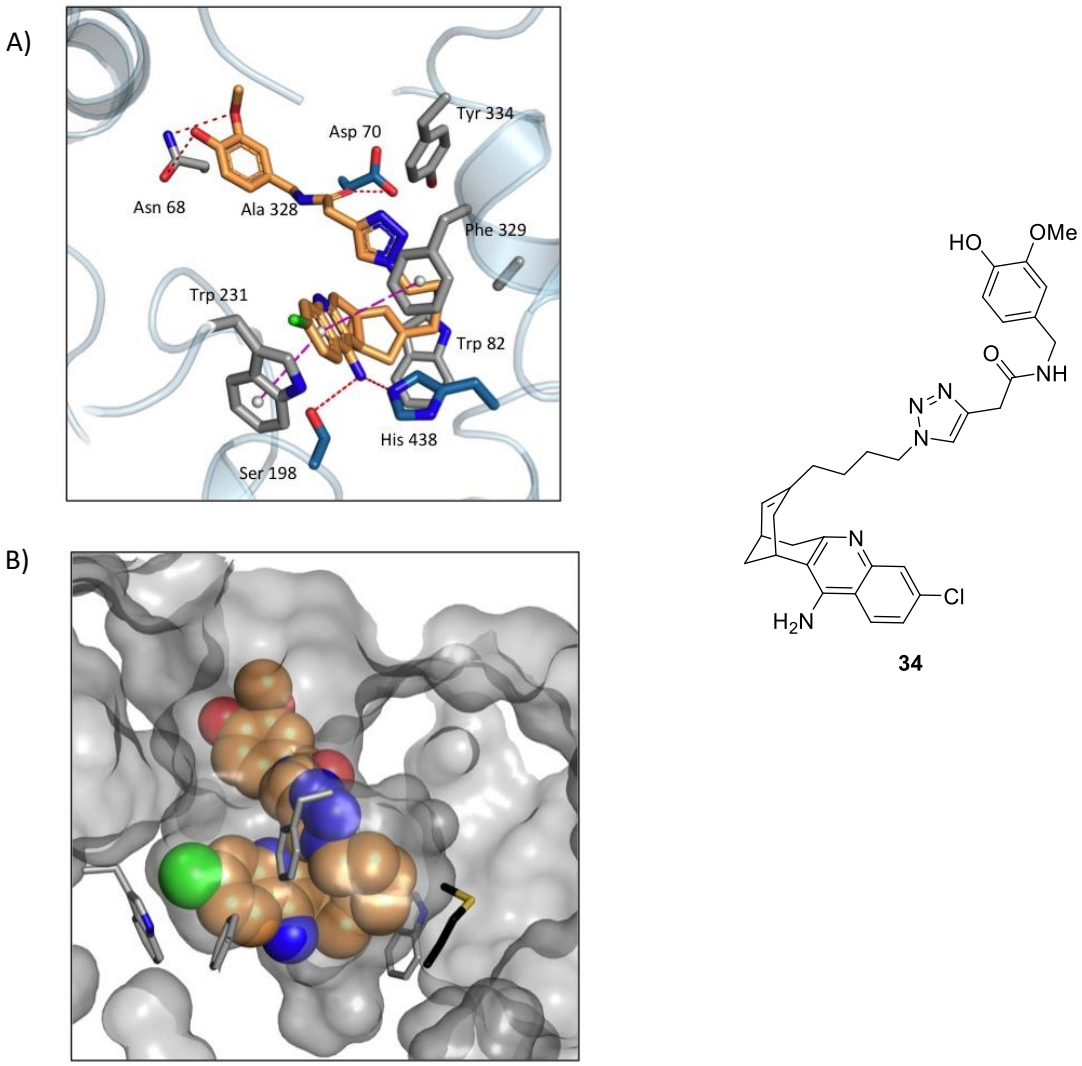

*Figure 76: (A) Crystal structure of **34** with hBChE (B) Surface representation of **34** inside the BChE active site*

7. Conclusion

In collaboration with the Professor Muñoz-Torrero's team, a new series of 9 conjugated MTDLs linking a potent AChE inhibitor and an antioxidant has been designed and biologically evaluated *in vitro.* The lead compound **34** presented interesting inhibitory activities towards cholinesterases in the nanomolar scale and moderated antioxidant properties. Our collaborators (Dr Jacques-Philippe Colletier and Dr. Nicolas Coquelle, IBS, Grenoble) were able to resolve the crystal structure of *Tc*AChE et *h*BChE in complex with compound **34** which enlightened us about the ligand activity toward BChE, indeed, it was reported that the aniline in position 12 of the ligand was capable to go inside the acyl pocket and disrupt the catalytic triad.

As part of my thesis, I managed to optimize some of the steps such as the deprotection of **47** and the purification method to give pure **34**, and the last step giving the key alkyne **49** of the synthetic pathway and synthesize compound **34** in a larger scale in 16 steps with an overall yield of 1% in prevision of *in* vivo studies leading to a publication. 150 mg of compound 34 have been sent to Pr. Inestrosa's team for in vivo evaluations. The evaluations will be performed on two types of AβPPswe/PS-1 double transgenic mice's group which express the mutant APPswe (K595N/M596L) and PSEN1ΔE9, one of young mice (5 month-old) and another set of old mice (10 month-old). Locomotor and stress behaviour (Large open-field (LOF) test), novel object recognition (NOR) and novel object localization (NOL), memory flexibility will be evaluated and the concentrations of Aβ will be determined.

Chapter II: Development of combined MTDLs based on the Rivastigmine scaffold

1. Aim of the project

In this second project, granted by the experience and expertise we gathered in the field of complex linker conjugated MTLDs synthesis, we decided to tackle the challenge of the development of new series of smaller combined MTDLs, more likely to reach all the required drugability parameters. In order to reach this goal, the strategy was based on the use of two known pharmacophores bearing a common moiety to obtain such combined MTDLs (Figure 77).

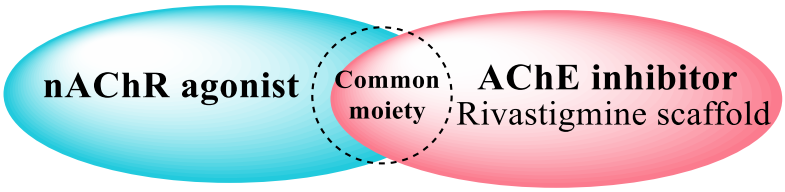

Figure 77: Structure of the MTDLs series

The main advantages of this type of combined MTDL ligands are:

- the small molecular weights respecting the Lipinski's rules of five[272],
- a good CNS MPO score[273,274],
- a lower structural complexity and an easier synthesis.

Indeed, one of our goals was to develop a shorter and high yielding synthetic pathway as compared to the synthetic efforts required for the access to linker conjugated MTDLs we previously designed in the team. The synthesis of this type of combined ligands was a new project I was assigned to tackle in Professor Renard's team. Considering Pr. Renard's team expertise in the development of AChE inhibitors, and the pivotal role of this enzyme inhibition to minimize AD impacts, we designed our new series with a pharmacophore offering this property. In collaboration with Pr. Routier's team in ICOA Orléans, who has a long expertise in the development of nAChR agonists, considering their proven efficacy to counteract CNS related disorders, we selected an α7 nAChR agonist as second pharmacophore.

---

[272] Lipinski, C. A.; Lombardo, F.; Dominy, B. W.; Feeney, P. J. Experimental and Computational Approaches to Estimate Solubility and Permeability in Drug Discovery and Development Settings1PII of Original Article: S0169-409X(96)00423-1. The Article Was Originally Published in Advanced Drug Delivery Reviews 23 (1997) 3–25.1. *Adv. Drug Deliv. Rev.* **2001**, *46* (1), 3–26.

[273] Wager, T. T.; Hou, X.; Verhoest, P. R.; Villalobos, A. Central Nervous System Multiparameter Optimization Desirability: Application in Drug Discovery. *ACS Chem. Neurosci.* **2016**, *7* (6), 767–775.

[274] Wager, T. T.; Hou, X.; Verhoest, P. R.; Villalobos, A. Moving beyond Rules: The Development of a Central Nervous System Multiparameter Optimization (CNS MPO) Approach To Enable Alignment of Druglike Properties. *ACS Chem. Neurosci.* **2010**, *1* (6), 435–449.

2. Nicotinic receptor

2.1. Overall structure

nAChR are integral allosteric membrane proteins of 290 kDa made up of five subunits (identical or homologous) arranged symmetrically around an ionic channel[275], in the context of my PhD and for the sake of clarity, only α7 nAChR's structure will be discussed, since this family of nAChR was chosen as a target for the second pharmacophore. Early electron microscopy observation of fish electric organ nAChR showed that the nAChR pentamer is a cylinder of 8 nm diameter and 16 nm length[276]. Even though no human α7 nAChR structure has been solved to date, the X-ray crystallography of AChBP structure gave a viable template of human nAChR[277] (Figure 78). Indeed, AChBP, a soluble protein discovered in the freshwater snail *Lymnaea stagnalis*[278], displays a high degree of conservation of amino acids present at the binding site[279], despites a lower overall sequence identity with nAChRs (around 30%)[280]. AChBP crystal structure shows that AChBP subunits are folded as β-sandwiches constituted by a 6-strand inner sheet and a 4-strand outer sheet connected by a conserved loop that includes two bridged cysteines, also found in all animal nAChRs[281]. Moreover, every AChBP molecule possesses 5 nicotinic ligand binding sites located between the subunits.

[275] Hucho, F.; Changeux, J. P. Molecular Weight and Quaternary Structure of the Cholinergic Receptor Protein Extracted by Detergents from Electrophorus Electricus Electric Tissue. *FEBS Lett.* **1973**, *38* (1), 11–15.
[276] Cartaud, J.; Benedetti, E. L.; Cohen, J. B.; Meunier, J. C.; Changeux, J. P. Presence of a Lattice Structure in Membrane Fragments Rich in Nicotinic Receptor Protein from the Electric Organ of Torpedo Marmorata. *FEBS Lett.* **1973**, *33* (1), 109–113.
[277] Dellisanti, C. D.; Yao, Y.; Stroud, J. C.; Wang, Z.-Z.; Chen, L. Crystal Structure of the Extracellular Domain of NAChR Alpha1 Bound to Alpha-Bungarotoxin at 1.94 A Resolution. *Nat. Neurosci.* **2007**, *10* (8), 953–962.
[278] Smit, A. B.; Syed, N. I.; Schaap, D.; van Minnen, J.; Klumperman, J.; Kits, K. S.; Lodder, H.; van der Schors, R. C.; van Elk, R.; Sorgedrager, B.; Brejc, K.; Sixma, T. K.; Geraerts, W. P. A Glia-Derived Acetylcholine-Binding Protein That Modulates Synaptic Transmission. *Nature* **2001**, *411* (6835), 261–268.
[279] Shahsavar, A.; Gajhede, M.; Kastrup, J. S.; Balle, T. Structural Studies of Nicotinic Acetylcholine Receptors: Using Acetylcholine-Binding Protein as a Structural Surrogate. *Basic Clin. Pharmacol. Toxicol.* **2016**, *118* (6), 399–407.
[280] Hansen, S. B.; Talley, T. T.; Radic, Z.; Taylor, P. Structural and Ligand Recognition Characteristics of an Acetylcholine-Binding Protein from Aplysia Californica. *J. Biol. Chem.* **2004**, *279* (23), 24197–24202.
[281] Tasneem, A.; Iyer, L. M.; Jakobsson, E.; Aravind, L. Identification of the Prokaryotic Ligand-Gated Ion Channels and Their Implications for the Mechanisms and Origins of Animal Cys-Loop Ion Channels. *Genome Biol.* **2005**, *6* (1), R4.

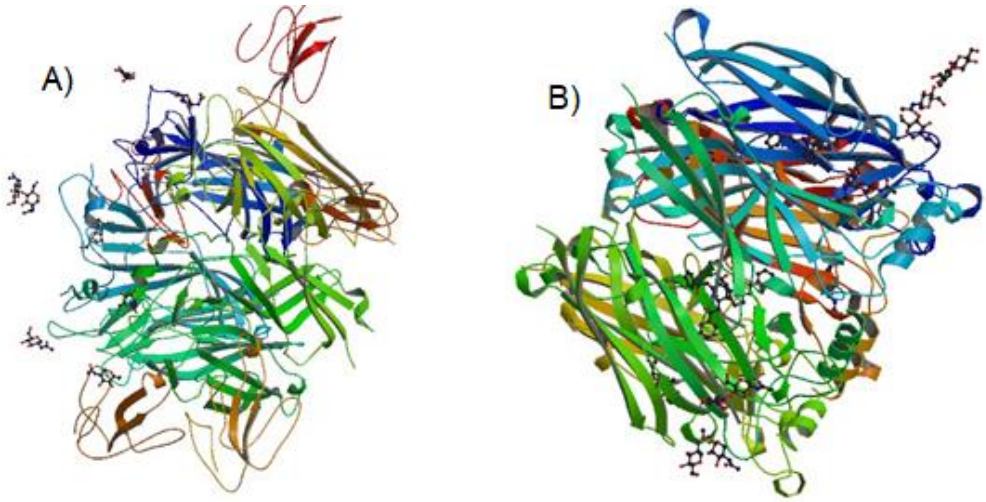

Figure 78: (A) α7 nAChR chimera in complex with alpha bungarotoxin (PDB 4HQP)[282] and (B) α7 AChBP in complex with Iobeline (PDB 5AFH)[283]

2.2. Binding sites

2.2.1. Orthosteric binding site

The site used to bind ACh and nicotine is an orthosteric binding site found in the extracellular domain between the receptor subunits and is composed of identical α-type subunits[284] (Figure 79).

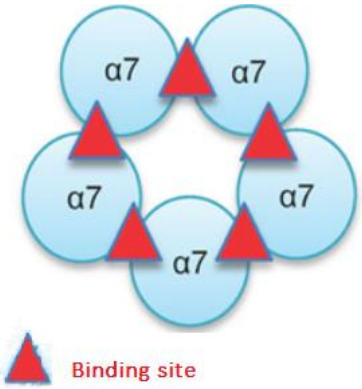

Figure 79: Schematic representation of an α7 nAChR[285]

[282] Li, S. X.; Cheng, K.; Gomoto, R.; Bren, N.; Huang, S.; Sine, S.; Chen, L. Structural Principles for Alpha-Neurotoxin Binding to and Selectivity among Nicotinic Receptors. *BE Publ.*

[283] Spurny, R.; Debaveye, S.; Farinha, A.; Veys, K.; Vos, A. M.; Gossas, T.; Atack, J.; Bertrand, S.; Bertrand, D.; Danielson, U. H.; Tresadern, G.; Ulens, C. Molecular Blueprint of Allosteric Binding Sites in a Homologue of the Agonist-Binding Domain of the Alpha7 Nicotinic Acetylcholine Receptor. *Proc.Natl.Acad.Sci.USA* **2015**, *112*, E2543.

[284] Corringer, P.-J.; Galzi, J.-L.; Eiselé, J.-L.; Bertrand, S.; Changeux, J.-P.; Bertrand, D. Identification of a New Component of the Agonist Binding Site of the Nicotinic 7 Homooligomeric Receptor. *J. Biol. Chem.* **1995**, *270* (20), 11749–11752.

[285] Hendrickson, L. M.; Guildford, M. J.; Tapper, A. R. Neuronal Nicotinic Acetylcholine Receptors: Common Molecular Substrates of Nicotine and Alcohol Dependence. *Front. Psychiatry* **2013**, *4*.

It has been described as a series of "loops" bordering the binding site that could be divided in two groups: loops A, B and C from the principal component and loops D, E and F from the complementary component. Because α7 nAChRs are homopentamers, their binding sites are identical and made up of aromatic residues such as Tyr97, Tyr157, Tyr196, Tyr203, Trp155 and Trp57, bridged cysteines Cys198 and Cys199 and a disulphide bridge[286]. This last moiety gives to the binding site an electronegative character neutralizing the positive charges carried by most of the nicotinic ligands[287]. Moreover, a cation-π interaction between the ACh's ammonium centre and Trp155 was proven to be involved in ACh binding to the receptors[288]. Indeed, the ammonium is placed in the centre of an "aromatic box" composed of most of the aromatic residues (Figure 80).

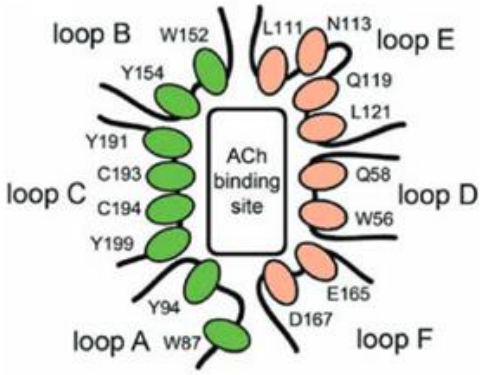

Figure 80: Schematic representation of ACh binding site of AChBP[286]

2.2.2. Ion channel binding site

Channel blockers constitute an important category of nicotinic drugs exerting valuable therapeutic actions, they bind to the transmembrane domain of nAChRs and prevent ion flux by sterically occluding the channel pore[289]. Determined high-resolution X-ray structures of nAChRs[290] have confirmed that the channel blocker binding sites are found in the transmembrane channel which is made up of stacked pentameric rings of homologous aminoacids. A well-known example of channel blocker is

[286] Charon, A. T. and S. α7 Nicotinic Acetylcholine Receptors: A Therapeutic Target in the Structure Era http://www.eurekaselect.com/97180/article.

[287] Dennis, M.; Giraudat, J.; Kotzyba-Hibert, F.; Goeldner, M.; Hirth, C.; Chang, J. Y.; Lazure, C.; Chrétien, M.; Changeux, J. P. Amino Acids of the Torpedo Marmorata Acetylcholine Receptor Alpha Subunit Labeled by a Photoaffinity Ligand for the Acetylcholine Binding Site. *Biochemistry* **1988**, *27* (7), 2346–2357.

[288] Dougherty, D. A.; Stauffer, D. A. Acetylcholine Binding by a Synthetic Receptor: Implications for Biological Recognition. *Science* **1990**, *250* (4987), 1558–1560.

[289] Cecchini, M.; Changeux, J.-P. The Nicotinic Acetylcholine Receptor and Its Prokaryotic Homologues: Structure, Conformational Transitions & Allosteric Modulation. *Neuropharmacology* **2015**, *96*, 137–149.

[290] Giraudat, J.; Dennis, M.; Heidmann, T.; Chang, J. Y.; Changeux, J. P. Structure of the High-Affinity Binding Site for Noncompetitive Blockers of the Acetylcholine Receptor: Serine-262 of the Delta Subunit Is Labeled by [3H]Chlorpromazine. *Proc. Natl. Acad. Sci.* **1986**, *83* (8), 2719–2723.

mecamylamine (Figure 81), a non-competitive nAChR antagonist developed by AstraZeneca to tackle addiction, mood disorders, cognitive impairment and attention deficit hyperactivity disorder[291].

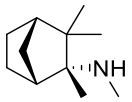

mecamylamine

Figure 81: Structure of mecamylamine, a channel blocker

2.2.3. Allosteric character of nAChRs[292]

2.2.3.1. Allosteric binding sites

nAChRs are the first chemically identified neurotransmitter receptor, ion channel and ligand-gated ion channel, their mode of action has the characteristics of an allosteric mechanism[293] : even without an agonist, the protein undergoes reversible transitions, involving at least two states[294], and a conformational selection between these states takes place when the receptor is in presence of an agonist. The allosteric nature of nAChRs induces structural reorganization altering the shape of various ligand binding pockets, including the ACh binding site. These modulatory sites, with positive or negative effects on the signal transduction mechanism, are found in every domain of the nAChRs.
In 1992, Mulle et *al.*[295] discovered that Ca^{2+} ions were the first positive allosteric modulator (PAM) recognised with α7 nAChR at the level of sites located in the extracellular domain, at the subunit interfaces, below the orthosteric ACh site, near the transmembrane domain. Moreover, other allosteric modulatory sites have been discovered in the transmembrane domain which accommodates pharmacological agents regulating the receptor activity. Finally, allosteric sites have also been found in the intracellular domain and these binding sites might be pivotal sites for the stabilisation and

[291] Nickell, J. R.; Grinevich, V. P.; Siripurapu, K. B.; Smith, A. M.; Dwoskin, L. P. Potential Therapeutic Uses of Mecamylamine and Its Stereoisomers. *Pharmacol. Biochem. Behav.* **2013**, *108*, 28–43.
[292] Changeux, J.-P. The Nicotinic Acetylcholine Receptor: A Typical 'Allosteric Machine.' *Philos. Trans. R. Soc. B Biol. Sci.* **2018**, *373* (1749), 20170174.
[293] Monod, J.; Wyman, J.; Changeux, J.-P. On the Nature of Allosteric Transitions: A Plausible Model. *J. Mol. Biol.* **1965**, *12* (1), 88–118.
[294] Changeux, J.-P.; Taly, A. Nicotinic Receptors, Allosteric Proteins and Medicine. *Trends Mol. Med.* **2008**, *14* (3), 93–102.
[295] Mulle, C.; Léna, C.; Changeux, J.-P. Potentiation of Nicotinic Receptor Response by External Calcium in Rat Central Neurons. *Neuron* **1992**, *8* (5), 937–945.

modulation of the receptor functions, particularly when interacting with G-proteins and, hence, G-protein-coupled receptors[296] (Figure 82).

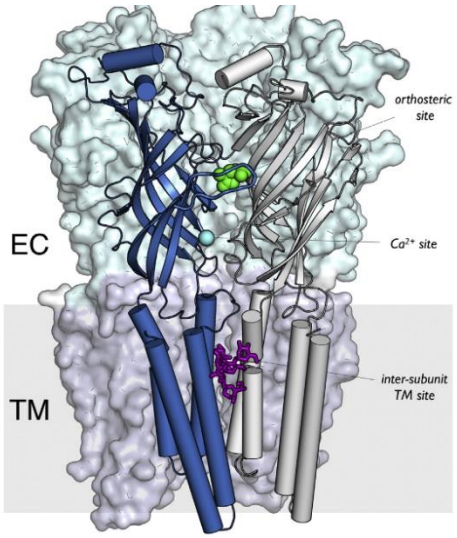

Figure 82: Ligand-binding sites in nAChRs[289] (EC = extracellular domain; TM= transmembrane domain)

2.2.3.2. Modulation of α7 nAChRs

When the receptor is in presence of high concentrations of neurotransmitters, it undergoes conformational transitions known as the gating isomerisation or active state, in this state, the α7 nAChR is highly permeable to Ca^{2+}. After responding to their agonists, the receptors' actions are terminated either by the removal of the ligand leading to a resting state in which the ion gate is closed or by a fast desensitization[297] in which the orthosteric site is still occupied by the neurotransmitter, but the ion channel is closed. In order to be able to interact again with other neurotransmitter, the receptor must transit to a resting state in which the orthosteric binding site is empty (Figure 83).

[296] Kabbani, N.; Woll, M. P.; Levenson, R.; Lindstrom, J. M.; Changeux, J.-P. Intracellular Complexes of the 2 Subunit of the Nicotinic Acetylcholine Receptor in Brain Identified by Proteomics. *Proc. Natl. Acad. Sci.* **2007**, *104* (51), 20570–20575.

[297] Corradi, J.; Bouzat, C. Understanding the Bases of Function and Modulation of 7 Nicotinic Receptors: Implications for Drug Discovery. *Mol. Pharmacol.* **2016**, *90* (3), 288–299.

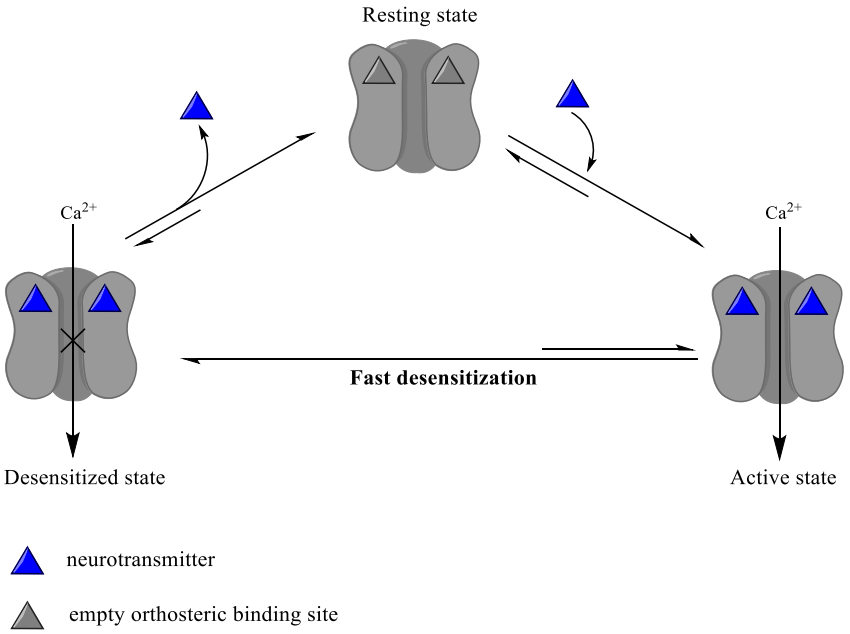

Figure 83: Schematic representation of α7 nAChR modulation mechanism (adapted from Basak et al.[298])

2.2.3.3. nAChRs allosteric modulators

Various α7 nAChRs PAM have been designed in order to potentiate α7 nAChRs ion channel opening and thus current in presence of ACh and they can be divided in two types:

- type I PAM which mainly enhance agonist-evoked peak current without delaying desensitisation and without reactivating properties toward the receptor (Figure 84),
- type II PAM able to delay desensitisation and reactivate desensitized receptors (Figure 85).

AVL-3288 is a type I α7 nAChRs PAM currently in phase I clinical trial for schizophrenia and schizoaffective disorder[299]. Studies in rodent models have shown that this promising compound was able to correct sensory deficits and improve cognition with or without the presence of an agonist[300].

[298] Basak, S.; Schmandt, N.; Gicheru, Y.; Chakrapani, S. Crystal Structure and Dynamics of a Lipid-Induced Potential Desensitized-State of a Pentameric Ligand-Gated Channel. *eLife* **2017**, *6*.
[299] Gee, K. W.; Olincy, A.; Kanner, R.; Johnson, L.; Hogenkamp, D.; Harris, J.; Tran, M.; Edmonds, S. A.; Sauer, W.; Yoshimura, R.; Johnstone, T.; Freedman, R. First in Human Trial of a Type I Positive Allosteric Modulator of Alpha7-Nicotinic Acetylcholine Receptors: Pharmacokinetics, Safety, and Evidence for Neurocognitive Effect of AVL-3288. *J. Psychopharmacol. (Oxf.)* **2017**, *31* (4), 434–441.
[300] Ng, H. J.; Whittemore, E. R.; Tran, M. B.; Hogenkamp, D. J.; Broide, R. S.; Johnstone, T. B.; Zheng, L.; Stevens, K. E.; Gee, K. W. Nootropic 7 Nicotinic Receptor Allosteric Modulator Derived from GABAA Receptor Modulators. *Proc. Natl. Acad. Sci.* **2007**, *104* (19), 8059–8064.

NS1738 designed by NeuroSearch and LY2087101[301] developed by Eli Lilly are also type I α7 nAChRs PAM, NS1738 was proven to increase the peak amplitude of ACh-evoked currents[302].

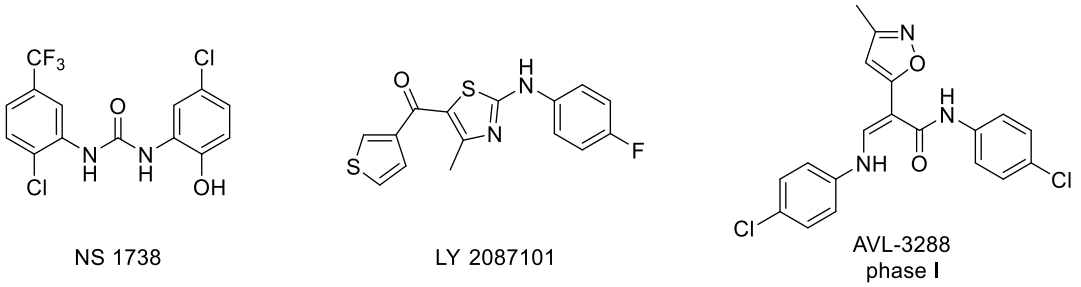

Figure 84: Examples of type I α7 nAChRs PAM

The first designed selective type II α7 nAChRs PAM was PNU-120596 developed by Pfizer. This compound displayed the capacity to potentiate the α7 nAChR peak current and to delay sensitization of α7 nAChRs[303]. Despite the fact that PNU-120596 was able to increase the precognitive effects of AChEI in rodent and non-human primates, it was not advance in clinical trials due to its high toxicity induced by an excessively high calcium influx[304]. Concerning A-867744 developed by AbbVie[305] and TQS[306], they both displayed α7 potentiation effects *in vitro* and precognition effects *in vivo*.

[301] Broad, L. M.; Zwart, R.; Pearson, K. H.; Lee, M.; Wallace, L.; McPhie, G. I.; Emkey, R.; Hollinshead, S. P.; Dell, C. P.; Baker, S. R.; Sher, E. Identification and Pharmacological Profile of a New Class of Selective Nicotinic Acetylcholine Receptor Potentiators. *J. Pharmacol. Exp. Ther.* **2006**, *318* (3), 1108–1117.

[302] Timmermann, D. B.; Grønlien, J. H.; Kohlhaas, K. L.; Nielsen, E. Ø.; Dam, E.; Jørgensen, T. D.; Ahring, P. K.; Peters, D.; Holst, D.; Chrsitensen, J. K.; Malysz, J.; Briggs, C. A.; Gopalakrishnan, M.; Olsen, G. M. An Allosteric Modulator of the A7 Nicotinic Acetylcholine Receptor Possessing Cognition-Enhancing Properties in Vivo. *J. Pharmacol. Exp. Ther.* **2007**, *323* (1), 294–307.

[303] Hurst, R. S.; Hajós, M.; Raggenbass, M.; Wall, T. M.; Higdon, N. R.; Lawson, J. A.; Rutherford-Root, K. L.; Berkenpas, M. B.; Hoffmann, W. E.; Piotrowski, D. W.; Groppi, V. E.; Allaman, G.; Ogier, R.; Bertrand, S.; Bertrand, D.; Arneric, S. P. A Novel Positive Allosteric Modulator of the A7 Neuronal Nicotinic Acetylcholine Receptor: In Vitro and In Vivo Characterization. *J. Neurosci.* **2005**, *25* (17), 4396–4405.

[304] Callahan, P. M.; Hutchings, E. J.; Kille, N. J.; Chapman, J. M.; Terry, A. V. Positive Allosteric Modulator of Alpha 7 Nicotinic-Acetylcholine Receptors, PNU-120596 Augments the Effects of Donepezil on Learning and Memory in Aged Rodents and Non-Human Primates. *Neuropharmacology* **2013**, *67*, 201–212.

[305] Malysz, J.; Grønlien, J. H.; Anderson, D. J.; Håkerud, M.; Thorin-Hagene, K.; Ween, H.; Wetterstrand, C.; Briggs, C. A.; Faghih, R.; Bunnelle, W. H.; Gopalakrishnan, M. In Vitro Pharmacological Characterization of a Novel Allosteric Modulator of A7 Neuronal Acetylcholine Receptor, 4-(5-(4-Chlorophenyl)-2-Methyl-3-Propionyl-1 *H* -Pyrrol-1-Yl)Benzenesulfonamide (A-867744), Exhibiting Unique Pharmacological Profile. *J. Pharmacol. Exp. Ther.* **2009**, *330* (1), 257–267.

[306] Dinklo, T.; Shaban, H.; Thuring, J. W.; Lavreysen, H.; Stevens, K. E.; Zheng, L.; Mackie, C.; Grantham, C.; Vandenberk, I.; Meulders, G.; Peeters, L.; Verachtert, H.; De Prins, E.; Lesage, A. S. J. Characterization of 2-[[4-Fluoro-3-(Trifluoromethyl)Phenyl]Amino]-4-(4-Pyridinyl)-5-Thiazolemethanol (JNJ-1930942), a Novel Positive Allosteric Modulator of the α 7 Nicotinic Acetylcholine Receptor. *J. Pharmacol. Exp. Ther.* **2011**, *336* (2), 560–574.

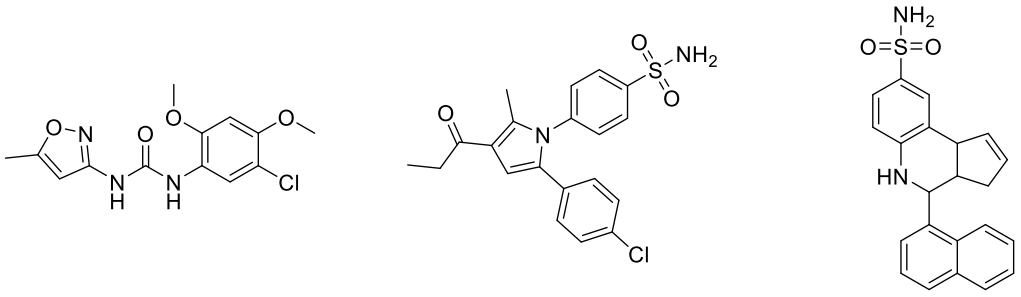

Figure 85: Examples of type II α7 nAChRs PAM

As a conclusion, α7 nAChRs agonists and PAMs appear to be a viable therapeutic strategy against CNS-related pathologies, nevertheless, their mode of action, binding sites and overall structures are diverse, SAR studies failed to lead to a rationalization of the pharmacophores structural requirements, and the complexity of the nAChRs structure and their allosteric character thus significantly complicate the drug design. Indeed, the structure reorganization and the fact that no human nAChR crystal structure has been determined yet must be considered during the development of drugs targeting nAChRs.

3. Chosen structures

3.1. α7 nAChRs agonists

Our first choice was to develop combined MTDL including an α7 nAChRs agonist scaffold. We designed our MTDLs with the help of our collaborators in the ICOA (Orléans). Indeed, Professor Routier's team has a large expertise in the development of α7 nAChRs especially compounds displaying a quinuclidine fragment and a triazole core. Moreover, they developed a library of compounds able to bind to α7 nAChRs bearing either a tropane, a quinazoline or a quinuclidine moiety[307]. They also put their efforts in the development of another α7 nAChRs agonists series with a 1,2,3-triazole core which is a well-known amide bond bioisoster and they were able to synthesize 30 new compounds bearing this core and a quinuclidine fragment. SAR studies showed that the quinuclidine fragment was essential to obtain good biological *in vitro* results. They also showed that the (R)- configuration was more active

[307] Pin, F.; Vercouillie, J.; Ouach, A.; Mavel, S.; Gulhan, Z.; Chicheri, G.; Jarry, C.; Massip, S.; Deloye, J.-B.; Guilloteau, D.; Suzenet, F.; Chalon, S.; Routier, S. Design of A7 Nicotinic Acetylcholine Receptor Ligands in Quinuclidine, Tropane and Quinazoline Series. Chemistry, Molecular Modeling, Radiochemistry, in Vitro and in Rats Evaluations of a [18F] Quinuclidine Derivative. *Eur. J. Med. Chem.* **2014**, *82*, 214–224.

and that a phenyl **(R)-69**, thiophene **(R)-70** or a benzofuran **(R)-71** could be attached to the triazole core and lead to good α7 nAChRs binding ability in *in vitro* assays[308] (Figure 86).

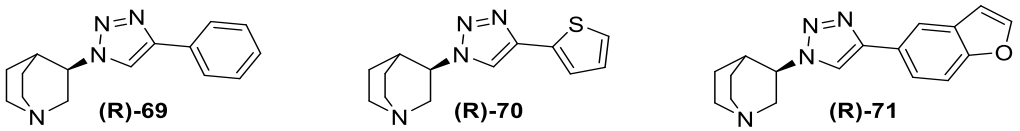

K_i = 8 +/- 4 nM K_i = 9.5 +/- 3 nM K_i = 3 +/- 1 nM

Figure 86: α7 nAChR agonists developed by Routier et al.[308]

Thus, once we had all this information in hands, we decided to work on a small fragment, easy to synthesize and displaying good biological results as a monomer structure. The fragment **(R)-69** we chose to work on has a 1,2,3-triazole core, bears a quinuclidine moiety, which is also found in a series of already developed α7 nAChR agonists, and a phenyl ring.

3.2. AChE inhibitor

Even though we now know that AD is a multifactorial disease, achieving an efficient AChE inhibition has been the main strategy used to develop treatments against AD for years. Indeed, inhibiting AChE could help restoring the ACh levels, a key neurotransmitter, in the brain. To be effective, we decided to base our inhibitor scaffold on one well-known AChE inhibitor (e.g. Tacrine, Rivastigmine, Galantamine, Donepezil). After observing the structures of these four main AChE inhibitors, we had to choose the one fulfilling all the criteria:

- small pharmacophore,
- easy synthesis,
- common moiety with the other chosen pharmacophore (α7 nAChRs agonist).

We thus turned our attention towards the Rivastigmine scaffold because all the criteria were fulfilled but also because it was a scaffold that attracted less attention for MTDLs, and that was not tackled in the group, and we were interested by the challenge.

[308] Ouach, A.; Pin, F.; Bertrand, E.; Vercouillie, J.; Gulhan, Z.; Mothes, C.; Deloye, J.-B.; Guilloteau, D.; Suzenet, F.; Chalon, S.; Routier, S. Design of A7 Nicotinic Acetylcholine Receptor Ligands Using the (Het)Aryl-1,2,3-Triazole Core: Synthesis, in Vitro Evaluation and SAR Studies. *Eur. J. Med. Chem.* **2016**, *107*, 153–164.

Nevertheless, a few Rivastigmine-based or carbamate-based MTDLs have been designed and evaluated in the past years (Figure 87). Weinstock et *al*.[309] developed compound **72** by combining the *N*-ethyl-*N*-methylcarbamate fragment of Rivastigmine with the *N*-propargyl-(1R)-aminoindanone fragment of the rasagiline, an anti-Parkinson drug. The resulting new MTDL has been evaluated and showed a good AChE inhibitory activity in addition to a MAO-A/B inhibitory activity, it could also be noted that compound **72** enhances cognition and reduces oxidative stress. Then, carbamate-based derivatives such as compounds **73** and **74** have been designed by Sterling et *al*.[310], the structures of these MTDLs were also based on a combination of a carbamate with a rasagiline moiety and are close to the structure of compound **72**. Both compound **73** and **74** displayed promising inhibitory activities toward AChE and MAO-A/B, with a slightly better IC_{50} on AChE for compound **74** .

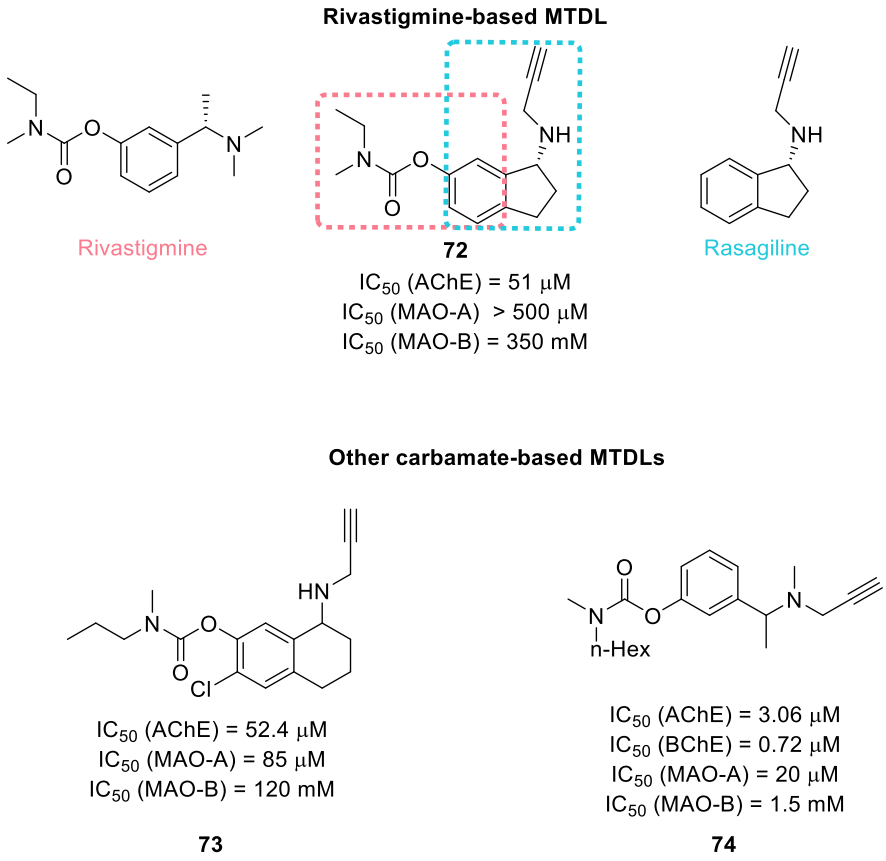

Figure 87: Examples of carbamate-based MTDLs

[309] Weinstock, M.; Goren, T.; Youdim, M. B. H. Development of a Novel Neuroprotective Drug (TV3326) for the Treatment of Alzheimer's Disease, with Cholinesterase and Monoamine Oxidase Inhibitory Activities. *Drug Dev. Res.* **2000**, *50* (3–4), 216–222.

[310] Sterling, J.; Herzig, Y.; Goren, T.; Finkelstein, N.; Lerner, D.; Goldenberg, W.; Miskolczi, I.; Molnar, S.; Rantal, F.; Tamas, T.; Toth, G.; Zagyva, A.; Zekany, A.; Lavian, G.; Gross, A.; Friedman, R.; Razin, M.; Huang, W.; Krais, B.; Chorev, M.; Youdim, M. B.; Weinstock, M. Novel Dual Inhibitors of AChE and MAO Derived from Hydroxy Aminoindan and Phenethylamine as Potential Treatment for Alzheimer's Disease. *J. Med. Chem.* **2002**, *45* (24), 5260–5279.

The carbamate moiety has thus proved to be a promising fragment to use for the design of MTDLs against AD targeting AChE, but to this date, such Rivastigmine based pharmacophore remains underused in the development of new anti-AD drugs.

Hence, in this context, we decided to work on this particular field of research with these two promising pharmacophore scaffolds bearing a common moiety which will allow us to reduce the MTDL's molecular weight and develop combined MTDLs (Figure 88).

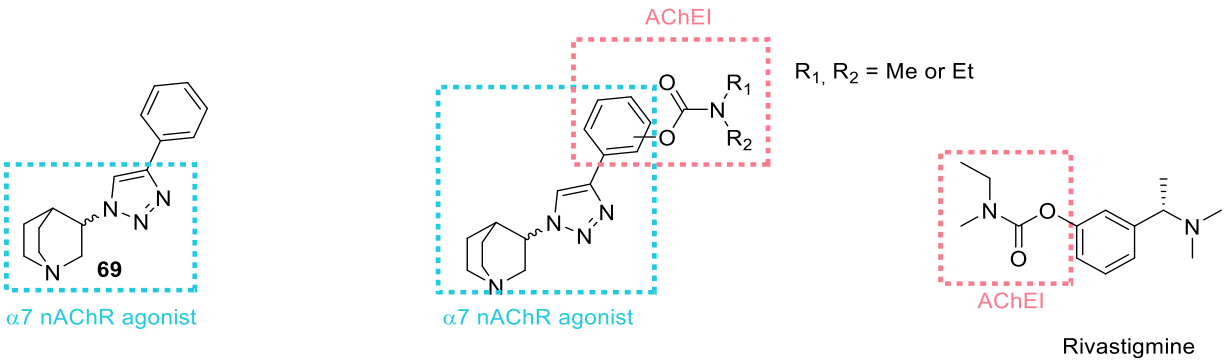

Figure 88: Chosen structure for the α7 nAChRs agonist / AChE inhibitor MTDLs

4. The steps of *in silico* drug design

4.1. Predict the BBB crossing

When developing drugs against CNS-related pathologies, one of the main challenges is to design molecules able to cross the blood brain barrier (BBB). Empirical laws (Lipinski's rules), physico-chemical properties computational evaluation (CNS MPO Score) and database based softwares (Percepta) have been developed to predict the ligands behaviour towards the BBB.

4.1.1. BBB structure

The BBB (Figure 89) is a semipermeable highly selective structure separating the circulating blood from the brain and extracellular fluid in the CNS[311]. It allows the passage of some molecules by passive diffusion but restricts the passage of pathogens and large or lipophobic molecules into the cerebrospinal fluid, only small polar or hydrophobic molecules can pass[312]. Between the blood and the brain, endothelial cells are attached together by tight junctions forming the BBB. These junctions are

[311] Daneman, R.; Prat, A. The Blood–Brain Barrier. *Cold Spring Harb. Perspect. Biol.* **2015**, *7* (1), a020412.
[312] Stamatovic, S. M.; Andjelkovic, R. F. K. and A. V. Brain Endothelial Cell-Cell Junctions: How to "Open" the Blood Brain Barrier http://www.eurekaselect.com/67655/article.

made up of smaller subunits that are transmembrane proteins like occludins, claudins or junctional adhesion molecules. Moreover, barrier's cells actively transport essential metabolic products like glucose, amino acids, purine bases, nucleoside or cholines by using specific transport proteins[312].

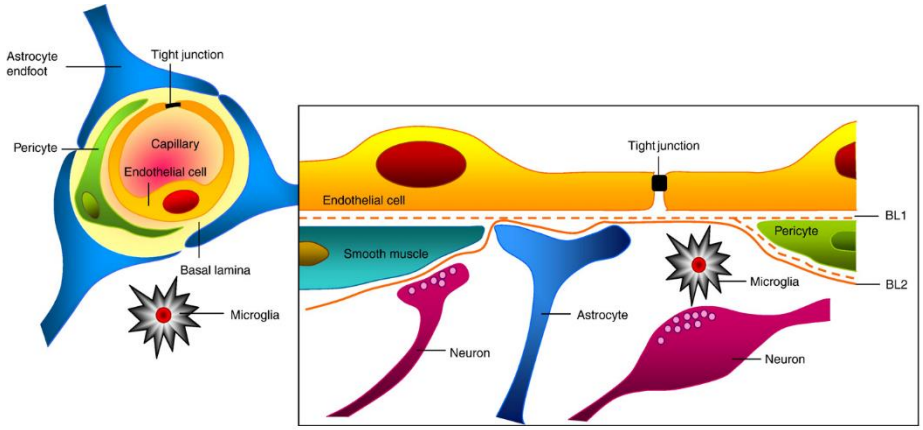

Figure 89: Representation of the BBB[313]

4.1.2. Lipinski's rule of five

Lipinski et *al.* designed in 2001 empirical rules to describe molecular properties to evaluate molecules druglikeness. Based on the observation that most orally available drugs are relatively small and lipophilic molecules, they established the four empirical following rules[272]. The molecule is unlikely to be a good orally available drug if it has :

- more than 5 H-bond donors,
- more than 10 H-bond acceptors,
- a molecular mass over 500 g/mol
- an octanol-water partition coefficient log P higher than 5

Nevertheless, in the past years it has been shown that defining the druglikeness of a compound by only following these four rules was misleading. For example, the number of FDA-approved drugs with a MW over 500 g/mol has increased while the number of FDA-approved drugs with a MW below 500 g/mol has stayed relatively constant (Figure 90).

[313] Abbott, N. J.; Patabendige, A. A. K.; Dolman, D. E. M.; Yusof, S. R.; Begley, D. J. Structure and Function of the Blood–Brain Barrier. *Neurobiol. Dis.* **2010**, *37* (1), 13–25.

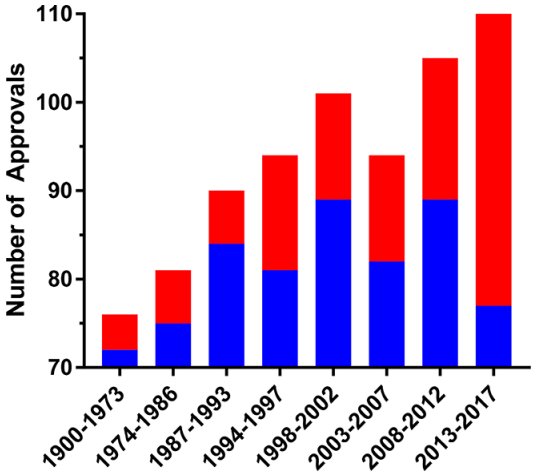

Figure 90: Number of FDA-approved oral drugs by time period (drugs with MW less than 500 are in blue and those above 500 are in red) [314]

Even if the parameters empirically determined by Lipinski et *al*. are important, the strategies currently used to design active drugs against several pathologies have changed with the development of next generation peptides based drugs or even small proteins drugs, oligonucleotides, fatty acid conjugation (to extend drugs' half-life) or nanoparticles and these rules only apply to classical small molecules in drug design[314].

4.1.3. CNS MPO score[273,274]

In 2010, Wager et *al*. designed a new tool focused on the alignment of major druglike attribute for drugs able to reach the CNS, the Central Nervous System Multiparameter optimisation score (CNS MPO score). They developed an algorithm using 6 key physicochemical properties (which can be calculated from the compound structure using different computational tools, or on Chemicalise.com):

- lipophilicity, calculated partition coefficient (CLogP),
- calculated distribution coefficient at pH = 7.4 (CLogD),
- molecular weight (MW),
- topological polar surface area (TPSA),
- number of hydrogen bond donors (HBD),
- most basic centre (pKa).

All these evaluated properties are weighted equally, with a score ranging from 0.0 to 1.0 for each property and thus a CNS MPO score of a molecule can range from 0.0 to 6.0. Moreover, Wager et *al.*

[314] Shultz, M. D. Two Decades under the Influence of the Rule of Five and the Changing Properties of Approved Oral Drugs. *J. Med. Chem.* **2019**, *62* (4), 1701–1714.

evaluated their new algorithm on a set of drugs and candidates (Figure 91) and brought to light that 74% of drugs had MPO scores over 4, a higher score when compared to the candidates (only 60%). This study suggested that CNS MPO score might be a potent tool to increase the probability of CNS targeted drugs survival to clinical trials.

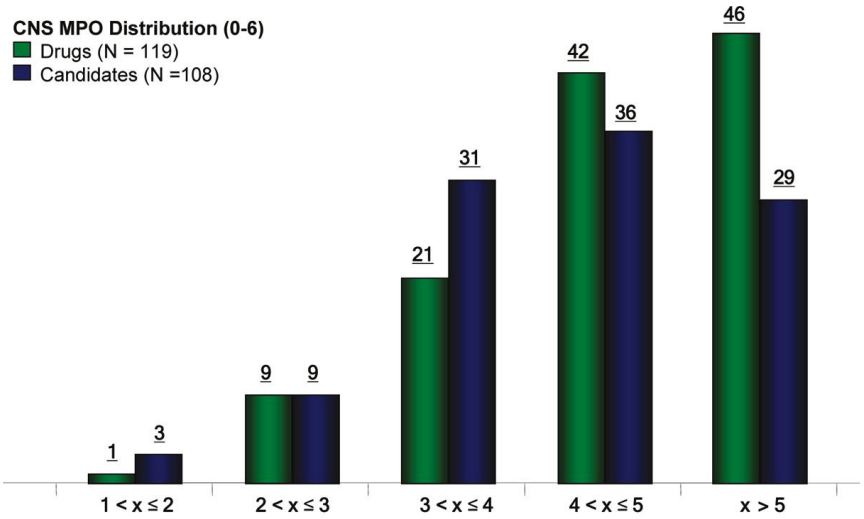

Figure 91: CNS MPO desirability score[274]

4.1.4. Percepta software[315]

Based on the same concept, ACD labs developed a software displaying tools to predict all the drug's properties (molecular properties, physicochemical, ADME and Tox). In the professor Renard's team, this software is used to predict the compounds brain penetration for CNS activity by giving plasma/brain equilibration rates and comparing the predicted compounds properties to known CNS active and inactive drugs. The module was developed using *in vivo* data of rates of passive diffusion across the BBB for more than 200 compounds expressed as LogPS (permeability surface) constants between -5 and -1 (Figure 92) and LogBB (Brain Barrier) determined by ratio of total drug concentrations in tissues and plasma at steady-state concentration. Calculations are performed using essential physiochemical properties such as lipophilicity, ionization constant, number of H-bonds and molecular weight. Fraction unbound in brain tissue (f_u), brain/plasma equilibration rate and Log(PS* f_u) defined as the rate required to achieve equilibrium by Liu et *al*.[316] are the three additional parameters evaluated and calculated by this model.

[315] Lanevskij, K.; Japertas, P.; Didziapetris, R.; Petrauskas, A. Ionization-Specific Prediction of Blood–Brain Permeability. *J. Pharm. Sci.* **2009**, *98* (1), 122–134.

[316] Liu, X.; Smith, B. J.; Chen, C.; Callegari, E.; Becker, S. L.; Chen, X.; Cianfrogna, J.; Doran, A. C.; Doran, S. D.; Gibbs, J. P.; Hosea, N.; Liu, J.; Nelson, F. R.; Szewc, M. A.; Van Deusen, J. Use of a Physiologically Based Pharmacokinetic Model to Study the Time to Reach Brain Equilibrium: An Experimental Analysis of the Role of

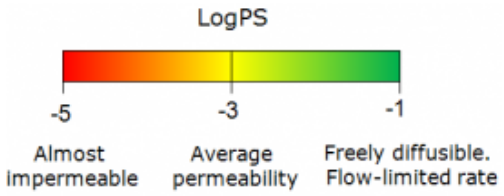

Figure 92: Scale of LogPS (adapted from ACDLab technical document)

4.2. CADD - A potent tool in drug discovery

As it was mentioned in the general introduction, over the past years, the cost of drug design and development has significantly increased along with high rates of clinical trial failures. Hence, to tackle this issue, the *in silico* approach has been developed to evaluate small molecules interactions with multiple targets (enzymes, proteins, etc). As shown on Figure 93, computer aided drug design (CADD) can be used to various goals like pharmacophore screening to find novel small molecules interacting with the receptors or to build innovative MTDLs, structures optimisation by QSAR studies, discovery or validation to predict druggability. In our work, we used CADD to predict the designed ligands binding affinities to AChE and to visualise their position inside the pocket's enzyme. As already mentioned, we did not use CADD to predict the desired ligands binding ability towards α7 nAChR, due to the multiple potential modes of interaction. We also performed such calculation to predict their druggability.

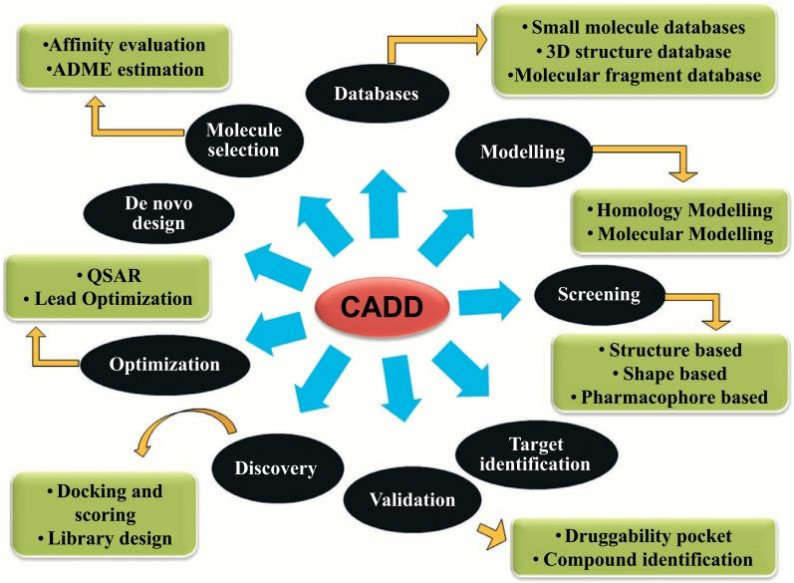

Figure 93: Overview of computer aided drug designing aims[317]

Blood-Brain Barrier Permeability, Plasma Protein Binding, and Brain Tissue Binding. *J. Pharmacol. Exp. Ther.* **2005**, *313* (3), 1254–1262.

[317] Aarthy, M.; Panwar, U.; Selvaraj, C.; Singh, S. K. Advantages of Structure-Based Drug Design Approaches in Neurological Disorders. *Curr. Neuropharmacol.* **2017**, *15* (8), 1136–1155.

4.2.1. Docking protocol

To choose the more promising structures to synthesize, we decided to perform *in silico* studies to evaluate ligand's binding to AChE (by introducing rigid or with flexible residues depending on the ligands we were evaluating). We have made the choice to work only on the AChE binding and not on the other targets, especially the α7 nAChR which structure and potential allosteric binding pockets as well as their potential effect on the receptors remain unknown.

Docking studies are divided in 5 steps:

- Choice and preparation of the target (protein, enzyme, etc)
- Choice and preparation of the ligands
- Docking calculation
- Evaluation of the results
- Visualisation of the docked ligands

Choice and preparation of the target

To provide a more realistic estimation of what could really happen, the starting point should be a co-crystal structure of the enzyme-ligand complexes where the known ligand must be structurally close to the MTDL which has to be evaluated. Such structures can be found in the protein data bank (PDB), a database gathering the X-ray crystallographic structures of proteins or nucleic acid obtained by biologists and biochemists on different biomolecules.

Once the choice of the enzyme structure in the protein data base to start with is made, thanks to a software (AutoDock tool), the target must be prepared. Indeed, the point is to remove the water molecules and the ligand of the co-crystal structure, and to determine which residue is protonated at physiological pH to add the corresponding polar hydrogen, and thus have an accurate vision of the charge of each residue.

Then, a box must be chosen, it means that the active site of the enzyme will be defined by 3 coordinates (X, Y, Z) defining a "box" where the docking will take place, and the ligand could be placed. If the box is too small, the docking will not be accurate and the possible conformations of the ligand inside the enzyme is limited, but if the box is too large, the calculation will be long and tedious.

Choice and preparation of the ligands

Once the target prepared, the ligands three-dimensional structures must be determined, and this happens in two steps. First, the ligands are designed with ChemBioDraw, the polar residues can be protonated or deprotonated if needed. This is achieved through the use of the Chemicalize.fr software, which enables to evaluate the protonation states of the ligands at pH 7.4. In a second time, the energy

levels of the ligands are minimized with Chem3D which uses a Merck Molecular Force Field, MMFF94[318].

Docking calculation

Once the target and the ligand are ready to be docked, thanks to AutoDock Vina[319] software, the docking calculations can be launched. AutoDock Vina is a suite of automated docking tools designed to predict energy levels of a small molecules such as drug candidates bound to a receptor of known 3D structure. The main programme is used to perform the docking of the ligands to a set of grids calculated by the software describing the target enzyme, in this case, the AChE. This software scoring function has been designed by combining knowledge-based potentials using the PDBbind database which gathers binding affinity data (K_D, K_i and IC_{50}) for 1359 protein-ligand complexes[320] with empirical scoring functions, more precisely by using the AMBER force field (assisted model building with energy refinement)[321]. Moreover, this type of hybrid scoring function has been widely inspired by X-score, an empirical scoring function for structure-based binding affinity predictions[322]. X-score includes in its scoring terms accounting for deformation penalty, Van de Waals interactions, hydrogen bonding and hydrophobic effects, this last parameter is calculated through three different algorithms leading to an improvement of the docking accuracy when compared to conventional force field computation.

Evaluation of the results

After the calculations, we will obtain evaluation of binding affinities of the chosen ligand in different conformation (usually 9) within the active site of the enzyme. These results are viewed as a text file with negative energy values in kcal/mol. The calculation considers intramolecular forces of the covalent binding (length of the link, angle of the link, dihedral angle) and non-covalent binding intermolecular forces (electrostatic, H-bond, dipolar interactions, hydrophobicity, Van der Waals). Reasonably, the given results with the lowest values should be the more stable conformations displaying a higher number, and stronger interactions.

---

[318] Halgren, T. A. Merck Molecular Force Field. I. Basis, Form, Scope, Parameterization, and Performance of MMFF94. *J. Comput. Chem.* **1996**, *17* (5–6), 490–519.

[319] Trott, O.; Olson, A. J. AutoDock Vina: Improving the Speed and Accuracy of Docking with a New Scoring Function, Efficient Optimization and Multithreading. *J. Comput. Chem.* **2010**, *31* (2), 455–461.

[320] Wang, R.; Fang, X.; Lu, Y.; Wang, S. The PDBbind Database: Collection of Binding Affinities for Protein−Ligand Complexes with Known Three-Dimensional Structures. *J. Med. Chem.* **2004**, *47* (12), 2977–2980.

[321] Cornell, W. D.; Cieplak, P.; Bayly, C. I.; Gould, I. R.; Merz, K. M.; Ferguson, D. M.; Spellmeyer, D. C.; Fox, T.; Caldwell, J. W.; Kollman, P. A. A Second Generation Force Field for the Simulation of Proteins, Nucleic Acids, and Organic Molecules. *J. Am. Chem. Soc.* **1995**, *117* (19), 5179–5197.

[322] Wang, R.; Lai, L.; Wang, S. Further Development and Validation of Empirical Scoring Functions for Structure-Based Binding Affinity Prediction. *J. Comput. Aided Mol. Des.* **2002**, *16* (1), 11–26.

Visualisation of the results

To be able to visualize the different predicted conformations, different softwares can be used, like Pymol which enables to see the position of the ligand inside the catalytic pocket or like Discovery studio which enables to visualize the interactions of the ligand with the enzymes' residues or within residues. The visualization is an important step of the studies allowing us to rationalize the binding energy values previously obtained, to evaluate the positioning of the ligand inside the pocket and its different interactions with the residues of the target.

5. Design and synthesis of the first family of Stigmine derivatives

5.1. In silico evaluations

The carbamate moiety could be placed on any position relative to the triazole (-o, -m or -p). Due to the strong steric hindrance and blocked configuration of the whole molecule induced by the relative position of the carbamate moiety, the "ortho" family was not investigated. Nitrogen substituents R_1 and R_2 could be either methyl or ethyl group. The selected structure presents one stereocenter, thus in order to select the structures to synthesize, we performed docking studies on 12 derivatives (6 with a (R) stereocenter and their (S) enantiomers) of a Stigmine derivative linked with an α7 nAChRs agonist (Figure 94). The docking was made with *m*AChE (PDB 1Q84)[323] structure containing flexible residues (Trp86, Tyr72, Tyr124, Tyr337, Tyr341). *In silico* investigations gave us essential pieces of information concerning the MTDLs we designed. The three main results that needed to be taken into account were:

- the binding affinity between the ligand and the enzyme,
- the proximity of the AChE catalytic serine (Ser203) with the ligand's carbamate,
- the interactions of the whole structure with the main residues of the enzyme.

[323] RCSB PDB - 1Q84: Crystal structure of the mouse acetylcholinesterase-TZ2PA6 anti complex https://www.rcsb.org/structure/1Q84.

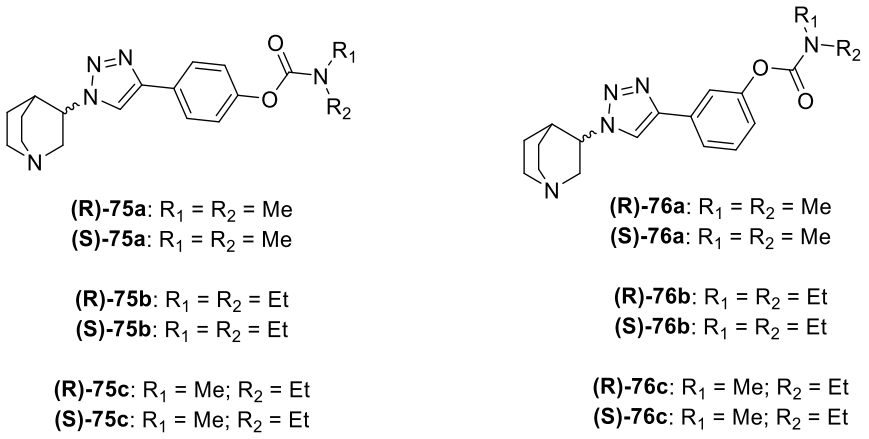

Figure 94: MTDLs evaluated in silico

5.1.1. Binding affinity and proximity with Ser203

After following the protocol given previously, we obtained the following results for the 12 compounds compiled in Table 5. This first evaluation brought to light that varying the quinuclidine's configuration didn't affect the results in a significant manner.

The binding affinities of the desired MTDLs were similar compared to the Rivastigmine's binding affinities. Moreover, the two types of derivatives were well positioned inside the enzymatic pocket and the quinuclidine fragment could also interact with the enzyme's peripheral site (Figure 95). Nevertheless, it could be notified that derivatives **(R)-75c** and **(R)-76c** (entries 4 and 7) displayed a significant stronger empirical binding energy when bound to AChE. On the other hand, the meta derivatives apart from **(R)-76c** (entry 7) would bring the carbamate closer to the catalytic serine because of their preferential conformation. Indeed, as shown on Figure 95, the ligand **(R)-76a**'s angle enables the MTDLs with a carbamate in the meta position to better interact with the catalytic serine.

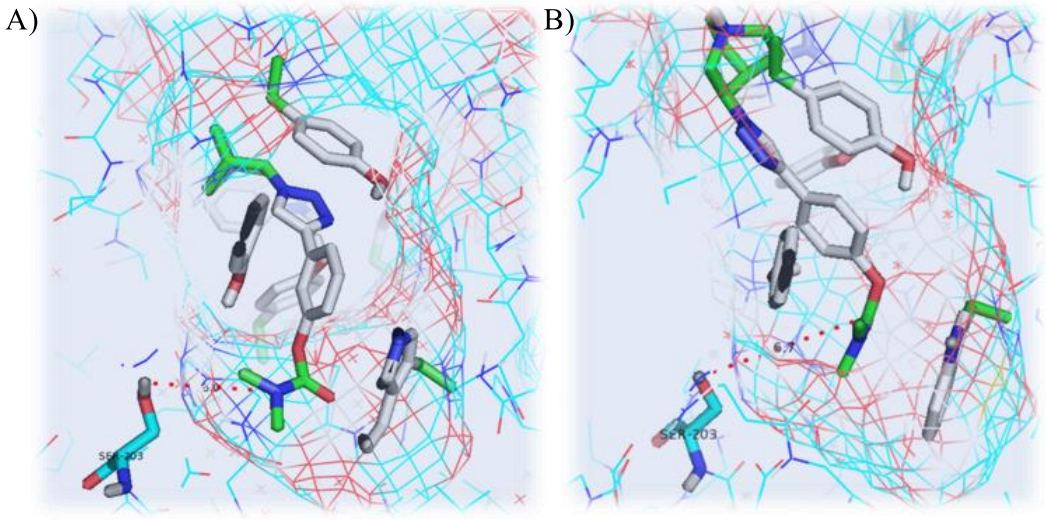

Figure 95: Visualisation of most stabilized conformation for compounds (A) ***(R)-75a*** *and (B)* ***(R)-76a*** *within the enzymatic pocket as predicted by AutodockVina and represented with PyMol*

Entry	Compound	R_1	R_2	E_{bind} (kcal/mol)	Carbamate reactive carbon distance to Oxygen atom of Ser203 (Å)
1	**Rivastigmine**	Me	Et	-7.5	8.7
2	**(R)-75a**	Me	Me	-7.5	6.7
3	**(R)- 75b**	Et	Et	-7.4	6.9
4	**(R)- 75c**	Me	Et	-10.2	8.7
5	**(R)-76a**	Me	Me	-6.1	5.0
6	**(R)- 76b**	Et	Et	-7.3	4.9
7	**(R)- 76c**	Me	Et	-9.5	12.8
8	**(S)- 75a**	Me	Me	-7.4	6.8
9	**(S)- 75b**	Et	Et	-7.4	6.9
10	**(S)- 75c**	Me	Et	-10.4	8.9
11	**(S)- 76a**	Me	Me	-6.2	5.0
12	**(S)- 76b**	Et	Et	-7.1	5.0
13	**(S)- 76c**	Me	Et	-9.5	13.1

Table 5: Docking results of ***(R)-75a-c, (R)-76a-c, (S)-75a-c*** *and* ***(S)-76a-c***

5.1.2. Interaction with the main AChE residues

Due to the striking similarity of results between the derivatives, only interactions between a representative of the meta and para substituted compounds **(R)-75a** and **(R)-76a** with AChE will be discussed but the results could be extended to all other derivatives (Table 6).

Entry	Type of interaction	"para" family (R)-75a-c	"meta" family (R)-76a-c
1	π-π interaction	Tyr341	Tyr341 Tyr124
2	π- lone pair interaction	Tyr337	
3	π -σ interaction	Trp86	
4	π-cation interaction		Tyr286

*Table 6: Main interactions predicted in silico for compounds **(R)-75a-c** and **(R)-76a-c***

5.1.2.1. Interactions predicted for the "para" derivatives family

Concerning the interactions between AChE main residues and the para derivatives (Figure 96), we could observe π -π interactions between Tyr341 and the phenyl ring of the ligand (entry 1). The phenyl also interacted with Tyr337 in a π-lone pair interaction type (entry 2). Moreover, the ligand's carbamate was predicted to interact with Trp86 through a π-σ interaction (entry 3).

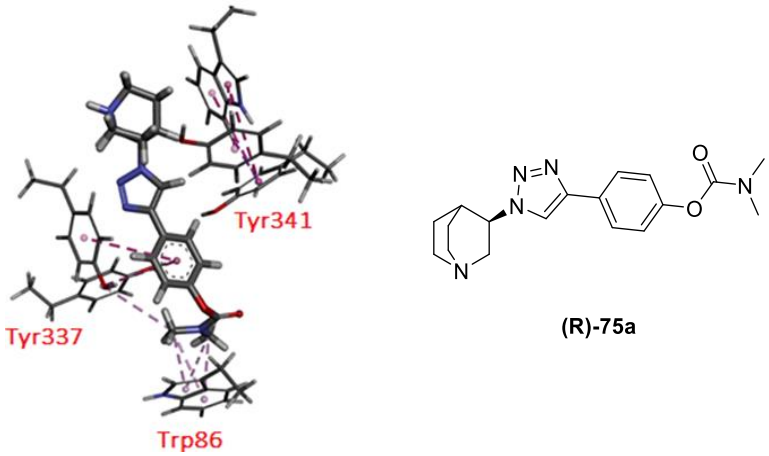

*Figure 96: Representation of predicted interactions between mAChE residues and **(R)-75a***

5.1.2.2. Main interactions predicted in silico for with the "meta" derivatives family

In the case of the meta derivatives (Figure 97), less interactions were found which could explain some of the lower binding energies as compared to these we obtained previously. Indeed, we only predicted a π -π interaction between the triazole core and Tyr341 and Tyr124 (entry 1), and a π – cation interaction between the Trp286 and the protonated amine of the quinuclidine (entry 4). Surprisingly, we couldn't observe neither the ligand's carbamate nor phenyl ring interactions with residues of the enzyme. This could be explained by the conformation of the ligand and the carbamate position which probably hinder the optimal placement of the ligand inside the catalytic site.

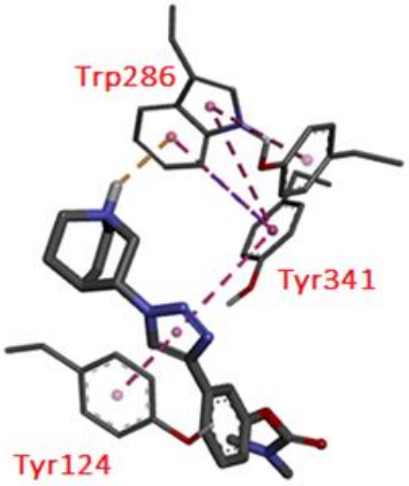

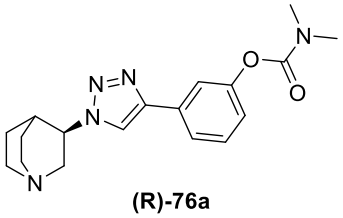

Figure 97: Representation of predicted interactions between mAChE residues and ***(R)-76a***

To date, only two co-crystal structures of Rivastigmine with *Tc*AChE have been disclosed in the literature, the first one was determined by Bar-On et *al*.[324] in 2002 (PDB : 1GQR) but displays the structure of Rivastigmine after the cleavage of the carbamyle leaving group (NAP) (Figure 98). The second one concerns analogue metabolites of Rivastigmine (PDB 6EUE) which were developed by Dighe et *al.*[325] in 2019.

[324] Bar-On, P.; Millard, C. B.; Harel, M.; Dvir, H.; Enz, A.; Sussman, J. L.; Silman, I. Kinetic and Structural Studies on the Interaction of Cholinesterases with the Anti-Alzheimer Drug Rivastigmine † , ‡. *Biochemistry* **2002**, *41* (11), 3555–3564.

[325] Dighe, S. N.; Mora, E. D. la; Chan, S.; Kantham, S.; McColl, G.; Miles, J. A.; Veliyath, S. K.; Sreenivas, B. Y.; Nassar, Z. D.; Silman, I.; Sussman, J. L.; Weik, M.; McGeary, R. P.; Parat, M.-O.; Brazzolotto, X.; Ross, B. P. Rivastigmine and Metabolite Analogues with Putative Alzheimer's Disease-Modifying Properties in a Caenorhabditis Elegans Model. *Commun. Chem.* **2019**, *2* (1), 1–14.

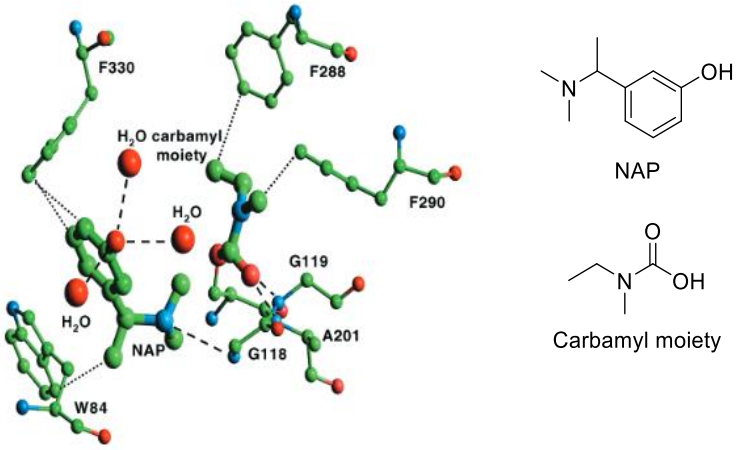

Figure 98: Active site of TcAChE after inhibition with Rivastigmine (adapted from Bar-On et al.[324])

Due to the lack of information concerning the interactions of Rivastigmine with AChE, it was decided to perform docking studies with the Rivastigmine structure itself (Figure 99) to be able to compare the results with the one obtained for the designed MTDLs. Apart from the position of the Rivastigmine which is close to the one observed for the various designed MTDLs, we observed several interactions with the main AChE residues found either in the MTDLs study or in the Rivastigmine study. Indeed, concerning Rivastigmine, the phenyl ring was predicted to perform a π-stacking interaction with Tyr341 and Tyr124 while the ethyl substituent of the carbamate displayed a π-sigma interaction with Trp86 which are interactions already predicted for the designed MTDLs and the enzyme. Moreover, a H-bond formation has also been predicted between Tyr124 and the Rivastigmine's oxygen.

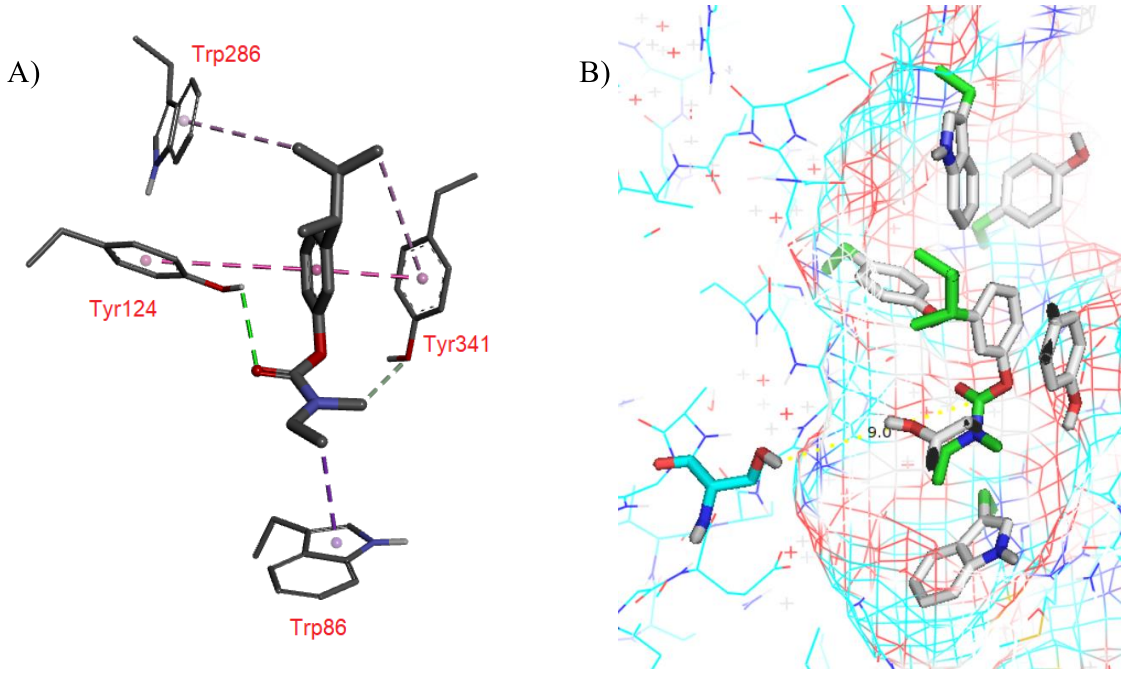

Figure 99: Docking prediction of Rivastigmine within mAChE (A) main interactions (B) snapshot of Rivastigmine position in the active site

5.2. Predicting ability to cross the BBB

5.2.1. CNS MPO scores

Besides the fact that all the derivatives are in accordance with the Lipinski's rules, CNS MPO scores have been determined for all the compounds of the series and showed the same results of 5.4/6 which are closed to the result obtained for Rivastigmine, the parent compound (Table 7). Hence, the 12 proposed MTDLs have promising pharmacologic profiles.

Entry	Compound	CLogP	CLogD	TPSA (Å²)	MW g/mol	HBD	pKa	CNS MPO score
1	Rivastigmine	2.41	1.00	32.78	250.34	0	8.8	**5.2**
2	**(R)-75a** and **(R)-76a**	2.15	0.38	63.49	341.41	0	9.17	**5.4**
3	**(R)-75b** and **(R)-76b**	2.86	1.10	63.49	369.47	0	9.17	**5.4**
4	**(R)-75c** and **(R)-76c**	2.51	0.74	63.49	355.44	0	9.17	**5.4**

Result can be extended to the (S) enantiomers
Physico-chemical properties obtained using Chemicalize.com

*Table 7: Physicochemical properties and CNS MPO score of Rivastigmine, **(R)-75a-c** and **(R)-76a-c***

5.2.2. Percepta software CNS activity prediction

The last *in silico* study that had to performed was the evaluation of the compounds ability to penetrate the brain and be CNS active by using the Percepta software. It could be noted that the relative position of the carbamate on the molecule did not affect the predicted results (Table 8). It could also be noted that the calculated Percepta evaluated LogP and pKa are close to the ones found when evaluating the CNS MPO scores, which shows a logical link between the CNS MPO score and the results obtained with the Percepta software. Indeed, some of the physicochemical properties used to calculate CNS MPO scores are also used to predict the BBB penetrations of potential novel drugs by Percepta software.

Entry	Compound	LogP	pKa	f_u	LogPS	LogBB	Log(PS*f_u)	Brain penetration for CNS activity
1	Rivastigmine	2.29	8.62	0.66	-1.9	0.5	-2.6	Sufficient
2	**(R)-75a** and **(R)-76a**	1.71	9.30	0.23	-2.6	-0.21	-3.0	Sufficient
3	**(R)-75b** and **(R)-76b**	2.55	9.30	0.18	-2.2	0.06	-3.0	Sufficient
4	**(R)-75c** and **(R)-76c**	2.18	9.30	0.19	-2.4	-0.09	-3.0	Sufficient

Result can be extended to the (S) enantiomers

Table 8: Physicochemical properties determined with Percepta of Rivastigmine, ***(R)-75a-c*** *and* ***(R)-76a-c***

As it is shown on Figure 100, all the designed MTDLs appeared to be promising compounds able to passively cross the BBB according to the Percepta software prediction. Moreover, compound **(R)-75b** (and compounds **(R)-76b**) (Figure 100 – (B)) displayed the best results concerning their predicited aptitude to be CNS active. This study showed us that even though all the MTDLs have shown interesting results, the carbamate's substitution can affect the brain penetration : a carbamate substituted by two ethyl groups seems to be the optimal structure for this type of ligands, according to the predictive softwares we used.

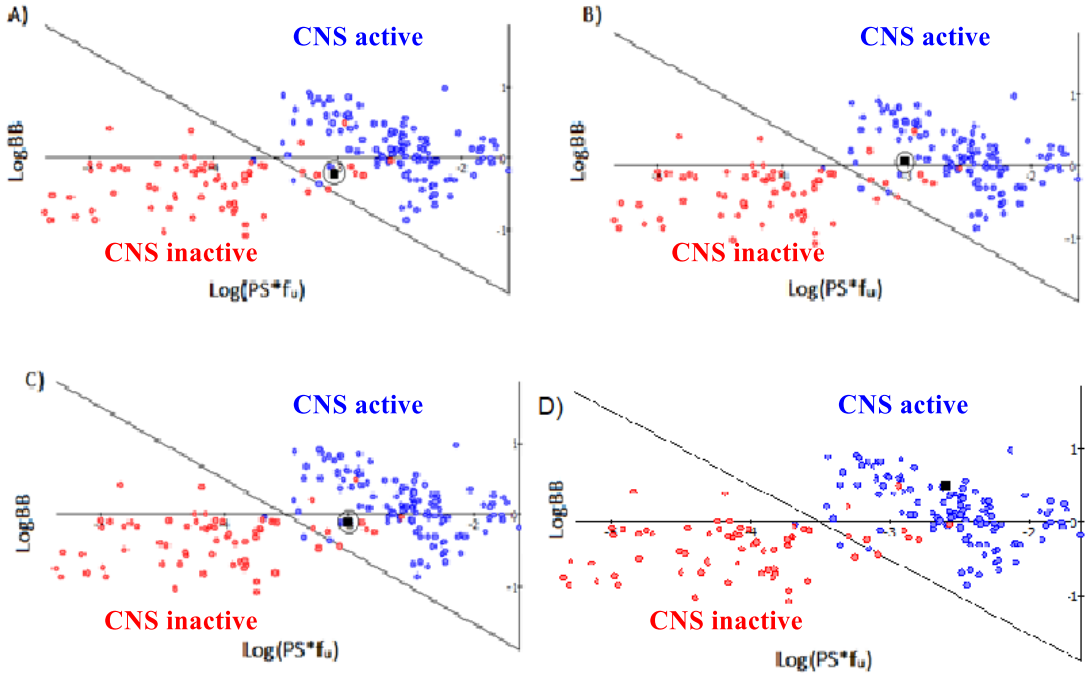

Figure 100: Results of Brain penetration for CNS activity for (A) ***(R)-75a*** *(B)* ***(R)-75b*** *(C)* ***(R)-75c*** *(D) Rivastigmine (red dots represent CNS inactive compounds, blue dots represent CNS active compounds and the circled black dot represent the tested compound)*

Hence, these computing evaluations have brought to light that the designed MTDLs were all promising compounds potentially able to interact with AChE, regardless of the substituent type or position. Moreover, the CNS MPO scores and results obtained from the Percepta software showed interesting properties concerning the ability of all compounds to cross the BBB an act directly at the CNS. We thus decided to undertake the synthesis of all compounds.

5.3. Synthesis of Stigmine's derivatives (series 1)

5.3.1. Retrosynthetic route

In order to obtain the new series of MTDLs **75a**-c and **76a-c** and their enantiomers **(R)-75a-c** and **(R)-76a-c** and **(S)-75a-c** and **(S)-76a-c** bearing a carbamate function, we decided to develop a convergent synthetic pathway using the Copper(I) catalysed Huisgen cycloaddition as a key step of the synthesis (Scheme 18). As seen earlier, 1,2,3-triazole is one of the most common bioisosters of amide bonds,

and, due to its easy synthetic access since Sharpless[326] and Meldal[327] have shown that the Huisgen cycloaddition between azides and alkynes yielding such scaffolds could be copper catalysed, with a perfect control of the isomer formed (1-4 vs 1-5 substituted triazole ring), its use in medicinal chemistry has increased. This abundance is also supported by practical structural features such as a good stability to basic and acid hydrolysis and reductive or oxidative conditions[328]. Moreover, this heterocycle displays a noticeable dipolar moment which could induce hydrogen bonds formation and is prompt to favour pi-stacking interactions with the target and thus should enhance the MTDLs activity[329].

Once racemic and enantiopure azides **77, (R)-77**, **(S)-77** and the desired alkynes **78a-c** and **79a-c** are obtained, we should thus be able to link easily the two parts of the MTDLs by the desired 1-4 substituted triazole ring formation through catalysed regioselective Huisgen cycloaddition, in order to yield the targeted new series of compounds against AD.

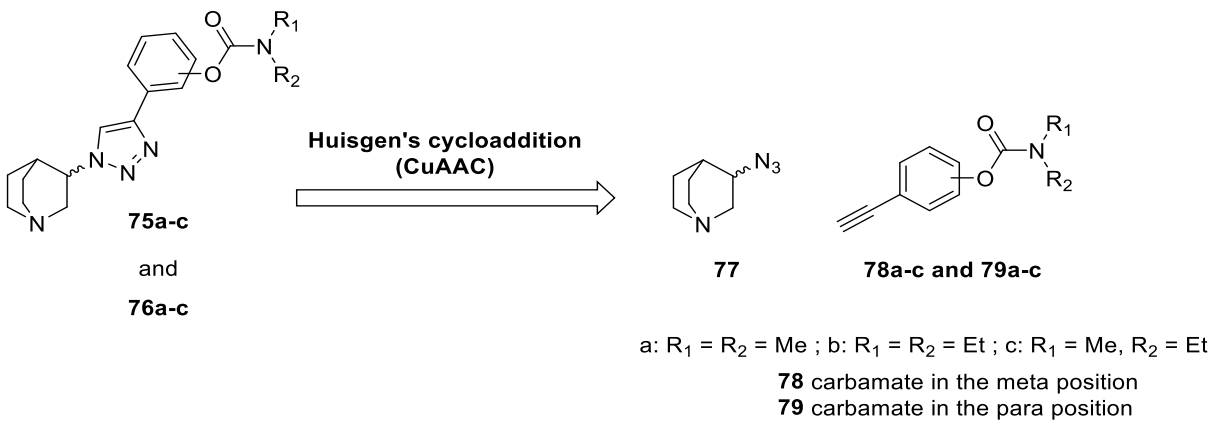

*Scheme 18: **75a**-c and **76a-c** retrosynthesis*

[326] Rostovtsev, V. V.; Green, L. G.; Fokin, V. V.; Sharpless, K. B. A Stepwise Huisgen Cycloaddition Process: Copper(I)-Catalyzed Regioselective "Ligation" of Azides and Terminal Alkynes. *Angew. Chem. Int. Ed.* **2002**, *41* (14), 2596–2599.

[327] Tornøe, C. W.; Sanderson, S. J.; Mottram, J. C.; Coombs, G. H.; Meldal, M. Combinatorial Library of Peptidotriazoles: Identification of [1,2,3]-Triazole Inhibitors against a Recombinant Leishmania Mexicana Cysteine Protease. *J. Comb. Chem.* **2004**, *6* (3), 312–324.

[328] Bourne, Y.; Kolb, H. C.; Radić, Z.; Sharpless, K. B.; Taylor, P.; Marchot, P. Freeze-Frame Inhibitor Captures Acetylcholinesterase in a Unique Conformation. *Proc. Natl. Acad. Sci. U. S. A.* **2004**, *101* (6), 1449–1454.

[329] Whiting, M.; Muldoon, J.; Lin, Y.-C.; Silverman, S. M.; Lindstrom, W.; Olson, A. J.; Kolb, H. C.; Finn, M. G.; Sharpless, K. B.; Elder, J. H.; Fokin, V. V. Inhibitors of HIV-1 Protease by Using in Situ Click Chemistry. *Angew. Chem. Int. Ed Engl.* **2006**, *45* (9), 1435–1439.

5.3.2. Azide Synthesis

5.3.2.1. Racemic azidoquinuclidine synthesis

Based on the work of Berdini et *al.*, 3-aminoquinuclidine **81** was obtained through a one steps process: reductive amination of commercially available 3-quinuclidinone **80**, with a large excess of ammonium formate and imine reduction achieved by catalytic hydrogenation (Pd/C) in order to obtain the primary amine **81** in a quantitative yield[330]. The second step consisted in a diazotransfer reaction to form the azide from the amine. Freshly prepared triflyl azide as a transfer agent was used, in presence of potassium carbonate through a Cu(II) salts[331,332] catalysed process (Scheme 19). Triflyl azide was prepared according to the protocol described of Titz et *al*.[333] who developed a safe method to synthesize this potentially explosive reagent. Indeed, by replacing the dichloromethane as solvent by toluene, the formation of hazardous side products such as azidochloromethane and diazidomethane could be avoided. We managed to obtain the racemic 3-azidoquinuclidine **77**, in pure form, yet in a modest isolated yield, since even though most of the organic azides are stable in various conditions, compounds with multiple azide functions, or displaying low molecular weight like compound **77** tend to be volatile or even explosive as was proven by Bräse et *al*.[334] Thus, in our hands, azide **77** was favourably directly used in the next steps without purification.

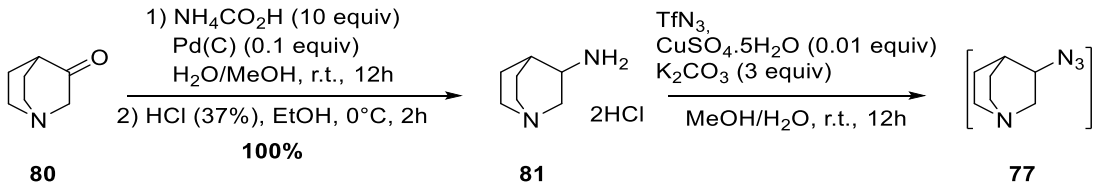

*Scheme 19: Synthesis of **77***

The mechanism of the diazotransfer reaction converting amine **81** into azide **77** has been studied by different groups. Pandiakumar et *al*. showed that the mechanism was not a simple azide (-N_3) transfer

[330] Berdini, V.; Cesta, M. C.; Curti, R.; D'Anniballe, G.; Bello, N. D.; Nano, G.; Nicolini, L.; Topai, A.; Allegretti, M. A Modified Palladium Catalysed Reductive Amination Procedure. *Tetrahedron* **2002**, *58* (28), 5669–5674.
[331] Alper, P. B.; Hung, S.-C.; Wong, C.-H. Metal Catalyzed Diazo Transfer for the Synthesis of Azides from Amines. *Tetrahedron Lett.* **1996**, *37* (34), 6029–6032.
[332] Nyffeler, P. T.; Liang, C.-H.; Koeller, K. M.; Wong, C.-H. The Chemistry of Amine−Azide Interconversion: Catalytic Diazotransfer and Regioselective Azide Reduction. *J. Am. Chem. Soc.* **2002**, *124* (36), 10773–10778.
[333] Titz, A.; Radic, Z.; Schwardt, O.; Ernst, B. A Safe and Convenient Method for the Preparation of Triflyl Azide, and Its Use in Diazo Transfer Reactions to Primary Amines. *Tetrahedron Lett.* **2006**, *47* (14), 2383–2385.
[334] Bräse, S.; Gil, C.; Knepper, K.; Zimmermann, V. Organic Azides: An Exploding Diversity of a Unique Class of Compounds. *Angew. Chem. Int. Ed Engl.* **2005**, *44* (33), 5188–5240.

through a S_Ni pathway[335] (Scheme 20) but that the diazo (-N=N) moiety was transferred from the diazotransfer agent's nitrogen to the primary amine.

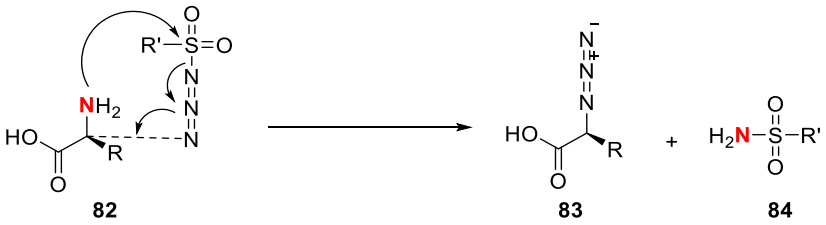

Scheme 20: Wrong S_ni diazotransfer mechanism[335]

They also confirmed the hypothesis given by Nyffeler et *al*.[332] that the attack of the amine group occurred on the terminal nitrogen of the transfer agent. And they thus hypothesised that, taking into account the copper(II) salts catalysis, the mechanism involves a transfer of the two terminal nitrogen atoms of the triflyl azide, through an intermediate 5 members metallocycle (Scheme 21).

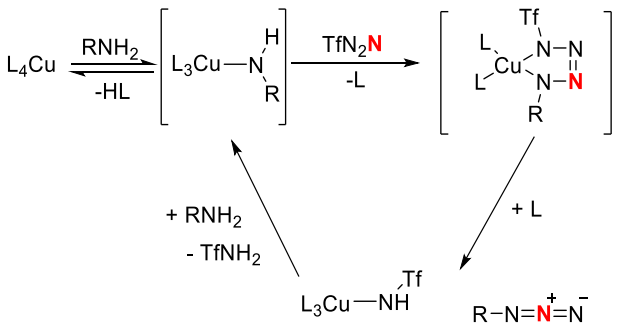

Scheme 21: Plausible postulated diazotransfer mechanism[332]

5.3.2.2. Enantiopure azidoquinuclidine synthesis

As it was shown previously by the Professor Routier's team, α7 nAChR agonists bearing a quinuclidine have better affinities when the (R)-enantiomer is used. For most of them, the binding affinity is in the nanomolar range, which is promising for the expected values of our MTDLs[308].

However, because of the enantiopure starting material **(R)-81** cost (90€/g), we decided to work on a diastereoselective synthetic pathway from the commercially available and cheap ketone. This synthesis consisted in a diastereoselective reduction of compounds **86** obtained from ketone **80** and a chiral auxiliary.

[335] Pandiakumar, A. K.; Sarma, S. P.; Samuelson, A. G. Mechanistic Studies on the Diazo Transfer Reaction. *Tetrahedron Lett.* **2014**, *55* (18), 2917–2920.

Our first idea was to synthesise compound **86** bearing a (S)-methylbenzylamine as a chiral auxiliary. Starting by a condensation between the ketone **80** and (S)-phenethylamine, we managed to isolate imine **85** with a low 25 % yield which could be potentially explained by stability issues. The next step was a diastereoselective reduction of compound **85**. We decided to perform it with L-selectride in order to use mild conditions (Scheme 22). Unfortunately, we were not able to obtain compound **86** but only degradation products too complex to be identified.

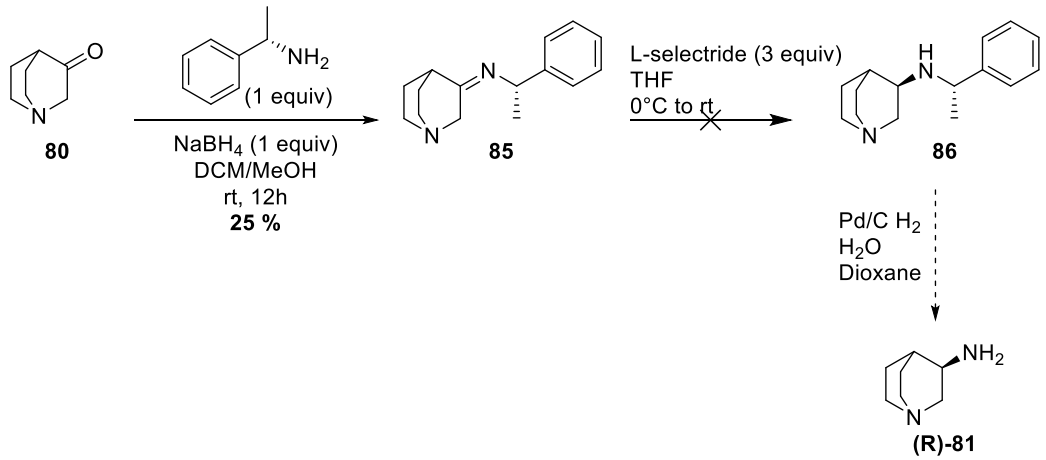

*Scheme 22: First Synthetic pathway to **(R)-81***

Because of the obtained products' complexity, we decided to try another synthetic pathway. We changed the chiral auxiliary and used (R)-2-methylpropane-2-sulfinamide to induce a diastereoselective reaction[336]. However, we could not synthesise compound **87** despite our attempts to perform a condensation between ketone **80** and (R)-2-methylpropane-2-sulfinamide, even with using a strong Lewis acid such as tetraethoxytitane(IV) (Scheme 23). Here again, we only obtained a complex mixture of unidentified degradation products.

[336] Ruano, J. L. G.; Alemán, J.; Parra, A.; Cid, M. B. Preparation of N-p-Tolylsulfonyl-(E)-1-Phenylethylideneimine. In *Organic Syntheses*; American Cancer Society, **2007**; pp 129–138.

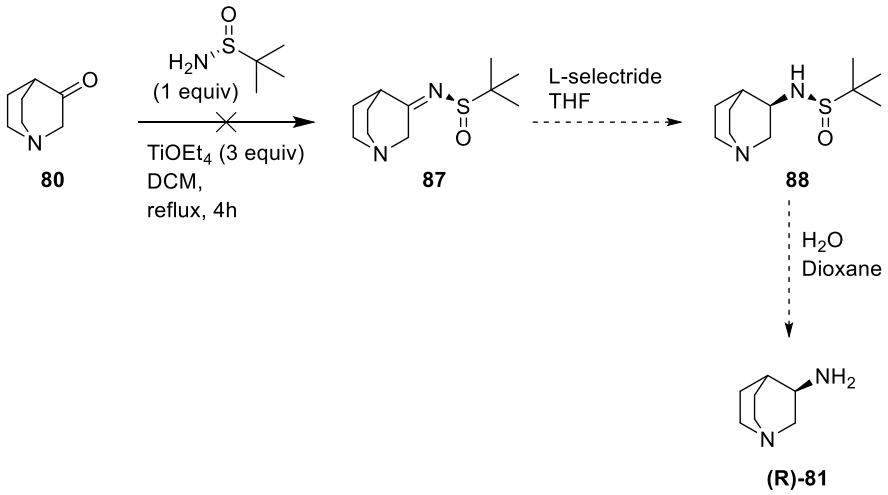

*Scheme 23: Second synthetic pathway to **(R)-81***

Hence, a direct access to enantiopure 3-aminoquinuclidine being not straightforward, we decided to synthesise (S)-3-azidoquinuclidine **(S)-77** and (R)-3-azidoquinuclidine **(R)-77** from respectively commercially available (S)-3-aminoquinuclidine **(S)-81** and (R)-3-aminoquinuclidine **(R)-81** following the same diazotransfer procedure used to synthesise the racemic 3-azidoquinuclidine **77** (Scheme 19). Yields obtained were in agreement with the process on racemic mixture, and we observed the same issues with the enantiopure compounds that were already observed with the racemic 3-azidoquinuclidine **77** concerning their instability and volatility. For this reason, we will assume that the conversions of amines **81**, **(S)-81** and **(R)-81** into the azide **77**, **(S)-77** and **(R)-77** were total in the following steps of the synthesis.

5.3.3. Alkynes 78a-c and 79a-c synthesis

Once we managed to synthesize azides **77**, **(S)-77** and **(R)-77**, we had to work on the an easily feasible and convergent synthetic pathway to obtain the alkynes bearing a carbamate group. First, we had to synthesize one of the carbamates precursors, the methyl(ethyl) carbamoyl chloride, which was not commercially available (Scheme 24). In one easy step developed by Fuchs et *al.*[337], we obtained **91c** from triphosgene **89** and *N*-methylethanamine **90** in presence of sodium bicarbonate in a quantitative yield and without any purification required.

[337] Fuchs, M.; Koszelewski, D.; Tauber, K.; Kroutil, W.; Faber, K. Chemoenzymatic Asymmetric Total Synthesis of (S)-Rivastigmine Using ω-Transaminases. *Chem. Commun.* **2010**, *46* (30), 5500–5502.

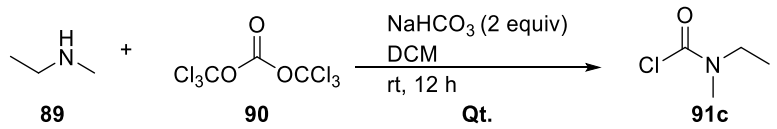

*Scheme 24: Synthesis of carbamoyl chloride **91c***

Our first attempt to synthesize the alkynes was to use a Sonogashira coupling reaction between trimethylsilylacetylene and the bromophenols bearing the desired carbamate moiety. Yet, our first attempts, and the experience of the laboratory on Sonogashira coupling reactions led us to realize that this carbamate moiety was interfering with the halogen residue during the Sonogashira cross coupling process. Thus, we changed our approach and decided to begin with the Pd-catalysed cross coupling reaction prior to the carbamoylation of the phenol (Scheme 25). The desired alkynes were synthesized in only 3 steps following the same synthetic pathway for all of them, with modest to good yields.

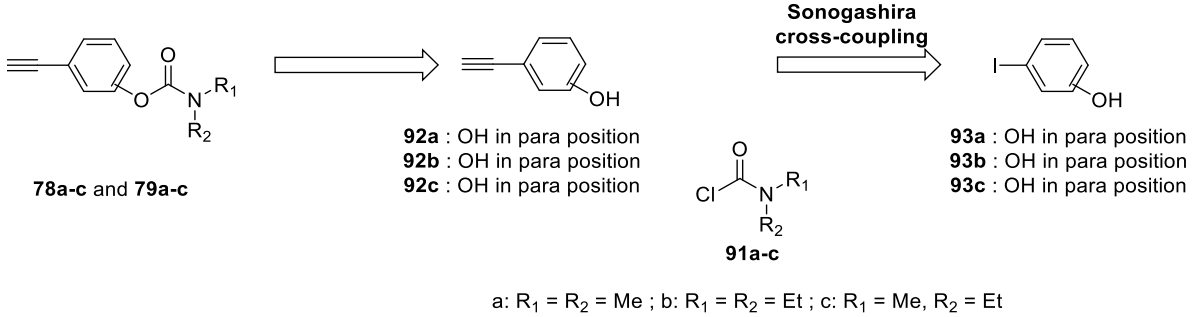

*Scheme 25: Retrosynthetic pathway for alkynes **78a-c** and **79a-c***

After a Pd-catalyzed Sonogashira coupling[338] reaction between iodophenols **93a-c** and trimethylsilylacetylene in present of a catalytic amount of a tetrakis(triphenylphosphine)palladium (0), we performed a deprotection of the obtained compounds, using tetrabutylammonium fluoride in order to obtain alkynes **92a-c**[339]. The following step was a carbamoylation reaction of the phenol on the alkynes and the corresponding carbamoyl chloride with potassium carbonate[340] giving us a series of new 6 alkynes **78a-c** and **79a-c** bearing respectively the *N,N*-dimethyl carbamate **91a**, the *N,N*-diethyl carbamate **91b** and the *N,N*-methylethyl carbamate **91c** substituted in positions meta and para (Scheme 26).

[338] Mercey, G.; Verdelet, T.; Saint-André, G.; Gillon, E.; Wagner, A.; Baati, R.; Jean, L.; Nachon, F.; Renard, P.-Y. First Efficient Uncharged Reactivators for the Dephosphylation of Poisoned Human Acetylcholinesterase. *Chem. Commun.* **2011**, *47* (18), 5295.

[339] Tassano, E.; Alama, A.; Basso, A.; Dondo, G.; Galatini, A.; Riva, R.; Banfi, L. Conjugation of Hydroxytyrosol with Other Natural Phenolic Fragments: From Waste to Antioxidants and Antitumour Compounds. *Eur. J. Org. Chem.* **2015**, *2015* (30), 6710–6726.

[340] John, A.; Nicholas, K. M. Palladium Catalyzed C–H Functionalization of *O* -Arylcarbamates: Selective *Ortho* -Bromination Using NBS. *J. Org. Chem.* **2012**, *77* (13), 5600–5605.

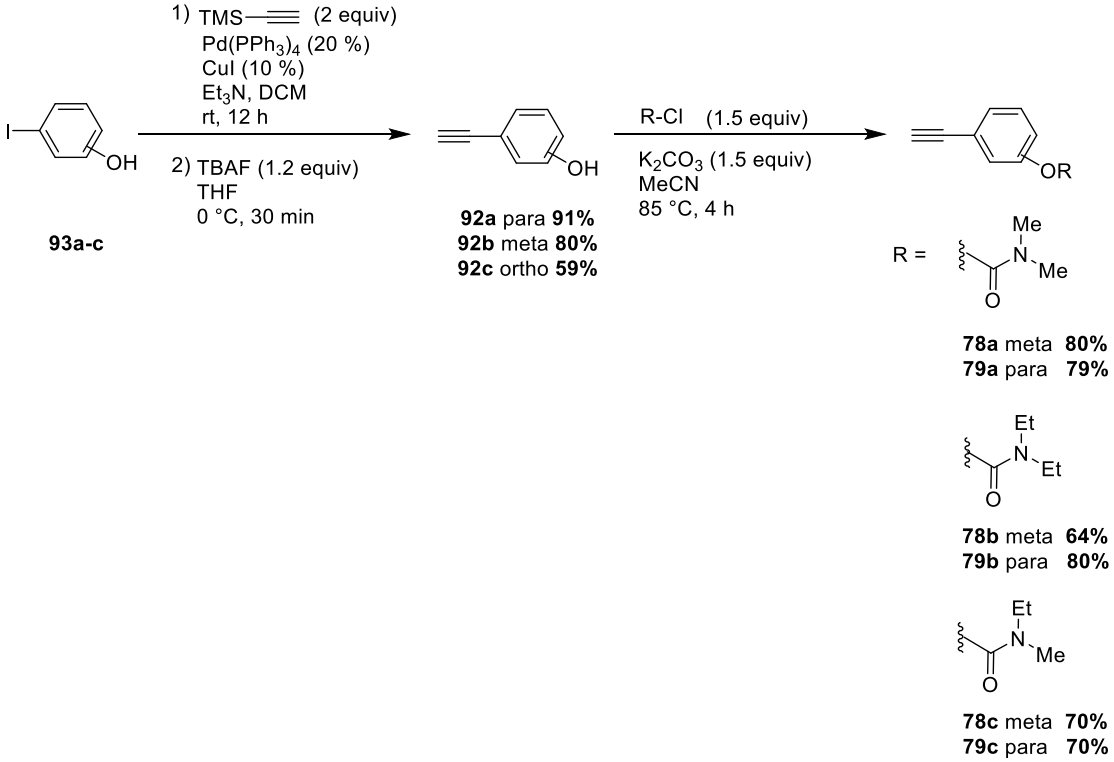

*Scheme 26: Alkynes **78a-c** and **79a-c** synthesis*

At the beginning of the project, alkynes bearing the carbamate in the ortho position were also targeted. Yet, we realised that, even if, the accordingly substituted alkyne could be obtained, steric hindrance induced by the carbamate position will preclude performing the CuAAC, the last step of the synthetic scheme. Nevertheless, we managed to obtain the 6 other alkynes (meta and para substituted) in only 3 steps with overall yields ranging from 51 to 73%.

5.3.4. Final key step of the synthesis: The Copper catalysed Huisgen cycloaddition

With the racemic and enantiopure azidoquinuclidines and the different alkynes in hands, we could perform the Huisgen cycloaddition using catalytic amounts of Cu(II)[341] salts, through in situ reduction of the Cu(II) salts by sodium ascorbate as a reductive agent to obtain catalytically active Cu(I) derivatives. Thus, a new series of 18 MTDLs was obtained with yields ranging from 9 to 36% (6 new ligands were synthesized, either as racemic mixtures **75a-c** and **76a-c** or each one of the enantiopure form **(R)-75a-c** and **(R)-76a-c** and **(S)-75a-c** and **(S)-76a-c**) (Scheme 27).

[341] Sarasamkan, J.; Scheunemann, M.; Apaijai, N.; Palee, S.; Parichatikanond, W.; Arunrungvichian, K.; Fischer, S.; Chattipakorn, S.; Deuther-Conrad, W.; Schüürmann, G.; Brust, P.; Vajragupta, O. Varying Chirality Across Nicotinic Acetylcholine Receptor Subtypes: Selective Binding of Quinuclidine Triazole Compounds. *ACS Med. Chem. Lett.* **2016**, *7* (10), 890–895.

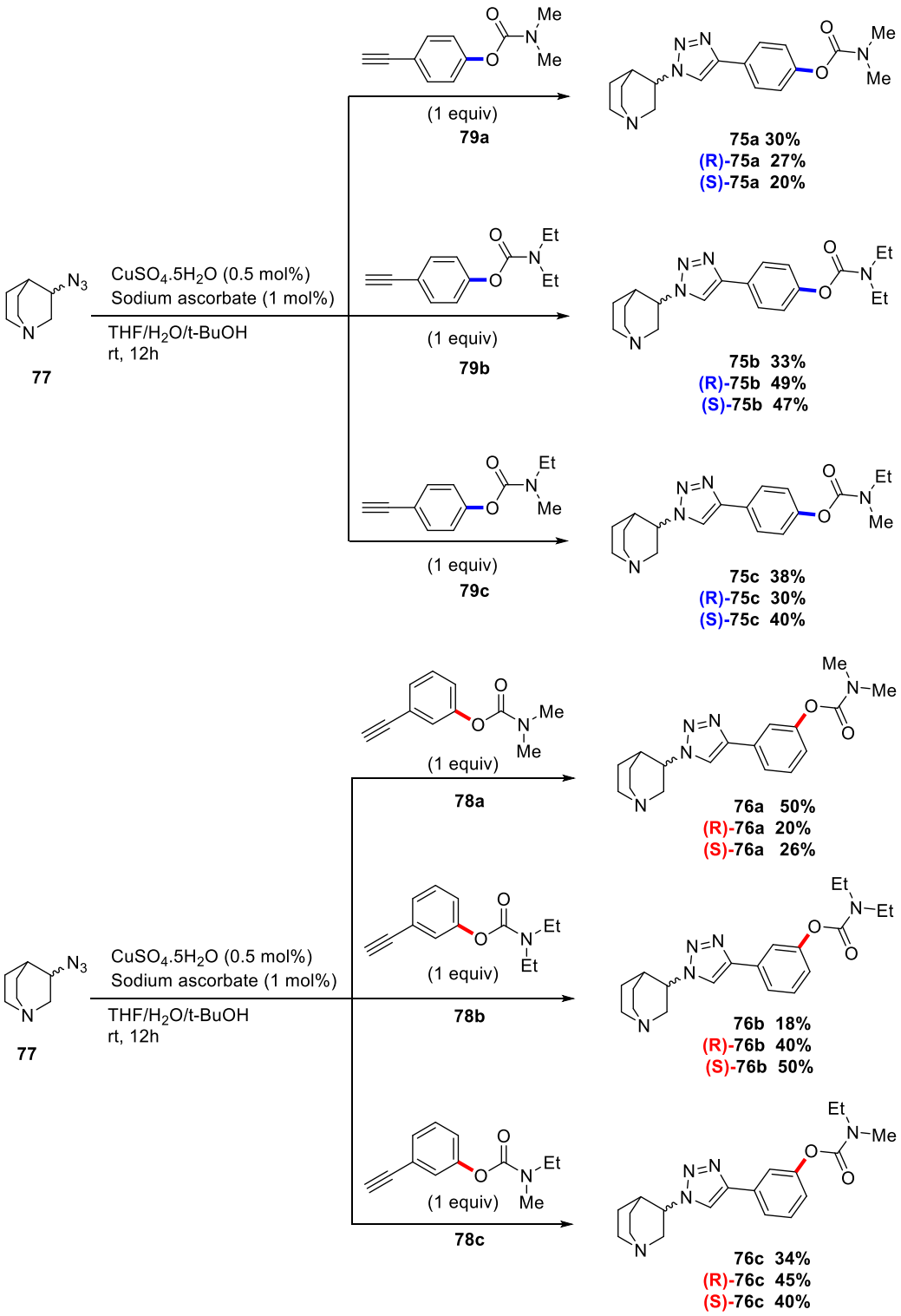

Scheme 27: Final step of MTDLs synthesis

Our efforts to rationalise the different global yields we obtained for the MTDLs series yet failed. Indeed, the unreproducible and variable yields we obtained for the azide intermediate precluded such a rationalization. This poor reproducibility could be directly assigned to the azide formation step and the high volatility and lack of stability of this key intermediate. Thus, these poor reproducibility issues had

a direct impact on the global MTDLs yields. The following global yields were obtained for the different targeted MTDLs (Table 9).

Entry	Compound	Number of steps	Overall yield (%)
1	**75a**		22
2	**76a**		32
3	**75b**	6	24
4	**76b**		9
5	**75c**		24
6	**76c**		19
7	**(R)-75a**		19
8	**(R)-76a**		13
9	**(R)-75b**	5	36
10	**(R)-76b**		20
11	**(R)-75c**		19
12	**(R)-76c**		25
13	**(S)-75a**		14
14	**(S)-76a**		16
15	**(S)-75b**	5	34
16	**(S)-76b**		25
17	**(S)-75c**		25
18	**(S)-76c**		22

Table 9: Global yields obtained for the 18 targeted MTDLs

As a conclusion, we managed to obtain 6 new racemic combined MTDLs in 6 steps with global yields from 9% to 32% (entries 1 to 6) and their enantiopure analogues in 5 steps with overall yields from 13% to 36% for the (R) derivatives (entries 7 to 12) and global yields from 14% to 34% for the (S) analogues (entry 13 to 18).

6. Biological results

6.1. Binding affinity toward α-7 nAChR

The 12 enantiopure compounds **(R)-75a-c** and **(R)-76a-c** and their enantiomers **(S)-75a-c** and **(S)-76a-c** were evaluated for their binding affinities toward α7 nAChR by the Pr. Chalon's team (CHU de Tours)

and reported in Table 10. Experiments were performed on male Wistar rats beheaded on the day of the assay and both frontal cortices of each animal were removed and kept on ice. Binding was determined by incubating proteins extracts from the frontal cortices (25 µg), radiolabelled [^{125}I]α-bungarotoxin (2 nM) , a known competitive antagonist of nAChR in the presence or not of each tested compound (10^{-6} to 10^{-10} M). K_i values corresponding to the ability of each compound to compete for nAChR binding with bungarotoxin were calculated according to Cheng and Prusoff procedure[342]. Assays were repeated in triplicate.

A first thing to observe is that, as expected, all the (R) compounds (entry 2 to 7) have significant better affinities toward α7 nAChR than the (S) compounds (entry 8 to 13). Indeed, the best candidate of the (S) series has a binding affinity of 13 nM (entry 9) whereas the lowest value for the (R) series is 2.3 nM (entry 6). We can also note as an unexpected and gratifying result that our most promising compound (entry 2) shows a better binding affinity that the monomer (entry 1) we based our work on. Indeed, the values ranges from 8 nM for the known α7 nAChR agonist (entry 1) to 0.35 nM for compound **(R)-75a** (entry 2). One of the main risks when associating two pharmacophores when developing MTDLs is that the combined compounds displays a decrease or even total loss of one of the targeted biological activities. On the contrary in our case, it seems that that the carbamate moiety, initially introduced on the α7 nAChR ligand in order to add an AChE inhibitory activity, tends to increase the ligand affinity toward the receptor.

[342] Yung-Chi, C.; Prusoff, W. H. Relationship between the Inhibition Constant (KI) and the Concentration of Inhibitor Which Causes 50 per Cent Inhibition (I50) of an Enzymatic Reaction. *Biochem. Pharmacol.* **1973**, *22* (23), 3099–3108.

Entry	Compound	K_i (nM)[a,b]
1	**(R)-69** (reminder)	8 ± 4
2	**(R)-75a**	**0.35 ± 0.05**
3	**(R)-76a**	1.5 ± 0.4
4	**(R)-75b**	1 ± 0.2
5	**(R)-76b**	2.1 ± 1
6	**(R)-75c**	2.3 ± 1
7	**(R)-76c**	1.8 ± 0.2
8	**(S)-75a**	25 ± 8
9	**(S)-76a**	13 ± 3
10	**(S)-75b**	15 ± 5
11	**(S)-76b**	17 ± 3
12	**(S)-75c**	20 ± 5
13	**(S)-76c**	15 ± 3

[a] Values are expressed as an average of 3 values from 3 independent experiments +/- SEM; [b] Binding determined by incubating proteins extracts from the frontal cortices (25µg), radiolabelled [125I]α-bungarotoxin (2 nM) and the tested compounds (10^{-6} to 10^{-10} M). Ki values were calculated according to Cheng and Prusoff procedure[342]

*Table 10: Affinity of **(R)-75a-c, (R)-76a-c, (S)-75a-c** and **(S)-76a-c** toward a7 nAChRs*

6.2. AChE inhibition

Cholinesterases inhibition were evaluated for the 6 (R) enantiomers by the Pr. Bartolini's team on human AChE and BChE and the preliminary data are reported in Table 11, unfortunately (S) enantiomers could not be evaluated due to a contamination of the series. The capacity to inhibit AChE and BChE activities were assessed using the Ellman's method[343]. Initial rate assays were performed at 37 °C with a Jasco V-530 double beam spectrophotometer. Stock solution of the tested compounds (3 mM) were prepared in methanol and diluted in methanol. The assay solution consisted of a 0.1 M

[343] Ellman, G. L.; Courtney, K. D.; Andres, V.; Featherstone, R. M. A New and Rapid Colorimetric Determination of Acetylcholinesterase Activity. *Biochem. Pharmacol.* **1961**, *7* (2), 88–95.

phosphate buffer, pH 8.0, with the addition of 340 µM 5,5'-dithiobis(2-nitrobenzoic acid), 0.02 unit/mL human recombinant AChE (Sigma Chemical) or human serum BChE (Sigma Chemical), and 550 µM substrate (acetylthiocholine iodide – ACTh or butyrylthiocholine iodide - BTCh, respectively). Assay solutions with and without inhibitor were preincubated at 37 °C for 40 min in the case of *h*AChE-based assay and of 20 min in the case of *h*BChE-based assay followed by the addition of substrate. Blank solutions containing all components except *h*AChE or *h*BChE were prepared in parallel to account for the non-enzymatic hydrolysis of the substrate.

The results of these assays showed that the combined MTDL displays an equal or even higher inhibition potency towards cholinesterases: compound **(R)-76a** (entry 3) and **(R)-75b** (entry 4) display an almost 10 time more efficient inhibitory activity against *h*AChE as compared to Rivastigmine. Compound **(R)-76a** also exerted a high inhibitory activity toward *h*BChE compared to the known inhibitory activity of Rivastigmine against BChE, this added property could also have a positive effect against cholinergic deficit and lead us to the conclusion that compound **(R)-76a** seemed to be the best candidate of the series. Moreover, time-dependent inhibition profile of **(R)-75b** has been first determined in order to define the necessary incubation time to evaluate inhibitory potency toward *h*AChE of the other derivatives (Figure 101). The Stigmine derivatives cholinesterase inhibition mechanism is a slow and reversible process as we already mentioned. Hence, the results obtained for compound **(R)-75b** which must be incubated for 40 minutes to reach 50% of inhibition are in accordance with what could be expected for carbamate-based AChEI.

Entry	Compound	IC_{50} *h*AChE (µM)[a]	IC_{50} *h*BChE (µM)[b]
1	**Rivastigmine**	48	54
2	**(R)-75a**	64.2 ± 1.5	191 ± 32
3	**(R)-76a**	**5.32 ± 0.67**	**2.74 ± 0.08**
4	**(R)-75b**	**4.98 ± 0.21**	**nd[c]**
5	**(R)-76b**	177 ± 34	nd
6	**(R)-75c**	nd	nd
7	**(R)-76c**	56.5 ± 1.9	nd

[a]incubation time of 40 min; [b]incubation time of 20 min; [c]not determined

Values are expressed as an average of 3 values from 3 independent experiments +/- SEM

Stock solution of the tested compound (3 mM) was prepared in methanol and diluted in methanol. Assays solutions of a 0.1 M phosphate buffer, pH 8.0, with the addition of 340 µM 5,5'-dithiobis(2-nitrobenzoic acid), 0.02 unit/mL human recombinant AChE (Sigma Chemical) or human serum BChE (Sigma Chemical), and 550 µM substrate (acetylthiocholine iodide – ACTh or butyrylthiocholine iodide - BTCh, respectively). Assay solutions with and without inhibitor were preincubated at 37 °C followed by the addition of substrate.

*Table 11: Cholinesterases Inhibition potency of **(R)-75a-c** and **(R)-76a-c***

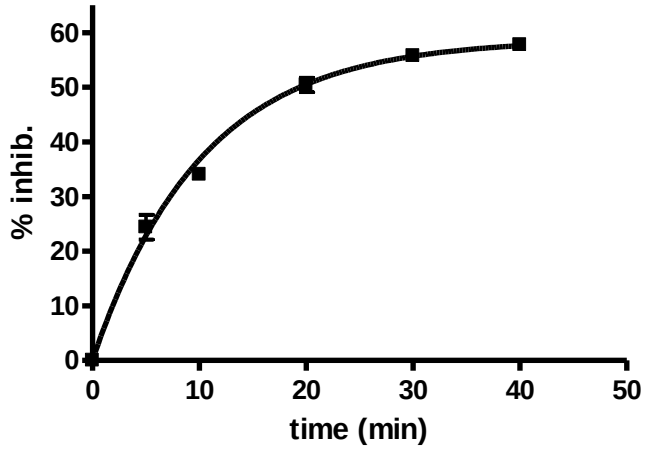

Stopped time assay performed, in which AChE and **(R)-75b** at a concentration of 6.0 µM, a value close to its IC_{50} value, were mixed in the assay buffer at pH 8.0. After 5, 10, 20, 30 and 40 minutes incubation at 37 °C, the determination of residual activity of the AChE-catalyzed hydrolysis of ATCh was carried out by Ellman's method[343].

*Figure 101: time-dependent inhibition profile of **(R)-75b***

We were particularly pleased to observe that for some of the synthesized MTDLs displayed a better AChE inhibition potency (up to one order of magnitude) that parent carbamate Rivastigmine. These results could be explained by the additional interactions which were predicted in the preliminary *in silico* studies between the quinuclidine fragment and peripherical site of the enzyme. Only crystal structures of the enzyme in interaction with the MTDLs could confirm these hypotheses. These studies are in progress in Martin Weik's team (IBS, Grenoble), a longtime collaborator of Pr. Renard's team for AChE and BChE structures determination.

The biological evaluations of the MTDLs affinities toward α7 nAChRs and inhibitory potency against AChE have shown global encouraging results, and two compounds have shown to be the most promising, **(R)-76a** and **(R)-76b** (Figure 102). Indeed, these results allowed us to obtain conjugates between an α7 nAChR agonist pharmacophore with an AChE inhibitor pharmacophore with increased properties compared to both the parent monomers. The IC_{50} values toward *h*AChE decreased from 50 µM to values around 5 µM. For the α7 nAChR, affinities decreased from 8 nM for the monomer parent to values around 1 nM for the MTDLs. These results have brought to light that a rational choice of each pharmacophore, besides its known activity toward its designated receptor, could assist the other pharmacophore in order to increase its biological properties.

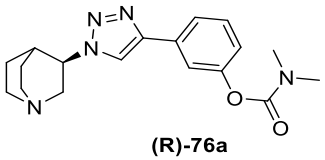

(R)-76a

IC_{50} (*h*AChE) = 5.32 μM
IC_{50} (*h*BChE) = 2.74 μM
K_i (α7 nAChR) = 1.5 nM

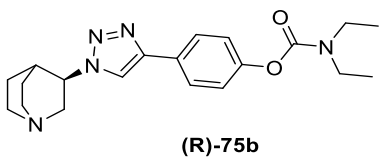

(R)-75b

IC_{50} (*h*AChE) = 4.98 μM
K_i (α7 nAChR) = 1.0 nM

Figure 102: Most promising MTDLs obtained for the series

Since the phenol is released once AChE or BChE is inhibited, we will also need to evaluate the biological properties of these parent compounds towards α7 nAChR. The preliminary results we obtained only display a binding affinity for the MTDL with α7 nAChR, for the carbamate and the phenols, the next step will be to undertake electrophysiological experiments in order to evaluate the effect of the MTDL (agonist / antagonist / allosteric modulator) on the receptor. These experiments will be undertaken by Dr. Romulo Araoz and Dr. Denis Servent's team at CEA Saclay. This team possesses the know-how on HiClamp experiments on xenopus ovocytes overexpressing the human α7 nAChR and has already evaluated the effect of some of the MTDLs synthesized in Pr. Renard's team.

The set-up of these assays required an additional amount of the most promising MTDLs. I, thus, following the synthetic pathway we optimized, performed an upscaled synthesis of the following compounds (Table 12):

Entry	Compound	Structure	Isolated mass (mg)
1	**(R)-76a**	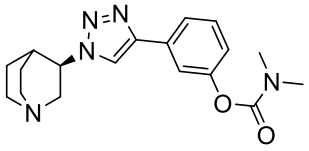	30
2	**(R)-75b**	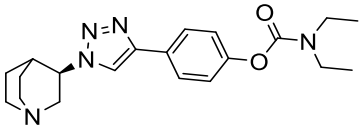	80

*Table 12: Upscale synthesis of **(R)-76a** and **(R)-75b***

If an agonist activity or an allosteric modulation is observed, the next step will be to evaluate the BBB crossing ability for the best compounds obtained (a collaboration with Pr. Marie-Pierre Dehouck, Université d'Artois has been set up to this end). If the *in silico* prediction are confirmed, *in vivo* studies will be undertaken, but finding an industrial partner able to further develop these molecules would be the best strategy.

7. Synthesis of Stigmine's derivatives with an optimised linker

7.1. Rational choice a new linker

The promising binding affinities of the MTDLs **(R)-75a-c** and **(R)-76a-c** with α7 nAChRs determined by Pr Sylvie Chalon's team, lead us to go one step further in order to increase these values by combining Pr Routier's expertise on α7 nAChRs and the expertise we gained in the development of combined MTDLs using CuAAC. Our preliminary results have shown that combining two pharmacophores, a carbamate and a quinuclidine, could end up in an increase of both the molecules affinity toward α7 nAChRs, and AChE inhibition potency. Moreover, it has been recently shown by Pr. Routier's team that adding a phenyl ring substituted in the meta position as represented in compound **(R)-94** could increase the binding affinity as compared to the monomer **(R)-69** bearing only one phenyl ring or a substituent in the para position (Figure 103)[344].

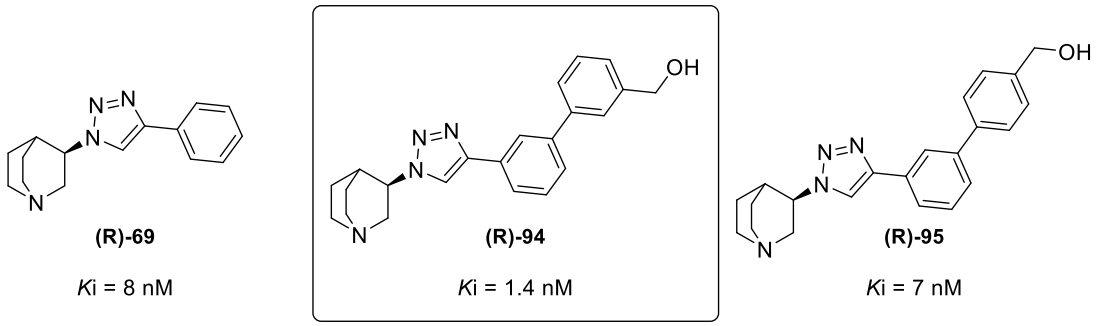

Figure 103: Second generation α-7 nAChR agonists developed by Routier et al.

Before beginning the synthesis of these new MTDLs, we decided to perform some docking studies. The aim was to check if increasing the size of the linker could lead to a modification of the position of the molecule inside AChE catalytic site, and thus, could change significantly the AChE inhibition activity of the MTDLs.

[344] Ouach, A.; Vercouillie, J.; Bertrand, E.; Rodrigues, N.; Pin, F.; Serriere, S.; Boiaryna, L.; Chartier, A.; Percina, N.; Tangpong, P.; Gulhan, Z.; Mothes, C.; Deloye, J.-B.; Guilloteau, D.; Page, G.; Suzenet, F.; Buron, F.; Chalon, S.; Routier, S. Bis(Het)Aryl-1,2,3-Triazole Quinuclidines as A7 Nicotinic Acetylcholine Receptor Ligands: Synthesis, Structure Affinity Relationships, Agonism Activity, [18F]-Radiolabeling and PET Study in Rats. *Eur. J. Med. Chem.* **2019**, *179*, 449–469.

7.1.1. Docking studies

Following the previously explained procedure, we prepared the target, and the different possible ligands by varying the relative position of the phenyl rings and the substituents of the carbamates (12 possible combinations of each enantiomer) (Figure 104).

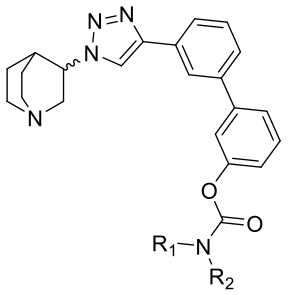

(R)-96a: $R_1 = R_2 = Me$
(S)-96a: $R_1 = R_2 = Me$

(R)-96b: $R_1 = R_2 = Et$
(S)-96b: $R_1 = R_2 = Et$

(R)-96c: $R_1 = Me$; $R_2 = Et$
(S)-96c: $R_1 = Me$; $R_2 = Et$

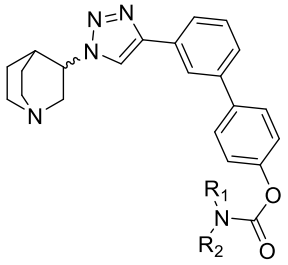

(R)-97a: $R_1 = R_2 = Me$
(S)-97a: $R_1 = R_2 = Me$

(R)-97b: $R_1 = R_2 = Et$
(S)-97b: $R_1 = R_2 = Et$

(R)-97c: $R_1 = Me$; $R_2 = Et$
(S)-97c: $R_1 = Me$; $R_2 = Et$

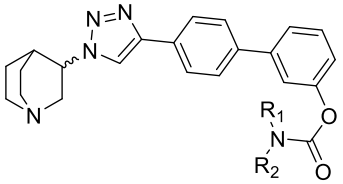

(R)-98a: $R_1 = R_2 = Me$
(S)-98a: $R_1 = R_2 = Me$

(R)-98b: $R_1 = R_2 = Et$
(S)-98b: $R_1 = R_2 = Et$

(R)-98c: $R_1 = Me$; $R_2 = Et$
(S)-98c: $R_1 = Me$; $R_2 = Et$

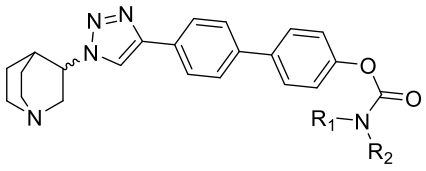

(R)-99a: $R_1 = R_2 = Me$
(S)-99a: $R_1 = R_2 = Me$

(R)-99b: $R_1 = R_2 = Et$
(S)-99b: $R_1 = R_2 = Et$

(R)-99c: $R_1 = Me$; $R_2 = Et$
(S)-99c: $R_1 = Me$; $R_2 = Et$

Figure 104: Structures of the MTDLs evaluated in silico

The three key points to evaluate during this study were:

- the binding energy value,
- the interactions with the main useful residues of the enzyme,
- the proximity of the carbamate with the catalytic serine (Ser203).

We used a semi-rigid model of the enzyme starting from the same crystal structure of *m*AChE (PDB 1Q84)[323] and we choose to give flexibility to the most important catalytic site residues of the target which could be involved in the ligands interaction (Trp86, Tyr72, Tyr124, Tyr337, Tyr341).

7.1.1.1. Binding affinity and proximity with Ser203

After completion of the 24 docking simulations, we obtained the following results listed in Table 13. Once again, the quinuclidine's configuration didn't affect the values and only (R) enantiomers values are reported in the table.

Entry	Compound	Relative position of the carbamate	R_1	R_2	E_{bind} (kcal/mol)	Carbamate - Ser203 distance (Å)
1	**Rivastigmine**	-meta	Me	Et	-7.5	8.7
2	**(R)-96a**	-meta	Me	Me	-12.7	5.0
3	**(R)-96b**	-meta	Et	Et	-12.2	5.3
4	**(R)-96c**	-meta	Me	Et	-12.3	5.0
5	**(R)-97a**	-para	Me	Me	-12.4	6. 8
6	**(R)-97b**	-para	Et	Et	-12.3	6.9
7	**(R)-97c**	-para	Me	Et	-12.4	6.9
8	**(R)-98a**	-meta	Me	Me	-13.2	5.0
9	**(R)-98b**	-meta	Et	Et	-12.2	4.9
10	**(R)-98c**	-meta	Me	Et	12.5	4.9
11	**(R)-99a**	-para	Me	Me	-12.3	6.4
12	**(R)-99b**	-para	Et	Et	-12.2	6.9
13	**(R)-99c**	-para	Me	Et	-12.2	6.5

*Table 13: Docking results for **(R)-96a-c, (R)-97a-c, (R)-98a-c** and **(R)-99a-c***

Adding a phenyl ring to the structure, regardless to its position, increased the predicted binding affinities by approximatively 5 kcal/mol as compared to Rivastigmine, and decreased the predicted distance between the MTDL's carbamate and AChE catalytic serine (Figure 105). Moreover, compared to the results obtained for the first series of carbamate-based derivatives, even though the carbamate-serine distance remained unchanged, the predicted binding affinities with *m*AChE for this second series of MTDLs were also improved by approximatively 5 kcal/mol. This observation was in accordance with the idea that adding a phenyl ring to the structure could lead to an increased stabilisation of the ligand inside the enzymatic pocket through new interactions with the main AChE residues.

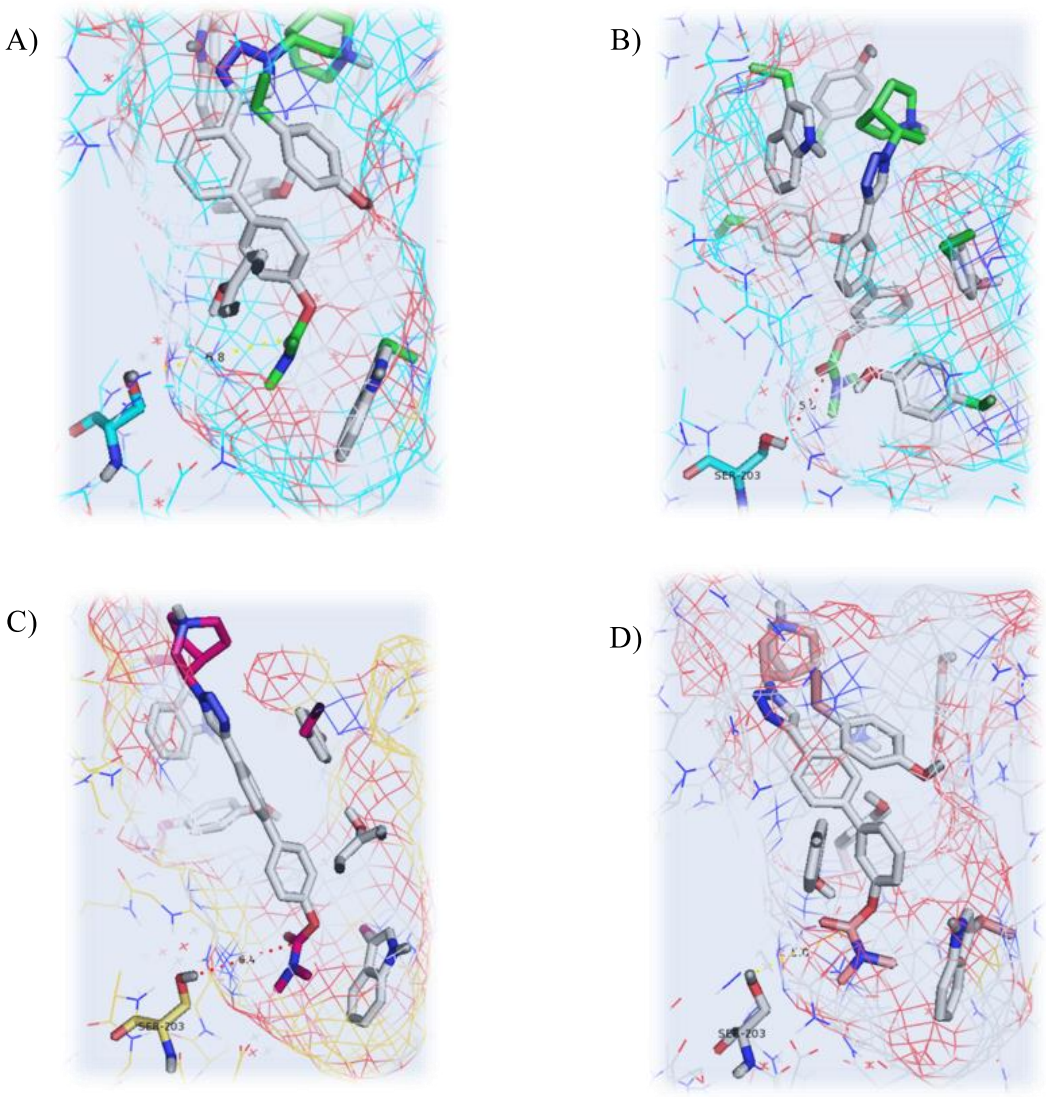

Figure 105: Visualisation of representative docking results for (A) ***(R)-96a*** *and (B)* ***(R)-97a*** *(C)* ***(R)-98a*** *(D)* ***(R)-99a*** *inside AChE catalytic site with PyMol*

7.1.1.2. Interaction with the main AChE residues

Due to the high similarities of the designed MTDLs, we will only discuss the results obtained for **(R)-96a, (R)-97a, (R)-98a** and **(R)-99a** compiled in Table 14**.** These results can be extended to the rest of the series.

Entry	Type of interaction	(R)-96a-c	(R)-97a-c	(R)-98a-c	(R)-99a-c
1	π-π interaction	Trp286 Tyr124 Tyr337 Tyr341	Trp286 Tyr341 Tyr124 Tyr337	Trp286 Tyr124 Tyr341 Tyr337	Trp286 Trp341 Trp286 Tyr124 Tyr341 Tyr337
2	π -σ interaction	Trp86		Trp86	
3	H-bond		Tyr337		Tyr337

*Table 14: In silico interactions predicted for **(R)-96a-c, (R)-97a-c, (R)-98a-c** and **(R)-99a-c***

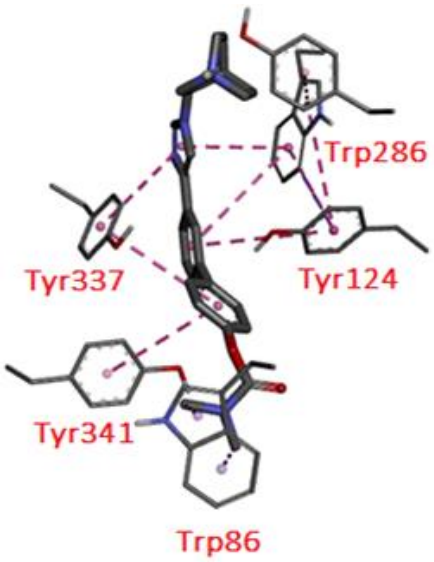

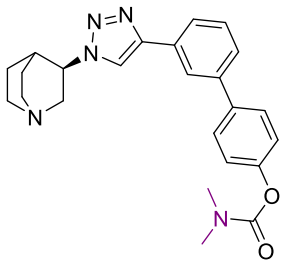

(R)-96a

*Figure 106: Representation of predicted interactions between mAChE and **(R)-96a***

For compound **(R)-96a** (and its analogues **(R)-96b** and **(R)-96c**), displaying the second phenyl ring at the meta position towards the triazole moiety, and the carbamate at the para position of this second phenyl ring, two types of interactions are reported in Figure 106: π-π stacking (in pink) and π-σ (in

purple). The phenyl ring directly linked to the triazole moiety is predicted to undergo π-π stacking interactions with Trp286 and Tyr124, Tyr337 whereas Tyr341 is predicted to interact with the phenyl ring bearing the carbamate (entry 1). Moreover, Trp86 is predicted to interact with the two methyl of the carbamate in a π-σ-type interaction (entry 2).

Concerning **(R)-97a** (and its analogues **(R)-97b to (R)-97c**), displaying the second phenyl ring at the meta position towards the triazole moiety, and the carbamate at the meta position of this second phenyl ring, we also observed two types of interactions (Figure 107). First, there is a H-bond formation (in green) between the carbamate's oxygen and the Tyr337 (entry 3). Then, we observed various π-π stacking (in pink) between the AChE residues and the triazole moiety and the two phenyl rings. Indeed, the triazole ring interacts with Trp286 and Tyr341. The phenyl directly linked to the triazole, for its part, is predicted to undergo π-π stacking interactions with Trp286 and Tyr124. Finally, the second phenyl ring bearing the carbamate interacts in the same way with Tyr341 and Tyr 337 (entry 1).

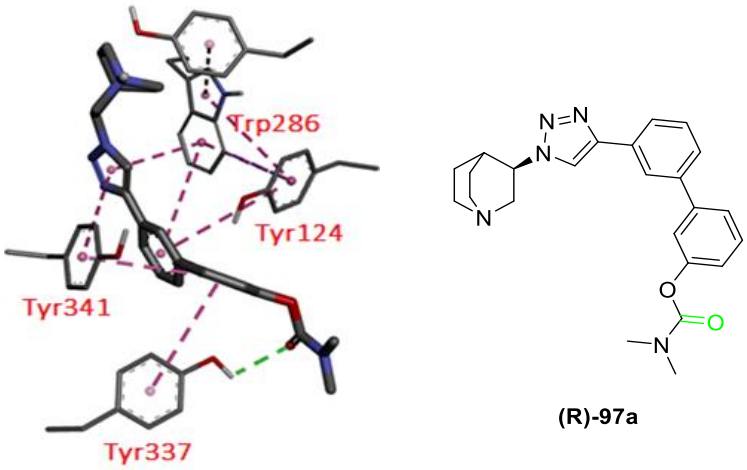

*Figure 107: Representation of predicted interactions between mAChE and **(R)-97a***

Regarding compound **(R)-98a** (and its analogues **(R)-98b** and **(R)-98c**), displaying the second phenyl ring at the para position towards the triazole moiety, and the carbamate at the meta position of this second phenyl ring, the main predicted interactions are π-π type interactions (in pink) (Figure 108). Indeed, the triazole moiety interacts with Trp286, the phenyl ring directly linked to the triazole is predicted to interact with Tyr341 and Tyr124 while the second phenyl ring bearing the carbamate is predicted to interact with Trp86 and Tyr337 (entry 1). Moreover, Tyr337 is also predicted to interact with the carbamate's oxygen *via* a H-bond (entry 3) (in green).

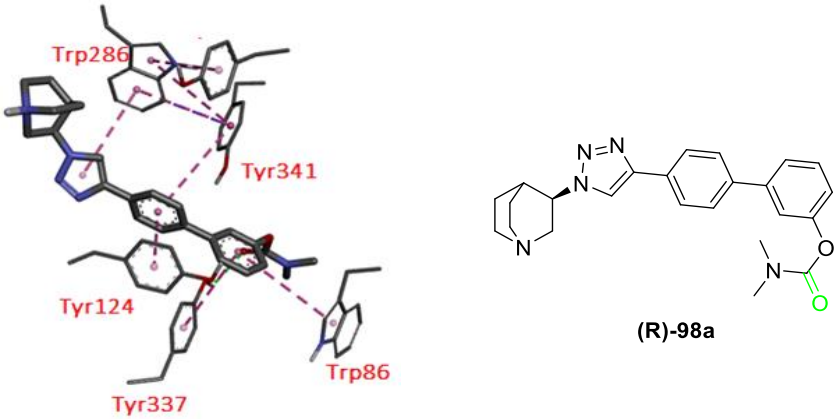

*Figure 108: Representation of predicted interactions between between mAChE and **(R)-98a***

Eventually, for compound **(R)-99a** (and its analogues **(R)-99b** and **(R)-99c**), displaying the second phenyl ring at the para position towards the triazole moiety, and the carbamate at the para position of this second phenyl ring, besides a predicted π-σ interaction (in purple) between one of the carbamate's methyl and Trp86 (entry 2), all the other predicted interactions include the phenyl rings and π-π stacking type interactions (Figure 109). Indeed, the phenyl ring directly linked to the triazole moiety is predicted to interact with Trp286 and Tyr124, while the second phenyl ring bearing the carbamate is predicted to interact with Tyr341 and Tyr337 (entry 1).

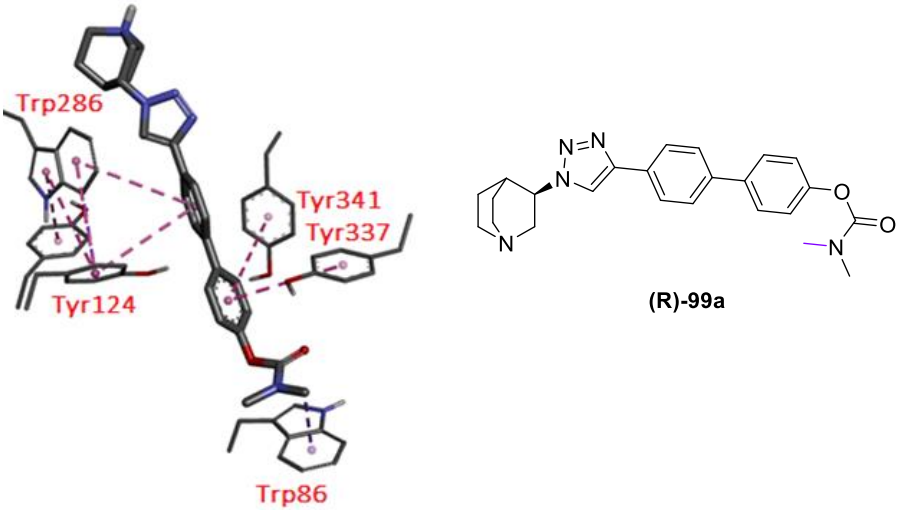

Figure 109: Representation of predicted interactions between mAChE and **(R)-99a**

Finally, in comparison with the results obtained for Rivastigmine and explained in the first part of this chapter (Figure 99 – p.174), the interactions between the MTDLs and the enzyme were, as it was expected, close to the ones observed for the parent compound. Moreover, we observed that adding a second phenyl moiety lead to an increased binding energy between the tested MTDLs and the enzyme, indeed, by modifying the MTDLs structures through the addition of a second phenyl ring, we designed

a new series of ligands with more possible interactions with the main AChE residues. Moreover, extending the size of the moiety between the two pharmacophores could also lead to interactions between the designed ligands and the AChE peripheral site which could give to the newly designed molecules other biological activities such as, for example, AChE-induced Aβ aggregate inhibition properties.

7.1.2. Predicting properties to cross the BBB

7.1.2.1. CNS MPO score

After verifying that all the MTDLs **(R)-96a-c, (R)-97a-c, (R)-98a-c** and **(R)-99a-c** followed the Lipinski's rules, CNS MPO scores were calculated and are reported in Table 15 (results can be extended for the respective (S)-enantiomers). It can be observed that adding a phenyl ring to the structure lowers the score compared to the first series derivatives and four of the compounds (entry 3 and 6) obtained a low CNS MPO score under 4. This decrease could be explained by the LogP and LogD values drastic increase, indeed, a high cLogP (or cLogD) is an indicator of the lipophilic character's increase for the MTDL.

However, Waring has shown that the theoretical optimal range of lipophilicity (logD value) was situated between 1 and 3[345], granting our new MTDLs derivative with good physicochemical profiles even if their CNS MPO scores are lower than expected.

[345] Waring, M. J. Lipophilicity in Drug Discovery. *Expert Opin. Drug Discov.* **2010**, *5* (3), 235–248.

Entry	Compound	CLogP	CLogD	TPSA (Å²)	MW g/mol	HBD	pKa	CNS MPO score
1	**(R)-75a** and **(R)-76a** (Reminder)	2.15	0.38	63.49	341.41	0	9.17	**5.4**
2	**(R)-96a** and **(R)-97a**	3.80	2.03	63.49	417.51	0	9.17	**4.6**
3	**(R)-96b** and **(R)-97b**	4.51	2.74	63.49	445.56	0	9.17	**3.7**
4	**(R)-96c** and **(R)-97c**	4.15	2.39	63.49	431.54	0	9.17	**4.1**
5	**(R)-98a** and **(R)-99a**	3.80	2.03	63.49	417.51	0	9.17	**4.6**
6	**(R)-98b** and **(R)-99b**	4.51	2.74	63.49	445.56	0	9.17	**3.7**
7	**(R)-98c** and **(R)-99c**	4.15	2.39	63.49	431.54	0	9.17	**4.1**

*Table 15: Physicochemical properties and CNS MPO scores computed for **(R)-96a-c, (R)-97a-c, (R)-98a-c** and **(R)-99a-c***

7.1.2.2. Percepta software CNS activity prediction

As it was done for the first series of MTDLs we developed, the predicted properties of the MTDLs designed in this second part were also calculated and are reported in Table 16. It is important to notice that adding a phenyl ring to the structures increased the values of LogP, as it was previously demonstrated for the CNS MPO scores calculations, inducing a better value of LogPS. The remaining physicochemical properties do not seem to differ from the results obtained for the first series.

Entry	Compound	LogP	pKa	f_u	LogPS	LogBB	Log ($PS*f_u$)	Brain penetration for CNS activity
1	**(R)-75a** and **(R)-76a** (Reminder)	1.71	9.30	0.23	-2.6	-0.21	-3.0	Sufficient
2	**(R)-96a** and **(R)-97a**	3.36	9.32	0.070	-1.9	0.08	-3.1	Sufficient
3	**(R)-96b** and **(R)-97b**	4.19	9.32	0.051	-1.6	0.39	-3.3	Sufficient
4	**(R)-96c** and **(R)-97c**	3.76	9.32	0.059	-1.7	0.23	-3.2	Sufficient
5	**(R)-98a** and **(R)-99a**	3.21	9.31	0.068	-1.9	-0.01	-3.1	Sufficient
6	**(R)-98b** and **(R)-99b**	4.03	9.31	0.046	-1.6	0.27	-3.2	Sufficient
7	**(R)-98c** and **(R)-99c**	3.61	9.31	0.058	-1.8	0.14	-3.2	Sufficient

*Table 16: Physicochemical properties determined with Percepta software for **(R)-96a-c, (R)-97a-c, (R)-98a-c** and **(R)-99a-c***

The results obtained and presented in Figure 110 were, as it could be expected, closed to the results obtained for the first series. Indeed, these calculations showed that all the MTDLs have promising predicted properties to cross the BBB and it appears that compounds carrying a carbamate substituted by two ethyl groups **(R)-96b** (and **(R)-97b**) and **(R)-98b** (and **(R)-99b**) (B and E Figure 110) could be the most viable compounds to penetrate the BBB.

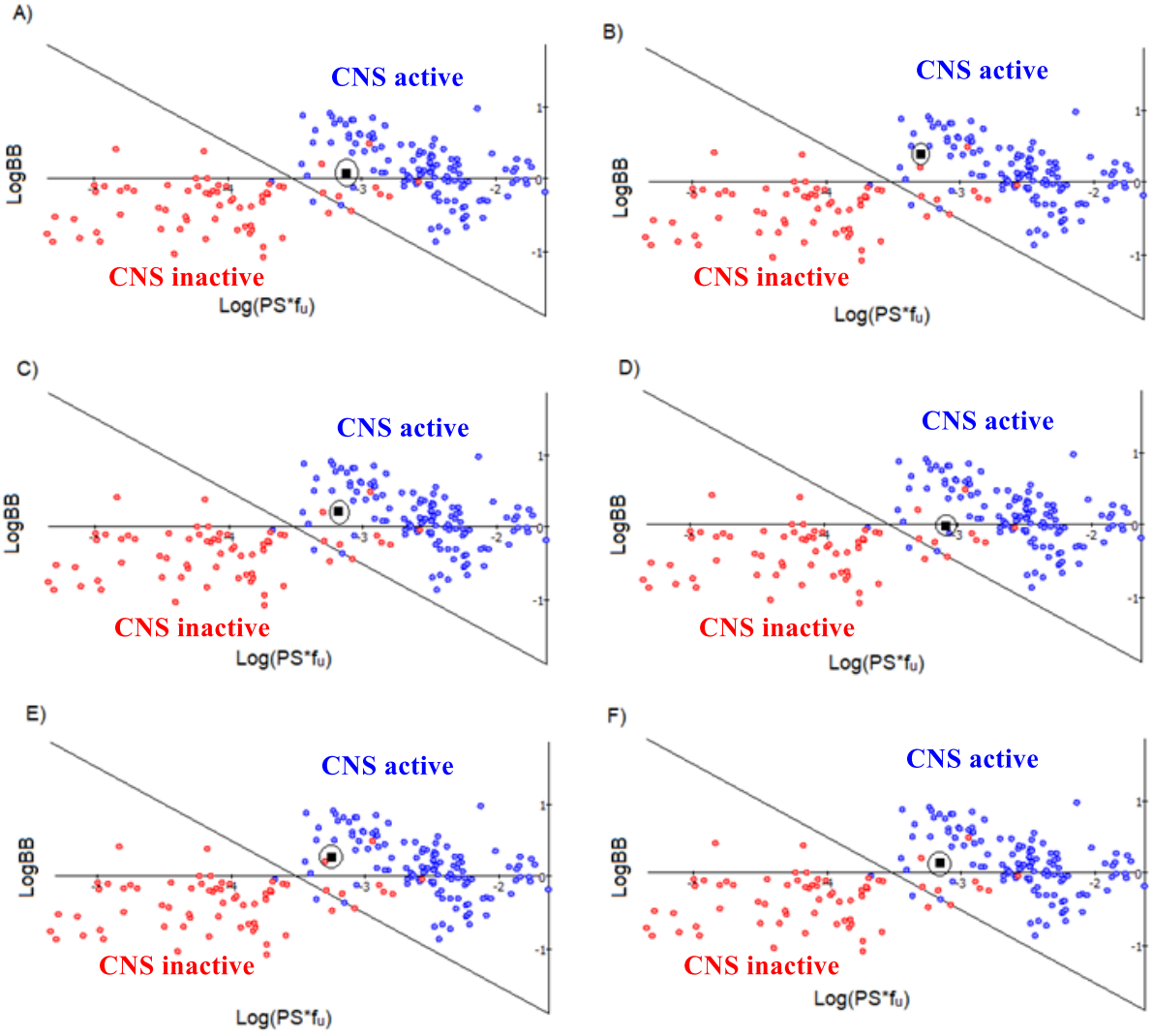

Figure 110: Results of Brain penetration prediction for CNS activity for (A) ***(R)-96a*** *(B)* ***(R)-96b*** *(C)* ***(R)-96c*** *(D)* ***(R)-98a*** *(E)* ***(R)-98b*** *(F)* ***(R)-98c*** *(red dots represent CNS inactive compounds, blue dots represent CNS active compounds and the circled black dot represent the evaluated compound*

With these results in hands and as a rational choice, we decided to develop a new series of MTDLs based on the stigmine's scaffold with a longer linker composed of two phenyls. The phenyl addition could increase the MTDLs affinity for AChE, and thus inhibitory activity (shown by docking experiments) and α7 nAChR (shown by Routier et *al*. experiments). Moreover, increasing the length between the two pharmacophores could lead to additional interactions between the quinuclidine moiety and AChE peripherical site.

At this time of the project, we decided to study only the (R)-enantiomers. Indeed, it was already experimentally showed that these enantiomers had the best binding affinities toward α-7 nAChRs and the docking studies did not show any significant differences between the two series.

7.2. New series synthesis

The first step of our study was to synthesize the bromoalkynes **101a** and **101b** from the corresponding commercially available aldehydes **100a** and **100b**

Our first approach to obtain **101a-b** was to perform a Seyfert-Gilbert homologation[344] using the Bestmann-Ohira reagent synthesized in the laboratory (Scheme 28). Unfortunately, we were not able to isolate the expected product and only obtained complex NMR signals, we were not able to confirm if we formed any expected alkyne.

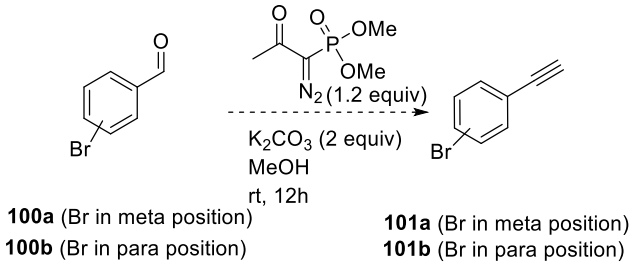

Scheme 28: First attempt for the synthesis of alkynes **101a** and **101b**

We changed our approach and found another pathway described in the literature by Liu et *al*.[346] The strategy was to synthesize the 1,1-dibromoalkene from the aldehyde, followed by a Corey-Fuchs elimination to yield the targeted alkyne. We performed a Ramirez' olefination of commercially available bromoaldehydes **100a** and **100b** with tetrabromomethane and triphenylphosphine and obtained the corresponding 1,1-dibromo alkenes **102a** and **102b** with global yields of *ca.* 50% (Scheme 29). These modest yields could be explained by the difficulties we had to purify the product. Indeed, after completion of the reaction, it is challenging to be able to separate the desired products from the remaining tetrabromomethane, moreover, the quantity of triphenylphosphine oxide formed during the reaction proved to be an issue when up-scaling the reactions. Once we had the desired alkenes, we performed a Corey-Fuchs reaction following the strategy proposed by Liu et *al*. who developed Corey-Fuchs reaction conditions avoiding the use of a strong base and low or high temperatures, therefore, amenable for a wide range of substrates. Their method was appropriate in our case, since the use of a strong lithium based base such as *n*-BuLi could have led to a halogen-metal exchange and thus the loss of the bromine atom, essential for the rest of the synthesis. Their method using tetrabutylammonium fluoride in presence of water, and triphenyl phosphine allowed us to obtain the desired alkynes **101a** and **101b** with good yields without observing the bromoalkyne formation.

[346] Liu, S.; Chen, X.; Hu, Y.; Yuan, L.; Chen, S.; Wu, P.; Wang, W.; Zhang, S.; Zhang, W. An Efficient Method for the Production of Terminal Alkynes from 1,1-Dibromo-1-Alkenes and Its Application in the Total Synthesis of Natural Product Dihydroxerulin. *Adv. Synth. Catal.* **2015**, *357* (2–3), 553–560.

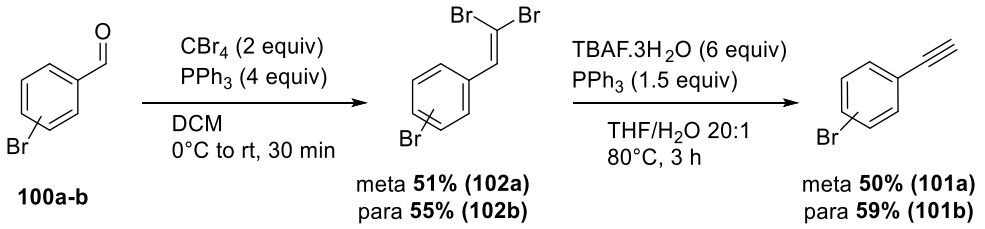

*Scheme 29: Synthesis of alkynes **101a** and **101b***

Liu et *al*. proposed a mechanism for the Corey-Fuchs reaction when TBAF is used as a base and in presence of water, according to their studies, the HO^- appeared to come from the hydrolysis of TBAF (Scheme 30). Indeed, after optimisation of the reaction conditions, they highlighted the importance of water in the solvent mixture, and Katsumura also reported that TBAF.$3H_2O$ promoted the generation of terminal alkyne **101a** over bromoalkyne **103**[346].

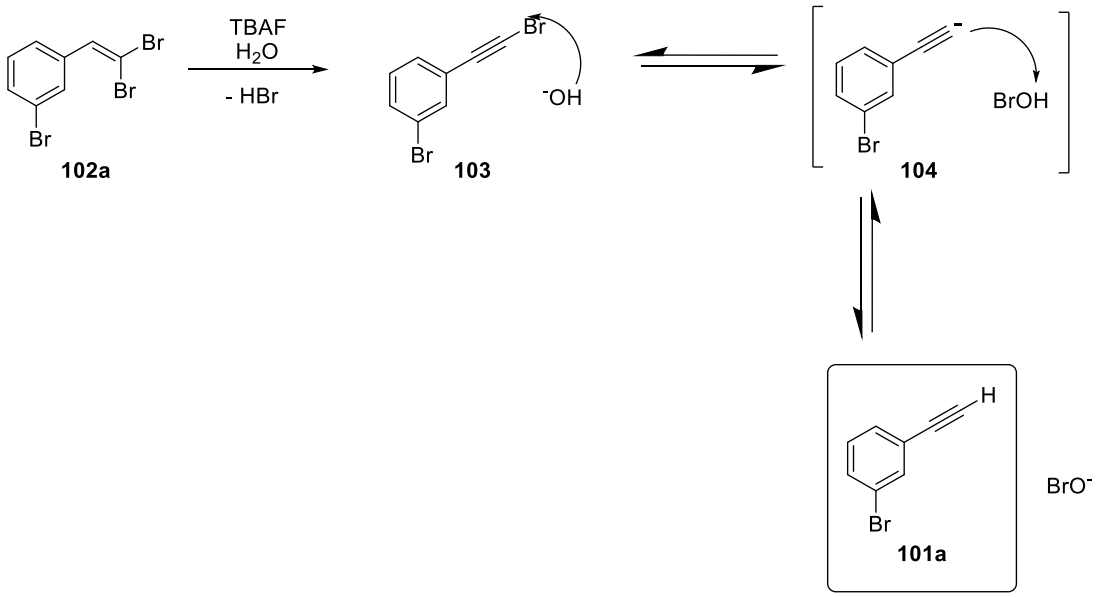

Scheme 30: Proposed mechanism for the Corey-Fuchs reaction under Liu et al.[346] reaction conditions

Once we had compounds **101a-b** in hand, we were able to perform the Copper-catalysed Huisgen's cycloaddition with the (R)-azidoquinuclidine **(R)-77**, using the same reaction conditions we previously presented (Scheme 31)[341]. We obtained compounds **(R)-105a** and **(R)-105b** with poor to good yields. Here again, the yields difference we obtained for the formation of the two compounds could not be explained rationally, apart from the fact that the azide is an unstable and volatile compound.

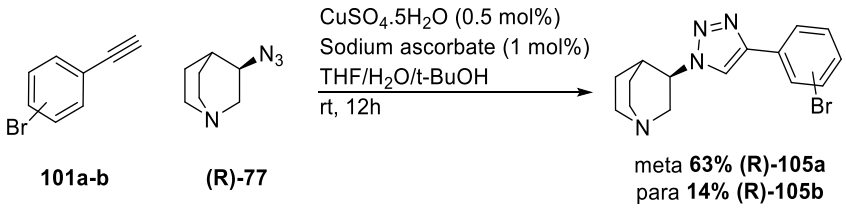

*Scheme 31: Huisgen cycloaddition for **(R)-105a** and **(R)-105b***

Once we managed to obtain compound **(R)-105a** by a CuAAC reaction, we could add the second phenyl ring. Based on the work of Pr. Routier's team, we performed a Suzuki-Myaura reaction between **(R)-105a** and respectively the 3-hydroxyphenylboronic acid **106** for **(R)-108** and 4-phenylboronic acid **107** for **(R)-109**, using tetrakis(triphenylphosphine)palladium [344] catalysis under microwave irradiations (Scheme 32). This optimized synthetic strategy allowed us to obtain readily the two desired compounds in good yields without any step optimisation.

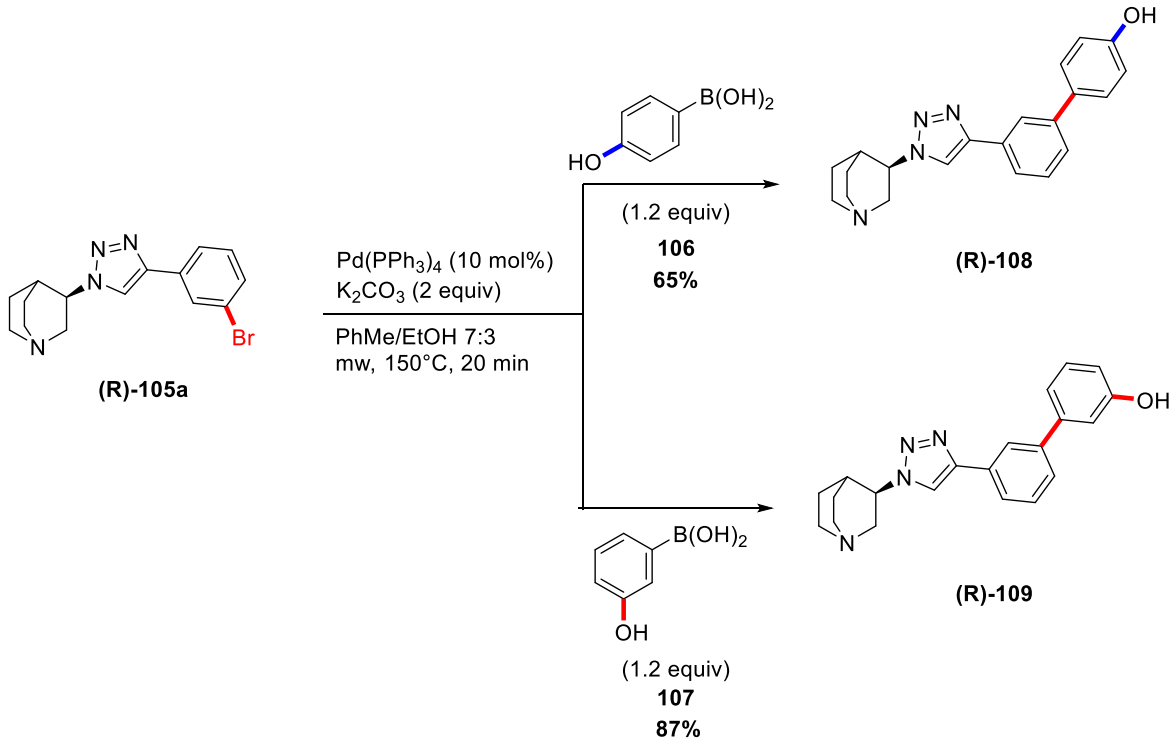

*Scheme 32: Suzuki-Myaura coupling reaction allowing access to **(R)-108** and **(R)-1098***

Building on this success, we decided to synthesize compound **(R)-110** and **(R)-111** from **(R)-105b** using the same synthetic pathway (Scheme 33). Once again, we readily obtained the two key intermediates in good yields.

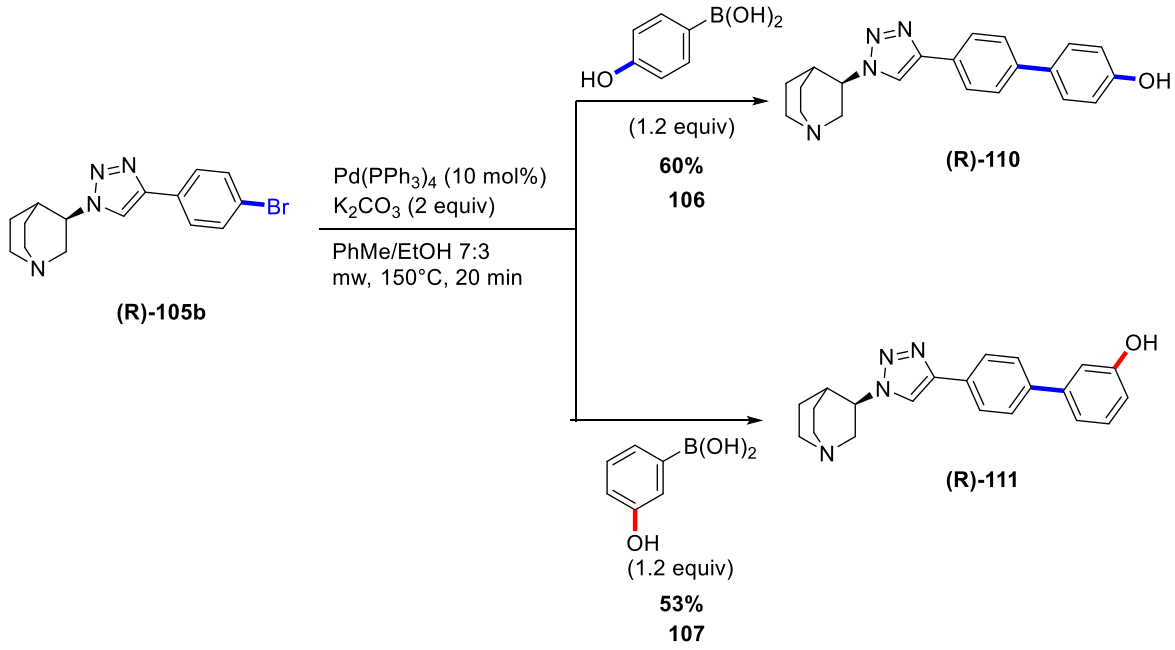

*Scheme 33: Suzuki-Myaura coupling reaction allowing access to **(R)-110** and **(R)-111***

The last step of our synthesis of this new series of MTDLs was the carbamate addition on the second phenyl ring (Scheme 34). By using the same conditions, we already optimized for the first MTDL series, we were able to obtain 6 new MTDLs bearing a quinuclidine fragment and the different carbamates derivatives.

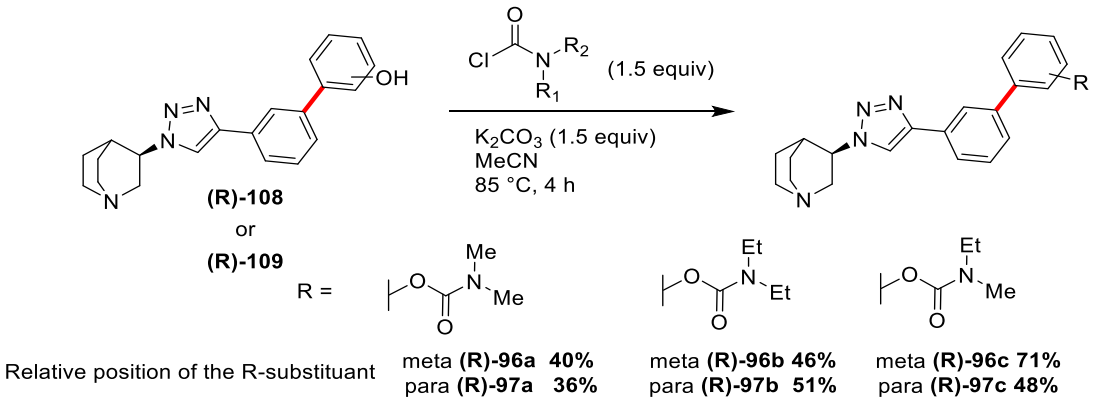

*Scheme 34: Last step of the synthesis to **(R)-96a-c** and **(R)-97a-c***

Due to the lack of time, we had to make a choice concerning the MTDLs to synthesize. We focused on the first series bearing the second phenyl ring in position 3, because the structure was the closest to the α7 nAChRs agonist structure developed by Pr. Routier's team. However, we wanted to design MTDLs with the second phenyl in position 4 (Scheme 35) to be able to evaluate whether this difference in substitution position had an influence for the MTDLs biological activities but we obtained only 4 out

of 6 carbamates, the lack of time did not allow us to synthesize the diethyl carbamate based compounds.

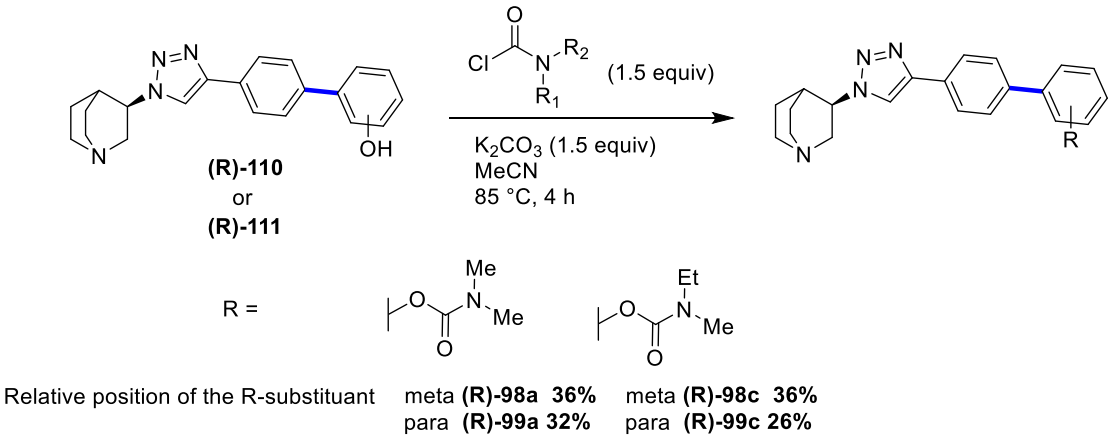

*Scheme 35: Last step of the synthesis to **(R)-98a/c** and **(R)-99a/c***

We thus were able to synthesize 10 new combined MTDLs based on the diphenyl linker, these compounds were obtained in 6 steps with the corresponding total yields from **(R)-81** displayed on Table 17.

Entry	Compound	Number of steps	Global yield (%)
1	**(R)-96a**		4
2	**(R)-97a**		6
3	**(R)-96b**	6	5
4	**(R)-97b**		6
5	**(R)-96c**		5
6	**(R)-97c**		10
7	**(R)-98a**		1
8	**(R)-99a**	6	1
9	**(R)-98c**		1
10	**(R)-99c**		0.8

Table 17: Global yields obtained for the 10 out of 12 targeted MTDLs

One step remained to be undertaken to obtain the two remaining compounds to achieve this second combined MTDL series. The *in vitro* biological evaluation for the 10 obtained compounds is in progress both for cholinesterase inhibition and α7 nAChR binding affinity.

8. Partial conclusion and perspective on the project.

As a conclusion, after *in silico* evaluations, we managed to develop two short synthetic pathways able to yield two new combined MTDLs series against AD based on stigmine based AChE inhibitors and quinuclidine based α7 nAChR agonists.

- For the first series of Stigmine derivatives, we managed to obtain 18 new compounds (6 racemic and their enantiopure analogues). We obtained the 6 racemic compounds in 6 steps with global yields ranging from 9 to 32% and the enantiopure ligands were synthesized in 5 steps with global yields ranging from 13 to 36%, in both pathways, CuAAC was used as a key synthetic step. Preliminary *in vitro* biological evaluation were performed on these new MTDLs (cholinesterase inhibition profile and α7 nAChR affinity), and we obtained promising results with two lead compounds **(R)-76a** and **(R)-75b** showing interesting *in vitro* results (Figure 111), with improvement of the activity on the two targets as compared to the parent compounds they are derived from. Further experiments are currently in progress in order to evaluated in more details their biological activities, such as their ability to cross the BBB or their precise activity on α7 nAChRs (agonist, antagonist or allosteric modulation).

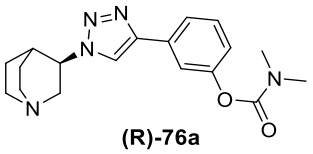

(R)-76a

IC_{50} (*h*AChE) = 5.32 μM
IC_{50} (*h*BChE) = 2.74 μM
K_i (α7 nAChR) = 1.5 nM

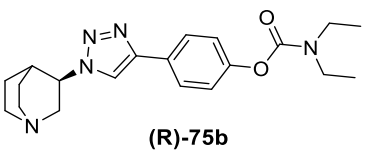

(R)-75b

IC_{50} (*h*AChE) = 4.98 μM
K_i (α7 nAChR) = 1.0 nM

Figure 111: Lead compounds for the first combined MTDLs series.

- For the second series, 10 out of 12 targeted compounds were obtained, through a more complex synthetic access, but we developed a 6 steps synthesis with yields ranging from 0.8 to 10%. We have been able to show that the Suzuki-Myaura reaction can be used on different boronic acids in order to add a phenyl ring to the desired MTDLs. For the last two compounds, only one step remained to be achieved. For this second series of combined MTDL, biological assays need to be performed and activities will be compared to these obtained for the first series in order to evaluate the added value of the additional phenyl ring for the design of new MTDLs targeting α7 nAChRs and AChE.

However, even though the two synthesis we developed are short and relatively effective, one bottleneck has been identified: the formation of the mandatory azide **77** and its enantiomer analogues **(R)-77** and **(S)-77** required to link the two pharmacophores with the triazole moiety needs to be improved. According to the literature, it could be possible to form the unstable azide *in situ* to circumvent the volatility and instability issues. Different groups have studied the *in situ* formation of a triazole starting from an amine and an alkyne[347,348,349,350]. Beckmann et *al*. were the first to develop this kind of one step one-pot procedure with a variety of commercially available amines (Scheme 36). Based on the simple reaction between benzylamine and phenylacetylene, they managed to optimize the reaction conditions and obtained good yields under microwave irradiations[347].

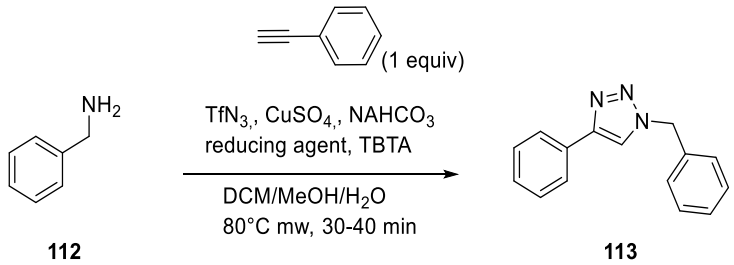

Entry	Amine (equiv)	$CuSO_4$ (mol %)	Reducing agent (mol %)	TBTA (mol %)	Yield
1	1.5	2	10 (of Na ascorbate)	10	93
2	1.0	10	30 (of Cu powder)	/	82

Scheme 36*: Optimized reaction conditions for the one-pot diazo-transfer and Huisgen cycloaddition*

We evaluated such a one-pot two steps strategy in order to increase the reaction yields and have a repeatable process. The racemic 3-aminoquinuclidine **81** and the desired alkyne **79a** were set in presence of the diazo transfer agent (TfN_3) with two catalytic sources of copper at two different oxidative states, Cu(II) and Cu(0), namely $CuSO_4$ and Cu powder, during 30 min at 80°C, under

[347] Beckmann, H. S. G.; Wittmann, V. One-Pot Procedure for Diazo Transfer and Azide−Alkyne Cycloaddition: Triazole Linkages from Amines. *Org. Lett.* **2007**, *9* (1), 1–4.
[348] Smith, N. M.; Greaves, M. J.; Jewell, R.; Perry, M. W. D.; Stocks, M. J.; Stonehouse, J. P. One-Pot, Three-Component Copper-Catalysed 'Click' Triazole Synthesis Utilising the Inexpensive, Shelf-Stable Diazotransfer Reagent Imidazole-1-Sulfonyl Azide Hydrochloride. *Synlett* **2009**, *2009* (9), 1391–1394.
[349] Maisonneuve, S.; Xie, J. One-Pot Synthesis of 1,4-Disubstituted 1,2,3-Triazoles from Aldehydes and Amines. *Synlett* **2009**, *2009* (18), 2977–2981.
[350] Johansson, J. R.; Lincoln, P.; Nordén, B.; Kann, N. Sequential One-Pot Ruthenium-Catalyzed Azide−Alkyne Cycloaddition from Primary Alkyl Halides and Sodium Azide. *J. Org. Chem.* **2011**, *76* (7), 2355–2359.

microwave irradiations. Using this process, we were able to obtain the MTDL **75a** in only one step and with a good 78% yield (Scheme 37), to be compared to the 22% yield obtained in the two steps process.

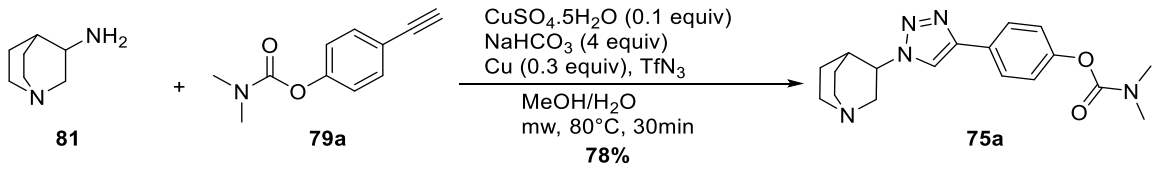

Scheme 37*: One-pot synthesis of* ***75a***

Unfortunately, when we tried the same experiment with the commercially available enantiopure 3-aminoquinuclidines, we could not obtain the desired MTDLs. When each enantiopure amine was put under these reaction conditions, they did not react at all. We did not have time to look for a rational explanation for this unexpected negative result (a difference in the protonation state of the amine could be suspected). Yet, based on our successful assay on the racemic mixture, and on the one-pot two steps procedures described in the literature, we should be able to find appropriate reaction conditions to perform the CuAAC. Once this step optimized, we will have a robust, rapid and convergent synthetic pathway for the two series of a new MTDLs against AD.

Another approach to circumvent the instability and volatility of the azido intermediate would be to base our synthesis on Maisonneuve and Xie work[349]. They managed to synthesize disubstituted 1,2,3-triazoles directly from aldehyde and amines. They managed to develop an innovative one-pot, three-step synthesis from various aldehydes and amines. Their method has a large range of applications and can be used on aryl aldehydes but also on glycosyl aldehydes. For the azide precursors, aminoesters, dipeptides or C-glycosyl amines have been used. Starting from an aldehyde, they performed a Seyfert-Gilbert homologation with the Bestmann-Ohira reagent, followed by the diazotransfer with the imidazole-1-sulfonyl azide as a transfer agent. The last step was the copper catalysed cycloaddition with $CuSO_4$ as a source of copper (Scheme 38).

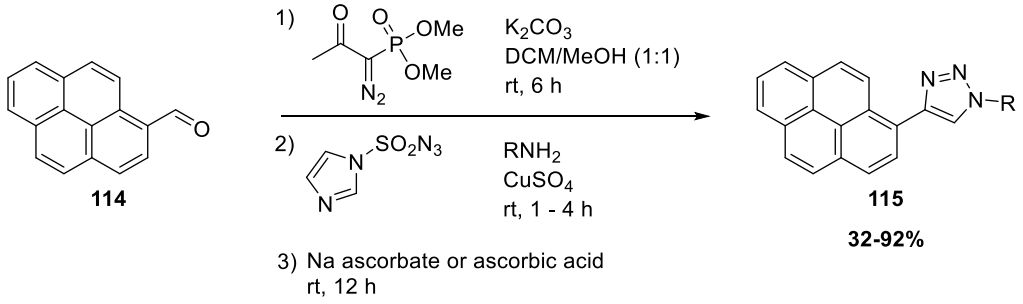

Scheme 38: three-step one-pot synthesis of ***115*** *by Maisonneuve et al.*[349]

We could imagine this procedure for our compounds, in order to obtain **(R)-75a-c** and **(R)-76a-c** from 3-aminoquinuclidine **(R)-81** and the commercially available hydroxybenzaldehydes and then perform the carbamate addition to exemplify and obtain our first MTDLs series with better yields and a shorter synthetic pathway (Scheme 39).

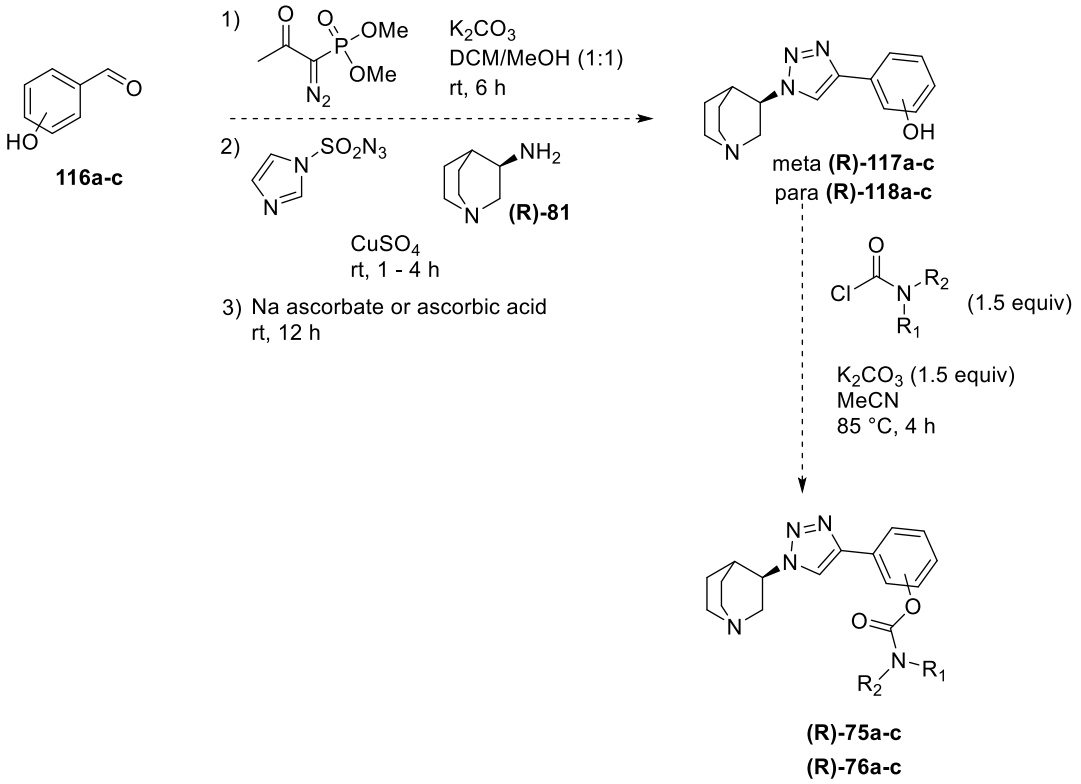

*Scheme 39: Proposed two steps synthetic access to **(R)-75a-c** and **(R)-76a-c***

Chapter III: Conception of combined MTDLs based on the Donepezil scaffold

1. Aim and context of the project

In this third project, we tackled a new challenge of designing and synthesising novel combined MTDLs based on another well-known AChEI, Donepezil. Given the encouraging results obtained in the previous chapter, it was decided to keep the quinuclidine moiety developed by our collaborator, Pr. Routier, as an α7 nAChRs agonist and to combine it to the Donepezil scaffold by the same common moiety used in the previous series of combined MTDLs (Figure 112).

Figure 112: Structure of new combined MTDLs

2. Chosen structures

2.1. Donepezil – a potent and selective AChE inhibitor

Donepezil is part of the four FDA-approved drugs against mild to moderate AD as a reversible non-competitive AChE inhibitor since 1996. Sugimoto et *al*.[351] designed a new class of AChE inhibitor carrying a *N*-benzylpiperidine and an indanone which exerted a long lasting action against *h*AChE and high selectivity toward *h*AChE compared to BChE (Figure 113).

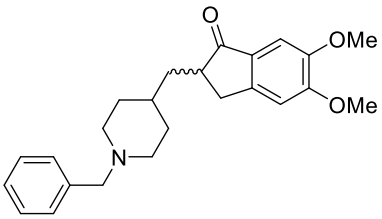

IC_{50} (*h*AChE) = 5.7nM
IC_{50} (*h*BChE) = 4100 nM

Figure 113: Donepezil structure

Initially, their objective was to synthesise a non-toxic derivative of tacrine and during the screening process they encountered *N*-benzylpiperazine scaffold **119** as a promising AChE inhibitor, in addition,

[351] Sugimoto, H.; Yamanish, Y.; Iimura, Y.; Kawakami, Y. Donepezil Hydrochloride (E2020) and Other Acetylcholinesterase Inhibitors. *Curr. Med. Chem.* **2000**, *7* (3), 303–339.

further studies showed that a replacement of *N*-benzylpiperazine by *N*-benzylpiperidine led to a drastic increase of the anti-AChE activity of the molecules (AChE IC_{50} = 12600 nM for **119** and AChE IC_{50} = 55 nM for **120**) (Figure 114).

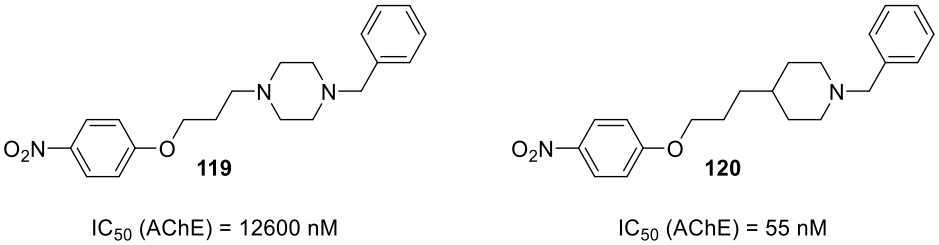

*Figure 114: Structures of studies N-benzylpiperazine **119** and N-benzylpiperidine **120** fragments*

Moreover, numerous therapeutic assays have brought to light that a 5 mg/day dose of Donepezil tends to increase cognitive functions in patients with mild to moderate AD without showing major adverse effects. Indeed, a 12-week study proved that Donepezil administration was not associated with any clinically significant adverse effects, the most commonly reported side effects were nausea, diarrhoea, constipation, gastric upset and dizziness, displayed during a 14- week phase II clinical trials[352].

Another great interest concerning Donepezil is its dual-site inhibition property (peripheral and catalytic site) able to lead to an inhibition of Aβ aggregation. Indeed, the dimethoxy indanone moiety of Donepezil has the capacity to bind to AChE PAS, known to trigger Aβ aggregation, therefore, facilitating the fibril formation. The crystal structure of Donepezil with *Tc*AChE obtained by Kryger et *al.*[353] in 1999, with *h*AChE obtained by Cheung et *al.*[354] in 2012 (Figure 115) and recent docking studies[355] have shown that while the piperidine ring of Donepezil, positioned in the narrow gorge, interacts with various AChE residues such as Tyr337, Phe338, Tyr341 or His447, the benzyl ring binds to Trp86 found in the catalytic pocket of the enzyme. In addition, it has been shown that the indanone ring of the molecules interacts with Trp286 which is located in the AChE PAS (*h*AChE aminoacid residues number used in the text)[355].

[352] Rogers, S. L.; Friedhoff, L. T. The Efficacy and Safety of Donepezil in Patients with Alzheimer's Disease: Results of a US Multicentre, Randomized, Double-Blind, Placebo-Controlled Trial. *Dement. Geriatr. Cogn. Disord.* **1996**, *7* (6), 293–303.

[353] Kryger, G.; Silman, I.; Sussman, J. L. Structure of Acetylcholinesterase Complexed with E2020 (Aricept®): Implications for the Design of New Anti-Alzheimer Drugs. *Structure* **1999**, *7* (3), 297–307.

[354] Cheung, J.; Rudolph, M. J.; Burshteyn, F.; Cassidy, M. S.; Gary, E. N.; Love, J.; Franklin, M. C.; Height, J. J. Structures of Human Acetylcholinesterase in Complex with Pharmacologically Important Ligands. *J.Med.Chem.* **2012**, *55*, 10282–10286.

[355] Li, Q.; He, S.; Chen, Y.; Feng, F.; Qu, W.; Sun, H. Donepezil-Based Multi-Functional Cholinesterase Inhibitors for Treatment of Alzheimer's Disease. *Eur. J. Med. Chem.* **2018**, *158*, 463–477.

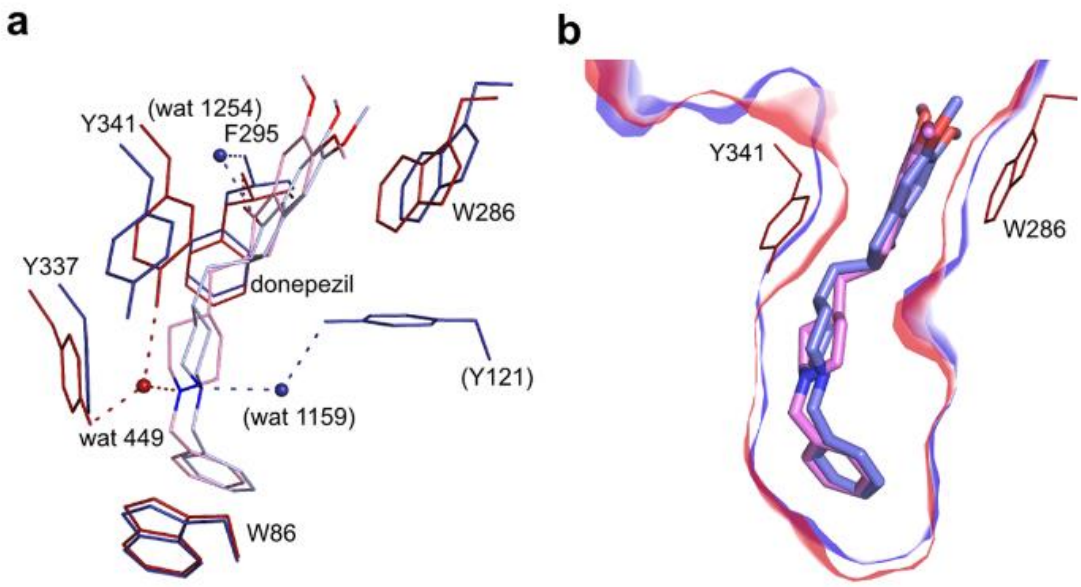

Figure 115: Structure of Donepezil with hAChE[354] (a) Donepezil is shown in stereo view with residues from TcAChE (solved at 2.5 Å) superimposed. Donepezil nitrogen and oxygen atoms are coloured blue and red, respectively, while carbon atoms are coloured pink in the human-bound conformer and light blue in the Torpedo-bound conformer. Residue numbering refers to human acetylcholinesterase, with equivalent numbers for TcAChE in parentheses (b) Active site gorge of the superimposed hAChE and TcAChE in complex with Donepezil (residues W286 and Y341 of the hAChE are shown as sticks and TcAChE residues are omitted for clarity

Because of the dual-binding properties of Donepezil with AChE, research groups have worked on structural modifications of Donepezil in order to increase the protective activity against Aβ aggregation to the already known AChE inhibition potency of Donepezil (Figure 116). As a first example, Wang et *al*.[356] designed a melatonin-Donepezil hybrid **121** in which the Donepezil benzyl fragment will interact with the catalytic site and the melatonin will be located at PAS. Indeed, studies have shown that melatonin, an endogenous neurohormone, exerted high antioxidant properties[357] and more importantly an Aβ aggregation inhibition activity by disturbing Asp^--His^+ salt bridges of Aβ[358]. The novel molecule **121** obtained displayed a good non-selective AChE inhibition (IC_{50} AChE = 0.273 µM) and BChE inhibition (IC_{50} BChE = 0.056 µM) coupled with a promising inhibition of self-induced Aβ

[356] Wang, J.; Wang, Z.-M.; Li, X.-M.; Li, F.; Wu, J.-J.; Kong, L.-Y.; Wang, X.-B. Synthesis and Evaluation of Multi-Target-Directed Ligands for the Treatment of Alzheimer's Disease Based on the Fusion of Donepezil and Melatonin. *Bioorg. Med. Chem.* **2016**, *24* (18), 4324–4338.

[357] Chojnacki, J. E.; Liu, K.; Yan, X.; Toldo, S.; Selden, T.; Estrada, M.; Rodríguez-Franco, M. I.; Halquist, M. S.; Ye, D.; Zhang, S. Discovery of 5-(4-Hydroxyphenyl)-3-Oxo-Pentanoic Acid [2-(5-Methoxy-1H-Indol-3-Yl)-Ethyl]-Amide as a Neuroprotectant for Alzheimer's Disease by Hybridization of Curcumin and Melatonin. *ACS Chem. Neurosci.* **2014**, *5* (8), 690–699.

[358] Stevens, C. B.; Hanna, J. M.; Lammi, R. K. Synthesis of Tetrahydroxybiphenyls and Tetrahydroxyterphenyls and Their Evaluation as Amyloid-β Aggregation Inhibitors. *Bioorg. Med. Chem. Lett.* **2013**, *23* (6), 1703–1706.

aggregation. Next, Meena et *al*.[359] designed compound **122** by structurally modifying Donepezil scaffold through the addition of a nicotine moiety, this choice was based on the knowledge that electron rich substituents on aromatic rings and heterocycles containing a nitrogen could play an important role in Aβ aggregation inhibition coupled with antioxidant activity[360]. Indeed, compound **120** was evaluated and showed a potent and selective AChE inhibition (IC_{50} AChE = 2.13 µM versus IC_{50} BChE = 81.70 µM) combined with a high inhibition of self-induced Aβ aggregation of 85.5% at a 25 µM concentration. Finally, based on the knowledge that the dimethoxyindanone moiety of Donepezil interacts with the AChE PAS, which is closely related to Aβ aggregation, Yerdelen et *al*.[361], reported a series of 5,6-dimethoxy-indanone-2-carboxamide derivatives amongst which compound **123** was one of the most promising because of its strong capacity to selectively inhibit AChE (IC_{50} AChE = 0.08 µM versus IC_{50} BChE = 3.21 µM). Moreover, compound **123** displayed a high potency to inhibit self-induced Aβ aggregation with more than 55% of $Aβ_{1-42}$ aggregation inhibition at a 25 µM concentration.

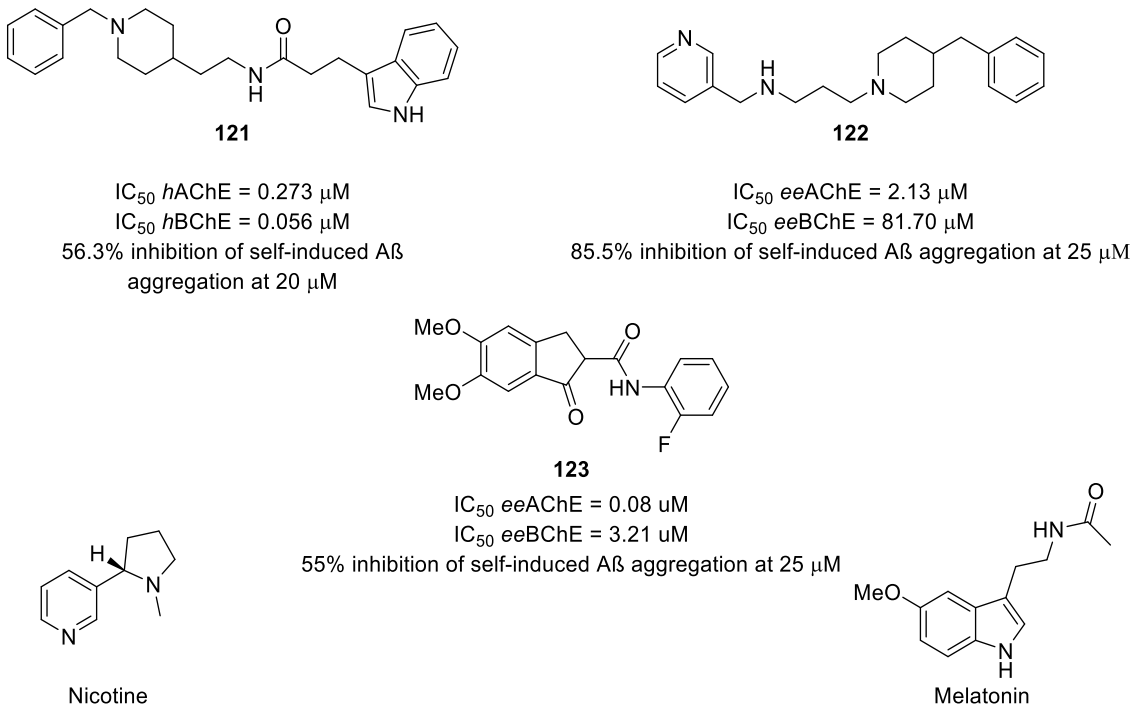

Figure 116: Examples of Donepezil-based ChE inhibitors with additional Aβ self-aggregation inhibition potency

[359] Meena, P.; Nemaysh, V.; Khatri, M.; Manral, A.; Luthra, P. M.; Tiwari, M. Synthesis, Biological Evaluation and Molecular Docking Study of Novel Piperidine and Piperazine Derivatives as Multi-Targeted Agents to Treat Alzheimer's Disease. *Bioorg. Med. Chem.* **2015**, *23* (5), 1135–1148.

[360] Salomon, A. R.; Marcinowski, K. J.; Friedland, R. P.; Zagorski, M. G. Nicotine Inhibits Amyloid Formation by the β-Peptide. *Biochemistry* **1996**, *35* (42), 13568–13578.

[361] Yerdelen, K. O.; Koca, M.; Anil, B.; Sevindik, H.; Kasap, Z.; Halici, Z.; Turkaydin, K.; Gunesacar, G. Synthesis of Donepezil-Based Multifunctional Agents for the Treatment of Alzheimer's Disease. *Bioorg. Med. Chem. Lett.* **2015**, *25* (23), 5576–5582.

2.2. Donepezil-based MTDLs

For the last decade, various research teams have worked on the development of Donepezil-based MTDLs targeting AChE (catalytic site and PAS) and other receptors involved in CNS-related pathologies (Figure 117). For example, Xu et *al*.[362] designed a family of MTDLs by combining a Donepezil moiety with a ferulic acid fragment giving **124** as the lead compound of the family with satisfying AChE inhibitory properties (IC_{50} AChE = 0.321 µM) simultaneously with antioxidant activity close to the one of ferulic acid (IC_{50} DPPH = 24.9 µM). In 2016, Li et *al*.[355] investigated, designed and biologically evaluated a series of Donepezil-like compounds displaying potent inhibitory activities against AChE, BChE and both MAO-A and MAO-B, among which compound **125** revealed to be the most promising molecule (IC_{50} AChE = 0.22 µM, IC_{50} BChE = 1.23 µM, IC_{50} MAO-A = 13.4 µM, IC_{50} MAO-B = 3.14 µM) ,able to cross the BBB and displaying low cell toxicity on PC12 cells. Because of their capacity to improve memory performance, subtype 4 of serotonin receptor (5-HT_4R) agonists have been investigated in the research of AD treatment, indeed, Rochais et *al*.[363] designed compound **126** as a fused MTDL targeting AChE and this class of receptor, which displayed promising activity and selectivity toward AChE against BChE (IC_{50} AChE = 8.5 nM) as a fusion of Donepezil and a an already known 5-HT_4R agonist (RS67333). As a last example, compound **127** was developed by Zhu et *al*.[364] as a dual inhibitor of AChE and BACE-1 based on a combination of the active Donepezil moiety with a diaminobenzyl subunit able to inhibit BACE-1, and the final MTDL expressed promising inhibitory activities toward AChE and BACE-1 (IC_{50} AChE = 1.83 µM, IC_{50} BACE-1 = 0.567 µM).

[362] Xu, W.; Wang, X.-B.; Wang, Z.-M.; Wu, J.-J.; Li, F.; Wang, J.; Kong, L.-Y. Synthesis and Evaluation of Donepezil–Ferulic Acid Hybrids as Multi-Target-Directed Ligands against Alzheimer's Disease. *MedChemComm* **2016**, *7* (5), 990–998.

[363] Rochais, C.; Lecoutey, C.; Gaven, F.; Giannoni, P.; Hamidouche, K.; Hedou, D.; Dubost, E.; Genest, D.; Yahiaoui, S.; Freret, T.; Bouet, V.; Dauphin, F.; Sopkova de Oliveira Santos, J.; Ballandonne, C.; Corvaisier, S.; Malzert-Fréon, A.; Legay, R.; Boulouard, M.; Claeysen, S.; Dallemagne, P. Novel Multitarget-Directed Ligands (MTDLs) with Acetylcholinesterase (AChE) Inhibitory and Serotonergic Subtype 4 Receptor (5-HT4R) Agonist Activities As Potential Agents against Alzheimer's Disease: The Design of Donecopride. *J. Med. Chem.* **2015**, *58* (7), 3172–3187.

[364] Zhu, Y.; Xiao, K.; Ma, L.; Xiong, B.; Fu, Y.; Yu, H.; Wang, W.; Wang, X.; Hu, D.; Peng, H.; Li, J.; Gong, Q.; Chai, Q.; Tang, X.; Zhang, H.; Li, J.; Shen, J. Design, Synthesis and Biological Evaluation of Novel Dual Inhibitors of Acetylcholinesterase and Beta-Secretase. *Bioorg. Med. Chem.* **2009**, *17* (4), 1600–1613.

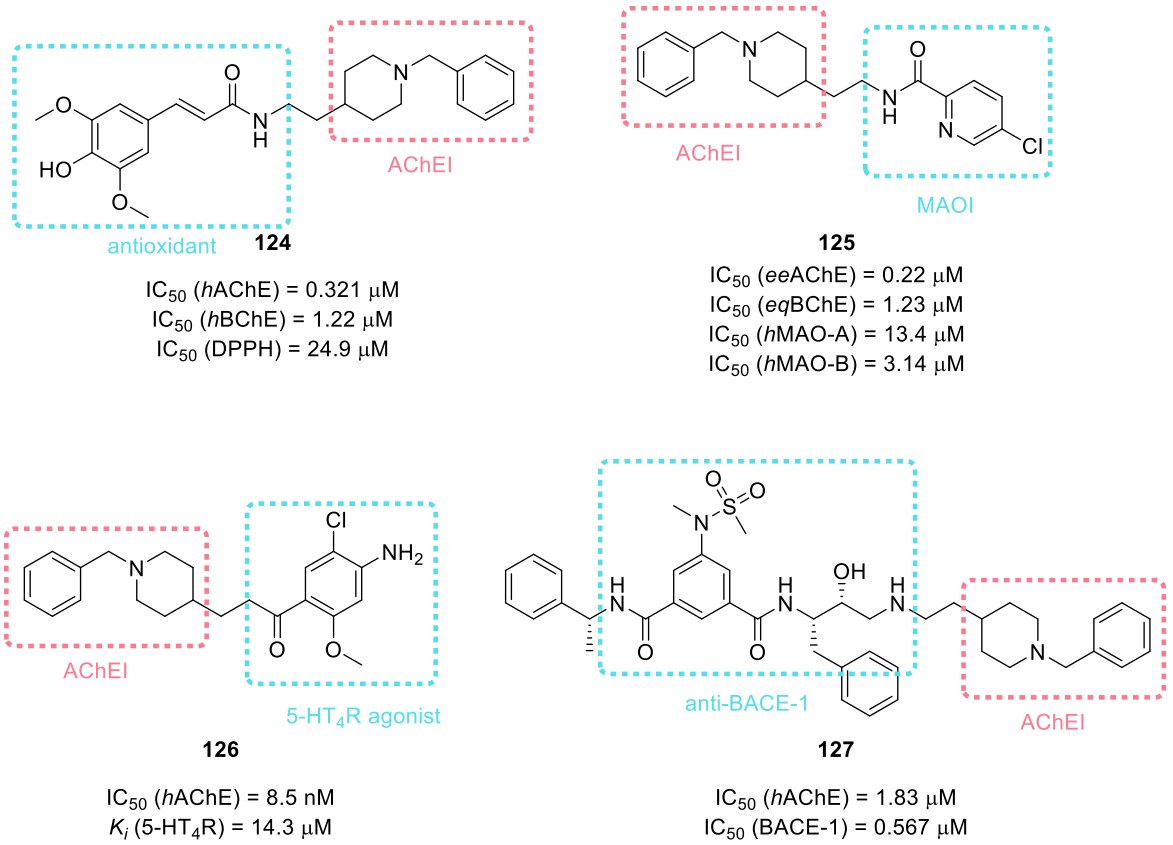

Figure 117: Examples of Donepezil based MTDLs (MAOI = MAO inhibitor)

As a conclusion, Donepezil moiety has been widely used in the past decade as a potent AChE inhibitor in the design of innovative MTDLs because of its potency and ability to bind with AChE both at the catalytic and peripherical sites, giving the molecule an additional protective activity against Aβ aggregation. In this context, using the active Donepezil fragment combined to a quinuclidine moiety able to interact with α-7 nAChRs to build a MTDLs appears to be a judicious choice.

Two different MTDL series have thus been designed (Figure 118), with the quinuclidine attached in place of one of the two dimethoxy substituents of Donepezil, since this moiety points towards AChE PAS. The first series has been designed with a flexible linker between the ketone (which key role in binding to AChE gorge residues has been proven in the various X-ray crystallographic data obtained with Donepezil bound to AChE), and the second one with the complete indanone moiety. For this second series, the synthesis will be led on the diastereomeric mixture with the mixture of the two absolute configurations at the asymmetric centre on the indanone moiety of Donepezil. Since it has been shown that at physiological pH, this indanone could easily undergo racemization, and although

only one of the two enantiomers of Donepezil tightly bind to AChE binding site, this compound is administrated as a racemic mixture[365].

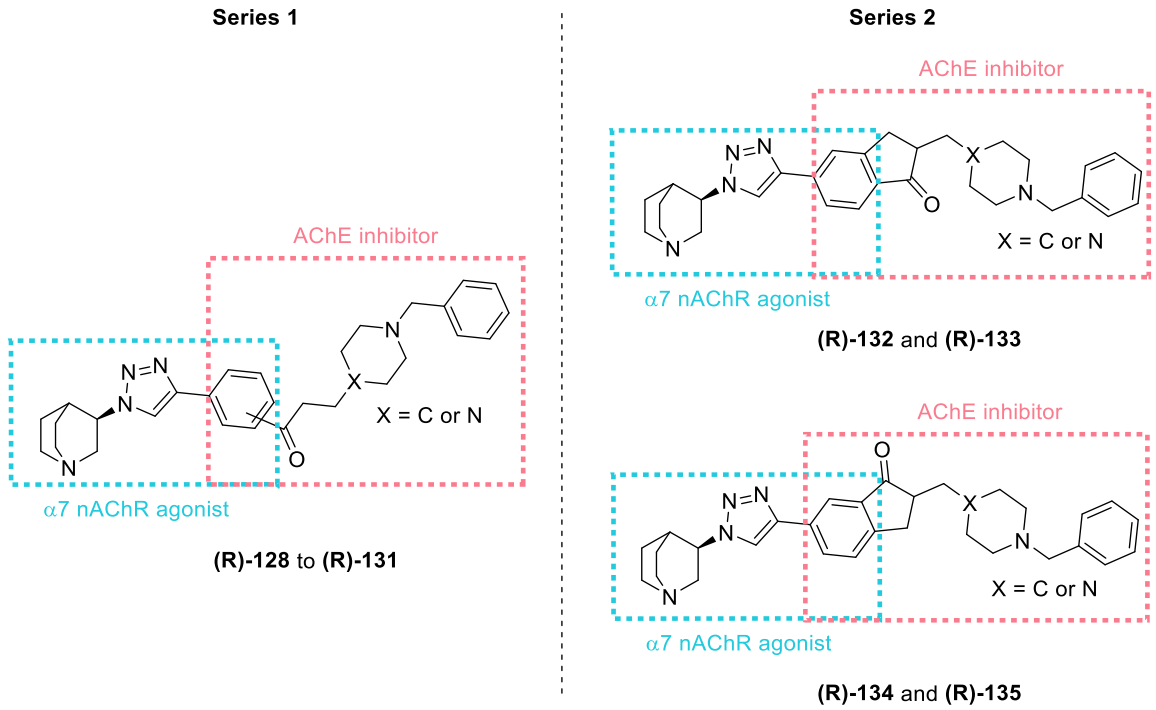

Figure 118: Structures of the targeted combined MTDLs

3. Preliminary studies

3.1. Series 1

The first series of possible MTDLs we designed is represented in Figure 119. The two differences are the attachment point of the quinuclidine moiety, and either a *N*-benzylpiperazine or *N*-benzylpiperidine moiety. E ach compound has been evaluated *in silico*. The binding affinities toward a rigid model of AChE, the position inside the enzyme binding site, the CNS MPO score and the probability to cross the BBB of compounds **(R)-128** to **(R)-131** were assayed to evaluate their profile as drug candidates.

[365] Matsui, K.; Oda, Y.; Ohe, H.; Tanaka, S.; Asakawa, N. Direct Determination of E2020 Enantiomers in Plasma by Liquid Chromatography-Mass Spectrometry and Column-Switching Techniques. *J. Chromatogr. A* **1995**, *694* (1), 209–218.

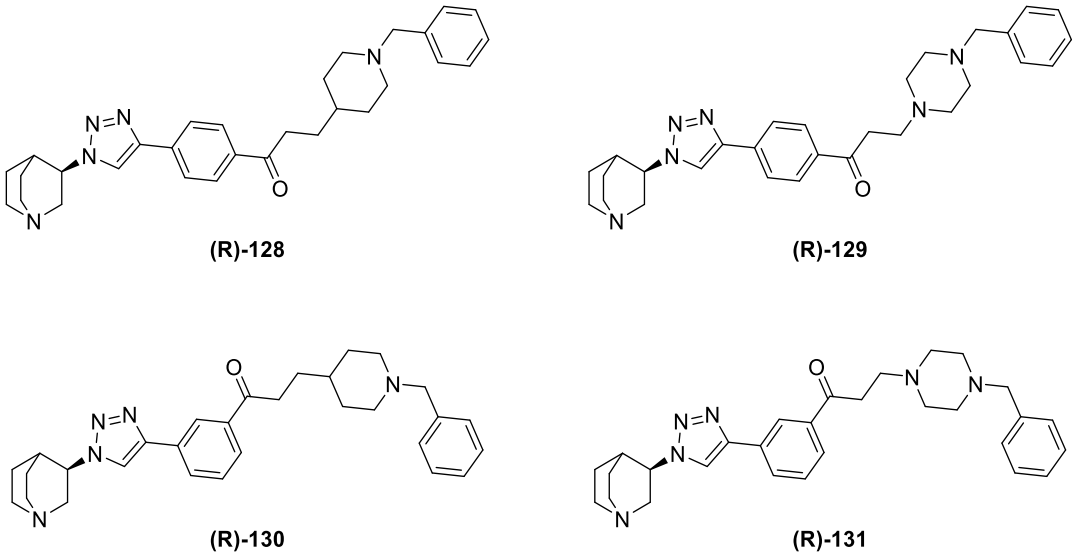

Figure 119: First series of Donepezil based MTDLs

3.1.1. Docking studies

The procedure explained in chapter II was used to evaluate the binding affinities and the position of the combined MTDLs inside the chosen enzyme, *rh*AChE. The starting point for the docking experiment was this time a crystal structure of this enzyme co-crystalized with Donepezil (PDB 4EY7)[354]. The predicted binding energies are reported in Table 18. Noteworthy, the binding mode and positioning predicted for Donepezil corresponds to the one observed in the crystal structure we started from.

Entry	Compound	E_{bind} (kcal/mol)
1	**Donepezil**	-11.6
2	**(R)-128**	-12.7
3	**(R)-129**	-11.6
4	**(R)-130**	-13.1
5	**(R)-131**	-12.2

*Table 18: Docking results for compounds **(R)-128**, **(R)-129**, **(R)-130** and **(R)-131***

It can be noted that compounds **(R)-128** (Figure 120-A), **(R)-129** (Figure 120-B), **(R)-130** (Figure 120-C) and **(R)-131** (Figure 120-D) have obtained encouraging results, both in terms of binding energy and

positioning within the enzyme binding site, compared to the reported binding affinity of Donepezil (entry 1).

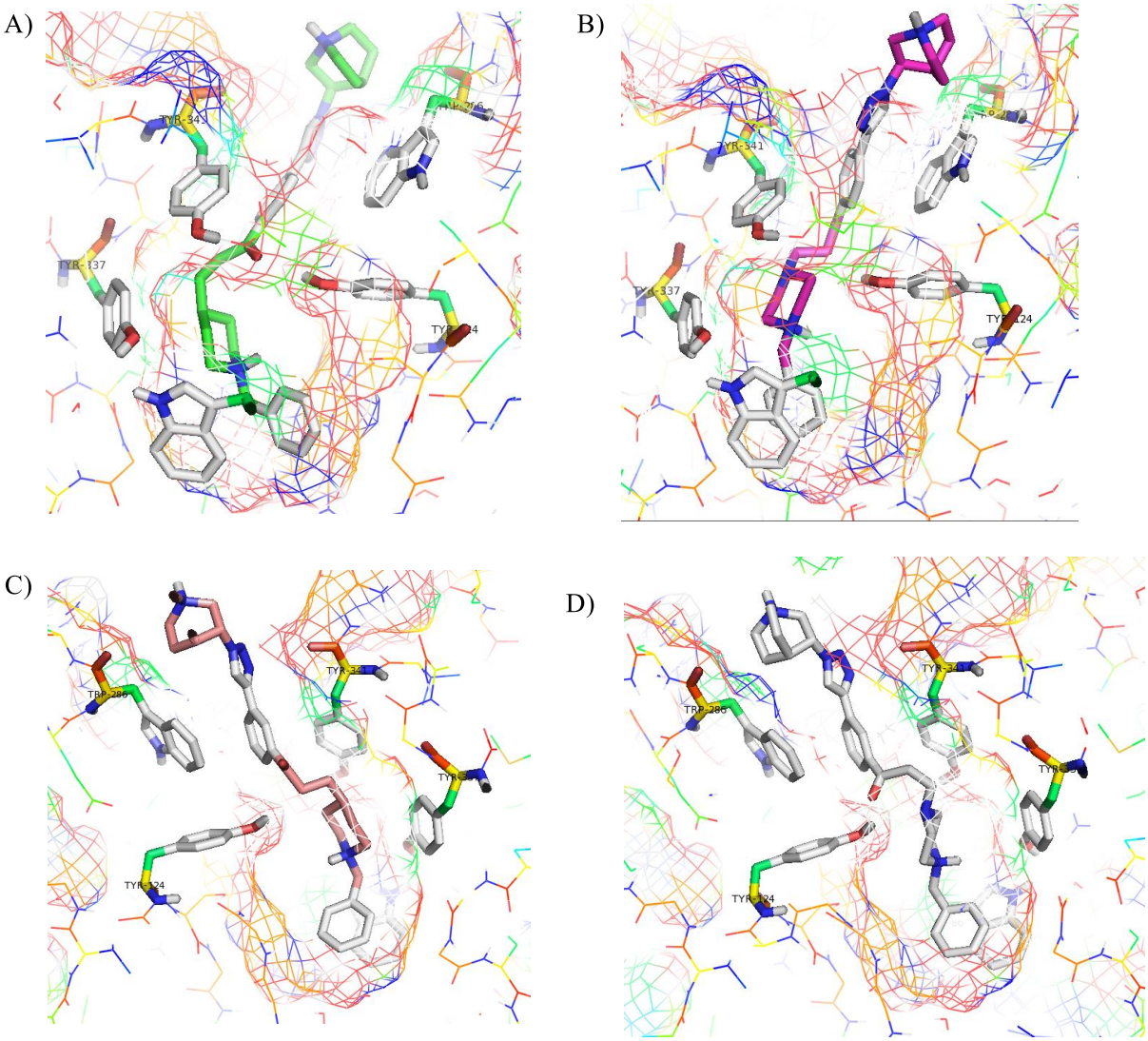

Figure 120: Docking of rhAChE with (A) ***(R)-128*** *(B)* ***(R)-129*** *(C)* ***(R)-130*** *(D)* ***(R)-131*** *(Trp286, Tyr124, Tyr341, Tyr337 and Trp86 are represented in sticks)*

The interactions of compounds **(R)-128**, **(R)-129**, **(R)-130** and **(R)-131** with the main residues of *rh*AChE were visualised using Discovery software and are reported in Table 19.

Entry	Type of interaction	Donepezil	(R)-128	(R)-129	(R)-130	(R)-131
1	π-stacking interaction	Trp86 Trp286	Trp286 Tyr341	Trp86 His447 Trp286 Tyr72	Trp286 Trp86 His447	Trp286 Trp86
2	H-bond	Tyr124 Tyr341 Tyr337	Arg296 Tyr124	Phe295	Phe295	Tyr124
3	Carbon-hydrogen				Ser293	Ser293
4	π- cation		Trp86	Asp74 Tyr37	Trp86 Tyr337	Asp74
5	π-sigma		Trp86			

*Table 19: Interactions predicted between rhAChE and **(R)-128**, **(R)-129**, **(R)-130** and **(R)-131***

Concerning compound **(R)-128** (Figure 121), the predominant interactions predicted with the enzyme were π-stacking interactions (entry 1). Indeed, it can be observed that the phenyl attached to the triazole was predicted to interact with Trp286 and Tyr341, and the second phenyl carried by the piperidine bounded with Trp86 which also interacts with the protonated hydrogen of the piperidine through π- cation interaction (entry 4) . Moreover, H-bonds interactions (entry 2) were predicted between Tyr124 and the ketone of **(R)-128** and between one of the triazole ring's nitrogen and Arg296.

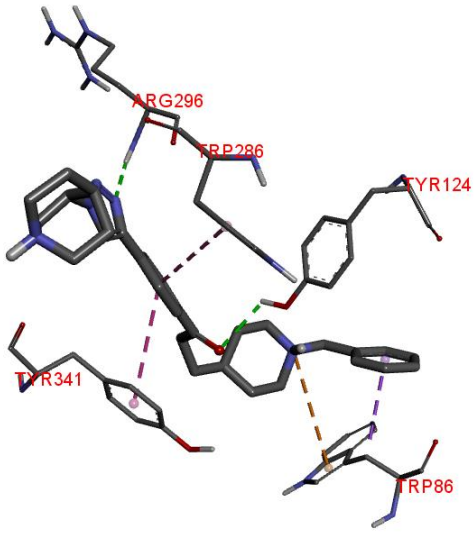

Figure 121: Representation of interactions between rhAChE and ***(R)-128***

Compound **(R)-129**'s triazole has been predicted to interact with Tyr72 through π-stacking interactions while the phenyl it carries has been predicted to π-stack with Trp286, moreover, the second phenyl carried by the piperazine appeared to π-stack with two residues: Trp86 and His447 (entry 1). Moreover, **(R)-129**'s ketone was predicted to interact with Phe295 *via* H-bond interactions (entry 2) while the protonated nitrogen of the piperazine appeared to interact with Asp74 and Tyr337 through π- cation interactions (entry 4), finally, Tyr337 has been predicted to interact with the hydrogen of this protonated nitrogen through a carbon-hydrogen bond (entry 3) (Figure 122).

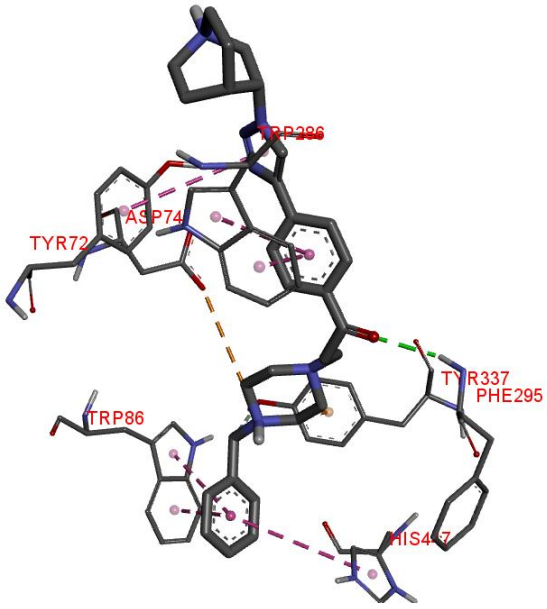

Figure 122: Representation of interactions between rhAChE and ***(R)-129***

Compound **(R)-130**'s phenyl carried by the triazole moiety has been predicted to π-stack with Trp286 while the second phenyl carried by the piperidine was predicted to interact with Trp86 and His447 in the same way (entry 1). Moreover, Trp337 and Trp86 have been predicted to interact with the protonated piperidine's nitrogen through π- cation interactions (entry 4). It must be noted that the quinuclidine appeared to do carbon-hydrogen bonds with Ser293 (entry 3). finally, a H-bond could be observed between the ketone of compound **(R)-130** and the amide of Phe295 (entry 2) (Figure 123).

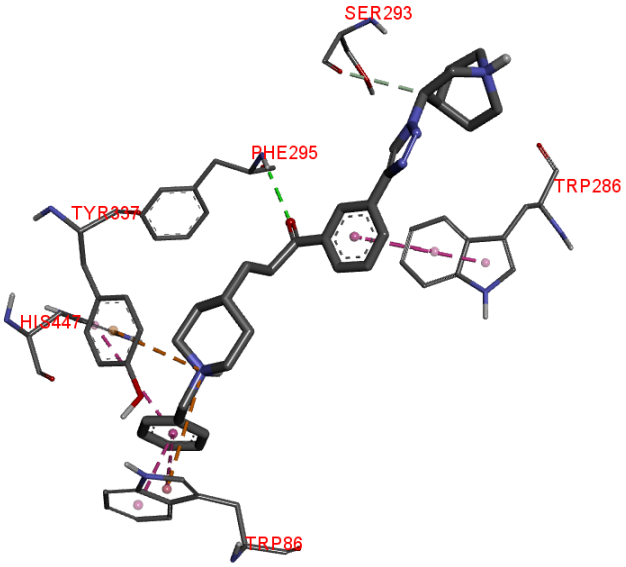

*Figure 123: Representation of interactions between rhAChE and **(R)-130***

Regarding the last tested compound of this study, compound **(R)-131**, three main interactions have been predicted: π-stacking (entry 1)and H-bond formation (entry 2). Firstly, the phenyl carried by the triazole moiety π-stacked with Trp286 which also π-stacked with the triazole moiety, while the second phenyl of the molecule, carried by the piperazine, π-stacked with Trp86. Two H-bonds were predicted to be formed between Tyr124 and simultaneously the ketone and the non-protonated piperazine nitrogen. Finally, two other type of interactions have been predicted: a π-cation interaction between Asp74 (entry 4) and the piperazine's protonated nitrogen and a carbon-hydrogen bond between Ser293 and the quinuclidine moiety (entry 3) (Figure 124).

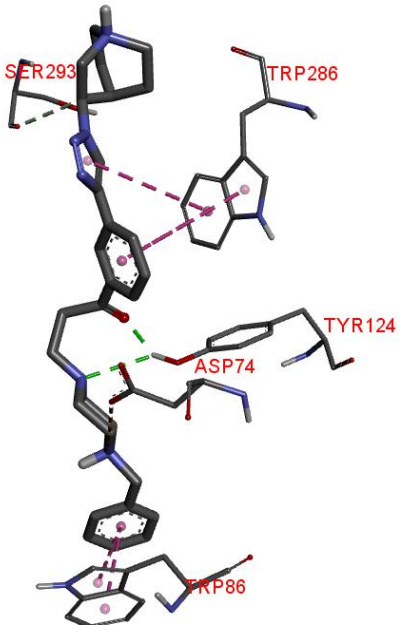

Figure 124: Representation of interactions between rhAChE and ***(R)-131***

As a result of this study, it is important to note that the predicted placement and interactions predicted for compounds **(R)-128**, **(R)-129**, **(R)-130** and **(R)-131** were close to the known information concerning Donepezil interactions with *rh*AChE. Indeed, the crystal structure of AChE bound to Donepezil (Figure 125) determined by Cheung et *al.*[354], we took as starting point, has shown that the benzyl interacts with Trp86 while the phenyl ring of the indanone π-stacks with Trp286 in the PAS, which are similar interactions to the ones we determined *in silico* for our newly designed MTDLs. Other interactions between the piperidine and Tyr337 and Tyr341 (H-bonds) were also displayed in Cheung et *al*. study, as well as the H-bonding interaction between indanone ketone and amide of Phe295.

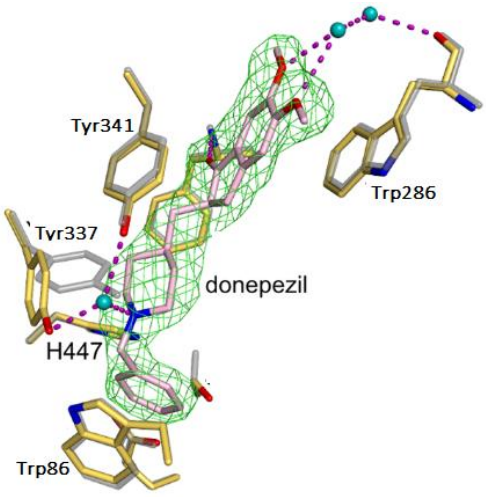

Figure 125: rhAChE active site with bound Donepezil (adapted from Cheung et al.[354]*)*

3.1.2. CNS MPO score computation

It has been verified that all the studied compounds respected the Lipinski's rules and their CNS MPO scores have been calculated from 6 of their physicochemical properties[366,367] (Table 20). Because of the high molecular weight and strong pKa values of the new series of combined MTDLs, the obtained results were lower than what was calculated in the previous project, nevertheless, the calculations displayed good CNS MPO scores for compound **(R)-129** (entry 3) and compound **(R)-131** (entry 5). Concerning compound **(R)-128** (entry 2) and compound **(R)-130** (entry 4), the scores were shown to be slightly lower because of a high logP value added to the size of the molecule and the high pKa, yet still within an acceptable score. Moreover, Donepezil, the parent monomer (entry 1) displayed a score of 4.4, a value in accordance with the scores obtained for compounds **(R)-129** and **(R)-131**, with also physico-chemical properties close to the one obtained for the all series.

Entry	Compound	CLogP	CLogD	TPSA (Å²)	MW g/mol	HBD	pKa	CNS MPO score
1	**Donepezil**	4.21	2.48	38.77	379.5	0	9.12	**4.4**
2	**(R)-128**	4.83	1.23	54.26	483.66	0	9.5	**3.5**
3	**(R)-129**	3.69	1.44	57.50	484.65	0	9.18	**4.2**
4	**(R)-130**	4.83	1.70	54.26	483.66	0	9.34	**3.5**
5	**(R)-131**	3.69	1.89	57.50	484.65	0	8.72	**4.4**

All physico-chemical properties were obtained from chemicalize.com

*Table 20: Physicochemical properties and CNS MPO scores evaluated for compounds **(R)-128**, **(R)-129**, **(R)-130** and **(R)-131***

[366] Wager, T. T.; Hou, X.; Verhoest, P. R.; Villalobos, A. Central Nervous System Multiparameter Optimization Desirability: Application in Drug Discovery. *ACS Chem. Neurosci.* **2016**, *7* (6), 767–775.

[367] Wager, T. T.; Hou, X.; Verhoest, P. R.; Villalobos, A. Moving beyond Rules: The Development of a Central Nervous System Multiparameter Optimization (CNS MPO) Approach To Enable Alignment of Druglike Properties. *ACS Chem. Neurosci.* **2010**, *1* (6), 435–449.

3.1.3. Percepta software analysis of the compounds[368]

To complete the *in silico* studies on compounds **(R)-128**, **(R)-129**, **(R)-130** and **(R)-131**, calculations *via* the percepta software were performed and the results are reported in Table 21. The LogP and most basic pKa values obtained were closed to the one obtained for the calculation of CNS MPO scores, and the evaluation show that even if compound **(R)-128** (entry 1) and **(R)-130** (entry 3) displayed low CNS MPO scores, the calculated probability for them to cross the BBB remained sufficient.

Entry	Compound	LogP	pKa	f_u	LogPS	LogBB	Log(PS*f_u)	Brain penetration for CNS activity
1	**(R)-128**	4.10	9.28	0.036	-1.6	0.20	-3.2	Sufficient
2	**(R)-129**	2.85	9.28	0.16	-2.1	0.16	-3.1	Sufficient
3	**(R)-130**	4.03	9.30	0.044	-1.6	0.25	-3.2	Sufficient
4	**(R)-131**	2.78	9.30	0.17	-2.2	0.15	-3.1	Sufficient

*Table 21: Physicochemical properties determined with Percepta software for **(R)-128**, **(R)-129**, **(R)-130** and **(R)-131***

Moreover, the representations given in Figure 126 have shown that the presence of a *N*-benzylpiperazine or a *N*-benzylpiperidine and their relative positions did not affect the chances of the four compounds to cross the BBB. Indeed, every compound was represented with the CNS active group of compounds (represented with blue dots).

[368] Lanevskij, K.; Japertas, P.; Didziapetris, R.; Petrauskas, A. Ionization-Specific Prediction of Blood–Brain Permeability. *J. Pharm. Sci.* **2009**, *98* (1), 122–134.

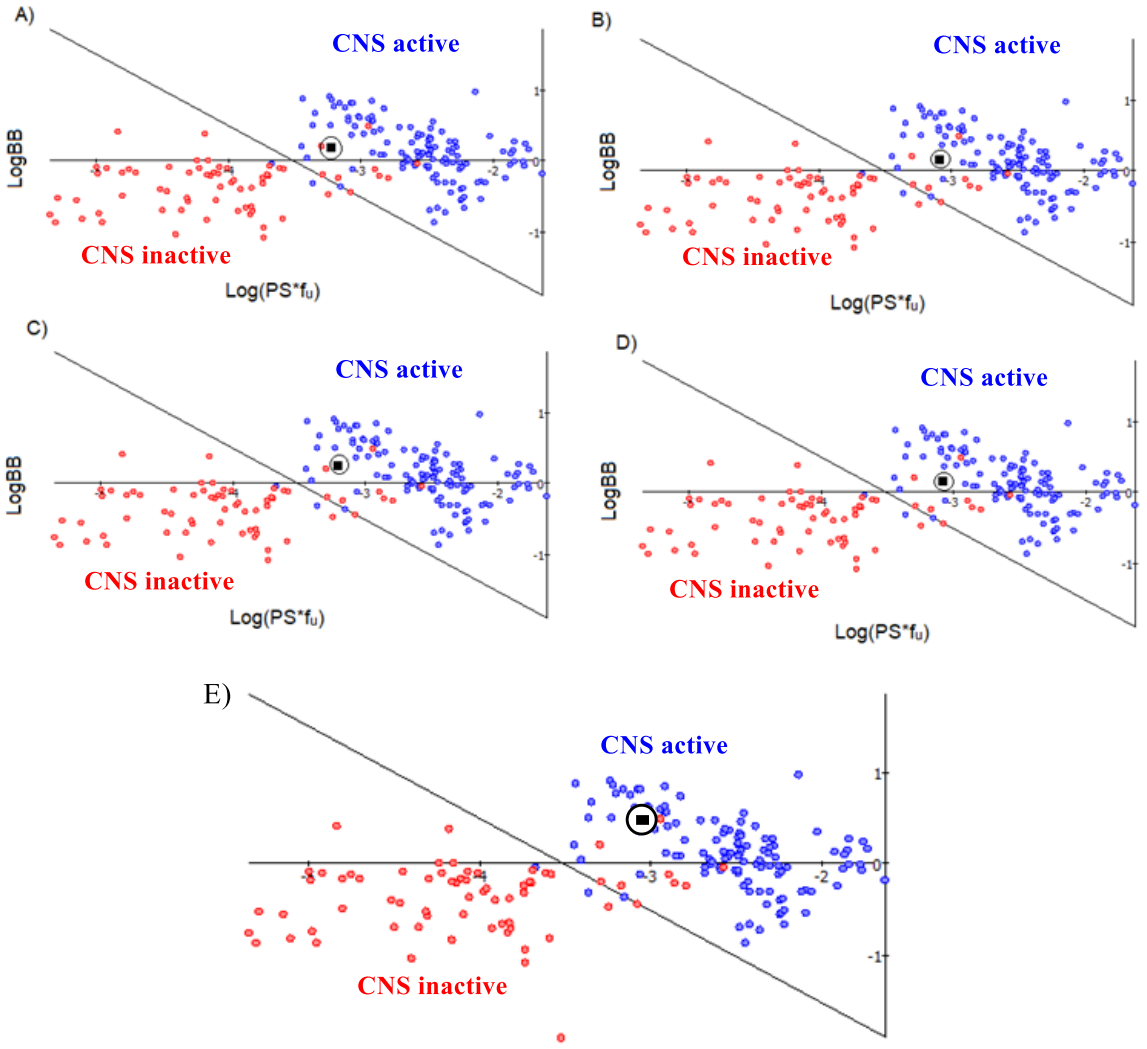

Figure 126: Results of Brain penetration computed ability for CNS activity for (A) ***(R)-128*** *(B)* ***(R)-129*** *(C)* ***(R)-130*** *(D)* ***(R)-131*** *(E) Donepezil (red dots represent CNS inactive compounds, blue dots represent CNS active compounds and the circled black dot represent the tested compound)*

3.2. Series 2

As part of the project of designing innovative Donepezil-based combined MTDLs, a second series carrying the whole indanone moiety was also evaluated *in silico* to predict the profile of compounds **(R)-132** to **(R)-135** (Figure 127). Since Donepezil is a chiral compound, but which stereocenter is prompted to racemization at physiological pH, this series was designed as a diastereomeric mixture, but for the docking experiments, the most active compound bearing the (R) absolute configuration at the second stereocenter was used. As for the first Donepezil based MTDL, the differences are in the attachment point for the triazole moiety and the N-benzylpiperazine or N-benzylpiperidine moiety.

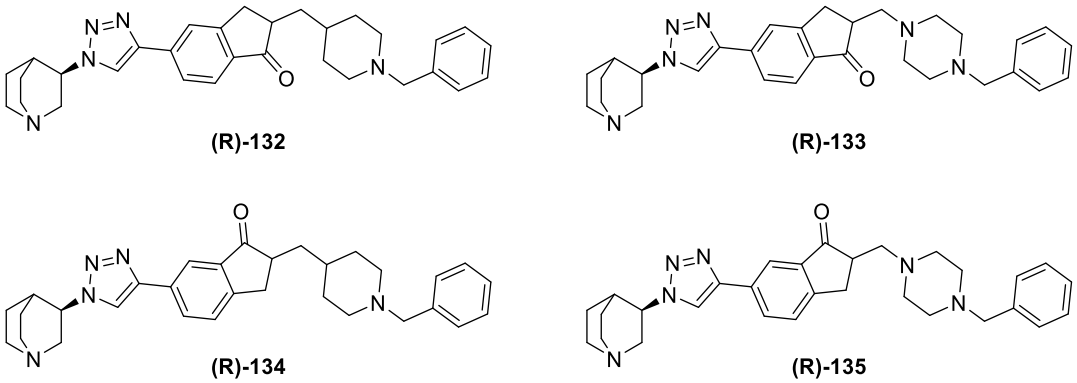

Figure 127: Second series of Donepezil based MTDLs

3.2.1. Docking studies

Using the procedure described in chapter II, compounds **(R)-132** to **(R)-135** were docked with a rigid model of *rh*AChE (PDB 4EY7)[354] to determine their binding affinities toward the enzyme, the results are reported in Table 22.

Entry	Compound	E_{bind} (kcal/mol)
1	**Donepezil**	-11.6
2	**(R)-132**	-13.1
3	**(R)-133**	-12.6
4	**(R)-134**	-13.0
5	**(R)-135**	-12.8

*Table 22: Docking results for compounds **(R)-132**, **(R)-133**, **(R)-134** and **(R)-135***

It can be noticed that the binding affinities toward AChE predicted for all the newly designed MTDLs (entries 2 to 5) were slightly better than the binding affinity displayed by Donepezil (entry 1). Moreover, compounds **(R)-132** (Figure 128-A), **(R)-133** (Figure 128-B), **(R)-134** (Figure 128-C) and **(R)-135** (Figure 128-D) all appeared to be well oriented inside the enzyme binding pocket and the quinuclidine fragment was found to be located at the PAS.

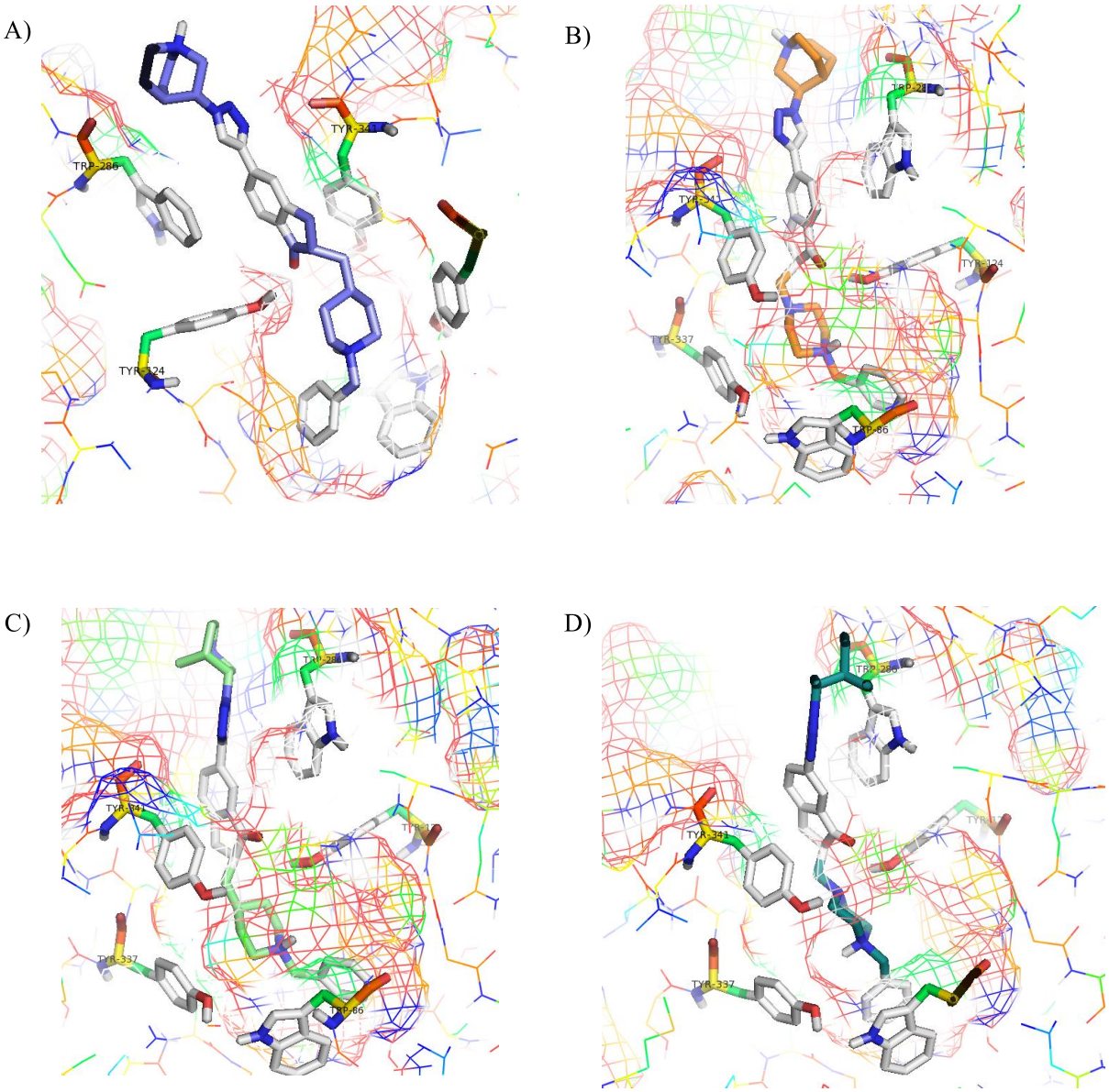

Figure 128: Docking of rhAChE with (A) ***(R)-132*** *(B)* ***(R)-133*** *(C)* ***(R)-134*** *(D)* ***(R)-135*** *(Trp286, Tyr124, Tyr341, Tyr337 and Trp86 are represented in sticks)*

Interactions between the newly designed MTDLs and the main residues of *rh*AChE were visualised with Discovery software and are reported in Table 23.

Entry	Type of interaction	Donepezil	(R)-132	(R)-133	(R)-134	(R)-135
1	π-stacking	Trp86 Trp286	Tyr341 Trp286	Trp286 Tyr341	Trp286 Tyr341	Trp286 Tyr72 Trp86 His447
2	π- alkyl				Val294	
3	H-bond	Tyr124 Tyr341 Tyr337	Tyr124	Tyr124	Tyr124	Tyr124 Asp74
4	Carbon-hydrogen			Gln291	Trp286	
5	π-sigma			Trp86		Tyr341

*Table 23: Interactions predicted between rhAChE and **(R)-132**, **(R)-133**, **(R)-134** and **(R)-135***

Concerning the interactions between compound **(R)-132** and *rh*AChE (Figure 129), a potential π-stacking interaction could be observed between the phenyl ring of the indanone and simultaneously Tyr341 and Trp286 (entry 1) and Tyr124 has been predicted to interact with the ketone fragment through H-bond interactions (entry 3) (Figure 129).

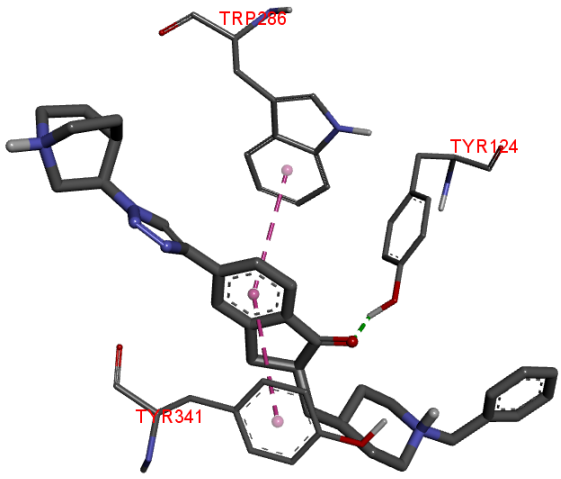

*Figure 129: Representation of predicted interactions between rhAChE and **(R)-132***

Compound **(R)-133**'s predicted interactions with *rh*AChE could be summarized as followed (Figure 130). π-stacking was foreseen between the ligand and various residues such as Trp286 and Tyr341

interacting with the phenyl fragment of the indanone (entry 1) and Gln291 interacting with the quinuclidine moiety through a carbon-hydrogen bond (entry 4). In addition, the compound's ketone has been predicted to interact with Tyr124 *via* a H-bond formation (entry 3) (Figure 130).

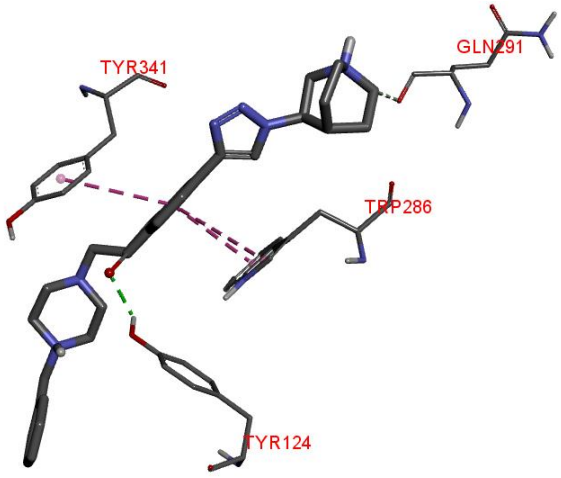

*Figure 130: Representation of predicted interactions between rhAChE and **(R)-133***

Compound **(R)-134** (Figure 131) was mainly predicted to display π-stacking interactions, indeed, the phenyl ring of the indanone should interact with Tyr341 and Trp286 (entry 1) while Trp286 also should interact with the triazole moiety through carbon-hydrogen bonds (entry 4). Moreover, the phenyl ring should also interact with Val294 through π-alkyl interactions (entry 2) (Figure 131).

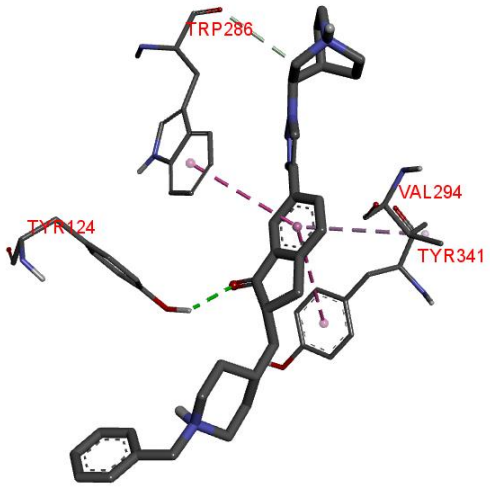

*Figure 131: Representation of predicted interactions between rhAChE and **(R)-134***

Regarding compound **(R)-135** (Figure 132), the phenyl ring part of the indanone moiety appeared to be proned to π-stack with Trp286 while the benzyl of the molecule, the one carried by the piperazine, to π-stack with Trp86 and His447 (entry 1) and the protonated nitrogen of the piperazine moiety

seemed to bind with Asp74 through a H-bond interaction while the second nitrogen of the piperazine appeared to bind with Tyr124 in the same way (entry 3). Finally, the carbon between the indanone and the piperazine moiety has been predicted to interact with Tyr341 through π-sigma interactions (Figure 132).

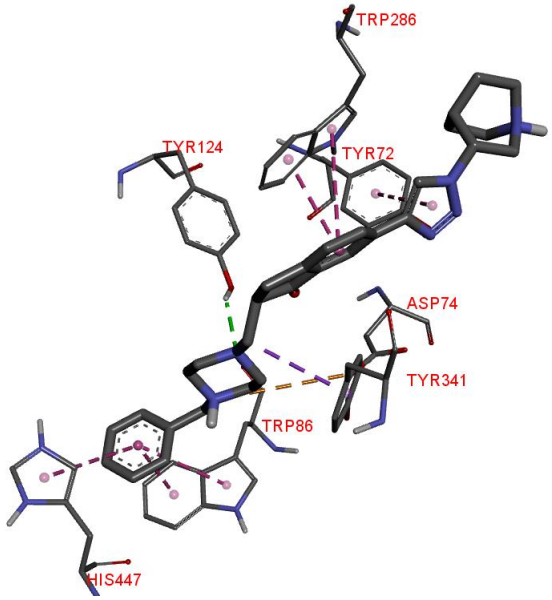

*Figure 132: Representation of interactions predicted between rhAChE and **(R)-135***

With these various results in hands, we were able to reach the same conclusion as for the first series, indeed, the predicted interactions of compounds **(R)-132** to **(R)-135** were similar to the one displayed for Donepezil structure (Figure 125 – p.12), meaning that adding a new pharmacophore to the Donepezil fragment did not seem to disrupt the interactions of this AChEI with the enzyme.

3.2.2. CNS MPO score computation

Besides the fact that compounds **(R)-132** to **(R)-135** respected the Lipinski's rules, their CNS MPO scores were calculated and reported in All physico-chemical *properties were obtained from chemicalize.com*

Table 24 along with their main physicochemical properties.

The obtained results were similar to those previously obtained for the first series of Donepezil based MTDL, compounds **(R)-132** (entry 2) and compound **(R)-134** (entry 4) displayed lower scores because of a higher molecular weight coupled with a strong LogP value, nevertheless, compounds **(R)-133** (entry 3) and compound **(R)-135** (entry 5), despite their size, expressed better CNS MPO scores thanks to a lower LogP value and pKa. Once again, the scores and main physicochemical properties values of the four tested compounds were in accordance with the score and physicochemical properties displayed by the parent monomer Donepezil (entry 1).

Entry	Compound	CLogP	CLogD	TPSA (Å²)	MW g/mol	HBD	pKa	CNS MPO score
1	**Donepezil**	4.21	2.48	38.77	379.5	0	9.12	**4.4**
2	**(R)-132**	4.98	1.49	54.26	495.67	0	9.45	**3.3**
3	**(R)-133**	3.83	1.57	57.50	496.66	0	9.18	**4.0**
4	**(R)-134**	4.98	1.96	54.26	495.67	0	9.26	**3.4**
5	**(R)-135**	3.83	2.04	57.50	496.66	0	8.72	**4.2**

All physico-chemical properties were obtained from chemicalize.com

*Table 24: Physicochemical properties and CNS MPO scores of **(R)-132**, **(R)-133**, **(R)-134** and **(R)-135***

3.2.3. Percepta software CNS activity prediction

Passive BBB penetration ability for compounds **(R)-132**, **(R)-133**, **(R)-134** and **(R)-135** has been predicted based on calculated physicochemical properties reported in Table 25. It is important to note that calculated LogP and most basic pKa values are in accordance with the values used to previously evaluate the CNS MPO scores and despite a lower CNS MPO score, compounds **(R)-132** (entry 1) and **(R)-134** (entry 3) obtained more encouraging prediction in this study, enough to be considered CNS active.

Entry	Compound	LogP	pKa	f_u	LogPS	LogBB	Log(PS*f_u)	Brain penetration for CNS activity
1	**(R)-132**	4.10	9.28	0.036	-1.6	0.20	-3.2	Sufficient
2	**(R)-133**	4.39	9.31	0.042	-1.5	0.41	-3.3	Sufficient
3	**(R)-134**	2.80	9.31	0.18	-2.2	0.19	-3.1	Sufficient
4	**(R)-135**	2.75	9.31	0.18	-2.2	0.16	-3.1	Sufficient

*Table 25: Physicochemical properties determined with Percepta software for **(R)-132**, **(R)-133**, **(R)-134** and **(R)-135***

The four tested compounds displayed promising ability concerning their aptitude to cross the BBB, indeed, they all obtained scores close to -3 (Figure 133) and were all positioned in the CNS active compounds group (represented with blue dots). Apparently, changing the *N*-benzylpiperidine of compounds **(R)-132** and **(R)-134** by a *N*-benzylpiperazine in compounds **(R)-133** and **(R)-135** did not affect the predicted properties of the ligands to cross the BBB, moreover, the relative position of the *N*-benzylpiperidine (or *N*-benzylpiperazine) fragment did not appear to induce a major change either.

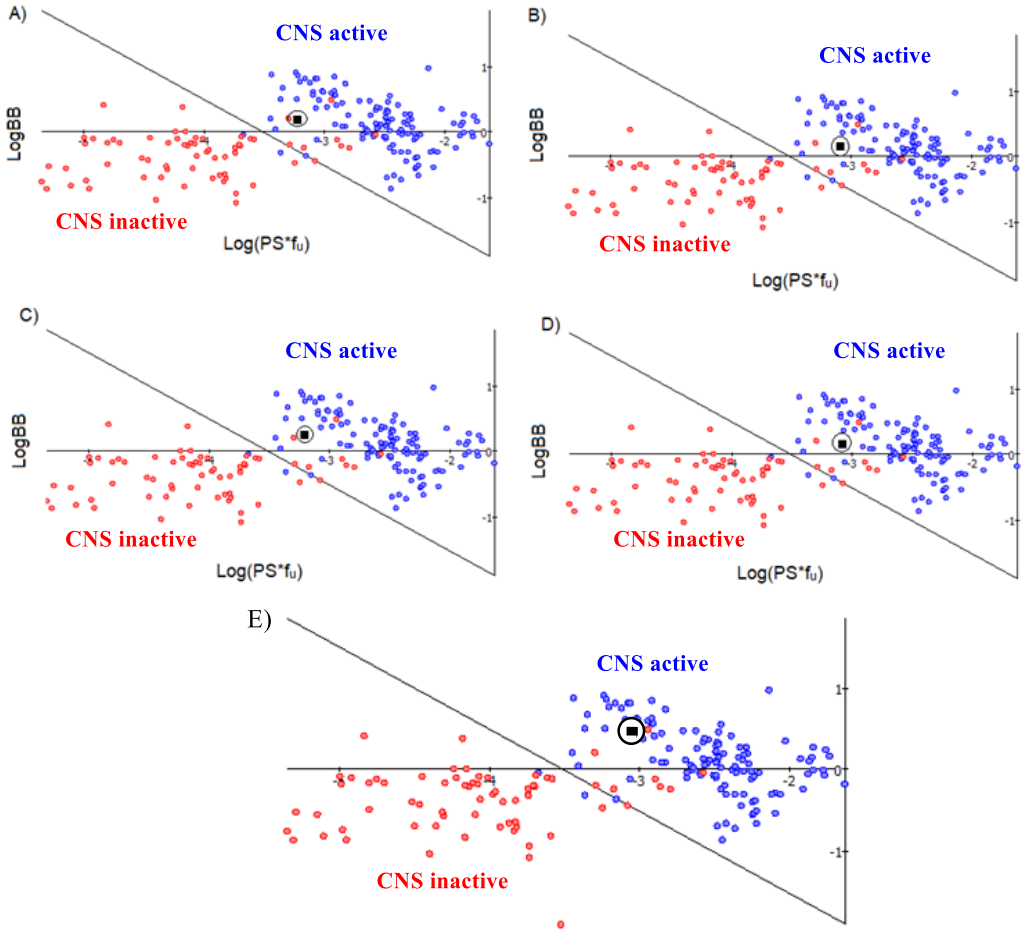

Figure 133: Results of Brain penetration prediction for CNS activity for (A) ***(R)-132*** *(B)* ***(R)-133*** *(C)* ***(R)-134*** *(D)* ***(R)-135*** *(E) Donepezil (red dots represent CNS inactive compounds, blue dots represent CNS active compounds and the circled black dot represent the tested compound)*

Hence, these studies have brought to light that the phenyl and benzyl rings of compounds **(R)-128**, **(R)-129**, **(R)-130** and **(R)-131** of the first series and of compounds **(R)-132**, **(R)-133**, **(R)-134** and **(R)-135** of the second series were of pivotal importance to induce an appropriate binding of the compounds inside AChE catalytic pocket due to the numerous interactions in which they were predicted to be involved with the main residues of the enzyme. Moreover, the chosen size of the compounds (and thus the length of the linker between the two pharmacophores) appeared to be the right choice, indeed, interactions between the quinuclidine moiety and AChE PAS could be considered with these types of

combined MTDLs and could possibly offer the molecules a higher affinity for the enzyme, more potential binding interactions and additional biological properties. Moreover, the studies concerning their physicochemical properties, either using CNS MPO score calculation or Percepta software representation, were encouraging for all the eight compounds. Nevertheless, as it was described by Sugimoto et *al*.[351], the most optimal structure of Donepezil as a AChEI is the one carrying a *N*-benzylpiperidine, which is thus why we first focused our synthetic efforts on compounds **(R)-128**, **(R)-130**, **(R)-132** and **(R)-134**.

4. Synthesis of the Donepezil based MTDLs

For the sake of clarity, the synthesis of the two series of combined Donepezil-based MTDLs will be presented separately but the investigations were performed in parallel.

4.1. Series 1

4.1.1. First approach to (R)-128 and (R)-130

4.1.1.1. Retrosynthetic scheme

To obtain the first series of combined MTDLs **(R)-128** and **(R)-130** based on a Donepezil scaffold we designed and validate with *in silico* evaluations, the rational approach was to use our gained expertise in the development of Copper(I) catalysed Huisgen cycloaddition protocols. After obtaining the (R)-azidoquinuclidine **(R)-77** using the protocol described in chapter II[369,370] and the required alkynes **136** and **137**, the two partners could be easily conjugated in the last synthetic step through a CuAAC[371] yielding the desired 1,2,3-triazole moiety (Figure 134).

[369] Alper, P. B.; Hung, S.-C.; Wong, C.-H. Metal Catalyzed Diazo Transfer for the Synthesis of Azides from Amines. *Tetrahedron Lett.* **1996**, *37* (34), 6029–6032.
[370] Nyffeler, P. T.; Liang, C.-H.; Koeller, K. M.; Wong, C.-H. The Chemistry of Amine−Azide Interconversion: Catalytic Diazotransfer and Regioselective Azide Reduction. *J. Am. Chem. Soc.* **2002**, *124* (36), 10773–10778.
[371] Sarasamkan, J.; Scheunemann, M.; Apaijai, N.; Palee, S.; Parichatikanond, W.; Arunrungvichian, K.; Fischer, S.; Chattipakorn, S.; Deuther-Conrad, W.; Schüürmann, G.; Brust, P.; Vajragupta, O. Varying Chirality Across Nicotinic Acetylcholine Receptor Subtypes: Selective Binding of Quinuclidine Triazole Compounds. *ACS Med. Chem. Lett.* **2016**, *7* (10), 890–895.

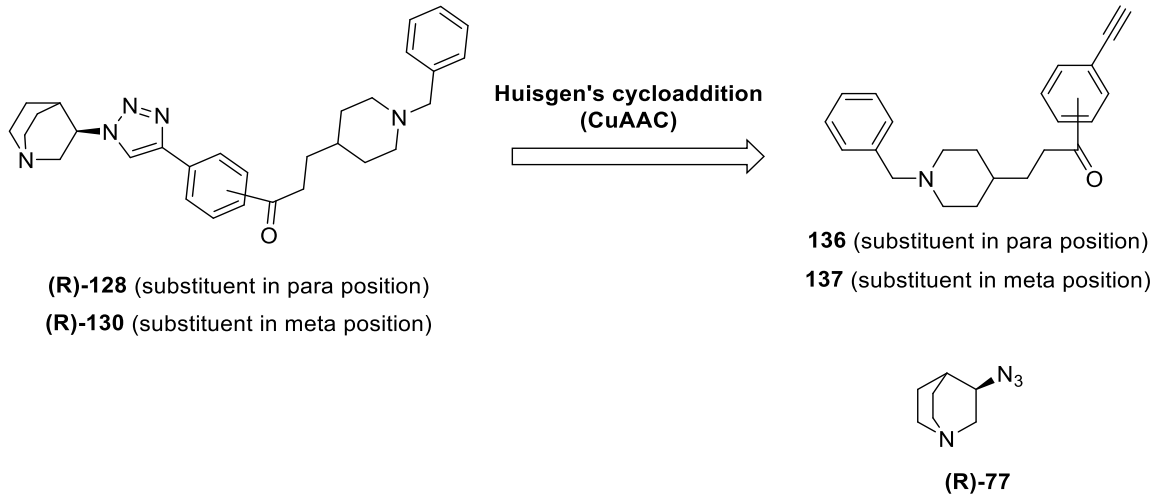

*Figure 134: Retrosynthetic pathway to **(R)-128** and **(R)-130***

*4.1.1.2. Synthesis of **136***

In a first intend, we decided to focus on the development of a robust synthetic pathway for one compound. Based on the docking experiment and starting materials available, we have chosen to work on compound **136** where the alkyne is in the para position, to simplify the synthetic process (Figure 135). The retrosynthetic strategy (Figure 135) could be summarized as follow: reduction and deprotection of the alkyne **138** should offer target product. Alkyne moiety could be obtained through Sonogashira cross coupling reaction, and the corresponding alcohol could be formed by an aldolization reaction between aldehyde **140** (readily obtained from commercially available alcohol **142**), and commercially available 4-bromoacetophenone **141**. The aldolization/dehydration pathway was chosen based on the work of Nagel et *al.*[372], moreover, our bibliographic researches on recent literature[373,374,375] lead to the conclusion that it was the predominant and more effective pathway to synthesise this type of donepezil moiety.

[372] Nagel, A. A.; Liston, D. R.; Jung, S.; Mahar, M.; Vincent, L. A.; Chapin, D.; Chen, Y. L.; Hubbard, S.; Ives, J. L. Design and Synthesis of 1-Heteroaryl-3-(1-Benzyl-4-Piperidinyl)Propan-1-One Derivatives as Potent, Selective Acetylcholinesterase Inhibitors. *J. Med. Chem.* **1995**, *38* (7), 1084–1089.

[373] Yan, J.; Hu, J.; Liu, A.; He, L.; Li, X.; Wei, H. Design, Synthesis, and Evaluation of Multitarget-Directed Ligands against Alzheimer's Disease Based on the Fusion of Donepezil and Curcumin. *Bioorg. Med. Chem.* **2017**, *25* (12), 2946–2955.

[374] Laroche, B.; Saito, Y.; Ishitani, H.; Kobayashi, S. Basic Anion-Exchange Resin-Catalyzed Aldol Condensation of Aromatic Ketones with Aldehydes in Continuous Flow. *Org. Process Res. Dev.* **2019**, *23* (5), 961–967.

[375] Green, K.; Fosso, M.; Garneau-Tsodikova, S. Multifunctional Donepezil Analogues as Cholinesterase and BACE1 Inhibitors. *Molecules* **2018**, *23* (12), 3252.

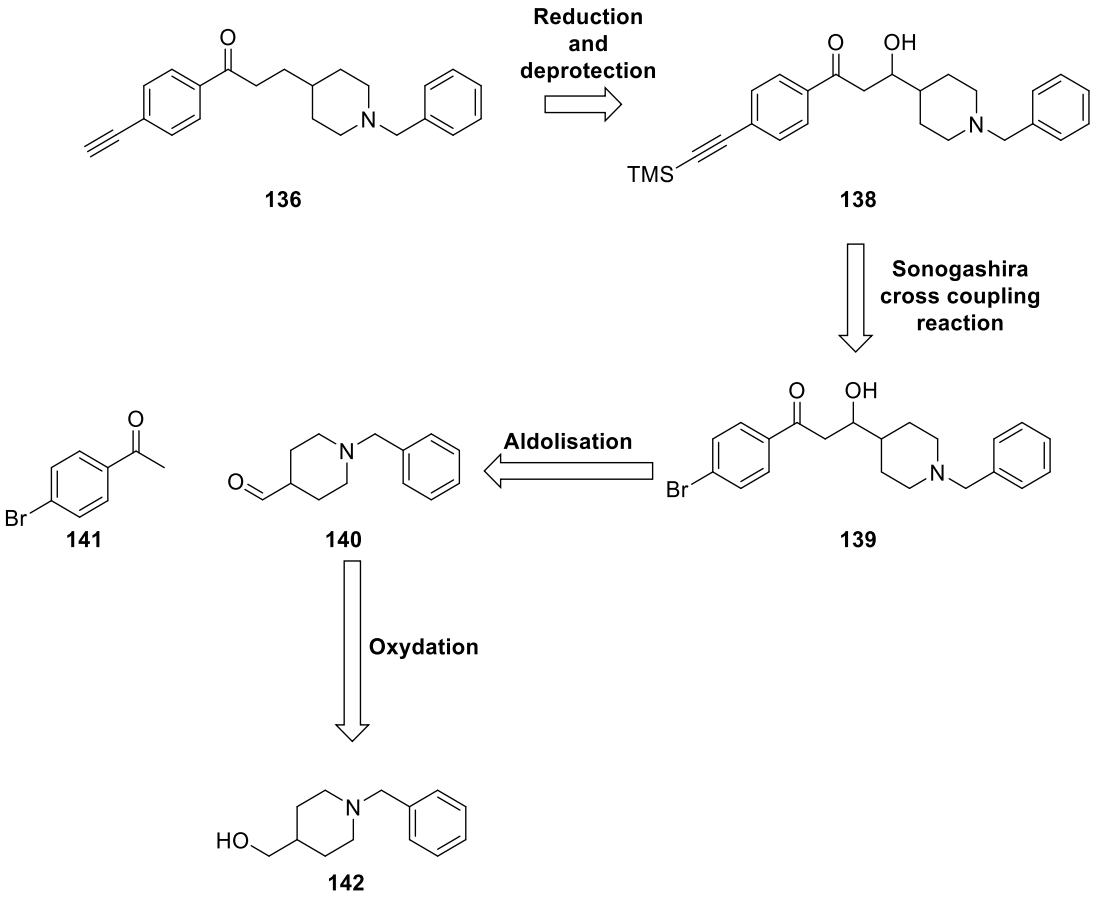

*Figure 135: Proposed synthetic route to **136***

Firstly, Swern oxidation of commercially available (1-benzylpiperidin-4-yl)methanol **142** using oxalyl chloride **143** and DMSO in presence of triethylamine in dichloromethane, offered the corresponding aldehyde **140**[376] in gram-scale with an excellent yield of 95%. The next step was an aldolization reaction between aldehyde **140** and the aromatic ketone **141** using basic conditions in THF[372]. LiHMDS was chosen as a base, and compound **139** was obtained in a low 16% yield which could be explained by the high dependence of the reaction to the quality of the base. Indeed, it was observed that, although such reaction has been described with similar compounds, we observed that with LiHMDS we had in stock (which was an already used bottle of LiHMDS), the reaction mixture was mainly composed of side products (or degradation products) giving complex NMR signals not allowing us to elucidate their structures. Finally, based on our expertise in the development of efficient Sonogashira coupling conditions, we tried to perform the coupling between compound **139** and ethynyltrimethylsilane in presence of copper(I) iodide with palladium tetrakis triphenylphosphine as the catalytic source of

[376] van Greunen, D. G.; Cordier, W.; Nell, M.; van der Westhuyzen, C.; Steenkamp, V.; Panayides, J.-L.; Riley, D. L. Targeting Alzheimer's Disease by Investigating Previously Unexplored Chemical Space Surrounding the Cholinesterase Inhibitor Donepezil. *Eur. J. Med. Chem.* **2017**, *127*, 671–690.

Pd(0), in a mixture composed of dichloromethane and triethylamine[377]. Yet, despite our efforts, only the starting materials and the ethynyltrimethylsilane homocoupling product were recovered.

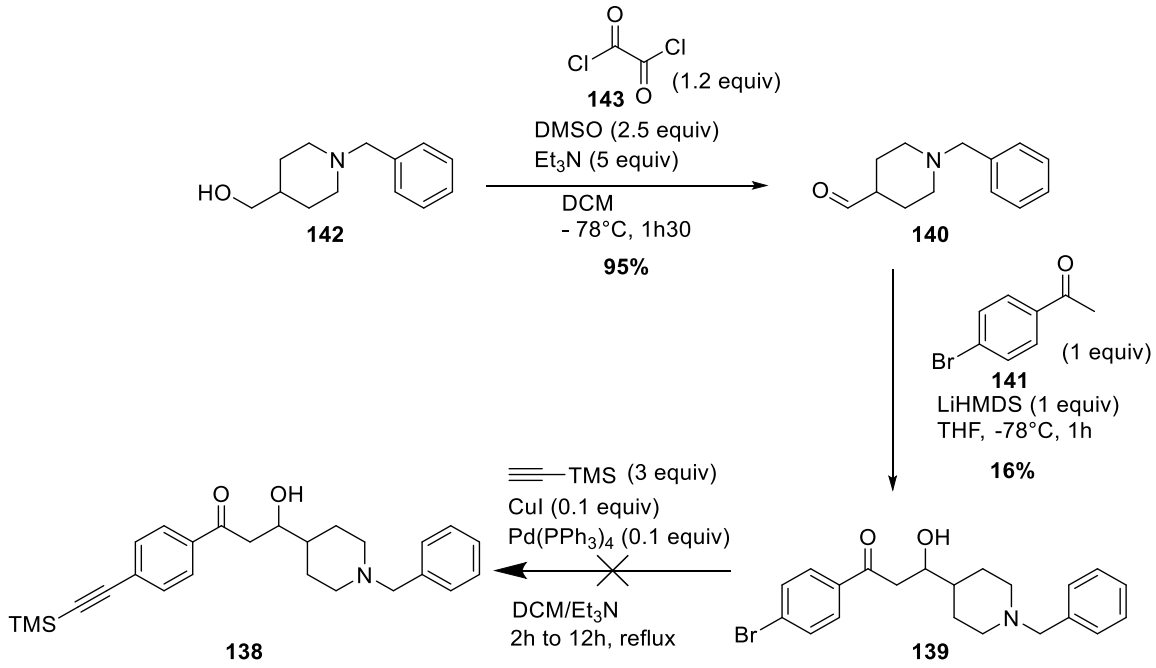

*Scheme 40: First synthetic pathway to **138***

4.1.1.3. Screening Sonogashira cross coupling reaction conditions

Despite a longer time of reaction (from 2h to 12h) to obtain compound **138**, the conversion rate as estimated through ^{1}H NMR spectra of quenched samples of crude reaction mixture, could not be increased higher than 10% under these reactions conditions. At this point of the project, we decided to find out optimized reaction conditions for the Sonogashira coupling step. The 1-(3-bromophenyl)ethan-1-one **144** was used as a test compound to evaluate the best conditions to perform the reaction, and obtained results are reported in
Table 26.

[377] Mercey, G.; Verdelet, T.; Saint-André, G.; Gillon, E.; Wagner, A.; Baati, R.; Jean, L.; Nachon, F.; Renard, P.-Y. First Efficient Uncharged Reactivators for the Dephosphylation of Poisoned Human Acetylcholinesterase. *Chem. Commun. Camb. Engl.* **2011**, *47* (18), 5295–5297.

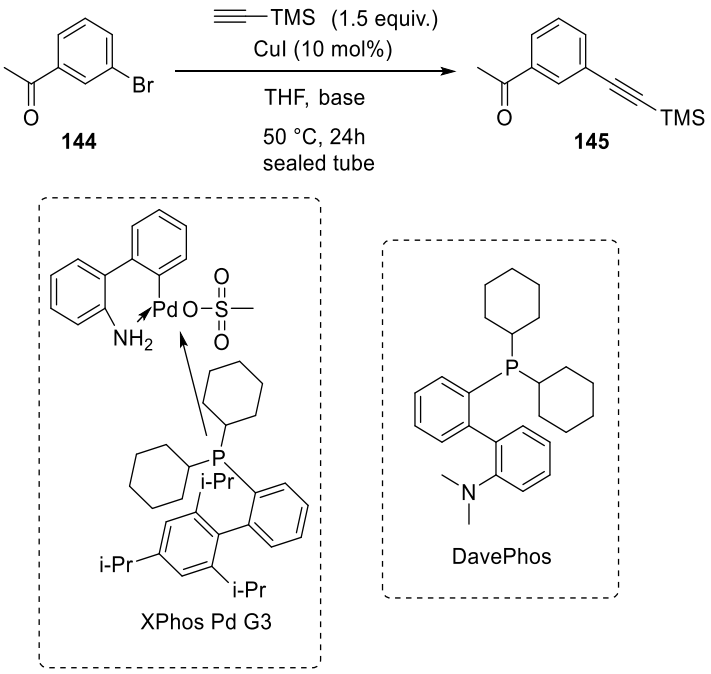

Scheme 41: Test reaction for the Sonogashira coupling

Entry	Base	Palladium source	Phosphine	Conversion (%)
1	Et_3N	$Pd(PPh_3)_4$ (10 mol%)	/	0
2	Et_3N	$Pd(dppf)Cl_2$ complex with DCM (10 mol%)	/	0
3	Et_3N	XPhos Pd, G3 (10 mol%)	/	5
4	Et_3N	$PdCl_2$ (5 mol%)	DavePhos (10 mol%)	38
5	**Et_3N**	**$Pd(OAc)_2$ (5 mol%)**	**DavePhos (10 mol%)**	**46**
6	Et_3N	$Pd_2(dba)_3$ (2.5 mol%)	DavePhos (10 mol%)	45
7	Cs_2CO_3	$Pd(OAc)_2$ (5 mol%)	DavePhos (10 mol%)	0
8	Cs_2CO_3	$Pd_2(dba)$ (2.5 mol%)	DavePhos (10 mol%)	0

*Table 26: Screening condition for the Sonogashira coupling to **145***

Sonogashira coupling is a sensitive reaction (due to the unstable character of Pd(0) complexes), thus must usually be run in mild, air-free and moisture-free conditions in presence of a base, acting as the solvent, in order to neutralize the hydrogen halide produced during the coupling. Based on our expertise, we first decided to keep the triethylamine as a base and performed the reactions in THF to be able to heat the mixture, and we varied the palladium source by using instead of $Pd(PPh_3)_4$, a $Pd(dppf)Cl_2$ complex with dichloromethane (entry 2) and commercially available Buchwald precatalyst, XPhos Pd G3, an air, moisture, and thermally stable complex of bulky phosphine and Pd(II) (entry 3)[378]. In the literature[379,380], $Pd(dppf)Cl_2$ complex with dichloromethane was proven to be an efficient precatalyst for this type of coupling and, in our study, it seemed relevant to evaluate the efficiency of such a bidentate ligand. Moreover, XPhos Pd G3 was also investigated because of its low sensitivity toward oxygen that could be found in the reaction mixture, which allowed us to minimize degradation (through oxidation) or even complexation of the precatalyst. Yet, neither heating with $Pd(PPh_3)_4$ nor use of these two Pd(II) sources significantly improved the conversion rate of **144**. The second strategy we used to optimise the procedure was to use separate palladium (II) source and phosphine in presence of triethylamine (entry 4), with $PdCl_2$ as Pd source and Davephos as the phosphine, we managed to obtain a 38% conversion of **144**, a promising result but which still requires improvement to be implemented at this stage of the synthesis. Building on this improvement, we decided to try other sources of palladium (either Pd(0) or Pd(II) species) available in the laboratory coupled with the most promising phosphine, DavePhos, and triethylamine, as shown on entry 5 and 6, the conversion was once again improved, and we obtained either using a Pd(II) source, namely $Pd(OAc)_2$ or a Pd(0) source, namely $Pd_2(dba)_3$, in both cases conversions around 45%. The last parameter we assayed was the replacement of the base, changing the triethylamine by cesium carbonate (entry 7 and 8), unfortunately, this base modification ended up in a drastic drop in conversion (down to 0%). As a conclusion of this short study, we managed to obtain a Sonogashira cross coupling reaction procedure allowing to reach a conversion of **144** of 46% NMR (entry 5) but we estimated that such a modest result was insufficient and decided to change the synthetic strategy.

[378] Anderson, K. W.; Buchwald, S. L. General Catalysts for the Suzuki-Miyaura and Sonogashira Coupling Reactions of Aryl Chlorides and for the Coupling of Challenging Substrate Combinations in Water. *Angew. Chem. Int. Ed.* **2005**, *44* (38), 6173–6177.

[379] Chinchilla, R.; Nájera, C. The Sonogashira Reaction: A Booming Methodology in Synthetic Organic Chemistry †. *Chem. Rev.* **2007**, *107* (3), 874–922.

[380] Zou, G.; Zhu, J.; Tang, J. Cross-Coupling of Arylboronic Acids with Terminal Alkynes in Air. *Tetrahedron Lett.* **2003**, *44* (48), 8709–8711.

4.1.2. New approach to (R)-128 and (R)-130

4.1.2.1. Retrosynthetic pathway

After finding out that the first strategy we developed presented at least two bottlenecks (at the aldolization and Sonogashira cross coupling steps), to efficiently obtain combined MTDLs **(R)-128** and **(R)-130**, we designed a new synthetic pathway where the Copper(I)-catalysed Huisgen's cycloaddition is not the final step but a pivotal point introduced earlier in the procedure (Figure 136). The newly developed retrosynthesis scheme could be summarized in the three following key steps: an aldolization of **(R)-146** (or **(R)-147**) and aldehyde **140**, previously obtained, followed by a reduction should lead to compound **(R)-128** (or **(R)-130**). Ketone **(R)-146** (or **(R)-147**) could be obtained from the corresponding alkyne **148** (or **149**) and azide **(R)-77** through a Copper(I)-catalysed Huisgen's cycloaddition following the procedure used in the previous chapter, and a Sonogashira cross-coupling between ketone **150** (or **151**) ,bearing a triflate instead of a bromine, and ethynyltrimethylsilane should offer compound **148** (or **149**).

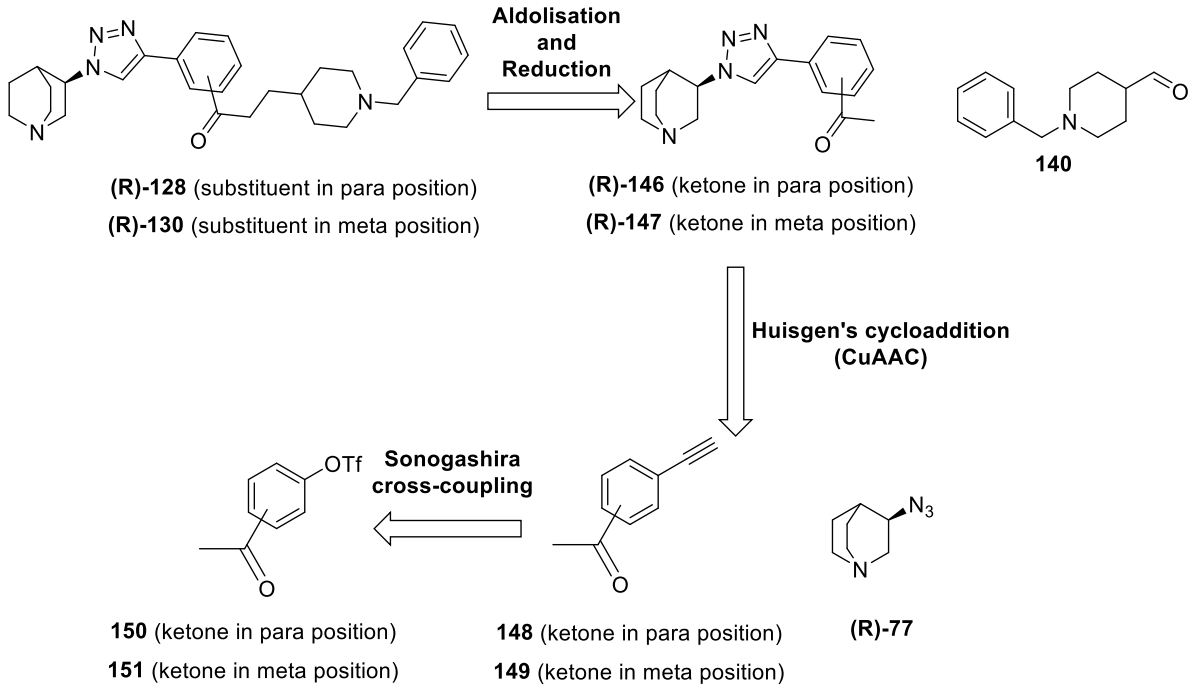

*Figure 136: Proposed retrosynthetic access to **(R)-128** and **(R)-130***

*4.1.2.2. Alkyne **148** and **149** synthesis*

As mentioned in the retrosynthetic analysis, we decided to perform the Sonogashira cross coupling reaction using a triflate instead of the bromine derivative, thus, commercially available 4-hydroxyacetophenone **152** and 3-hydroxyacetophenone **153** were put in presence of

trifluoromethanesulfonic anhydride and triethylamine (4 equiv.) in dichloromethane[381] to give respectively compounds **150** and **151** bearing a triflate function in good 71% and 78% yields. Then, a Sonogashira coupling, using the non-optimized but more affordable procedure (in presence of $PdCl_2(PPh_3)_2$ in refluxing DMF) was performed between ethynyltrimethylsilane and compounds **150** and **151**, followed by a deprotection of the terminal alkyne using potassium carbonate to provide alkynes **148** and **149** in 3 steps with acceptable 25% and 26% overall yields over the three steps in a 400 mg scale (Scheme 42).

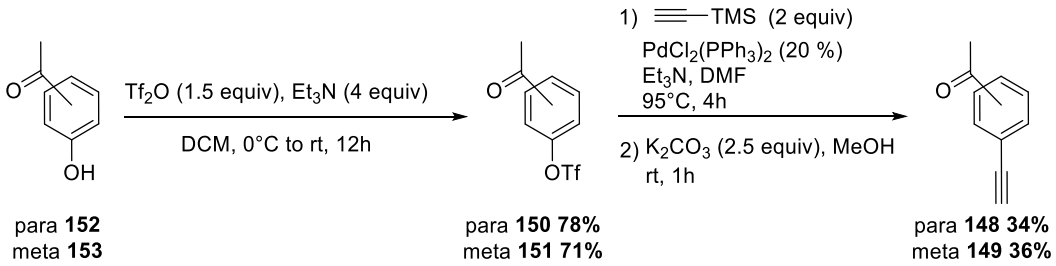

*Scheme 42: Synthesis of alkynes **148** and **149***

*4.1.2.3. Synthesis of **(R)-147***

With alkyne **148** and **149** in hands, we decided to first continue the synthesis with only alkyne **149** to build a viable synthetic pathway applicable to other substrates (Scheme 43). Our first attempt to process to the aldolization reaction between ketone **149** and aldehyde **140** in basic conditions as previously reported[372]. unfortunately failed, and we were not able to recover the desired key compound **137**. This result was afterwards easily explained by the small pKa difference between the hydrogens of the methylketone moiety (pKa = 24.7) and the one of the free alkyne (pKa = 25) present in the same compound **149**, as compared with the pKa of the base we chose (pKa_{LiHMDS} = 25). In order to get rid of this interfering free alkyne, in view of the failed experiment, it was decided to perform first the Copper(I) catalysed Huisgen cycloaddition between the newly obtained alkyne **149** and the (R)-azidoquinuclidine **(R)-77** (obtained as previously through a diazaotransfert on (R)-aminoquinuclidine **(R)-81**). The CuAAC reaction was led in the same conditions as previously reported in this manuscript and the key intermediate **(R)-147**, was synthesised in 26% yield.

[381] Dürr, A. B.; Yin, G.; Kalvet, I.; Napoly, F.; Schoenebeck, F. Nickel-Catalyzed Trifluoromethylthiolation of Csp2–O Bonds. *Chem. Sci.* **2016**, *7* (2), 1076–1081.

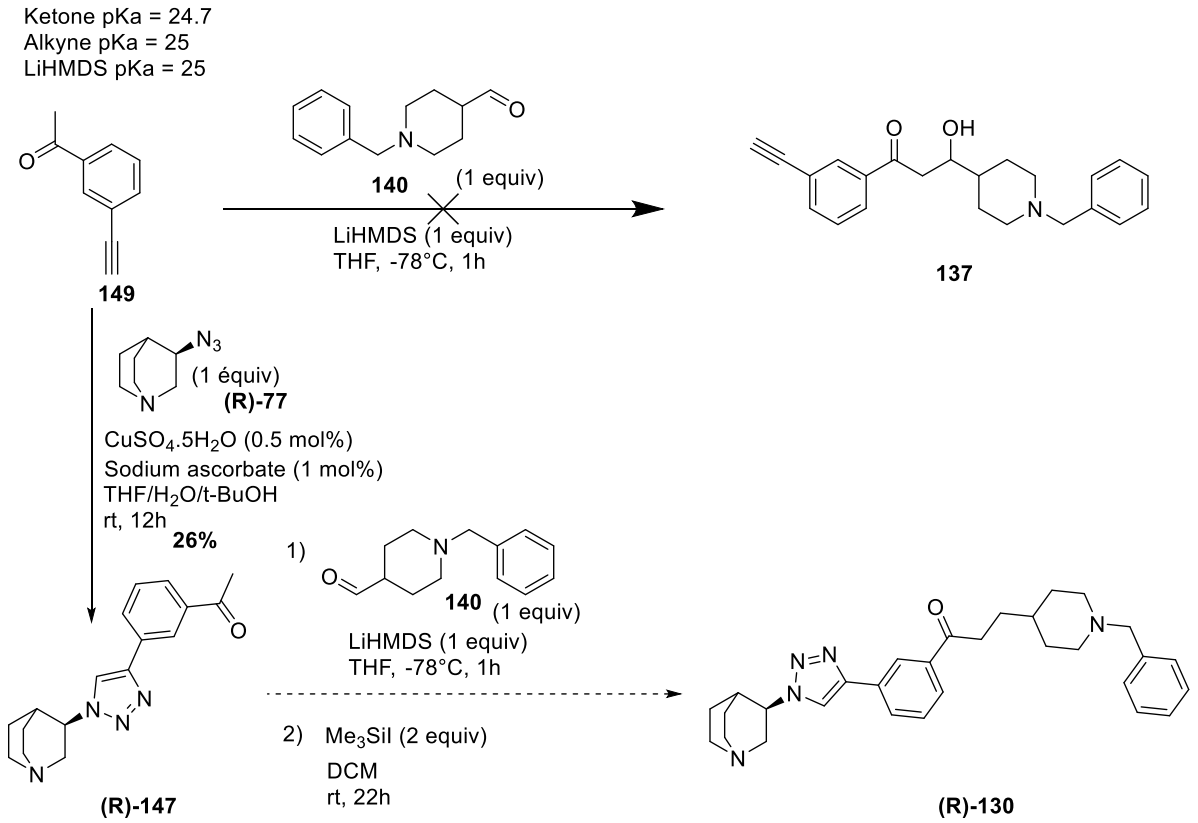

*Scheme 43: Synthesis of **(R)-147** and further work to obtain **(R)-130***

With this key intermediate in hands, the next step will be to proceed to the aldolization reaction it between ketone **(R)-147** and aldehyde **140** using the previously displayed basic conditions, then proceed to a reduction of the ketol following the procedure described by Richard Roberts[382] (use an excess iodotrimethylsilane in DCM) to have access to the MTDL **(R)-130**. Regioisomer MTDL **(R)-128** could be obtained following the same synthetic route. If these two last steps are successfully achieved, optimization of the whole synthetic process could be undertaken: for the aldolization reaction, the base used could be changed for a bulkier one such as LiTMP, or other aldolization processes (such as the use of enamines) preventing the use of basic aldolization conditions with an aldehyde able to form an enol, conditions known to end up with aldehyde auto condensation and polymerization issues. For the Sonogashira cross coupling reaction, yields could be improved using the optimized conditions described in paragraph 4.1.1.3 ($Pd(OAc)_2$ or Pd_2dba_3 as the Pd source and Davephos as a ligand).

[382] Roberts, R. S. Studies on the Phenyldimethylsilyllithium Reagent and Its Applications to Organic Synthesis. Ph.D., University of Cambridge, **1997**.

4.2. Series 2

4.2.1. First approach to (R)-132 and (R)-134

4.2.1.1. Retrosynthetic pathway

In parallel to the development of combined MTDLs **(R)-128** and **(R)-130**, we designed a strategy to access combined MTDLs **(R)-132** and **(R)-134** through the same pathway using Copper(I) catalysed Huisgen cycloaddition to link the two partners **(R)-77** and **154** (or **155**) *via* the formation of a 1,2,3-triazole moiety (Figure 137). As a first example of the series, MTDL **(R)-134** was chosen as a first synthetic target in order to validate the synthetic pathway before applying it on the other substituents.

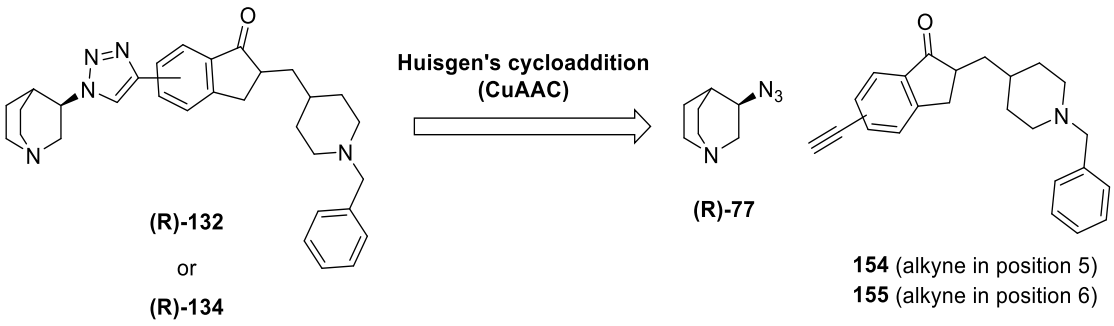

*Figure 137: Retrosynthetic pathway to **(R)-132** and **(R)-134***

*4.2.1.2. Synthesis of the Donepezil moiety **154** or **155***

The synthesis of Donepezil based MTDLs began with the preparation of the Donepezil moiety **154**. To achieve the formation of this moiety, the first step was to prepare the aldehyde **159** from commercially available ethyl isonipecoate based on a synthesis previously developed in the team by Doctor Renou during his PhD[383] (Scheme 44).

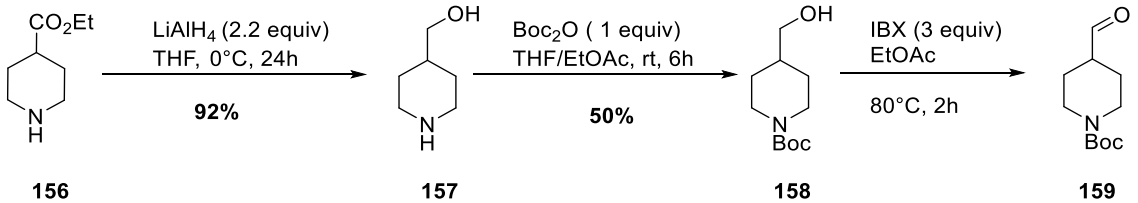

*Scheme 44: Synthesis of **159***

[383] Renou, J.; Dias, J.; Mercey, G.; Verdelet, T.; Rousseau, C.; Gastellier, A.-J.; Arboléas, M.; Touvrey-Loiodice, M.; Baati, R.; Jean, L.; Nachon, F.; Renard, P.-Y. Synthesis and in Vitro Evaluation of Donepezil-Based Reactivators and Analogues for Nerve Agent-Inhibited Human Acetylcholinesterase. *RSC Adv.* **2016**, *6* (22), 17929–17940.

Alcohol **157** was obtained from ethyl isonipecoate **156** through the reduction of the ethyl ester using $LiAlH_4$ in THF with an excellent 92% yield. Next, the secondary amine of compound **157** was protected as a Boc-carbamate to give compound **158** in 50% yield. This alcohol was **158** finally oxidized in aldehyde **159** through the use of 2-iodoxybenzoic acid giving the unstable aldehyde **159**, which was used without further purification in the following steps of the synthesis. To obtain the Donepezil moiety **154** an aldolization-crotonization process was performed between aldehyde **159** and 5-bromoindanone **160** in presence of an aqueous solution of sodium hydroxide as a base, the required water / DCM mixture needed in this process required the additional use of tetra-*n*-butylammonium bromide as a phase transfer catalyst. The aldolization-crotonization process gave compound **161** in 44% yield. With this Donepezil moiety **161** in hands, a Sonogashira cross coupling reaction was assayed, yet, as shown previously with the acyclic MTDL series, despite various attempts, compound **162** could not be obtained and only ethynyltrimethylsilane homocoupling product was observed along with the recovery of the starting material **161** (Scheme 45).

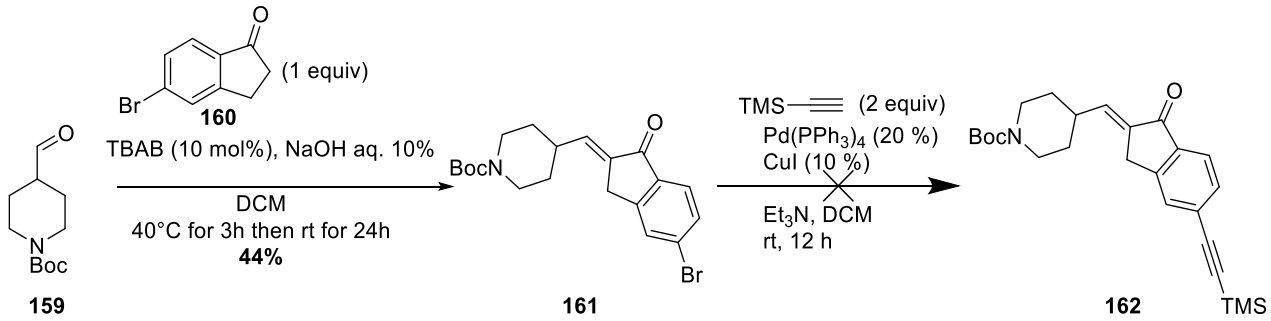

*Scheme 45: Attempt synthesis of **162***

4.2.1.3. Screening Sonogashira cross coupling reaction conditions on 5-bromoindanone derivatives.

As a model compound, 5-bromoindanone **160** was used in this study to evaluate the reaction conditions for the Sonogashira cross-coupling step required to access to alkyne **154** or **155**. Main results are reported on Table 27.

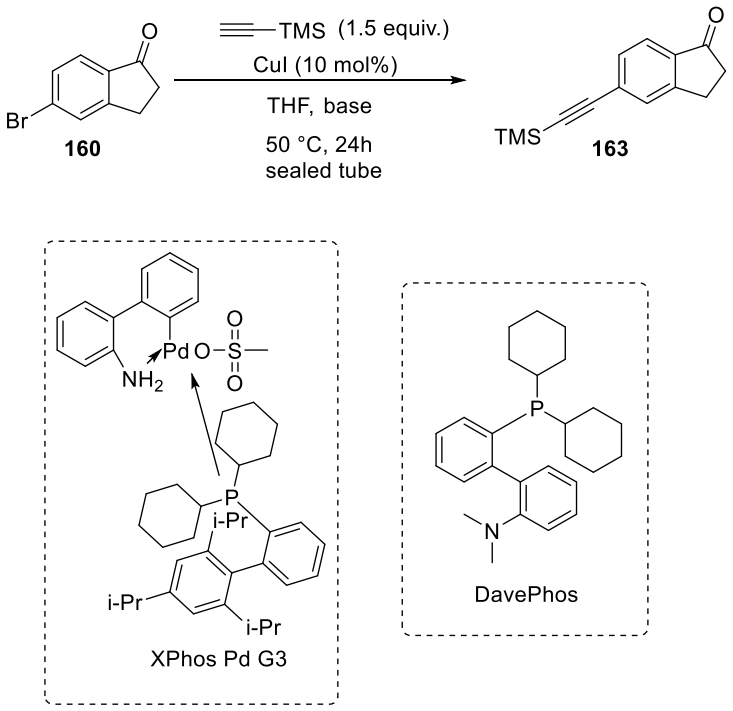

Scheme 46: Test reaction for the Sonogashira coupling

Entry	Base	Palladium source	Phosphine	Conversion (%)
1	Et_3N	Pd $(PPh_3)_4$ (10 mol%)	/	0
2	Et_3N	Pd(dppf)Cl_2 complex with DCM (10 mol%)	/	0
3	Et_3N	XPhos Pd, G3 (10 mol%)	/	< 5
4	**Et_3N**	**$PdCl_2$ (5 mol%)**	**DavePhos (10 mol%)**	**41**

Table 27: Conditions assayed for Sonogashira cross coupling reaction optimization

Based on our results on the synthesis of **145**, the acyclic ketone analogue of **163**, we already observed that triethylamine was the base giving the best results during the assays and it was not modified during the Sonogashira cross coupling reaction conditions optimization assays we performed. It can be noted that the reaction conditions where a pre-formed Pd-ligand complex was used, such as Pd$(PPh_3)_4$ (entry 1), Pd(dppf)Cl_2 complex with dichloromethane (entry 2) or XPhos Pd, G3 (entry 3), no product was formed and the starting material was recovered as it stands, and without noticeable degradation. Yet, when distinct source of palladium such as $PdCl_2$ and phosphine like DavePhos were used, the conversion of **160 s**ignificantly increased (entry 4). Unfortunately, the maximum conversion we

obtained could be estimated to reach only around 40% which precluded this synthetic route and required the implementation of another synthetic strategy.

4.2.2. New approach to (R)-132 and (R)-134

4.2.2.1. Second retrosynthetic strategy to access to (R)-132 and (R)-134

As for the synthesis of MTDLs **(R)-128** and **(R)-130**, a new strategy was designed to tackle the challenge of obtaining combined MTDLs **(R)-132** and **(R)-134** (Scheme 47). The Copper(I) catalysed Huisgen cycloaddition will be used at an earlier key step of the synthetic pathway between azide **(R)-77** and alkynes **166** and **167**, followed by an aldol based coupling of the obtained compounds **(R)-164** and **(R)-165** bearing a triazole with aldehyde **140**.

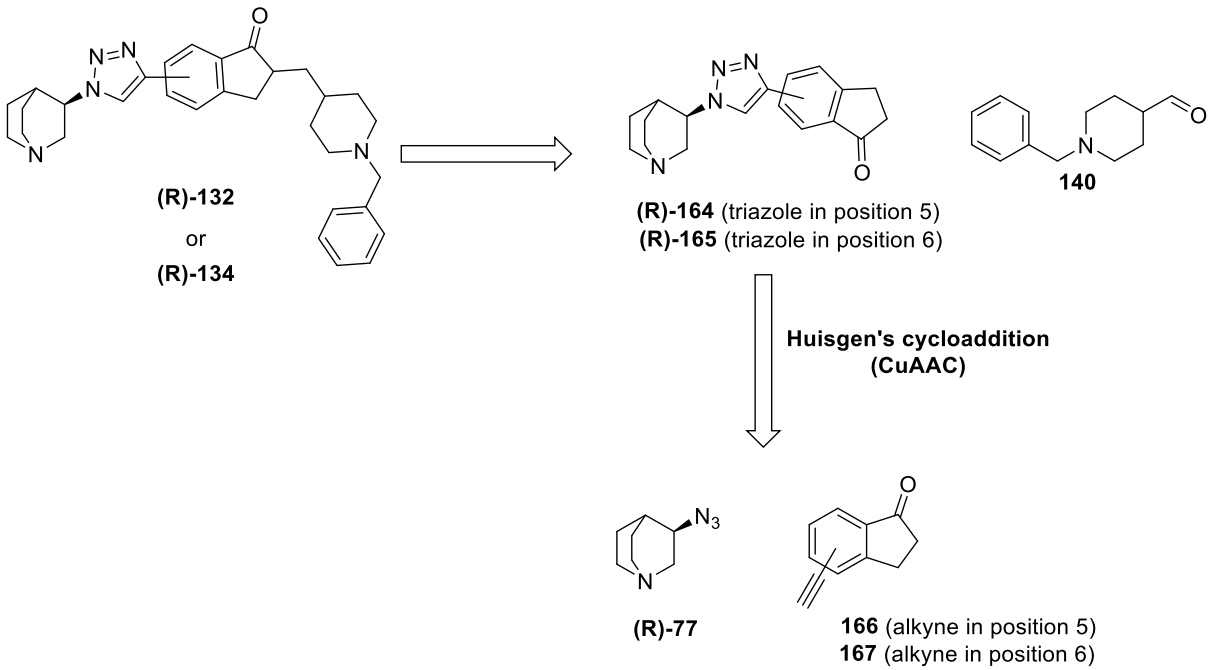

*Scheme 47: New retrosynthesis strategy to **(R)-132** and **(R)-134***

*4.2.2.2. Synthesis of alkynes **166** and **167***

Phenols carried by commercially available 5-hydroxyindanone **168** and 6-hydroxyindanone **169** were activated as triflates in presence of trifluoromethanesulfonic anhydride in triethylamine and dichloromethane[381] to give compounds **170** and **171** in good yields. The newly obtained compounds were then coupled with ethynyltrimethylsilane *via* a conventional Sonogashira coupling catalysed by $PdCl_2(PPh_3)_2$ in a mixture of dimethylformamide and triethylamine, and deprotected in presence of

potassium carbonate, giving the final alkynes **166** and **167** in decent yields. The two alkynes were prepared in 3 steps with overall yields of respectively 46% and 37% (Scheme 48).

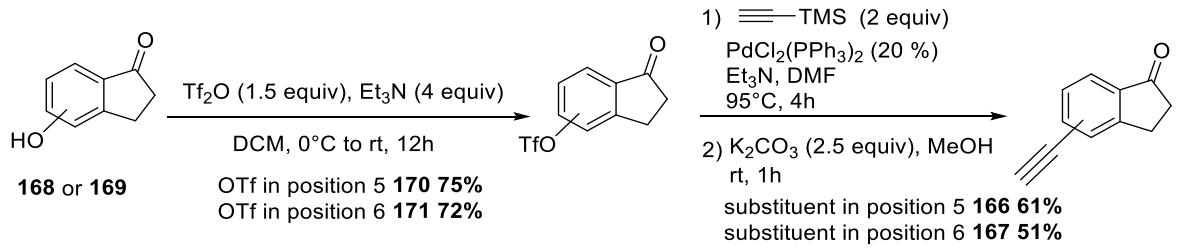

*Scheme 48: Synthesis of **166** and **167***

*4.2.2.3. Attempted synthesis of a pivotal compound **172***

We first assayed the aldolization reaction on the alkynylated indanones with the previously obtained aldehyde **140**, in order to evaluate the influence of the free alkyne on this reaction. The attempt was first performed with only alkyne **166** but did not show any expected result. Indeed, the first assayed conditions using sodium methanolate[384] in methanol and THF to achieve the aldolization – crotonization reaction, despite an extended reaction time of 12h instead of 3h , allowed us only to recover the starting materials. The second attempt using a stronger base, sodium hydride in THF was also unsuccessful, and we were not able to obtain the desired compound **172** but only a highly complex mixture we were not able to identify.(Scheme 49).

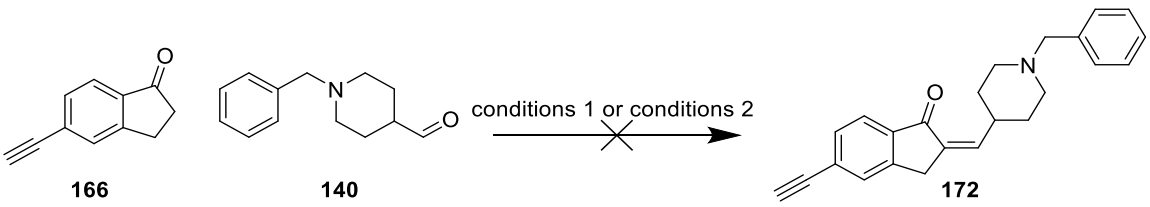

*Scheme 49: Attempt synthesis of **172***

*4.2.2.4. Attempt synthesis of **(R)-164** and **(R)-165** by CuAAC*

Due to the technical impossibility to obtain the desired intermediate **172**, it was decided, as previously reported with the first series of Donepezil based MTDL, to firstly perform the CuAAC reaction between

[384] Barbe, G.; Charette, A. B. Highly Chemoselective Metal-Free Reduction of Tertiary Amides. *J. Am. Chem. Soc.* **2008**, *130* (1), 18–19.

alkynes **166** and **167** and (R)-3-azidoquinuclidine **(R)-77** obtained from (R)-3-aminoquinuclidine **(R)-81**. NMR analyses of the crude reaction mixtures showed that key intermediates **(R)-164** and **(R)-165** were obtained with a conversion of approximatively 70% for both of the intermediates (equivalent to around 130 mg for each compound). Indeed, in the crude ^{1}H NMR spectra, we could observe the characteristic aromatic signals from the triazole core protons and a shift of the asymmetric carbon aliphatic protons of **(R)-164** and **(R)-165**. Yet, we were unable to isolate these two compounds which decomposed upon the silica gel chromatography purification steps and seemed too unstable to be easily purified by this chromatographic method. By lack of time, these CuAAC reactions and the purification procedures to obtain **(R)-164** and **(R)-165** could not be achieved.

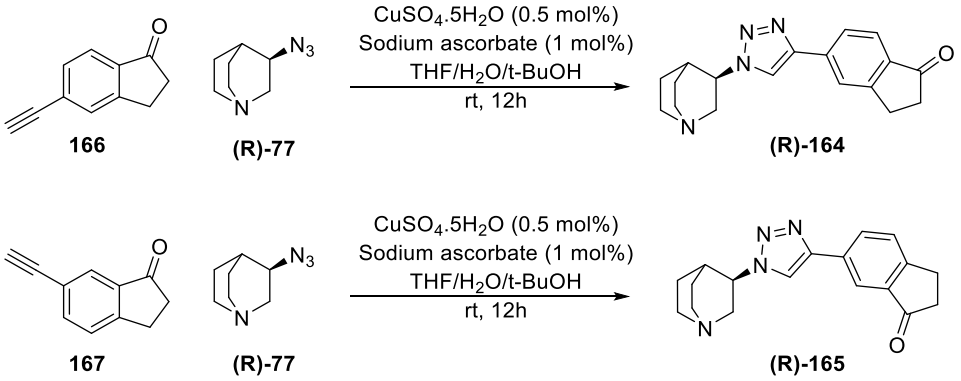

*Scheme 50: Assayed CuAAC reactions to obtain **(R)-164** and **(R)-165***

5. Partial conclusion and perspectives

As a conclusion on this third project, even though we didn't manage to obtain the expected novel Donepezil based MTDLs due to a lack of time and unexpected synthetic bottlenecks, we developed promising synthetic pathways for both series. Concerning the first series of MTDLs **(R)-128** and **(R)-130**, we obtained a key intermediate **(R)-147** in 4 steps with an overall 6% yield and only two step remains to be completed to obtain MTDLs **(R)-130** through an aldolization followed by a reduction of the ketol with TMSI. Moreover, another quicker synthetic strategy could be considered, indeed, after an activation of alcohol **142** into the mesylate **173**, an alkylation of **(R)-147** with LDA could lead directly to the desired MTDL **(R)-130** (the same synthetic pathways could be used to obtain its regioisomer **(R)-128** from already synthesized alkyne **148**) (Scheme 51).

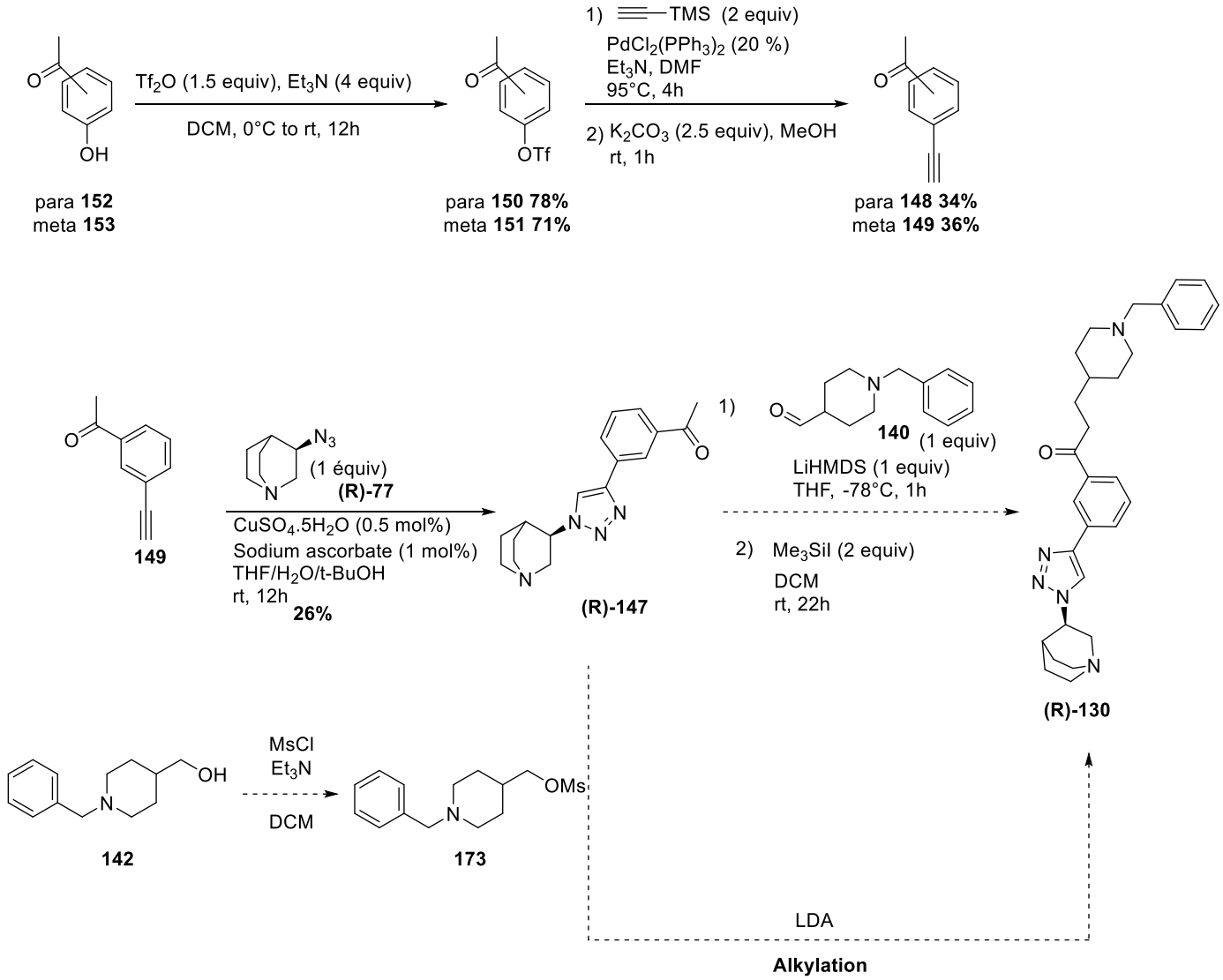

*Scheme 51: summarized synthesis to **(R)-147** and further steps to **(R)-130***

Regarding the second series, we had to face several challenges allowing us to better understand which synthetic pathway should be undertaken. Moreover, even though **(R)-164** and **(R)-165** proved too unstable to be easily purified by conventional silica gel chromatography, ^{1}H NMR analysis of the crude reaction mixtures are encouraging, since the two key intermediates were formed during the reaction. With an optimized purification step and compounds **(R)-164** and **(R)-165** in hands, it would be possible to achieve the synthesis as exposed on Scheme 52. From compound **(R)-164** resulting from the CuAAC reaction performed between azide **(R)-77** and alkyne **166**, it would be possible to obtain the key aldol intermediate following a procedure previously described by Barbe and Charette[384], the resulting aldol could either undergo a crotonization reaction followed by the Pd catalysed reduction of the olefin, or a reduction of the ketol with an excess of TMSI as exposed for the first series to give the final MTDL **(R)-134** and by extension MTDL **(R)-132**. As shown for the first series of Donepezil-based MTDLs, final

compound **(R)-134** and by extension the regioisomer **(R)-132**, could also be obtained through an alkylation of compound **(R)-164** (and **(R)-165**) with the activated mesylate **173** in presence of LDA.
As noted in the introduction of this chapter, taking into account the low pKa of the indanone moiety of Donepezil, it has been shown that the asymmetric centre epimerizes at physiological pH, thus we can assume that MTDLs **(R)-132** and **(R)-134** could be obtained as 1/1 diastereosisomers mixtures, a diastereoselective aldolization reaction is thus not required (but could be undertaken if need be).

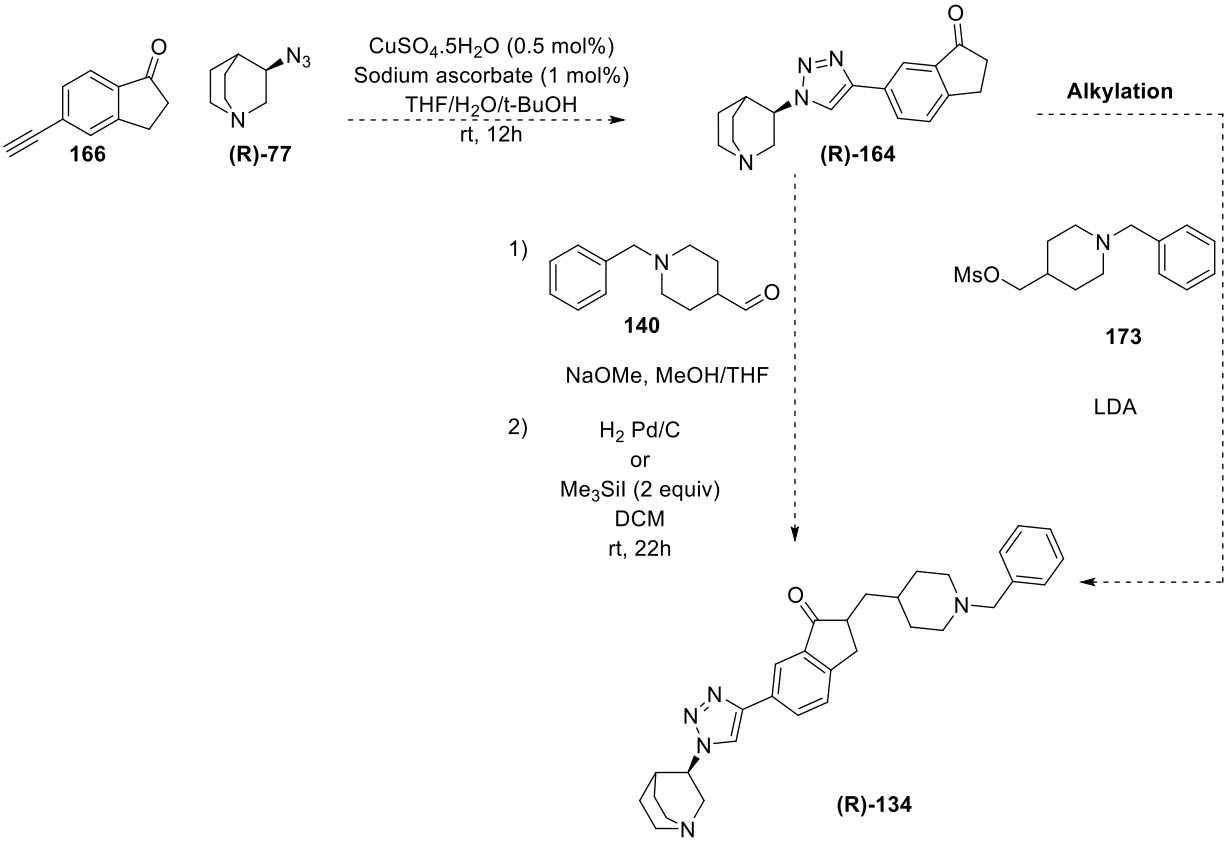

*Scheme 52: Further work to obtain **(R)-132** and **(R)-134***

Concerning the perspective of this project, meanwhile we tried to design new routes to obtain combined MTDLs **(R)-128**, **(R)-130**, **(R)-132** and **(R)-134**, we also briefly worked on the development of *N*-benzyl-piperazine based MTDLs **(R)-129**, **(R)-131**, **(R)-133** and **(R)-135**. Even though, the docking results were less conclusive, managing to synthesise these compounds could provide important information on the *in vitro* activities between *N*-benzyl piperidine based MTDLs **(R)-128**, **(R)-130**, **(R)-132** and **(R)-134** and *N*-benzyl piperazine based MTDLs **(R)-129**, **(R)-131**, **(R)-133** and **(R)-135.** For this purpose, we attempted to attach commercially available 1-benzypiperazine **174** with either compound **170** and **171** (entries 1 and 2) or alkynes **163** and **175** (entries 3 and 4) through an acid catalysed iminium based aldol type reaction. Indanone derivatives were thus set in presence of

paraformaldehyde in acidic conditions[385], unfortunately the desired intermediates were not obtained and NMR spectra only displayed complex signals implying a degradation of the starting materials (Table 28).

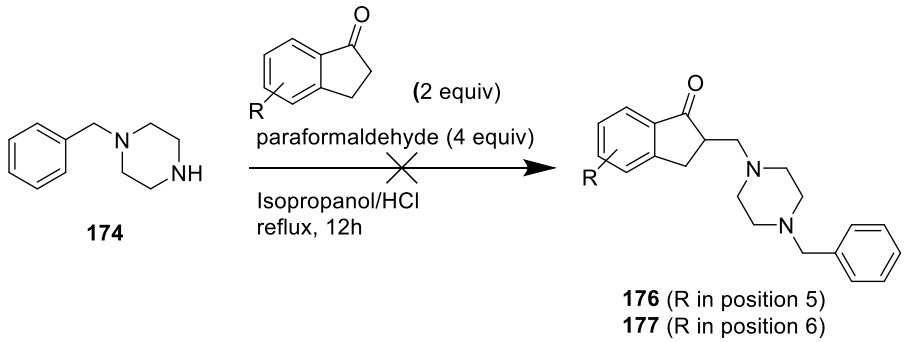

Entry	Compound	R	Relative position of the R substituent	Result
1	**170**	OTf	Position 5	No desired product
2	**171**	OTf	Position 6	No desired product
3	**163**	Protected alkyne	Position 5	No desired product
4	**175**	Protected alkyne	Position 6	No desired product

*Table 28: Assays to obtain piperazine based intermediates **176** and **177***

The same experiments in the same conditions were performed in parallel between compounds **145**, **150**, **151** and **178** and 1-benzypiperazine **174**, sadly, the obtained results were similar to what was obtained previously (Table 29). When 1-benzylpiperazine was set in reaction with compounds **150** and **151**, NMR spectra showed complex signals assuming that only degradation products were recovered. On the contrary, when the reaction was performed with alkynes **145** and **178**, no degradation was witnessed but the starting materials were recovered without any trace of the formation of the targeted intermediates. These reactions thus still need to be implemented in order to complete MTDL series, and other aldolization akin reactions need to be assayed.

[385] Learmonth, D. A.; Soares, D. S. P. M. Substituted Nitrated Catechols, Their Use in the Treatment of Some Central and Peripheral Nervous System Disorders and Pharmaceutical Compositions Containing Them. WO0198250 (A1), December 27, **2001.**

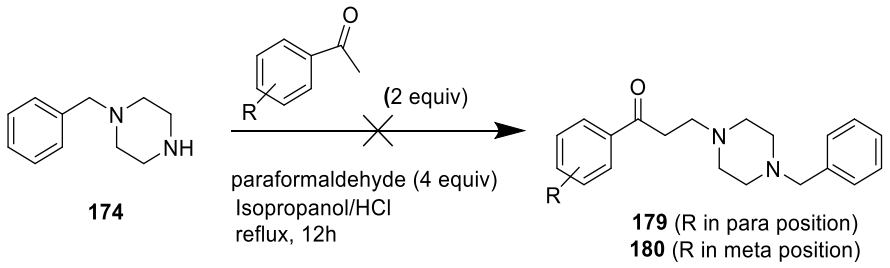

Entry	Compound	R	Relative position of the R substituent	Result
1	**150**	OTf	Para	No desired product
2	**151**	OTf	Meta	No desired product
3	**178**	Protected alkyne	Para	Starting material
4	**145**	Protected alkyne	Meta	Starting material

*Table 29: Assays performed to obtain N-benzylpiperazine based intermediates **179** and **180***

General conclusion

1. Background and PhD objectives

Alzheimer disease is a complex and multifactorial neurodegenerative disease discovered in 1906 by Doctor Alois Alzheimer characterised by a loss of memory and cognition. Worldwide, AD is the first cause of dementia for patients over 75 years old, moreover, the number of people with AD is dramatically increasing and could reach 135.5 million in 2050. Even though AD is a highly complex disease, scientists have been able to determine the two main histopathologies involved. The first described histopathology is the formation of β-amyloid plaques through the fibrillation of Aβ peptide, a peptide issued of the cleavage of APP by β-secretases and γ-secretases in an amyloidogenic pathway. In addition, studies have shown that there is a strong affinity between the Aβ peptide and the homomeric α7-nAChR facilitating peptide's aggregation and the inhibition of neuroprotection signals. The second lesion is characterised by the neurofibrillary degeneration induced by the protein Tau hyperphosphorylation which leads to a loss of affinity with the microtubules, weakening the cytoskeleton causing neuronal death. Despite a better understanding of the biochemical mechanism involved in this CNS-related pathology, only three AChE inhibitors are available in the market (Donepezil, Galantamine and Rivastigmine) and one NMDA antagonist (Memantine). Unfortunately, all these drugs have only a palliative role, and act only in the early stages of AD. Even though, numerous molecules have been developed in the past years (almost 100 molecules were involved in phase I, II, III and IV clinical trials), there hasn't been any new drug commercialised in the past decade due to toxicity, various adverse effects and the lack of activity of assayed molecules, and AD remains incurable. Nevertheless, to tackle this new challenge, researchers have begun to adopt a new approach, the multi target-directed ligand approach, indeed, due to the multifactorial character of the pathology of AD, designing new drugs composed of two pharmacophores able to act on various targets of the pathology appeared to be a promising way toward innovative treatment of such CNS-related disorders. My PhD project falls within this particular context. Three different approach were undertaken. By collaborating with Professor Muñoz-Torrero (University of Barcelona), a novel and promising Huprine-Capsaicin heterodimer has been designed and biologically evaluated. Moreover, arising from another collaboration with Professor Routier (ICOA of Orléans) and Professor Chalon (CHU of Tours), the design and development of two innovative combined MTDLs families targeting AChE and α7 nAChRs simultaneously was tackled.

2. Objectif 1: Synthesis of an Huprine-Capsaicin heterodimer

2.1. Review of the results

In this first project of my PhD, I worked on the synthesis of a conjugated MTDL combining a Huprine fragment and a capsaicin fragment connected with a triazole based linker (Figure 138). Based on the research of Doctor Chao, Doctor Oukoloff and Doctor Bouet, former researchers in the team, I performed the up-scaled synthesis of a heterodimer bearing a Huprine scaffold, known to be a potent inhibitor of AChE, and a capsaicin moiety proven to have high antioxidant properties. Compound **34** had already been synthesised in the team by Doctor Bouet, nevertheless, an upscale of the synthesis was required in order to obtain **34** in a larger scale in prevision of the *in vivo* assays required, and this up-scale proved challenging.

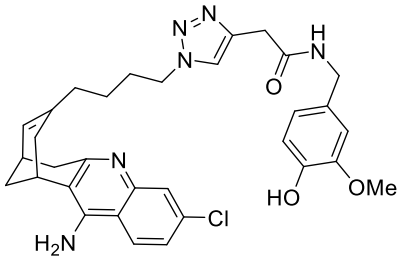

34

*Figure 138: Structure of MTDL **34***

In order to obtain compound **34** (Figure 138), the work was divided in two main achievements, the alkyne **49** synthesis in 18% on a 400 mg scale and the huprine scaffold **48** synthesis bearing an azide was obtained in 10 steps with an overall yield of 2%. The pivotal step to obtain compound **34** was the association of the two partners **48** and **49** through a Copper(I)-catalysed Huisgen cycloaddition giving the final MTDL **34** in 15 steps in 150 mg scale using a convergent and efficient synthetic pathway (Scheme 53).

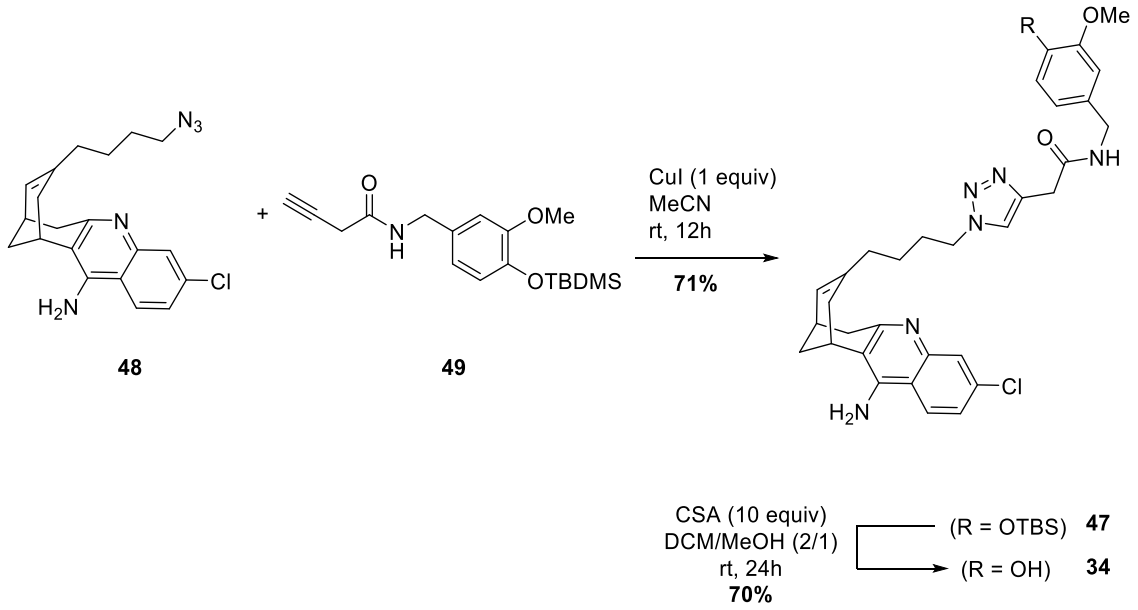

*Scheme 53: Final steps of the MTDL **34** synthesis*

In vitro assays have been performed on an entire series of conjugated AChEI – antioxidant MTDLs, with the antioxidant moiety attached at different positions and with different linker length, but compound **34** seemed to be the most promising. Indeed, besides its potent inhibition of AChE, in the low nM range and close to the values already observed for patent huprine Y, compound **34** displayed also a very promising 7 nM IC_{50} inhibition potency for BChE. Moreover, compound **34** appeared to be a promising MTDL, since attachment of the huprine moiety had little influence on the antioxidant properties as compared to non-substituted capsaicin moiety. It should also be noted that, despite a > 500g/mol molecular weight (587 g/mol), ranking **34** outside Lipinski rules range, evaluation of compound **34** druglikeness gave clues that this compound might have great chances to cross the BBB (Table 30).

Entry	Compound	IC_{50} (nM) (*h*AChE)	IC_{50} (nM) (*h*BChE)	Selectivity ratio	IC_{50} (µM) (DPPH)	P_e (10^{-6} cm s^{-1})
1	Huprine Y	1.07 +/- 0.05	181 +/- 15	169.2	nd[b]	23.8 +/- 2.7 (CNS+)
2	Capsaicin	>200 000	na[a]	/	50.3 +/- 8.3	10.3 +/- 1.2 (CNS+)
3	**34**	1.06 +/- 0.26	7.3 +/- 0.6	6.9	92.0 +/- 12.4	8.8 +/- 1.3 (CNS+)

[a]not active; [b]not determined

Table 30: In vitro evaluation of **34**

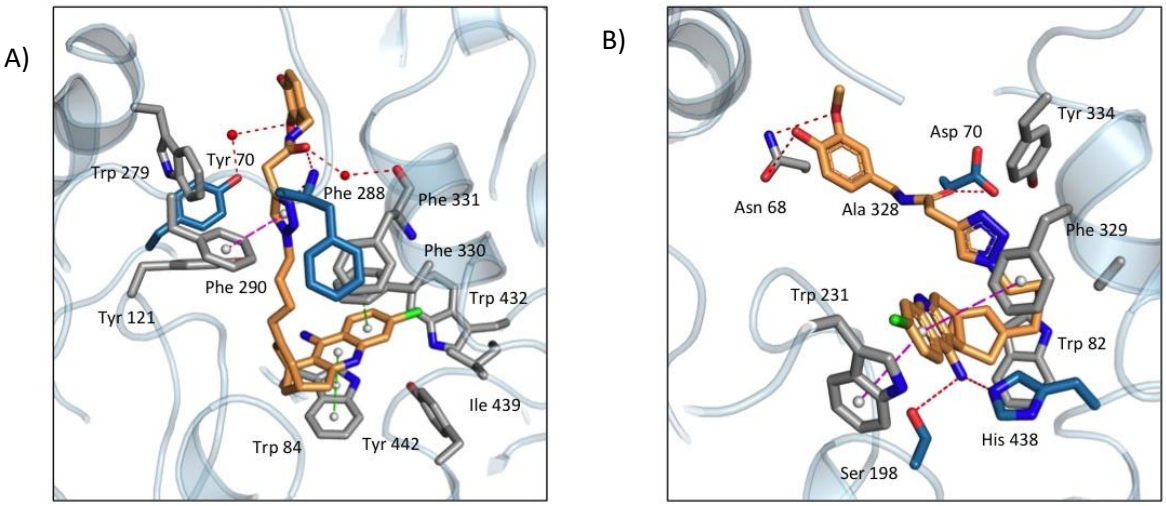

Figure 139: Crystal structures TcAChE (A) and hBChE (B) in complex with

In addition, crystal structures of *Tc*AChE and *h*BChE in complex with compound **34** were obtained by our partner Dr. Jacques-Philippe Colletier, Dr. Nicolas Coquelle and Dr. Martin Weik at IBS (Grenoble), and predicted interactions with each of the enzymes were observed (Figure 139). These structural determinations brought to light that the aniline moiety in position 12 of MTDL **34** was able to fit in BChE acyl pocket, fitting between Ser198 and His448 and to disrupt the catalytic triad, which could explain the potency of **34** as an inhibitor of both AChE and BChE.

2.2. Perspectives

Approximatively 150 mg of MTDL **34** were synthesised for *in vivo* assays. indeed, with the exciting *in vitro* results obtained for the conjugated MTDL **34** related to its potent AChE inhibition and its antioxidant character, our collaborators in Pr. Inestrosa's team (Pontificia Universidad Católica de Chile, Santiago, Chili) are currently evaluating the *in vivo* activity of this new heterodimer on two types of AβPPswe/PS-1 double transgenic mice's group expressing the mutant APPswe (K595N/M596L) and PSEN1ΔE9, one of young mice (5 month-old) and another set of old mice (10 month-old). Various tests (LOF, NOR, NOL, memory flexibility test and detection and quantification of Aβ) will be performed.

3. Objective 2: Design and synthesis of an innovative Rivastigmine-based MTDL family

3.1. Review of the results

In this second project, we designed in collaboration with Pr. Routier's team (UMR CNRS 7311 ICOA, Orléans), new combined MTDLs combining an AChE inhibitor, the Rivastigmine fragment, and an α7 nAChR agonist, the quinuclidine fragment (Figure 140). The first pharmacophore targeting AChE was chosen for its long lasting AChE inhibition due to a slowly reversible covalent inhibition mechanism through carbamoylation of the catalytic serine, and the nAChR agonist moiety made up of a quinuclidine and a triazole fragment was chosen as the second pharmacophore because of its proven efficiency to counteract CNS-related pathologies. The strategy was to design combined MTDLs sharing a common moiety of each parent pharmacophore in order to decrease the molecular weight of the drug candidate and to improve its CNS activity profile.

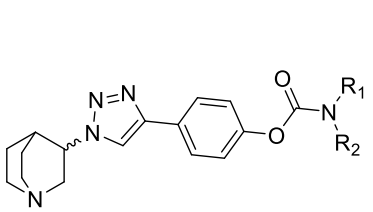

75a: $R_1 = R_2$ = Me **22%**
(R)-75a: $R_1 = R_2$ = Me **19%**
(S)-75a: $R_1 = R_2$ = Me **14%**

75b: $R_1 = R_2$ = Et **24%**
(R)-75b: $R_1 = R_2$ = Et **36%**
(S)-75b: $R_1 = R_2$ = Et **34%**

75c: R_1 = Me; R_2 = Et **24%**
(R)-75c: R_1 = Me; R_2 = Et **19%**
(S)-75c: R_1 = Me; R_2 = Et **25%**

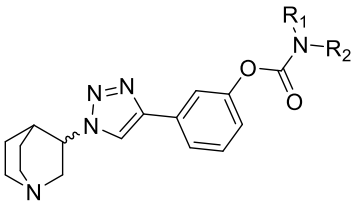

76a: $R_1 = R_2$ = Me **32%**
(R)-76a: $R_1 = R_2$ = Me **13%**
(S)-76a: $R_1 = R_2$ = Me **16%**

76b: $R_1 = R_2$ = Et **9%**
(R)-76b: $R_1 = R_2$ = Et **20%**
(S)-76b: $R_1 = R_2$ = Et **25%**

76c: R_1 = Me; R_2 = Et **19%**
(R)-76c: R_1 = Me; R_2 = Et **25%**
(S)-76c: R_1 = Me; R_2 = Et **22%**

Figure 140: New family of MTDLs

After a validation of the structures through *in silico* evaluations (docking with AChE, CNS MPO score computation and evaluation of the BBB permeation with Percepta), we worked on the development of a robust synthetic pathway to obtain the 18 combined MTDLs of a new Rivastigmine-based family **75a-c** and **76a-c** and their corresponding enantiomers **(R)-75a-c** and **(R)-76a-c** and **(S)-75a-c** and **(S)-76a-c** in 5 steps with overall yields ranging from 9% to 36% (Figure 140). The limiting step is the formation of quinuclidine azide, which proved highly unstable, and different strategies in which the azide was formed *in situ* were considered to have acceptable and reproducible yields. One attempt

was made and gave an encouraging result with an improved yield compared to the two steps process in the synthesis of **75a** from **81** and **78a** (Scheme 54).

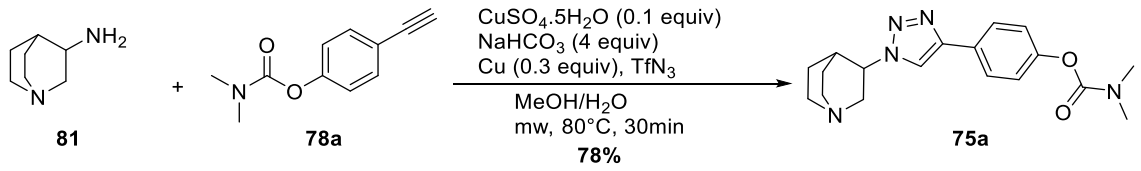

*Scheme 54: One-pot synthesis of **75a***

The molecules of this series were evaluated *in vitro* for their binding to α7 nAChR by Pr. Chalon (UMR INSERM 1253, iBrain, Tours), and it appeared, as expected and already brought to light by Pr. Routier, that the (R) enantiomers had a better affinity toward α7 nAChRs. From that point, the 6 (R) enantiomers were also evaluated for their potency to inhibit cholinesterases by Pr. Bartolini's team (University of Bologna, Italy)(Table 31). The first thing to notice was that the affinities toward α7 nAChRs were increased compared to the parent compound for all the MTDLs of the family and all the new molecules displayed values at a nanomolar level and even subnanomolar for **(R)-75a** (entry 3). Moreover, we saw that two compounds appeared more promising than the others, given the IC_{50} results. Indeed compound **(R)-76a** (entry 4) and **(R)-75b** (entry 5) also displayed the best results concerning their ability to inhibit AChE (and BChE for **(R)-76a**). As MTDLs targeting AChE and α7 nAChRs simultaneously, these two molecules represented in Figure 141 in appeared to have the most promising dual action.

Entry	Compound	K_i (nM) α7 nAChRs	IC_{50} hAChE (µM)[a]	IC_{50} hBChE (µM)[b]
1	**(R)-69** (reminder)	8 ± 4	nd[c]	nd
2	Rivastigmine	nd	48	54
3	**(R)-75a**	0.35 ± 0.05	64.2 ± 1.5	191 ± 32
4	**(R)-76a**	**1.5 ± 0.4**	**5.32 ± 0.67**	**2.74 ± 0.08**
5	**(R)-75b**	**1 ± 0.2**	**4.98 ± 0.21**	**nd**
6	**(R)-76b**	2.1 ± 1	177 ± 34	nd
7	**(R)-75c**	2.3 ± 1	56.5 ± 1.9	nd
8	**(R)-76c**	1.8 ± 0.2	nd	nd

[a]incubation time of 40 min; [b]incubation time of 20 min; [c]not determined

Table 31: In vitro assays for compounds **(R)-75a-c** and **(R)-76a-c**

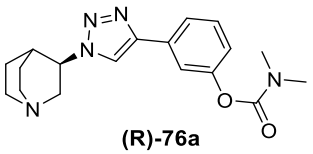

(R)-76a

IC_{50} (*h*AChE) = 5.32 µM
IC_{50} (*h*BChE) = 2.74 µM
K_i (α7 nAChR) = 1.5 nM

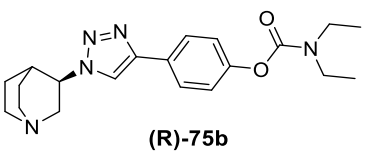

(R)-75b

IC_{50} (*h*AChE) = 4.98 µM
K_i (α7 nAChR) = 1.0 nM

*Figure 141: Structure of **(R)-76a** and **(R)-75b***

In the same project, building on this first success, we attempted to optimise the structure of the new MTDLs by modulating the common moiety. Based on the expertise of our collaborator Pr. Routier, it was decided to add a phenyl ring to the common moiety while the active fragments remained unchanged. After an evaluation of the structure *in silico*, we managed to synthesise 10 new MTDLs in 6 steps with overall yields from 0.8% to 10% (Figure 142). Once again, the limiting step was the azide formation. *In vitro* evaluations of the activity of these drug candidates towards AChE, BChE and α7 nAChRs are currently in progress.

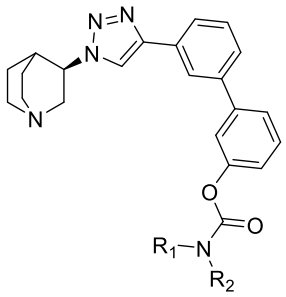

(R)-96a: $R_1 = R_2$ = Me **6%**
(R)-96b: $R_1 = R_2$ = Et **6%**
(R)-96c: R_1 = Me; R_2 = Et **10%**

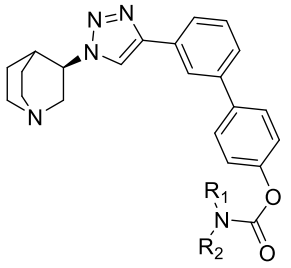

(R)-97a: $R_1 = R_2$ = Me **4%**
(R)-97b: $R_1 = R_2$ = Et **5%**
(R)-97c: R_1 = Me; R_2 = Et **5%**

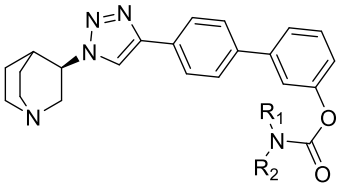

(R)-98a: $R_1 = R_2$ = Me **1%**
(R)-98c: R_1 = Me; R_2 = Et **1%**

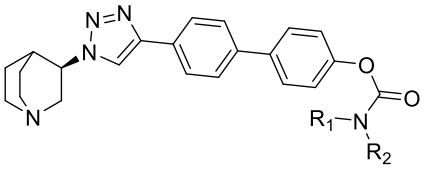

(R)-99a: $R_1 = R_2$ = Me **1%**
(R)-99c: R_1 = Me; R_2 = Et **0.8%**

*Figure 142: Structures of MTDLs **(R)-96a-c, (R)-97a-c, (R)-98a/c** and **(R)-99a/c***

3.2. Perspectives

From this study we obtained two new series of Rivastigmine-based MTDLs among which two compounds appeared to be particularly efficient, aside from further biological evaluations and the development of a one-pot synthesis of the 1,2,3-triazole core we discussed in chapter III which could allow us to perform gram-scale synthesis for *in vivo* evaluations, we could optimise the structure by varying the α7 nAChRs agonist structure to give new combined MTDLs. Based on Pr. Routier's expertise who designed a potent α-7 nAChRs agonist with a thiophene linked to the triazole (Figure 143), we could study a third series of combined Rivastigmine-based ligands represented in Figure 144.

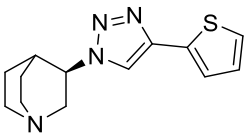

(R)-70
K_i = 9.5 +/- 3 nM

Figure 143: α-7 nAChRs designed by Routier et al.

In prevision of this work, preliminary studies have been performed and every potential compound exerted good *in silico* results with binding energies around 9.5 kcal/mol, a sufficient proximity of the

carbamate moiety with the catalytic serine (Ser203) of *m*AChE and promising CNS MPO scores (Figure 144).

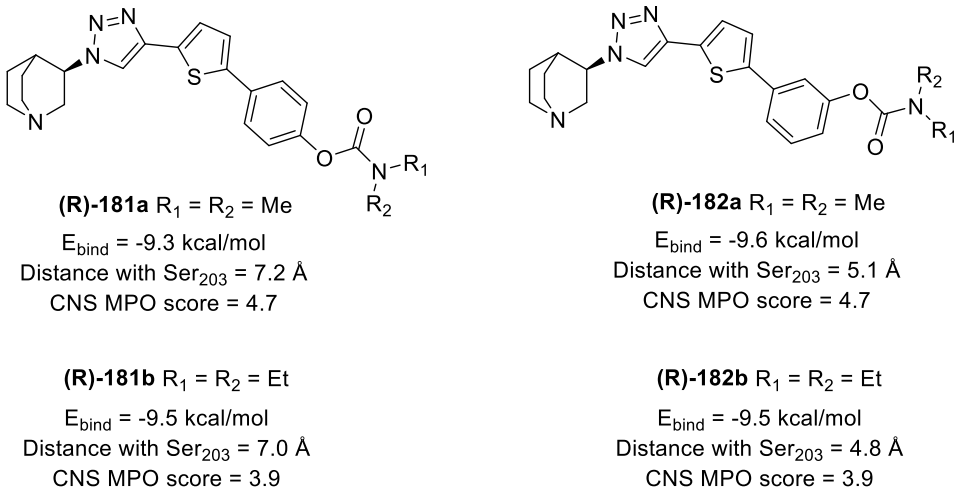

Figure 144: Structure and in silico evaluations of a new series of combined MTDLs

Once the docking was performed on compounds **(R)-181a-b** and **(R)-182a-b**, the Discovery software was used to visualise the different possible interactions with the main AChE residues and are reported in Table 32.

Entry	Type of interaction	(R)-181a	(R)-181b	(R)-182a	(R)-182b
1	π-π interaction	Trp286	Tyr341	Trp286	Tyr337
		Tyr341	Tyr337	Tyr341	Tyr341
		Tyr337		Tyr337	Trp286
3	π -σ interaction			Trp86	
4	π-donor				Tyr124
5	H-bond	Tyr337	Tyr337		
6	Sulphur-X		Tyr124		

*Table 32: Interactions of **(R)-181a-b** and **(R)-182a-b** with AChE main residues*

Concerning compound **(R)-181a**, π-π interactions (entry 1) were predicted between Trp286 and the triazole core of the structure, Ty341 and the phenyl ring and the newly added thiophene and finally π-

π interactions could be noted between the phenyl ring and Tyr337 also involved in a H-bond (entry 5) with the double bounded oxygen of the carbamate.

Then, compound **(R)-181b** is foreseen to display various interactions such as π-π interactions (entry 1) between Tyr341 and the phenyl ring and the thiophene, Tyr337 and the phenyl ring and Tyr337 also could be involved in a H-bond (entry 5) with the double bounded oxygen of the carbamate. A novel interaction was also noted, indeed, Tyr124 seemed to interact with the sulphur atom of the thiophene in a sulphur-X interaction type (entry 6).

Regarding compound **(R)-182a**, we could note that Trp286 was predicted to interact in a π-π type with the triazole moiety and the thiophene, Tyr341 was predicted to be involved in π-π interactions with the thiophene and the phenyl ring also interacting with Tyr337 (entry 1). Finally, Trp86 was predicted to interact with the methyl groups of the carbamate in a π -σ interaction (entry 3).

Compound **(R)-182b** displayed predicted π-π interactions (entry 1) involving 3 AChE residues: Tyr337 with the phenyl ring, Tyr341 with the phenyl ring and the thiophene, Trp86 with the thiophene. A π-donor interaction between Tyr124 and the phenyl ring was also shown (entry4).

Based on our expertise in the design of combined MTDLs and Professor Routier's expertise in the design and synthesis of α-7 nAChRs agonists carrying a quinuclidine fragment, as an example, compound **(R)-181a** could be obtained through a similar route to the one designed for the other quinuclidine based MTDL : a Copper(I)-catalysed Huisgen cycloaddition between azide **(R)-77** and alkyne **183** could allow formation of the triazole moiety, alkyne **183** could be obtained in two steps through a Suzuki Miyaura coupling between alkyne **184** and 4-hydroxyboronic acid **107** followed by an acylation reaction of **184** with the carbamoyl chloride **91a** (Figure 145).

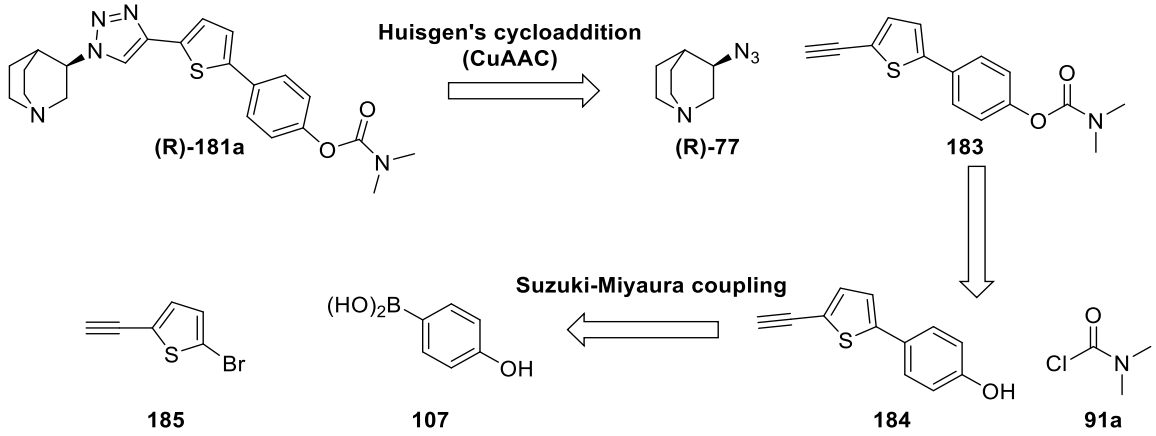

Figure 145: Proposed retrosynthetic route to **(R)-181a**

4. Objective 3: Design and synthesis of an innovative Donepezil-based MTDL family

4.1. Review of the results

Finally, in the last project of my PhD, we began to work on the design and synthesis of combined Donepezil-based MTDLs based on the association of another AChE inhibitor, the Donepezil fragment, and the same α-7 nAChRs agonist pharmacophore, the quinuclidine fragment associated with a triazole moiety. The project, even if at its early stage, could be divided in two main parts: the synthesis of flexible chain based **(R)-128** and **(R)-130** and the synthesis of indanone based **(R)-132** and **(R)-134** (Figure 146). This last family will be synthesized as a diastereoisomers mixture, since it has been shown that the indanone moiety was prompt to epimerize in physiological conditions.

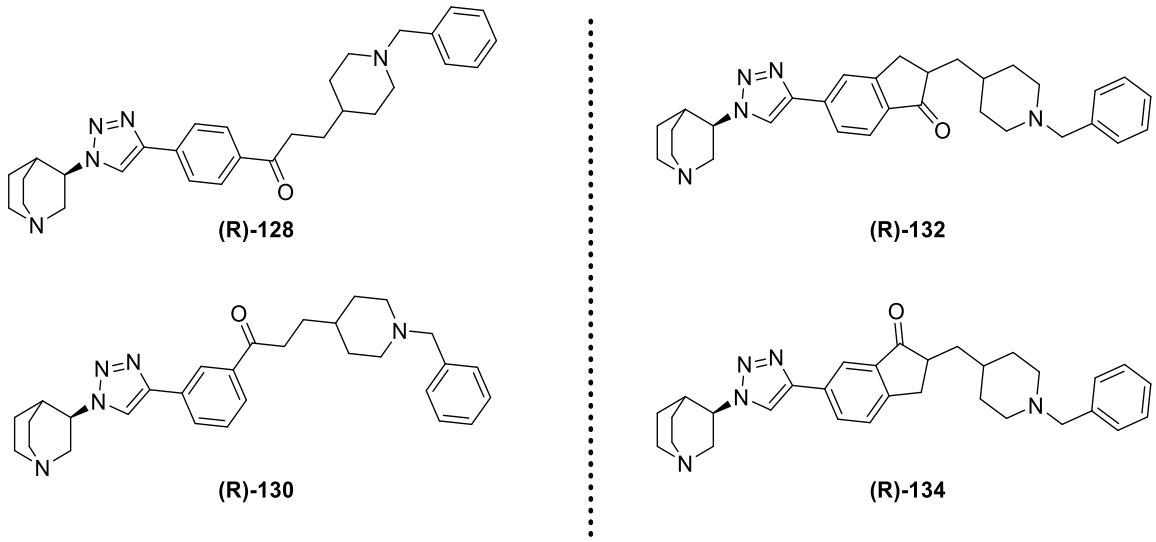

*Figure 146: Structures of **(R)-128**, **(R)-130**, **(R)-132** and **(R)-134***

Concerning the first two MTDLs **(R)-128** and **(R)-130**, after a validation of the structures *via in silico* evaluations, we managed to obtain the pivotal intermediate **(R)-147** (Figure 147), one step away from the final expected MTDL **(R)-130**. This intermediate was obtained in 4 steps with 7% overall yield, with two limiting steps: the azide formation and the Sonogashira cross coupling reaction for the required alkyne introduction. Intermediate **(R)-147** could yield expected MTDL **(R)-130** through one additional enol aldolization / reduction. If this last reaction fails, a simple alkylation of the enol of acetophenone enolate could be an alternate strategy, the aldehyde being then replaced by an activated alcohol (Tosylate, Mesylate), or an alkyl bromide. Once the limiting Sonogashira cross coupling reaction has been optimized, the synthetic strategy will be further applied to synthesise the (R) enantiomer analogues **(R)-128** and **(R)-130.**

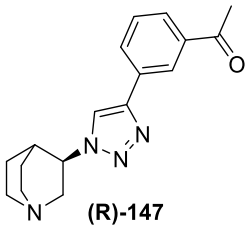

*Figure 147: Structure of **(R)-147***

Regarding the targeted indanone based two other analogues **(R)-132** and **(R)-134** of the Donepezil-based family, we managed to obtain alkynes **166** and **167** in 3 steps with overall 46% and 37% yields using the synthetic pathway investigated and developed in the first part of the project. Even though, two attempts of coupling the newly obtained alkyne **166** with the previously obtained aldehyde **140** were performed by using either sodium methanolate in methanol and THF or sodium hydride in THF, the key intermediate **172** was not reached (Scheme 55).

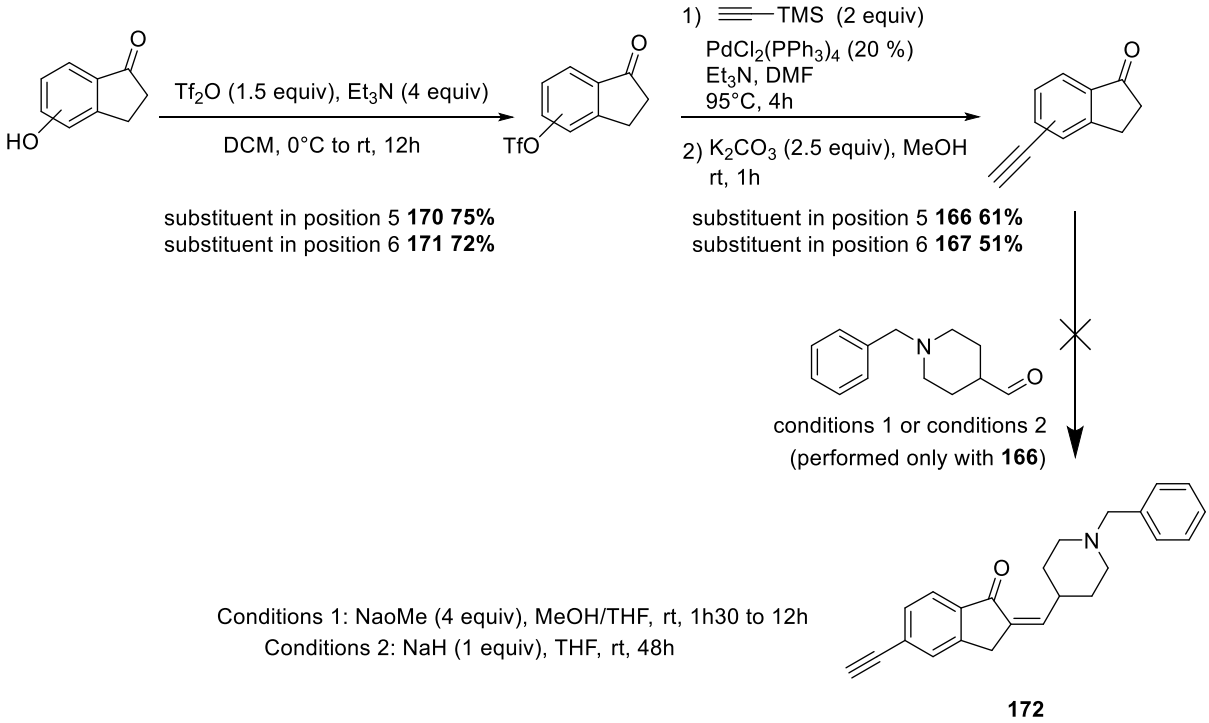

*Scheme 55: Attempted synthesis of **172***

In a revised retrosynthetic strategy, we decided to perform the CuAAC step before the aldolization reaction step, our attempt to perform this Copper(I) catalysed Huisgen cycloaddition between respectively **166** and **(R)-77** and **167** and **(R)-77** brought to light a stability issue of the resulting compounds, indeed, according to NMR assays the expected products were formed but their appeared to be unstable on silica gel (Scheme 56).

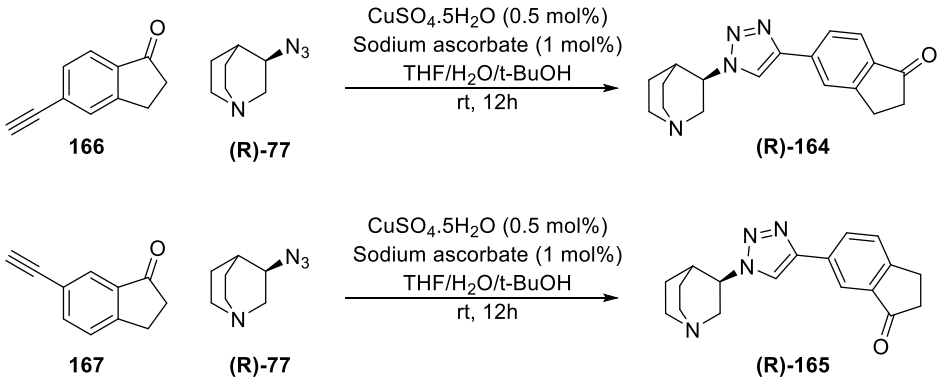

*Scheme 56: CuAAC to obtain **(R)-164** and **(R)-165***

4.2. Perspectives

In this last project of my PhD, the first perspective is to develop a viable synthetic pathway in both cases. For compounds **(R)-128** and **(R)-130**, we must find appropriate aldolization reaction conditions to couple aldehyde **140** with ketone **(R)-147** followed by a reduction of the ketol to give the final MTDLs, as shown on Scheme 57 for example. For this last step, we can, rely on the results described by Nagel et *al.* who developed an efficient synthesis of Donepezil derivatives[386]. Alternatively, another aldolization related reaction can be undertaken, for instance by using a secondary amine to form then enamine of ketone **(R)-147** , or a primary amine followed by a basic treatment to form the azaenolate. Use of a Lewis acid in order to form the silylenol ether could be a back-up solution, but we have to deal with the tertiary amine. Another possibility would be to perform an enolate alkylation instead of the aldolization by replacing the aldehyde by a halogenated compound or an activated alcohol.

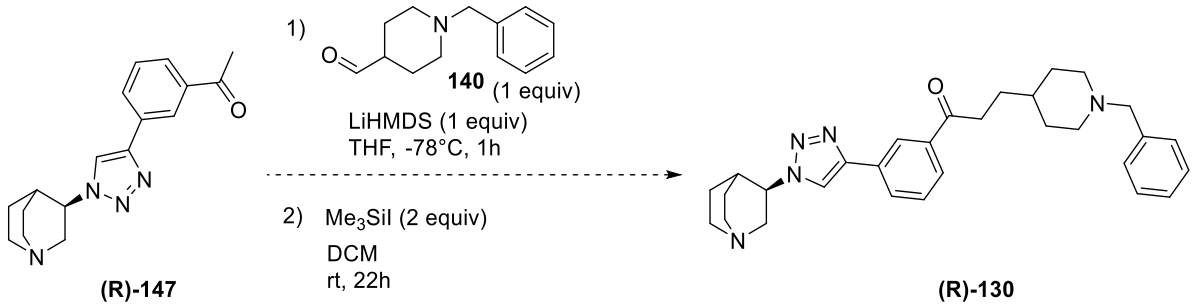

*Scheme 57: Possible synthesis of **(R)-130***

For the second series of Donepezil based MTDL based on an indanone moiety, more efforts have to be undertaken, since one additional reaction step has to be secured, namely the CuAAC reaction which

[386] Nagel, A. A.; Liston, D. R.; Jung, S.; Mahar, M.; Vincent, L. A.; Chapin, D.; Chen, Y. L.; Hubbard, S.; Ives, J. L. Design and Synthesis of 1-Heteroaryl-3-(1-Benzyl-4-Piperidinyl)Propan-1-One Derivatives as Potent, Selective Acetylcholinesterase Inhibitors. *J. Med. Chem.* **1995**, *38* (7), 1084–1089.

unexpectedly gave unstable triazoles intermediates. Yet, NMR assays gave us hope, indeed, we managed to synthesise but not to isolate pure pivotal intermediates **(R)-164** and **(R)-165**. Hence, a synthesis with an optimised purification step followed by the coupling of the indanones **(R)-164** and **(R)-165** and aldehyde **140** and a reduction step could lead to the obtention of MTDLs **(R)-132** and **(R)-134** (Scheme 52).

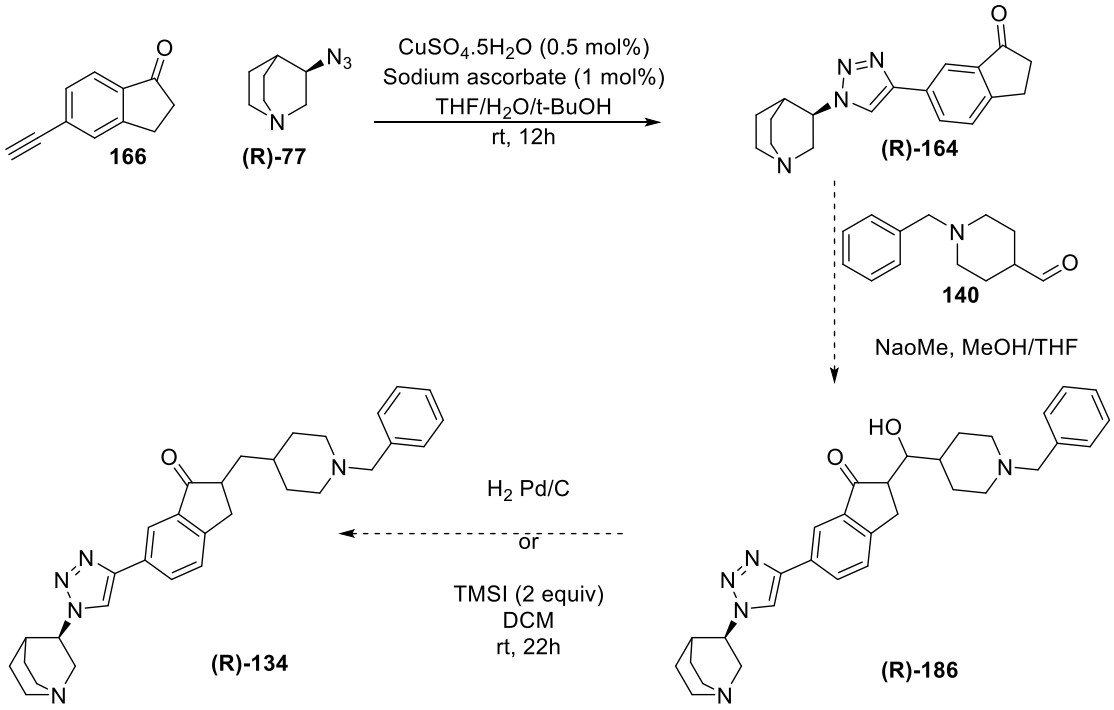

*Scheme 58: Further work to obtain **(R)-134** (and **(R)-132**)*

With these four MTDLs **(R)-128**, **(R)-130, (R)-132** and **(R)-134** in hands, we would able to perform in vitro evaluation of their activity toward the two chosen targets, AChE and α7 nAChRs. These studies would allow us to observe the possible positive synergic effect of combining a Donepezil moiety and a quinuclidine fragment. Moreover, we would be able to determine the importance of an indanone moiety as in compounds **(R)-132** and **(R)-134** in the structure compared to compounds **(R)-128** and **(R)-130**.

5. Global perspectives

Granted by the expertise we gathered in the field of combined and combined MTDLs synthesis in the treatment of AD, we imagined other combinations of pharmacophores. Firstly, it could be possible to increase the potency of carbamate-based MTDLs against AChE by varying the substituents of the carbamate's nitrogen while keeping the same α7 nAChR agonist moiety (Figure 148).Indeed, Sterling

et *al.*[387] designed in 2002 dual inhibitors of AChE and MAO **187** from the Rivastigmine scaffold, and during their investigations, they observed that the nature of the nitrogen substituents seemed to directly influence AChE inhibitory activity. They brought to light that an aromatic substituent lead to the best IC_{50} values while a substitution with methyl and ethyl groups lead to a loss of activity. Thus, carbamate-based compounds such as **(R)-188** could be promising and have increased AChE inhibitory activities compared to the MTDLs that were designed during my PhD.

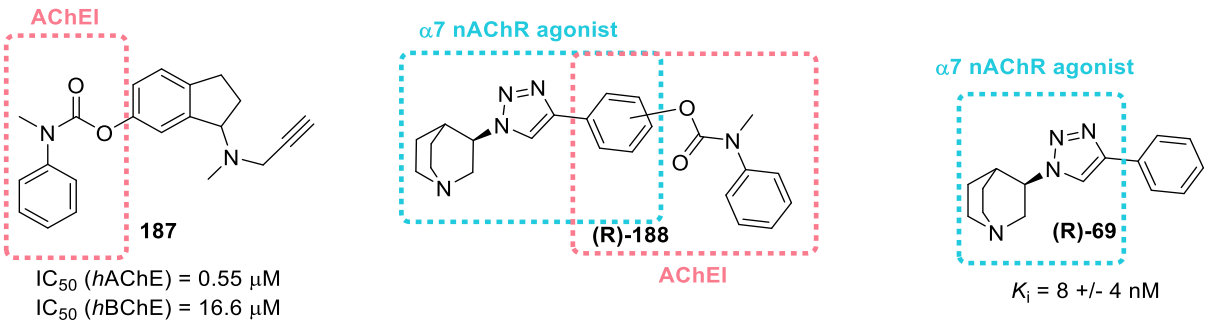

Figure 148: Other possible structures of urea-based MTDLs

Another pathway to follow in the design of MTDLs against AD could be to investigate other α7 nAChR agonists as secondary pharmacophores, our researches lead us to the conclusion that the quinuclidine scaffold was the most potent and efficient. Nevertheless, based on the structures of TC-5619[388], MEM3454[389] and Encenicline[390,391], three known α7 nAChR partial or full agonists, two new families of Donepezil-based MTDLs **189** and carbamate-based MTDLs **190** could be investigated and designed to give small MTDLs (Figure 149).

---

[387] Sterling, J.; Herzig, Y.; Goren, T.; Finkelstein, N.; Lerner, D.; Goldenberg, W.; Miskolczi, I.; Molnar, S.; Rantal, F.; Tamas, T.; Toth, G.; Zagyva, A.; Zekany, A.; Lavian, G.; Gross, A.; Friedman, R.; Razin, M.; Huang, W.; Krais, B.; Chorev, M.; Youdim, M. B.; Weinstock, M. Novel Dual Inhibitors of AChE and MAO Derived from Hydroxy Aminoindan and Phenethylamine as Potential Treatment for Alzheimer's Disease. *J. Med. Chem.* **2002**, *45* (24), 5260–5279.

[388] Hauser, T. A.; Kucinski, A.; Jordan, K. G.; Gatto, G. J.; Wersinger, S. R.; Hesse, R. A.; Stachowiak, E. K.; Stachowiak, M. K.; Papke, R. L.; Lippiello, P. M.; Bencherif, M. TC-5619: An Alpha7 Neuronal Nicotinic Receptor-Selective Agonist That Demonstrates Efficacy in Animal Models of the Positive and Negative Symptoms and Cognitive Dysfunction of Schizophrenia. *Biochem. Pharmacol.* **2009**, *78* (7), 803–812.

[389] Huang, M.; Felix, A. R.; Kwon, S.; Lowe, D.; Wallace, T.; Santarelli, L.; Meltzer, H. Y. The Alpha-7 Nicotinic Receptor Partial Agonist/5-HT3 Antagonist RG3487 Enhances Cortical and Hippocampal Dopamine and Acetylcholine Release. *Psychopharmacology (Berl.)* **2014**, *231* (10), 2199–2210.

[390] Huang, M.; Felix, A. R.; Flood, D. G.; Bhuvaneswaran, C.; Hilt, D.; Koenig, G.; Meltzer, H. Y. The Novel A7 Nicotinic Acetylcholine Receptor Agonist EVP-6124 Enhances Dopamine, Acetylcholine, and Glutamate Efflux in Rat Cortex and Nucleus Accumbens. *Psychopharmacology (Berl.)* **2014**, *231* (23), 4541–4551.

[391] Prickaerts, J.; van Goethem, N. P.; Chesworth, R.; Shapiro, G.; Boess, F. G.; Methfessel, C.; Reneerkens, O. A. H.; Flood, D. G.; Hilt, D.; Gawryl, M.; Bertrand, S.; Bertrand, D.; König, G. EVP-6124, a Novel and Selective A7 Nicotinic Acetylcholine Receptor Partial Agonist, Improves Memory Performance by Potentiating the Acetylcholine Response of A7 Nicotinic Acetylcholine Receptors. *Neuropharmacology* **2012**, *62* (2), 1099–1110.

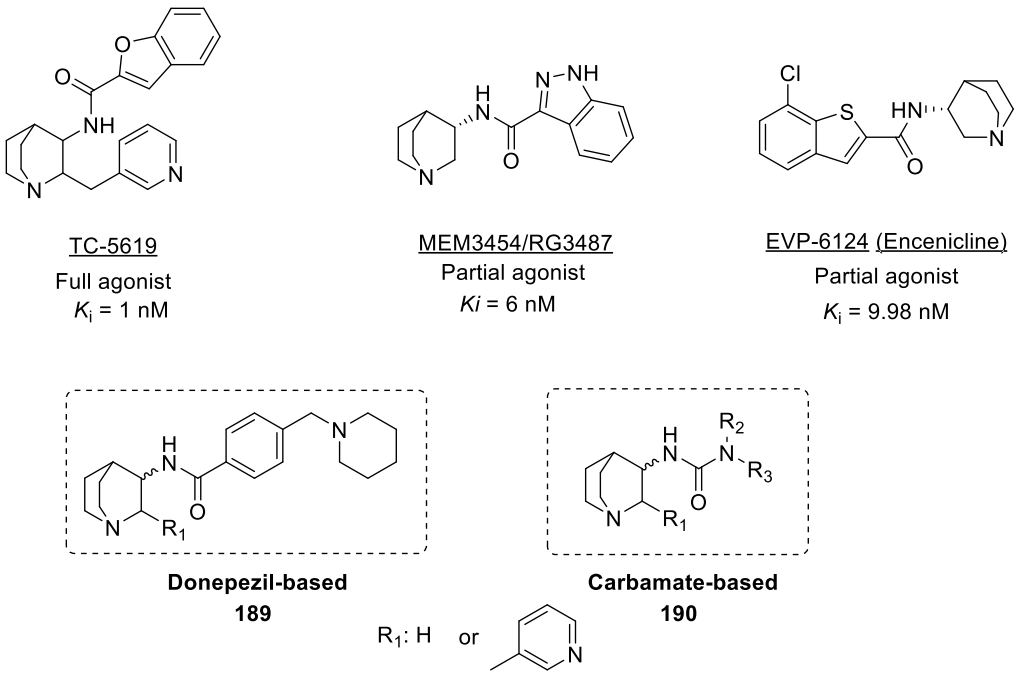

Figure 149: Possible structures of Donepezil-based and carbamate-based MTDLs

Finally, a totally different approach would be to associate two pharmacophores with none of them targeting AChE, but another main biological target involved in CNS-related disorders. Given the previous encouraging results obtained with the quinuclidine moiety as an α7 nAChR agonists, a fusion of flavonoid-based scaffolds **191**, **192** or **193** designed by Chimenti et *al.*[392] with this moiety could lead to new MTDLs **(R)-194** with several biological properties such as MAO inhibitory activity, α7 nAChR agonist properties and even antioxidant properties (Figure 150).

[392] Chimenti, F.; Fioravanti, R.; Bolasco, A.; Chimenti, P.; Secci, D.; Rossi, F.; Yáñez, M.; Orallo, F.; Ortuso, F.; Alcaro, S.; Cirilli, R.; Ferretti, R.; Sanna, M. L. A New Series of Flavones, Thioflavones, and Flavanones as Selective Monoamine Oxidase-B Inhibitors. *Bioorg. Med. Chem.* **2010**, *18* (3), 1273–1279.

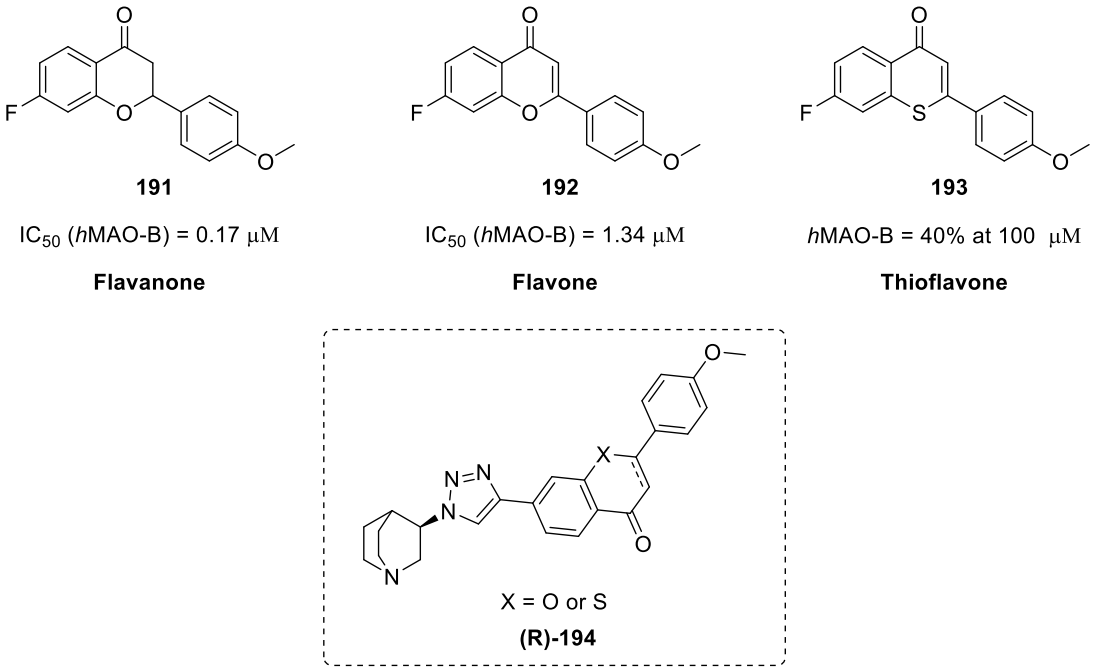

Figure 150: Combined MTDLs targeting MAO-B with α7 nAChR agonists properties

Experimental part

Chemistry

Chemical and reagents

All reagents were supplied by Sigma-Aldrich, TCI, Alfa Aesar and Acros organic and used without further purification. CH_3CN, THF, toluene, DCM and Et_2O were dried over alumina cartridges using a solvent purification system MBRAUN MB SPS-800®. Other solvents were dried by standard procedures (1,2-DCE: distillation over CaH_2; THF: distillation over sodium benzophenone and Et_3N dried and stored over KOH). Flash-column chromatography purifications were performed either on Geduran® Si 60 silica gel (40-63 µm) from Merck Millipore or Macherey-Nagel. Thin Layer chromatography (TLC) were carried out on Merck DC Kieselgel 60 F-254 aluminium sheets. Compounds were visualized by UV lamp illumination (λ = 254 or 365 nm) and/or staining with $KMnO_4$, phosphomolybdic acid (PMA), cerium ammonium molybdate (CAM) or ninhydrin.

Instruments

^1H and ^{13}C NMR spectra were recorded at 298 K on a Bruker DPX 300 spectrometer (Bruker, Wissembourg, France). Chemical shifts are expressed in parts per million (ppm), and the residual solvent peak was used for calibration. J values are expressed in Hz. Peaks are annotated as follow: s = singled, d = doublet, t = triplet, m = multiplet, br = broad. Mass spectra were obtained with a Finnigan LCQ Advantage MAX (ion trap) apparatus equipped with an electrospray source. High-resolution mass spectra (HRMS) were recorded either with a Thermo LTQ Orbitrap XL apparatus equipped with an ESI source. GC/MS analyses were acquired on a Shimadzu QP2010 with electron impact ionization (70eV) and a quadrupole analyzer. GC/FID analyses were done on a Shimadzu GC2014 or SCION GC436. Quantitative analyses were obtained by usage of a linear alkane as internal standard (C12, C14 or C18). General method for GC and GC/MS routine analysis. Realized on a 30 meters DB5-MS (95% PDMS, 5% diphenylsiloxane), with 0.25 mm ID and 0.25 µm film thickness. Helium carrier was set at 1.7 mL/min constant flow rate. Oven program : 150°C for 2 minutes, then 20 K/min up to 270°C, and a final isotherm for 17 more minutes. Total analysis time : 25 minutes. In case of MS analysis, detection ranged from m/z 50 to 500, with a 4.5 min solvent cut time.

Analytic HPLC (Thermo Hypersil GOLD C18 column, 5 µm, 2.1 × 100 mm) was performed with CH_3CN and 0.1% aq. TFA as eluents [100% aq. TFA (5 min), then linear gradient from 0% to 80% (40 min) CH_3CN] at a flow rate of 0.25 mL/min. UV/Vis detection was achieved with the "Max Plot" (i.e., chromatogram at absorbance maximum for each compound) mode (220-700 nm).

Semi-preparative RP-HPLC (Syncronis Thermoscientific C18 column, 5 µm, 21.2 x 250 mm) with MeCN and aq. 10 mM AcONH as eluents [40% MeCN (5min), followed by linear gradient from 40% to 100% (35 min) of MeCN] at a flow rate of 1 mL/min. Dual visible detection was achieved at 250 and 550 nm.

Optical rotations were recorder on a Perkin Emler 341 polarimeter using the sodium D line (589 nm) and the concentration given in g.100 mL^{-1} and the values in unit deg.mL.cm^{-1}. g^{-1}. Reactions under microwave conditions were carried out in an Anton Paar Monowave 300 apparatus equipped with an infrared external temperature sensor and a stirrer. Melting points were measured with a Stuart SMP30 melting-point apparatus.

Biochemistry

AChE inhibition Assay

The inhibitory activity on human cholinesterases was evaluated spectrophotometrically by the method of Ellman et *al*[393]. AChE stock solution was prepared by dissolving human recombinant AChE (E.C.3.1.1.7) lyophilized powder (Sigma, Italy) in 0.1 M phosphate buffer (pH = 8.0) containing Triton X-100 0.1%. Stock solution of BChE (E.C. 3.1.1.8) from human serum (Sigma, Italy) was prepared by dissolving the lyophilized powder in an aqueous solution of gelatine 0.1%. Stock solutions of the tested compounds (1 mM for compounds in chapter I and 3 nM for compounds in chapter II) were prepared in MeOH and diluted in MeOH. Five increasing concentrations of each inhibitor were used, able to give an inhibition of the enzymatic activity in the range of 20–80%. The assay solution consisted of a 0.1 M phosphate buffer pH 8.0, with the addition of 340 μM 5,5'-dithio-bis(2-nitrobenzoic acid), 0.02 unit/mL of human recombinant AChE, or BChE from human serum and 550 μM of substrate (acetylthiocholine iodide (ATCh) or butyrylthiocholine iodide (BTCh), respectively). Assay solutions with and without inhibitor were preincubated at 37 ºC for 20 min followed by the addition of substrate. Blank solutions containing all components except AChE or BChE were prepared in parallel to account for the non-enzymatic hydrolysis of the substrate. Initial rate assays were performed at 37 °C with a Jasco V-530 double beam Spectrophotometer: the rate of increase in the absorbance at 412 nm was followed for 210 s. The velocity in the presence and absence of inhibitor were compared and % inhibition was calculated. The results were plotted by placing the percentage of inhibition in function of the decimal log of the final inhibitor concentration. Linear regression and IC_{50} values were calculated using Microcal Origin 3.5 software (Microcal Software, Inc).

Evaluation of the time-dependent carbamoylation of *h*AChE

The stopped time assay was performed, in which AChE and the tested compound at a concentration of 6.0 μM, a value close to its IC_{50} value, were mixed in the assay buffer at pH 8.0. After 5, 10, 20, 30

[393] Ellman, G. L.; Courtney, K. D.; Andres, V.; Featherstone, R. M. A New and Rapid Colorimetric Determination of Acetylcholinesterase Activity. *Biochem. Pharmacol.* **1961**, *7* (2), 88–95.

and 40 minutes incubation at 37 °C, the determination of residual activity of the AChE-catalyzed hydrolysis of ATCh was carried out by Ellman's method.[1] A parallel control (i.e., no inhibitors in the mixture) allowed to adjust activities measured at the same incubation times.

BACE-1 inhibition Assay

β-Secretase (BACE-1, Sigma) inhibition studies were performed by employing a peptide mimicking APP sequence as substrate (Methoxycoumarin-Ser-Glu-Val-Asn-Leu-Asp-Ala-Glu-Phe-Lys-dinitrophenyl, M-2420, Bachem, Germany). The following procedure was employed: 5 µL of test compound (or DMSO, if preparing a control well) were pre-incubated with 175 µL of enzyme (in 20 mM sodium acetate pH 4.5 containing CHAPS 0.1% w/v) for 1 h at rt. The substrate (3 µM, final concentration) was then added and left to react for 15 min. The fluorescence signal was read at λ_{em} = 405 nm (λ_{exc} = 320 nm). The DMSO concentration in the final mixture was maintained below 5% (v/v) to guarantee no significant loss of enzyme activity. The background signal was measured in control wells containing all the reagents, except BACE-1 and subtracted. The fluorescence intensities with and without inhibitor were compared and the percent inhibition due to the presence of test compounds was calculated by the following expression: $100 - (IF_i/IF_o \times 100)$ where IF_i and IF_o are the fluorescence intensities obtained for BACE-1 in the presence and in the absence of inhibitor, respectively. To demonstrate inhibition of BACE-1 activity a peptidomimetic inhibitor (β-secretase inhibitor IV, Calbiochem) was serially diluted into the reactions' wells (IC_{50} = 13.0 ± 0.1 nM).

DPPH radical scavenging activity Assay

Radical scavenging activity of the capsaicin–huprine hybrids was determined by DPPH assay. Four different concentrations of the compounds (3–100 µM) dissolved in DMSO were incubated with a methanolic solution of DPPH (100 µM). The final concentration of DMSO was kept below 1%. After 30 min of incubation at rt in the dark, the absorbance at 517 nm was measured by a spectrophotometer. The percent inhibition for each concentration was calculated by comparison with the absorbance of DPPH solution. Dose–response curves were plotted and IC_{50} values were calculated by the software CurveExpert version 1.34 for Windows. The average values represent the mean of 3 experiments.

BBB permeation Assay

The parallel artificial membrane permeation assay for blood–brain barrier described by Di et *al.*[394] was used to assess the brain penetration of the HC hybrids. The *in vitro* permeability (P_e) of the synthesized

[394] Di, L.; Kerns, E. H.; Fan, K.; McConnell, O. J.; Carter, G. T. High Throughput Artificial Membrane Permeability Assay for Blood-Brain Barrier. *Eur. J. Med. Chem.* **2003**, *38* (3), 223–232.

hybrids and fourteen commercial drugs through lipid extract of porcine brain membrane was determined using a mixture of phosphate-buffered saline (PBS)/EtOH 70:30. Assay validation was made by comparison of the experimental and reported P_e values of the commercial drugs, which showed a good correlation: P_e (exp) = 1.4974 P_e (lit) − 0.8434 (R^2 = 0. 9428). From this equation and taking into account the limits established by Di *et al.* for BBB permeation, the following ranges of permeability were established: compounds of high BBB permeation (CNS+): P_e (10^{-6} cm s^{-1}) > 5.1; compounds of low BBB permeation (CNS–): P_e (10^{-6} cm s^{-1}) < 2.1, and compounds of uncertain BBB permeation (CNS±): 5.1 > P_e (10^{-6} cm s^{-1}) > 2.1.

nAChRs binding affinity Assay

Animals were killed by decapitation on the day of the assay and both frontal cortices of each animal were removed on ice and weighed (2 rats were used for each experiment). The tissue was homogenized in 10 vol of a pH 7.4 HEPES 15 mM buffer containing 120 mM NaCl, 5.4 mM KCl, 0.8 mM $MgCl_2$ and 1.8 mM $CaCl_2$ using an Ultraturrax T25. After 45.000x g centrifugation at 4°C for 10 min (J2-21M/E, Beckman), the supernatant was eliminated, and the pellet was suspended in 2 mL of the same buffer. The protein concentration was measured according to Bradford using bovine serum albumin as standard. For competition studies, [^{125}I]α-bungarotoxin (2 nM) was incubated in the presence or absence of each tested compound (10^{-6} to 10^{-10} M) with 25 mg protein in a total volume of 1 mL in a pH 7.4 TriseHCl buffer (50 mM TriseHCl, 120 mM NaCl, 5 mM KCl, 1mM $MgCl_2$ and 2.5mM $CaCl_2$) for 3h at 22°C. After incubation, samples were diluted in 3 mL of TriseHCl buffer at 4°C and then rapidly filtered through Whatman GF/C fiber filters soaked with 0.05% polyethylenimine (Sigma, St Quentin-Fallavier, France). The filters were washed twice with 3 mL of 4 °C buffer, and the residual radioactivity was measured in a gcounter (2480 Gamma counter Wizard, Perkin Elmer). The IC_{50} values were determined graphically for each compound and the *K*i calculated according to Cheng & Prusoff[395].

[395] Yung-Chi, C.; Prusoff, W. H. Relationship between the Inhibition Constant (KI) and the Concentration of Inhibitor Which Causes 50 per Cent Inhibition (I50) of an Enzymatic Reaction. *Biochem. Pharmacol.* **1973**, *22* (23), 3099–3108.

General procedures

General procedure A: Sonogashira cross coupling with $Pd(PPh_3)_4$

A solution of triethylamine and DCM (2/1 v/v, 0.2 M) was degassed with Argon for 15 min. Then iodophenol (1 equiv), CuI (0.1 equiv), Pd(triphenylphosphine) tetrakis palladium (0.02 equiv) were added. Trimethylsilylacetylene (2 equiv) was added and the mixture was stirred overnight at room temperature and kept away from light. After completion determined by TLC analysis, the solution was concentrated under reduced pressure, diluted with H_2O, extracted with Et_2O (x2). Organics layers were combined, dried over $MgSO_4$, filtered, and concentrated under reduced pressure. The crude oil was purified by column chromatography (PE/EtOAc 90/10, v/v) to yield the desired protected alkyne.
Then, a solution of protected alkyne (1 equiv) in THF (0.25 M) was cooled at 0 °C, tetrabutylammonium fluoride (1.2 equiv) was added dropwise and the solution was stirred 30 min at room temperature. After completion determined by TLC analysis, the solution was diluted with NH_4Cl sat, extracted with EtOAc (x2). Organics layers were combined, dried over $MgSO_4$, filtered, and concentrated under reduced pressure. The crude oil was purified by column chromatography (PE/EtOAc 90/10, v/v) to yield the desired product.

General procedure B: Carbamate formation

A solution of alkyne (1 equiv), carbamyl chloride **91a-c** (1.5 equiv), K_2CO_3 (1.5 equiv) in MeCN (0.15 M) was put under reflux for 4 h. After completion determined by TLC analysis, the solution was concentrated under reduced pressure, diluted with H_2O, extracted with Et_2O (x2). Organic layers were combined, dried over $MgSO_4$, filtered, and concentrated under reduced pressure. The crude oil was purified by column chromatography (PE/EtOAc 80/20, v/v) to yield the product.

General procedure C: Copper(II)-catalyzed alkyne-azide cycloaddition (Click chemistry)

To a solution of sodium azide (8 equiv) in water was added toluene (1/1 v/v 0.3 M). The mixture was cooled to 0 °C. Trifluoromethanesulfonic anhydride (1.6 equiv) was added dropwise and the resulting mixture was stirred at 0 °C for 2h. The reaction mixture was poured into water and extracted with toluene (2x) to yield TfN_3 which was directly used in the following diazo transfer reaction. 3-aminoquinuclidine dihydrochloride **81** (1 equiv), K_2CO_3 (1 equiv), $CuSO_4.5H_2O$ (0.01 equiv) were dissolved in a minimum amount of water. Then, TfN_3 was added, followed by the addition of methanol (0.13 M) to obtain a homogeneous system. The reaction mixture was stirred at room temperature for 12h. The reaction mixture was poured into water and extracted with DCM. The combined organic layers were washed with water and brine and dried over Na_2SO_4. The solvent was reduced under *vacuo*

to afford azidoquinuclidine **77**. Then, to a solution of azidoquinuclidine **77** (1 equiv) in THF was added terminal alkyne (1 equiv) in t-BuOH followed by the addition of $CuSO_4.5H_2O$ (0.05 equiv) in water and sodium ascorbate (0.01 equiv) (THF/Water/t-BuOH 1/1/1 v/v/v 0.1 M). The reaction mixture was stirred at room temperature for 12h. The crude product was poured into water, extracted with DCM (4x). The combined organic layers were washed with water and brine, dried over Na_2SO_4, and concentrated under *vacuo.* The residue obtained was purified by column chromatography (DCM/MeOH 80/20, v/v).

General procedure D: Olefination

To a solution of bromobenzaldehyde (1 equiv) in dry DCM (0.5 M), CBr_4 (2 equiv) was added, the mixture was cooled at 0°C. Then, a solution of PPh_3 (4 equiv) in dry DCM (0.5 M) was added dropwise. The reacting mixture was stirred for 30 min at room temperature. After completion determined by TLC analysis, the solution was concentrated under reduced pressure, the crude product was purified by column chromatography (Cyclohexane 100) to yield the product.

General procedure E: Corey-Fuchs

To a solution of olefin (1 equiv) in a mixture THF/ H_2O (20/1 v/v 0.2 M), TBAF.3 H_2O (6 equiv) and PPh_3 (1.5 equiv) were added. Then, the reacting mixture was stirred at 80°C in a sealed tube for 2h30. After completion determined by TLC analysis, the solution was diluted with H_2O, extracted with EtOAc (x3). Organics layers were combined, dried over Na_2SO_4, filtered, and concentrated under reduced pressure. The crude oil was purified by column chromatography (Cyclohexane 100) to yield the product.

General procedure F: Suzuki-Myaura cross coupling

To a mixture of derivative **105a-b** (1 equiv) in toluene and EtOH (7/3 v/v 0.1 M) were successively added the desired boronic acid (1.2 eq.), K_2CO_3 (2.0 eq.) and $Pd(PPh_3)_4$ (10 mol %). The reaction mixture was degassed with Ar and irradiated under microwave for 20 minutes at 150°C. After cooling, the volatiles were removed under reduced pressure and the crude material purified by flash chromatography (DCM/MeOH 80/20, v/v).

General procedure G: Triflate addition

To a solution of 3'-hydroxyacetophenone (1 equiv) in dry DCM (0.9 M), was added Et_3N (4 equiv). The solution was cooled to 0°C. Trifluoromethanesulfonic anhydride (1.5 equiv) was added slowly. After 2h at 0°C, the reacting mixture was stirred at rt for 12h. After completion determined by TLC analysis, the solution was diluted with water, extracted with DCM (x3). Organics layers were combined, dried over

$MgSO_4$, filtered, and concentrated under reduced pressure. The crude oil was purified by column chromatography (Cyclohexane/Et_2O 90/10, v/v).

General procedure H: Sonogashira cross coupling with $PdCl_2(PPh_3)_2$

A solution of triflate derivative (1 equiv) in dry DMF and Et_3N (7/3 v/v 0.3 M) was degazed with argon for 10 min. Ethynyltrimethylsilane (2 equiv) and $PdCl_2(PPh_3)_2$ (0.05 equiv) were added to the mixture. The reaction mixture was stirred at reflux for 4h. After completion determined by TLC analysis, the solution was cooled to rt, diluted with water and extracted with EtOAc. The organic layers were combined, washed with NaCl sat., dried over $MgSO_4$, filtered and concentrated under reduced pressure. The crude oil was purified by column chromatography (Cyclohexane/Et_2O 80/20, v/v).

General procedure I: TMS deprotection with K_2CO_3

To a solution of protected alkyne (1 equiv) in dry MeOH (0.3 M), was added K_2CO_3 (2.5 equiv). The solution was stirred at rt for 1h. After completion determined by TLC analysis, the solution was concentrated under reduced pressure, diluted with H_2O, extracted with DCM (x3). Organic layers were combined, dried over $MgSO_4$, filtered, and concentrated under reduced pressure. The crude oil was purified by column chromatography (Cyclohexane/Et_2O 80/20, v/v)

Mass spectrometry analysis are missing for several compounds due to a technical issue with the spectrophotometer of the institute, HRMS analysis are scheduled to be performed in another institute soon.

4-hydroxy-3-methoxybenzonitrile (51)

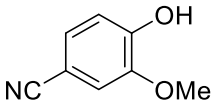

$C_8H_7NO_2$
Molecular Weight: 149,15 g/mol

To a solution of vanillin **50** (3 g, 19.7 mmol) in acetic acid (15 mL) was added hydroxylamine hydrochloride (2.05 g, 29.55 mmol, 1.5 equiv). The reaction mixture was stirred at 120°C for 1h. The white solution became orange. After cooling down to room temperature, the solution was poured into Et_2O. Then, it was washed with water and aq. 5% NaOH, and extracted with Et_2O. The organic layers were dried over $MgSO_4$ and concentrated under reduced pressure, after what, the crude product was recrystallized from toluene to give **51** (2.74 g, 93%) as a white solid.

^{1}H NMR (300 MHz, $CDCl_3$) δ 7.17 (dd, *J* = 1.2 Hz, 8.1 Hz, 1H), 7.02 (s, 1H), 6.91 (d, 8.4 Hz, 1H), 6.18 (br, OH), 3.86 (s, 3H).

NMR spectrum are in accordance with those reported previously:
Thompson, R.; Doggrell, S.; Hoberg, J. O. Potassium Channel Activators Based on the Benzopyran Substructure: Synthesis and Activity of the C-8 Substituent. *Bioorg. Med. Chem.* **2003**, *11* (8), 1663–1668.

4-((tert-butyldimethylsilyl)oxy)-3-methoxybenzonitrile (52)

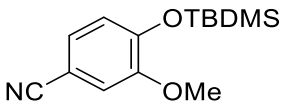

$C_{14}H_{21}NO_2Si$
Molecular Weight: 263,41 g/mol

A solution of **51** (2.74 g, 18.3 mmol) was prepared in dry DCM (120 mL) with imidazole (1.38 g, 20.17 mmol, 1.1 equiv). TBDMSCl (3.04 g, 20.17 mmol, 1.1 equiv) and DMAP (223.6 mg, 1.83 mmol, 0.1 equiv) were added. The reaction mixture was stirred at rt for 3h. After that time, the mixture was quenched with water and extracted with DCM. The organic layers were washed with water, brine and dried over $MgSO_4$ and concentrated under reduced pressure to obtain **52** (4.8 g, 100%) as a brown oil.

^{1}H NMR (300 MHz, $CDCl_3$) δ 7.18 (dd, *J* = 1.8 Hz, 6.3 Hz, 1H), 7.08 (d, *J* = 1.8 Hz, 1H), 6.89 (d, 8.1 Hz, 1H), 3.82 (s, 3H), 0.99 (s, 9H), 0.17 (s, 6H).

NMR spectrum are in accordance with those reported previously:

Teague, S. J.; Barber, S. Synthesis of 6-Substituted 5-Cyano-7-Hydroxy-2-Carboxybenzofurans. *Tetrahedron Lett.* **2010**, *51* (36), 4720–4722.

(4-((tert-butyldimethylsilyl)oxy)-3-methoxyphenyl)methanamine (53)

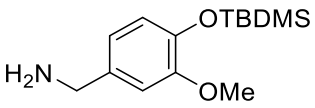

$C_{14}H_{25}NO_2Si$
Molecular Weight: 267,44 g/mol

A solution of **52** (4.8 g, 18.25 mmol) in dry THF (180 mL) was prepared and cooled down to 0°C. $LiAlH_4$ (1.038 g, 27.37 mmol, 1.5 equiv) was added in small portions. The reaction mixture was stirred for 30 min at 0°C and 18h at rt. The aluminium salts were hydrolyzed with H_2O (1 mL), aq. 10% NaOH (1 mL) and again H_2O (3 mL). The mixture was filtered through a pad of celite and washed with EtOAc and Et_2O and evaporated under reduced pressure. The crude orange oil was used in the next step without further purification.

1H NMR (300 MHz, CDCl3) δ 6.85 (s, 1H), 6.81 (m, 2H), 3.80 (s, 3H), 2.52 (s, br), 0.98 (s, 9H), 0.14 (s, 6H).

NMR spectrum are in accordance with those reported previously:

Cole, A. G.; Metzger, A.; Brescia, M.-R.; Qin, L.-Y.; Appell, K. C.; Brain, C. T.; Hallett, A.; Ganju, P.; Denholm, A. A.; Wareing, J. R.; Ritchie, T. J.; Drake, G. M.; Bevan, S. J.; MacGloinn, A.; McBryde, A.; Patel, V.; Oakley, P. J.; Nunez, X.; Gstach, H.; Schneider, P.; Baldwin, J. J.; Dolle, R. E.; McDonald, E.; Henderson, I. Sulfonamido-Aryl Ethers as Bradykinin B1 Receptor Antagonists. *Bioorg. Med. Chem. Lett.* **2009**, *19* (1), 119–122.

N-(4-((tert-butyldimethylsilyl)oxy)-3-methoxybenzyl)but-3-ynamide (49)

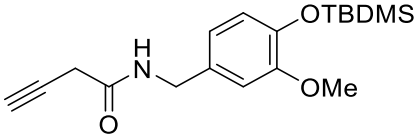

$C_{18}H_{27}NO_3Si$
Molecular Weight: 333,50 g/mol

To a solution of $Na_2Cr_2O_7$ (0.085 g, 0.285 mmol, 0.01 mmol) in HNO_3 (0.09 mL) and H_2O (25 mL), was added $NaIO_4$ (13.4 g, 62.7 mmol, 2.2 equiv). The solution was cooled down to 0°C and stirred for 15 min. Then, a solution of 3-butynol **53** (2 g, 28.5 mmol, 1 equiv) in H_2O (25 mL) was added dropwise and

the mixture was stirred at rt for 12h, then, the reaction mixture was extracted with Et_2O (6x40 mL). The combined organic layers were dried over $MgSO_4$, filtered and concentrated under reduced pressure. The obtained pink solid was diluted in DCM and concentrated under reduced pressure (4 times) to give 3-butynoic acid **55** as a white solid (2 g, 83%). Then, to a solution of amine **53** (1.92 g, 7.16 mmol) in dry DCM (36 mmol), 3-butynoic acid **55** (602 mg, 7.16 mmol, 1 equiv) and EDC. HCl (1.37 g, 7.16 mmol, 1 equiv) were added successively. The reaction mixture was stirred at rt for 2h. After completion determined by TLC, the mixture was quenched with H_2O and extracted with DCM. The organic layers were washed with H_2O and brine, dried over $MgSO_4$ and concentrated under reduced pressure. The crude product was purified by flash column chromatography on silica gel (PE/EtOAc, 80/20 to 70/30, v/v) to give **49** (455 mg, 20%) as an orange solid.

^{1}H NMR (300 MHz, $CDCl_3$) δ 6.85-6.67 (m, 3H), 4.39 (d, *J* = 5.7 Hz, 2H), 3.79 (s, 3H), 3.26 (d, *J* = 2.7 Hz, 2H), 2.33 (t, *J* = 2.7 Hz, 1H), 0.98 (s, 9H), 0.14 (s, 6H); **^{13}C NMR (75 MHz, $CDCl_3$) δ** 166.0, 151.2, 144.7, 131.1, 121.0, 120.2, 111.9, 77.5, 74.4, 55.6, 43.9, 27.5, 25.8, 18.6, -4.5; **MS (ESI+)** (*m/z*) 334 $[M+H]^+$.

Tetramethyl 3,7-dihydroxybicyclo[3.3.1]nona-2,7-diene-2,4,6,8-tetracarboxylate (59)

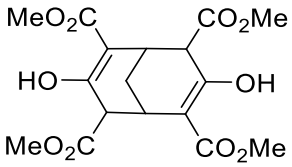

$C_{17}H_{20}O_{10}$
Molecular Weight: 384,34 g/mol

A mixture of 1,1,3,3-tetramethoxypropane **56** (60 g, 365 mmol, 1 equiv.) and aq. 2 M HCl (182 mL) was stirred at rt for 1.5h. To this mixture cooled at 0 °C was added successively and carefully an aq. 5 N NaOH within 30 min (pH = 7.5) and MeOH (183 mL). At 0 °C, dimethyl-3-oxoglutarate **57** (127.3 g, 731 mmol, 2 equiv.) was added slowly, followed by addition of MeOH (127 mL). The reaction mixture was allowed to warm to rt and stirred for 3 days. The reaction mixture was acidified to pH = 2.5 with HCl 37%. Filtrating fraction wise, washing with H2O and drying at desiccator in presence of P_2O_5 to afford the desired tetra ester **59**, as white-grey solid (82 g, 58%).

^{1}H NMR (300 MHz, $CDCl_3$) δ 12.34 (s, 2H), 3.84 (s, 6H), 3.77 (s, 6H), 3.30 (s, 2H), 3.23 (t, *J* = 3.3 Hz, 2H), 1.94 (t, *J* = 3.3 Hz, 2H) ; **^{13}C NMR (75 MHz, $CDCl_3$) δ** 171.8, 170.8, 168.1, 102.0, 52.7, 52.2, 50.3, 30.1, 22.5; **GC-MS** (*m/z*) 384 $[M]^+$.

Spectral data are in accordance with those reported previously:

Bertz, S. H. Series on Chemistry under Physiological Conditions. Part 7. Tetramethyl 3,7-Dihydroxybicyclo[3.3.1]Nona-2,6-Diene-2,4,6,8-Tetracarboxylate: A Useful Companion to Meerwein's Ester. Topological Analysis of Bicyclo[3.3.1]Nonane Synthesis. *J. Org. Chem.* **1985**, *50* (19), 3585–3592.

Bicyclo[3.3.1]nonane-3,7-dione (60)

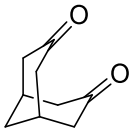

$C_9H_{12}O_2$
Molecular Weight: 152,19 g/mol

A suspension of **59** (60 g, 130 mmol) in a HCl 37% (130 mL), H2O (72 mL) and glacial acetic acid (72mL) was heated at 100 °C for 6h. After cooling at rt., the reaction mixture was poured into crushed ice (200 g) and extracted with DCM (3 x 100 mL). The combined organic layer was washed with aq. sat. $NaHCO_3$ until pH 7, then washed with H_2O (2 x 100 mL) and brine. The organic layer was dried over $MgSO_4$, filtered and concentrated under reduced pressure to give a brown solid. This crude product was dissolved in acetone (80 mL) and precipitated salts were filtered. The filtrate was concentrated and washed with acetone/Et2O (5/95, v/v) to afford the desired diketone **60** as a beige solid (10.6 g, 45%).

^{1}H NMR (300 MHz, $CDCl_3$) δ 2.96-2.92 (m, 2H), 2.69–2.62 (m, 4H), 2.50-2.45 (m, 4H), 2.23–2.27 (m, 2H); **^{13}C NMR (75 MHz, $CDCl_3$) δ** 209, 48.2, 33.0, 31.8; **GC-MS** (*m/z*) 152 $[M]^+$.

Spiro[bicyclo[3.3.1]nonane-3,2'-[1,3]dioxolan]-7-one (61)

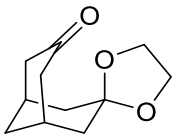

$C_{11}H_{16}O_3$
Molecular Weight: 196,25 g/mol

To a solution of diketone **60** (4g, 26.28 mmol) in dry DCM (520 mL) with molecular sieves 4 Å at 0°C, was added $BF_3{\cdot}Et_2O$ (6.48 mL, 52.6 mmol, 2 equiv.) and ethylene glycol (7.5 mL, 131.44 mmol, 5 equiv.). The reaction mixture was heated at 40°C for 15h. After completion determined by TLC analysis, the solution was cooled down and filtered to remove residues. The solution was washed with aq. sat. $NaHCO_3$, extracted with DCM (4x). The combined organic layers were washed with water and brine, dried over $MgSO_4$, and concentrated under *vacuo* to obtain **61** as a white solid (3.46g, 67%).

^{1}H NMR (300 MHz, $CDCl_3$) δ 3.95–3.88 (m, 2H), 3.86–3.80 (m, 2H), 2.53–2.44 (m, 4H), 2.34 (dd, *J* = 18.4, 6.6 Hz, 2H), 1.88–1.72 (m, 6H).

Spectral data are in accordance with those reported previously:
Tomizawa, M.; Shibuya, M.; Iwabuchi, Y. Highly Enantioselective Organocatalytic Oxidative Kinetic Resolution of Secondary Alcohols Using Chirally Modified AZADOs. *Org. Lett.* **2009**, *11* (8), 1829–1831.

Spiro[bicyclo[3.3.1]non[6]ene-3,2'-[1,3]dioxolan]-7-yl trifluoromethanesulfonate (62)

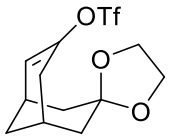

$C_{12}H_{15}F_3O_5S$
Molecular Weight: 328,30 g/mol

To a solution of **61** (2.82g, 14.41 mmol) in dry THF (58 mL), NaHMDS (0.6 M in toluene, 64.83 mL, 26.78 mmol, 2.5 equiv) was added dropwise at -78°C. The solution was stirred at -78°C for 1.5h. Then, the solution of *N*-phenylbis(trifluoromethane) sulfonimide (6.5 g, 18.2 mmol, 1.7 equiv.) was added and the reaction mixture was stirred at -78 °C for 5 h, quenched with a sat. aq. $NaHCO_3$ and allowed warm up to rt and extracted with Et_2O. The combined organic layers were washed with water and brine, dried over $MgSO_4$, and concentrated under *vacuo*. The crude product was purified by flash chromatography on silica gel (PE/EtOAc, 95/5, v/v) to yield desired product **62** as a colourless oil (3.99 g, 85%).

^{1}H NMR (300 MHz, $CDCl_3$) δ 5.80 (d, *J* = 10.2 Hz, 1H), 3.96 (m, 4H), 2.66 (m, 3H), 2.32 (d, *J* = 17.5 Hz, 1H), 1.72–1.84 (m, 5H), 1.62 (dt, *J* = 12.8, 2.7 Hz, 1H); **^{13}C NMR (75 MHz, $CDCl_3$) δ** 150.0, 121.0, 118.7, 107.9, 64.9, 63.3, 41.6, 38.1, 33.4, 30.2, 29.3, 28.3; **MS(CI)** (*m/z*) 329 (100) $[M+H]^+$

tert-Butyl-4-(spiro[bicyclo[3.3.1]non[6]ene-3,2'-[1,3]dioxolane]-7-yl)butanoate (63)

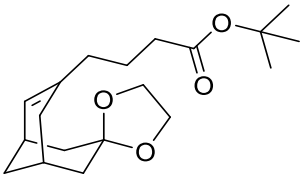

$C_{19}H_{30}O_4$
Molecular Weight: 322,45 g/mol

In the two-necked dry round-bottomed flask under Ar atmosphere, 9-BBN (0.5 M in THF, 58.8 mL, 29 mmol, 2.4 equiv.) was added dropwise at 0 °C to the alkene derivative (2.34 mL, 14.5 mmol, 1.2 equiv.)

and this solution was stirred at 0 °C for 30 min and at 80 °C for 2 h. Then, this solution was cooled down to rt and quenched with H_2O (3 mL). The solution of **62** (3.99 g, 12.1 mmol, 1 equiv.) in dry THF (4 mL) was added and the mixture was degassed and backfilled with Ar during 5 min, then catalyst PdCl2(dppf)·DCM (0.99 g, 0.121 mmol, 0.1 equiv.) and K_3PO_4 (3.85 g, 18.15 mmol, 1.5 equiv.) were introduced. This mixture was heated at 80 °C overnight. After cooling down to rt, H_2O and EtOAc were added to the reaction mixture, and residues were extracted with EtOAc and washed with H_2O and brine, dried with $MgSO_4$ and concentrated under reduced pressure. The crude product was purified by flash chromatography on silica gel (PE/EtOAc, 90/10, v/v) to yield desired product **63** as a yellow oil (2.80 g, 72%).

^{1}H NMR (300 MHz, $CDCl_3$) δ 5.45 (d, *J* = 5.8 Hz, 1H), 3.95–3.65 (m, 4H), 2.46–2.07 (m, 5H), 1.92 (m, 3H), 1.84–1.51 (m, 8H), 1.44 (s, 9H); **^{13}C NMR (75 MHz, $CDCl_3$) δ** 173.7, 137.1, 125.1, 109.0, 79.8, 64.6, 62.9, 42.0, 39.1, 36.8, 35.1, 34.5, 31.3, 29.3, 28.2, 27.7, 23.1; **MS (CI)** *(m/z)* 322 (100) $[M]^+$.

4-((1R,5R)-spiro[bicyclo[3.3.1]nonane-3,2'-[1,3]dioxolan]-6-en-7-yl)butan-1-ol (64)

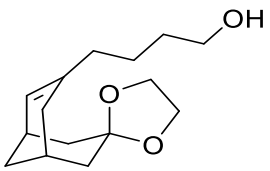

$C_{15}H_{24}O_3$
Molecular Weight: 252,35 g/mol

To a cooled suspension of $LiAlH_4$ (1.1 g, 28.9 mmol, 3 equiv) in dry Et_2O (60 mL), was added dropwise a solution of **63** (2.8 g, 8.68 mmol, 1 equiv) in dry Et_2O (10 mL). The reaction mixture was stirred at 0°C for 2h then quenched with H_2O (3.6 mL), then an aqueous solution of NaOH (5 M, 3.6 mL) and H_2O (3.6 mL). The mixture was dried with $MgSO_4$. The filtrate was concentrated under reduced pressure to afford **64** as a yellow oil (2.18 g, 100%).

^{1}H NMR (300 MHz, $CDCl_3$) δ 5.44 (d, *J* = 5.6 Hz, 1H), 3.93-3.65 (m, 3H), 3.59 (t, *J* = 6.4 Hz, 2H), 2.36 (s, 1H), 2.25-2.12 (m, 2H), 1.89 (dt, *J* = 22.3, 6.6 Hz, 4H), 1.73 (dd, *J* = 10.2, 3.5 Hz, 4H), 1.68-1.35 (m, 8H); **^{13}C NMR (75 MHz, $CDCl_3$) δ** 137.7, 124.2, 109.0, 64.5, 62.9, 62.7, 41.89, 39.0, 37.0, 34.6, 31.3, 29.2, 27.7, 23.6; **HRMS (ESI^+)** (*m/z*) calcd. for $C_{15}H_{25}O_3^+$ $[M+H]^+$ 253.1798 found 253.1794.

7-(4-Hydroxybutyl)bicyclo[3.3.1]non-6-en-3-one (65)

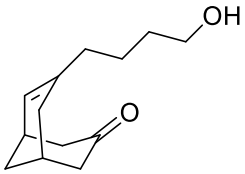

$C_{13}H_{20}O_2$
Molecular Weight: 208,30 g/mol

A solution of **64** (2.18 g, 8.6 mmol, 1 equiv.) in acetone (25 mL) was prepared to which paratoluenosulfonic acid (0.164 g, 0.86 mmol, 0.1 equiv.) was added. This solution was stirred at rt for 4 h. Then, the reaction mixture was extracted with EtOAc (3 × 30 mL) and the combined organic layer was washed with H2O and then dried with $MgSO_4$. The solvent was removed under reduced pressure. The crude product was purified by flash column chromatography on silica gel (PE /EtOAc 60/40, v/v) to give the desired product **65** as a colourless oil (1.46 g, 81%).

^{1}H NMR (300 MHz, $CDCl_3$) δ 5.42 (d, *J* = 5.7 Hz, 1H), 3.69–3.51 (m, 2H), 2.67 (s, 1H), 2.58 (s, 1H), 2.47 (m, 2H), 2.35–2.19 (m, 4H), 2.03–1.78 (m, 5H), 1.53–1.34 (m, 4H); **^{13}C NMR (75 MHz, $CDCl_3$) δ** 213.0, 136.4, 124.9, 62.7, 49.2, 46.8, 36.7, 35.5, 32.04, 31.39, 30.5, 30.4, 23.6; **MS (ESI$^-$)** (*m/z*) 207 (100) [M–H]$^-$.

4-(12-Amino-3-chloro-6,7,10,11-tetrahydro-7,11-methanocycloocta[b]quinolin-9 yl)butan-1-ol (67)

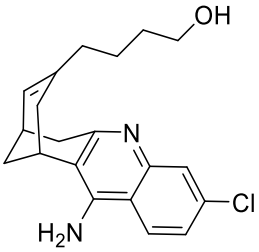

$C_{20}H_{23}ClN_2O$
Molecular Weight: 342,87 g/mol

In the two-necked dry round-bottomed flask, a suspension of 2-amino-4-chlorobenzonitrile **66** (1.709 g, 11.23 mmol, 1.6 equiv.) in dry 1,2-DCE (70 mL) was prepared and $AlCl_3$ (1.6 g, 11.94 mmol, 1.7 equiv.) was added in one portion. This mixture was stirred for 10 min then a solution of **65** (1.46 g, 7 mmol, 1 equiv.) in 1,2-DCE (14 mL) was added dropwise within 5 min, then the mixture was refluxed at 95 °C for 16 h. After cooling down to rt, THF was added, followed by H_2O and aq. 5 M NaOH, this mixture was stirred for another 30 min and organic solvents were evaporated under reduced pressure. Residues were taken up in EtOAc and extracted with EtOAc, then organic phases were washed with

H_2O, brine and dried with $MgSO_4$ and concentrated under reduced pressure. The crude product was purified by flash chromatography on silica gel (PE /EtOAc, 1:/, v/v EtOAc/MeOH 90/10 to 85/15, v/v) to give **67** (960 mg, 40%) as a yellowish solid.

^{1}H NMR (300 MHz, $CDCl_3$) δ 7.82 (d, *J* = 2.1 Hz, 1H), 7.61 (d, *J* = 9.0 Hz, 1H), 7.24 (dd, *J* = 9.0, 2.1 Hz, 1H), 5.48 (d, *J* = 5.1 Hz, 1H), 4.85 (br. s), 3.47 (t, *J* = 17.4 Hz, 2H), 3.19–3.16 (m, 1H), 3.09 (dd, *J* = 17.4, 5.3 Hz, 1H), 2.91 (d, *J* = 17.5 Hz, 1H), 2.72–2.68 (m, 1H), 2.60–2.40 (br.s, 1H), 2.41 (dd, *J* = 16.9, 4.3 Hz, 1H), 1.98–1.90 (m, 3H), 1.80–1.75 (m, 2H), 1.30–1.21 (m, 4H); **HRMS (ESI$^+$)** (*m/z*) calcd. for $C_{20}H_{24}{}^{35}ClN_2O^+$ $[M+H]^+$ 343.1572, found 343.1570.

Spectral data are in accordance with those reported previously:

Ronco, C.; Sorin, G.; Nachon, F.; Foucault, R.; Jean, L.; Romieu, A.; Renard, P. Y. Synthesis and Structure-Activity Relationship of Huprine Derivatives as Human Acetylcholinesterase Inhibitors. *Bioorg. Med. Chem.* **2009**, *17* (13), 4523–4536.

Ronco, C.; Foucault, R.; Gillon, E.; Bohn, P.; Nachon, F.; Jean, L.; Renard, P.-Y. New Huprine Derivatives Functionalized at Position 9 as Highly Potent Acetylcholinesterase Inhibitors. *ChemMedChem* **2011**, *6* (5), 876–888.

Ronco, C.; Carletti, E.; Colletier, J. P.; Weik, M.; Nachon, F.; Jean, L.; Renard, P. Y. Huprine Derivatives as Sub-Nanomolar Human Acetylcholinesterase Inhibitors: From Rational Design to Validation by X-Ray Crystallography. *ChemMedChem* **2012**, *7* (3), 400–405.

4-((7R,11R)-12-amino-3-chloro-6,7,10,11-tetrahydro-7,11-methanocycloocta[b]quinolin-9-yl)butyl methanesulfonate (68)

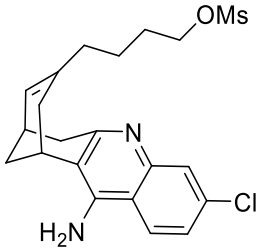

$C_{21}H_{25}ClN_2O_3S$
Molecular Weight: 420,95 g/mol

To a solution of **67** (791 mg, 2.31 mmol) in dry THF (21 mL), MsCl (0.27 mL, 3.46 mmol, 1.5 equiv) and Et_3N (0.48 mL, 3.46 mmol, 1.5 equiv) were added at 0°C. The reaction mixture was stirred at 0°C for 30 min. Then, it was quenched with sat. aq. $NaHCO_3$ and extracted with EtOAc. The organic layers were washed with H_2O and brine and dried over $MgSO_4$. The crude product was used without further purification for the next step.

9-(4-Azidobutyl)-3-chloro-6,7,10,11-tetrahydro-7,11-methanocycloocta[b]quinolin-12-amine (48)

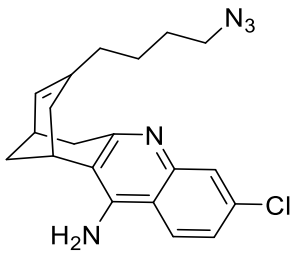

$C_{20}H_{22}ClN_5$
Molecular Weight: 367,88 g/mol

To a solution of **68** (790 mg, 1.88 mmol, 1 equiv) in dry DMF (19 mL), NaN_3 (366.73 mg, 5.64 mmol, 3 equiv) was added. The reaction mixture was stirred at 90°C overnight. After completion determined by TLC, the mixture was allowed to cool down to rt and quenched with H_2O. Then, it was extracted with EtOAc. The organic layers were washed with H_2O, brine and dried over $MgSO_4$, and concentrated under reduced pressure. The crude product was purified by flash chromatography on silica gel (PE/EtOAc, 60/40, v/v then EtOAc/MeOH 9/1 v/v) to give **48** (414 mg, 60%) as an orange solid.

^{1}H NMR (300 MHz, $CDCl_3$) δ 7.84 (d, *J* = 2.1 Hz, 1H), 7.63 (d, *J* = 9.0 Hz, 1H), 7.27 (dd, *J* = 9.0, 2.1 Hz, 1H), 5.52 (d, *J* = 5.3 Hz, 1H), 4.82 (br.s), 3.21–3.19 (m, 1H), 3.11 (dd, *J* = 17.5, 5.6 Hz, 1H), 3.10–3.07 (m, 2H), 2.93 (d, *J* = 17.5 Hz, 1H), 2.77–2.73 (m, 1H), 2.45 (dd, *J* = 16.9, 4.5 Hz, 1H), 2.02–1.94 (m, 3H), 1.82 (t, *J* = 6.6 Hz, 2H), 1.35–1.28 (m, 4H); **HRMS (ESI$^+$)** (*m/z*) calcd. for $C_{20}H_{23}{}^{35}ClN_5{}^+$ $[M+H]^+$ 368.1636 found 368.1632.

Spectral data are in accordance with those reported previously:
Ronco, C.; Carletti, E.; Colletier, J. P.; Weik, M.; Nachon, F.; Jean, L.; Renard, P. Y. Huprine Derivatives as Sub-Nanomolar Human Acetylcholinesterase Inhibitors: From Rational Design to Validation by X-Ray Crystallography. *ChemMedChem* **2012**, *7* (3), 400–405.

2-(1-(4-((7R,11R)-12-amino-3-chloro-6,7,10,11-tetrahydro-7,11-methanocycloocta[b]quinolin-9-yl)butyl)-1H-1,2,3-triazol-4-yl)-N-(4-((tert-butyldimethylsilyl)oxy)-3-methoxybenzyl)acetamide (47)

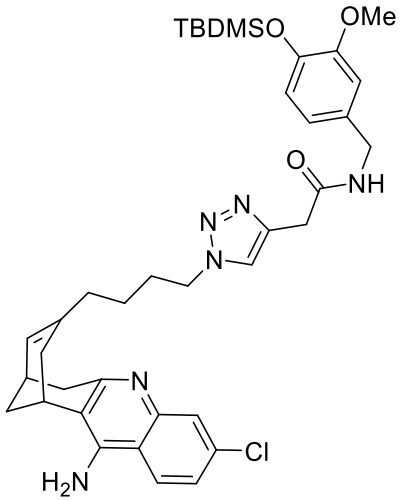

$C_{38}H_{49}ClN_6O_3Si$
Molecular Weight: 701,38 g/mol

A solution of azide **48** (374.5 mg, 1.02 mmol) and alkyne **49** (403.8 mg, 1.22 mmol, 1.2 equiv) was prepared in HPLC grade MeCN (34 mL). CuI (194.26 mg, 1.02 mmol, 1 equiv) was added to the solution and the reaction mixture was stirred at rt for 12h. The reaction mixture was concentrated under reduced pressure and the crude product was purified by flash column on silica gel (DCM/MeOH, 98/2 to 80/20, v/v) to give **47** (507 mg, 71%) as a yellow solid.

^{1}H NMR (CD_3OD, 300 MHz) δ 8.33 (d, *J* = 9.1 Hz, 1H), 7.69 (d, *J* = 2.1 Hz, 2H), 7.57 (dd, *J* = 2.0 Hz, *J* = 9.1 Hz, 2H), 6.90 (d, *J* = 7.9 Hz, 1H), 6.74 (d, *J* = 1.1 Hz, 2H), 5.58 (d, br.), 4.36 (d, *J* = 11.5 Hz, 2H), 4.21 (t, *J* = 6.9 Hz, 2H), 3.76 (s, 3H), 3.30-3.02 (m, 4H), 2.90-2.82 (m, 2H), 2.82 (m, 1H), 2.41-2.37 (m, 1H), 1.97-1.92 (m, 6H), 1.72-1.51 (m, 2H), 0.97 (s, 9H), 0.10 (s, 6H); **^{13}C NMR (CD_3OD, 75 MHz) δ** 171.8, 155.4, 154.2, 152.3, 145.4, 141.1, 139.5, 137.8, 133.5, 127.2, 126.0, 125.9, 124.6, 124.4, 121.7, 121.0, 120.6, 115.4, 112.9, 99.4, 55.9, 53.2, 50.9, 44.2, 37.1, 36.8, 33.7, 30.0, 29.5, 28.4, 27.6, 26.2, 24.9, 19.3, -4.5; **MS (ESI+)** (*m/z*) 702 $[M+H]^+$.

2-(1-(4-((7R,11R)-12-amino-3-chloro-6,7,10,11-tetrahydro-7,11-methanocycloocta[b]quinolin-9-yl)butyl)-1H-1,2,3-triazol-4-yl)-N-(4-hydroxy-3-methoxybenzyl)acetamide (34)

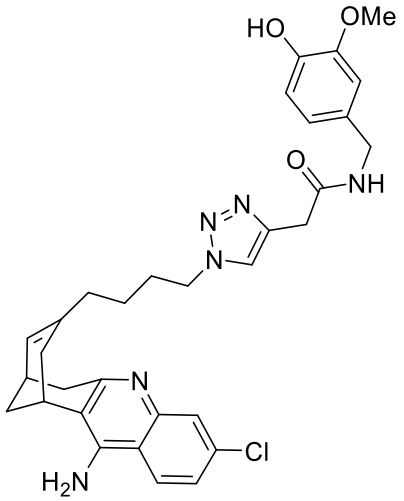

$C_{32}H_{35}ClN_6O_3$
Molecular Weight: 587,12 g/mol

To a solution of **47** (50 mg, 0.07 mmol) in dry DCM (2.4 mL), CSA (165 mg, 0.7 mmol, 10 equiv) and MeOH (1 mL) were added. The reaction mixture was stirred at rt for 24h.Progress of the reaction was checked by HPLC. Reaction mixture was quenched with aq. sat. NaHCO3, extracted with DCM. Organic layers were dried over Na_2SO_4 and concentrated under reduced pressure. The crude product was purified by semi-preparative with MeCN and aq. AcONH (10 mM) (0% MeCN followed by linear gradient from 40% to 45% of MeCN in 20 min with a flow rate of 1mL/min). Dual visible detection was achieved at 230 and 550 nm to give **34** (29 mg, 70%) as a beige solid.

^{1}H NMR (300 MHz, CD_3OD) *δ* 8.33 (d, *J* = 9.1 Hz, 1H), 7.67 (d, *J* = 1.9 Hz, 1H), , 7.63 (s, 1H) , 7.42 (dd, *J* = 9.1 Hz, *J* = 1.9 Hz, 1H) , 6.86 (s, 1H) , 6.71 (m, 2H), 5.59 (d, *J* = 5.7 Hz,1H) , 4.29 (s, 2H) , 4.17 (t, *J* = 6.9 Hz, 2H) , 3.81 (s, 3H) , 3.66 (s, 2H) , 3.30 (m, 1H) , 3.11 (dd, *J* = 18.0 Hz, *J* = 5.4 Hz, 1H) , 2.82 (d, *J* = 18.0 Hz, 1H), 2.74 (m, 1H) , 2.37 (dd, *J* = 17.0 Hz, *J* = 3.3 Hz, 1H), 2.10-1.87 (complex signal, 5H), 1.61 (m, 2H), 1.30 (m, 2H); **^{13}C NMR (75 MHz, CD_3OD) *δ*** 24.8, 25.4, 27.5, 28.1, 29.3, 30.0, 33.6, 36.0, 37.0, 50.8, 56.4, 112.4, 115.4, 116.1 , 119.3, 121.3, 125.7, 126.3, 127.7, 131.1, 135.4, 137.9, 139.5 , 140.5, 140.6, 149.0, 153.0, 156.7, 171.4 ; **HRMS (ESI$^+$)** calcd for $C_{32}H_{35}{}^{35}ClN_6O_3{}^+$ $[M]^+$ 587.2532 found 587.2534.

Ethyl(methyl)carbamic chloride (91c)

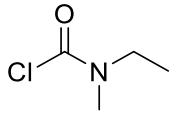

C_4H_8ClNO
Molecular Weight: 121,56 g/mol

To a solution of triphosgene **90** (500 mg, 8.4 mmol, 1 equiv) in DCM (8 mL) was added sodium bicarbonate (1.4g, 16.8 mmol, 2 equiv). The mixture was cooled at – 10°C and a solution of ethylmethylamine **89** (1.6 g, 5.6 mmol, 0.6 equiv) in DCM (1.5 mL) was added dropwise. The resulting mixture was stirred at room temperature for 12h. After completion determined by TLC analysis, the solution was filtered. The filtrate was concentrated under reduced pressure to give **91c** as a yellow oil (1.02 g, 100%).

^{1}H NMR (300 MHz, $CDCl_3$) δ 3.48 (dq, *J* = 21.3, 7.2 Hz, 2H), 3.07 (d, *J* = 26.1 Hz, 3H), 1.21 (dt, *J* = 14.6, 7.2 Hz, 3H); **^{13}C NMR (75 MHz, $CDCl_3$) *δ*** 149.2, 149.0, 47.9, 46.3, 37.8, 36.0, 12.9, 12.2 (each carbon gives 2 signals because of the 2 rotamers of the amide).

Spectral data are in accordance with those reported previously:
Fuchs, M.; Koszelewski, D.; Tauber, K.; Kroutil, W.; Faber, K. Chemoenzymatic Asymmetric Total Synthesis of (S)-Rivastigmine Using ω-Transaminases. *Chem. Commun.* **2010**, *46* (30), 5500–5502.

4-ethynylphenol (92a)

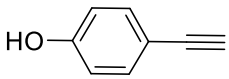

C_8H_6O
Molecular Weight: 118,13 g/mol

92a was obtained from 4-iodophenol **93a** (200 mg, 1.04 mmol) following the general procedure A and isolated as a purple oil (111.7 mg, 91%).

^{1}H NMR (300 MHz, $CDCl_3$) δ 7.37 (d*, J* = 8.8 Hz, 2H), 7.07 (br s, -OH), 6.78 (d, *J* = 8.8 Hz, 2H), 3.01 (s, 1H); **^{13}C NMR (75 MHz, $CDCl_3$) δ** 156.4, 131.5, 115.3, 114.1, 83.8, 75.9.

Spectral data are in accordance with those reported previously:
Pirali, T.; Gatti, S.; Di Brisco, R.; Tacchi, S.; Zaninetti, R.; Brunelli, E.; Massarotti, A.; Sorba, G.; Canonico, P. L.; Moro, L.; Genazzani, A. A.; Tron, G. C.; Billington, R. A. Estrogenic Analogues Synthesized by Click Chemistry. *ChemMedChem* **2007**, *2* (4), 437–440.

3-ethynylphenol (92b)

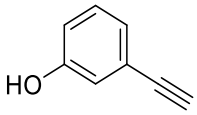

C_8H_6O
Molecular Weight: 118,13 g/mol

92b was obtained from 3-iodophenol **93b** (200 mg, 1.04 mmol) following the general procedure A and isolated as a yellow oil (98.28 mg, 80%).

^{1}H NMR (300 MHz, $CDCl_3$) δ 7.30-6.80 (m, 4H), 3.14 (s, 1H); **^{13}C NMR (75 MHz, $CDCl_3$) δ** 155.6, 129.8, 124.7, 123.4, 119.1, 116.7, 83.7, 77.7.

Spectral data are in accordance with those reported previously:
Pirali, T.; Gatti, S.; Di Brisco, R.; Tacchi, S.; Zaninetti, R.; Brunelli, E.; Massarotti, A.; Sorba, G.; Canonico, P. L.; Moro, L.; Genazzani, A. A.; Tron, G. C.; Billington, R. A. Estrogenic Analogues Synthesized by Click Chemistry. *ChemMedChem* **2007**, *2* (4), 437–440.

2-ethynylphenol (92c)

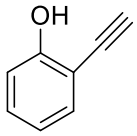

C_8H_6O
Molecular Weight: 118,13 g/mol

92c was obtained from 2-iodophenol **93c** (200 mg, 1.04 mmol) following the general procedure A and isolated as a yellow oil (72.48 mg, 59%).

^{1}H NMR (300 MHz, $CDCl_3$) δ 7.37 (dd, *J* = 7.7/1.6 Hz, 1H), 7.27 (t, *J* = 7.4 Hz, 1H), 6.94 (d, *J* = 8.2 Hz, 1H), 6.83 (td, J = 7.7/1.1 Hz, 1H), 5.90 (br s, OH), 3.46 (s, 1H); **^{13}C NMR (75 MHz, $CDCl_3$) δ** 157.4, 132.3, 131.1, 120.5, 115.0, 108.4, 84.5, 78.5.

Spectral data are in accordance with those reported previously:
Pirali, T.; Gatti, S.; Di Brisco, R.; Tacchi, S.; Zaninetti, R.; Brunelli, E.; Massarotti, A.; Sorba, G.; Canonico, P. L.; Moro, L.; Genazzani, A. A.; Tron, G. C.; Billington, R. A. Estrogenic Analogues Synthesized by Click Chemistry. *ChemMedChem* **2007**, *2* (4), 437–440.

3-ethynylphenyl dimethylcarbamate (78a)

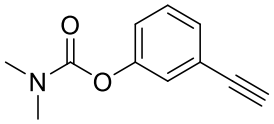

$C_{11}H_{11}NO_2$
Molecular Weight: 189,21

78a was obtained from **92b** (300 mg, 2.55 mmol) and **91a** following the general procedure B and isolated as a yellow oil (385.9 mg, 80%).

^{1}H NMR (300 MHz, $CDCl_3$) δ 7.32 – 7.29 (m, 2H), 7.26 – 7.24 (m, 1H), 7.12 (dt, *J* = 6.6, 2.5 Hz, 1H), 3.09 (s, 3H), 3.06 (s, 1H), 3.01 (s, 3H); **^{13}C NMR (75 MHz, $CDCl_3$)** δ 154.6, 151.3, 129.1, 125.5, 123.3, 122.7, 82.9, 77.8, 36.8, 36.5; **HRMS (ESI$^+$)** (*m/z*) calcd. for $C_{11}H_{12}NO_2^+$ [M+H$^+$] 190.0790 found 190.0792.

3-ethynylphenyl diethylcarbamate (78b)

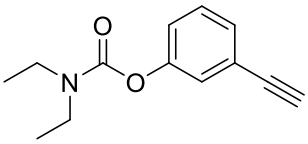

$C_{13}H_{15}NO_2$
Molecular Weight: 217,26 g/mol

78b was obtained from **92b** (300 mg, 2.55 mmol) and **91b** following the general procedure B and isolated as a yellow oil (354 mg, 64%).

^{1}H NMR (300 MHz, $CDCl_3$) δ 7.26 – 7.22 (m, 2H), 7.20 (t, *J* = 1.7 Hz, 1H), 7.12 – 7.03 (m, 1H), 3.48 – 3.24 (m, 4H), 3.00 (s, 1H), 1.28 – 1.06 (m, 6H); **^{13}C NMR (75 MHz, $CDCl_3$) δ** 153.9, 151.4, 129.2, 128.9, 125.5, 123.2, 122.8, 82.9, 77.7, 42.2, 12.9; **HRMS (ESI$^+$)** (*m/z*) calcd. for $C_{13}H_{16}NO_2^+$ [M+H$^+$] 218.1103 found 218.1174.

3-ethynylphenyl ethyl(methyl)carbamate (78c)

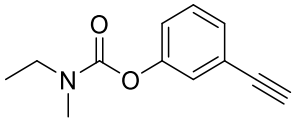

$C_{12}H_{13}NO_2$
Molecular Weight: 203,24 g/mol

78c was obtained from **92b** (200 mg, 1.76 mmol) and **91c** following the general procedure B and isolated as a yellow oil (251 mg, 70%).

^{1}H NMR (300 MHz, $CDCl_3$) δ 7.32 – 7.28 (m, 2H), 7.25 (s, 1H), 7.15 – 7.10 (m, 1H), 3.51 – 3.35 (m, 2H), 3.09 – 2.95 (m, 4H), 1.27 – 1.14 (m, 3H); **^{13}C NMR (75 MHz, $CDCl_3$) δ** 151.5, 138.2, 124.1, 88.9, 44.2, 34.3, 33.9, 13.3, 12.5 (three carbons are missing despite an extended acquisition time); **HRMS (ESI^+)** : (*m/z*) calcd. for $C_{12}H_{14}NO_2^+$ [M+H^+] 204.1032 found 204.1032.

4-ethynylphenyl dimethylcarbamate (79a)

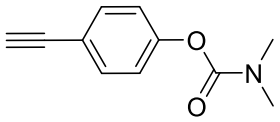

$C_{11}H_{11}NO_2$
Molecular Weight: 189,21 g/mol

79a was obtained from **92a** (300 mg, 2.55 mmol) and **91a** following the general procedure B and isolated as a white solid (381 mg, 79%).

^{1}H NMR (300 MHz, $CDCl_3$) δ 7.51 – 7.45 (m, 2H), 7.11 – 7.05 (m, 2H), 3.05 (d, *J* = 25.1 Hz, 6H), 3.04 (s, 1H); **^{13}C NMR (75 MHz, $CDCl_3$)** δ 154.5, 151.9, 133.3, 121.9, 119.1, 83.21, 77.1, 36.7; **HRMS (ESI^+)** (*m/z*) calcd. for $C_{11}H_{12}NO_2^+$ [M+H^+] 190.0790 found 190,0866.

4-ethynylphenyl diethylcarbamate (79b)

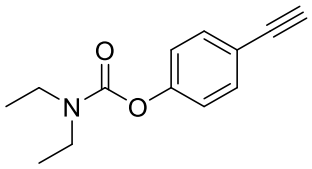

$C_{13}H_{15}NO_2$
Molecular Weight: 217,26 g/mol

79b was obtained from **92a** (300 mg, 2.55 mmol) and **91b** following the general procedure B and isolated as a white solid (443 mg, 80%)**.**

^{1}H NMR (300 MHz, $CDCl_3$) δ 7.44 – 7.38 (m, 2H), 7.05 – 6.99 (m, 2H), 3.34 (dd, *J* = 12.4, 6.5 Hz, 4H), 2.97 (s, 1H), 1.20 – 1.11 (m, 6H); **^{13}C NMR (75 MHz, $CDCl_3$) δ** 153.8, 152, 133.3, 121.9, 118.9, 83.3, 77.0, 42.4, 13.5; **HRMS (ESI^+)** (*m/z*) calcd. for $C_{13}H_{16}NO_2^+$ [M+H^+] 218.1103 found 218.1180.

4-ethynylphenyl ethyl(methyl)carbamate (79c)

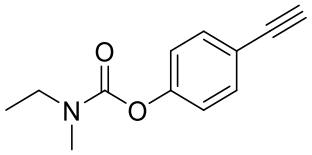

$C_{12}H_{13}NO_2$
Molecular Weight: 203,24 g/mol

79c was obtained from **92a** (200 mg, 1.76 mmol) and **91c** following the general procedure B and isolated as a yellow oil (251 mg, 70%).

^{1}H NMR (300 MHz, $CDCl_3$) δ 7.48 (d, *J* = 8.89 Hz, 2H), 7.09 (d, *J* = 7.2 Hz, 2H), 3.44 (dq, *J* = 14.1, 6.9 Hz, 2H), 3.03 (dd, *J* = 13.7, 7.5 Hz, 4H), 1.21 (dt, *J* = 13.9, 7.0 Hz, 3H); **^{13}C NMR (75 MHz, $CDCl_3$) δ** 154.3, 151.4, 129.1, 125.5, 123.3, 122.8, 82.92, 77.8, 44.2, 34.4, 33.9, 29.8. **HRMS (ESI^+)** (*m/z*) calcd. for $C_{12}H_{14}NO_2^+$ [M+H$^+$] 204.1032 found 204.1030.

4-(1-(quinuclidin-3-yl)-1H-1,2,3-triazol-4-yl)phenyl dimethylcarbamate (75a)

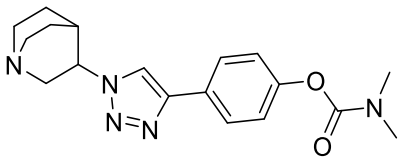

$C_{18}H_{23}N_5O_2$
Molecular Weight: 341,41 g/mol

75a was obtained from alkyne **79a** (83.25 mg, 0.44 mmol, 1 equiv) and 3-aminoquinuclidine **81** (100 mg, 0.44 mmol, 1 equiv) following the general procedure C and isolated as a brown powder (45 mg, 30%).

^{1}H NMR (300 MHz, $CDCl_3$) δ 7.83 (d, *J* = 9 Hz, 2H), 7.78 (s, 1H), 7.19 (d, *J* = 9 Hz, 2H), 4.65 (s, 1H), 3.71 (m, 1H), 3.50 (m, 1H), 3.07 (d, *J* = 30 Hz, 6H), 2.95 (m, 4H), 2.29 (m, 1H), 1.80 (m, 4H); **^{13}C NMR (75 MHz, $CDCl_3$)** δ 154.9, 151.6, 147.2, 127.8, 126.7, 122.3, 119.1, 58.2, 52.4, 46.9, 36.7, 28.2, 19.9 (two carbons are missing despite an extended acquisition time); **HRMS (ESI^+)** (*m/z*)calcd. for $C_{18}H_{24}N_5O_2^+$ [M+H]$^+$ 342.1925 found 342.1924; **mp** = 170 °C

(R)-4-(1-(quinuclidin-3-yl)-1H-1,2,3-triazol-4-yl)phenyl dimethylcarbamate ((R)-75a)

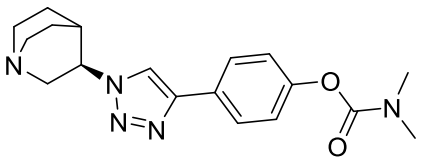

$C_{18}H_{23}N_5O_2$
Molecular Weight: 341,41 g/mol

(R)-75a was obtained from alkyne **79a** (83.25 mg, 0.44 mmol, 1 equiv) and 3-aminoquinuclidine **(R)-81** (100 mg, 0.44 mmol, 1 equiv) following the general procedure C and isolated as a brown powder (40.1 mg, 27%).

NMR and MS data were in accordance with those reported above for **75a**
$[\alpha]_D$ = 19.25 (c = 0.05 in $CHCl_3$ at 22 °C)

(S)-4-(1-(quinuclidin-3-yl)-1H-1,2,3-triazol-4-yl)phenyl dimethylcarbamate ((S)-75a)

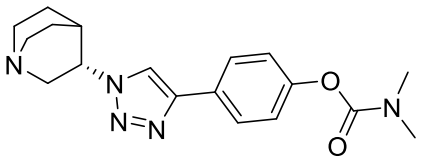

$C_{18}H_{23}N_5O_2$
Molecular Weight: 341,41 g/mol

(S)-75a was obtained from alkyne **79a** (83.25 mg, 0.44 mmol, 1 equiv) and 3-aminoquinuclidine **(S)-81** (100 mg, 0.44 mmol, 1 equiv) following the general procedure C and isolated as a brown powder (30 mg, 20%).

NMR and MS data were in accordance with those reported above for **75a**
$[\alpha]_D$ = - 18.30 (c = 0.05 in $CHCl_3$ at 22 °C)

4-(1-(quinuclidin-3-yl)-1H-1,2,3-triazol-4-yl)phenyl diethylcarbamate (75b)

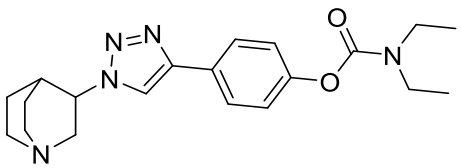

$C_{20}H_{27}N_5O_2$
Molecular Weight: 369,47 g/mol

75b was obtained from alkyne **79b** (95.5 mg, 0.44 mmol, 1 equiv) and 3-aminoquinuclidine **81** (100mg, 0.44 mmol, 1 equiv) following the general procedure C and isolated as a yellow oil (53.57 mg, 33%).

^{1}H NMR (300 MHz, $CDCl_3$) δ 7.83 (d, *J* = 9 Hz, 2H), 7.78 (s, 1H), 7.19 (d, *J* = 9 Hz, 2H), 4.65 (s, 1H), 3.71 (m, 1H), 3.45 (m, 6H), 2.92 (m, 4H), 2.20 (m, 2H), 1.66 (m, 3H), 1.24 (m, 5H); **^{13}C NMR (75 MHz, $CDCl_3$)** δ 154.1, 151.5, 147.1, 127.7, 126.6, 122.2, 119.1, 58.2, 52.4, 47.1, 42.2, 28.2, 20.0, 13.9 (two carbons are missing despite an extended acquisition time); **HRMS (ESI^+)** (*m/z*)calcd. for $C_{20}H_{28}N_5O_2^+$ $[M+H]^+$ 370.2165 found 370.2242.

(R)-4-(1-(quinuclidin-3-yl)-1H-1,2,3-triazol-4-yl)phenyl diethylcarbamate ((R)-75b)

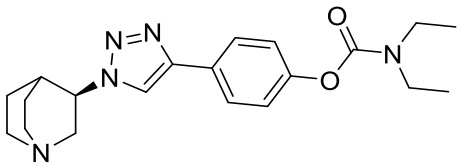

$C_{20}H_{27}N_5O_2$
Molecular Weight: 369,47 g/mol

(R)-75b was obtained from alkyne **79b** (95.5 mg, 0.44 mmol, 1 equiv) and 3-aminoquinuclidine **(R)-81** (100mg, 0.44 mmol, 1 equiv) following the general procedure C and isolated as a yellow oil (79.38 mg, 49%).

NMR and MS data were in accordance with those reported above for **75b**
$[\alpha]_D$ = 19.25 (c = 0.05 in $CHCl_3$ at 22 °C)

(S)-4-(1-(quinuclidin-3-yl)-1H-1,2,3-triazol-4-yl)phenyl diethylcarbamate ((S)-75b)

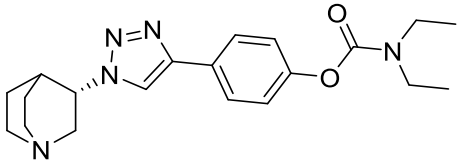

$C_{20}H_{27}N_5O_2$
Molecular Weight: 369,47 g/mol

(S)-75b was obtained from alkyne **79b** (95.5 mg, 0.44 mmol, 1 equiv) and 3-aminoquinuclidine **(S)-81** (100mg, 0.44 mmol, 1 equiv) following the general procedure C and isolated as a yellow oil (76.14 mg, 47%).

NMR and MS data were in accordance with those reported above for **75b**
$[\alpha]_D$ = - 19.45 (c = 0.05 in $CHCl_3$ at 22 °C)

4-(1-(quinuclidin-3-yl)-1H-1,2,3-triazol-4-yl)phenyl ethyl(methyl)carbamate (75c)

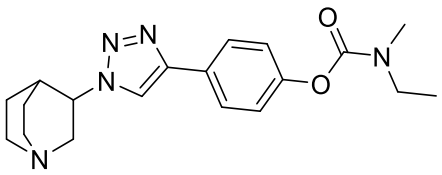

$C_{19}H_{25}N_5O_2$
Molecular Weight: 355,44 g/mol

75c was obtained from alkyne **79c** (83.25 mg, 0.44 mmol, 1 equiv) and 3-aminoquinuclidine **81** (100 mg, 0.44 mmol, 1 equiv) following the general procedure C and isolated as a brown powder (59.58 mg, 38%).

^{1}H NMR (300 MHz, $CDCl_3$) δ 7.82 (d, *J* = 9.21 Hz, 2H), 7.78 (s, 1H), 7.19 (d, *J* = 7.8 Hz, 2H), 4.65 (m, 1H), 3.72 (dd, *J* = 13.9, 4.1 Hz, 1H), 3.55 – 3.35 (m, 3H), 3.08 – 2.97 (m, 3H), 2.96 – 2.87 (m, 2H), 2.28 (dt, *J* = 6.1, 3.0 Hz, 1H), 1.87 – 1.61 (m, 4H), 1.54 – 1.41 (m, 1H), 1.31 – 1.11 (m, 4H); **^{13}C NMR (75 MHz, $CDCl_3$) δ** 151.6, 147.3, 126.7, 122.3, 119.3, 57.7, 53.6, 52.2, 47.2, 46.2, 44.2, 38.3, 28.1, 25.4, 23.6, 19.7, 18.9 (two carbons are missing despite an extended acquisition time); **HRMS (ESI$^+$)** (*m/z*) calcd. for $C_{19}H_{26}N_5O_2^+$ $[M+H]^+$ 356.2008 found 356.1968; **mp** = 143.3 °C

(R)-4-(1-(quinuclidin-3-yl)-1H-1,2,3-triazol-4-yl)phenyl ethyl(methyl)carbamate ((R)-75c)

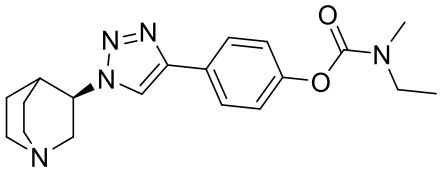

$C_{19}H_{25}N_5O_2$
Molecular Weight: 355,44 g/mol

(R)-75c was obtained from alkyne **79c** (83.25 mg, 0.44 mmol, 1 equiv) and 3-aminoquinuclidine **(R)-81** (100 mg, 0.44 mmol, 1 equiv) following the general procedure C and isolated as a brown powder (46.48 mg, 30%).

NMR and MS data were in accordance with those reported above for **75c**
$[\alpha]_D$ = 12.16 (c = 0.05 in $CHCl_3$ at 23 °C)

(S)-4-(1-(quinuclidin-3-yl)-1H-1,2,3-triazol-4-yl)phenyl ethyl(methyl)carbamate ((S)-75c)

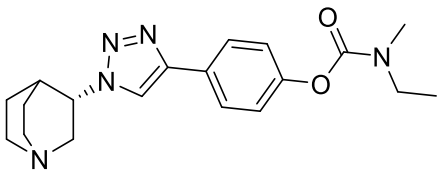

$C_{19}H_{25}N_5O_2$
Molecular Weight: 355,44 g/mol

(S)-75c was obtained from alkyne **79c** (83.25 mg, 0.44 mmol, 1 equiv) and 3-aminoquinuclidine **(S)-81** (100 mg, 0.44 mmol, 1 equiv) following the general procedure C and isolated as a brown powder (62.40 mg, 40%).

NMR and MS data were in accordance with those reported above for **75c**
$[\alpha]_D$ = - 16.20 (c = 0.05 in $CHCl_3$ at 23 °C)

3-(1-(quinuclidin-3-yl)-1H-1,2,3-triazol-4-yl)phenyl dimethylcarbamate (76a)

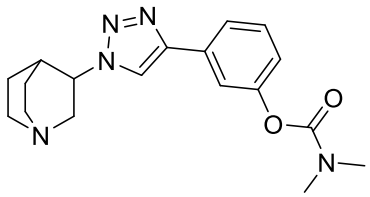

$C_{18}H_{23}N_5O_2$
Molecular Weight: 341,41 g/mol

76a was obtained from alkyne **78a** (83.25 mg, 0.44 mmol, 1 equiv) and 3-aminoquinuclidine **81** (100 mg, 0.44 mmol, 1 equiv) following the general procedure C and isolated as a brown powder (75 mg, 50%).

^{1}H NMR (300 MHz, $CDCl_3$) δ 7.81 (s, 1H), 7.68 (d, 1H), 7.58 – 7.55 (m, 1H), 7.39 (t, *J* = 7.9 Hz, 1H), 7.08 (ddd, *J* = 8.1, 2.4, 1.0 Hz, 1H), 4.67 – 4.59 (m, 1H), 3.74 – 3.62 (m, 2H), 3.47 (ddd, *J* = 12.0, 9.8, 1.7 Hz, 1H), 3.06 (d, 6H), 2.97 – 2.89 (m, 3H), 2.69 – 2.60 (m, 2H), 2.28 – 2.19 (m, 1H), 2.01 – 1.94 (m, 2H); **^{13}C NMR (75 MHz, $CDCl_3$)** δ 154.9, 152.1, 147, 132, 129.8, 122.5, 121.5, 119.5, 119.2, 58.2, 52.5, 47.1, 36.7, 28.1, 19.9 (two carbons are missing despite an extended acquisition time); **HRMS (ESI$^+$)** (*m/z*) calcd. for $C_{18}H_{24}N_5O_2^+$ $[M+H]^+$ 342.1925 found 342.1928; **mp** = 132.2 °C

(R)-3-(1-(quinuclidin-3-yl)-1H-1,2,3-triazol-4-yl)phenyl dimethylcarbamate ((R)-76a)

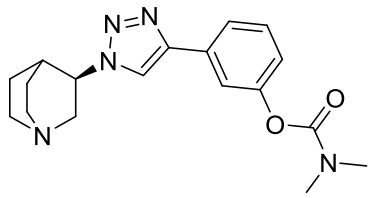

$C_{18}H_{23}N_5O_2$
Molecular Weight: 341,41 g/mol

(R)-76a was obtained from alkyne **78a** (83.25 mg, 0.44 mmol, 1 equiv) and 3-aminoquinuclidine **(R)-81** (100 mg, 0.44 mmol, 1 equiv) following the general procedure C and isolated as a brown powder (30 mg, 20%).

NMR and MS data were in accordance with those reported above for **76a**
$[\alpha]_D$ = 15.05 (c = 0.05 in $CHCl_3$ at 23 °C)

(S)-3-(1-(quinuclidin-3-yl)-1H-1,2,3-triazol-4-yl)phenyl dimethylcarbamate ((S)-76a)

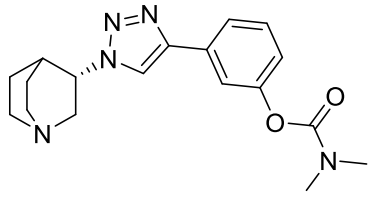

$C_{18}H_{23}N_5O_2$
Molecular Weight: 341,41 g/mol

(S)-76a was obtained from alkyne **78a** (83.25 mg, 0.44 mmol, 1 equiv) and 3-aminoquinuclidine **(S)-81** (100 mg, 0.44 mmol, 1 equiv) following the general procedure C and isolated as a brown powder (39 mg, 26%).

NMR and MS data were in accordance with those reported above for **76a**
$[\alpha]_D$ = - 20.05 (c = 0.05 in $CHCl_3$ at 23 °C)

3-(1-(quinuclidin-3-yl)-1H-1,2,3-triazol-4-yl)phenyl diethylcarbamate (76b)

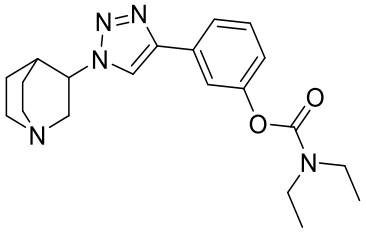

$C_{20}H_{27}N_5O_2$
Molecular Weight: 369,46 g/mol

76b was obtained from alkyne **78b** (95.5 mg, 0.44 mmol, 1 equiv) and 3-aminoquinuclidine **81** (100 mg, 0.44 mmol, 1 equiv) following the general procedure C and isolated as a yellow oil (29.22 mg, 18%).

^{1}H NMR (300 MHz, $CDCl_3$) δ 7.83 (s, 1H), 7.71 – 7.66 (m, 1H), 7.60 – 7.57 (m, 1H), 7.41 (t, *J* = 7.9 Hz, 1H), 7.11 (ddd, *J* = 8.1, 2.4, 1.0 Hz, 1H), 4.67 (dd, *J* = 6.4, 3.4 Hz, 1H), 3.79 – 3.73 (m, 2H), 3.70 (d, *J* = 10.3 Hz, 2H), 3.62 (dd, *J* = 5.5, 3.6 Hz, 1H), 3.58 – 3.50 (m, 1H), 3.43 (dd, *J* = 18.0, 8.1 Hz, 4H), 3.28 – 3.10 (m, 2H), 2.99 – 2.83 (m, 6H), 2.77 – 2.68 (m, 1H), 2.29 (dd, *J* = 6.2, 3.1 Hz, 1H), 2.04 (dt, *J* = 6.4, 3.2 Hz, 1H); **^{13}C NMR (75 MHz, $CDCl_3$)** δ 154.2, 152, 146.9, 131.9, 129.7, 122.4, 121.5, 119.5, 119.2, 58.3, 52.4, 47.2, 42.3, 28.1, 25.8, 13.9 (two carbons are missing despite an extended acquisition time); **HRMS** (*m/z*) calcd. for $C_{20}H_{28}N_5O_2^+$ $[M+H]^+$ 370.2165 found 370.2248.

(R)-3-(1-(quinuclidin-3-yl)-1H-1,2,3-triazol-4-yl)phenyl diethylcarbamate ((R)-76b)

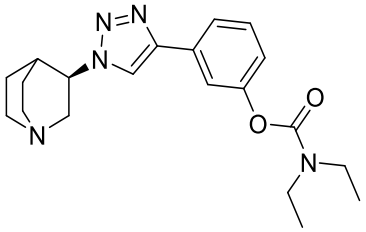

$C_{20}H_{27}N_5O_2$
Molecular Weight: 369,46 g/mol

(R)-76 was obtained from alkyne **78b** (95.5 mg, 0.44 mmol, 1 equiv) and 3-aminoquinuclidine **(R)-81**, (100 mg, 0.44 mmol, 1 equiv) following the general procedure C and isolated as a yellow oil (64.8 mg, 40%).

NMR and MS data were in accordance with those reported above for **76b**
$[\alpha]_D$ = 22.01 (c = 0.05 in $CHCl_3$ at 22 °C)

(S)-3-(1-(quinuclidin-3-yl)-1H-1,2,3-triazol-4-yl)phenyl diethylcarbamate ((S)-76b)

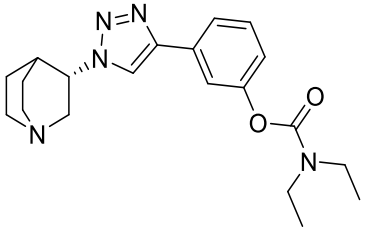

$C_{20}H_{27}N_5O_2$
Molecular Weight: 369,46 g/mol

(S)-76b was obtained from alkyne **78b** (95.5 mg, 0.44 mmol, 1 equiv) and 3-aminoquinuclidine **(S)-81**, (100 mg, 0.44 mmol, 1 equiv) following the general procedure C and isolated as a yellow oil (81.1 mg, 50%).

NMR and MS data were in accordance with those reported above for **76b**
$[\alpha]_D$ = - 20.01 (c = 0.05 in $CHCl_3$ at 22 °C)

3-(1-(quinuclidin-3-yl)-1H-1,2,3-triazol-4-yl)phenyl ethyl(methyl)carbamate (76c)

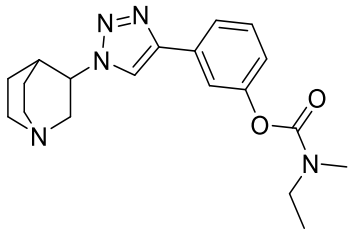

$C_{19}H_{25}N_5O_2$
Molecular Weight: 355,44 g/mol

76c was obtained from alkyne **78c** (83.25 mg, 0.44 mmol, 1 equiv) and 3-aminoquinuclidine **81** (100 mg, 0.44 mmol, 1 equiv) following the general procedure C and isolated as a yellow oil (53.1 mg, 34%).

^{1}H NMR (300 MHz, $CDCl_3$) δ 7.84 (s, 1H), 7.66 – 7.62 (m, 1H), 7.55 (s, 1H), 7.36 (t, *J* = 7.9 Hz, 1H), 7.06 (d, *J* = 8.1 Hz, 1H), 4.72 – 4.59 (m, 1H), 3.77 – 3.62 (m, 2H), 3.54 – 3.33 (m, 3H), 3.26 – 3.09 (m, 1H), 2.96 (dd, *J* = 23.3, 15.8 Hz, 6H), 2.24 (dd, *J* = 6.1, 3.0 Hz, 1H), 1.85 – 1.69 (m, 3H), 1.65 – 1.53 (m, 1H), 1.51 – 1.34 (m, 2H); **^{13}C NMR (75 MHz, $CDCl_3$) δ** 152.0, 146.9, 129.7, 122.4, 121.5, 119.6, 119.1, 58.5, 58.1, 54.0, 52.3, 47.06, 46.4, 44.2, 28.1, 25.6, 24.6, 19.8, 13.3; **HRMS (ESI$^+$)** (*m/z*) calcd. for $C_{19}H_{26}N_5O_2^+$ $[M+H]^+$ 356.2008 found 356.2002.

(R)-3-(1-(quinuclidin-3-yl)-1H-1,2,3-triazol-4-yl)phenyl ethyl(methyl)carbamate ((R)-76c)

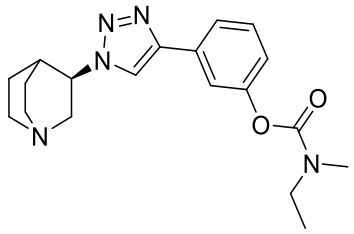

$C_{19}H_{25}N_5O_2$
Molecular Weight: 355,44 g/mol

(R)-76c was obtained from alkyne **78c** (83.25 mg, 0.44 mmol, 1 equiv) and 3-aminoquinuclidine **(R)-81** (100 mg, 0.44 mmol, 1 equiv) following the general procedure C and isolated as a yellow oil (70.1 mg, 45%).

NMR and MS data were in accordance with those reported above for **76c**
$[\alpha]_D$ = 10.92 (c = 0.05 in $CHCl_3$ at 23 °C)

(S)-3-(1-(quinuclidin-3-yl)-1H-1,2,3-triazol-4-yl)phenyl ethyl(methyl)carbamate ((S)-76c)

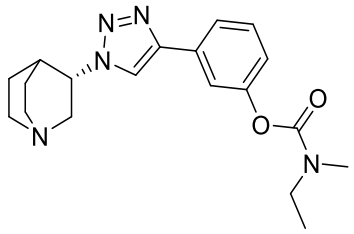

$C_{19}H_{25}N_5O_2$
Molecular Weight: 355,44 g/mol

(S)-76c was obtained from alkyne **78c** (83.25 mg, 0.44 mmol, 1 equiv) and 3-aminoquinuclidine **(S)-81** (100 mg, 0.44 mmol, 1 equiv) following the general procedure C and isolated as a yellow oil (62.4 mg, 40%).

NMR and MS data were in accordance with those reported above for **76c**
$[\alpha]_D$ = - 9.54 (c = 0.05 in $CHCl_3$ at 23 °C)

1-bromo-3-(2,2-dibromovinyl)benzene (102a)

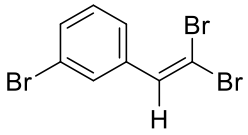

$C_8H_5Br_3$
Molecular Weight: 340,84 g/mol

102a was obtained from 3-bromobenzaldehyde **100a** (2g, 10.8 mmol, 1 equiv) following the general procedure D and isolated as a yellow oil (1.89 g, 51%).

^{1}H NMR (300 MHz, $CDCl_3$) δ 7.73 (t, *J* = 1.5 Hz, 1H), 7.56 – 7.44 (m, 3H), 7.32 – 7.28 (m, 1H).

Spectral data are in accordance with those reported previously:
Horibe, H.; Fukuda, Y.; Kondo, K.; Okuno, H.; Murakami, Y.; Aoyama, T. Asymmetric Kumada–Corriu Cross-Coupling Reaction with Pd2(Dba)3 and an N–Ar Axially Chiral Mimetic-Type Ligand Catalyst. *Tetrahedron* **2004**, *60* (47), 10701–10709.

1-bromo-4-(2,2-dibromovinyl)benzene (102b)

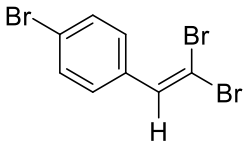

$C_8H_5Br_3$
Molecular Weight: 340,84 g/mol

102b was obtained from 4-bromobenzaldehyde **100b** (2g, 10.8 mmol, 1 equiv) following the general procedure D and isolated as a yellow oil (2.04 g, 55%).

^{1}H NMR (300 MHz, $CDCl_3$) δ 7.53 – 7.47 (m, 2H), 7.42 (d, *J* = 2.4 Hz, 2H), 7.40 – 7.38 (m, 1H); **^{13}C NMR (75 MHz, $CDCl_3$) δ** 135.8, 134.2, 131.7, 130.0, 122.7, 90.7.

Spectral data are in accordance with those reported previously:
Pawluć, P.; Hreczycho, G.; Walkowiak, J.; Marciniec, B. A New Facile Synthesis of 1,1-Dibromo-2-Arylethenes. *Synlett* **2007**, *2007* (13), 2061–2064

1-bromo-3-ethynylbenzene (101a)

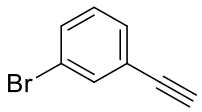

C_8H_5Br
Molecular Weight: 181,03 g/mol

101a was obtained from **102a** (500mg, 1.45 mmol, 1 equiv) following the general procedure E and isolated as a colorless oil (131 mg, 50%).

^{1}H NMR (300 MHz, $CDCl_3$) δ 7.64 (t, *J* = 1.7 Hz, 1H), 7.49 (ddd, *J* = 8.1, 1.9, 1.1 Hz, 1H), 7.45 – 7.38 (m, 1H), 7.19 (t, *J* = 7.9 Hz, 1H), 3.12 (s, 1H).

Spectral data are in accordance with those reported previously:
Malamas, M. S.; Barnes, K.; Johnson, M.; Hui, Y.; Zhou, P.; Turner, J.; Hu, Y.; Wagner, E.; Fan, K.; Chopra, R.; Olland, A.; Bard, J.; Pangalos, M.; Reinhart, P.; Robichaud, A. J. Di-Substituted Pyridinyl Aminohydantoins as Potent and Highly Selective Human β-Secretase (BACE1) Inhibitors. *Bioorg. Med. Chem.* **2010**, *18* (2), 630–639.

1-bromo-4-ethynylbenzene (101b)

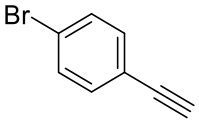

C_8H_5Br
Molecular Weight: 181,03 g/mol

101b was obtained from **102b** (1g, 2.9 mmol, 1 equiv) following the general procedure E and isolated as a colorless oil (308 mg, 59%).

^{1}H NMR (300 MHz, $CDCl_3$) δ 7.49 – 7.43 (m, 2H), 7.38 – 7.32 (m, 2H), 3.12 (s, 1H).

Spectral data are in accordance with those reported previously:
Kuang, C.; Yang, Q.; Senboku, H.; Tokuda, M. Synthesis of (Z)-1-Bromo-1-Alkenes and Terminal Alkynes from Anti-2,3-Dibromoalkanoic Acids by Microwave-Induced Reaction. *Tetrahedron* **2005**, *61* (16), 4043–4052.

(R)-3-(4-(3-bromophenyl)-1H-1,2,3-triazol-1-yl)quinuclidine ((R)-105a)

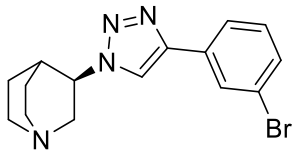

$C_{15}H_{17}BrN_4$
Molecular Weight: 333,23 g/mol

(R)-105a was obtained from **101a** (150 mg, 0.66 mmol, 1 equiv) and (R)-3-aminoquinuclidine **(R)-81** (119.5 mg, 0.66 mmol, 1 equiv) following general procedure C and isolated as a white solid (138.46 mg, 63%).

^{1}H NMR (300 MHz, MeOD) δ 8.45 (s, 1H), 7.98 (t, *J* = 1.7 Hz, 1H), 7.79 – 7.72 (m, 1H), 7.43 (ddd, *J* = 8.0, 1.9, 1.0 Hz, 1H), 7.29 (t, *J* = 7.9 Hz, 1H), 4.82 (s, 1H), 3.84 – 3.68 (m, 1H), 3.59 – 3.44 (m, 1H), 3.30 (s, 1H), 3.08 – 2.87 (m, 3H), 2.25 (d, *J* = 2.6 Hz, 1H), 1.86 (s, 2H), 1.56 (s, 2H).

Spectral data are in accordance with those reported previously:
Ouach, A.; Vercouillie, J.; Bertrand, E.; Rodrigues, N.; Pin, F.; Serriere, S.; Boiaryna, L.; Chartier, A.; Percina, N.; Tangpong, P.; Gulhan, Z.; Mothes, C.; Deloye, J.-B.; Guilloteau, D.; Page, G.; Suzenet, F.; Buron, F.; Chalon, S.; Routier, S. Bis(Het)Aryl-1,2,3-Triazole Quinuclidines as A7 Nicotinic Acetylcholine Receptor Ligands: Synthesis, Structure Affinity Relationships, Agonism Activity, [18F]-Radiolabeling and PET Study in Rats. *Eur. J. Med. Chem.* **2019**, *179*, 449–469.

(R)-3-(4-(4-bromophenyl)-1H-1,2,3-triazol-1-yl)quinuclidine ((R)-105b)

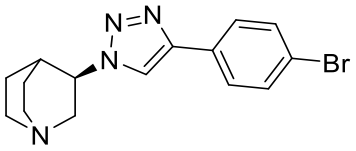

$C_{15}H_{17}BrN_4$
Molecular Weight: 333,23 g/mol

(R)-105b was obtained from **101b** (150 mg, 0.66 mmol, 1 equiv) and (R)-3-aminoquinuclidine **(R)-81** (119.5 mg, 0.66 mmol, 1 equiv) following general procedure C and isolated as a white solid (31.1 mg, 14%).

^{1}H NMR (300 MHz, MeOD) δ 8.47 (s, 1H), 7.76 (d, *J = 8.5* Hz, 2H), 7.63 – 7.54 (d, *J = 8.6* Hz, 2H), 4.91 – 4.86 (m, 1H), 3.77 (dd, *J* = 13.9, 4.2 Hz, 1H), 3.58 – 3.45 (m, 1H), 3.15 (d, *J* = 14.7 Hz, 1H), 3.02 – 2.89 (m, 3H), 2.31 (dd, *J* = 6.2, 3.1 Hz, 1H), 1.96 – 1.85 (m, 2H), 1.68 – 1.53 (m, 2H).

Spectral data are in accordance with those reported previously:

Ouach, A.; Vercouillie, J.; Bertrand, E.; Rodrigues, N.; Pin, F.; Serriere, S.; Boiaryna, L.; Chartier, A.; Percina, N.; Tangpong, P.; Gulhan, Z.; Mothes, C.; Deloye, J.-B.; Guilloteau, D.; Page, G.; Suzenet, F.; Buron, F.; Chalon, S.; Routier, S. Bis(Het)Aryl-1,2,3-Triazole Quinuclidines as A7 Nicotinic Acetylcholine Receptor Ligands: Synthesis, Structure Affinity Relationships, Agonism Activity, [18F]-Radiolabeling and PET Study in Rats. *Eur. J. Med. Chem.* **2019**, *179*, 449–469.

(R)-3'-(1-(quinuclidin-3-yl)-1H-1,2,3-triazol-4-yl)-[1,1'-biphenyl]-4-ol ((R)-108)

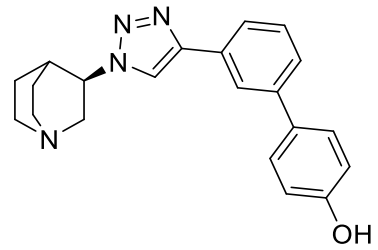

$C_{21}H_{22}N_4O$
Molecular Weight: 346,43 g/mol

(R)-108 was obtained from **(R)-105a** (15.2 mg, 0.045 mmol, 1 equiv) and 4-hydroxyphenylboronic acid **106** (7.45 mg, 0.055 mmol, 1.2 equiv) following general procedure F and isolated as a yellow oil (10.15 mg, 65%).

^{1}H NMR (300 MHz, MeOD) δ 8.59 – 8.48 (m, 1H), 7.88 – 7.81 (m, 1H), 7.77 – 7.31 (m, 5H), 6.90 – 6.87 (m, 1H), 5.13 – 5.03 (m, 1H), 4.03 (d, *J* = 14.1 Hz, 1H), 3.81 – 3.48 (m, 2H), 3.35 (s, 2H), 3.25 – 3.14 (m, 3H), 2.50 – 2.41 (m, 1H), 2.06 (s, 2H), 1.81 – 1.70 (m, 2H); **HRMS (ESI$^+$)** (*m/z*) calcd. for $C_{21}H_{23}N_4O^+$ [M+H$^+$] 347.1794 in progress; **[α]$_D$** = - 28.51 (c = 0.05 in $CHCl_3$ at 23 °C).

Despite an extended time of acquisition, ^{13}C NMR experiment could not be performed on compound **(R)-108**.

(R)-3'-(1-(quinuclidin-3-yl)-1H-1,2,3-triazol-4-yl)-[1,1'-biphenyl]-3-ol ((R)-109)

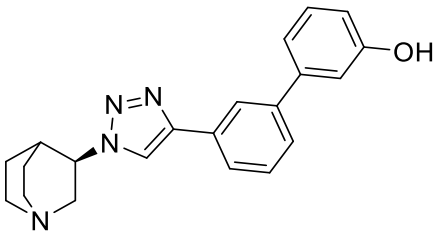

$C_{21}H_{22}N_4O$
Molecular Weight: 346,43 g/mol

(R)-109 was obtained from **(R)-105a** (50 mg, 0.15 mmol, 1 equiv) and 3-hydroxyphenylboronic acid **107** (24.82 mg, 0.18 mmol, 1.2 equiv) following general procedure F and isolated as a yellow oil (45.19 mg, 87%).

^{1}H NMR (300 MHz, MeOD) δ 8.51 (s, 1H), 7.80 (dd, *J* = 13.3, 7.8 Hz, 1H), 7.56 (d, *J* = 7.0 Hz, 1H), 7.51 – 7.38 (m, 1H), 7.26 (t, *J* = 7.8 Hz, 1H), 7.17 – 7.08 (m, 2H), 6.83 – 6.77 (m, 1H), 5.01 – 4.91 (m, 1H), 3.88 (dd, *J* = 14.2, 4.7 Hz, 1H), 3.66 – 3.53 (m, 1H), 3.35 (s, 1H), 3.29 – 3.15 (m, 1H), 3.10 – 3.01 (m, 3H), 2.42 – 2.32 (m, 2H), 1.96 (dd, *J* = 8.5, 4.1 Hz, 2H), 1.76 – 1.55 (m, 2H); **^{13}C NMR (75 MHz, MeOD) δ** 159.0, 148.9, 143.3, 132.1, 130.9, 130.5, 130.0, 127.9, 125.6, 125.2, 122.0, 119.3, 115.6, 114.9, 58.5, 52.0, 47.8, 47.5, 29.0, 25.1, 20.0; **HRMS (ESI$^+$)** (*m/z*) calcd. for $C_{21}H_{23}N_4O^+$ [M+H$^+$] 347.1794 in progress; **$[\alpha]_D$** = - 33.3 (c = 0.05 in $CHCl_3$ at 23 °C).

(R)-4'-(1-(quinuclidin-3-yl)-1H-1,2,3-triazol-4-yl)-[1,1'-biphenyl]-4-ol ((R)-110)

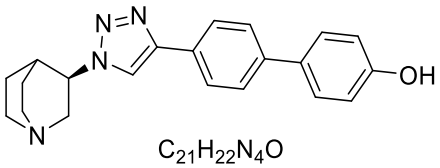

$C_{21}H_{22}N_4O$
Molecular Weight: 346,43 g/mol

(R)-110 was obtained from **(R)-105b** (27 mg, 0.08 mmol, 1 equiv) and 4-hydroxyphenylboronic acid **106** (13.42 mg, 0.097 mmol, 1.2 equiv) following general procedure F and isolated as a yellow oil (16.60 mg, 60%).

^{1}H NMR (300 MHz, MeOD) δ 8.06 (dd, *J* = 8.3, 2.4 Hz, 1H), 7.88 (d, *J* = 8.4 Hz, 1H), 7.78 – 7.40 (m, 5H), 6.91 – 6.82 (m, 1H), 5.22 (s, 1H), 4.32 – 4.11 (m, 1H), 3.88 (d, *J* = 18.8 Hz, 1H), 3.55 (dd, *J* = 13.1, 6.6 Hz, 1H), 3.43 – 3.33 (m, 2H), 3.08 (dd, *J* = 5.2, 3.6 Hz, 1H), 2.63 – 2.47 (m, 1H), 2.36 – 2.23 (m, 1H), 2.15 (t, *J* = 19.6 Hz, 1H), 2.04 (d, *J* = 10.0 Hz, 2H), 1.86 (s, 2H); **^{13}C NMR (75 MHz, MeOD) δ** 158.5, 149.0, 142.4, 133.9, 133.15, 132.9, 130.1, 130.0, 129.0, 127.9, 123.8, 122.5, 116.7, 51.2, 47.5, 47.8, 33.0, 32.9, 30.7,

28.5, 18.9; **HRMS (ESI$^+$)** (*m/z*) calcd. for $C_{21}H_{23}N_4O^+$ [M+H$^+$] 347.1794 in progress; **[α]$_D$** = - 35.5 (c = 0.05 in $CHCl_3$ at 23 °C).

(R)-4'-(1-(quinuclidin-3-yl)-1H-1,2,3-triazol-4-yl)-[1,1'-biphenyl]-3-ol ((R)-111)

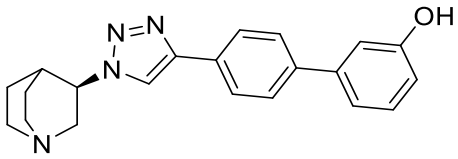

$C_{21}H_{22}N_4O$
Molecular Weight: 346,43 g/mol

(R)-111 was obtained from **(R)-105b** (31.1 mg, 0.09 mmol, 1 equiv) and 3-hydroxyphenylboronic acid **107** (15.24 mg, 0.11 mmol, 1.2 equiv) following general procedure F and isolated as a yellow oil (16.63 mg, 53%).

^{1}H NMR (300 MHz, MeOD) δ 8.67 – 8.42 (m, 1H), 8.05 (dd, *J* = 8.5, 2.7 Hz, 1H), 7.86 (ddd, *J* = 12.9, 8.2, 4.8 Hz, 1H), 7.80 – 7.51 (m, 4H), 7.50 – 7.41 (m, 1H), 5.06 – 4.97 (m, 1H), 4.00 – 3.85 (m, 1H), 3.67 (ddd, *J* = 12.9, 8.5, 2.6 Hz, 1H), 3.34 (d, *J* = 5.6 Hz, 1H), 3.11 (dd, *J* = 15.9, 7.0 Hz, 3H), 2.45 – 2.37 (m, 1H), 2.07 – 1.93 (m, 2H), 1.71 (d, *J* = 4.1 Hz, 2H), 1.26 (d, *J* = 2.8 Hz, 2H); **^{13}C NMR (75 MHz, MeOD) δ** 133.9, 133.7, 133.2, 133.0, 130.1, 130.0, 129.9, 129.4, 128.4, 127.0, 126.8, 126.7, 58.5, 51.9, 47.8, 47.5, 29.0, 25.1, 24.9, 19.9; **HRMS (ESI$^+$)** (*m/z*) calcd. for $C_{21}H_{23}N_4O^+$ [M+H$^+$] 347.1794 in progress; **[α]$_D$** = - 28.92 (c = 0.05 in $CHCl_3$ at 23 °C).

(R)-3'-(1-(quinuclidin-3-yl)-1H-1,2,3-triazol-4-yl)-[1,1'-biphenyl]-3-yl dimethylcarbamate ((R)-96a)

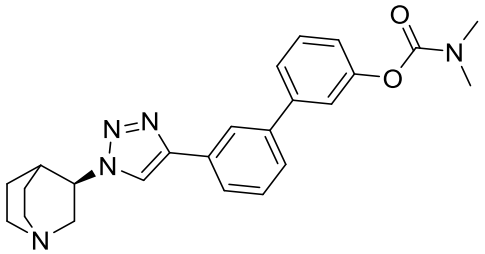

$C_{24}H_{27}N_5O_2$
Molecular Weight: 417,50 g/mol

(R)-96a was obtained from **(R)-109** (30 mg, 0.08 mmol, 1 equiv) and dimethylcarbamoyl chloride **91a** (0.13 mmol, 1.5 equiv) following general procedure B and isolated as a pale yellow oil (13.34 mg, 40%).

^{1}H NMR (300 MHz, MeOD) δ 8.54 (s, 1H), 8.12 (t, *J* = 1.5 Hz, 1H), 7.89 – 7.81 (m, 1H), 7.66 – 7.42 (m, 4H), 7.12 (ddd, *J* = 8.0, 2.3, 1.1 Hz, 1H), 4.93 – 4.86 (m, 1H), 3.78 (dd, *J* = 14.2, 5.0 Hz, 1H), 3.52 (ddd, *J*

= 14.3, 9.9, 2.3 Hz, 1H), 3.34 (d, *J* = 5.4 Hz, 1H), 3.16 (s, 3H), 3.05 – 2.89 (m, 6H), 2.32 (dd, *J* = 6.1, 3.0 Hz, 2H), 1.92 (dd, *J* = 9.7, 4.8 Hz, 2H), 1.69 – 1.55 (m, 2H); **^{13}C NMR (75 MHz, MeOD) δ** 156.8, 153.4, 148.6, 143.4, 142.2, 132.4, 130.7, 127.9, 125.9, 125.2, 122.5, 122.0, 121.6, 59.2, 52.4, 47.8, 47.5, 36.8, 29.2, 25.97, 20.5 (2 carbon signals are missing despite an extended acquisition time); **HRMS (ESI$^+$)** (*m/z*) calcd. for $C_{24}H_{28}N_5O_2^+$ [M+H$^+$] 418.2165 in progress; **[α]$_D$** = 26.7 (c = 0.05 in $CHCl_3$ at 23 °C).

(R)-3'-(1-(quinuclidin-3-yl)-1H-1,2,3-triazol-4-yl)-[1,1'-biphenyl]-3-yl diethylcarbamate ((R)-96b)

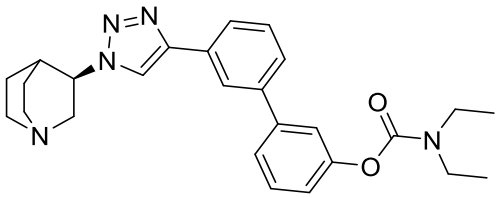

$C_{26}H_{31}N_5O_2$
Molecular Weight: 445,57 g/mol

(R)-96b was obtained from **(R)-109** (10.00 mg, 0.03 mmol, 1 equiv) and diethylcarbamoyl chloride **91b** (0.04 mmol, 1.5 equiv) following general procedure B and isolated as a pale yellow oil (6.14 mg, 46%).

^{1}H NMR (300 MHz, MeOD) δ 8.56 (d, *J* = 3.2 Hz, 1H), 8.13 (d, *J* = 1.6 Hz, 1H), 7.86 (d, *J* = 7.7 Hz, 1H), 7.64 (dd, *J* = 6.5, 1.6 Hz, 1H), 7.60 – 7.43 (m, 3H), 7.12 (ddd, *J* = 7.9, 2.2, 1.0 Hz, 1H), 4.95 (dd, *J* = 12.2, 7.2 Hz, 1H), 3.88 (dd, *J* = 14.2, 4.9 Hz, 1H), 3.67 – 3.49 (m, 4H), 3.48 – 3.37 (m, 3H), 3.35 (s, 2H), 3.11 – 2.97 (m, 4H), 2.38 (dd, *J* = 6.2, 3.0 Hz, 1H), 2.02 – 1.91 (m, 3H), 1.67 (dt, *J* = 25.9, 12.8 Hz, 4H); **^{13}C NMR (75 MHz, MeOD) δ** 154.7, 151.9, 147.3, 142.1, 140.8, 130.9, 129.4, 126.6, 124.6, 123.8, 121.2, 120.6, 120.1, 57.4, 50.8, 46.4, 46.1, 42.1, 29.4, 27.7, 24.1, 22.6, 18.8. (1 carbon signals are missing despite an extended acquisition time); **HRMS (ESI$^+$)** (*m/z*) calcd. for $C_{26}H_{32}N_5O_2^+$ [M+H$^+$] 446.2478 in progress; **[α]$_D$** = 22.6 (c = 0.05 in $CHCl_3$ at 23 °C).

(R)-3'-(1-(quinuclidin-3-yl)-1H-1,2,3-triazol-4-yl)-[1,1'-biphenyl]-3-yl ethyl(methyl)carbamate ((R)-96c)

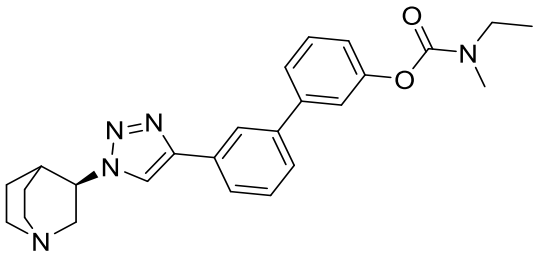

$C_{25}H_{29}N_5O_2$
Molecular Weight: 431,54 g/mol

(R)-96c was obtained from **(R)-109** (10.00 mg, 0.03 mmol, 1 equiv) and **91c** (0.04 mmol, 1.5 equiv) following general procedure B and isolated as a yellow oil (9.18 mg, 71%).

^{1}H NMR (300 MHz, MeOD) δ 8.56 (s, 1H), 8.13 (d, *J* = 1.6 Hz, 1H), 7.89 – 7.83 (m, 1H), 7.68 – 7.41 (m, 4H), 7.12 (dd, *J* = 8.0, 1.2 Hz, 1H), 4.96 – 4.87 (m, 1H), 3.81 (dd, *J* = 14.3, 5.0 Hz, 1H), 3.61 – 3.48 (m, 2H), 3.43 (dd, *J* = 14.3, 7.3 Hz, 1H), 3.23 – 3.11 (m, 2H), 3.04 – 2.92 (m, 4H), 2.35 (dd, *J* = 6.2, 3.1 Hz, 2H), 1.94 (dd, *J* = 9.3, 4.3 Hz, 3H), 1.76 – 1.56 (m, 3H), 1.21 (t, *J* = 7.1 Hz, 2H); **^{13}C NMR (75 MHz, MeOD) δ** 148.4, 143.7, 138.5, 137.2, 127.4, 125.9, 125.7, 123.0, 121.0, 120.30, 120.1, 117.5, 117.0, 54.1, 47.4, 42.8, 42.5, 40.2, 25.7, 24.2, 20.9, 15.4. (three carbon signals are missing despite an extended acquisition time); **HRMS (ESI$^+$)** (*m/z*) calcd. for $C_{25}H_{30}N_5O_2^+$ [M+H$^+$] 432.2321 in progress; **[α]$_D$** = 43.32 (c = 0.05 in $CHCl_3$ at 23 °C).

(R)-3'-(1-(quinuclidin-3-yl)-1H-1,2,3-triazol-4-yl)-[1,1'-biphenyl]-4-yl dimethylcarbamate ((R)-97a)

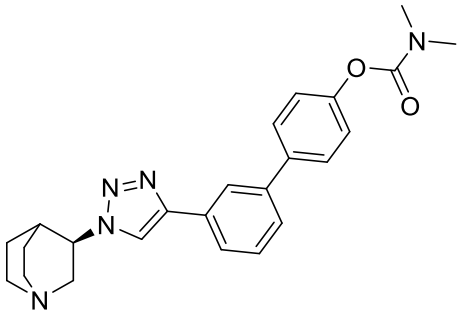

$C_{24}H_{27}N_5O_2$
Molecular Weight: 417,51 g/mol

(R)-97a was obtained from **(R)-108** (10.00 mg, 0.03 mmol, 1 equiv) and dimethylcarbamoyl chloride **91a** (0.04 mmol, 1.5 equiv) following general procedure B and isolated as a pale yellow oil (4.5 mg, 36%).

^{1}H NMR (300 MHz, MeOD) δ 8.55 (s, 1H), 8.12 (t, *J* = 1.6 Hz, 1H), 7.87 – 7.80 (m, 5H),7.25 – 7.18 (m, 1H), 4.99 – 4.90 (m, 1H), 3.86 (dd, *J* = 14.4, 4.6 Hz, 1H), 3.67 – 3.51 (m, 1H), 3.23 (d, *J* = 12.5 Hz, 2H), 3.15 (s, 2H), 3.09 – 2.96 (m, 6H), 2.41 – 2.30 (m, 1H), 2.01 – 1.89 (m, 2H), 1.66 (d, *J* = 12.3 Hz, 3H); **^{13}C NMR (75 MHz, MeOD) δ** 148.8, 142.4, 139.3, 133.9, 132.3, 130.6, 130.3, 129.0, 127.9, 126.7, 125.6, 123.3, 122.5, 58.9, 52.2, 47.8, 47.5, 36.8, 29.1, 25.6, 20.6, 14.5. (one carbon signal is missing despite an extended acquisition time); **HRMS (ESI^{+})** (*m/z*) calcd. for $C_{24}H_{28}N_5O_2^{+}$ [M+H^{+}] 418.2165 in progress; **$[\alpha]_D$** = 31.2 (c = 0.05 in $CHCl_3$ at 23 °C).

(R)-3'-(1-(quinuclidin-3-yl)-1H-1,2,3-triazol-4-yl)-[1,1'-biphenyl]-4-yl diethylcarbamate ((R)-97b)

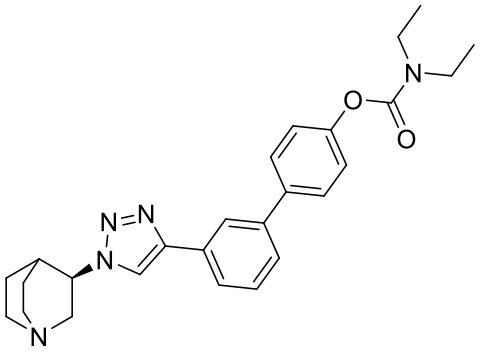

$C_{26}H_{31}N_5O_2$
Molecular Weight: 445,57 g/mol

(R)-97b was obtained from **(R)-108** (10.00 mg, 0.023 mmol, 1 equiv) and diethylcarbamoyl chloride **91b** (0.033 mmol, 1.5 equiv) following general procedure B and isolated as a colourless oil (5.22 mg, 51%).

^{1}H NMR (300 MHz, MeOD) δ 8.65 (s, 1H), 7.84 (d, *J* = 7.7 Hz, 1H), 7.73 (d, *J* = 8.6 Hz, 2H), 7.67 – 7.61 (m, 1H), 7.51 (ddd, *J* = 21.7, 12.3, 6.6 Hz, 2H), 7.22 (d, *J* = 8.7 Hz, 1H), 5.33 (s, 1H), 4.31 (dd, *J* = 14.1, 4.3 Hz, 1H), 3.99 (t, *J* = 12.2 Hz, 1H), 3.70 – 3.36 (m, 8H), 3.34 (d, *J* = 6.1 Hz, 5H), 2.63 (dd, *J* = 6.5, 3.2 Hz, 1H), 2.21 (dt, *J* = 18.6, 9.1 Hz, 2H), 2.00 – 1.84 (m, 2H), 1.51 (d, *J* = 7.3 Hz, 2H); **HRMS (ESI^{+})** (*m/z*) calcd. for $C_{26}H_{32}N_5O_2^{+}$ [M+H^{+}] 446.2478 in progress; **$[\alpha]_D$** = - 34.5 (c = 0.05 in $CHCl_3$ at 23 °C).

Compound **(R)-97b** was obtained in too low quantities to perform ^{13}C NMR experiment.

(R)-3'-(1-(quinuclidin-3-yl)-1H-1,2,3-triazol-4-yl)-[1,1'-biphenyl]-4-yl ethyl(methyl)carbamate ((R)-97c)

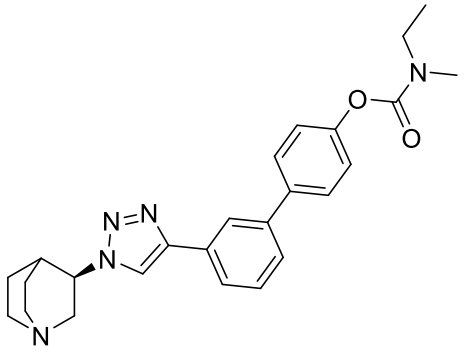

$C_{25}H_{29}N_5O_2$
Molecular Weight: 431,54 g/mol

(R)-97c was obtained from **(R)-108** (10.00 mg, 0.03 mmol, 1 equiv) and **91c** (0.045 mmol, 1.5 equiv) following general procedure B and isolated as a colourless oil (6.2 mg, 48%).

^{1}H NMR (300 MHz, MeOD) δ 8.55 (s, 1H), 8.12 (s, 1H), 7.88 – 7.80 (m, 1H), 7.75 – 7.68 (m, 2H), 7.67 – 7.39 (m, 3H), 7.22 (d, *J* = 8.6 Hz, 1H), 4.91 (s, 1H), 3.81 (dd, *J* = 14.2, 4.6 Hz, 1H), 3.62 – 3.37 (m, 3H), 3.28 – 3.17 (m, 1H), 3.11 (d, *J* = 14.1 Hz, 1H), 2.99 (d, *J* = 13.1 Hz, 4H), 2.34 (dt, *J* = 5.6, 2.9 Hz, 1H), 2.00 – 1.85 (m, 2H), 1.79 – 1.49 (m, 3H), 1.30 (d, *J* = 5.7 Hz, 3H); **^{13}C NMR (75 MHz, MeOD) δ** 152.6, 148.7, 142.4,138.7, 132.3, 130.6, 130.0, 129.0, 127.9, 126.7, 125.4, 123.3, 122.5, 58.9, 52.4, 47.8, 47.5, 45.2, 34.5, 30.7, 29.2, 25.9, 20.5 (two carbons are missing despite an extended acquisition time); **HRMS (ESI$^+$)** (*m/z*) calcd. for $C_{25}H_{30}N_5O_2^+$ [M+H$^+$] 432.2321 in progress; **[α]$_D$** = - 44.5 (c = 0.05 in $CHCl_3$ at 23 °C).

(R)-4'-(1-(quinuclidin-3-yl)-1H-1,2,3-triazol-4-yl)-[1,1'-biphenyl]-3-yl dimethylcarbamate ((R)-98a)

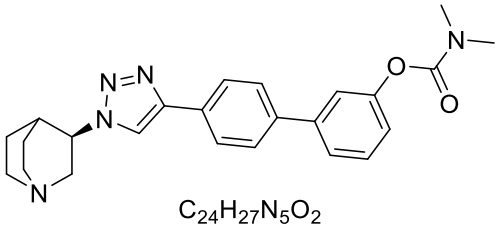

$C_{24}H_{27}N_5O_2$
Molecular Weight: 417,50 g/mol

(R)-98a was obtained from **(R)-111** (16.63 mg, 0.05 mmol, 1 equiv) and dimethylcarbamoyl chloride **91a** (0.07 mmol, 1.5 equiv) following general procedure B and isolated as a white solid (7.5 mg, 36%).

^{1}H NMR (300 MHz, MeOD) δ 8.38 (d, *J* = 5.2 Hz, 1H), 7.86 – 7.79 (m, 2H), 7.65 – 7.59 (m, 2H), 7.46 – 7.29 (m, 2H), 7.00 (ddd, *J* = 7.9, 2.3, 1.2 Hz, 1H), 4.84 – 4.76 (m, 1H), 3.71 (dd, *J* = 14.2, 5.1 Hz, 1H), 3.44

(ddd, *J* = 14.2, 9.9, 2.3 Hz, 1H), 3.25 (s, 1H), 3.06 (s, 3H), 2.95 – 2.85 (m, 6H), 2.24 (dd, *J* = 6.2, 3.1 Hz, 2H), 1.88 – 1.78 (m, 2H), 1.61 – 1.48 (m, 2H); **^{13}C NMR (75 MHz, MeOD) δ** 155.4, 152.0, 147.0, 141.8, 139.9, 129.7, 129.4, 127.1, 125.8, 123.5, 120.9, 120.5, 119ij.9, 57.7, 50.9, 46.4, 46.1, 35.5, 35.3, 27.8, 24.4, 19.0. . (1 carbon signal is missing despite an extended acquisition time); **HRMS (ESI$^+$)** (*m/z*) calcd. for $C_{24}H_{28}N_5O_2^+$ [M+H$^+$] 418.2165 in progress; **mp** = 139.9 °C; **[α]$_D$** = 108.12 (c = 0.05 in $CHCl_3$ at 23 °C).

(R)-4'-(1-(quinuclidin-3-yl)-1H-1,2,3-triazol-4-yl)-[1,1'-biphenyl]-3-yl ethyl(methyl)carbamate ((R)-98c)

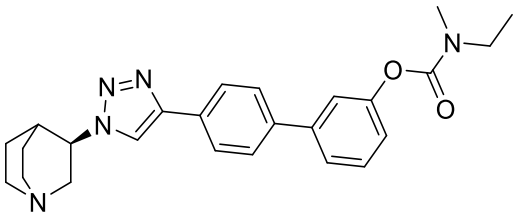

$C_{25}H_{29}N_5O_2$
Molecular Weight: 431,54 g/mol

(R)-98c was obtained from **(R)-111** (6 mg, 0.017 mmol, 1 equiv) and **91c** (0.026 mmol, 1.5 equiv) following general procedure B and isolated as a colourless oil (2.63 mg, 36%).

^{1}H NMR (300 MHz, MeOD) δ 8.54 (d, *J* = 7.0 Hz, 1H), 7.95 (d, *J* = 8.3 Hz, 1H), 7.74 (d, *J* = 8.4 Hz, 1H), 7.68 – 7.38 (m, 5H), 5.22 (s, 1H), 3.59 – 3.49 (m, 3H), 3.43 – 3.34 (m, 4H), 3.07 (d, 3H), 2.55 (d, *J* = 16.7 Hz, 2H), 2.36 – 2.24 (m, 2H), 2.22 – 2.10 (m, *J* = 13.3 Hz, 2H), 2.03 (s, 2H), 1.87 (s, 2H); **HRMS (ESI$^+$)** (*m/z*) calcd. for $C_{25}H_{30}N_5O_2^+$ [M+H$^+$] 432.2321 in progress; **[α]$_D$** = 160.35 (c = 0.05 in $CHCl_3$ at 23 °C).

Compound **(R)-98c** was obtained in too low quantities to perform ^{13}C NMR experiment.

(R)-3'-(1-(quinuclidin-3-yl)-1H-1,2,3-triazol-4-yl)-[1,1'-biphenyl]-4-yl diethylcarbamate ((R)-99a)

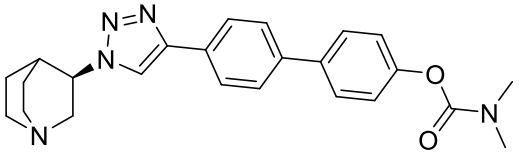

$C_{24}H_{27}N_5O_2$
Molecular Weight: 417,51 g/mol

(R)-99a was obtained from **(R)-110** (4.5 mg, 0.013 mmol, 1 equiv) and dimethylcarbamoyl chloride **91a** (0.02 mmol, 1.5 equiv) following general procedure B and isolated as a colourless oil (1.73 mg, 32%).

^{1}H NMR (300 MHz, MeOD) δ 8.48 (d, *J* = 30.1 Hz, 1H), 7.95 (d, *J* = 5.8 Hz, 1H), 7.69 – 7.42 (m, 5H), 7.10 (d, *J* = 8.7 Hz, 1H), 5.08 – 4.99 (m, 1H), 3.43 (d, *J* = 6.3 Hz, 2H), 3.08 – 2.86 (m, 4H), 2.40 (s, 1H), 2.21 (s, 2H), 2.01 (s, 4H), 1.70 (s, 2H), 1.50 (s, 3H); **HRMS (ESI$^+$)** (*m/z*) calcd. for $C_{24}H_{28}N_5O_2^+$ [M+H$^+$] 418.2165 in progress; **$[\alpha]_D$** = 128.5 (c = 0.05 in $CHCl_3$ at 23 °C).

Compound **(R)-99a** was obtained in too low quantities to perform ^{13}C NMR experiment.

(R)-4'-(1-(quinuclidin-3-yl)-1H-1,2,3-triazol-4-yl)-[1,1'-biphenyl]-4-yl ethyl(methyl)carbamate ((R)-99c)

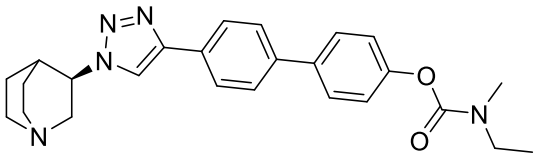

$C_{25}H_{29}N_5O_2$
Molecular Weight: 431,54 g/mol

(R)-99c was obtained from **(R)-110** (4.5 mg, 0.013 mmol, 1 equiv) and **91c** (0.02 mmol, 1.5 equiv) following general procedure B and isolated as a colourless oil (1.5 mg, 26%).

^{1}H NMR (300 MHz, MeOD) δ 8.62 (s, 1H), 8.06 (d, *J* = 8.4 Hz, 1H), 7.77 – 7.62 (m, 5H), 7.59 (dd, *J* = 7.0, 2.2 Hz, 1H), 5.35 (s, 1H), 4.22 (d, *J* = 6.6 Hz, 1H), 3.65 (s, 1H), 3.55 (dd, *J* = 12.5, 5.8 Hz, 1H), 2.42 (s, 2H), 2.25 (d, *J* = 24.9 Hz, 3H), 2.03 (s, 3H), 1.66 (m, 9H); **HRMS (ESI$^+$)** (*m/z*) calcd. for $C_{25}H_{30}N_5O_2^+$ [M+H$^+$] 432.2321 in progress; **$[\alpha]_D$** = 140.24 (c = 0.05 in $CHCl_3$ at 23 °C).

Compound **(R)-99c** was obtained in too low quantities to perform ^{13}C NMR experiment.

1-benzylpiperidine-4-carbaldehyde (140)

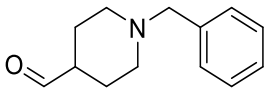

$C_{13}H_{17}NO$
Molecular Weight: 203,29 g/mol

A solution of oxalyl chloride **143** (0.45 mL, 5.2 mmol, 1.2 equiv) in dry DCM (6 mL) was cooled down to -78°C and a solution of DMSO (0.77 mL, 10.8 mmol, 2.5 equiv) in dry DCM (5 mL) was added dropwise. The reaction mixture was stirred at -78°C for 30 min and a solution of compound **142** (883 mg, 4.3 mmol, 1 equiv) in dry DCM (5 mL) was added dropwise. The resulting mixture was stirred at -78°C for another 30 min, Et_3N (3 mL, 21.7 mmol, 5 equiv) was added dropwise to the mixture which was stirred

for another 30 min at -78°C. The mixture was allowed to cool down to rt and water was added, the mixture was extracted with EtOAc, the combined organic layers were washed with water and brine and dried over Na_2SO_4. The solvent was removed under reduce pressure to give compound **140** as a yellow oil used without further purification (831.7 mg, 95%).

^{1}H NMR (300 MHz, $CDCl_3$) δ 9.63 (s, 1H), 7.32 – 7.27 (m, 5H), 3.49 (s, 2H), 2.85 – 2.76 (m, 2H), 2.27 – 2.19 (m, 1H), 2.09 (td, *J* = 11.2, 2.5 Hz, 2H), 1.91 – 1.82 (m, 2H), 1.74 – 1.59 (m, 2H).

Spectral data are in accordance with those reported previously:
Woo Lee, H.; Leol Yoo, C.; Uk Lee, S.; Kwon Kang, S. Effective Procedure for the Oxidative Cleavage of Olefins by OsO4-NaIO4. *HETEROCYCLES* **2009**, *78* (7), 1837.

3-(1-benzylpiperidin-4-yl)-1-(4-bromophenyl)-3-hydroxypropan-1-one (139)

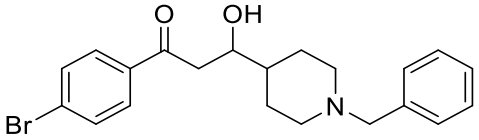

$C_{21}H_{24}BrNO_2$
Molecular Weight: 402,33 g/mol

To a solution of LiHMDS 1M in THF (2 mL, 2 mmol, 1 equiv) was added a solution of 4'-bromoacetophenone **141** (398 mg, 2 mmol, 1 equiv) in dry THF (5 mL) at -78°C. The mixture was stirred at that temperature for 15 min followed by the addition of a solution of compound **140** (415.7 mg, 2 mmol, 1 equiv) in dry THF (5 mL). The resulting mixture was stirred at -78°C for another 45 min. After completion determined by TLC, water (20 mL) was added to the mixture which was, then, allowed to warm up at rt. The pH was adjusted at pH = 4 with an aq. solution of HCl and the reaction mixture was extracted with EtOAc. The combined organic layer's pH was adjusted at pH = 9.5 with an aq. solution of NaOH, dried over Na_2SO_4 and the solvent was evaporated under reduce pressure to give compound **139** as a colourless oil without further purification (128 mg, 16%).

4-acetylphenyl trifluoromethanesulfonate (150)

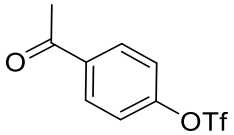

$C_9H_7F_3O_4S$
MolecularWeight: 268,21 g/mol

150 was obtained from 4-hydroxyaetophenone **152** (2 g, 14.7 mmol, 1 equiv) following the general procedure G and isolated as an orange solid (3.05 g, 78%).

^{1}H NMR (300 MHz, $CDCl_3$) δ 8.08 – 8.02 (m, 2H), 7.40 – 7.36 (m, 2H), 2.62 (s, 3H); **^{13}C NMR (75 MHz, $CDCl_3$)** δ 196.1, 152.5, 136.0, 130.7, 121.7, 116.6, 26.6.

The NMR spectra matched those reported in the literature for 4-acethylphenyl trifluoromethanesulfonate [CAS: 109613-00-5].

3-acetylphenyl trifluoromethanesulfonate (151)

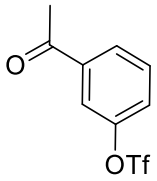

$C_9H_7F_3O_4S$
Molecular Weight:268,21 g/mol

151 was obtained from 3-hydroxyacetophenone **153** (2 g, 14.7 mmol, 1 equiv) following the general procedure G and isolated as a brown oil (2.7 g, 71%).

^{1}H NMR (300 MHz, $CDCl_3$) δ 8.00 – 7.95 (m, 1H), 7.87 – 7.84 (m, 1H), 7.62 – 7.56 (m, 1H), 7.49 (ddd, *J* = 8.3, 2.5, 1.0 Hz, 1H), 2.60 (s, 3H); **^{13}C NMR (75 MHz, $CDCl_3$)** δ 195.9, 149.9, 139.4, 130.8, 128.3, 125.9, 121.1, 116.7, 26.8.

The NMR spectra matched those reported in the literature for 3-acethylphenyl trifluoromethanesulfonate [CAS: 138313-22-1].

1-(4-((trimethylsilyl)ethynyl)phenyl)ethenone (178)

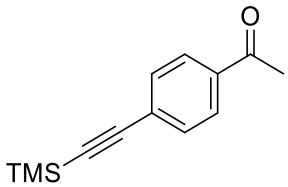

$C_{13}H_{16}OSi$
Molecular Weight: 216,35 g/mol

178 was obtained from **150** (2 g, 7.46 mmol, 1 equiv) following the general procedure H and isolated as an orange solid (1.07 g, 73%).

^{1}H NMR (300 MHz, $CDCl_3$) δ 7.91 – 7.86 (m, 2H), 7.56 – 7.51 (m, 2H), 2.59 (s, 3H), 0.26 (s, 9H).

Spectral data are in accordance with those reported previously:
Torborg, C.; Zapf, A.; Beller, M. Palladium Catalysts for Highly Selective Sonogashira Reactions of Aryl and Heteroaryl Bromides. *ChemSusChem* **2008**, *1* (1–2), 91–96.

1-(3-((trimethylsilyl)ethynyl)phenyl)ethenone (145)

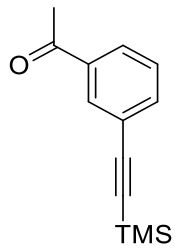

$C_{13}H_{16}OSi$
Molecular Weight: 216,36 g/mol

145 was obtained from **151** (2 g, 7.46 mmol, 1 equiv) following the general procedure H and isolated as an orange oil (1.3 g, 89%).

^{1}H NMR (300 MHz, $CDCl_3$) δ 8.04 (t, *J* = 1.5 Hz, 1H), 7.90 (dt, 1H), 7.64 (dt, 1H), 7.41 (t, *J* = 7.8 Hz, 1H), 2.60 (s, 3H), 0.26 (s, 9H).

Spectral data are in accordance with those reported previously:
Riva, B.; Griglio, A.; Serafini, M.; Cordero-Sanchez, C.; Aprile, S.; Di Paola, R.; Gugliandolo, E.; Alansary, D.; Biocotino, I.; Lim, D.; Grosa, G.; Galli, U.; Niemeyer, B.; Sorba, G.; Canonico, P. L.; Cuzzocrea, S.; Genazzani, A. A.; Pirali, T. Pyrtriazoles, a Novel Class of Store-Operated Calcium Entry Modulators: Discovery, Biological Profiling, and in Vivo Proof-of-Concept Efficacy in Acute Pancreatitis. *J. Med. Chem.* **2018**, *61* (21), 9756–9783.

1-(4-ethynylphenyl)ethenone (148)

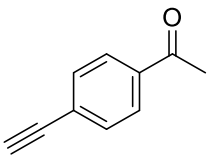

$C_{10}H_8O$
Molecular Weight: 144,17 g/mol

148 was obtained from **178** (1 g, 5.1 mmol, 1 equiv) following the general procedure I and isolated as a brown oil (380 mg, 60%).

^{1}H NMR (300 MHz, $CDCl_3$) δ 7.93 – 7.89 (m, 2H), 7.59 – 7.55 (m, 2H), 3.25 (s, 1H), 2.60 (s, 3H); **^{13}C NMR (75 MHz, $CDCl_3$)** δ 197.4, 136.9, 132.4, 128.3, 127.1, 82.9, 80.5, 26.7.; **mp :** 68.3 °C.

Spectral data are in accordance with those reported previously:
Kabalka, G. W.; Zhou, L.-L.; Wang, L.; Pagni, R. M. A Microwave-Enhanced, Solventless Mannich Condensation of Terminal Alkynes and Secondary Amines with Para-Formaldehyde on Cuprous Iodide Doped Alumina. *Tetrahedron* **2006**, *62* (5), 857–867.

1-(3-ethynylphenyl)ethenone (149)

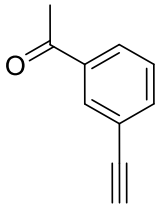

$C_{10}H_8O$
Molecular Weight: 144,17 g/mol

149 was obtained from **145** (1.3 g, 6.6 mmol, 1 equiv) following the general procedure I and isolated as a yellow solid (380 mg, 46%).

^{1}H NMR (300 MHz, $CDCl_3$) δ 8.06 (dd, *J* = 3.4, 1.9 Hz, 1H), 7.96 – 7.91 (m, 1H), 7.69 – 7.65 (m, 1H), 7.47 – 7.40 (m, 1H), 3.13 (s, 1H), 2.60 (s, 3H); **^{13}C NMR (75 MHz, $CDCl_3$) δ** 197.3, 137.3, 136.5, 132.2, 128.8, 128.5, 122.9, 82.7, 78.4, 26.7.; **mp**: 55.5 °C.

Spectral data are in accordance with those reported previously:
Riva, B.; Griglio, A.; Serafini, M.; Cordero-Sanchez, C.; Aprile, S.; Di Paola, R.; Gugliandolo, E.; Alansary, D.; Biocotino, I.; Lim, D.; Grosa, G.; Galli, U.; Niemeyer, B.; Sorba, G.; Canonico, P. L.; Cuzzocrea, S.; Genazzani, A. A.; Pirali, T. Pyrtriazoles, a Novel Class of Store-Operated Calcium Entry Modulators: Discovery, Biological Profiling, and in Vivo Proof-of-Concept Efficacy in Acute Pancreatitis. *J. Med. Chem.* **2018**, *61* (21), 9756–9783.

1-(3-(1-(quinuclidin-3-yl)-1H-1,2,3-triazol-4-yl)phenyl)ethenone ((R)-147)

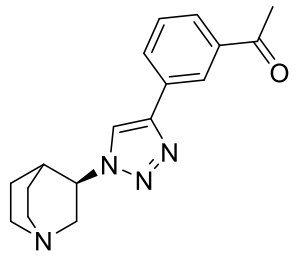

$C_{17}H_{20}N_4O$
Molecular Weight: 296,37 g/mol

(R)-147 was obtained from alkyne **149** and (R)-3-aminoquinuclidine **(R)-81** (200 mg, 1 mmol, 1 equiv) by following the general procedure C, as a white solid (77 mg, 26%).

^{1}H NMR (300 MHz, $CDCl_3$) δ 8.38 (t, *J* = 1.6 Hz, 1H), 8.14 – 8.08 (m, 1H), 7.95 – 7.88 (m, 2H), 7.54 (t, *J* = 7.8 Hz, 1H), 4.75 – 4.64 (m, 1H), 3.72 (dt, *J* = 11.0, 5.7 Hz, 1H), 3.53 (ddd, *J* = 14.4, 9.8, 2.2 Hz, 1H), 3.25 – 3.09 (m, 1H), 3.02 – 2.87 (m, 3H), 2.66 (s, 3H), 2.31 (dd, *J* = 6.2, 3.1 Hz, 1H), 1.92 – 1.61 (m, 3H), 1.57 – 1.42 (m, 1H); **^{13}C NMR (75 MHz, $CDCl_3$)** δ 198.1, 146.9, 137.7, 131.4, 130.3, 129.4, 128.2, 125.5, 119.6, 58.6, 52.7, 47.4, 47.1, 28.3, 26.9, 26.1, 20.1; **GC-MS** (*m/z*) 296 (2) 268 (20) 97 (100) 82 (20) 69 (20) 55 (20); **mp :** 65.6 °C.

piperidin-4-ylmethanol (157)

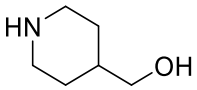

$C_6H_{13}NO$
Molecular Weight: 115,18 g/mol

To solution of $LiAlH_4$ (1.05 g, 27.6 mmol, 2.2 equiv) in dry THF (50 mL) at 0°C was added ethyl piperidine-4-carboxylate **156** (2 g, 12.7 mmol, 1 equiv). The reaction mixture was stirred at rt. for 24 h. After completion determined by TLC analysis, H_2O (2 mL) was added, followed by aq. NaOH (15%, 2 mL) and H_2O (5 mL). The resulting mixture was stirred at rt. for 1 h and filtrated. The filtrate was dried over $MgSO_4$ and concentrated under reduced pressure to give a colourless oil (1.3 g, 92%).

^{1}H NMR (300 MHz, $CDCl_3$) δ 3.38 (d, *J* = 6.4 Hz, 2H), 3.07-3.01 (m, 2H), 2.59-2.50 (m, 2H), 1.70-1.66 (m, 2H), 1.64-1.42 (m, 1H), 1.03-0.90 (m, 2H); **^{13}C NMR (75 MHz, $CDCl_3$) δ** 67.6, 46.3, 39.1, 30.0.

Spectral data are in accordance with those reported previously:

Renou, J.; Dias, J.; Mercey, G.; Verdelet, T.; Rousseau, C.; Gastellier, A.-J.; Arboléas, M.; Touvrey-Loiodice, M.; Baati, R.; Jean, L.; Nachon, F.; Renard, P.-Y. Synthesis and in Vitro Evaluation of Donepezil-Based Reactivators and Analogues for Nerve Agent-Inhibited Human Acetylcholinesterase. *RSC Adv.* **2016**, *6* (22), 17929–17940.

tert-butyl 4-(hydroxymethyl)piperidine-1-carboxylate (158)

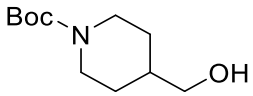

$C_{11}H_{21}NO_3$
Molecular Weight: 215,29 g/mol

To a solution of **157** (1.3 g, 11.3 mmol, 1 equiv) in THF (17 mL) and EtOAc (40 mL), was slowly added di-tert-butylcarbamate (2.57 g, 11.3 mmol, 1 equiv) and the resulting mixture was stirred at rt for 6h. The mixture was successively washed with sat. aq. $NaHCO_3$ and brine. The organic layer was dried over $MgSO_4$ and the solvent was removed under reduced pressure. The crude oil was purified by column chromatography (PE/EtOAc 50/50, v/v) to give compound **158** as a white solid (1.22 g, 50%).

^{1}H NMR (300 MHz, $CDCl_3$) δ 4.15 (d, *J* = 11.4 Hz, 2H), 3.53 (d, *J* = 6.0 Hz, 2H), 2.73 (t, *J* = 12.1 Hz, 2H), 1.76 (s, 1H), 1.69 (dt, *J* = 15.0, 12.2 Hz, 3H), 1.48 (s, 9H), 1.18 (ddd, *J* = 22.4, 12.6, 6.6 Hz, 2H).

Spectral data are in accordance with those reported previously:

Renou, J.; Dias, J.; Mercey, G.; Verdelet, T.; Rousseau, C.; Gastellier, A.-J.; Arboléas, M.; Touvrey-Loiodice, M.; Baati, R.; Jean, L.; Nachon, F.; Renard, P.-Y. Synthesis and in Vitro Evaluation of Donepezil-Based Reactivators and Analogues for Nerve Agent-Inhibited Human Acetylcholinesterase. *RSC Adv.* **2016**, *6* (22), 17929–17940.

tert-butyl 4-formylpiperidine-1-carboxylate (159)

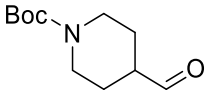

$C_{11}H_{19}NO_3$
Molecular Weight: 213,28 g/mol

To a solution of **158** (300 mg, 1.4 mmol, 1 equiv) in dry EtOAc was added 2-iodoxybenzoic acid (1.18 g, 4.2 mmol, 3 equiv) and the resulting mixture was stirred at 80°C for 2h and after completion determined by ^{1}H NMR, was allowed to cool down to rt. The solid was filtered, washed with EtOAc and

the solvent was evaporated under reduce pressure to give the crude aldehyde which was used in the next step of the synthesis without further purification.

tert-butyl-4-((5-bromo-1-oxo-1,3-dihydro-2H-inden-2-ylidene)methyl)piperidine-1-carboxylate (161)

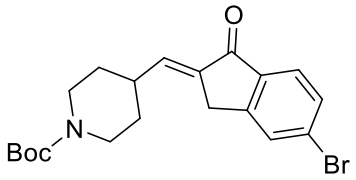

$C_{20}H_{24}BrNO_3$
Molecular Weight: 406,32 g/mol

To a solution of **159** (490 mg, 2.3 mmol, 1 equiv) in dry DCM were successively added 5-bromoindanone **160** (388.3 mg, 1.84 mmol, 0.8 equiv), tetra-n-butylammonium bromide (7.4 mg, 0.023 mmol, 0.01 equiv) and NaOH aq. 10% (3.2 mL). The resulting mixture was stirred at reflux for 5h and allowed to cool down to rt before being evaporated under reduced pressure. The obtained crude oil was recrystallized in MeOH to give compound **161** as a brown solid (410.9 mg, 44%).

^{1}H NMR (300 MHz, $CDCl_3$) δ 7.72 (d, *J* = 8.1 Hz, 1H), 7.67 (s, 1H), 7.55 (d, *J* = 8.1 Hz, 1H), 6.72 (d, *J* = 9.7 Hz, 1H), 4.12 (s, 2H), 3.70 (s, 2H), 2.82 (t, *J* = 12.2 Hz, 2H), 2.49 (d, *J* = 9.7 Hz, 1H), 1.70 (d, *J* = 10.5 Hz, 2H), 1.57 (s, 2H), 1.47 (s, 9H).

3-oxo-2,3-dihydro-1H-inden-5-yl trifluoromethanesulfonate (171)

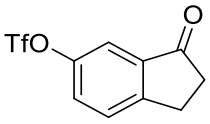

$C_{10}H_7F_3O_4S$
Molecular Weight: 280,22 g/mol

171 was obtained from 6-hydroxyindanone **169** (500 mg, 3.37 mmol, 1 equiv) following the general procedure G and isolated as a brown oil (678.4 mg, 72%).

^{1}H NMR (300 MHz, $CDCl_3$) δ 7.84 (d, *J* = 8.4 Hz, 1H), 7.41 (s, 1H), 7.28 (dd, *J* = 8.6, 2.3 Hz, 1H), 3.25 – 3.16 (m, 2H), 2.80 – 2.73 (m, 2H);**^{13}C NMR (75 MHz, $CDCl_3$) δ** 204.9, 154.7, 149.2, 139.1, 128.7, 127.6, 121.0, 116.6, 36.9, 25.7.

1-oxo-2,3-dihydro-1H-inden-5-yl trifluoromethanesulfonate (170)

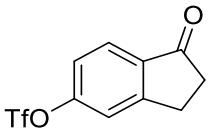

$C_{10}H_7F_3O_4S$
Molecular Weight: 280,22 g/mol

170 was obtained from 5-hydroxyindanone **168** (1 g, 6.7 mmol, 1 equiv) following the general procedure G and isolated as a yellow oil (1.407 g, 75%).

^{1}H NMR (300 MHz, $CDCl_3$) δ 7.82 (d, *J* = 9.3 Hz, 1H), 7.51-7.48 (m, 2H), 3.26-3.15 (m, 2H), 2.79 (t, *J* = 5.9 Hz, 2H);**^{13}C NMR (75 MHz, $CDCl_3$) δ** 204.7, 157.3, 153.8, 137.0, 126.0, 121.0, 119.9, 116.7, 36.5, 26.0.

Spectral data are in accordance with those reported previously:
Maegawa, T.; Kitamura, Y.; Sako, S.; Udzu, T.; Sakurai, A.; Tanaka, A.; Kobayashi, Y.; Endo, K.; Bora, U.; Kurita, T.; Kozaki, A.; Monguchi, Y.; Sajiki, H. Heterogeneous Pd/C-Catalyzed Ligand-Free, Room-Temperature Suzuki–Miyaura Coupling Reactions in Aqueous Media. *Chem. – Eur. J.* **2007**, *13* (20), 5937–5943.

6-((trimethylsilyl)ethynyl)-2,3-dihydro-1H-inden-1-one (175)

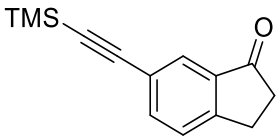

$C_{14}H_{16}OSi$
Molecular Weight: 228,37 g/mol

175 was obtained from **171** (600 mg, 2.14 mmol, 1 equiv) following the general procedure H and isolated as a yellow oil (292.75 mg, 60%).

^{1}H NMR (300 MHz, $CDCl_3$) δ 7.83 (d, *J* = 0.8 Hz, 1H), 7.64 (dd, *J* = 7.9, 1.6 Hz, 1H), 7.40 (dd, *J* = 7.9, 0.7 Hz, 1H), 3.12 (dd, *J* = 10.6, 4.4 Hz, 2H), 2.70 (ddd, *J* = 5.9, 5.3, 3.3 Hz, 2H), 0.25 (s, 9H); **^{13}C NMR (75 MHz, $CDCl_3$) δ** 206.1, 155.1, 137.0, 136.2, 127.4, 126.8, 122.7, 104.0, 95.3, 36.5, 26.0, -0.1.

5-((trimethylsilyl)ethynyl)-2,3-dihydro-1H-inden-1-one (163)

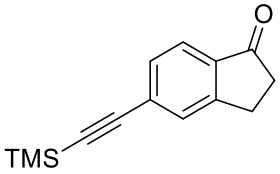

$C_{14}H_{16}OSi$
Molecular Weight: 228,37 g/mol

163 was obtained from **170** (1.2 g, 4.28 mmol, 1 equiv) following the general procedure H and isolated as a yellow oil (683 mg, 70%).

^{1}H NMR (300 MHz, $CDCl_3$) δ 7.68 (d, *J* = 8.0 Hz, 1H), 7.57 (s, 1H), 7.47 – 7.41 (m, 1H), 3.12 (dd, *J* = 12.2, 6.5 Hz, 2H), 2.70 (ddd, *J* = 5.9, 5.2, 3.3 Hz, 2H), 0.26 (s, 9H);**^{13}C NMR (75 MHz, $CDCl_3$) δ** 206.2, 154.9, 136.8, 131.3, 130.5, 129.5, 123.7, 104.4, 98.4, 36.4, 25.7, -0.1.

Spectral data are in accordance with those reported previously:
Ortega, R.; Hübner, H.; Gmeiner, P.; Masaguer, C. F. Aromatic Ring Functionalization of Benzolactam Derivatives: New Potent Dopamine D3 Receptor Ligands. *Bioorg. Med. Chem. Lett.* **2011**, *21* (9), 2670–2674.

6-ethynyl-2,3-dihydro-1H-inden-1-one (167)

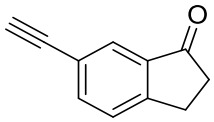

$C_{11}H_8O$
Molecular Weight: 156,18 g/mol

167 was obtained from **175** (150 mg, 0.66 mmol, 1 equiv) following the general procedure I and isolated as a yellow oil (87.51mg, 85%).

^{1}H NMR (300 MHz, $CDCl_3$) δ 7.87 (s, 1H), 7.68 (dd, *J* = 7.9, 1.6 Hz, 1H), 7.45 (d, *J* = 8.0 Hz, 1H), 3.15 (dd, *J* = 11.1, 5.2 Hz, 3H), 3.10 (s, 1H), 2.74 – 2.69 (m, 1H); **^{13}C NMR (75 MHz, $CDCl_3$) δ** 205.4, 155.0, 133.4, 132.6, 130.2, 128.0, 126.8, 84.5, 82.3, 33.7, 22.8; **mp** = 88.8 °C.

5-ethynyl-2,3-dihydro-1H-inden-1-one (166)

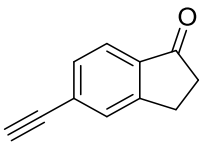

$C_{11}H_8O$
Molecular Weight: 156,18 g/mol

166 was obtained from **163** (150 mg, 0.66 mmol, 1 equiv) following the general procedure I and isolated as a yellow oil (90.60 mg, 88%).

^{1}H NMR (300 MHz, $CDCl_3$) δ 7.75 (dd, *J* = 7.7, 0.6 Hz, 1H), 7.55 (s, 1H), 7.42 (d, *J* = 8.8 Hz, 1H), 3.22 (s, 1H), 3.14-3.09 (m, 2H), 2.78-2.72 (m, 2H);**^{13}C NMR (75 MHz, $CDCl_3$) δ** 204.0, 154.9, 134.2, 133.6, 131.2, 129.2, 126.2, 83.6, 81.4, 34.3, 23.6.

Spectral data are in accordance with those reported previously:
Ortega, R.; Hübner, H.; Gmeiner, P.; Masaguer, C. F. Aromatic Ring Functionalization of Benzolactam Derivatives: New Potent Dopamine D3 Receptor Ligands. *Bioorg. Med. Chem. Lett.* **2011**, *21* (9), 2670–2674.

References

The manuscript references are listed following their appearance order, thus, the number are different from the one given in the text.

(1) Historique de la maladie d'Alzheimer : découverte, identification ... *Fondation Vaincre Alzheimer*.

(2) Alzheimer, A. über eigenartige Krankheitsfälle des späteren Alters. *Z. Für Gesamte Neurol. Psychiatr.* **1911**, *4* (1), 356.

(3) Fischer, O. Miliare Nekrosen mit drusigen Wucherungen der Neurofibril-len, eine regelma¨ssige Vera¨nderung der Hirnrinde bei seniler. *R DemenzMonatsschr Psychiat Neurol* **1907**, *22*, 361–372.

(4) Perusini, G. U¨ber klinisch und histologisch eigenartige psychischeErkrankungen des spa¨teren Lebensalters. *Nissl-Alzheimers HistolHistopathol Arb Hirnr* **1909**, *3*, 297–351.

(5) Glenner, G. G.; Wong, C. W. Alzheimer's Disease: Initial Report of the Purification and Characterization of a Novel Cerebrovascular Amyloid Protein. *Biochem. Biophys. Res. Commun.* **1984**, *120* (3), 885–890.

(6) Brion, J. P.; Passareiro, H.; Nunez, J.; Flament Durand, J. Mise en évidence immunologique de la protéine tau au niveau des lésions de dégénérescence neurofibrillaire de la maladie d'Alzheimer. *Arch. Biol. (Liege)* **1985**, *95*, 229–235.

(7) World Alzheimer Report 2015: The Global Impact of Dementia | Alzheimer's Disease International https://www.alz.co.uk/research/world-report-2015.

(8) Les symptômes de la maladie d'Alzheimer https://www.francealzheimer.org/maladie-dalzheimer-vos-questions-nos-reponses/symptomes-de-maladie-dalzheimer/.

(9) Diagnostic de la maladie d'Alzheimer. *Fondation pour la Recherche sur Alzheimer*.

(10) Salvatore, C.; Cerasa, A.; Castiglioni, I. MRI Characterizes the Progressive Course of AD and Predicts Conversion to Alzheimer's Dementia 24 Months Before Probable Diagnosis. *Front. Aging Neurosci.* **2018**, *10*.

(11) Sperling, R. A.; Jack, C. R.; Black, S. E.; Frosch, M. P.; Greenberg, S. M.; Hyman, B. T.; Scheltens, P.; Carrillo, M. C.; Thies, W.; Bednar, M. M.; et al. Amyloid-Related Imaging Abnormalities in Amyloid-Modifying Therapeutic Trials: Recommendations from the Alzheimer's Association Research Roundtable Workgroup. *Alzheimers Dement.* **2011**, *7* (4), 367–385.

(12) Ledig, C.; Schuh, A.; Guerrero, R.; Heckemann, R. A.; Rueckert, D. Structural Brain Imaging in Alzheimer's Disease and Mild Cognitive Impairment: Biomarker Analysis and Shared Morphometry Database. *Sci. Rep.* **2018**, *8* (1), 11258.

(13) Oukoloff, K.; Cieslikiewicz-Bouet, M.; Chao, S.; Da Costa Branquinho, E.; Bouteiller, C.; Jean, L.; Renard, P.-Y. PET and SPECT Radiotracers for Alzheimer's Disease. *Curr. Med. Chem.* **2015**, *22* (28), 3278–3304.

(14) Nordberg, A.; Rinne, J. O.; Kadir, A.; Långström, B. The Use of PET in Alzheimer Disease. *Nat. Rev. Neurol.* **2010**, *6* (2), 78–87.

(15) Schilling, L. P.; Zimmer, E. R.; Shin, M.; Leuzy, A.; Pascoal, T. A.; Benedet, A. L.; Borelli, W. V.; Palmini, A.; Gauthier, S.; Rosa-Neto, P. Imaging Alzheimer's Disease Pathophysiology with PET. *Dement. Neuropsychol.* **2016**, *10* (2), 79–90.

(16) Fischer, F. U.; Wolf, D.; Scheurich, A.; Fellgiebel, A.; Alzheimer's Disease Neuroimaging Initiative. Altered Whole-Brain White Matter Networks in Preclinical Alzheimer's Disease. *NeuroImage Clin.* **2015**, *8*, 660–666.

(17) Syed, Y. Y.; Deeks, E. [(18)F]Florbetaben: A Review in β-Amyloid PET Imaging in Cognitive Impairment. *CNS Drugs* **2015**, *29* (7), 605–613.

(18) Thal, D. R.; Beach, T. G.; Zanette, M.; Heurling, K.; Chakrabarty, A.; Ismail, A.; Smith, A. P. L.; Buckley, C. [(18)F]Flutemetamol Amyloid Positron Emission Tomography in Preclinical and

Symptomatic Alzheimer's Disease: Specific Detection of Advanced Phases of Amyloid-β Pathology. *Alzheimers Dement. J. Alzheimers Assoc.* **2015**, *11* (8), 975–985.

(19) Schonhaut, D. R.; McMillan, C. T.; Spina, S.; Dickerson, B. C.; Siderowf, A.; Devous, M. D.; Tsai, R.; Winer, J.; Russell, D. S.; Litvan, I.; et al. 18F-Flortaucipir Tau PET Distinguishes Established Progressive Supranuclear Palsy from Controls and Parkinson's Disease: A Multicenter Study. *Ann. Neurol.* **2017**, *82* (4), 622–634.

(20) Chiotis, K.; Saint-Aubert, L.; Savitcheva, I.; Jelic, V.; Andersen, P.; Jonasson, M.; Eriksson, J.; Lubberink, M.; Almkvist, O.; Wall, A.; et al. Imaging In-Vivo Tau Pathology in Alzheimer's Disease with THK5317 PET in a Multimodal Paradigm. *Eur. J. Nucl. Med. Mol. Imaging* **2016**, *43*, 1686–1699.

(21) Having a lumbar puncture https://www.alzheimers.org.uk/research/take-part-research/lumbar-puncture.

(22) Colovic, M. B.; Krstic, D. Z.; Lazarevic-Pasti, T. D.; Bondzic, A. M.; Vasic, V. M. Acetylcholinesterase Inhibitors: Pharmacology and Toxicology. *Curr. Neuropharmacol.* **2013**, *11* (3), 315–335.

(23) Acetylcholine Transmitter | Physiology Plus http://physiologyplus.com/acetylcholine-transmitter/.

(24) Bowen, D. M.; Smith, C. B.; White, P.; Davison, A. N. NEUROTRANSMITTER-RELATED ENZYMES AND INDICES OF HYPOXIA IN SENILE DEMENTIA AND OTHER ABIOTROPHIES. *Brain* **1976**, *99* (3), 459–496.

(25) Sugimoto, H.; Yamanishi, Y.; Iimura, Y.; Kawakami, Y. Donepezil Hydrochloride (E2020) and Other Acetylcholinesterase Inhibitors. *Curr. Med. Chem.* **2000**, *7* (3), 303–339.

(26) Sims, N. R.; Bowen, D. M.; Allen, S. J.; Smith, C. C. T.; Neary, D.; Thomas, D. J.; Davison, A. N. Presynaptic Cholinergic Dysfunction in Patients with Dementia. *J. Neurochem.* **1983**, *40* (2), 503–509.

(27) Ladner, C. J.; Lee, J. M. Pharmacological Drug Treatment of Alzheimer Disease: The Cholinergic Hypothesis Revisited. *J. Neuropathol. Exp. Neurol.* **1998**, *57* (8), 719–731.

(28) Hardy, J. The Amyloid Hypothesis for Alzheimer's Disease: A Critical Reappraisal. *J. Neurochem.* **2009**, *110* (4), 1129–1134.

(29) Les plaques amyloïdes — Site des ressources d'ACCES pour enseigner la Science de la Vie et de la Terre http://acces.ens-lyon.fr/acces/thematiques/neurosciences/actualisation-des-connaissances/maladies-et-traitements/alzheimer/la-maladie-dalzheimer-a-lechelle-cellulaire-et-moleculaire/les-palques.

(30) De Strooper, B. Proteases and Proteolysis in Alzheimer Disease: A Multifactorial View on the Disease Process. *Physiol. Rev.* **2010**, *90* (2), 465–494.

(31) Ubhi, K.; Masliah, E. Alzheimer's Disease: Recent Advances and Future Perspectives. *J. Alzheimers Dis. JAD* **2013**, *33 Suppl 1*, S185-194.

(32) Schreck, J. S.; Yuan, J.-M. Statistical Mechanical Treatments of Protein Amyloid Formation. *Int. J. Mol. Sci.* **2013**, *14* (9), 17420–17452.

(33) Shankar, G. M.; Walsh, D. M. Alzheimer's Disease: Synaptic Dysfunction and Aβ. *Mol. Neurodegener.* **2009**, *4* (1), 48.

(34) Yu, W.; Mechawar, N.; Krantic, S.; Chabot, J.-G.; Quirion, R. Upregulation of Astrocytic A7 Nicotinic Receptors in Alzheimer's Disease Brain- Possible Relevant to Amyloid Pathology. *Mol. Neurodegener.* **2012**, *7* (1), O7.

(35) Sadigh-Eteghad, S.; Talebi, M.; Farhoudi, M.; Golzari, S. E. J.; Sabermarouf, B.; Mahmoudi, J. Beta-Amyloid Exhibits Antagonistic Effects on Alpha 7 Nicotinic Acetylcholine Receptors in Orchestrated Manner. *J. Med. Hypotheses Ideas* **2014**, *8* (2), 49–52.

(36) Buée, L.; Bussière, T.; Buée-Scherrer, V.; Delacourte, A.; Hof, P. R. Tau Protein Isoforms, Phosphorylation and Role in Neurodegenerative Disorders11These Authors Contributed Equally to This Work. *Brain Res. Rev.* **2000**, *33* (1), 95–130.

(37) Morishima-Kawashima, M.; Hasegawa, M.; Takio, K.; Suzuki, M.; Yoshida, H.; Titani, K.; Ihara, Y. Proline-Directed and Non-Proline-Directed Phosphorylation of PHF-Tau. *J. Biol. Chem.* **1995**, *270* (2), 823–829.

(38) Drechsel, D. N.; Hyman, A. A.; Cobb, M. H.; Kirschner, M. W. Modulation of the Dynamic Instability of Tubulin Assembly by the Microtubule-Associated Protein Tau. *Mol. Biol. Cell* **1992**, *3* (10), 1141–1154.

(39) Verwilst, P.; Kim, H. S.; Kim, S.; Kang, C.; Kim, J. S. Shedding Light on Tau Protein Aggregation: The Progress in Developing Highly Selective Fluorophores. *Chem. Soc. Rev.* **2018**, *47* (7), 2249–2265.

(40) Luna-Muñoz, J.; R, C.; M, C.; Flores-Rodriguez, P.; Avila, J.; R, S.; De la Cruz, F.; Mena, R.; A, M.; Floran, B. Phosphorylation of Tau Protein Associated as a Protective Mechanism in the Presence of Toxic, C-Terminally Truncated Tau in Alzheimer's Disease; 2013.

(41) Tumiatti, V.; Minarini, A.; Bolognesi, M. L.; Milelli, A.; Rosini, M.; Melchiorre, C. Tacrine Derivatives and Alzheimers Disease. *Curr. Med. Chem.* **2010**, *17* (17), 1825–1838.

(42) Bolognesi, M. L.; Cavalli, A.; Valgimigli, L.; Bartolini, M.; Rosini, M.; Andrisano, V.; Recanatini, M.; Melchiorre, C. Multi-Target-Directed Drug Design Strategy: From a Dual Binding Site Acetylcholinesterase Inhibitor to a Trifunctional Compound against Alzheimer's Disease. *J. Med. Chem.* **2007**, *50* (26), 6446–6449.

(43) Arrieta, J. L.; Artalejo, F. R. Methodology, Results and Quality of Clinical Trials of Tacrine in the Treatment of Alzheimer's Disease: A Systematic Review of the Literature. *Age Ageing* **1998**, *27* (2), 161–179.

(44) Summers, W. K.; Majovski, L. V.; Marsh, G. M.; Tachiki, K.; Kling, A. Oral Tetrahydroaminoacridine in Long-Term Treatment of Senile Dementia, Alzheimer Type. *N. Engl. J. Med.* **1986**, *315* (20), 1241–1245.

(45) Patocka, J.; Jun, D.; Kuca, K. Possible Role of Hydroxylated Metabolites of Tacrine in Drug Toxicity and Therapy of Alzheimer's Disease. *Curr. Drug Metab.* **2008**, *9* (4), 332–335.

(46) Rogers, S. L.; Friedhoff, L. T. The Efficacy and Safety of Donepezil in Patients with Alzheimer's Disease: Results of a US Multicentre, Randomized, Double-Blind, Placebo-Controlled Trial. *Dement. Geriatr. Cogn. Disord.* **1996**, *7* (6), 293–303.

(47) Marco-Contelles, J.; do Carmo Carreiras, M.; Rodríguez, C.; Villarroya, M.; García, A. G. Synthesis and Pharmacology of Galantamine. *Chem. Rev.* **2006**, *106* (1), 116–133.

(48) Lilienfeld, S. Galantamine--a Novel Cholinergic Drug with a Unique Dual Mode of Action for the Treatment of Patients with Alzheimer's Disease. *CNS Drug Rev.* **2002**, *8* (2), 159–176.

(49) Maelicke, A.; Samochocki, M.; Jostock, R.; Fehrenbacher, A.; Ludwig, J.; Albuquerque, E. X.; Zerlin, M. Allosteric Sensitization of Nicotinic Receptors by Galantamine, a New Treatment Strategy for Alzheimer's Disease. *Biol. Psychiatry* **2001**, *49* (3), 279–288.

(50) Cummings, J.; Lefèvre, G.; Small, G.; Appel-Dingemanse, S. Pharmacokinetic Rationale for the Rivastigmine Patch. *Neurology* **2007**, *69* (4 Suppl 1), S10-13.

(51) Jann, M. W. Rivastigmine, a New-Generation Cholinesterase Inhibitor for the Treatment of Alzheimer's Disease. *Pharmacotherapy* **2000**, *20* (1), 1–12.

(52) Bar-On, P.; Millard, C. B.; Harel, M.; Dvir, H.; Enz, A.; Sussman, J. L.; Silman, I. Kinetic and Structural Studies on the Interaction of Cholinesterases with the Anti-Alzheimer Drug Rivastigmine. *Biochemistry* **2002**, *41* (11), 3555–3564.

(53) Polinsky, R. J. Clinical Pharmacology of Rivastigmine: A New-Generation Acetylcholinesterase Inhibitor for the Treatment of Alzheimer's Disease. *Clin. Ther.* **1998**, *20* (4), 634–647.

(54) Maelicke, A. Memogain, a Pleasant, Highly Potent and Neuroprotective Novel Drug Treatment in Alzheimer's Disease. *Alzheimers Dement.* **2011**, *7* (4), S799.

(55) Maelicke, A.; Hoeffle-Maas, A.; Ludwig, J.; Maus, A.; Samochocki, M.; Jordis, U.; Koepke, A. K. E. Memogain Is a Galantamine Pro-Drug Having Dramatically Reduced Adverse Effects and Enhanced Efficacy. *J. Mol. Neurosci.* **2010**, *40* (1–2), 135–137.

(56) Zouridakis, M.; Zisimopoulou, P.; Poulas, K.; Tzartos, S. J. Recent Advances in Understanding the Structure of Nicotinic Acetylcholine Receptors. *IUBMB Life* **2009**, *61* (4), 407–423.

(57) Grando, S. A. Connections of Nicotine to Cancer. *Nat. Rev. Cancer* **2014**, *14* (6), 419–429.
(58) Karlin, A. Emerging Structure of the Nicotinic Acetylcholine Receptors. *Nat. Rev. Neurosci.* **2002**, *3* (2), 102–114.
(59) Metabolism http://www.chm.bris.ac.uk/motm/nicotine/E-metabolisme.html.
(60) Graham, A.; Court, J. A.; Martin-Ruiz, C. M.; Jaros, E.; Perry, R.; Volsen, S. G.; Bose, S.; Evans, N.; Ince, P.; Kuryatov, A.; et al. Immunohistochemical Localisation of Nicotinic Acetylcholine Receptor Subunits in Human Cerebellum. *Neuroscience* **2002**, *113* (3), 493–507.
(61) Paterson, D.; Nordberg, A. Neuronal Nicotinic Receptors in the Human Brain. *Prog. Neurobiol.* **2000**, *61* (1), 75–111.
(62) Yang, T.; Xiao, T.; Sun, Q.; Wang, K. The Current Agonists and Positive Allosteric Modulators of α 7 NAChR for CNS Indications in Clinical Trials. *Acta Pharm. Sin. B* **2017**, *7* (6), 611–622.
(63) Lape, R.; Colquhoun, D.; Sivilotti, L. G. On the Nature of Partial Agonism in the Nicotinic Receptor Superfamily. *Nature* **2008**, *454* (7205), 722–727.
(64) Sydserff, S.; Sutton, E. J.; Song, D.; Quirk, M. C.; Maciag, C.; Li, C.; Jonak, G.; Gurley, D.; Gordon, J. C.; Christian, E. P.; et al. Selective A7 Nicotinic Receptor Activation by AZD0328 Enhances Cortical Dopamine Release and Improves Learning and Attentional Processes. *Biochem. Pharmacol.* **2009**, *78* (7), 880–888.
(65) Zhou, D.; Zhang, M.; Ye, X.; Gu, C.; Piser, T. M.; Lanoue, B. A.; Schock, S. A.; Cheng, Y.-F.; Grimm, S. W. In Vitro Metabolism of A7 Neuronal Nicotinic Receptor Agonist AZD0328 and Enzyme Identification for Its N-Oxide Metabolite. *Xenobiotica* **2011**, *41* (3), 232–242.
(66) Study to Asses Pharmacodynamics, Pharmacokinetics, Safety and Tolerability of AZD0328 in Patients With Schizophrenia - Full Text View - ClinicalTrials.gov https://clinicaltrials.gov/ct2/show/NCT00669903.
(67) Bristow, L. J.; Easton, A. E.; Li, Y.-W.; Sivarao, D. V.; Lidge, R.; Jones, K. M.; Post-Munson, D.; Daly, C.; Lodge, N. J.; Gallagher, L.; et al. The Novel, Nicotinic Alpha7 Receptor Partial Agonist, BMS-933043, Improves Cognition and Sensory Processing in Preclinical Models of Schizophrenia. *PLOS ONE* **2016**, *11* (7), e0159996.
(68) Therapeutics | ALZFORUM https://www.alzforum.org/therapeutics.
(69) Huang, M.; Felix, A. R.; Flood, D. G.; Bhuvaneswaran, C.; Hilt, D.; Koenig, G.; Meltzer, H. Y. The Novel A7 Nicotinic Acetylcholine Receptor Agonist EVP-6124 Enhances Dopamine, Acetylcholine, and Glutamate Efflux in Rat Cortex and Nucleus Accumbens. *Psychopharmacology (Berl.)* **2014**, *231* (23), 4541–4551.
(70) Huang, M.; Felix, A. R.; Bhuvaneswaran, C.; Hilt, D.; König, G.; Meltzer, H. Y. The Alpha-7 Receptor Agonist EVP-6124 Increases Dopamine and Glutamate Efflux in Rat Medial Prefrontal Cortex and Nucleus Accumbens. *Biochem. Pharmacol.* **2011**, *82* (8), 1040.
(71) Prickaerts, J.; van Goethem, N. P.; Chesworth, R.; Shapiro, G.; Boess, F. G.; Methfessel, C.; Reneerkens, O. A. H.; Flood, D. G.; Hilt, D.; Gawryl, M.; et al. EVP-6124, a Novel and Selective A7 Nicotinic Acetylcholine Receptor Partial Agonist, Improves Memory Performance by Potentiating the Acetylcholine Response of A7 Nicotinic Acetylcholine Receptors. *Neuropharmacology* **2012**, *62* (2), 1099–1110.
(72) Huang, M.; Felix, A. R.; Kwon, S.; Lowe, D.; Wallace, T.; Santarelli, L.; Meltzer, H. Y. The Alpha-7 Nicotinic Receptor Partial Agonist/5-HT3 Antagonist RG3487 Enhances Cortical and Hippocampal Dopamine and Acetylcholine Release. *Psychopharmacology (Berl.)* **2014**, *231* (10), 2199–2210.
(73) Umbricht, D.; Keefe, R. S.; Murray, S.; Lowe, D. A.; Porter, R.; Garibaldi, G.; Santarelli, L. A Randomized, Placebo-Controlled Study Investigating the Nicotinic *α*7 Agonist, RG3487, for Cognitive Deficits in Schizophrenia. *Neuropsychopharmacology* **2014**, *39* (7), 1568–1577.
(74) Hauser, T. A.; Kucinski, A.; Jordan, K. G.; Gatto, G. J.; Wersinger, S. R.; Hesse, R. A.; Stachowiak, E. K.; Stachowiak, M. K.; Papke, R. L.; Lippiello, P. M.; et al. TC-5619: An Alpha7 Neuronal Nicotinic Receptor-Selective Agonist That Demonstrates Efficacy in Animal Models of the Positive and Negative Symptoms and Cognitive Dysfunction of Schizophrenia. *Biochem. Pharmacol.* **2009**, *78* (7), 803–812.

(75) Lieberman, J. A.; Dunbar, G.; Segreti, A. C.; Girgis, R. R.; Seoane, F.; Beaver, J. S.; Duan, N.; Hosford, D. A. A Randomized Exploratory Trial of an Alpha-7 Nicotinic Receptor Agonist (TC-5619) for Cognitive Enhancement in Schizophrenia. *Neuropsychopharmacology* **2013**, *38* (6), 968–975.

(76) Hosford, D.; Dvergsten, C.; Beaver, J.; Segreti, A. C.; Toler, S.; Farr, M. G.; Joseph, M.; Jett, J.; Lippiello, P.; Bencherif, M. P.3.d.018 Phase 2 Clinical Trial of TC-5619, an Alpha 7 Nicotinic Receptor Agonist in the Treatment of Negative and Cognitive Symptoms in Schizophrenia. *Eur. Neuropsychopharmacol.* **2014**, *24*, S531–S532.

(77) Walling, D.; Marder, S. R.; Kane, J.; Fleischhacker, W. W.; Keefe, R. S. E.; Hosford, D. A.; Dvergsten, C.; Segreti, A. C.; Beaver, J. S.; Toler, S. M.; et al. Phase 2 Trial of an Alpha-7 Nicotinic Receptor Agonist (TC-5619) in Negative and Cognitive Symptoms of Schizophrenia. *Schizophr. Bull.* **2016**, *42* (2), 335–343.

(78) Di Paolo, T.; Grégoire, L.; Feuerbach, D.; Elbast, W.; Weiss, M.; Gomez-Mancilla, B. AQW051, a Novel and Selective Nicotinic Acetylcholine Receptor A7 Partial Agonist, Reduces l-Dopa-Induced Dyskinesias and Extends the Duration of l-Dopa Effects in Parkinsonian Monkeys. *Parkinsonism Relat. Disord.* **2014**, *20* (11), 1119–1123.

(79) Trenkwalder, C.; Berg, D.; Rascol, O.; Eggert, K.; Ceballos-Baumann, A.; Corvol, J.-C.; Storch, A.; Zhang, L.; Azulay, J.-P.; Broussolle, E.; et al. A Placebo-Controlled Trial of AQW051 in Patients With Moderate to Severe Levodopa-Induced Dyskinesia. *Mov. Disord.* **2016**, *31* (7), 1049–1054.

(80) Avila, J. Muscarinic Receptors and Alzheimer's Disease. *Neurodegener. Dis. Manag.* **2011**, *1* (4), 267–269.

(81) Wess, J.; Eglen, R. M.; Gautam, D. Muscarinic Acetylcholine Receptors: Mutant Mice Provide New Insights for Drug Development. *Nat. Rev. Drug Discov.* **2007**, *6* (9), 721–733.

(82) Conn, P. J.; Jones, C. K.; Lindsley, C. W. Subtype-Selective Allosteric Modulators of Muscarinic Receptors for the Treatment of CNS Disorders. *Trends Pharmacol. Sci.* **2009**, *30* (3), 148–155.

(83) Züchner, T.; Perez-Polo, J. R.; Schliebs, R. Beta-Secretase BACE1 Is Differentially Controlled through Muscarinic Acetylcholine Receptor Signaling. *J. Neurosci. Res.* **2004**, *77* (2), 250–257.

(84) Liu, J.; Rasul, I.; Sun, Y.; Wu, G.; Li, L.; Premont, R. T.; Suo, W. Z. GRK5 Deficiency Leads to Reduced Hippocampal Acetylcholine Level via Impaired Presynaptic M2/M4 Autoreceptor Desensitization. *J. Biol. Chem.* **2009**, *284* (29), 19564–19571.

(85) Farías, G. G.; Godoy, J. A.; Hernández, F.; Avila, J.; Fisher, A.; Inestrosa, N. C. M1 Muscarinic Receptor Activation Protects Neurons from Beta-Amyloid Toxicity. A Role for Wnt Signaling Pathway. *Neurobiol. Dis.* **2004**, *17* (2), 337–348.

(86) Jiang, S.; Li, Y. L.; Zhang, C.; Zhao, Y.; Bu, G. D.; Xu, H.; Zhang, Y.-W. M1 Muscarinic Acetylcholine Receptor in Alzheimer's Disease. *Neurosci. Bull.* **2013**, *30*, 295–307.

(87) Alzheimer Europe - News - Science watch - Tuesday 18 September 2018 - Sosei and Allergan suspend clinical activities of HTL0018318 in AD https://www.alzheimer-europe.org/News/Science-watch/Tuesday-18-September-2018-Sosei-and-Allergan-suspend-clinical-activities-of-HTL0018318-in-AD.

(88) Hansen, K. B.; Yi, F.; Perszyk, R. E.; Furukawa, H.; Wollmuth, L. P.; Gibb, A. J.; Traynelis, S. F. Structure, Function, and Allosteric Modulation of NMDA Receptors. *J. Gen. Physiol.* **2018**, *150* (8), 1081–1105.

(89) Gielen, M. Fonctionnement des récepteurs-canaux du glutamate - Des proteines responsables de la transmission synaptique excitatrice. *médecine/sciences* **2010**, *26* (1), 65–72.

(90) Panatier, A.; Theodosis, D. T.; Mothet, J.-P.; Touquet, B.; Pollegioni, L.; Poulain, D. A.; Oliet, S. H. R. Glia-Derived D-Serine Controls NMDA Receptor Activity and Synaptic Memory. *Cell* **2006**, *125* (4), 775–784.

(91) Kleckner, N. W.; Dingledine, R. Requirement for Glycine in Activation of NMDA-Receptors Expressed in Xenopus Oocytes. *Science* **1988**, *241* (4867), 835–837.

(92) Snyder, E. M.; Nong, Y.; Almeida, C. G.; Paul, S.; Moran, T.; Choi, E. Y.; Nairn, A. C.; Salter, M. W.; Lombroso, P. J.; Gouras, G. K.; et al. Regulation of NMDA Receptor Trafficking by Amyloid-Beta. *Nat. Neurosci.* **2005**, *8* (8), 1051–1058.

(93) Plazas, P. V.; Savino, J.; Kracun, S.; Gomez-Casati, M. E.; Katz, E.; Parsons, C. G.; Millar, N. S.; Elgoyhen, A. B. Inhibition of the Alpha9alpha10 Nicotinic Cholinergic Receptor by Neramexane, an Open Channel Blocker of N-Methyl-D-Aspartate Receptors. *Eur. J. Pharmacol.* **2007**, *566* (1–3), 11–19.

(94) Lleó, A.; Berezovska, O.; Herl, L.; Raju, S.; Deng, A.; Bacskai, B. J.; Frosch, M. P.; Irizarry, M.; Hyman, B. T. Nonsteroidal Anti-Inflammatory Drugs Lower Abeta42 and Change Presenilin 1 Conformation. *Nat. Med.* **2004**, *10* (10), 1065–1066.

(95) Lim, G. P.; Yang, F.; Chu, T.; Chen, P.; Beech, W.; Teter, B.; Tran, T.; Ubeda, O.; Ashe, K. H.; Frautschy, S. A.; et al. Ibuprofen Suppresses Plaque Pathology and Inflammation in a Mouse Model for Alzheimer's Disease. *J. Neurosci. Off. J. Soc. Neurosci.* **2000**, *20* (15), 5709–5714.

(96) Hori, Y.; Takeda, S.; Cho, H.; Wegmann, S.; Shoup, T. M.; Takahashi, K.; Irimia, D.; Elmaleh, D. R.; Hyman, B. T.; Hudry, E. A Food and Drug Administration-Approved Asthma Therapeutic Agent Impacts Amyloid β in the Brain in a Transgenic Model of Alzheimer Disease. *J. Biol. Chem.* **2015**, *290* (4), 1966–1978.

(97) Stein, T. D.; Anders, N. J.; DeCarli, C.; Chan, S. L.; Mattson, M. P.; Johnson, J. A. Neutralization of Transthyretin Reverses the Neuroprotective Effects of Secreted Amyloid Precursor Protein (APP) in APPSw Mice Resulting in Tau Phosphorylation and Loss of Hippocampal Neurons: Support for the Amyloid Hypothesis. *J. Neurosci.* **2004**, *24* (35), 7707–7717.

(98) Tippmann, F.; Hundt, J.; Schneider, A.; Endres, K.; Fahrenholz, F. Up-Regulation of the Alpha-Secretase ADAM10 by Retinoic Acid Receptors and Acitretin. *FASEB J. Off. Publ. Fed. Am. Soc. Exp. Biol.* **2009**, *23* (6), 1643–1654.

(99) Endres, K.; Fahrenholz, F.; Lotz, J.; Hiemke, C.; Teipel, S.; Lieb, K.; Tüscher, O.; Fellgiebel, A. Increased CSF APPs-α Levels in Patients with Alzheimer Disease Treated with Acitretin. *Neurology* **2014**, *83* (21), 1930–1935.

(100)https://www.alzforum.org/therapeutics/

(101) Maier, W. A. Thalidomide Embryopathy and Limb Defects. *Arch. Dis. Child.* **1965**, *40* (210), 154–157.

(102) He, P.; Cheng, X.; Staufenbiel, M.; Li, R.; Shen, Y. Long-Term Treatment of Thalidomide Ameliorates Amyloid-like Pathology through Inhibition of β-Secretase in a Mouse Model of Alzheimer's Disease. *PloS One* **2013**, *8* (2), e55091.

(103) Neumann, U.; Ufer, M.; Jacobson, L. H.; Rouzade-Dominguez, M.-L.; Huledal, G.; Kolly, C.; Lüönd, R. M.; Machauer, R.; Veenstra, S. J.; Hurth, K.; et al. The BACE-1 Inhibitor CNP520 for Prevention Trials in Alzheimer's Disease. *EMBO Mol. Med.* **2018**, *10* (11).

(104) Wong, G. T.; Manfra, D.; Poulet, F. M.; Zhang, Q.; Josien, H.; Bara, T.; Engstrom, L.; Pinzon-Ortiz, M.; Fine, J. S.; Lee, H.-J. J.; et al. Chronic Treatment with the γ-Secretase Inhibitor LY-411,575 Inhibits β-Amyloid Peptide Production and Alters Lymphopoiesis and Intestinal Cell Differentiation. *J. Biol. Chem.* **2004**, *279* (13), 12876–12882.

(105) Rogers, K.; Felsenstein, K. M.; Hrdlicka, L.; Tu, Z.; Albayya, F.; Lee, W.; Hopp, S.; Miller, M.-J.; Spaulding, D.; Yang, Z.; et al. Modulation of γ-Secretase by EVP-0015962 Reduces Amyloid Deposition and Behavioral Deficits in Tg2576 Mice. *Mol. Neurodegener.* **2012**, *7*, 61.

(106) Nübling, G.; Bader, B.; Levin, J.; Hildebrandt, J.; Kretzschmar, H.; Giese, A. Synergistic Influence of Phosphorylation and Metal Ions on Tau Oligomer Formation and Coaggregation with α-Synuclein at the Single Molecule Level. *Mol. Neurodegener.* **2012**, *7* (1), 35.

(107) Hooper, C.; Markevich, V.; Plattner, F.; Killick, R.; Schofield, E.; Engel, T.; Hernandez, F.; Anderton, B.; Rosenblum, K.; Bliss, T.; et al. Glycogen Synthase Kinase-3 Inhibition Is Integral to Long-Term Potentiation. *Eur. J. Neurosci.* **2007**, *25* (1), 81–86.

(108) Gong, C.-X.; Iqbal, K. Hyperphosphorylation of Microtubule-Associated Protein Tau: A Promising Therapeutic Target for Alzheimer Disease. *Curr. Med. Chem.* **2008**, *15* (23), 2321–2328.

(109) Avila, J.; Hernández, F. GSK-3 Inhibitors for Alzheimer's Disease. *Expert Rev. Neurother.* **2007**, *7* (11), 1527–1533.
(110) Akoury, E.; Gajda, M.; Pickhardt, M.; Biernat, J.; Soraya, P.; Griesinger, C.; Mandelkow, E.; Zweckstetter, M. Inhibition of Tau Filament Formation by Conformational Modulation. *J. Am. Chem. Soc.* **2013**, *135* (7), 2853–2862.
(111) de Paula, V. de J. R.; Guimarães, F. M.; Diniz, B. S.; Forlenza, O. V. Neurobiological Pathways to Alzheimer's Disease: Amyloid-Beta, TAU Protein or Both? *Dement. Neuropsychol.* **2009**, *3* (3), 188–194.
(112) Jean, D. C.; Baas, P. W. It Cuts Two Ways: Microtubule Loss during Alzheimer Disease: Microtubule Loss during Alzheimer Disease. *EMBO J.* **2013**, *32* (22), 2900–2902.
(113) Nogales, E.; Wolf, S. G.; Khan, I. A.; Ludueña, R. F.; Downing, K. H. Structure of Tubulin at 6.5 Å and Location of the Taxol-Binding Site. *Nature* **1995**, *375* (6530), 424.
(114) Petersen, R. B.; Nunomura, A.; Lee, H.; Casadesus, G.; Perry, G.; Smith, M. A.; Zhu, X. Signal Transduction Cascades Associated with Oxidative Stress in Alzheimer's Disease. *J. Alzheimers Dis. JAD* **2007**, *11* (2), 143–152.
(115) Sutton, H. C.; Winterbourn, C. C. On the Participation of Higher Oxidation States of Iron and Copper in Fenton Reactions. *Free Radic. Biol. Med.* **1989**, *6* (1), 53–60.
(116) Connor, J. R.; Snyder, B. S.; Arosio, P.; Loeffler, D. A.; LeWitt, P. A Quantitative Analysis of Isoferritins in Select Regions of Aged, Parkinsonian, and Alzheimer's Diseased Brains. *J. Neurochem.* **1995**, *65* (2), 717–724.
(117) Dias-Santagata, D.; Fulga, T. A.; Duttaroy, A.; Feany, M. B. Oxidative Stress Mediates Tau-Induced Neurodegeneration in *Drosophila*. *J. Clin. Invest.* **2007**, *117* (1), 236–245.
(118) Paola, D.; Domenicotti, C.; Nitti, M.; Vitali, A.; Borghi, R.; Cottalasso, D.; Zaccheo, D.; Odetti, P.; Strocchi, P.; Marinari, U. M.; et al. Oxidative Stress Induces Increase in Intracellular Amyloid β-Protein Production and Selective Activation of BI and BII PKCs in NT2 Cells. *Biochem. Biophys. Res. Commun.* **2000**, *268* (2), 642–646.
(119) Wang, H.; Jiang, T.; Li, W.; Gao, N.; Zhang, T. Resveratrol Attenuates Oxidative Damage through Activating Mitophagy in an in Vitro Model of Alzheimer's Disease. *Toxicol. Lett.* **2018**, *282*, 100–108.
(120) Sawda, C.; Moussa, C.; Turner, R. S. Resveratrol for Alzheimer's Disease. *Ann. N. Y. Acad. Sci.* **2017**, *1403* (1), 142–149.
(121) Resveratrol Improves Memory in Overweight Adults | ALZFORUM https://www.alzforum.org/news/research-news/resveratrol-improves-memory-overweight-adults.
(122) Logovinsky, V.; Satlin, A.; Lai, R.; Swanson, C.; Kaplow, J.; Osswald, G.; Basun, H.; Lannfelt, L. Safety and Tolerability of BAN2401 - a Clinical Study in Alzheimer's Disease with a Protofibril Selective Aβ Antibody. *Alzheimers Res. Ther.* **2016**, *8* (1), 14.
(123) Söllvander, S.; Nikitidou, E.; Gallasch, L.; Zyśk, M.; Söderberg, L.; Sehlin, D.; Lannfelt, L.; Erlandsson, A. The Aβ Protofibril Selective Antibody MAb158 Prevents Accumulation of Aβ in Astrocytes and Rescues Neurons from Aβ-Induced Cell Death. *J. Neuroinflammation* **2018**, *15* (1), 98.
(124) Dodart, J.-C.; Bales, K. R.; Gannon, K. S.; Greene, S. J.; DeMattos, R. B.; Mathis, C.; DeLong, C. A.; Wu, S.; Wu, X.; Holtzman, D. M.; et al. Immunization Reverses Memory Deficits without Reducing Brain Abeta Burden in Alzheimer's Disease Model. *Nat. Neurosci.* **2002**, *5* (5), 452–457.
(125) Xue, H.; Li, J.; Xie, H.; Wang, Y. Review of Drug Repositioning Approaches and Resources. *Int. J. Biol. Sci.* **2018**, *14* (10), 1232–1244.
(126) Pammolli, F.; Magazzini, L.; Riccaboni, M. The Productivity Crisis in Pharmaceutical R&D. *Nat. Rev. Drug Discov.* **2011**, *10* (6), 428–438.
(127) Wang, J.; Ono, K.; Dickstein, D. L.; Arrieta-Cruz, I.; Zhao, W.; Qian, X.; Lamparello, A.; Subnani, R.; Ferruzzi, M.; Pavlides, C.; et al. Carvedilol as a Potential Novel Agent for the Treatment of Alzheimer's Disease. *Neurobiol. Aging* **2011**, *32* (12), 2321.e1-2321.e12.

(128) Serrano-Pozo, A.; Vega, G. L.; Lütjohann, D.; Locascio, J. J.; Tennis, M. K.; Deng, A.; Atri, A.; Hyman, B. T.; Irizarry, M. C.; Growdon, J. H. Effects of Simvastatin on Cholesterol Metabolism and Alzheimer Disease Biomarkers: *Alzheimer Dis. Assoc. Disord.* **2010**, 1.

(129) Haase, N.; Herse, F.; Spallek, B.; Haase, H.; Morano, I.; Qadri, F.; Szijártó, I. A.; Rohm, I.; Yilmaz, A.; Warrington, J. P.; et al. Amyloid-β Peptides Activate A1-Adrenergic Cardiovascular Receptors. *Hypertens. Dallas Tex 1979* **2013**, *62* (5), 966–972.

(130) Design of Hybrid Molecules for Drug Development - 1st Edition https://www.elsevier.com/books/design-of-hybrid-molecules-for-drug-development/decker/978-0-08-101011-2.

(131) Morphy, R.; Rankovic, Z. Designed Multiple Ligands. An Emerging Drug Discovery Paradigm. *J. Med. Chem.* **2005**, *48* (21), 6523–6543.

(132) Jacobson, K. A.; Xie, R.; Young, L.; Chang, L.; Liang, B. T. A Novel Pharmacological Approach to Treating Cardiac Ischemia. Binary Conjugates of A1 and A3 Adenosine Receptor Agonists. *J. Biol. Chem.* **2000**, *275* (39), 30272–30279.

(133) Montero, A.; Goya, P.; Jagerovic, N.; Callado, L. F.; Callado, L. F.; Meana, J. J.; Girón, R.; Goicoechea, C.; Martín, M. I. Guanidinium and Aminoimidazolinium Derivatives of N-(4-Piperidyl)Propanamides as Potential Ligands for Mu Opioid and I2-Imidazoline Receptors: Synthesis and Pharmacological Screening. *Bioorg. Med. Chem.* **2002**, *10* (4), 1009–1018.

(134) Ortiz, C. J. C.; de Freitas Silva, M.; Gontijo, V. S.; Viegas, F. P. D.; Dias, K. S. T.; Viegas, C. Design of Multi-Target Directed Ligands as a Modern Approach for the Development of Innovative Drug Candidates for Alzheimer's Disease. In *Multi-Target Drug Design Using Chem-Bioinformatic Approaches*; Roy, K., Ed.; Methods in Pharmacology and Toxicology; Springer New York: New York, NY, 2019; pp 255–351.

(135) Rosini, M.; Simoni, E.; Bartolini, M.; Cavalli, A.; Ceccarini, L.; Pascu, N.; McClymont, D. W.; Tarozzi, A.; Bolognesi, M. L.; Minarini, A.; et al. Inhibition of Acetylcholinesterase, β-Amyloid Aggregation, and NMDA Receptors in Alzheimer's Disease: A Promising Direction for the Multi-Target-Directed Ligands Gold Rush. *J. Med. Chem.* **2008**, *51* (15), 4381–4384.

(136) León, R.; Garcia, A. G.; Marco-Contelles, J. Recent Advances in the Multitarget-Directed Ligands Approach for the Treatment of Alzheimer's Disease. *Med. Res. Rev.* **2013**, *33* (1), 139–189.

(137) de Freitas Silva, M.; Dias, K. S. T.; Gontijo, V. S.; Ortiz, C. J. C.; Viegas, C. Multi-Target Directed Drugs as a Modern Approach for Drug Design Towards Alzheimer's Disease: An Update. *Curr. Med. Chem.* **2018**, *25* (29), 3491–3525.

(138) Alvarez, A.; Opazo, C.; Alarcón, R.; Garrido, J.; Inestrosa, N. C. Acetylcholinesterase Promotes the Aggregation of Amyloid-Beta-Peptide Fragments by Forming a Complex with the Growing Fibrils. *J. Mol. Biol.* **1997**, *272* (3), 348–361.

(139) De Ferrari, G. V.; Canales, M. A.; Shin, I.; Weiner, L. M.; Silman, I.; Inestrosa, N. C. A Structural Motif of Acetylcholinesterase That Promotes Amyloid Beta-Peptide Fibril Formation. *Biochemistry* **2001**, *40* (35), 10447–10457.

(140) Muñoz, F. J.; Inestrosa, N. C. Neurotoxicity of Acetylcholinesterase Amyloid Beta-Peptide Aggregates Is Dependent on the Type of Abeta Peptide and the AChE Concentration Present in the Complexes. *FEBS Lett.* **1999**, *450* (3), 205–209.

(141) Rodríguez-Franco, M. I.; Fernández-Bachiller, M. I.; Pérez, C.; Hernández-Ledesma, B.; Bartolomé, B. Novel Tacrine-Melatonin Hybrids as Dual-Acting Drugs for Alzheimer Disease, with Improved Acetylcholinesterase Inhibitory and Antioxidant Properties. *J. Med. Chem.* **2006**, *49* (2), 459–462.

(142) Fu, H.; Li, W.; Luo, J.; Lee, N. T. K.; Li, M.; Tsim, K. W. K.; Pang, Y.; Youdim, M. B. H.; Han, Y. Promising Anti-Alzheimer's Dimer Bis(7)-Tacrine Reduces β-Amyloid Generation by Directly Inhibiting BACE-1 Activity. *Biochem. Biophys. Res. Commun.* **2008**, *366* (3), 631–636.

(143) Kwon, Y. E.; Park, J. Y.; No, K. T.; Shin, J. H.; Lee, S. K.; Eun, J. S.; Yang, J. H.; Shin, T. Y.; Kim, D. K.; Chae, B. S.; et al. Synthesis, in Vitro Assay, and Molecular Modeling of New Piperidine Derivatives Having Dual Inhibitory Potency against Acetylcholinesterase and Aβ1–42

Aggregation for Alzheimer's Disease Therapeutics. *Bioorg. Med. Chem.* **2007**, *15* (20), 6596–6607.

(144) Camps, P.; Formosa, X.; Galdeano, C.; Gómez, T.; Muñoz-Torrero, D.; Scarpellini, M.; Viayna, E.; Badia, A.; Clos, M. V.; Camins, A.; et al. Novel Donepezil-Based Inhibitors of Acetyl- and Butyrylcholinesterase and Acetylcholinesterase-Induced β-Amyloid Aggregation. *J. Med. Chem.* **2008**, *51* (12), 3588–3598.

(145) Zha, G.-F.; Zhang, C.-P.; Qin, H.-L.; Jantan, I.; Sher, M.; Amjad, M. W.; Hussain, M. A.; Hussain, Z.; Bukhari, S. N. A. Biological Evaluation of Synthetic α,β-Unsaturated Carbonyl Based Cyclohexanone Derivatives as Neuroprotective Novel Inhibitors of Acetylcholinesterase, Butyrylcholinesterase and Amyloid-β Aggregation. *Bioorg. Med. Chem.* **2016**, *24* (10), 2352–2359.

(146) Prati, F.; Bottegoni, G.; Bolognesi, M. L.; Cavalli, A. BACE-1 Inhibitors: From Recent Single-Target Molecules to Multitarget Compounds for Alzheimer's Disease. *J. Med. Chem.* **2018**, *61* (3), 619–637.

(147) Piazzi, L.; Cavalli, A.; Colizzi, F.; Belluti, F.; Bartolini, M.; Mancini, F.; Recanatini, M.; Andrisano, V.; Rampa, A. Multi-Target-Directed Coumarin Derivatives: HAChE and BACE1 Inhibitors as Potential Anti-Alzheimer Compounds. *Bioorg. Med. Chem. Lett.* **2008**, *18* (1), 423–426.

(148) Zha, X.; Lamba, D.; Zhang, L.; Lou, Y.; Xu, C.; Kang, D.; Chen, L.; Xu, Y.; Zhang, L.; De Simone, A.; et al. Novel Tacrine–Benzofuran Hybrids as Potent Multitarget-Directed Ligands for the Treatment of Alzheimer's Disease: Design, Synthesis, Biological Evaluation, and X-Ray Crystallography. *J. Med. Chem.* **2016**, *59* (1), 114–131.

(149) Costanzo, P.; Cariati, L.; Desiderio, D.; Sgammato, R.; Lamberti, A.; Arcone, R.; Salerno, R.; Nardi, M.; Masullo, M.; Oliverio, M. Design, Synthesis, and Evaluation of Donepezil-Like Compounds as AChE and BACE-1 Inhibitors. *ACS Med. Chem. Lett.* **2016**, *7* (5), 470–475.

(150) Camps, P.; Formosa, X.; Galdeano, C.; Muñoz-Torrero, D.; Ramírez, L.; Gómez, E.; Isambert, N.; Lavilla, R.; Badia, A.; Clos, M. V.; et al. Pyrano[3,2-c]Quinoline−6-Chlorotacrine Hybrids as a Novel Family of Acetylcholinesterase- and β-Amyloid-Directed Anti-Alzheimer Compounds. *J. Med. Chem.* **2009**, *52* (17), 5365–5379.

(151) Cavalli, A.; Bolognesi, M. L.; Capsoni, S.; Andrisano, V.; Bartolini, M.; Margotti, E.; Cattaneo, A.; Recanatini, M.; Melchiorre, C. A Small Molecule Targeting the Multifactorial Nature of Alzheimer's Disease. *Angew. Chem. Int. Ed Engl.* **2007**, *46* (20), 3689–3692.

(152) Bolognesi, M. L.; Cavalli, A.; Melchiorre, C. Memoquin: A Multi-Target-Directed Ligand as an Innovative Therapeutic Opportunity for Alzheimer's Disease. *Neurotherapeutics* **2009**, *6* (1), 152–162.

(153) Huang, W.; Tang, L.; Shi, Y.; Huang, S.; Xu, L.; Sheng, R.; Wu, P.; Li, J.; Zhou, N.; Hu, Y. Searching for the Multi-Target-Directed Ligands against Alzheimer's Disease: Discovery of Quinoxaline-Based Hybrid Compounds with AChE, H3R and BACE 1 Inhibitory Activities. *Bioorg. Med. Chem.* **2011**, *19* (23), 7158–7167.

(154) Simoni, E.; Daniele, S.; Bottegoni, G.; Pizzirani, D.; Trincavelli, M. L.; Goldoni, L.; Tarozzo, G.; Reggiani, A.; Martini, C.; Piomelli, D.; et al. Combining Galantamine and Memantine in Multitargeted, New Chemical Entities Potentially Useful in Alzheimer's Disease. *J. Med. Chem.* **2012**, *55* (22), 9708–9721.

(155) Rook, Y.; Schmidtke, K.-U.; Gaube, F.; Schepmann, D.; Wünsch, B.; Heilmann, J.; Lehmann, J.; Winckler, T. Bivalent β-Carbolines as Potential Multitarget Anti-Alzheimer Agents. *J. Med. Chem.* **2010**, *53* (9), 3611–3617.

(156) Rosini, M.; Simoni, E.; Bartolini, M.; Cavalli, A.; Ceccarini, L.; Pascu, N.; McClymont, D. W.; Tarozzi, A.; Bolognesi, M. L.; Minarini, A.; et al. Inhibition of Acetylcholinesterase, β-Amyloid Aggregation, and NMDA Receptors in Alzheimer's Disease: A Promising Direction for the Multi-Target-Directed Ligands Gold Rush. *J. Med. Chem.* **2008**, *51* (15), 4381–4384.

(157) Rosini, M.; Andrisano, V.; Bartolini, M.; Bolognesi, M. L.; Hrelia, P.; Minarini, A.; Tarozzi, A.; Melchiorre, C. Rational Approach to Discover Multipotent Anti-Alzheimer Drugs. *J. Med. Chem.* **2005**, *48* (2), 360–363.

(158) Fang, L.; Kraus, B.; Lehmann, J.; Heilmann, J.; Zhang, Y.; Decker, M. Design and Synthesis of Tacrine-Ferulic Acid Hybrids as Multi-Potent Anti-Alzheimer Drug Candidates. *Bioorg. Med. Chem. Lett.* **2008**, *18* (9), 2905–2909.

(159) Fernández-Bachiller, M. I.; Pérez, C.; Campillo, N. E.; Páez, J. A.; González-Muñoz, G. C.; Usán, P.; García-Palomero, E.; López, M. G.; Villarroya, M.; García, A. G.; et al. Tacrine-Melatonin Hybrids as Multifunctional Agents for Alzheimer's Disease, with Cholinergic, Antioxidant, and Neuroprotective Properties. *ChemMedChem* **2009**, *4* (5), 828–841.

(160) Arce, M. P.; Rodríguez-Franco, M. I.; González-Muñoz, G. C.; Pérez, C.; López, B.; Villarroya, M.; López, M. G.; García, A. G.; Conde, S. Neuroprotective and Cholinergic Properties of Multifunctional Glutamic Acid Derivatives for the Treatment of Alzheimer's Disease. *J. Med. Chem.* **2009**, *52* (22), 7249–7257.

(161) Bolognesi, M. L.; Cavalli, A.; Bergamini, C.; Fato, R.; Lenaz, G.; Rosini, M.; Bartolini, M.; Andrisano, V.; Melchiorre, C. Toward a Rational Design of Multitarget-Directed Antioxidants: Merging Memoquin and Lipoic Acid Molecular Frameworks. *J. Med. Chem.* **2009**, *52* (23), 7883–7886.

(162) Oukoloff, K.; Coquelle, N.; Bartolini, M.; Naldi, M.; Le Guevel, R.; Bach, S.; Josselin, B.; Ruchaud, S.; Catto, M.; Pisani, L.; et al. Design, Biological Evaluation and X-Ray Crystallography of Nanomolar Multifunctional Ligands Targeting Simultaneously Acetylcholinesterase and Glycogen Synthase Kinase-3. *Eur. J. Med. Chem.* **2019**, *168*, 58–77.

(163) Reynolds, G. P.; Mason, S. L.; Meldrum, A.; De Keczer, S.; Parnes, H.; Eglen, R. M.; Wong, E. H. 5-Hydroxytryptamine (5-HT)4 Receptors in Post Mortem Human Brain Tissue: Distribution, Pharmacology and Effects of Neurodegenerative Diseases. *Br. J. Pharmacol.* **1995**, *114* (5), 993–998.

(164) Robert, S. J.; Zugaza, J. L.; Fischmeister, R.; Gardier, A. M.; Lezoualc'h, F. The Human Serotonin 5-HT4 Receptor Regulates Secretion of Non-Amyloidogenic Precursor Protein. *J. Biol. Chem.* **2001**, *276* (48), 44881–44888.

(165) Lecoutey, C.; Hedou, D.; Freret, T.; Giannoni, P.; Gaven, F.; Since, M.; Bouet, V.; Ballandonne, C.; Corvaisier, S.; Fréon, A. M.; et al. Design of Donecopride, a Dual Serotonin Subtype 4 Receptor Agonist/Acetylcholinesterase Inhibitor with Potential Interest for Alzheimer's Disease Treatment. *Proc. Natl. Acad. Sci.* **2014**, 201410315.

(166) Lalut, J.; Santoni, G.; Karila, D.; Lecoutey, C.; Davis, A.; Nachon, F.; Silman, I.; Sussman, J.; Weik, M.; Maurice, T.; et al. Novel Multitarget-Directed Ligands Targeting Acetylcholinesterase and Σ1 Receptors as Lead Compounds for Treatment of Alzheimer's Disease: Synthesis, Evaluation, and Structural Characterization of Their Complexes with Acetylcholinesterase. *Eur. J. Med. Chem.* **2019**, *162*, 234–248.

(167) Villard, V.; Espallergues, J.; Keller, E.; Vamvakides, A.; Maurice, T. Anti-Amnesic and Neuroprotective Potentials of the Mixed Muscarinic Receptor/Sigma 1 (Σ1) Ligand ANAVEX2-73, a Novel Aminotetrahydrofuran Derivative. *J. Psychopharmacol. Oxf. Engl.* **2011**, *25* (8), 1101–1117.

(168) Maurice, T. Protection by Sigma-1 Receptor Agonists Is Synergic with Donepezil, but Not with Memantine, in a Mouse Model of Amyloid-Induced Memory Impairments. *Behav. Brain Res.* **2016**, *296*, 270–278.

(169) Maurice, T.; Goguadze, N. Role of Σ1 Receptors in Learning and Memory and Alzheimer's Disease-Type Dementia. *Adv. Exp. Med. Biol.* **2017**, *964*, 213–233.

(170) Ronco, C.; Foucault, R.; Gillon, E.; Bohn, P.; Nachon, F.; Jean, L.; Renard, P.-Y. New Huprine Derivatives Functionalized at Position 9 as Highly Potent Acetylcholinesterase Inhibitors. *ChemMedChem* **2011**, *6* (5), 876–888.

(171) Ronco, C.; Carletti, E.; Colletier, J.-P.; Weik, M.; Nachon, F.; Jean, L.; Renard, P.-Y. Huprine Derivatives as Sub-Nanomolar Human Acetylcholinesterase Inhibitors: From Rational Design to Validation by X-Ray Crystallography. *ChemMedChem* **2012**, *7* (3), 400–405.

(172) Ronco, C.; Sorin, G.; Nachon, F.; Foucault, R.; Jean, L.; Romieu, A.; Renard, P. Y. Synthesis and Structure-Activity Relationship of Huprine Derivatives as Human Acetylcholinesterase Inhibitors. *Bioorg. Med. Chem.* **2009**, *17* (13), 4523–4536.

(173) Galdeano, C.; Coquelle, N.; Cieslikiewicz-Bouet, M.; Bartolini, M.; Pérez, B.; Clos, M. V.; Silman, I.; Jean, L.; Colletier, J.-P.; Renard, P.-Y.; et al. Increasing Polarity in Tacrine and Huprine Derivatives: Potent Anticholinesterase Agents for the Treatment of Myasthenia Gravis. *Molecules* **2018**, *23* (3), 634.

(174) Aráoz, R.; Bouet, M.; Bartolini, M.; Coquelle, N.; Colletier, J.-P.; Servent, D.; Molgo, J.; Jean, L.; Renard, P.-Y. Multi-Target Directed Ligands: Electrophysiological Characterization of an Anticholinesterase Inhibitor Coupled to an Agonist of A7 Nicotinic Acetylcholine Receptor. *Biochem. Pharmacol.* **2015**, *97* (4), 621.

(175) Oueis, E.; Nachon, F.; Sabot, C.; Renard, P.-Y. First Enzymatic Hydrolysis/Thio-Michael Addition Cascade Route to Synthesis of AChE Inhibitors. *Chem. Commun.* **2014**, *50* (16), 2043–2045.

(176) Viayna, E.; Sola, I.; Bartolini, M.; De Simone, A.; Tapia-Rojas, C.; Serrano, F. G.; Sabaté, R.; Juárez-Jiménez, J.; Pérez, B.; Luque, F. J.; et al. Synthesis and Multitarget Biological Profiling of a Novel Family of Rhein Derivatives as Disease-Modifying Anti-Alzheimer Agents. *J. Med. Chem.* **2014**, *57* (6), 2549–2567.

(177) Galdeano, C.; Viayna, E.; Sola, I.; Formosa, X.; Camps, P.; Badia, A.; Clos, M. V.; Relat, J.; Ratia, M.; Bartolini, M.; et al. Huprine–Tacrine Heterodimers as Anti-Amyloidogenic Compounds of Potential Interest against Alzheimer's and Prion Diseases. *J. Med. Chem.* **2012**, *55* (2), 661–669.

(178) Badia, A.; Baños, J. E.; Camps, P.; Contreras, J.; Görbig, D. M.; Muñoz-Torrero, D.; Simón, M.; Vivas, N. M. Synthesis and Evaluation of Tacrine–Huperzine a Hybrids as Acetylcholinesterase Inhibitors of Potential Interest for the Treatment of Alzheimer's Disease. *Bioorg. Med. Chem.* **1998**, *6* (4), 427–440.

(179) Silman, I.; Sussman, J. L. Acetylcholinesterase: "classical" and "Non-Classical" Functions and Pharmacology. *Curr. Opin. Pharmacol.* **2005**, *5* (3), 293–302.

(180) Van der Kloot, W.; Molgó, J.; Cameron, R.; Colasante, C. Vesicle Size and Transmitter Release at the Frog Neuromuscular Junction When Quantal Acetylcholine Content Is Increased or Decreased. *J. Physiol.* **2002**, *541* (Pt 2), 385–393.

(181) Colović, M. B.; Krstić, D. Z.; Lazarević-Pašti, T. D.; Bondžić, A. M.; Vasić, V. M. Acetylcholinesterase Inhibitors: Pharmacology and Toxicology. *Curr. Neuropharmacol.* **2013**, *11* (3), 315–335.

(182) Berg, J. M.; Tymoczko, J. L.; Stryer, L. Enzymes Are Powerful and Highly Specific Catalysts. *Biochem. 5th Ed.* **2002**.

(183) Sussman, J. L.; Harel, M.; Frolow, F.; Oefner, C.; Goldman, A.; Toker, L.; Silman, I. Atomic Structure of Acetylcholinesterase from Torpedo Californica: A Prototypic Acetylcholine-Binding Protein. *Science* **1991**, *253* (5022), 872–879.

(184) Marchot, P.; Ravelli, R. B.; Raves, M. L.; Bourne, Y.; Vellom, D. C.; Kanter, J.; Camp, S.; Sussman, J. L.; Taylor, P. Soluble Monomeric Acetylcholinesterase from Mouse: Expression, Purification, and Crystallization in Complex with Fasciculin. *Protein Sci. Publ. Protein Soc.* **1996**, *5* (4), 672–679.

(185) Harel, M.; Kryger, G.; Rosenberry, T. L.; Mallender, W. D.; Lewis, T.; Fletcher, R. J.; Guss, J. M.; Silman, I.; Sussman, J. L. Three-Dimensional Structures of Drosophila Melanogaster Acetylcholinesterase and of Its Complexes with Two Potent Inhibitors. *Protein Sci. Publ. Protein Soc.* **2000**, *9* (6), 1063–1072.

(186) Bourne, Y.; Grassi, J.; Bougis, P. E.; Marchot, P. Conformational Flexibility of the Acetylcholinesterase Tetramer Suggested by X-Ray Crystallography. *J. Biol. Chem.* **1999**, *274* (43), 30370–30376.

(187) Kryger, G.; Harel, M.; Giles, K.; Toker, L.; Velan, B.; Lazar, A.; Kronman, C.; Barak, D.; Ariel, N.; Shafferman, A.; et al. Structures of Recombinant Native and E202Q Mutant Human

Acetylcholinesterase Complexed with the Snake-Venom Toxin Fasciculin-II. *Acta Crystallogr. D Biol. Crystallogr.* **2000**, *56* (Pt 11), 1385–1394.

(188) Inestrosa, N. C.; Dinamarca, M. C.; Alvarez, A. Amyloid-Cholinesterase Interactions: Implications for Alzheimer's Disease. *FEBS J.* **2008**, *275* (4), 625–632.

(189) Cheung, J.; Rudolph, M. J.; Burshteyn, F.; Cassidy, M. S.; Gary, E. N.; Love, J.; Franklin, M. C.; Height, J. J. Structures of Human Acetylcholinesterase in Complex with Pharmacologically Important Ligands. *J. Med. Chem.* **2012**, *55* (22), 10282–10286.

(190) Ronco, C.; Carletti, E.; Colletier, J.-P.; Weik, M.; Nachon, F.; Jean, L.; Renard, P.-Y. Huprine Derivatives as Sub-Nanomolar Human Acetylcholinesterase Inhibitors: From Rational Design to Validation by X-Ray Crystallography. *ChemMedChem* **2012**, *7* (3), 400–405.

(191) Ollis, D. L.; Cheah, E.; Cygler, M.; Dijkstra, B.; Frolow, F.; Franken, S. M.; Harel, M.; Remington, S. J.; Silman, I.; Schrag, J. The Alpha/Beta Hydrolase Fold. *Protein Eng.* **1992**, *5* (3), 197–211.

(192) Radic, Z.; Pickering, N. A.; Vellom, D. C.; Camp, S.; Taylor, P. Three Distinct Domains in the Cholinesterase Molecule Confer Selectivity for Acetyl- and Butyrylcholinesterase Inhibitors. *Biochemistry* **1993**, *32* (45), 12074–12084.

(193) Zhang, Y.; Kua, J.; McCammon, J. A. Role of the Catalytic Triad and Oxyanion Hole in Acetylcholinesterase Catalysis: An Ab Initio QM/MM Study. *J. Am. Chem. Soc.* **2002**, *124* (35), 10572–10577.

(194) Froede, H. C.; Wilson, I. B. Direct Determination of Acetyl-Enzyme Intermediate in the Acetylcholinesterase-Catalyzed Hydrolysis of Acetylcholine and Acetylthiocholine. *J. Biol. Chem.* **1984**, *259* (17), 11010–11013.

(195) Bourne, Y.; Radić, Z.; Sulzenbacher, G.; Kim, E.; Taylor, P.; Marchot, P. Substrate and Product Trafficking through the Active Center Gorge of Acetylcholinesterase Analyzed by Crystallography and Equilibrium Binding. *J. Biol. Chem.* **2006**, *281* (39), 29256–29267.

(196) Saxena, A.; Raveh, L.; Ashani, Y.; Doctor, B. P. Structure of Glycan Moieties Responsible for the Extended Circulatory Life Time of Fetal Bovine Serum Acetylcholinesterase and Equine Serum Butyrylcholinesterase. *Biochemistry* **1997**, *36* (24), 7481–7489.

(197) Ma, J. C.; Dougherty, D. A. The Cation−π Interaction. *Chem. Rev.* **1997**, *97* (5), 1303–1324.

(198) Axelsen, P. H.; Harel, M.; Silman, I.; Sussman, J. L. Structure and Dynamics of the Active Site Gorge of Acetylcholinesterase: Synergistic Use of Molecular Dynamics Simulation and X-Ray Crystallography. *Protein Sci. Publ. Protein Soc.* **1994**, *3* (2), 188–197.

(199) Harel, M.; Schalk, I.; Ehret-Sabatier, L.; Bouet, F.; Goeldner, M.; Hirth, C.; Axelsen, P. H.; Silman, I.; Sussman, J. L. Quaternary Ligand Binding to Aromatic Residues in the Active-Site Gorge of Acetylcholinesterase. *Proc. Natl. Acad. Sci.* **1993**, *90* (19), 9031–9035.

(200) Barak, D.; Kronman, C.; Ordentlich, A.; Ariel, N.; Bromberg, A.; Marcus, D.; Lazar, A.; Velan, B.; Shafferman, A. Acetylcholinesterase Peripheral Anionic Site Degeneracy Conferred by Amino Acid Arrays Sharing a Common Core. *J. Biol. Chem.* **1994**, *269* (9), 6296–6305.

(201) Van Belle, D.; De Maria, L.; Iurcu, G.; Wodak, S. J. Pathways of Ligand Clearance in Acetylcholinesterase by Multiple Copy Sampling11Edited by I. B. Honig. *J. Mol. Biol.* **2000**, *298* (4), 705–726.

(202) Chatonnet, A.; Lockridge, O. Comparison of Butyrylcholinesterase and Acetylcholinesterase. *Biochem. J.* **1989**, *260* (3), 625–634.

(203) Li, B.; Stribley, J. A.; Ticu, A.; Xie, W.; Schopfer, L. M.; Hammond, P.; Brimijoin, S.; Hinrichs, S. H.; Lockridge, O. Abundant Tissue Butyrylcholinesterase and Its Possible Function in the Acetylcholinesterase Knockout Mouse. *J. Neurochem.* **2000**, *75* (3), 1320–1331.

(204) Manoharan, I.; Boopathy, R.; Darvesh, S.; Lockridge, O. A Medical Health Report on Individuals with Silent Butyrylcholinesterase in the Vysya Community of India. *Clin. Chim. Acta Int. J. Clin. Chem.* **2007**, *378* (1–2), 128–135.

(205) Greig, N. H.; Lahiri, D. K.; Sambamurti, K. Butyrylcholinesterase: An Important New Target in Alzheimer's Disease Therapy. *Int. Psychogeriatr.* **2002**, *14 Suppl 1*, 77–91.

(206) Rao, A. A.; Sridhar, G. R.; Das, U. N. Elevated Butyrylcholinesterase and Acetylcholinesterase May Predict the Development of Type 2 Diabetes Mellitus and Alzheimer's Disease. *Med. Hypotheses* **2007**, *69* (6), 1272–1276.

(207) Meden, A.; Knez, D.; Jukič, M.; Brazzolotto, X.; Gršič, M.; Pišlar, A.; Zahirović, A.; Kos, J.; Nachon, F.; Svete, J.; et al. Tryptophan-Derived Butyrylcholinesterase Inhibitors as Promising Leads against Alzheimer's Disease. *Chem. Commun.* **2019**, *55* (26), 3765–3768.

(208) Wajid, S.; Khatoon, A.; Khan, M. A.; Zafar, H.; Kanwal, S.; Atta-ur-Rahman; Choudhary, M. I.; Basha, F. Z. Microwave-Assisted Organic Synthesis, Structure–Activity Relationship, Kinetics and Molecular Docking Studies of Non-Cytotoxic Benzamide Derivatives as Selective Butyrylcholinesterase Inhibitors. *Bioorg. Med. Chem.* **2019**, *27* (18), 4030–4040.

(209) Allderdice, P. W.; Gardner, H. A.; Galutira, D.; Lockridge, O.; LaDu, B. N.; McAlpine, P. J. The Cloned Butyrylcholinesterase (BCHE) Gene Maps to a Single Chromosome Site, 3q26. *Genomics* **1991**, *11* (2), 452–454.

(210) Masson, P.; Lockridge, O. Butyrylcholinesterase for Protection from Organophosphorus Poisons: Catalytic Complexities and Hysteretic Behavior. *Arch. Biochem. Biophys.* **2010**, *494* (2), 107–120.

(211) Radic, Z.; Pickering, N. A.; Vellom, D. C.; Camp, S.; Taylor, P. Three Distinct Domains in the Cholinesterase Molecule Confer Selectivity for Acetyl- and Butyrylcholinesterase Inhibitors. *Biochemistry* **1993**, *32* (45), 12074–12084.

(212) Saxena, A.; Redman, A. M.; Jiang, X.; Lockridge, O.; Doctor, B. P. Differences in Active Site Gorge Dimensions of Cholinesterases Revealed by Binding of Inhibitors to Human Butyrylcholinesterase. *Biochemistry* **1997**, *36* (48), 14642–14651.

(213) Brazzolotto, X.; Wandhammer, M.; Ronco, C.; Trovaslet, M.; Jean, L.; Lockridge, O.; Renard, P. Y.; Nachon, F. Human Butyrylcholinesterase Produced in Insect Cells: Huprine-Based Affinity Purification and Crystal Structure. *FEBS J* **2012**, *279*, 2905–2916.

(214) Masson, P.; Xie, W.; Froment, M. T.; Levitsky, V.; Fortier, P. L.; Albaret, C.; Lockridge, O. Interaction between the Peripheral Site Residues of Human Butyrylcholinesterase, D70 and Y332, in Binding and Hydrolysis of Substrates. *Biochim. Biophys. Acta* **1999**, *1433* (1–2), 281–293.

(215) Masson, P.; Xie, W.; Froment, M. T.; Lockridge, O. Effects of Mutations of Active Site Residues and Amino Acids Interacting with the Omega Loop on Substrate Activation of Butyrylcholinesterase. *Biochim. Biophys. Acta* **2001**, *1544* (1–2), 166–176.

(216) Nachon, F.; Carletti, E.; Ronco, C.; Trovaslet, M.; Nicolet, Y.; Jean, L.; Renard, P.-Y. Crystal Structures of Human Cholinesterases in Complex with Huprine W and Tacrine: Elements of Specificity for Anti-Alzheimer's Drugs Targeting Acetyl- and Butyryl-Cholinesterase. *Biochem. J.* **2013**, *453* (3), 393–399.

(217) Ronco, C.; Foucault, R.; Gillon, E.; Bohn, P.; Nachon, F.; Jean, L.; Renard, P.-Y. New Huprine Derivatives Functionalized at Position 9 as Highly Potent Acetylcholinesterase Inhibitors. *ChemMedChem* **2011**, *6* (5), 876–888.

(218) Ronco, C.; Carletti, E.; Colletier, J. P.; Weik, M.; Nachon, F.; Jean, L.; Renard, P. Y. Huprine Derivatives as Sub-Nanomolar Human Acetylcholinesterase Inhibitors: From Rational Design to Validation by X-Ray Crystallography. *ChemMedChem* **2012**, *7* (3), 400–405.

(219) Camps, P.; El Achab, R.; Görbig, D. M.; Morral, J.; Muñoz-Torrero, D.; Badia, A.; Baños, J. E.; Vivas, N. M.; Barril, X.; Orozco, M.; et al. Synthesis, in Vitro Pharmacology, and Molecular Modeling of Very Potent Tacrine−Huperzine A Hybrids as Acetylcholinesterase Inhibitors of Potential Interest for the Treatment of Alzheimer's Disease. *J. Med. Chem.* **1999**, *42* (17), 3227–3242.

(220) Camps, P.; El Achab, R.; Morral, J.; Muñoz-Torrero, D.; Badia, A.; Baños, J. E.; Vivas, N. M.; Barril, X.; Orozco, M.; Luque, F. J. New Tacrine−Huperzine A Hybrids (Huprines): Highly Potent Tight-Binding Acetylcholinesterase Inhibitors of Interest for the Treatment of Alzheimer's Disease. *J. Med. Chem.* **2000**, *43* (24), 4657–4666.

(221) Ros, E.; Aleu, J.; Gómez de Aranda, I.; Muñoz-Torrero, D.; Camps, P.; Badia, A.; Marsal, J.; Solsona, C. The Pharmacology of Novel Acetylcholinesterase Inhibitors, (+/-)-Huprines Y and X, on the Torpedo Electric Organ. *Eur. J. Pharmacol.* **2001**, *421* (2), 77–84.
(222) Camps, P.; Cusack, B.; Mallender, W. D.; Achab, R. E.; Morral, J.; Muñoz-Torrero, D.; Rosenberry, T. L. Huprine X Is a Novel High-Affinity Inhibitor of Acetylcholinesterase That Is of Interest for Treatment of Alzheimer's Disease. *Mol. Pharmacol.* **2000**, *57* (2), 409–417.
(223) Muñoz-Torrero, D.; Pera, M.; Relat, J.; Ratia, M.; Galdeano, C.; Viayna, E.; Sola, I.; Formosa, X.; Camps, P.; Badia, A.; et al. Expanding the Multipotent Profile of Huprine-Tacrine Heterodimers as Disease-Modifying Anti-Alzheimer Agents. *Neurodegener. Dis.* **2012**, *10* (1–4), 96–99.
(224) Roman, S.; Badia, A.; Camps, P.; Clos, M. V. Potentiation Effects of (+/-)Huprine X, a New Acetylcholinesterase Inhibitor, on Nicotinic Receptors in Rat Cortical Synaptosomes. *Neuropharmacology* **2004**, *46* (1), 95–102.
(225) Canudas, A. M.; Pubill, D.; Sureda, F. X.; Verdaguer, E.; Camps, P.; Muñoz-Torrero, D.; Jiménez, A.; Camins, A.; Pallàs, M. Neuroprotective Effects of (±)-Huprine Y on in Vitro and in Vivo Models of Excitoxicity Damage. *Exp. Neurol.* **2003**, *180* (2), 123–130.
(226) Ratia, M.; Giménez-Llort, L.; Camps, P.; Muñoz-Torrero, D.; Clos, M.; Badia, A. Behavioural Effects and Regulation of PKCα and MAPK by Huprine X in Middle Aged Mice. *Pharmacol. Biochem. Behav.* **2010**, *95* (4), 485–493.
(227) Viayna, E.; Gómez, T.; Galdeano, C.; Ramírez, L.; Ratia, M.; Badia, A.; Clos, M. V.; Verdaguer, E.; Junyent, F.; Camins, A.; et al. Novel Huprine Derivatives with Inhibitory Activity toward β-Amyloid Aggregation and Formation as Disease-Modifying Anti-Alzheimer Drug Candidates. *ChemMedChem* **2010**, *5* (11), 1855–1870.
(228) Giménez-Llort, L.; Ratia, M.; Pérez, B.; Camps, P.; Muñoz-Torrero, D.; Badia, A.; Clos, M. V. AVCRI104P3, a Novel Multitarget Compound with Cognition-Enhancing and Anxiolytic Activities: Studies in Cognitively Poor Middle-Aged Mice. *Behav. Brain Res.* **2015**, *286*, 97–103.
(229) Viayna, E.; Sola, I.; Bartolini, M.; De Simone, A.; Tapia-Rojas, C.; Serrano, F. G.; Sabaté, R.; Juárez-Jiménez, J.; Pérez, B.; Luque, F. J.; et al. Synthesis and Multitarget Biological Profiling of a Novel Family of Rhein Derivatives as Disease-Modifying Anti-Alzheimer Agents. *J. Med. Chem.* **2014**, *57* (6), 2549–2567.
(230) Oukoloff, K.; Chao, S.; Cieslikiewicz-Bouet, M.; Mougeot, R.; Jean, L.; Renard, P.-Y. Improved Access to Huprine Derivatives Functionalized at Position 9. *Eur. J. Org. Chem.* **2016**, *2016* (7), 1337–1343.
(231) Ronco, C.; Jean, L.; Renard, P.-Y. Improved Synthetic Pathway for the Derivatization of Huprine Scaffold. *Tetrahedron* **2010**, *66* (37), 7399–7404.
(232) Patent WO2011124712A1.
(233) Bourne, Y.; Kolb, H. C.; Radic, Z.; Sharpless, K. B.; Taylor, P.; Marchot, P. Freeze-Frame Inhibitor Captures Acetylcholinesterase in a Unique Conformation. *Proc.Natl.Acad.Sci.Usa* **2004**, *101*, 1449–1454.
(234) ChemForAse. Home http://www.chemforase.com/products/hupresin.
(235) Brazzolotto, X.; Wandhammer, M.; Ronco, C.; Trovaslet, M.; Jean, L.; Lockridge, O.; Renard, P.-Y.; Nachon, F. Human Butyrylcholinesterase Produced in Insect Cells: Huprine-Based Affinity Purification and Crystal Structure. *FEBS J.* **2012**, *279* (16), 2905–2916.
(236) Alkanaimsh, S.; Corbin, J. M.; Kailemia, M. J.; Karuppanan, K.; Rodriguez, R. L.; Lebrilla, C. B.; McDonald, K. A.; Nandi, S. Purification and Site-Specific N-Glycosylation Analysis of Human Recombinant Butyrylcholinesterase from Nicotiana Benthamiana. *Biochem. Eng. J.* **2019**, *142*, 58–67.
(237) Schopfer, L. M.; Lockridge, O.; David, E.; Hinrichs, S. H. Purification of Human Butyrylcholinesterase from Frozen Cohn Fraction IV-4 by Ion Exchange and Hupresin Affinity Chromatography. *PLOS ONE* **2019**, *14* (1), e0209795.
(238) Onder, S.; David, E.; Tacal, O.; Schopfer, L. M.; Lockridge, O. Hupresin Retains Binding Capacity for Butyrylcholinesterase and Acetylcholinesterase after Sanitation with Sodium Hydroxide. *Front. Pharmacol.* **2017**, *8*.

(239) Nachon, F.; Brazzolotto, X.; Trovaslet, M.; Masson, P. Progress in the Development of Enzyme-Based Nerve Agent Bioscavengers. *Chem. Biol. Interact.* **2013**, *206* (3), 536–544.
(240) Chao, S.; Krejci, E.; Bernard, V.; Leroy, J.; Jean, L.; Renard, P.-Y. A Selective and Sensitive Near-Infrared Fluorescent Probe for Acetylcholinesterase Imaging. *Chem. Commun.* **2016**, *52* (77), 11599–11602.
(241) Feng, Y.; Wang, X. Antioxidant Therapies for Alzheimer's Disease. *Oxid. Med. Cell. Longev.* **2012**, *2012*.
(242) Colizzi, C. The Protective Effects of Polyphenols on Alzheimer's Disease: A Systematic Review. *Alzheimers Dement. Transl. Res. Clin. Interv.* **2019**, *5*, 184–196.
(243) Sharma, S. K.; Vij, A. S.; Sharma, M. Mechanisms and Clinical Uses of Capsaicin. *Eur. J. Pharmacol.* **2013**, *720* (1), 55–62.
(244) Adaszek, Ł.; Gadomska, D.; Mazurek, Ł.; Łyp, P.; Madany, J.; Winiarczyk, S. Properties of Capsaicin and Its Utility in Veterinary and Human Medicine. *Res. Vet. Sci.* **2019**, *123*, 14–19.
(245) Delanty, N.; Dichter, M. A. Antioxidant Therapy in Neurologic Disease. *Arch. Neurol.* **2000**, *57* (9), 1265–1270.
(246) Dairam, A.; Fogel, R.; Daya, S.; Limson, J. L. Antioxidant and Iron-Binding Properties of Curcumin, Capsaicin, and S-Allylcysteine Reduce Oxidative Stress in Rat Brain Homogenate. *J. Agric. Food Chem.* **2008**, *56* (9), 3350–3356.
(247) Jiang, X.; Jia, L.-W.; Li, X.-H.; Cheng, X.-S.; Xie, J.-Z.; Ma, Z.-W.; Xu, W.-J.; Liu, Y.; Yao, Y.; Du, L.-L.; et al. Capsaicin Ameliorates Stress-Induced Alzheimer's Disease-Like Pathological and Cognitive Impairments in Rats. *J. Alzheimers Dis.* **2013**, *35* (1), 91–105.
(248) Chen, D.; Daniel, K. G.; Kuhn, D. J.; Kazi, A.; Bhuiyan, M.; Li, L.; Wang, Z.; Wan, S. B.; Lam, W. H.; Chan, T. H.; et al. Green Tea and Tea Polyphenols in Cancer Prevention. *Front. Biosci. J. Virtual Libr.* **2004**, *9*, 2618–2631.
(249) Laughton, M. J.; Evans, P. J.; Moroney, M. A.; Hoult, J. R. S.; Halliwell, B. Inhibition of Mammalian 5-Lipoxygenase and Cyclo-Oxygenase by Flavonoids and Phenolic Dietary Additives. *Biochem. Pharmacol.* **1991**, *42* (9), 1673–1681.
(250) Kumar, S.; Pandey, A. K. Chemistry and Biological Activities of Flavonoids: An Overview. *Sci. World J.* **2013**, *2013*, 1–16.
(251) Bors, W.; Heller, W.; Michel, C.; Saran, M. [36] Flavonoids as Antioxidants: Determination of Radical-Scavenging Efficiencies. In *Methods in Enzymology*; Elsevier, 1990; Vol. 186, pp 343–355.
(252) Shimmyo, Y.; Kihara, T.; Akaike, A.; Niidome, T.; Sugimoto, H. Flavonols and Flavones as BACE-1 Inhibitors: Structure–Activity Relationship in Cell-Free, Cell-Based and in Silico Studies Reveal Novel Pharmacophore Features. *Biochim. Biophys. Acta BBA - Gen. Subj.* **2008**, *1780* (5), 819–825.
(253) Wang, J.; Yu, Z.; Yu, Q.; Kong, Q.; Zhang, N.; He, L.; Yi, Y. Study on Neuroprotective Capacity of Key Flavonoids of *Ampelopsis Grossedentata*. *J. Food Nutr. Res.* **2014**, *2* (12), 880–889.
(254) Okello, E. J.; Leylabi, R.; McDougall, G. J. Inhibition of Acetylcholinesterase by Green and White Tea and Their Simulated Intestinal Metabolites. *Food Funct.* **2012**, *3* (6), 651.
(255) Choi, Y.-T.; Jung, C.-H.; Lee, S.-R.; Bae, J.-H.; Baek, W.-K.; Suh, M.-H.; Park, J.; Park, C.-W.; Suh, S.-I. The Green Tea Polyphenol (−)-Epigallocatechin Gallate Attenuates β-Amyloid-Induced Neurotoxicity in Cultured Hippocampal Neurons. *Life Sci.* **2001**, *70* (5), 603–614.
(256) Wobst, H. J.; Sharma, A.; Diamond, M. I.; Wanker, E. E.; Bieschke, J. The Green Tea Polyphenol (−)-Epigallocatechin Gallate Prevents the Aggregation of Tau Protein into Toxic Oligomers at Substoichiometric Ratios. *FEBS Lett.* **2015**, *589* (1), 77–83.
(257) Niki, E. Role of Vitamin E as a Lipid-Soluble Peroxyl Radical Scavenger: In Vitro and in Vivo Evidence. *Free Radic. Biol. Med.* **2014**, *66*, 3–12.
(258) Ulatowski, L.; Parker, R.; Warrier, G.; Sultana, R.; Butterfield, D. A.; Manor, D. Vitamin E Is Essential for Purkinje Neuron Integrity. *Neuroscience* **2014**, *260*, 120–129.
(259) Valko, M.; Izakovic, M.; Mazur, M.; Rhodes, C. J.; Telser, J. Role of Oxygen Radicals in DNA Damage and Cancer Incidence. *Mol. Cell. Biochem.* **2004**, *266* (1/2), 37–56.

(260) Yatin, S. M.; Varadarajan, S.; Butterfield, D. A. Vitamin E Prevents Alzheimer's Amyloid Beta-Peptide (1-42)-Induced Neuronal Protein Oxidation and Reactive Oxygen Species Production. *J. Alzheimers Dis. JAD* **2000**, *2* (2), 123–131.

(261) Dysken, M. W.; Guarino, P. D.; Vertrees, J. E.; Asthana, S.; Sano, M.; Llorente, M.; Pallaki, M.; Love, S.; Schellenberg, G. D.; McCarten, J. R.; et al. Vitamin E and Memantine in Alzheimer's Disease: Clinical Trial Methods and Baseline Data. *Alzheimers Dement. J. Alzheimers Assoc.* **2014**, *10* (1), 36–44.

(262) Kryscio, R. J.; Abner, E. L.; Caban-Holt, A.; Lovell, M.; Goodman, P.; Darke, A. K.; Yee, M.; Crowley, J.; Schmitt, F. A. Association of Antioxidant Supplement Use and Dementia in the Prevention of Alzheimer's Disease by Vitamin E and Selenium Trial (PREADViSE). *JAMA Neurol.* **2017**, *74* (5), 567–573.

(263) Gao, S.; Jin, Y.; Hall, K. S.; Liang, C.; Unverzagt, F. W.; Ji, R.; Murrell, J. R.; Cao, J.; Shen, J.; Ma, F.; et al. Selenium Level and Cognitive Function in Rural Elderly Chinese. *Am. J. Epidemiol.* **2007**, *165* (8), 955–965.

(264) Arnaud, J.; Akbaraly, N. T.; Hininger, I.; Roussel, A.-M.; Berr, C. Factors Associated with Longitudinal Plasma Selenium Decline in the Elderly: The EVA Study. *J. Nutr. Biochem.* **2007**, *18* (7), 482–487.

(265) Rodrigues, R.; Petersen, R. B.; Perry, G. Parallels between Major Depressive Disorder and Alzheimer's Disease: Role of Oxidative Stress and Genetic Vulnerability. *Cell. Mol. Neurobiol.* **2014**, *34* (7), 925–949.

(266) Ellman, G. L.; Courtney, K. D.; Andres, V.; Featherstone, R. M. A New and Rapid Colorimetric Determination of Acetylcholinesterase Activity. *Biochem. Pharmacol.* **1961**, *7* (2), 88–95.

(267) Khorana, N.; Markmee, S.; Ingkaninan, K.; Ruchirawat, S.; Kitbunnadaj, R.; Pullagurla, M. R. Evaluation of a New Lead for Acetylcholinesterase Inhibition. *Med. Chem. Res.* **2008**, *18* (3), 231.

(268) Brand-Williams, W.; Cuvelier, M. E.; Berset, C. Use of a Free Radical Method to Evaluate Antioxidant Activity. *LWT - Food Sci. Technol.* **1995**, *28* (1), 25–30.

(269) Teixeira, J.; Gaspar, A.; Garrido, E. M.; Garrido, J.; Borges, F. Hydroxycinnamic Acid Antioxidants: An Electrochemical Overview. *BioMed Res. Int.* **2013**, *2013*, 1–11.

(270) Di, L.; Kerns, E. H.; Fan, K.; McConnell, O. J.; Carter, G. T. High Throughput Artificial Membrane Permeability Assay for Blood-Brain Barrier. *Eur. J. Med. Chem.* **2003**, *38* (3), 223–232.

(271) Lipinski, C. A.; Lombardo, F.; Dominy, B. W.; Feeney, P. J. Experimental and Computational Approaches to Estimate Solubility and Permeability in Drug Discovery and Development Settings1PII of Original Article: S0169-409X(96)00423-1. The Article Was Originally Published in Advanced Drug Delivery Reviews 23 (1997) 3–25.1. *Adv. Drug Deliv. Rev.* **2001**, *46* (1), 3–26.

(272) Wager, T. T.; Hou, X.; Verhoest, P. R.; Villalobos, A. Central Nervous System Multiparameter Optimization Desirability: Application in Drug Discovery. *ACS Chem. Neurosci.* **2016**, *7* (6), 767–775.

(273) Wager, T. T.; Hou, X.; Verhoest, P. R.; Villalobos, A. Moving beyond Rules: The Development of a Central Nervous System Multiparameter Optimization (CNS MPO) Approach To Enable Alignment of Druglike Properties. *ACS Chem. Neurosci.* **2010**, *1* (6), 435–449.

(274) Hucho, F.; Changeux, J. P. Molecular Weight and Quaternary Structure of the Cholinergic Receptor Protein Extracted by Detergents from Electrophorus Electricus Electric Tissue. *FEBS Lett.* **1973**, *38* (1), 11–15.

(275) Cartaud, J.; Benedetti, E. L.; Cohen, J. B.; Meunier, J. C.; Changeux, J. P. Presence of a Lattice Structure in Membrane Fragments Rich in Nicotinic Receptor Protein from the Electric Organ of Torpedo Marmorata. *FEBS Lett.* **1973**, *33* (1), 109–113.

(276) Dellisanti, C. D.; Yao, Y.; Stroud, J. C.; Wang, Z.-Z.; Chen, L. Crystal Structure of the Extracellular Domain of NAChR Alpha1 Bound to Alpha-Bungarotoxin at 1.94 A Resolution. *Nat. Neurosci.* **2007**, *10* (8), 953–962.

(277) Smit, A. B.; Syed, N. I.; Schaap, D.; van Minnen, J.; Klumperman, J.; Kits, K. S.; Lodder, H.; van der Schors, R. C.; van Elk, R.; Sorgedrager, B.; et al. A Glia-Derived Acetylcholine-Binding Protein That Modulates Synaptic Transmission. *Nature* **2001**, *411* (6835), 261–268.

(278) Shahsavar, A.; Gajhede, M.; Kastrup, J. S.; Balle, T. Structural Studies of Nicotinic Acetylcholine Receptors: Using Acetylcholine-Binding Protein as a Structural Surrogate. *Basic Clin. Pharmacol. Toxicol.* **2016**, *118* (6), 399–407.

(279) Hansen, S. B.; Talley, T. T.; Radic, Z.; Taylor, P. Structural and Ligand Recognition Characteristics of an Acetylcholine-Binding Protein from Aplysia Californica. *J. Biol. Chem.* **2004**, *279* (23), 24197–24202.

(280) Tasneem, A.; Iyer, L. M.; Jakobsson, E.; Aravind, L. Identification of the Prokaryotic Ligand-Gated Ion Channels and Their Implications for the Mechanisms and Origins of Animal Cys-Loop Ion Channels. *Genome Biol.* **2005**, *6* (1), R4.

(281) Li, S. X.; Cheng, K.; Gomoto, R.; Bren, N.; Huang, S.; Sine, S.; Chen, L. Structural Principles for Alpha-Neurotoxin Binding to and Selectivity among Nicotinic Receptors. *BE Publ.*

(282) Spurny, R.; Debaveye, S.; Farinha, A.; Veys, K.; Vos, A. M.; Gossas, T.; Atack, J.; Bertrand, S.; Bertrand, D.; Danielson, U. H.; et al. Molecular Blueprint of Allosteric Binding Sites in a Homologue of the Agonist-Binding Domain of the Alpha7 Nicotinic Acetylcholine Receptor. *Proc.Natl.Acad.Sci.USA* **2015**, *112*, E2543.

(283) Corringer, P.-J.; Galzi, J.-L.; Eiselé, J.-L.; Bertrand, S.; Changeux, J.-P.; Bertrand, D. Identification of a New Component of the Agonist Binding Site of the Nicotinic 7 Homooligomeric Receptor. *J. Biol. Chem.* **1995**, *270* (20), 11749–11752.

(284) Hendrickson, L. M.; Guildford, M. J.; Tapper, A. R. Neuronal Nicotinic Acetylcholine Receptors: Common Molecular Substrates of Nicotine and Alcohol Dependence. *Front. Psychiatry* **2013**, *4*.

(285) Charon, A. T. and S. α7 Nicotinic Acetylcholine Receptors: A Therapeutic Target in the Structure Era http://www.eurekaselect.com/97180/article.

(286) Dennis, M.; Giraudat, J.; Kotzyba-Hibert, F.; Goeldner, M.; Hirth, C.; Chang, J. Y.; Lazure, C.; Chrétien, M.; Changeux, J. P. Amino Acids of the Torpedo Marmorata Acetylcholine Receptor Alpha Subunit Labeled by a Photoaffinity Ligand for the Acetylcholine Binding Site. *Biochemistry* **1988**, *27* (7), 2346–2357.

(287) Dougherty, D. A.; Stauffer, D. A. Acetylcholine Binding by a Synthetic Receptor: Implications for Biological Recognition. *Science* **1990**, *250* (4987), 1558–1560.

(288) Cecchini, M.; Changeux, J.-P. The Nicotinic Acetylcholine Receptor and Its Prokaryotic Homologues: Structure, Conformational Transitions & Allosteric Modulation. *Neuropharmacology* **2015**, *96*, 137–149.

(289) Giraudat, J.; Dennis, M.; Heidmann, T.; Chang, J. Y.; Changeux, J. P. Structure of the High-Affinity Binding Site for Noncompetitive Blockers of the Acetylcholine Receptor: Serine-262 of the Delta Subunit Is Labeled by [3H]Chlorpromazine. *Proc. Natl. Acad. Sci.* **1986**, *83* (8), 2719–2723.

(290) Nickell, J. R.; Grinevich, V. P.; Siripurapu, K. B.; Smith, A. M.; Dwoskin, L. P. Potential Therapeutic Uses of Mecamylamine and Its Stereoisomers. *Pharmacol. Biochem. Behav.* **2013**, *108*, 28–43.

(291) Changeux, J.-P. The Nicotinic Acetylcholine Receptor: A Typical 'Allosteric Machine.' *Philos. Trans. R. Soc. B Biol. Sci.* **2018**, *373* (1749), 20170174.

(292) Monod, J.; Wyman, J.; Changeux, J.-P. On the Nature of Allosteric Transitions: A Plausible Model. *J. Mol. Biol.* **1965**, *12* (1), 88–118.

(293) Changeux, J.-P.; Taly, A. Nicotinic Receptors, Allosteric Proteins and Medicine. *Trends Mol. Med.* **2008**, *14* (3), 93–102.

(294) Mulle, C.; Léna, C.; Changeux, J.-P. Potentiation of Nicotinic Receptor Response by External Calcium in Rat Central Neurons. *Neuron* **1992**, *8* (5), 937–945.

(295) Kabbani, N.; Woll, M. P.; Levenson, R.; Lindstrom, J. M.; Changeux, J.-P. Intracellular Complexes of the 2 Subunit of the Nicotinic Acetylcholine Receptor in Brain Identified by Proteomics. *Proc. Natl. Acad. Sci.* **2007**, *104* (51), 20570–20575.

(296) Corradi, J.; Bouzat, C. Understanding the Bases of Function and Modulation of 7 Nicotinic Receptors: Implications for Drug Discovery. *Mol. Pharmacol.* **2016**, *90* (3), 288–299.

(297) Basak, S.; Schmandt, N.; Gicheru, Y.; Chakrapani, S. Crystal Structure and Dynamics of a Lipid-Induced Potential Desensitized-State of a Pentameric Ligand-Gated Channel. *eLife* **2017**, *6*.

(298) Gee, K. W.; Olincy, A.; Kanner, R.; Johnson, L.; Hogenkamp, D.; Harris, J.; Tran, M.; Edmonds, S. A.; Sauer, W.; Yoshimura, R.; et al. First in Human Trial of a Type I Positive Allosteric Modulator of Alpha7-Nicotinic Acetylcholine Receptors: Pharmacokinetics, Safety, and Evidence for Neurocognitive Effect of AVL-3288. *J. Psychopharmacol. (Oxf.)* **2017**, *31* (4), 434–441.

(299) Ng, H. J.; Whittemore, E. R.; Tran, M. B.; Hogenkamp, D. J.; Broide, R. S.; Johnstone, T. B.; Zheng, L.; Stevens, K. E.; Gee, K. W. Nootropic 7 Nicotinic Receptor Allosteric Modulator Derived from GABAA Receptor Modulators. *Proc. Natl. Acad. Sci.* **2007**, *104* (19), 8059–8064.

(300) Broad, L. M.; Zwart, R.; Pearson, K. H.; Lee, M.; Wallace, L.; McPhie, G. I.; Emkey, R.; Hollinshead, S. P.; Dell, C. P.; Baker, S. R.; et al. Identification and Pharmacological Profile of a New Class of Selective Nicotinic Acetylcholine Receptor Potentiators. *J. Pharmacol. Exp. Ther.* **2006**, *318* (3), 1108–1117.

(301) Timmermann, D. B.; Grønlien, J. H.; Kohlhaas, K. L.; Nielsen, E. Ø.; Dam, E.; Jørgensen, T. D.; Ahring, P. K.; Peters, D.; Holst, D.; Chrsitensen, J. K.; et al. An Allosteric Modulator of the A7 Nicotinic Acetylcholine Receptor Possessing Cognition-Enhancing Properties in Vivo. *J. Pharmacol. Exp. Ther.* **2007**, *323* (1), 294–307.

(302) Hurst, R. S.; Hajós, M.; Raggenbass, M.; Wall, T. M.; Higdon, N. R.; Lawson, J. A.; Rutherford-Root, K. L.; Berkenpas, M. B.; Hoffmann, W. E.; Piotrowski, D. W.; et al. A Novel Positive Allosteric Modulator of the A7 Neuronal Nicotinic Acetylcholine Receptor: In Vitro and In Vivo Characterization. *J. Neurosci.* **2005**, *25* (17), 4396–4405.

(303) Callahan, P. M.; Hutchings, E. J.; Kille, N. J.; Chapman, J. M.; Terry, A. V. Positive Allosteric Modulator of Alpha 7 Nicotinic-Acetylcholine Receptors, PNU-120596 Augments the Effects of Donepezil on Learning and Memory in Aged Rodents and Non-Human Primates. *Neuropharmacology* **2013**, *67*, 201–212.

(304) Malysz, J.; Grønlien, J. H.; Anderson, D. J.; Håkerud, M.; Thorin-Hagene, K.; Ween, H.; Wetterstrand, C.; Briggs, C. A.; Faghih, R.; Bunnelle, W. H.; et al. In Vitro Pharmacological Characterization of a Novel Allosteric Modulator of A7 Neuronal Acetylcholine Receptor, 4-(5-(4-Chlorophenyl)-2-Methyl-3-Propionyl-1 *H* -Pyrrol-1-Yl)Benzenesulfonamide (A-867744), Exhibiting Unique Pharmacological Profile. *J. Pharmacol. Exp. Ther.* **2009**, *330* (1), 257–267.

(305) Dinklo, T.; Shaban, H.; Thuring, J. W.; Lavreysen, H.; Stevens, K. E.; Zheng, L.; Mackie, C.; Grantham, C.; Vandenberk, I.; Meulders, G.; et al. Characterization of 2-[[4-Fluoro-3-(Trifluoromethyl)Phenyl]Amino]-4-(4-Pyridinyl)-5-Thiazolemethanol (JNJ-1930942), a Novel Positive Allosteric Modulator of the α_7 Nicotinic Acetylcholine Receptor. *J. Pharmacol. Exp. Ther.* **2011**, *336* (2), 560–574.

(306) Pin, F.; Vercouillie, J.; Ouach, A.; Mavel, S.; Gulhan, Z.; Chicheri, G.; Jarry, C.; Massip, S.; Deloye, J.-B.; Guilloteau, D.; et al. Design of A7 Nicotinic Acetylcholine Receptor Ligands in Quinuclidine, Tropane and Quinazoline Series. Chemistry, Molecular Modeling, Radiochemistry, in Vitro and in Rats Evaluations of a [18F] Quinuclidine Derivative. *Eur. J. Med. Chem.* **2014**, *82*, 214–224.

(307) Ouach, A.; Pin, F.; Bertrand, E.; Vercouillie, J.; Gulhan, Z.; Mothes, C.; Deloye, J.-B.; Guilloteau, D.; Suzenet, F.; Chalon, S.; et al. Design of A7 Nicotinic Acetylcholine Receptor Ligands Using the (Het)Aryl-1,2,3-Triazole Core: Synthesis, in Vitro Evaluation and SAR Studies. *Eur. J. Med. Chem.* **2016**, *107*, 153–164.

(308) Weinstock, M.; Goren, T.; Youdim, M. B. H. Development of a Novel Neuroprotective Drug (TV3326) for the Treatment of Alzheimer's Disease, with Cholinesterase and Monoamine Oxidase Inhibitory Activities. *Drug Dev. Res.* **2000**, *50* (3–4), 216–222.

(309) Sterling, J.; Herzig, Y.; Goren, T.; Finkelstein, N.; Lerner, D.; Goldenberg, W.; Miskolczi, I.; Molnar, S.; Rantal, F.; Tamas, T.; et al. Novel Dual Inhibitors of AChE and MAO Derived from Hydroxy Aminoindan and Phenethylamine as Potential Treatment for Alzheimer's Disease. *J. Med. Chem.* **2002**, *45* (24), 5260–5279.

(310) Daneman, R.; Prat, A. The Blood–Brain Barrier. *Cold Spring Harb. Perspect. Biol.* **2015**, *7* (1), a020412.

(311) Stamatovic, S. M.; Andjelkovic, R. F. K. and A. V. Brain Endothelial Cell-Cell Junctions: How to "Open" the Blood Brain Barrier http://www.eurekaselect.com/67655/article.

(312) Abbott, N. J.; Patabendige, A. A. K.; Dolman, D. E. M.; Yusof, S. R.; Begley, D. J. Structure and Function of the Blood–Brain Barrier. *Neurobiol. Dis.* **2010**, *37* (1), 13–25.

(313) Shultz, M. D. Two Decades under the Influence of the Rule of Five and the Changing Properties of Approved Oral Drugs. *J. Med. Chem.* **2019**, *62* (4), 1701–1714.

(314) Lanevskij, K.; Japertas, P.; Didziapetris, R.; Petrauskas, A. Ionization-Specific Prediction of Blood–Brain Permeability. *J. Pharm. Sci.* **2009**, *98* (1), 122–134.

(315) Liu, X.; Smith, B. J.; Chen, C.; Callegari, E.; Becker, S. L.; Chen, X.; Cianfrogna, J.; Doran, A. C.; Doran, S. D.; Gibbs, J. P.; et al. Use of a Physiologically Based Pharmacokinetic Model to Study the Time to Reach Brain Equilibrium: An Experimental Analysis of the Role of Blood-Brain Barrier Permeability, Plasma Protein Binding, and Brain Tissue Binding. *J. Pharmacol. Exp. Ther.* **2005**, *313* (3), 1254–1262.

(316) Aarthy, M.; Panwar, U.; Selvaraj, C.; Singh, S. K. Advantages of Structure-Based Drug Design Approaches in Neurological Disorders. *Curr. Neuropharmacol.* **2017**, *15* (8), 1136–1155.

(317) Halgren, T. A. Merck Molecular Force Field. I. Basis, Form, Scope, Parameterization, and Performance of MMFF94. *J. Comput. Chem.* **1996**, *17* (5–6), 490–519.

(318) Trott, O.; Olson, A. J. AutoDock Vina: Improving the Speed and Accuracy of Docking with a New Scoring Function, Efficient Optimization and Multithreading. *J. Comput. Chem.* **2010**, *31* (2), 455–461.

(319) Wang, R.; Fang, X.; Lu, Y.; Wang, S. The PDBbind Database: Collection of Binding Affinities for Protein−Ligand Complexes with Known Three-Dimensional Structures. *J. Med. Chem.* **2004**, *47* (12), 2977–2980.

(320) Cornell, W. D.; Cieplak, P.; Bayly, C. I.; Gould, I. R.; Merz, K. M.; Ferguson, D. M.; Spellmeyer, D. C.; Fox, T.; Caldwell, J. W.; Kollman, P. A. A Second Generation Force Field for the Simulation of Proteins, Nucleic Acids, and Organic Molecules. *J. Am. Chem. Soc.* **1995**, *117* (19), 5179–5197.

(321) Wang, R.; Lai, L.; Wang, S. Further Development and Validation of Empirical Scoring Functions for Structure-Based Binding Affinity Prediction. *J. Comput. Aided Mol. Des.* **2002**, *16* (1), 11–26.

(322) RCSB PDB - 1Q84: Crystal structure of the mouse acetylcholinesterase-TZ2PA6 anti complex https://www.rcsb.org/structure/1Q84.

(323) Bar-On, P.; Millard, C. B.; Harel, M.; Dvir, H.; Enz, A.; Sussman, J. L.; Silman, I. Kinetic and Structural Studies on the Interaction of Cholinesterases with the Anti-Alzheimer Drug Rivastigmine † , ‡. *Biochemistry* **2002**, *41* (11), 3555–3564.

(324) Dighe, S. N.; Mora, E. D. la; Chan, S.; Kantham, S.; McColl, G.; Miles, J. A.; Veliyath, S. K.; Sreenivas, B. Y.; Nassar, Z. D.; Silman, I.; et al. Rivastigmine and Metabolite Analogues with Putative Alzheimer's Disease-Modifying Properties in a Caenorhabditis Elegans Model. *Commun. Chem.* **2019**, *2* (1), 1–14.

(325) Rostovtsev, V. V.; Green, L. G.; Fokin, V. V.; Sharpless, K. B. A Stepwise Huisgen Cycloaddition Process: Copper(I)-Catalyzed Regioselective "Ligation" of Azides and Terminal Alkynes. *Angew. Chem. Int. Ed.* **2002**, *41* (14), 2596–2599.

(326) Tornøe, C. W.; Sanderson, S. J.; Mottram, J. C.; Coombs, G. H.; Meldal, M. Combinatorial Library of Peptidotriazoles: Identification of [1,2,3]-Triazole Inhibitors against a Recombinant Leishmania Mexicana Cysteine Protease. *J. Comb. Chem.* **2004**, *6* (3), 312–324.
(327) Bourne, Y.; Kolb, H. C.; Radić, Z.; Sharpless, K. B.; Taylor, P.; Marchot, P. Freeze-Frame Inhibitor Captures Acetylcholinesterase in a Unique Conformation. *Proc. Natl. Acad. Sci. U. S. A.* **2004**, *101* (6), 1449–1454.
(328) Whiting, M.; Muldoon, J.; Lin, Y.-C.; Silverman, S. M.; Lindstrom, W.; Olson, A. J.; Kolb, H. C.; Finn, M. G.; Sharpless, K. B.; Elder, J. H.; et al. Inhibitors of HIV-1 Protease by Using in Situ Click Chemistry. *Angew. Chem. Int. Ed Engl.* **2006**, *45* (9), 1435–1439.
(329) Berdini, V.; Cesta, M. C.; Curti, R.; D'Anniballe, G.; Bello, N. D.; Nano, G.; Nicolini, L.; Topai, A.; Allegretti, M. A Modified Palladium Catalysed Reductive Amination Procedure. *Tetrahedron* **2002**, *58* (28), 5669–5674.
(330) Alper, P. B.; Hung, S.-C.; Wong, C.-H. Metal Catalyzed Diazo Transfer for the Synthesis of Azides from Amines. *Tetrahedron Lett.* **1996**, *37* (34), 6029–6032.
(331) Nyffeler, P. T.; Liang, C.-H.; Koeller, K. M.; Wong, C.-H. The Chemistry of Amine−Azide Interconversion: Catalytic Diazotransfer and Regioselective Azide Reduction. *J. Am. Chem. Soc.* **2002**, *124* (36), 10773–10778.
(332) Titz, A.; Radic, Z.; Schwardt, O.; Ernst, B. A Safe and Convenient Method for the Preparation of Triflyl Azide, and Its Use in Diazo Transfer Reactions to Primary Amines. *Tetrahedron Lett.* **2006**, *47* (14), 2383–2385.
(333) Bräse, S.; Gil, C.; Knepper, K.; Zimmermann, V. Organic Azides: An Exploding Diversity of a Unique Class of Compounds. *Angew. Chem. Int. Ed Engl.* **2005**, *44* (33), 5188–5240.
(334) Pandiakumar, A. K.; Sarma, S. P.; Samuelson, A. G. Mechanistic Studies on the Diazo Transfer Reaction. *Tetrahedron Lett.* **2014**, *55* (18), 2917–2920.
(335) Ruano, J. L. G.; Alemán, J.; Parra, A.; Cid, M. B. Preparation of N-p-Tolylsulfonyl-(E)-1-Phenylethylideneimine. In *Organic Syntheses*; American Cancer Society, 2007; pp 129–138.
(336) Fuchs, M.; Koszelewski, D.; Tauber, K.; Kroutil, W.; Faber, K. Chemoenzymatic Asymmetric Total Synthesis of (S)-Rivastigmine Using ω-Transaminases. *Chem. Commun.* **2010**, *46* (30), 5500–5502.
(337) Mercey, G.; Verdelet, T.; Saint-André, G.; Gillon, E.; Wagner, A.; Baati, R.; Jean, L.; Nachon, F.; Renard, P.-Y. First Efficient Uncharged Reactivators for the Dephosphylation of Poisoned Human Acetylcholinesterase. *Chem. Commun.* **2011**, *47* (18), 5295.
(338) Tassano, E.; Alama, A.; Basso, A.; Dondo, G.; Galatini, A.; Riva, R.; Banfi, L. Conjugation of Hydroxytyrosol with Other Natural Phenolic Fragments: From Waste to Antioxidants and Antitumour Compounds. *Eur. J. Org. Chem.* **2015**, *2015* (30), 6710–6726.
(339) John, A.; Nicholas, K. M. Palladium Catalyzed C–H Functionalization of *O* -Arylcarbamates: Selective *Ortho* -Bromination Using NBS. *J. Org. Chem.* **2012**, *77* (13), 5600–5605.
(340) Sarasamkan, J.; Scheunemann, M.; Apaijai, N.; Palee, S.; Parichatikanond, W.; Arunrungvichian, K.; Fischer, S.; Chattipakorn, S.; Deuther-Conrad, W.; Schüürmann, G.; et al. Varying Chirality Across Nicotinic Acetylcholine Receptor Subtypes: Selective Binding of Quinuclidine Triazole Compounds. *ACS Med. Chem. Lett.* **2016**, *7* (10), 890–895.
(341) Yung-Chi, C.; Prusoff, W. H. Relationship between the Inhibition Constant (KI) and the Concentration of Inhibitor Which Causes 50 per Cent Inhibition (I50) of an Enzymatic Reaction. *Biochem. Pharmacol.* **1973**, *22* (23), 3099–3108.
(342) Ouach, A.; Vercouillie, J.; Bertrand, E.; Rodrigues, N.; Pin, F.; Serriere, S.; Boiaryna, L.; Chartier, A.; Percina, N.; Tangpong, P.; et al. Bis(Het)Aryl-1,2,3-Triazole Quinuclidines as A7 Nicotinic Acetylcholine Receptor Ligands: Synthesis, Structure Affinity Relationships, Agonism Activity, [18F]-Radiolabeling and PET Study in Rats. *Eur. J. Med. Chem.* **2019**, *179*, 449–469.
(343) Waring, M. J. Lipophilicity in Drug Discovery. *Expert Opin. Drug Discov.* **2010**, *5* (3), 235–248.
(344) Liu, S.; Chen, X.; Hu, Y.; Yuan, L.; Chen, S.; Wu, P.; Wang, W.; Zhang, S.; Zhang, W. An Efficient Method for the Production of Terminal Alkynes from 1,1-Dibromo-1-Alkenes and Its

Application in the Total Synthesis of Natural Product Dihydroxerulin. *Adv. Synth. Catal.* **2015**, *357* (2–3), 553–560.

(345) Beckmann, H. S. G.; Wittmann, V. One-Pot Procedure for Diazo Transfer and Azide−Alkyne Cycloaddition: Triazole Linkages from Amines. *Org. Lett.* **2007**, *9* (1), 1–4.

(346) Smith, N. M.; Greaves, M. J.; Jewell, R.; Perry, M. W. D.; Stocks, M. J.; Stonehouse, J. P. One-Pot, Three-Component Copper-Catalysed 'Click' Triazole Synthesis Utilising the Inexpensive, Shelf-Stable Diazotransfer Reagent Imidazole-1-Sulfonyl Azide Hydrochloride. *Synlett* **2009**, *2009* (9), 1391–1394.

(347) Maisonneuve, S.; Xie, J. One-Pot Synthesis of 1,4-Disubstituted 1,2,3-Triazoles from Aldehydes and Amines. *Synlett* **2009**, *2009* (18), 2977–2981.

(348) Johansson, J. R.; Lincoln, P.; Nordén, B.; Kann, N. Sequential One-Pot Ruthenium-Catalyzed Azide−Alkyne Cycloaddition from Primary Alkyl Halides and Sodium Azide. *J. Org. Chem.* **2011**, *76* (7), 2355–2359.

(349) Sugimoto, H.; Yamanish, Y.; Iimura, Y.; Kawakami, Y. Donepezil Hydrochloride (E2020) and Other Acetylcholinesterase Inhibitors. *Curr. Med. Chem.* **2000**, *7* (3), 303–339.

(350) Kryger, G.; Silman, I.; Sussman, J. L. Structure of Acetylcholinesterase Complexed with E2020 (Aricept®): Implications for the Design of New Anti-Alzheimer Drugs. *Structure* **1999**, *7* (3), 297–307.

(351) Cheung, J.; Rudolph, M. J.; Burshteyn, F.; Cassidy, M. S.; Gary, E. N.; Love, J.; Franklin, M. C.; Height, J. J. Structures of Human Acetylcholinesterase in Complex with Pharmacologically Important Ligands. *J.Med.Chem.* **2012**, *55*, 10282–10286.

(352) Li, Q.; He, S.; Chen, Y.; Feng, F.; Qu, W.; Sun, H. Donepezil-Based Multi-Functional Cholinesterase Inhibitors for Treatment of Alzheimer's Disease. *Eur. J. Med. Chem.* **2018**, *158*, 463–477.

(353) Wang, J.; Wang, Z.-M.; Li, X.-M.; Li, F.; Wu, J.-J.; Kong, L.-Y.; Wang, X.-B. Synthesis and Evaluation of Multi-Target-Directed Ligands for the Treatment of Alzheimer's Disease Based on the Fusion of Donepezil and Melatonin. *Bioorg. Med. Chem.* **2016**, *24* (18), 4324–4338.

(354) Chojnacki, J. E.; Liu, K.; Yan, X.; Toldo, S.; Selden, T.; Estrada, M.; Rodríguez-Franco, M. I.; Halquist, M. S.; Ye, D.; Zhang, S. Discovery of 5-(4-Hydroxyphenyl)-3-Oxo-Pentanoic Acid [2-(5-Methoxy-1H-Indol-3-Yl)-Ethyl]-Amide as a Neuroprotectant for Alzheimer's Disease by Hybridization of Curcumin and Melatonin. *ACS Chem. Neurosci.* **2014**, *5* (8), 690–699.

(355) Stevens, C. B.; Hanna, J. M.; Lammi, R. K. Synthesis of Tetrahydroxybiphenyls and Tetrahydroxyterphenyls and Their Evaluation as Amyloid-β Aggregation Inhibitors. *Bioorg. Med. Chem. Lett.* **2013**, *23* (6), 1703–1706.

(356) Meena, P.; Nemaysh, V.; Khatri, M.; Manral, A.; Luthra, P. M.; Tiwari, M. Synthesis, Biological Evaluation and Molecular Docking Study of Novel Piperidine and Piperazine Derivatives as Multi-Targeted Agents to Treat Alzheimer's Disease. *Bioorg. Med. Chem.* **2015**, *23* (5), 1135–1148.

(357) Salomon, A. R.; Marcinowski, K. J.; Friedland, R. P.; Zagorski, M. G. Nicotine Inhibits Amyloid Formation by the β-Peptide. *Biochemistry* **1996**, *35* (42), 13568–13578.

(358) Yerdelen, K. O.; Koca, M.; Anil, B.; Sevindik, H.; Kasap, Z.; Halici, Z.; Turkaydin, K.; Gunesacar, G. Synthesis of Donepezil-Based Multifunctional Agents for the Treatment of Alzheimer's Disease. *Bioorg. Med. Chem. Lett.* **2015**, *25* (23), 5576–5582.

(359) Xu, W.; Wang, X.-B.; Wang, Z.-M.; Wu, J.-J.; Li, F.; Wang, J.; Kong, L.-Y. Synthesis and Evaluation of Donepezil–Ferulic Acid Hybrids as Multi-Target-Directed Ligands against Alzheimer's Disease. *MedChemComm* **2016**, *7* (5), 990–998.

(360) Rochais, C.; Lecoutey, C.; Gaven, F.; Giannoni, P.; Hamidouche, K.; Hedou, D.; Dubost, E.; Genest, D.; Yahiaoui, S.; Freret, T.; et al. Novel Multitarget-Directed Ligands (MTDLs) with Acetylcholinesterase (AChE) Inhibitory and Serotonergic Subtype 4 Receptor (5-HT4R) Agonist Activities As Potential Agents against Alzheimer's Disease: The Design of Donecopride. *J. Med. Chem.* **2015**, *58* (7), 3172–3187.

(361) Zhu, Y.; Xiao, K.; Ma, L.; Xiong, B.; Fu, Y.; Yu, H.; Wang, W.; Wang, X.; Hu, D.; Peng, H.; et al. Design, Synthesis and Biological Evaluation of Novel Dual Inhibitors of Acetylcholinesterase and Beta-Secretase. *Bioorg. Med. Chem.* **2009**, *17* (4), 1600–1613.

(362) Matsui, K.; Oda, Y.; Ohe, H.; Tanaka, S.; Asakawa, N. Direct Determination of E2020 Enantiomers in Plasma by Liquid Chromatography-Mass Spectrometry and Column-Switching Techniques. *J. Chromatogr. A* **1995**, *694* (1), 209–218.

(363) Nagel, A. A.; Liston, D. R.; Jung, S.; Mahar, M.; Vincent, L. A.; Chapin, D.; Chen, Y. L.; Hubbard, S.; Ives, J. L. Design and Synthesis of 1-Heteroaryl-3-(1-Benzyl-4-Piperidinyl)Propan-1-One Derivatives as Potent, Selective Acetylcholinesterase Inhibitors. *J. Med. Chem.* **1995**, *38* (7), 1084–1089.

(364) Yan, J.; Hu, J.; Liu, A.; He, L.; Li, X.; Wei, H. Design, Synthesis, and Evaluation of Multitarget-Directed Ligands against Alzheimer's Disease Based on the Fusion of Donepezil and Curcumin. *Bioorg. Med. Chem.* **2017**, *25* (12), 2946–2955.

(365) Laroche, B.; Saito, Y.; Ishitani, H.; Kobayashi, S. Basic Anion-Exchange Resin-Catalyzed Aldol Condensation of Aromatic Ketones with Aldehydes in Continuous Flow. *Org. Process Res. Dev.* **2019**, *23* (5), 961–967.

(366) Green, K.; Fosso, M.; Garneau-Tsodikova, S. Multifunctional Donepezil Analogues as Cholinesterase and BACE1 Inhibitors. *Molecules* **2018**, *23* (12), 3252.

(367) van Greunen, D. G.; Cordier, W.; Nell, M.; van der Westhuyzen, C.; Steenkamp, V.; Panayides, J.-L.; Riley, D. L. Targeting Alzheimer's Disease by Investigating Previously Unexplored Chemical Space Surrounding the Cholinesterase Inhibitor Donepezil. *Eur. J. Med. Chem.* **2017**, *127*, 671–690.

(368) Mercey, G.; Verdelet, T.; Saint-André, G.; Gillon, E.; Wagner, A.; Baati, R.; Jean, L.; Nachon, F.; Renard, P.-Y. First Efficient Uncharged Reactivators for the Dephosphylation of Poisoned Human Acetylcholinesterase. *Chem. Commun. Camb. Engl.* **2011**, *47* (18), 5295–5297.

(369) Anderson, K. W.; Buchwald, S. L. General Catalysts for the Suzuki-Miyaura and Sonogashira Coupling Reactions of Aryl Chlorides and for the Coupling of Challenging Substrate Combinations in Water. *Angew. Chem. Int. Ed.* **2005**, *44* (38), 6173–6177.

(370) Chinchilla, R.; Nájera, C. The Sonogashira Reaction: A Booming Methodology in Synthetic Organic Chemistry †. *Chem. Rev.* **2007**, *107* (3), 874–922.

(371) Zou, G.; Zhu, J.; Tang, J. Cross-Coupling of Arylboronic Acids with Terminal Alkynes in Air. *Tetrahedron Lett.* **2003**, *44* (48), 8709–8711.

(372) Dürr, A. B.; Yin, G.; Kalvet, I.; Napoly, F.; Schoenebeck, F. Nickel-Catalyzed Trifluoromethylthiolation of Csp2–O Bonds. *Chem. Sci.* **2016**, *7* (2), 1076–1081.

(373) Roberts, R. S. Studies on the Phenyldimethylsilyllithium Reagent and Its Applications to Organic Synthesis. Ph.D., University of Cambridge, 1997.

(374) Renou, J.; Dias, J.; Mercey, G.; Verdelet, T.; Rousseau, C.; Gastellier, A.-J.; Arboléas, M.; Touvrey-Loiodice, M.; Baati, R.; Jean, L.; et al. Synthesis and in Vitro Evaluation of Donepezil-Based Reactivators and Analogues for Nerve Agent-Inhibited Human Acetylcholinesterase. *RSC Adv.* **2016**, *6* (22), 17929–17940.

(375) Barbe, G.; Charette, A. B. Highly Chemoselective Metal-Free Reduction of Tertiary Amides. *J. Am. Chem. Soc.* **2008**, *130* (1), 18–19.

(376) Learmonth, D. A.; Soares, D. S. P. M. Substituted Nitrated Catechols, Their Use in the Treatment of Some Central and Peripheral Nervous System Disorders and Pharmaceutical Compositions Containing Them. WO0198250 (A1), December 27, 2001.

(377) Prickaerts, J.; van Goethem, N. P.; Chesworth, R.; Shapiro, G.; Boess, F. G.; Methfessel, C.; Reneerkens, O. A. H.; Flood, D. G.; Hilt, D.; Gawryl, M.; et al. EVP-6124, a Novel and Selective A7 Nicotinic Acetylcholine Receptor Partial Agonist, Improves Memory Performance by Potentiating the Acetylcholine Response of A7 Nicotinic Acetylcholine Receptors. *Neuropharmacology* **2012**, *62* (2), 1099–1110.

(378) Chimenti, F.; Fioravanti, R.; Bolasco, A.; Chimenti, P.; Secci, D.; Rossi, F.; Yáñez, M.; Orallo, F.; Ortuso, F.; Alcaro, S.; et al. A New Series of Flavones, Thioflavones, and Flavanones as Selective Monoamine Oxidase-B Inhibitors. *Bioorg. Med. Chem.* **2010**, *18* (3), 1273–1279.

(379) Yung-Chi, C.; Prusoff, W. H. Relationship between the Inhibition Constant (KI) and the Concentration of Inhibitor Which Causes 50 per Cent Inhibition (I50) of an Enzymatic Reaction. *Biochem. Pharmacol.* **1973**, *22* (23), 3099–3108.

(380) Thompson, R.; Doggrell, S.; Hoberg, J. O. Potassium Channel Activators Based on the Benzopyran Substructure: Synthesis and Activity of the C-8 Substituent. *Bioorg. Med. Chem.* **2003**, *11* (8), 1663–1668.

(381) Teague, S. J.; Barber, S. Synthesis of 6-Substituted 5-Cyano-7-Hydroxy-2-Carboxybenzofurans. *Tetrahedron Lett.* **2010**, *51* (36), 4720–4722.

(382) Cole, A. G.; Metzger, A.; Brescia, M.-R.; Qin, L.-Y.; Appell, K. C.; Brain, C. T.; Hallett, A.; Ganju, P.; Denholm, A. A.; Wareing, J. R.; et al. Sulfonamido-Aryl Ethers as Bradykinin B1 Receptor Antagonists. *Bioorg. Med. Chem. Lett.* **2009**, *19* (1), 119–122.

(383) Bertz, S. H. Series on Chemistry under Physiological Conditions. Part 7. Tetramethyl 3,7-Dihydroxybicyclo[3.3.1]Nona-2,6-Diene-2,4,6,8-Tetracarboxylate: A Useful Companion to Meerwein's Ester. Topological Analysis of Bicyclo[3.3.1]Nonane Synthesis. *J. Org. Chem.* **1985**, *50* (19), 3585–3592.

(384) Tomizawa, M.; Shibuya, M.; Iwabuchi, Y. Highly Enantioselective Organocatalytic Oxidative Kinetic Resolution of Secondary Alcohols Using Chirally Modified AZADOs. *Org. Lett.* **2009**, *11* (8), 1829–1831.

(385) Pirali, T.; Gatti, S.; Di Brisco, R.; Tacchi, S.; Zaninetti, R.; Brunelli, E.; Massarotti, A.; Sorba, G.; Canonico, P. L.; Moro, L.; et al. Estrogenic Analogues Synthesized by Click Chemistry. *ChemMedChem* **2007**, *2* (4), 437–440.

(386) Horibe, H.; Fukuda, Y.; Kondo, K.; Okuno, H.; Murakami, Y.; Aoyama, T. Asymmetric Kumada–Corriu Cross-Coupling Reaction with Pd2(Dba)3 and an N–Ar Axially Chiral Mimetic-Type Ligand Catalyst. *Tetrahedron* **2004**, *60* (47), 10701–10709.

(387) Malamas, M. S.; Barnes, K.; Johnson, M.; Hui, Y.; Zhou, P.; Turner, J.; Hu, Y.; Wagner, E.; Fan, K.; Chopra, R.; et al. Di-Substituted Pyridinyl Aminohydantoins as Potent and Highly Selective Human β-Secretase (BACE1) Inhibitors. *Bioorg. Med. Chem.* **2010**, *18* (2), 630–639.

(388) Kuang, C.; Yang, Q.; Senboku, H.; Tokuda, M. Synthesis of (Z)-1-Bromo-1-Alkenes and Terminal Alkynes from Anti-2,3-Dibromoalkanoic Acids by Microwave-Induced Reaction. *Tetrahedron* **2005**, *61* (16), 4043–4052.

(389) Woo Lee, H.; Leol Yoo, C.; Uk Lee, S.; Kwon Kang, S. Effective Procedure for the Oxidative Cleavage of Olefins by OsO4-NaIO4. *HETEROCYCLES* **2009**, *78* (7), 1837.

(390) Torborg, C.; Zapf, A.; Beller, M. Palladium Catalysts for Highly Selective Sonogashira Reactions of Aryl and Heteroaryl Bromides. *ChemSusChem* **2008**, *1* (1–2), 91–96.

(391) Riva, B.; Griglio, A.; Serafini, M.; Cordero-Sanchez, C.; Aprile, S.; Di Paola, R.; Gugliandolo, E.; Alansary, D.; Biocotino, I.; Lim, D.; et al. Pyrtriazoles, a Novel Class of Store-Operated Calcium Entry Modulators: Discovery, Biological Profiling, and in Vivo Proof-of-Concept Efficacy in Acute Pancreatitis. *J. Med. Chem.* **2018**, *61* (21), 9756–9783.

(392) Kabalka, G. W.; Zhou, L.-L.; Wang, L.; Pagni, R. M. A Microwave-Enhanced, Solventless Mannich Condensation of Terminal Alkynes and Secondary Amines with Para-Formaldehyde on Cuprous Iodide Doped Alumina. *Tetrahedron* **2006**, *62* (5), 857–867.

(393) Maegawa, T.; Kitamura, Y.; Sako, S.; Udzu, T.; Sakurai, A.; Tanaka, A.; Kobayashi, Y.; Endo, K.; Bora, U.; Kurita, T.; et al. Heterogeneous Pd/C-Catalyzed Ligand-Free, Room-Temperature Suzuki–Miyaura Coupling Reactions in Aqueous Media. *Chem. – Eur. J.* **2007**, *13* (20), 5937–5943.

(394) Ortega, R.; Hübner, H.; Gmeiner, P.; Masaguer, C. F. Aromatic Ring Functionalization of Benzolactam Derivatives: New Potent Dopamine D3 Receptor Ligands. *Bioorg. Med. Chem. Lett.* **2011**, *21* (9), 2670–2674.

Résumé

La maladie d'Alzheimer (MA) est une maladie neurodégénérative complexe caractérisée par une perte progressive de la mémoire et de la cognition. C'est la première cause de démence chez le sujet âgé et affecte environs 4.6 millions de personnes par an, selon un rapport de l'association « Alzheimer's disease International », le nombre de patients pourrait s'élever à 135.5 millions en 2050. Du fait de sa complexité, la MA reste incurable et seuls 4 médicaments aux vertus palliatives dont 3 visant à inhiber l'acétylcholinestérase (AChE) ont reçu une autorisation de mise sur le marché à ce jour. L'approche multi-cible parait particulièrement adaptée du fait du grand nombre de cibles potentielles de la pathologie, et du caractère multifactoriel de la maladie. Cette approche consiste à associer sur une seule molécule, plusieurs pharmacophores afin qu'ils puissent agir simultanément sur différentes cibles impliquées dans le processus neurodégénératif. Dans ce contexte, en parallèle de la resynthèse d'un ligand multi-cible conjugué alliant un inhibiteur d'AChE (IAChE) et un antioxydant, deux nouvelles familles de ligands multi-cibles conjuguées, combinant un IAChE et un agoniste des récepteurs nicotiniques α7 (α7 nAChR) ont été conçues et leur synthèse abordée. Dans le cas de la première famille, le fragment ivastigmine a été choisi pour sa capacité à inhiber de manière pseudo-irréversible l'AChE et a été conjugué à un motif quinuclidine, un puissant agoniste des α7 nAChRs impliqués dans la MA. En combinant ces deux fragments, il a été observé que les propriétés biologiques *in vitro* de chaque pharmacophore étaient améliorées. La structure de la seconde famille est basée sur le Donepezil, un IAChE réversible de plus forte affinité, combiné au même motif quinuclidine que dans la série précédente. Si des intermédiaires avancés ont été obtenus, un ou deux étapes restent à finaliser pour finaliser la synthèse de cette troisième famille de MTDL.

Mots-clés : maladie d'Alzheimer, ligand multi-cibles, acétylcholinestérase, antioxydant, récepteur nicotinique α7, huprine, rivastigmine, donepezil.

Abstract

Alzheimer's disease (AD) is a complex neurodegenerative disease characterised by a progressive loss of memory and cognition. Nowadays, 4.6 million new patients are identified every year and according to the "Alzheimer's diseases International" association, the number of patients could reach 135.5 million in 2050. Due to its complexity, AD remains uncurable and only 4 palliative drugs, of which 3 are acetylcholinesterase (AChE) inhibitors (AChEI), have been approved by FDA to date. AD being a multifactorial illness, with many potential targets involved in the pathology, the MTDL approach seems promising. This strategy associates in one single molecule, different pharmacophores (at least) acting on different targets involved in this CNS-related disorder. In this context, in parallel with the upscaled synthesis of a conjugated MTDL combining an AChEI inhibitor and an antioxidant, two new families of conjugated MTDLs associating an AChEI and a α7 nicotinic receptor (α7 nAChR) agonist have been investigated. The structure of the first family was based on a Rivastigmine scaffold, known to be a pseudo-irreversible AChE inhibitor, and a quinuclidine fragment, a potent α7 nAChR agonist. By combining these two fragments, it was brought to light that the in vitro biological properties were improved on both targets. The second family was based on a donepezil fragment, a more potent AChEI, and the same quinuclidine fragment than in the first family. Advanced intermediates have been obtained, and two last steps remain to be achieved for the completion of this third MTDL series.

Keywords: Alzheimer's disease, multi-target directed ligand, acetylcholinesterase, antioxidant, α7 nicotinic receptor, huprine, rivastigmine, donepezil